

THE DEFORMATION CHARACTERISTICS OF
DEOXIDATION PRODUCTS IN HOT ROLLED STEEL.

A thesis submitted in application
for the degree of:
DOCTOR OF PHILOSOPHY
in
THE UNIVERSITY OF ASTON IN BIRMINGHAM
by
GRAHAM WARDLE

Department of Metallurgy and Materials,
The University of Aston in Birmingham,
Gosta Green, Birmingham. B4 7ET.
January, 1979.

THE DEFORMATION CHARACTERISTICS OF DEOXIDATION PRODUCTS
IN HOT ROLLED STEEL.

GRAHAM WARDIE.

THESIS : DOCTOR OF PHILOSOPHY - JANUARY 1979.

SUMMARY

The deoxidation of steel at 1600°C. was achieved by the use of Mn-Si-Al alloys. Steels containing silicate inclusions of various compositions were deformed by rolling, and the deformation of these inclusions was studied with reference to various parameters.

Electron-probe micro analysis revealed that the 'as cast' inclusion compositions varied with respect to inclusion size.

The 'Relative Plasticity indices' of deformed inclusions have been measured and related to inclusion size, composition, matrix strain and the temperature of deformation. In addition attention has been focussed upon the measurement of 'relative plasticity' values obtained from other orthogonal planes.

It was shown that inclusions less than approximately 2 μm in diameter did not deform under any of the imposed deformation conditions. The size of deformed inclusions was represented by the use of the square root of the product of their major and minor axes.

Inclusions rolled at the lower temperatures behaved in a 'brittle' or 'rigid' manner. There was a rapid transition from brittle to deformable behaviour over a narrow temperature range. This transition temperature was often shown to be well below any solidus/liquidus temperature encountered within the oxide system under study.

It was found that the value of 'relative plasticity index' was lowered as the degree of matrix deformation was increased. An explanation in part has been proposed on the basis of a change in strain rate during a multi-pass rolling programme.

The variation in plasticity index values measured on the various orthogonal planes has been attributed to non-plane strain deformation. Equations have been derived to relate measurements to the plane strain condition.

(INCLUSIONS : DEFORMATION : PLASTICITY-INDEX : SIZE :
COMPOSITION).

VOL. II.

CONTENTSVOLUME I

	Page
<u>SECTION 1 INTRODUCTION</u>	
1.1	Introduction 1
1.2	Present work 2
<u>SECTION 2 LITERATURE REVIEW</u>	
2.1	Deoxidation 4
2.1.1	Deoxidation processes 7
2.1.2	Inclusion classification 9
2.1.2.1	Inclusion origins 10
2.1.3	Deoxidation thermodynamics 11
2.1.3.1	Deoxidation equilibria 11
2.1.3.2	Manganese deoxidation 11
2.1.3.3	Silicon deoxidation 12
2.1.3.4	Manganese - silicon deoxidation 14
2.1.3.5	Aluminium deoxidation 15
2.1.3.6	Manganese - silicon - aluminium deoxidation 17
2.1.4	Kinetics of the deoxidation process 18
2.1.4.1	Deoxidant solution 20
2.1.4.2	Nucleation of deoxidation products 21
2.1.4.2.1	Complex deoxidation 23
2.1.4.3	Growth of nuclei 26

		Page
2.1.4.4	Elimination of inclusions	29
2.1.5	Formation of glassy and partially glassy deoxidation products	38
2.1.5.1	Phase separation and liquid immiscibility	42
2.1.5.2	Volume - temperature relationships	43
2.1.5.3	Nucleation and growth of crystals in a glass	43
2.1.6	Constitution of non-metallic inclusions in steel	45
2.2	Inclusion deformation	58
2.2.1	Introduction	58
2.2.2	Concept of a plasticity index	58
2.2.3	Measurement of inclusion plasticity	63
2.2.4	Factors influencing the inclusion plasticity index	66
2.2.4.1	The influence of inclusion and matrix strengths	69
2.2.4.2	Cavitation at inclusion/matrix interfaces	88
2.2.4.3	Degree of deformation	89
2.2.4.4	Inclusion size	94
2.2.4.5	Temperature of deformation	96
2.2.4.6	Strain rate	107

		Page
2.3	The influence of inclusions on steel properties	110
2.3.1	Influence upon strength, ductility and toughness	110
2.3.1.1	General theoretical considerations	111
2.3.1.2	Factors influencing the fracture process	113
2.3.1.2.1	Inclusion size	113
2.3.1.2.2	Interparticle spacing and volume fraction	115
2.3.1.2.3	Inclusion morphology	120
2.3.1.2.4	Deformation	121
2.3.1.2.5	Matrix/particle bond	126
2.3.1.3	Lamellar tearing	127
2.3.2	Impact resistance	128
2.3.3	Fatigue	132
2.3.4	Machinability	139
2.3.4.1	Inclusion type and morphology	139
2.3.4.2	Composition and deformability of inclusions	140
2.3.4.3	Volume fraction	140
2.3.4.4	Size and shape	141
2.3.5	Influence of inclusions on other properties	141

SECTION 3 EXPERIMENTAL PROCEDURE

3.1	Melting and casting procedure	143
3.1.1	Selection of experimental conditions	143
3.1.1.1	Melt material	143
3.1.1.2	Crucible material	144
3.1.2	Experimental equipment	145
3.1.2.1	Melting furnaces	145
3.1.2.2	Furnace atmospheres	147
3.1.3	Selection of deoxidant compositions	147
3.1.4	Preparation of deoxidant alloys	149
3.1.5	Experimental melts	149
3.1.5.1	Iron - oxygen alloys (melting procedure)	149
3.1.5.2	Sampling and deoxidation procedure	151
3.1.5.3	Casting technique	151
3.1.5.4	Sectioning of cast bars	152
3.1.6	Development of programme	152
3.2	Rolling procedures	154
3.2.1	Selection of experimental conditions	154
3.2.1.1	Sample reductions	154
3.2.1.2	Rolling temperatures	156
3.2.2	Experimental equipment	158
3.2.2.1	Rolling mill	158
3.2.2.2	Furnaces	158
3.2.3	Sectioning of rolled samples	159
3.2.4	Plasticine model system	159

		page
3.3	Heat treatment	161
3.3.1	Specimen size	161
3.3.2	Heat treatment temperatures	162
3.3.3	Heat treatment times	162
3.3.4	Heat treatment furnace	162
3.4	Quantitative analysis	163
3.4.1	Compositional analysis	163
3.4.1.1	Chemical analysis	163
3.4.1.2	Inclusion analysis	163
3.4.2	Metallography	166
3.4.2.1	Preparation of microstructures	166
3.4.2.2	Inclusion size and area distribution	166
3.4.2.3	Aspect ratio analysis	167
3.5	Electron metallography	169
3.5.1	Preparation of samples	169

SECTION 4 EXPERIMENTAL RESULTS

4.1	Analysis of starting material	171
4.2	Oxygen analysis	171
4.3	Deoxidant alloys	175
4.4	Melt and inclusion analyses	175
4.5	Inclusion size distribution and area content	185
4.6	Plasticity index analyses	195
4.7	Metallographic examination (as cast)	219
4.8	Metallographic examination (Hot rolled samples)	233

		page
4.9	Stereoscan examination of rolled structures	269
4.10	Heat treatment	280

VOLUME II

SECTION 5 DISCUSSION OF RESULTS

5.1.1	Product composition	306
5.1.1.1	Influence of (Mn:Si) deoxidant ratio upon product composition	306
5.1.1.2	Influence of aluminium upon product composition	313
5.1.2	Variation in 'as cast' inclusion composition	317
5.1.2.1	Variation with respect to position in the 'as cast' bar	317
5.1.2.2	Variation in composition with inclusion size	319
5.1.2.3	Variation in composition at small sizes and the presence of sulphur	333
5.1.3	Nucleation and growth of products	343
5.1.3.1	Inclusion size distributions	347
5.1.3.2	Summary of the results for inclusion composition and its effects upon coalescence	368
5.2	Heat treatment	375

		page
5.2.1	General observations	378
5.2.2	Developments of the heat treatment programme	379
5.3	Inclusion deformation	381
5.3.1	The behaviour of inclusion phases which did not plastically or fluidly deform at the hot rolling temperatures.	381
5.3.1.1	Plastic or fluid inclusion deformation	386
5.3.1.2	Representation of inclusion size	387
5.3.2	The effect of hot rolling upon inclusion deformation characteristics	392
5.3.3	The variation in inclusion plasticity index with temperature	392
5.3.3.1	Factors which influence the non- deformable/deformable transition curve	416
5.3.3.1.1	Viscosity	416
5.3.3.1.2	Precipitation	421
5.3.3.2	Inclusion deformation above the transition temperature	421
5.3.4	The variation in inclusion plasticity index with composition	427
5.3.5	The variation in inclusion plasticity index with size	439
5.3.5.1	Summary of the general features of plasticity index versus size relation ships and the factors which influence them	512

		page
5.3.5.1.1	Inclusion composition	514
5.3.5.1.2	Adiabatic heating effects	517
5.3.5.1.3	The ferrite to austenite transformation	518
5.3.5.1.4	The break up of large inclusions	525
5.3.5.1.5	The spheroidisation of deformed inclusions	528
5.3.5.1.6	Sectioning problems	541
5.3.5.1.7	Surface energy criterion	542
5.3.5.1.8	Effective stresses acting upon the inclusion	549
5.3.5.1.9	Deviation from plane strain	554
5.3.6	The variation of the inclusion plasticity index with the degree of matrix reduction	555
5.3.6.1	The effect of matrix/inclusion constraint	573
5.3.6.2	Inhomogeneous deformation of the matrix	578
5.3.6.3	Variation in inclusion strain across specimen width	610
5.3.7	The measurement of matrix strain	612
5.3.8	The deformation of inclusions within the roll throat	617
5.3.9	The variation in inclusion plasticity index with the plane of measurement	624

5.3.9.1	The variation of plasticity index with size for measurements on the (XZ) and (YZ) planes.	639
5.3.10	Some possible mechanisms of inclusion deformation.	647
5.4	Practical implications.	652
5.4.1	Machinability.	653
5.4.2	Surface quality of rolled products.	654
5.4.3	Implications to mechanical properties.	654

SECTION 6.

6.1	Conclusions.	655
6.2	Suggestions for further work.	661

<u>ACKNOWLEDGEMENTS.</u>	665
--------------------------	-----

<u>APPENDICES.</u>	666
--------------------	-----

A.3.1	668
A.3.2	671
A.3.3	674
A.4.1	675
A.4.2	721
A.4.3	777
A.5.1	781
A.5.2	782
A.5.3	784
A.5.4	785
A.5.4(a)	790

A.5.5

Page.

792

A.5.5(a)

803

REFERENCES.

804

5.1.1.

PRODUCT COMPOSITION

5.1.1.1.

Influence of (Mn : Si) deoxidant ratio upon product composition

Initial oxygen contents of melts prior to deoxidation were nominally constant at the 0.11 wt% level. Various additions of Mn - Si - Al deoxidants were made with different Mn:Si ratios (the maximum aluminium present in the melt after addition was approximately 0.066 wt%).

Table 5.1. indicates that as the Mn:Si ratio of the deoxidants increased then the MnO:SiO₂ ratio in the products increased linearly upto a Mn:Si ratio of approximately 5. Above this value the MnO:SiO₂ ratio appeared asymptotic, although figure 5.1. indicates there is a degree of scatter associated with these points. The oxide percentages relating to points attributable to this project are taken from table 4.5., which gives inclusion mean compositions for inclusions greater than 10 μm diameter (in order to lessen composition - size effects discussed later).

Ideally the data could be expressed as a graphical relationship between

$$\left(\frac{N^2 \text{MnO}}{N \text{SiO}_2} \right) \quad \text{versus} \quad \left(\frac{\% \text{Mn}^2}{\% \text{Si}} \right)$$

product. steel.

Table 5.1

Relationship between deoxidant (Mn/Si) ratio and (MnO/SiO₂) ratio of the product.

Melt	%Al** Addn.	$\frac{\%Mn^*}{\%Si}$ Deox	$\frac{\%MnO}{\%SiO_2}$ Prod	$\frac{\%Mn^2}{\%Si}$	$\frac{\%MnO^2}{\%SiO}$
A 6		2.25	1.30	4.32	72.84
A 6(2)		2.54	1.25	3.43	66.72
A 7		5.03	1.73	15.44	105.36
A 8		8.32	1.63	39.61	98.98
A 9	0.012	3.48	1.16	7.06	65.21
A10	0.011	5.67	1.59	20.80	90.37
A11	0.012	10.83	1.73	34.86	100.21
A12	0.020	1.56	0.63	0.62	20.16
A13	0.023	2.63	0.84	1.19	34.47
A13X	~	2.63	0.85	1.44	34.94
A14	0.026	7.12	1.31	38.72	55.60
A14(2)	0.026	7.12	1.18	5.39	77.97
A14C	0.026	7.12	1.25	12.25	61.34
A15	0.033	4.76	1.31	3.83	64.90
A16	0.028	1.49	0.67	0.73	22.13
A17	0.046	7.12	1.26*	3.04	50.75
A18	0.066	7.12	1.39	3.12	50.84

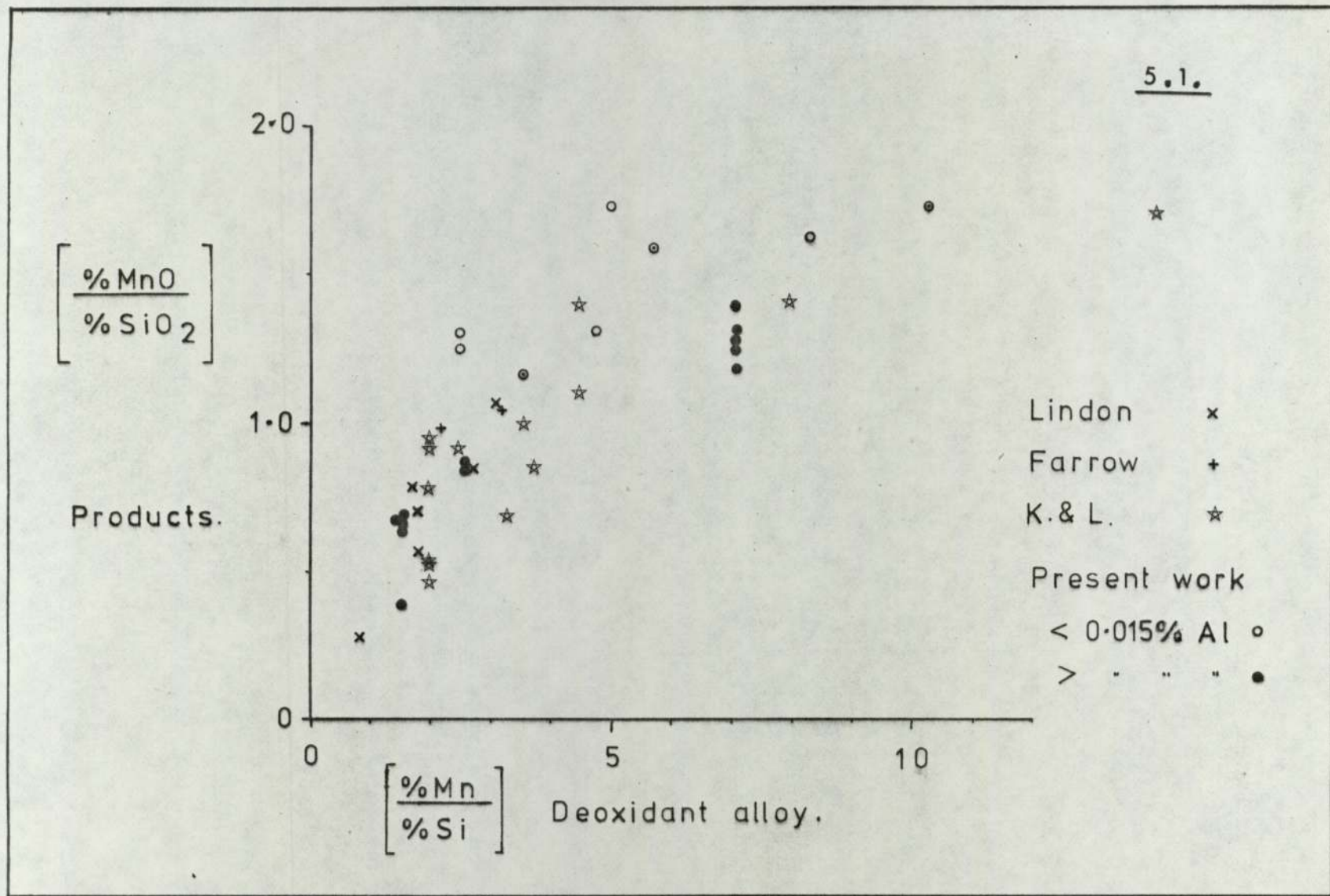
Table 5.1 (cont.)

Melt	%Al** Addn.	$\left[\frac{\%Mn^*}{\%Si}\right]$ Deox.	$\left[\frac{\%MnO}{\%SiO_2}\right]$ Prod.	$\frac{\%Mn^2}{\%Si}$	$\frac{\%MnO^2}{\%SiO}$
NIA12	0.020	1.56	0.64	1.00	19.52
CRA12	0.020	1.56	0.65	0.42	21.26
VA12	0.020	1.56	0.68	0.72	21.38
NI50A12	0.020	1.56	0.39	0.48	8.95

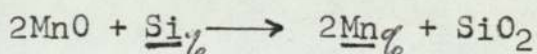
*Taken from table 4.3 chemically analysed
deoxidant alloy

$$\# \%Al = \left(\frac{\%Al \text{ in alloy}}{100} \right) \times \text{wt\% addition of alloy}$$

☆From rolled products



since the reaction for equilibrium between a melt containing manganese oxide and silica is given by



where

$$K = \frac{\% \text{Mn}^2 \cdot a_{\text{SiO}_2}}{a_{\text{MnO}}^2 \% \text{Si}}$$

Such a plot, using the results of chemical analysis only indicated a relationship which appeared to be valid for

$$\left(\frac{\% \text{Mn}^2}{\% \text{Si}} \right) \text{ steel} < 3 \quad \text{Fig. 5.2.}$$

However, it must be remembered that Mn analysis includes MnO, similarly Si and SiO₂.

i.e.

$$\frac{N^2 \text{MnO}}{N \text{SiO}_2} \sim 14 \left(\frac{\% \text{Mn}^2}{\% \text{Si}} \right)$$

where the slope of the graph is 14
Above a value of $\left(\frac{\% \text{Mn}^2}{\% \text{Si}} \right) = 3$ there was a large

degree of scatter associated with the points which varied between

$$50 < \frac{N^2 \text{MnO}}{N \text{SiO}_2} < 100+$$

However it did appear that the slope of the graph decreased possibly due to a change in the value of $\frac{\gamma_{\text{SiO}_2}}{\gamma_{\text{MnO}}^2}$ at higher $\left(\frac{\% \text{Mn}^2}{\% \text{Si}} \right)$ values.

Figure 5.1 . also contains data from the work of Lindon (9) and Farrow, and may be regarded as a generalized guide to the expected MnO:SiO₂ ratio for a given Mn:Si ratio in the deoxidant.

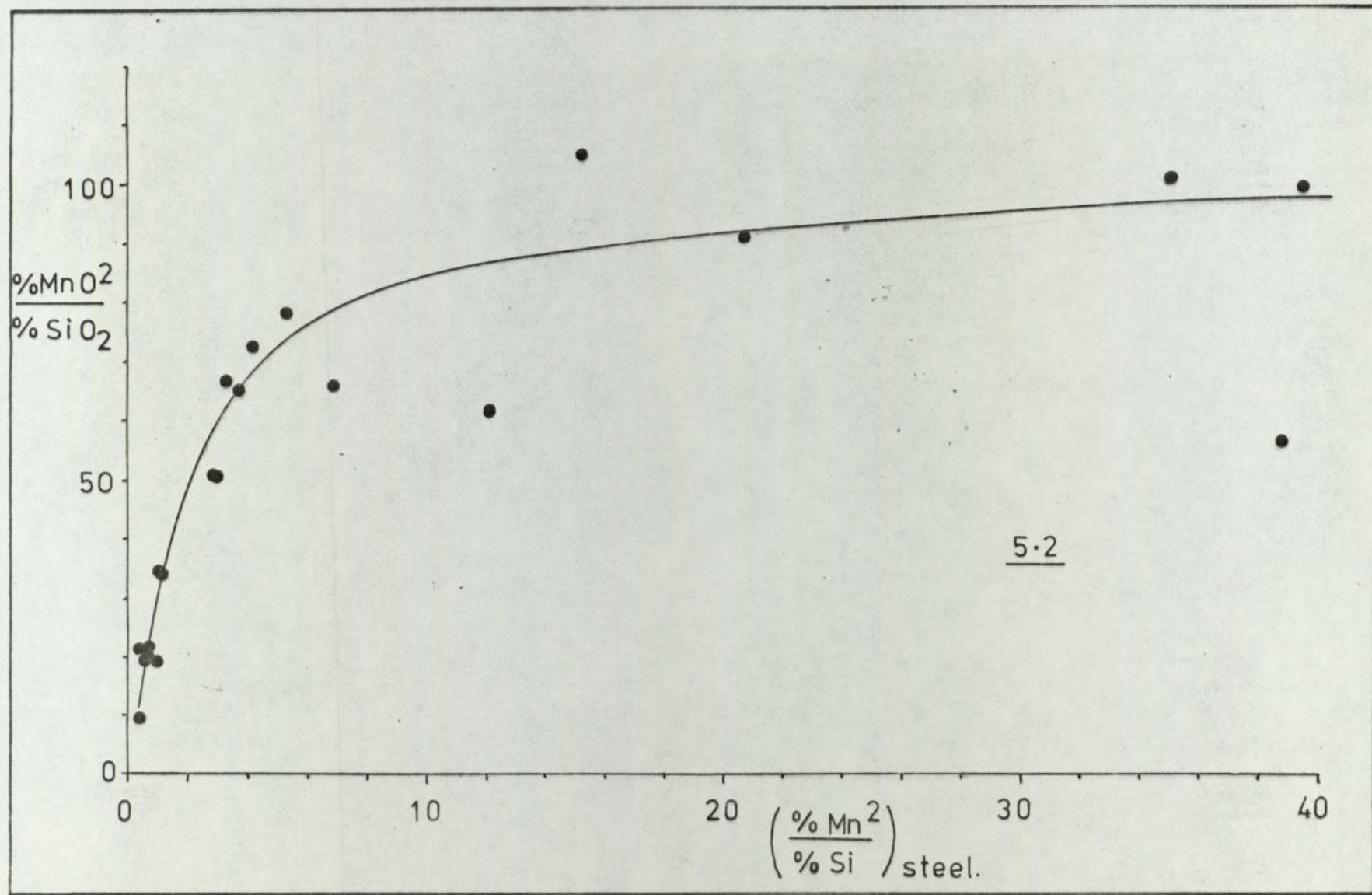


Table 5.1(a)

Relationship between deoxidant (Mn/Si) ratio and (MnO/SiO₂) ratio of the product.

(Results compiled from the data of Lindon (9) and Farrow (182))

Melt	%Al add ⁿ	$\frac{\%Mn}{\%Si}$ Deox	$\frac{\%MnO}{\%SiO_2}$ Prod
<u>Lindon</u>			
5E1	0.007	1.80	0.57
5E2	0.004	2.73	0.85
5E3	0.003	3.11	1.07
5E4	0.008	0.85	0.28
5E5	0.017	1.80	0.70
5E6	0.034	1.76	0.79
<u>Farrow</u>			
A	0.020	2.21	0.98
B	0.020	3.22	1.04

N.B. All melts deoxidised with Mn - Si - Al alloys

Data from Kiessling and Lange (79) has also been included. However, it should be emphasised that this data (table 5.2.) relates to Mn and Si levels in the steel phase via chemical analysis and is only presented as comparative data.

5.1.1.2. Influence of aluminium upon product composition.

Aluminium is the strongest of the deoxidants used in this system under study. Assuming that negligible residual aluminium contents are required for equilibrium, then for a given initial free oxygen level in the steel, it should be expected that increased levels of aluminium added would result in increased levels of alumina in the product. This should be expected until the stoichiometric alumina value was achieved.

However, in this system under study there are variable amounts of Mn and Si present, and in addition the only oxygen that the added aluminium and alumina in the product can be related to is the total oxygen at the time the deoxidant was added. It is therefore fortuitous that an approximately linear relationship exists between the alumina in the oxide products and the ratio

$$\frac{\%Al}{\%O_{total}} \quad \begin{array}{l} \text{(via the deoxidant)} \\ \text{(at the time the deoxidant was} \end{array}$$

(table 5.3 & fig.5.3.) added)

Table 5.2

Comparison between the Mn:Si ratio in the steel phase and the MnO:SiO₂ ratio in the inclusions for carbon steels studied by Kiessling and Lange

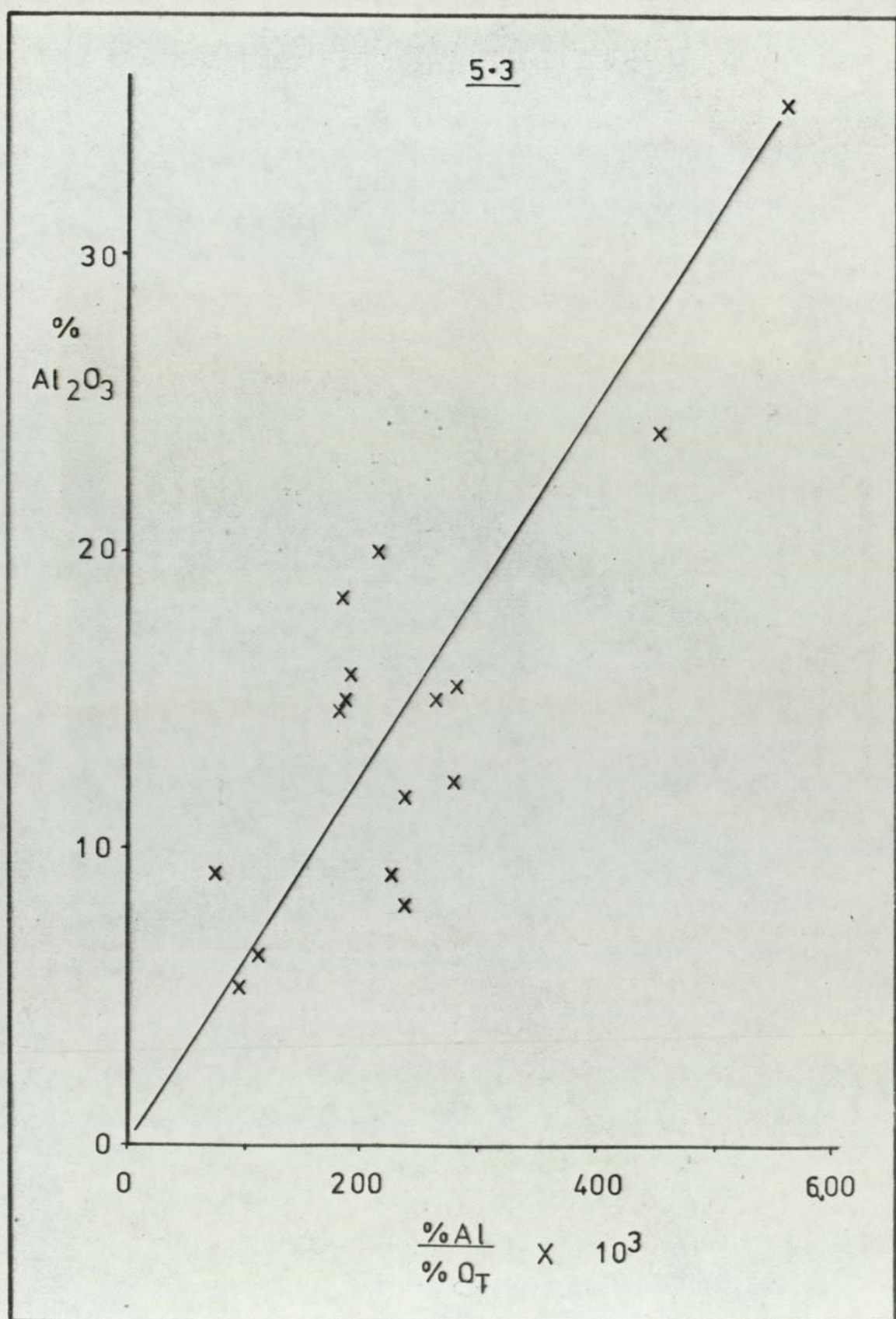
Mn:Si	MnO:SiO ₂
1.9	0.47
1.9	0.53
1.9	0.54
1.9	0.78
1.9	0.92
1.9	0.95
2.4	0.92
3.2	0.69
3.5	1.0
3.5	1.0
3.7	0.85
4.4	1.1
4.4	1.4
7.9	1.4
14	1.7
17	1.7

Table 5.3

Relationship between aluminium and oxygen contents of the melts and the amount of alumina present in the products.

Melt	%Al (via deox)	%O _T (Mo+Fe ₂ O ₃)	$\frac{(\%Al)}{(\%O_T)} \times 10^3$	%Al ₂ O ₃ (prods)
A 9	0.012	0.156	76.9	9.0
A10	0.011	0.113	97.3	5.2
A11	0.012	0.111	108.1	6.2
A12	0.020	0.109	183.5	14.3
A13	0.023	0.102	225.5	9.5
A13X	-	-	-	-
A14	0.026	0.093	279.6	15.2
A14(2)	0.026	0.11*	236.3	8.0
A14C	0.026	0.11*	236.2	10.8
A15	0.032	0.115	278.3	12.1
A16	0.028	0.106	264.1	15.0
A17	0.046	0.102	451.0	24.0
A18	0.066	0.118	559.3	35.6
NIA12	0.020	0.11*	181.8	18.4
CRA12	0.020	0.105	190.5	15.7
VA12	0.020	0.094	212.8	20.7
NI5IA12	0.020	0.11*	181.8	14.7

* Assumed oxygen level

5-3

5.1.2. Variation in 'as cast' inclusion compositions

5.1.2.1. Variation with respect to position in the 'as cast' bar.

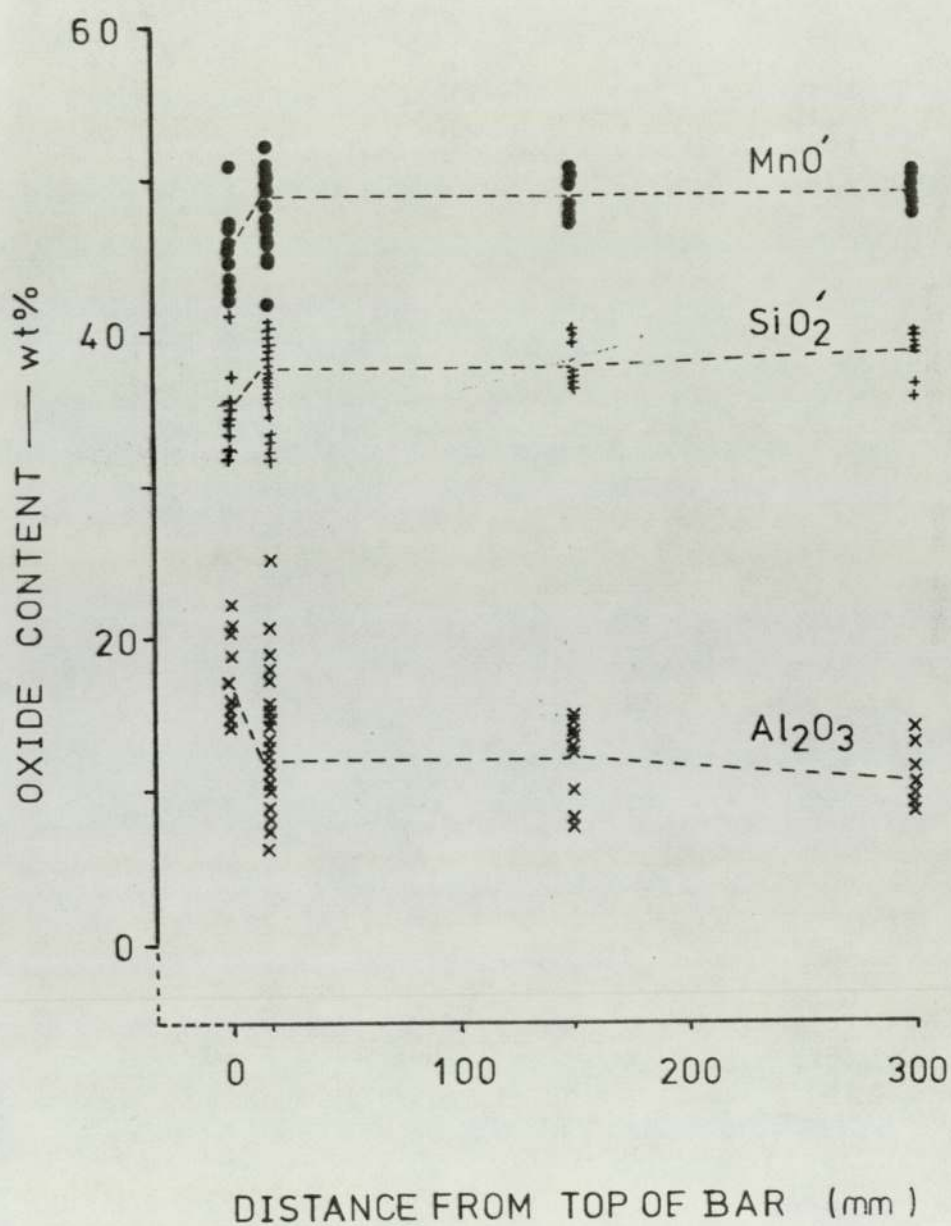
One of the conditions hoped for in these experiments was that there was a uniform inclusion composition throughout the 'as cast' bar. This was not found to be the case as has been shown from sections of the 'as cast' bar of melt Al5. (figure 4.7.)

Sections taken from various positions showed slight compositional variation within the bar. The most striking feature was that the highest level of alumina in the products existed within the topmost section. From the results contained in appendix 4.1 figure 5.4. was produced showing this compositional variation. It may be added that all the points plotted are analyses where the inclusion diameter is greater than 20 μm thus limiting the composition size effect.

The reasons why the topmost section is richest in alumina may be attributed to experimental procedure and the surface properties of the inclusions in the melt. The deoxidation procedure involves stirring the deoxidant into the melt and the solution of the deoxidant takes a finite time. Assuming that the first deoxidation products are richer in alumina, they will tend to agglomerate and coalesce as they rise to the surface layers of the melt (9). Therefore, when the melt is ready to be cast (after the stirring is completed). the larger inclusions

5.4.

Variation in inclusion composition
with position in 'as cast' bar.

MELT A15.

which are richer in alumina rise towards the top surface of the melt. Using the suction casting process the regions towards the top of the melt are taken to the top of the bar. There will of course be a degree of turbulence associated with the casting process, causing dissemination of large alumina rich products to be present throughout the bar. However, there is a finite cooling period in the bar, approximately 30 seconds (21) and the tendency will be for these larger alumina rich products to rise towards the upper region. The topmost region has been shown to contain a high volume fraction of inclusions in an earlier section. figure 4.7.

5.1.2.2. Variation in composition with inclusion size.

From early investigations it became evident that there was a variation in composition with respect to inclusion size. It was generally observed that the smaller inclusions were less rich in aluminium but had increased levels of silica present. It was, however, essential that variations due to heterogeneity of inclusions and matrix excitations were eliminated from the system.

Line scans across numerous glassy inclusions in the as cast state showed no apparent evidence of compositional variation across their diameters. It was assumed for the most part that these glassy inclusions were homogeneous. However, prior to any analysis, line scans, area scans and electron images were used for checking homogeneity. Heterogeneous inclusions were analysed using area or line scans within inclusions, although the results are more

suspect to errors due to small changes in Bragg angles when scanning.

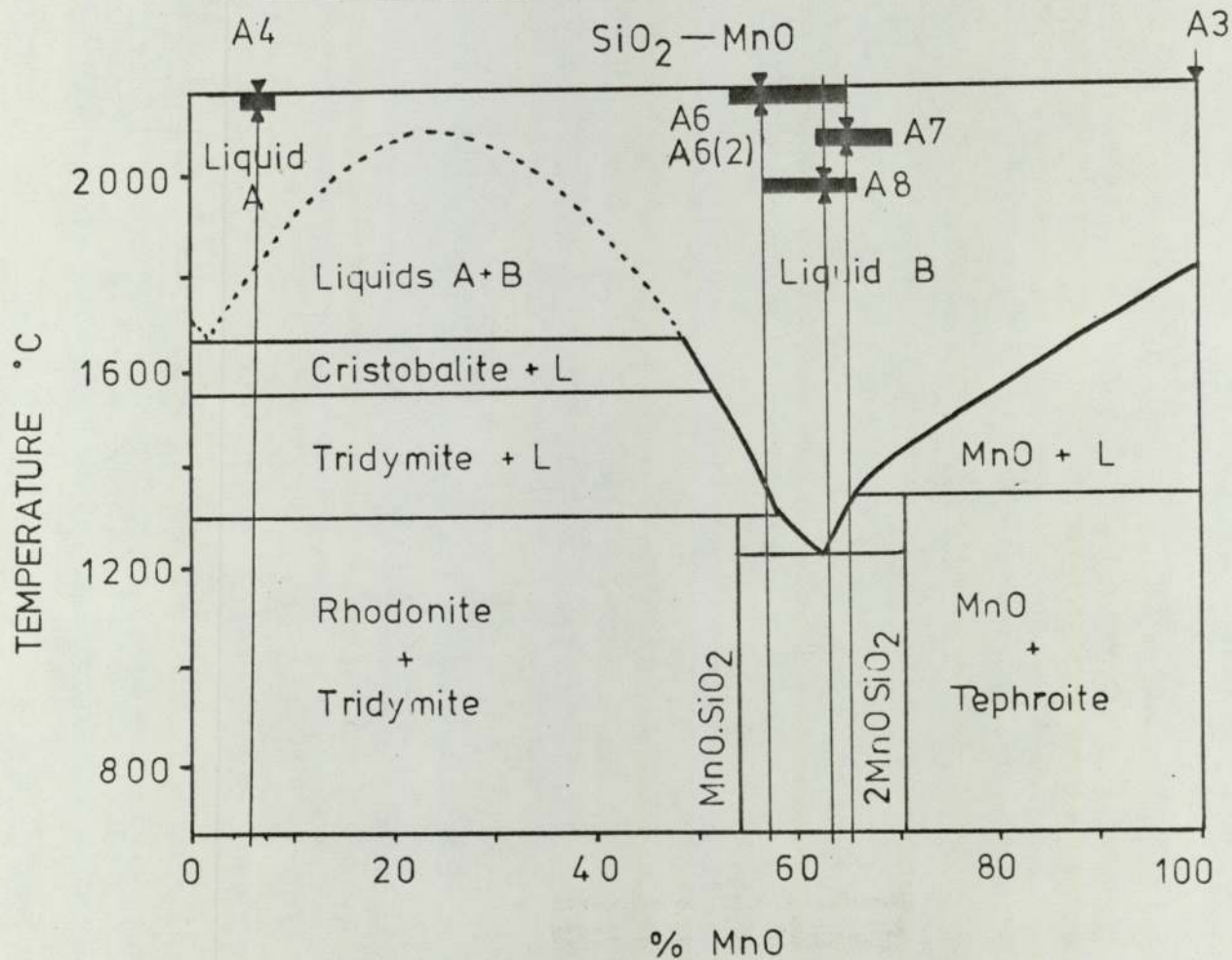
Inclusion compositions within melts deoxidised by Mn - Si alloys showed little systematic change in composition over their entire size range. Inclusions less than approximately 8 μm did show a variation in composition but this could be accounted for by matrix excitation at around the 5 μm level which would cause the apparent increase in FeO content, and decrease in MnO and SiO₂ contents. Figure 5.5 shows the compositional range

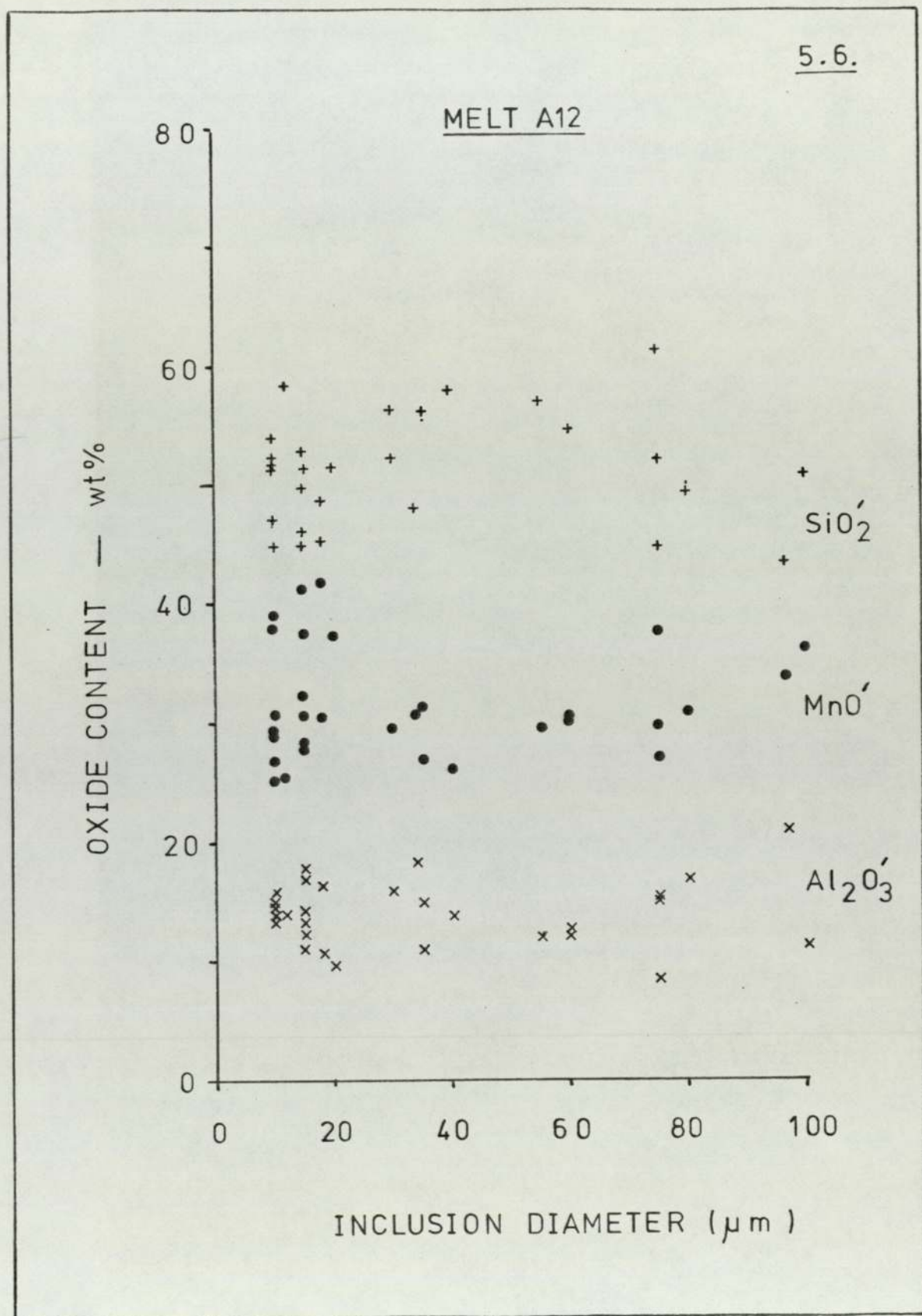
The melts which were deoxidised by aluminium containing alloys did not show such a narrow range of composition as was observed for the Mn - Si deoxidants. Variation in oxide contents of the order 20 wt% were observed (figures 5.6. - 5.15.)

Detailed composition size analyses were completed for several melts, and it became obvious that composition varied with size, particularly below 40 μm . Appendix 4.1 and figures 5.12-15. show that the general trend was that alumina decreased as size decreased. It was usually found that the silica increased with decrease in size, although the manganese oxide composition also varied to a lesser extent.

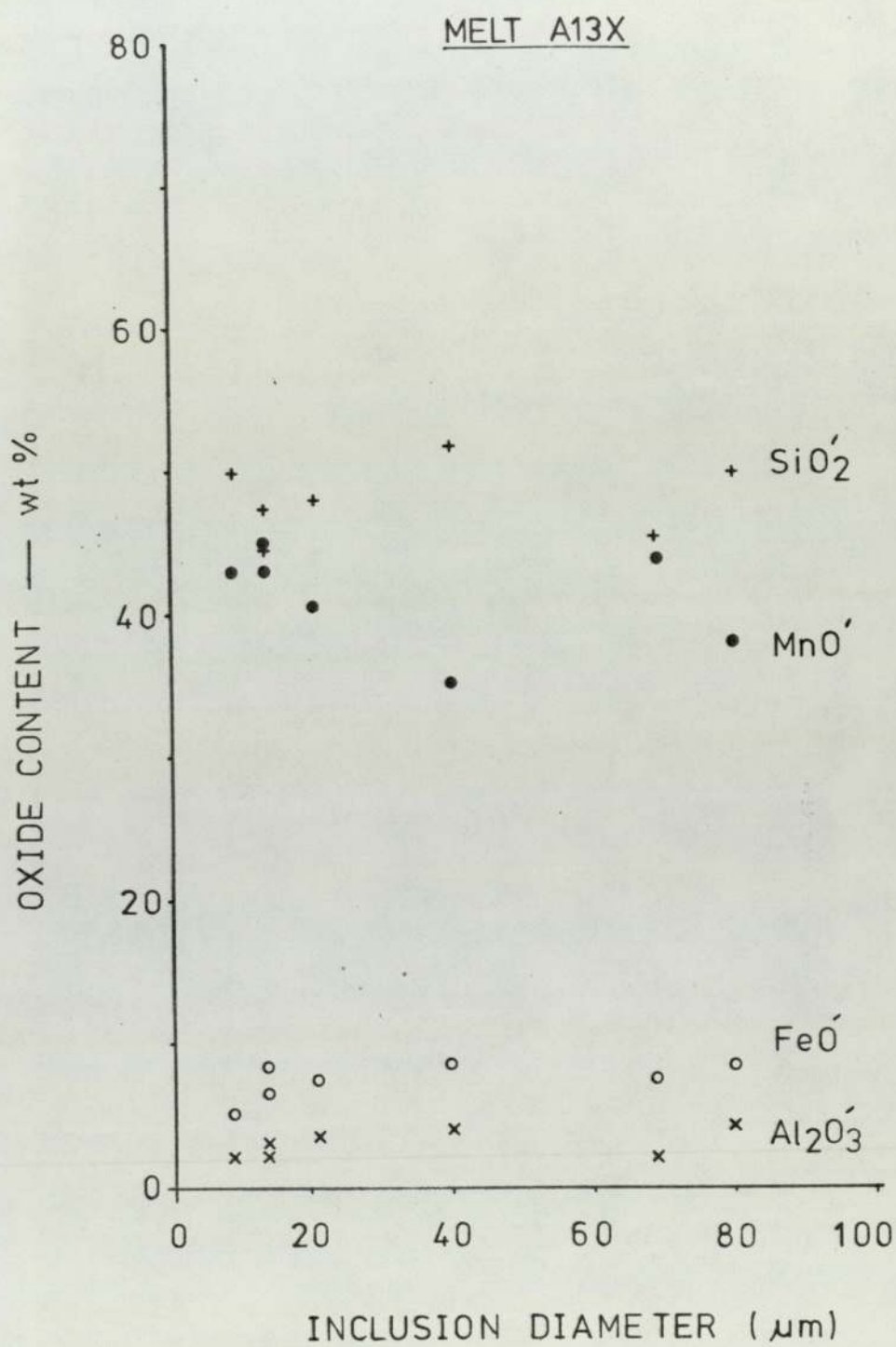
An explanation of the size - composition phenomenon may be based upon the deoxidising power of the elements present. If the initial products were alumina rich and had both time and ability to coalesce (as shown by Lindon (9)) then these inclusions should have been the largest

Figure.5.5. : Range of inclusion compositions encountered in Mn - Si deoxidised melts.

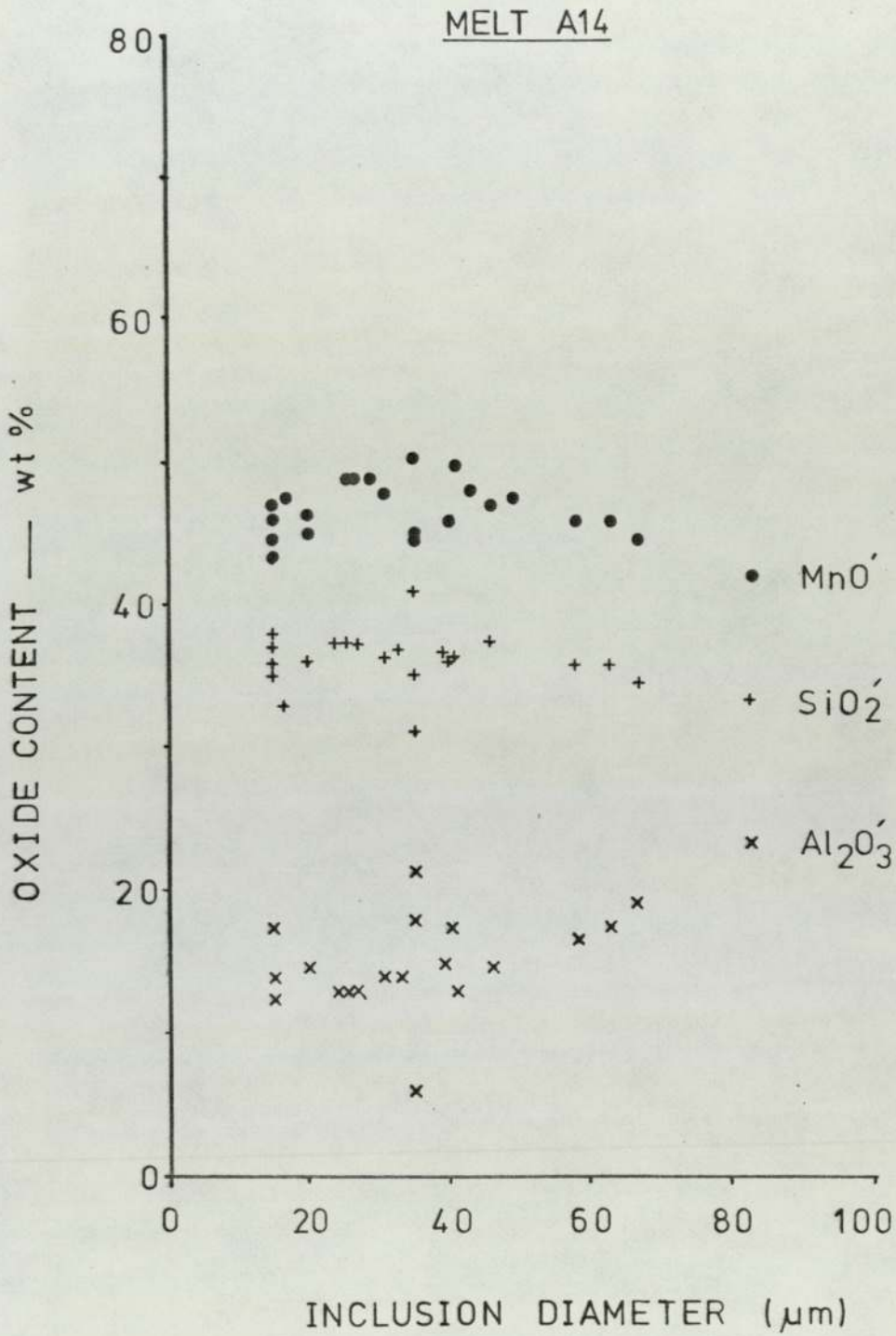




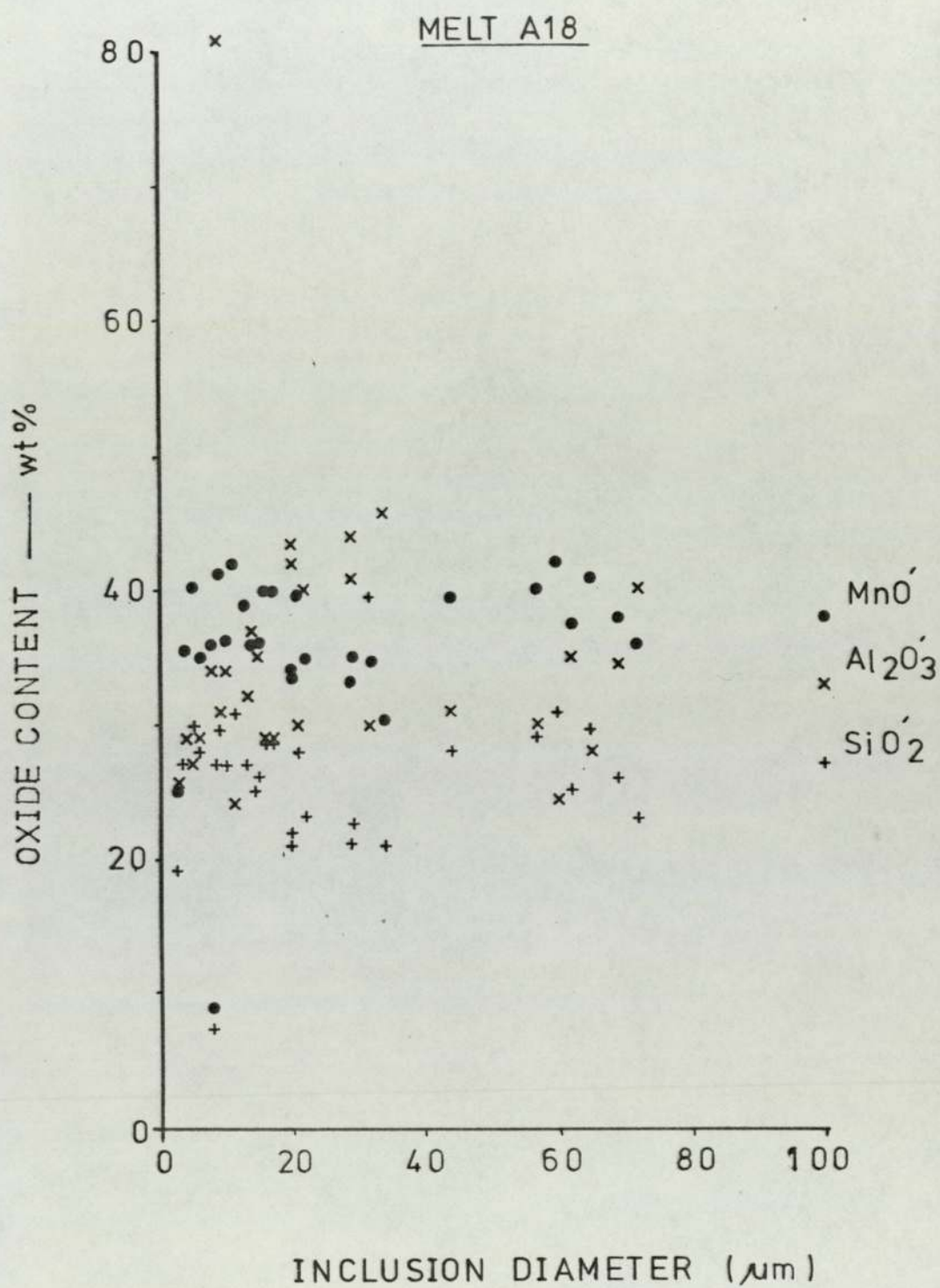
5.7.

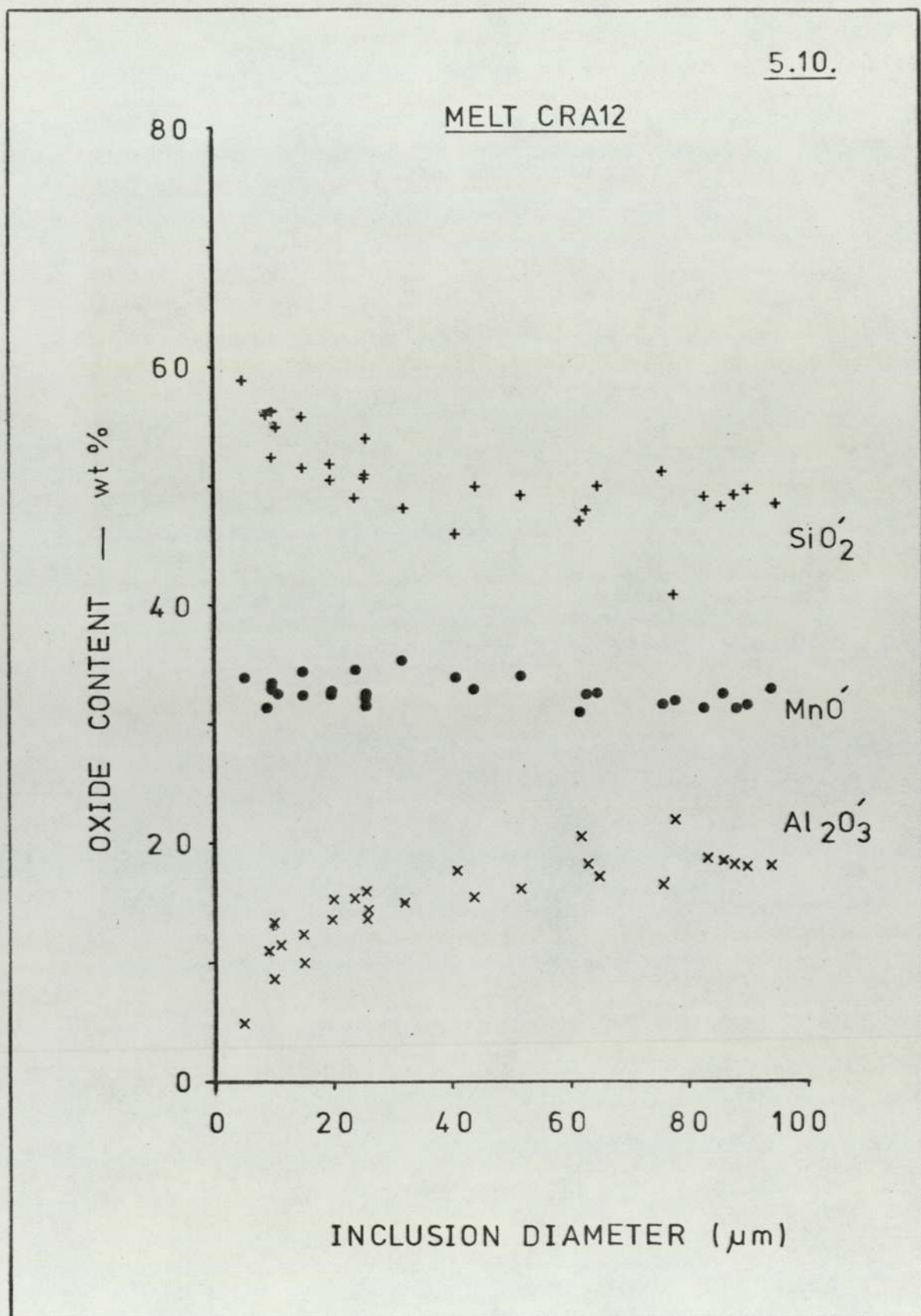


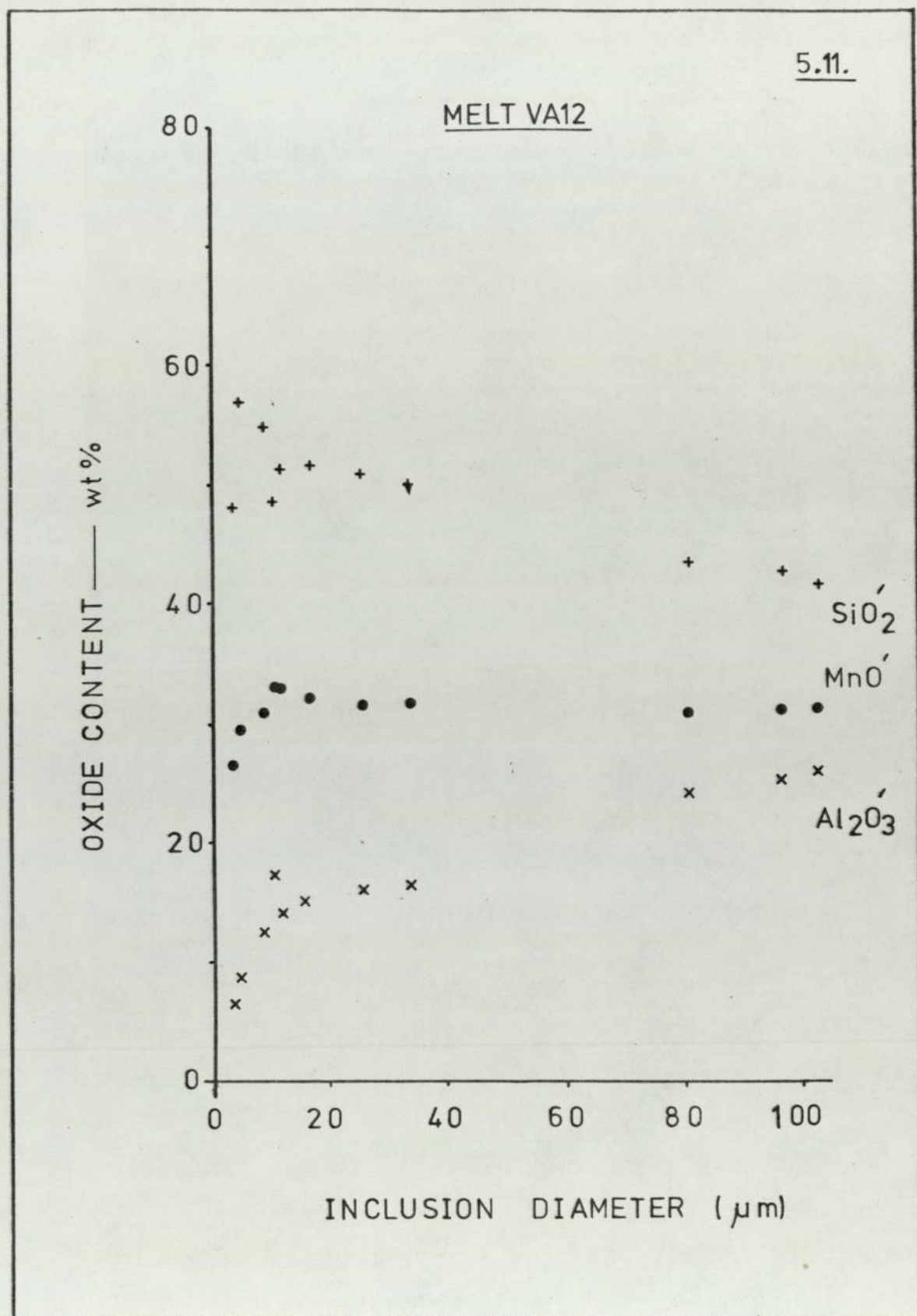
5.8.



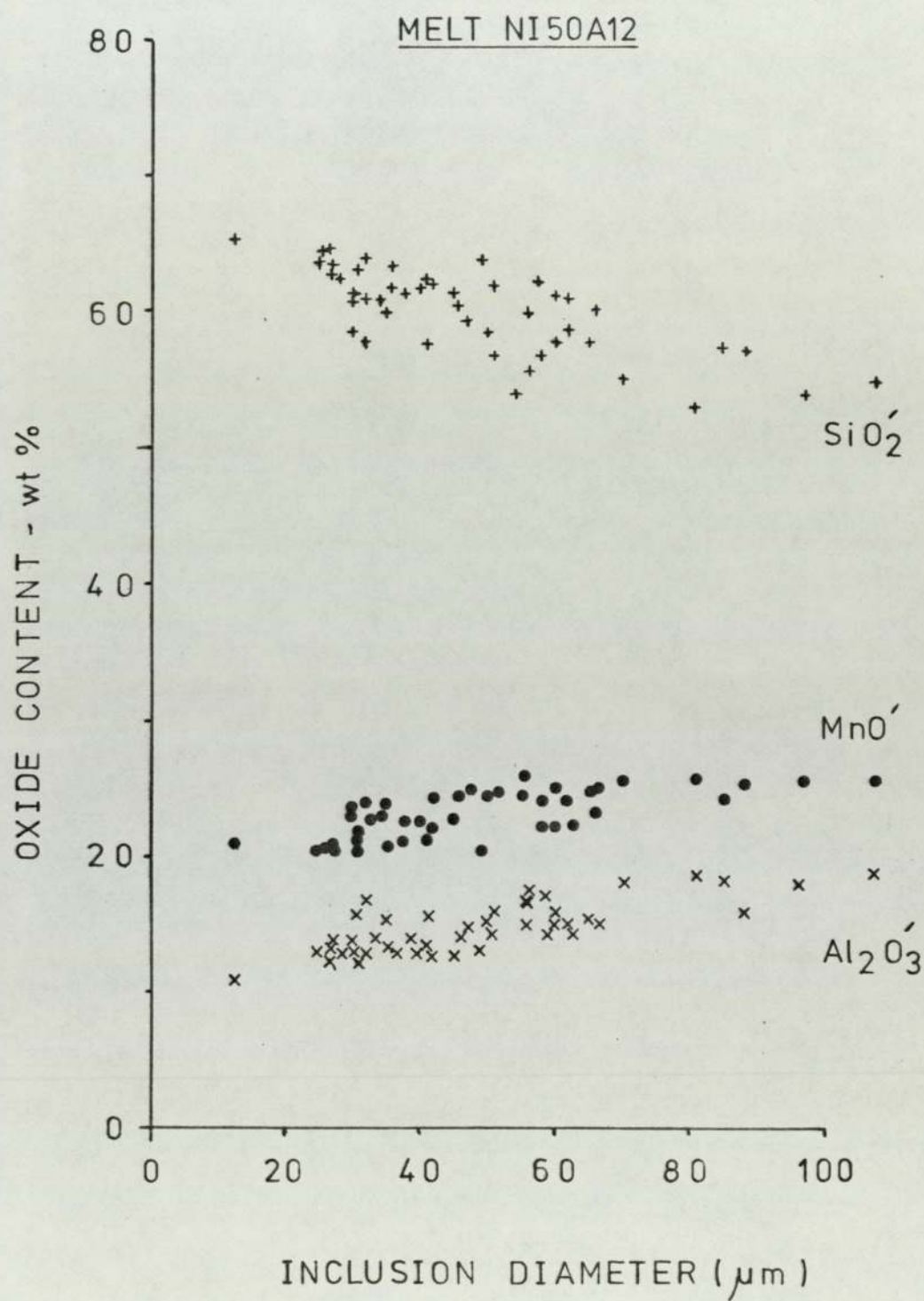
5.9.

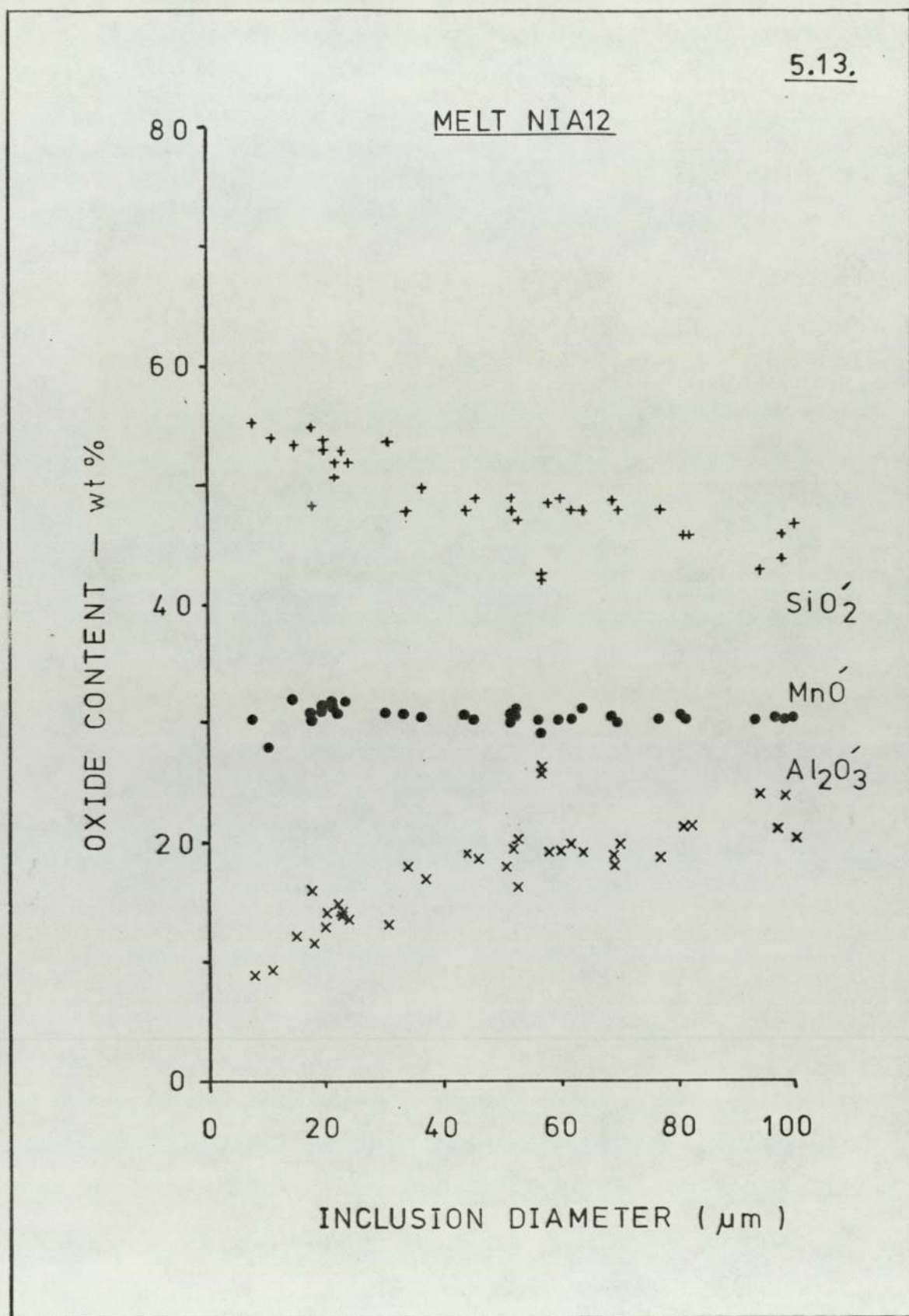




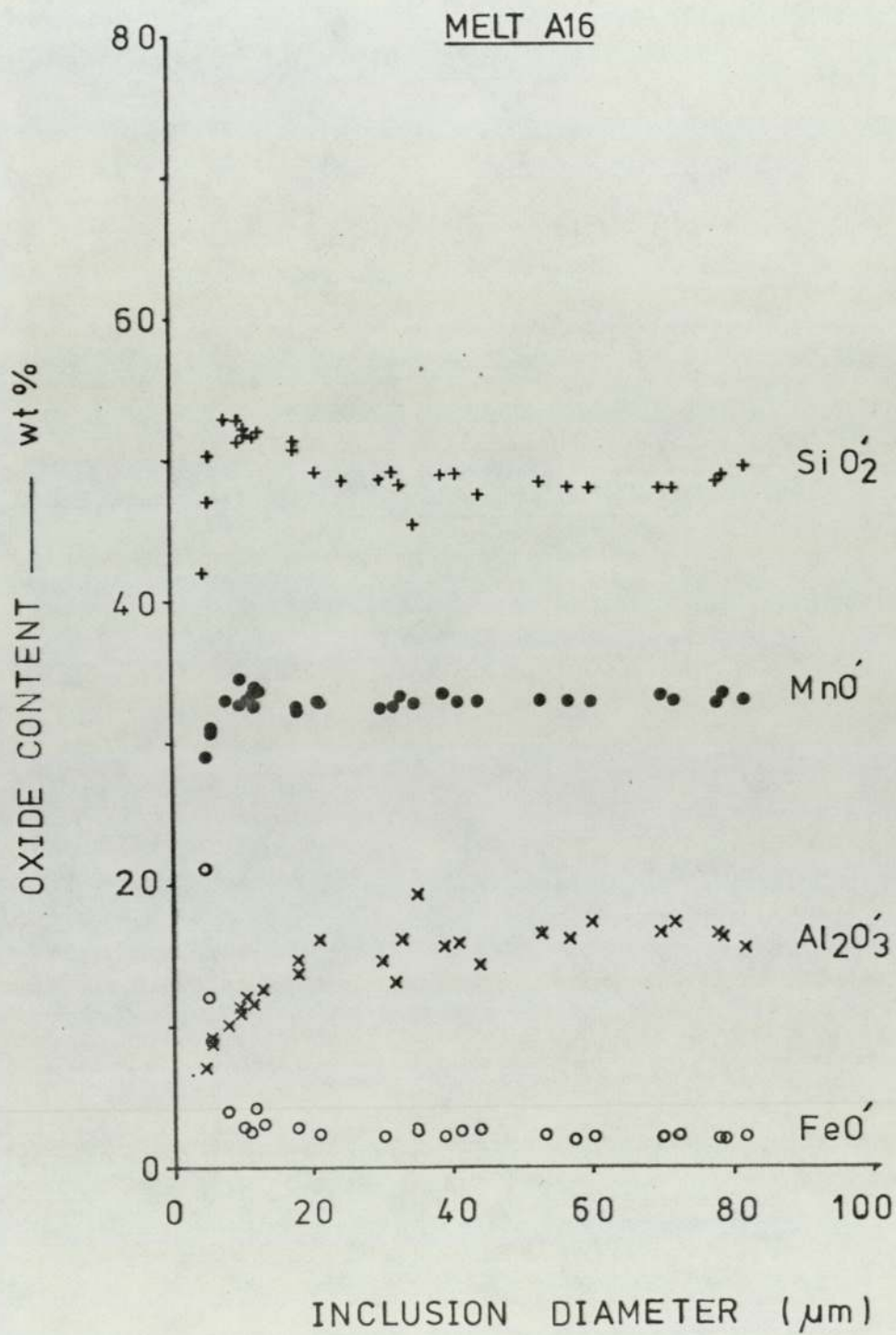


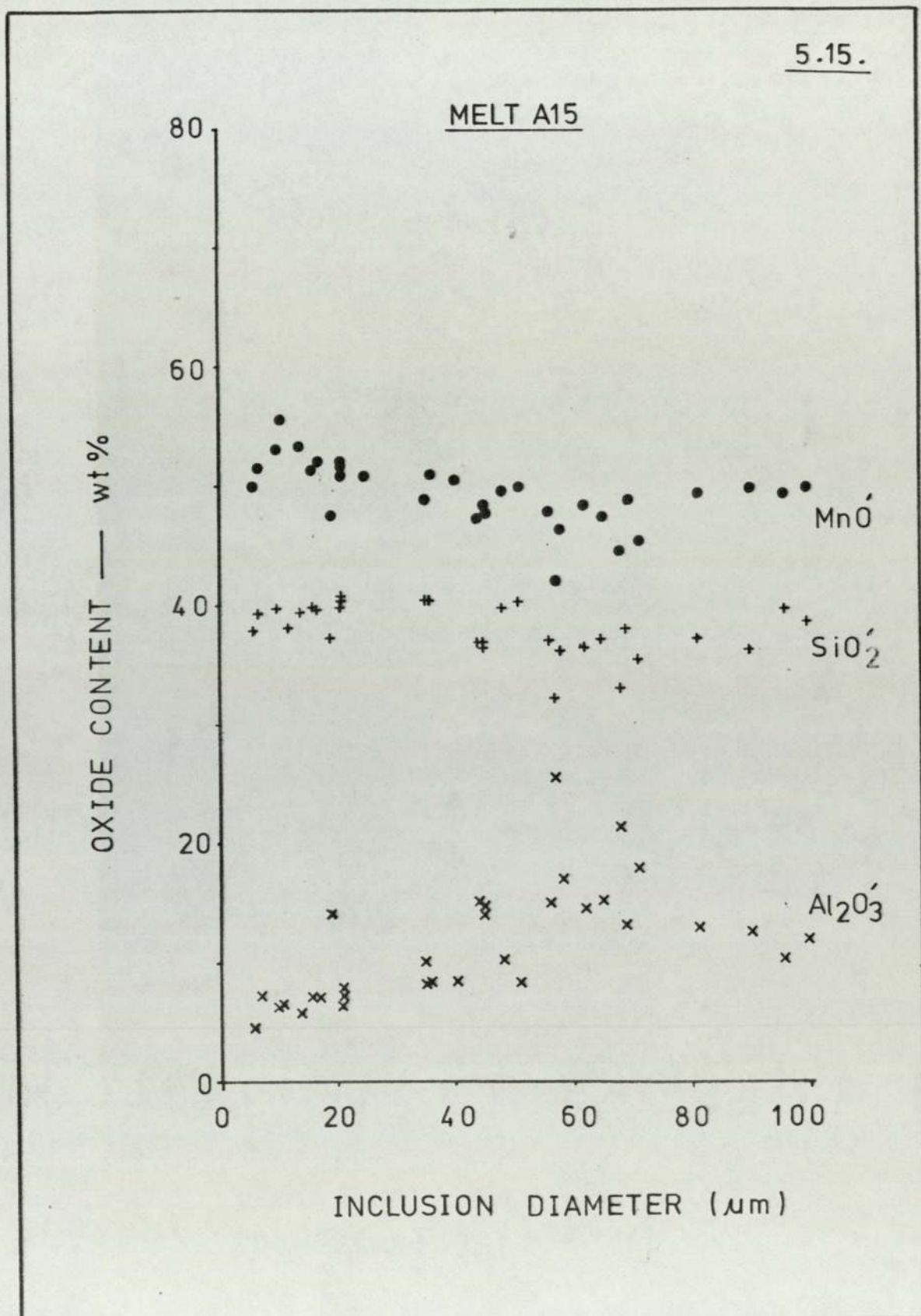
5.12.





5.14.





present in the system. As the Aluminium present in the melt was used up the next strongest deoxidant present was silicon and this began to take a more active role in the deoxidation process.

The degree to which silicon participated was obviously dictated by the amount present and its activity. However, it would generally be expected that melts containing products within the silica rich areas of the $\text{MnO} - \text{SiO}_2 - \text{Al}_2\text{O}_3$ system would have allowed silica to be far more effective. Similarly it would seem reasonable that manganese would play the predominant role in the manganese rich oxide system.

In order to see if there was any apparent effect of compositional variation with size, for inclusions within various regions of the $\text{MnO} - \text{SiO}_2 - \text{Al}_2\text{O}_3$ system, comparison was made between melts containing inclusions of similar level of alumina but with differing $\text{MnO} - \text{SiO}_2$ ratios. Such data was limited due to the number of analyses required to construct meaningful graphs. The comparison was limited also to the melts which contained the glassy 'as cast' inclusions.

Melt NI50A12 (richest in SiO_2) - figure 5.12.

It appeared that there was a steady increase in the percentage of silica present in the inclusions as the inclusion size decreased. There was also a noticeable decrease in the manganese oxide and alumina contents which corresponded to the increase in silica content.

Melts Al6 and N1A12 (Intermediate SiO₂ level) figures 5.13. & .14.

Unlike melt NI50A12 the increase in silica with decrease in inclusion size is less pronounced, and in melt Al6 there was only a slight increase in silica content at sizes less than 20 μm . In both melts Al6 and N1A12 the manganese oxide content remained constant for inclusion sizes greater than 10 μm . (N.B. Below 5 μm electron probe errors existed due to matrix excitation).

Melt Al5 (low SiO₂ Level), figure 5.15.

There was a slight indication that as the alumina content of the inclusions decreased with a decrease in size (i.e. from approximately 60 μm downwards) there was an increase in the manganese oxide level of the products. The silica level of the inclusions remaining approximately constant.

5.1.2.3. Variation in composition at small sizes, and the presence of sulphur.

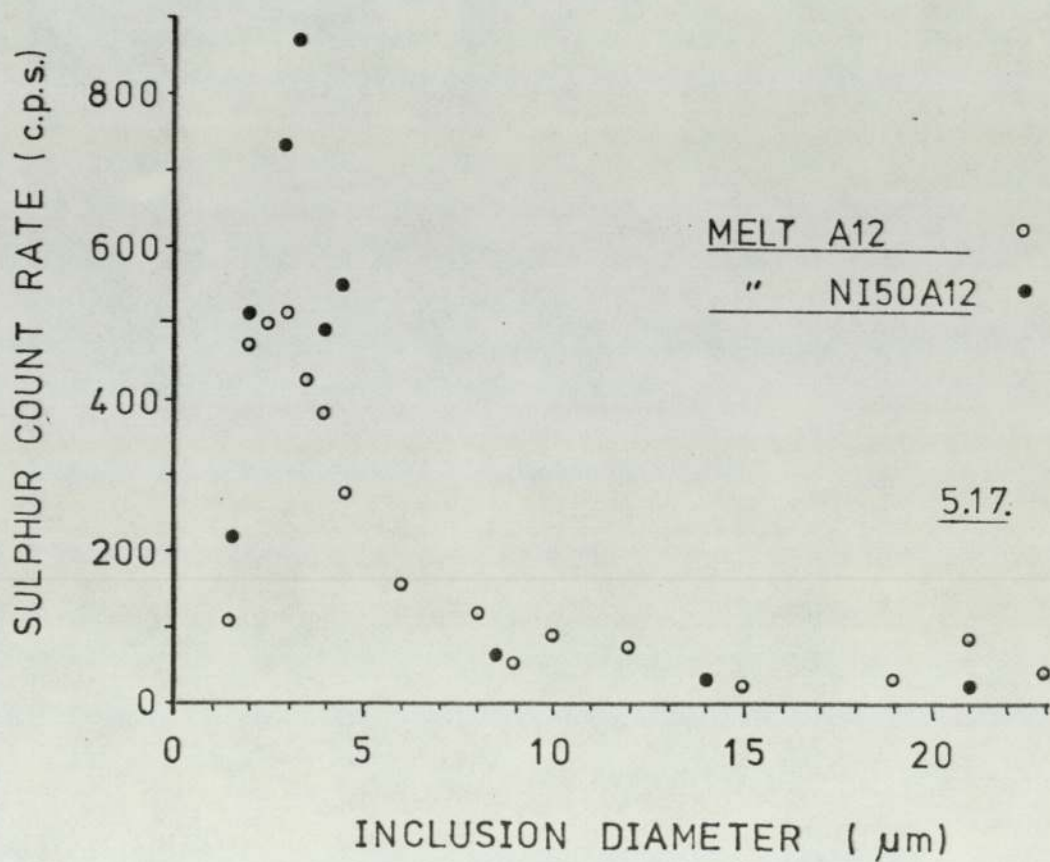
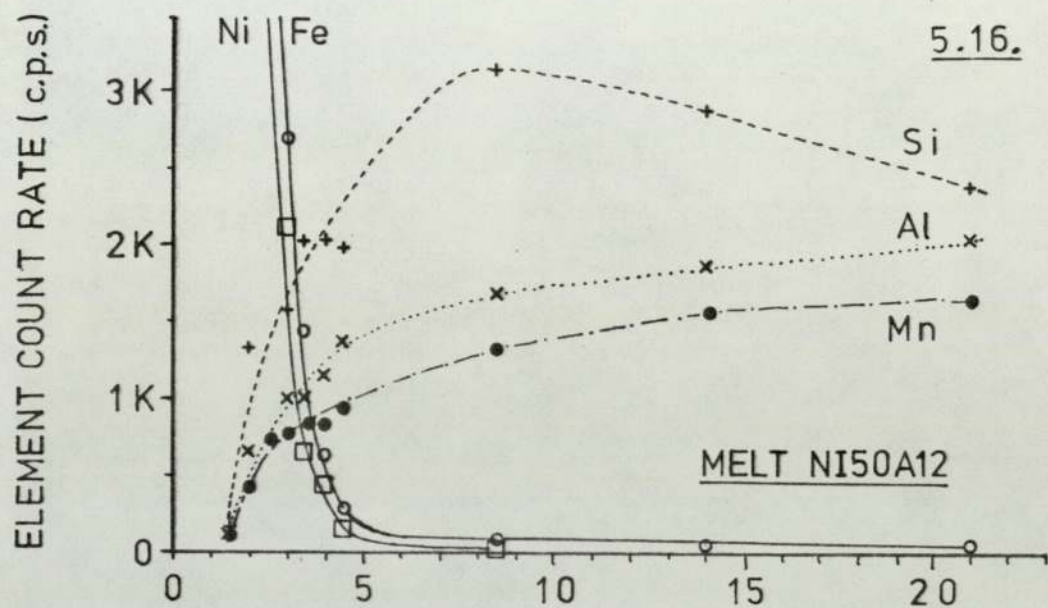
From the previous section it appeared that for inclusions below approximately 20 μm there was a compositional change. In previous work using similar deoxidants, but with 0.05% sulphur (i.e. approximately 10 times the amount in this work) present in the melt Trigwell (183) showed that oxide inclusions may be surrounded by manganese sulphide rims. In particular the presence of sulphide in the inclusion

phase increased as the size decreased.

In this work although the sulphur level in the melt was approximately 0.007 wt% it was thought appropriate to examine the smaller inclusions for sulphur content. This was regarded as essential since it is well known that the presence of sulphide and oxysulphides phases influence the deformation behaviour of inclusions.

Melt NI50Al2 was used initially for this investigation although sulphur levels at ^{Small} small sizes have been measured for melts Al2, NIA12 and VA12 (Appendix. 4.1.) The choice of melt NI50Al2 was on the basis that it had undergone a previous composition size analysis, and in addition it had been established that nickel was not present in the inclusion phase. Therefore, matrix excitation would be shown by a rapid increase in the nickel count rate. Since nickel is of similar atomic number to iron it was expected that the excitation of the ~~matrix~~ matrix would be seen. Also it was hoped it would indicate whether or not iron was present as FeO in the smaller inclusions.

Figure 5.16. shows the (observed minus background) count rates for each of the elements present for different inclusion sizes in melt NI50Al2. From these results it does appear that the silicon level increased as both aluminium and manganese decreased with decrease in size, for inclusions greater than 8 μm . Below 8 μm the silicon level decreased with decrease in size, as did the manganese and aluminium levels. This would appear to be due to the onset of matrix excitation which is shown by the iron and nickel count rates rapidly increasing at the 4 - 5 μm



sizes. It was also apparent that below $5\ \mu\text{m}$ sulphur (figure 5.17.) was present at low concentrations but increased with decrease in size. There appeared to be a peak in the sulphur count rate at around $3\ \mu\text{m}$ but this was more than likely due to attenuation of the sulphur counts since these inclusions had diameters in the region of the beam diameter ($1\frac{1}{2} - 2\ \mu\text{m}$). This effect has also been shown for melt Al2 (figure 5.17.), and data corrected for atomic number, absorption and fluorescence effects (appendix 4.1), for melts VA12 and NIA12 show this increase in sulphur level at small sizes reaching a value of approximately 5% at the $2 - 3\ \mu\text{m}$ level.

As has been shown the comparison of inclusion compositions is influenced by the observed matrix excitation. In order to compare compositions whilst compensating in part for matrix excitation a qualitative examination was performed on deformed glassy inclusions. Melt NIA12 which had been rolled at 900°C , was scanned for large deformed and small non deformed inclusions in proximity. Two inclusions were eventually found, one $6 \times 4\ \mu\text{m}$ and the larger one approximately $100 \times 4\ \mu\text{m}$ (plate 5.1.). Since both minor axes were the same size a line scan across the minor axes was hoped to compensate in part for matrix excitation. Qualitatively the line scans (plates 5.1.(a)-(m)) indicated that the smaller inclusion was

- i Very slightly less rich in manganese
- ii Less rich in aluminium

PLATES 5.1 (a) - (e)

MELT NI50Al2 ROLLED AT 900°C.

X1000

(a) ELECTRON IMAGE

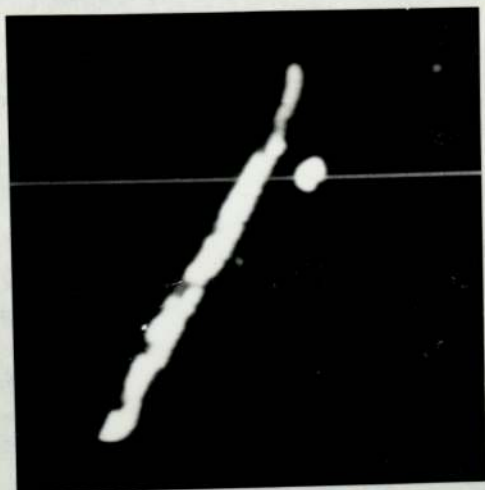
(b) Ni - SCAN

(c) Fe - SCAN

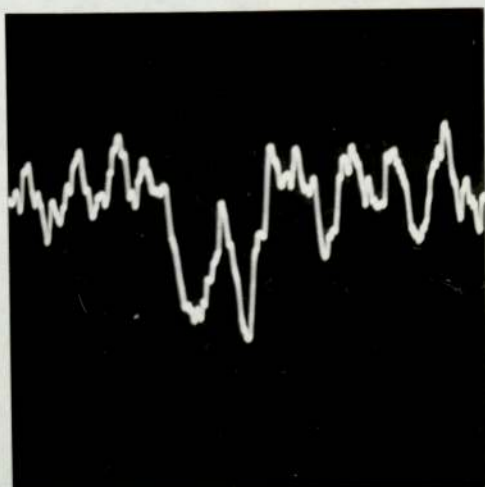
(d) Mn - XRAY

(e) Mn - SCAN

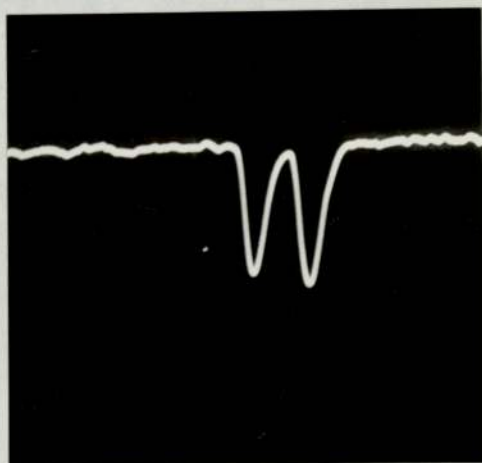
5.1.



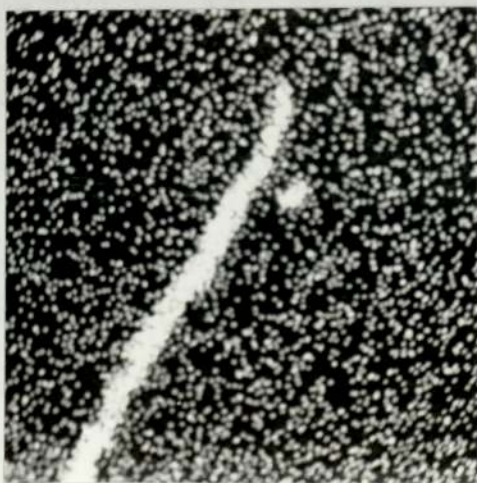
a



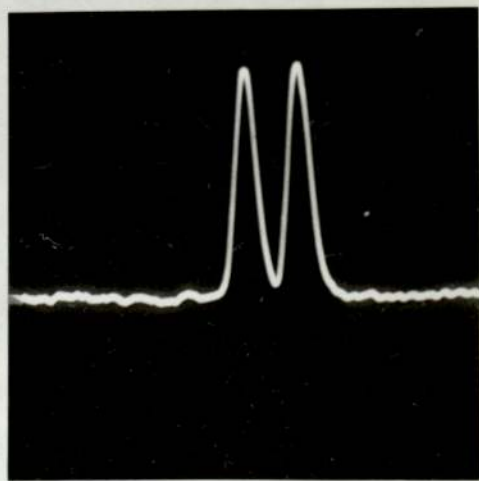
b



c



d



e

PLATES 5.1 (f) - (i)

MELT NI50Al2 ROLLED AT 900°C.

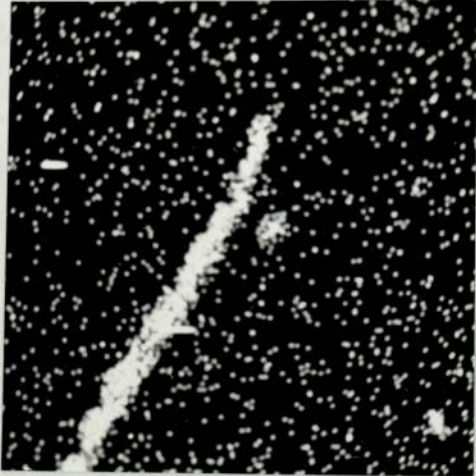
X1000

(f) Al - XRAY

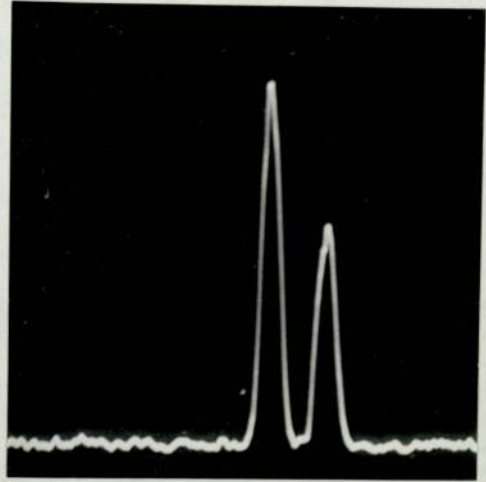
(g) Al - SCAN

(h) Si - XRAY

(i) Si - SCAN



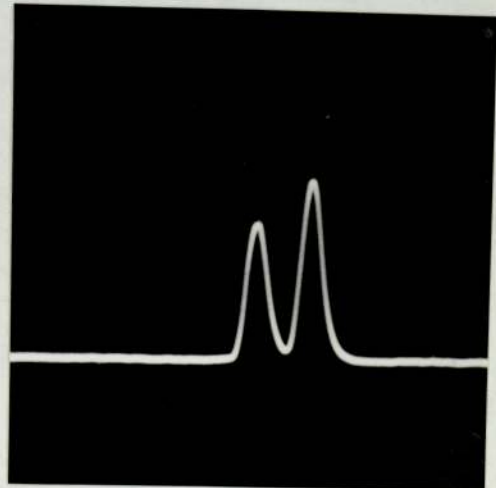
f



g



h



i

PLATES 5.1 (j) - (m)

MELT NI50A12 ROLLED AT 900°C.

X1000

(j) O - XRAY

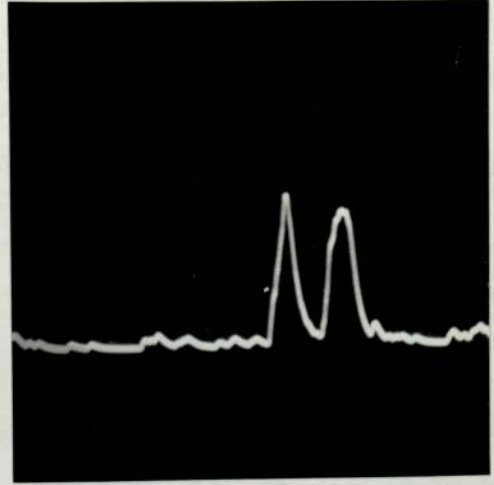
(k) O - SCAN

(l) S - XRAY

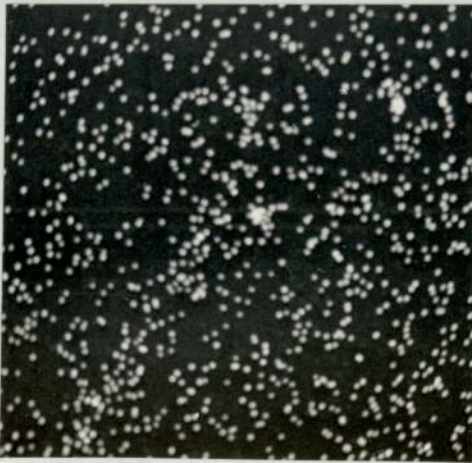
(m) S - SCAN



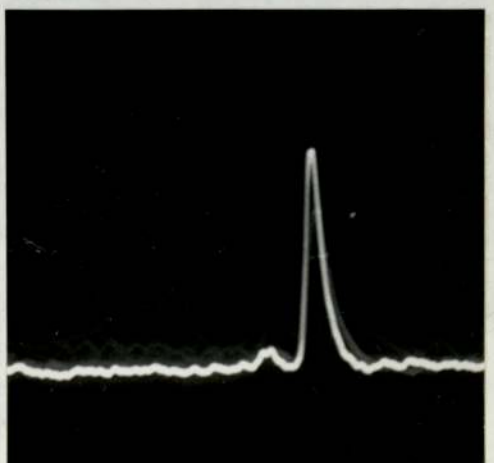
j



k



l



m

- iii. Richer in silicon.
- iv. Slightly less rich in oxygen.
- v. Richer in sulphur (Almost no S was present in the large inclusion).

This was what had been expected from the earlier investigations. However, there was a difference in the expected manganese levels. This may be accounted for if the smaller inclusion had manganese sulphide associated with it due to heat treatment at the rolling temperature although this was not directly evident.

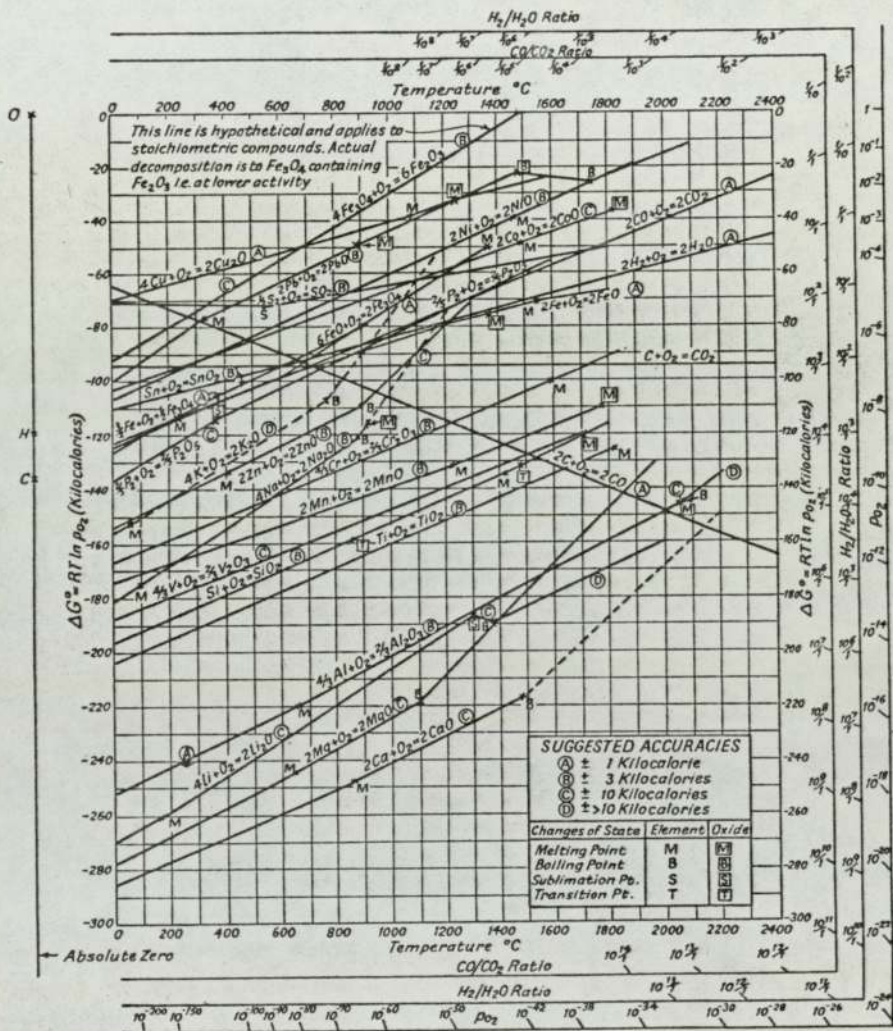
The presence of sulphur in the smaller inclusions may be accounted for by considering the thermodynamics of oxide and sulphide formation. From thermodynamic data (18) figures 5.18.&.19.) manganese sulphide is less stable than the oxides present. As such it would be expected that the sulphide phase would form later in the solidification process and nucleate on oxide phases present, as was observed by Trigwell (183).

5.1.3. Nucleation and growth of products.

From the present work, data was not available to calculate the degree of supersaturation for any specific oxide species. This was due in part to the inability of obtaining residual dissolved oxygen contents in the final melt, (the determined oxygen includes the deoxidation products which have remained in the cast steel).

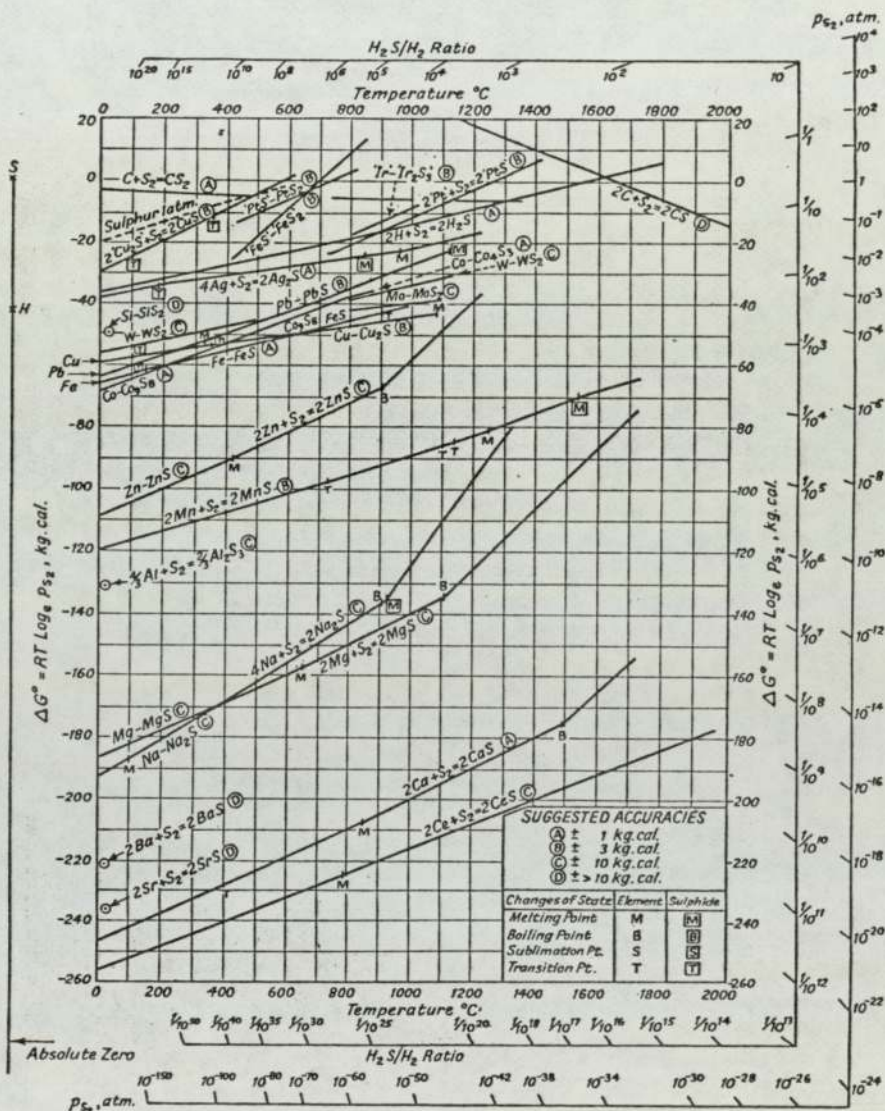
Lindon (9) did however show by calculation that in the present system ΔG (critical) for homogeneous

5.18



The standard free energy of formation of metallurgically important oxides as a function of temperature (from Darken and Gurry³²).

5.19



The standard free energy of formation of metallurgically important sulphides as a function of temperature (from Richardson and Jeffes⁴⁶).

nucleation was not reached for any specific oxide species (assuming that there was a homogeneous distribution of solutes initially).

Earlier work of Turkdogan (30) and Turpin and Elliott (48) had shown that as a deoxidant dissolves into the melt local conditions are favourable for obtaining ΔG values in excess of those required for homogeneous nucleation. In addition the presence of foreign nuclei (e.g. hercynite particles which may form due to melt crucible reactions at oxygen contents greater than 0.045% (33)) are known to aid deoxidation because they act as nucleation sites.

If the initial mixed oxide products form in areas of high deoxidant concentration a situation may exist which differs from that where there is a uniform distribution of oxygen and deoxidant. (i.e. there is a lower oxygen potential in the former situation).

The indications are, therefore, that oxides formed in these areas of high deoxidant concentration would have unstable compositions, and there would be a potential for compositional change as they moved into other regions of the melt, It would also seem likely that in this instance the smaller inclusions should be influenced to a greater extent, since they have a larger surface area to volume ratio. If so, this compositional instability may partially contribute to the observed variation of composition with size.

5.1.3.1. Inclusion size distributions.

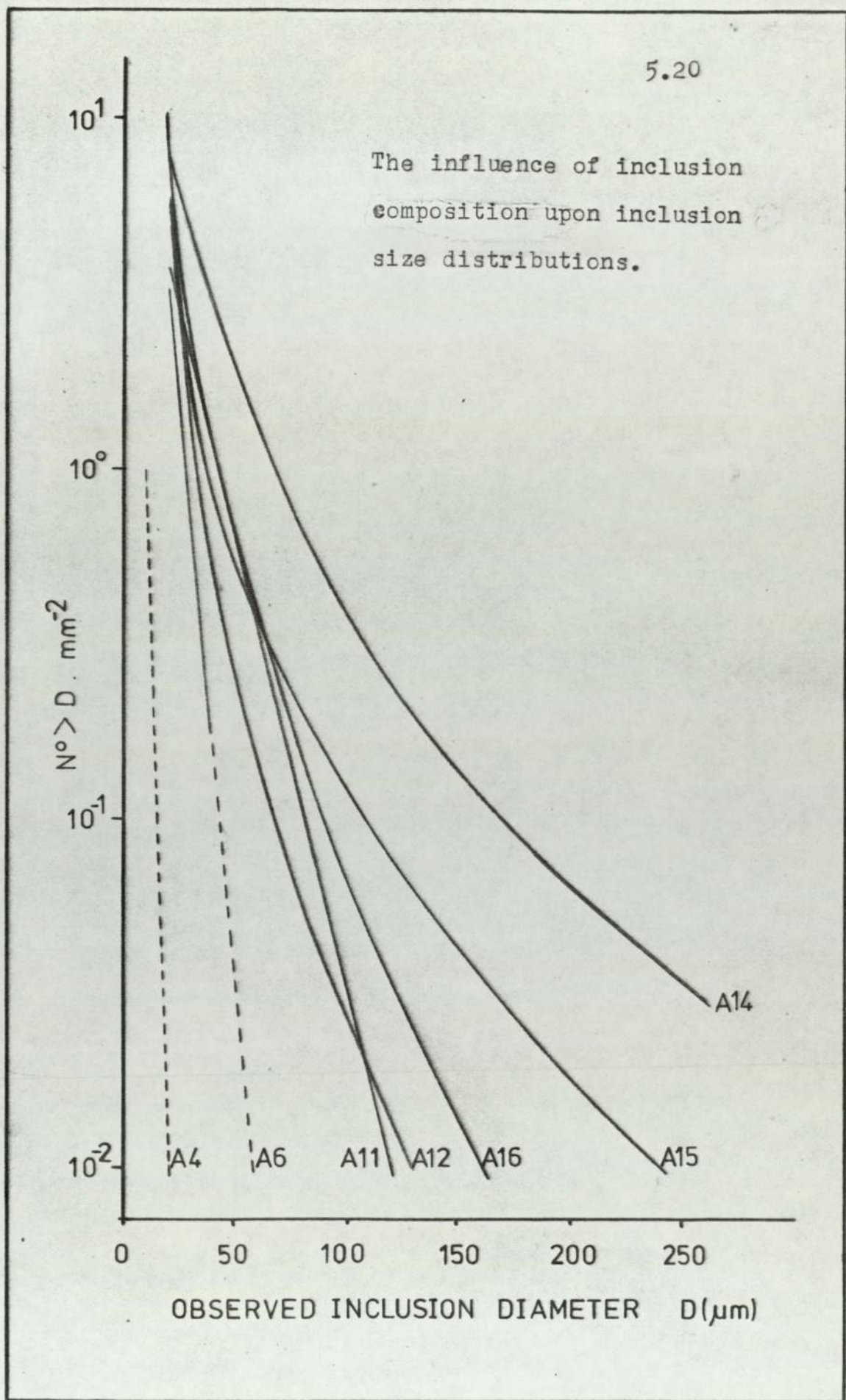
From metallographic data (tables 4.6, 8 and figures 5.20, 5.30) it appears that inclusion size distributions were influenced by inclusion composition. Size distributions in terms of number of inclusions greater than a given diameter per unit area would have been influenced by areas from which samples were taken from the 'as cast' bar. (An observation confirmed by Asante (103)). However, in this instance samples were taken approximately 8 - 10 cm from the top of the bar and samples from the various melts could be compared directly.

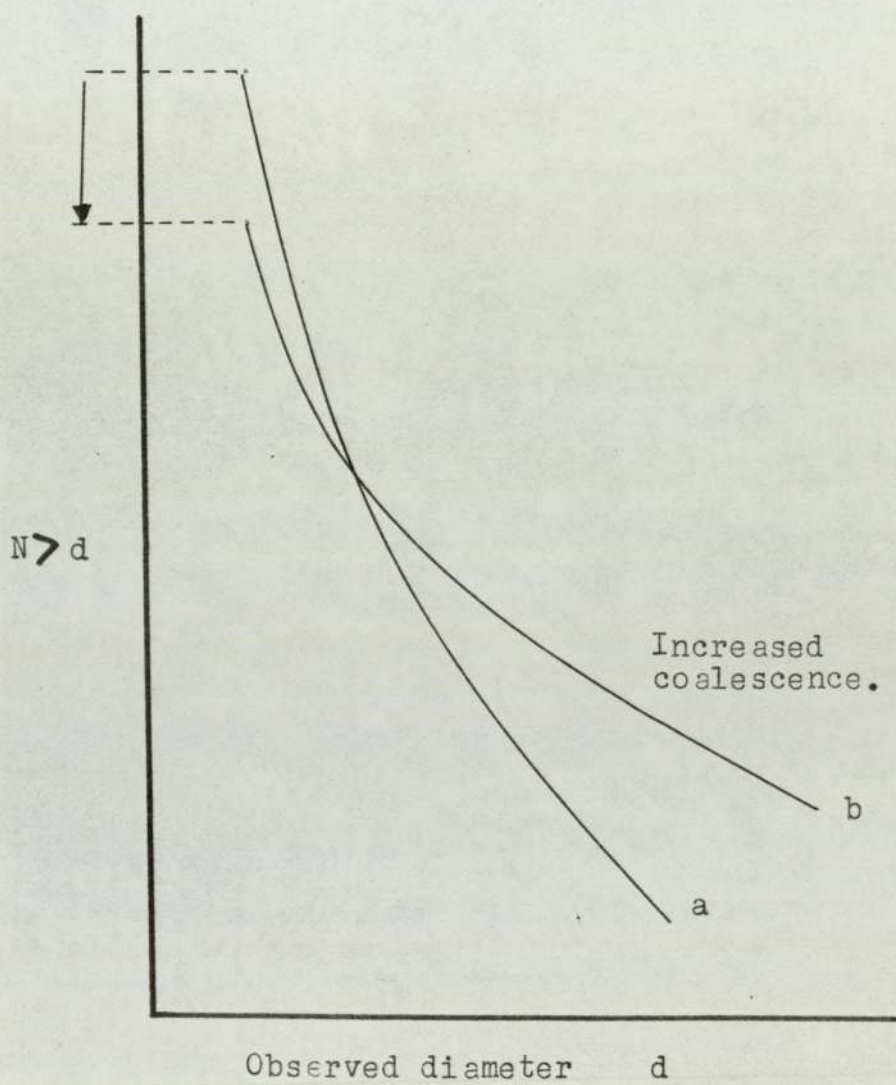
From nucleation and growth theory inclusions greater than $3\frac{1}{2}$ μm radius cannot be accounted for (9) and it is necessary to assume agglomeration and coalescence of particles. It has been pointed out earlier that in this experimental work, solidification was not instantaneous and particles had up to 40s in which agglomeration and coalescence could occur prior to solidification of the cast. This time was however constant for the data in these experiments and enabled a pseudocuantitative exercise to be performed.

The work of Kawawa et al (78) showed experimentally that if no change in particle size occurred by coalescence then inclusion size distribution could be related to the expression

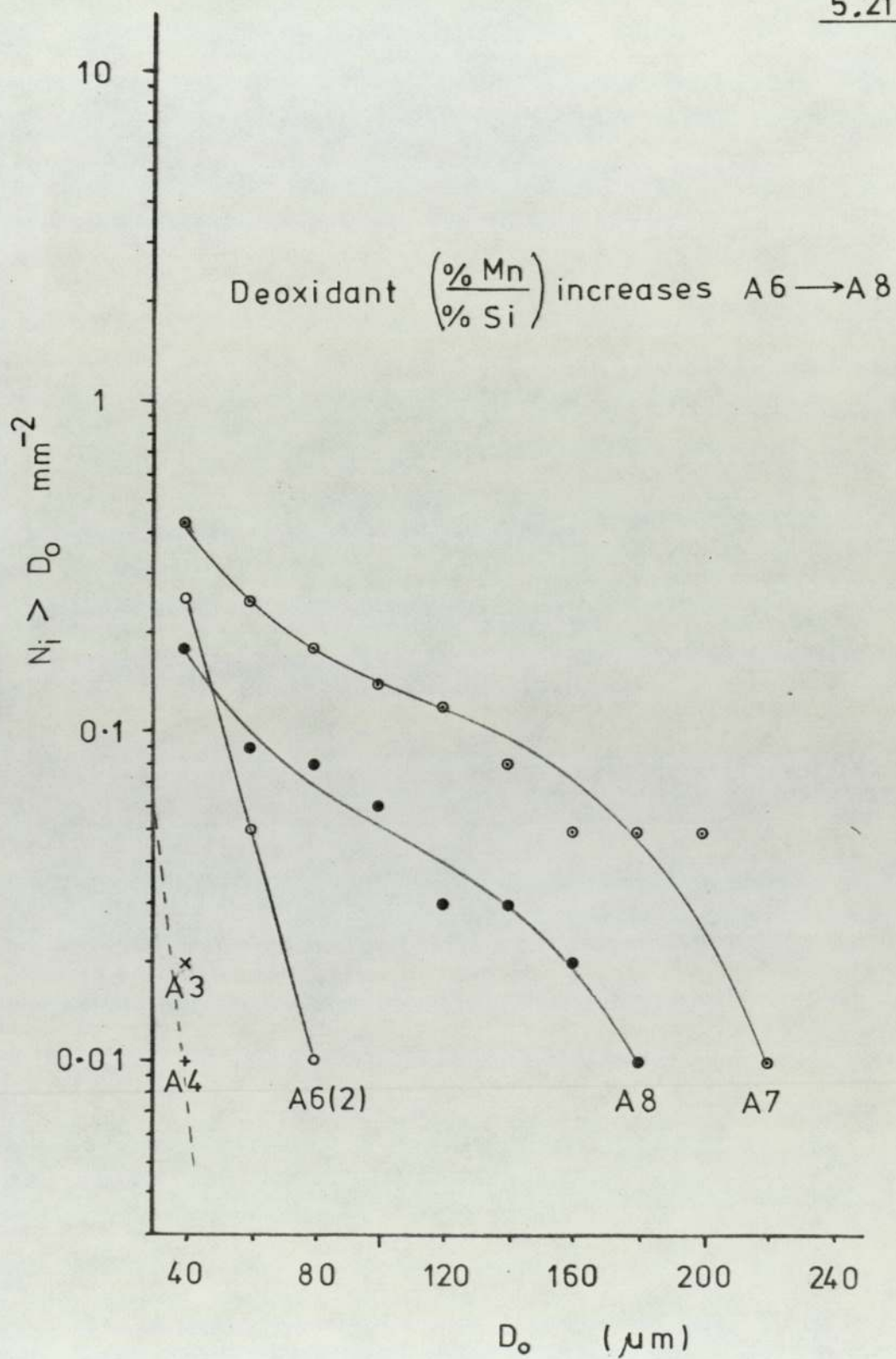
$$n = n_0 e^{-A\delta}$$

where n was the number of inclusions per unit area having a radius greater than δ , n_0 and A were constants.

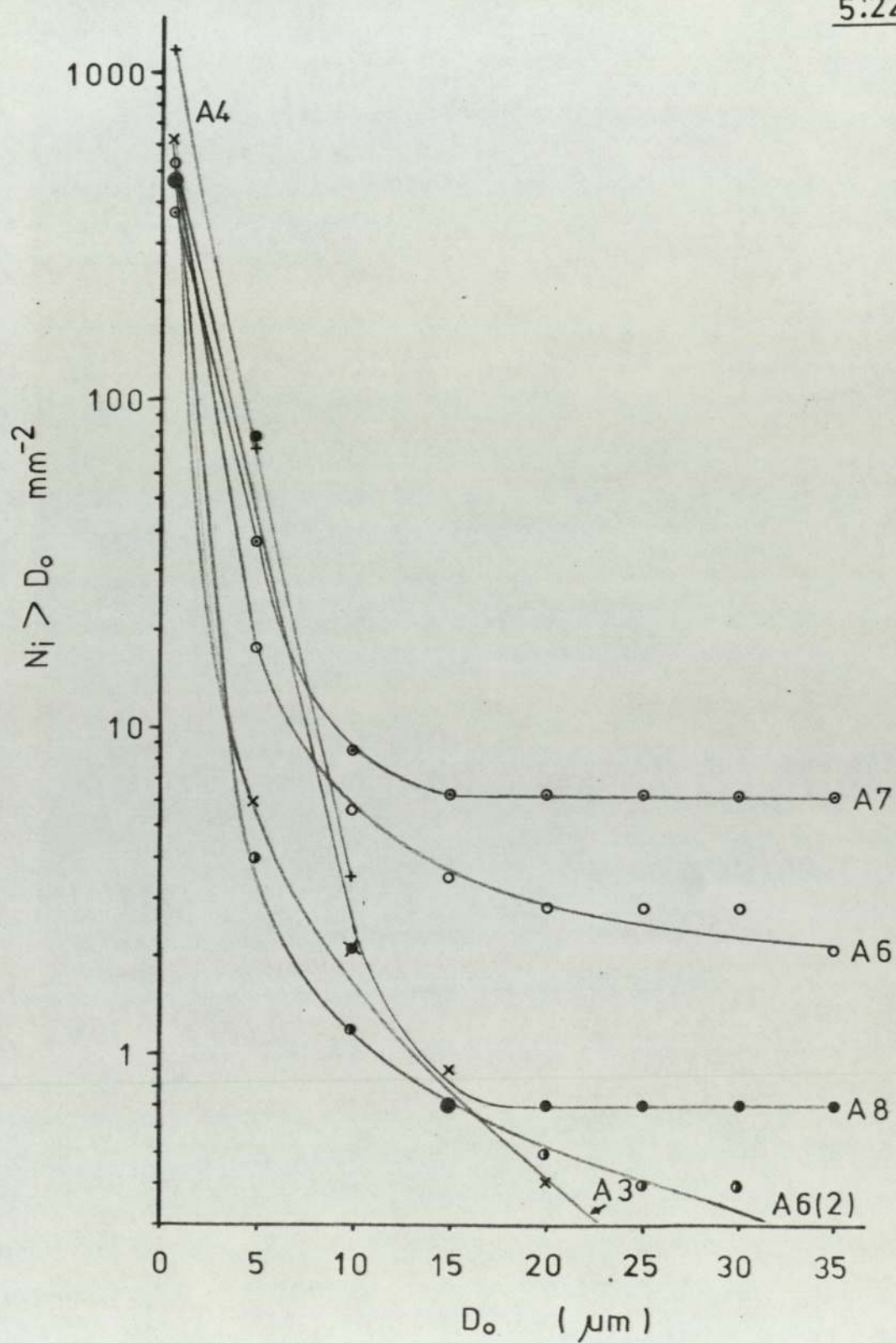


5.20(a).

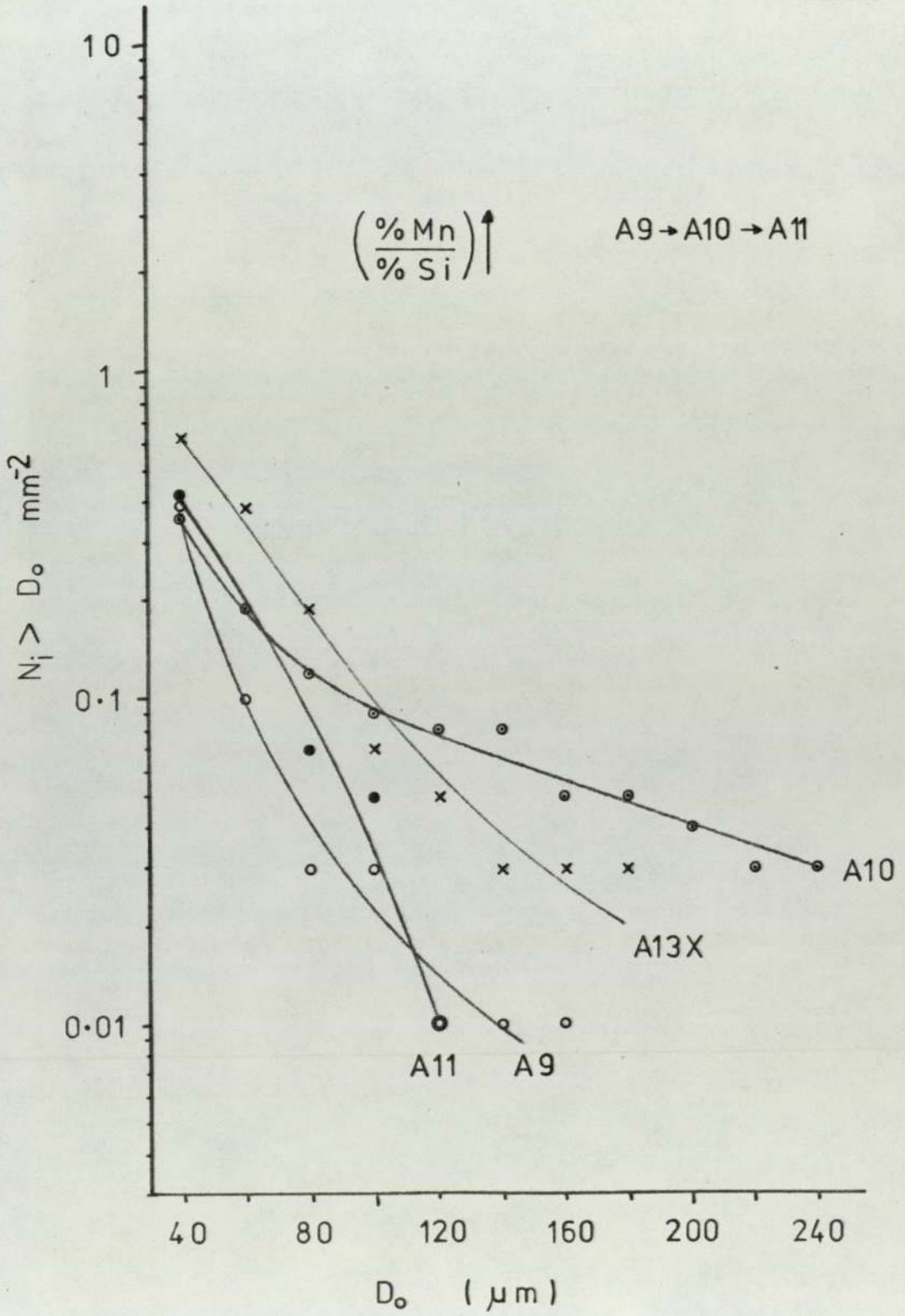
5.21.



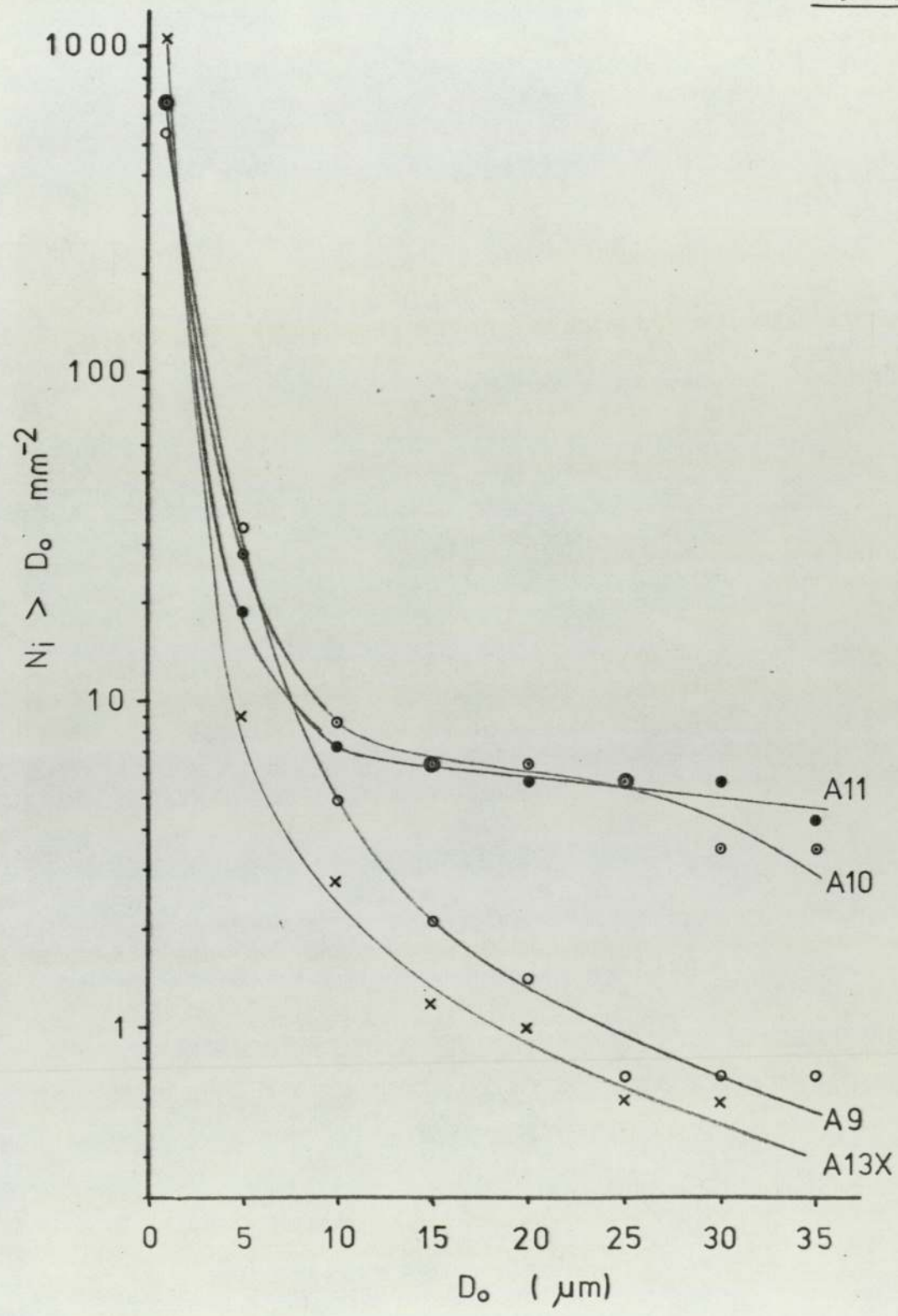
5:22.



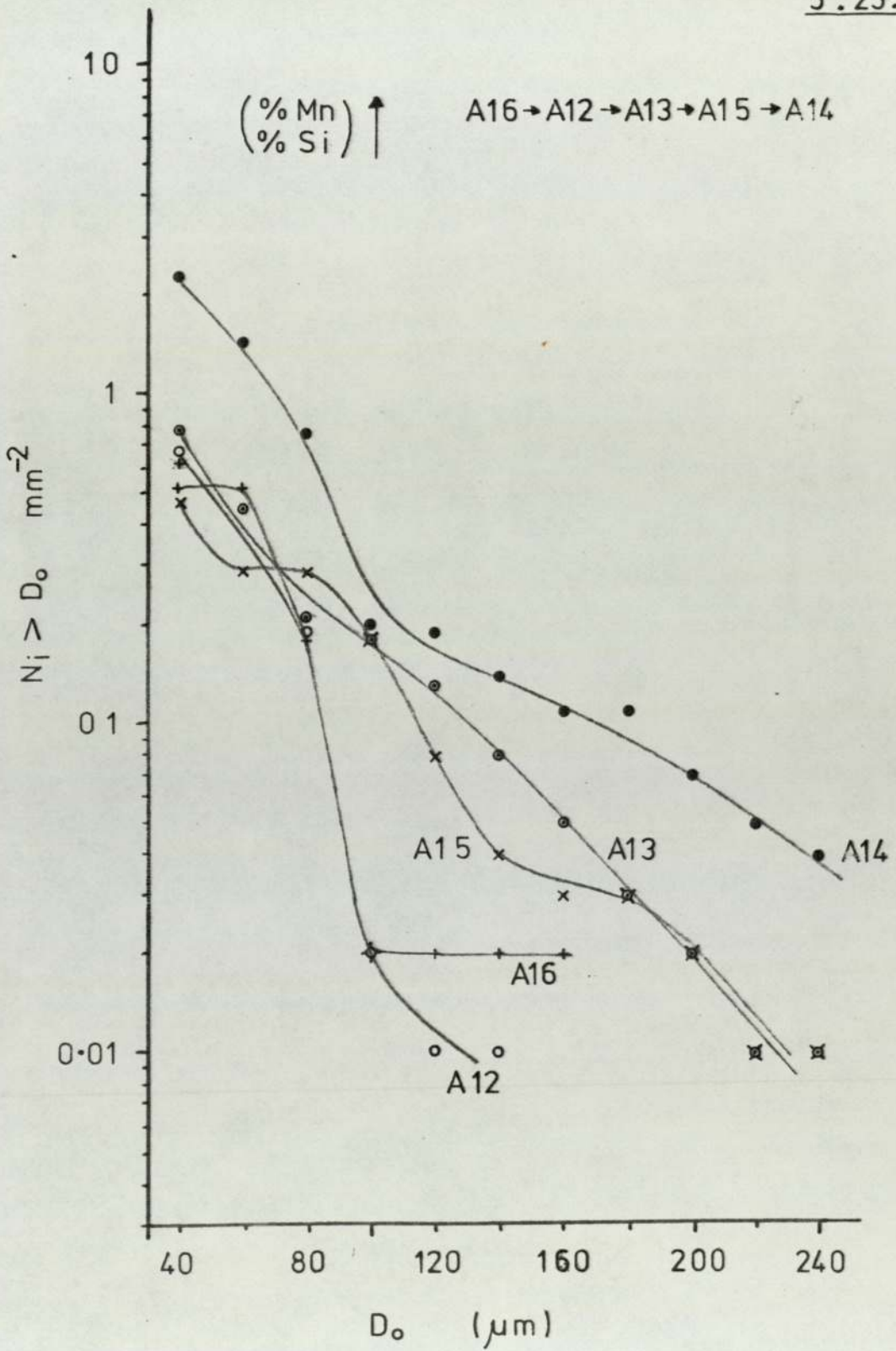
5.23.



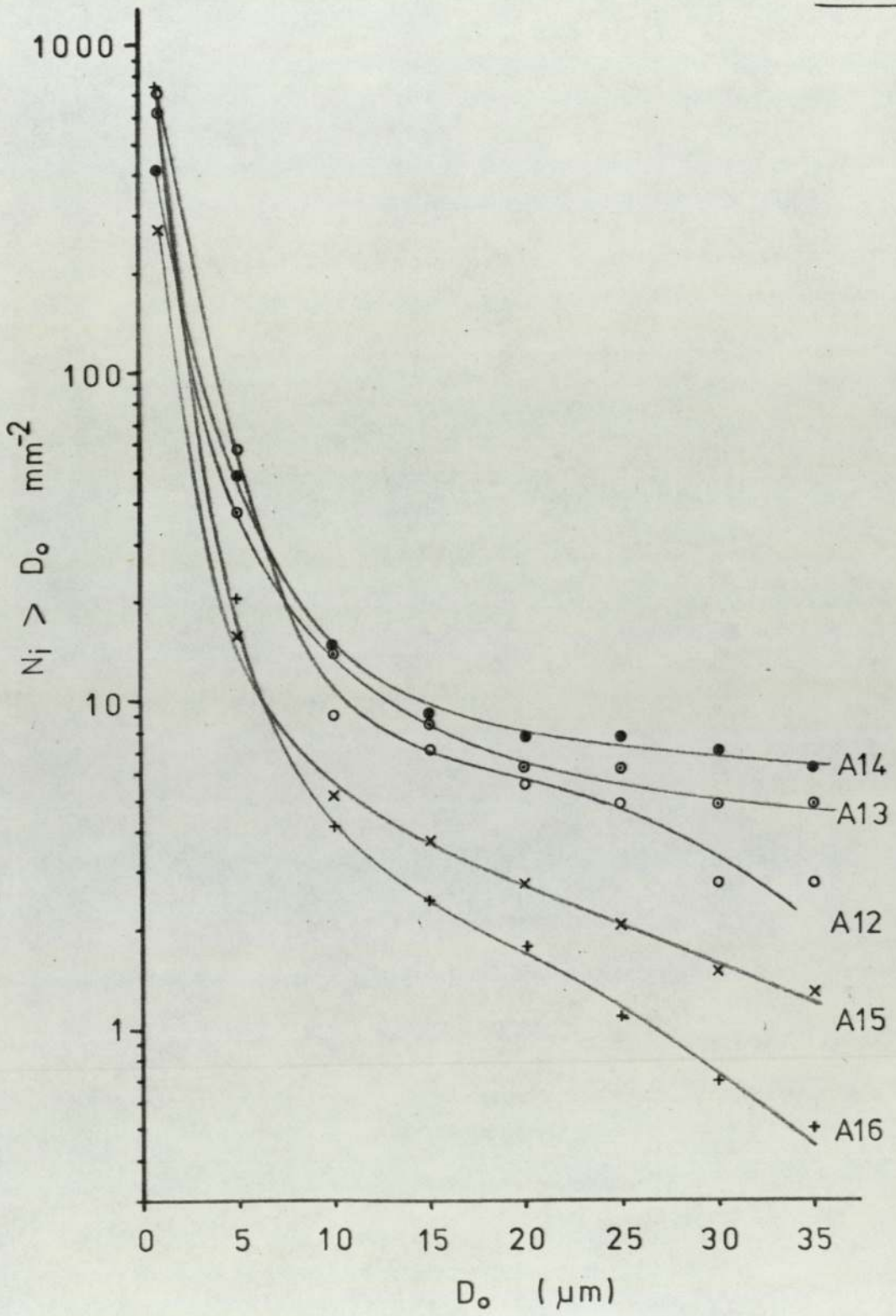
5.24.



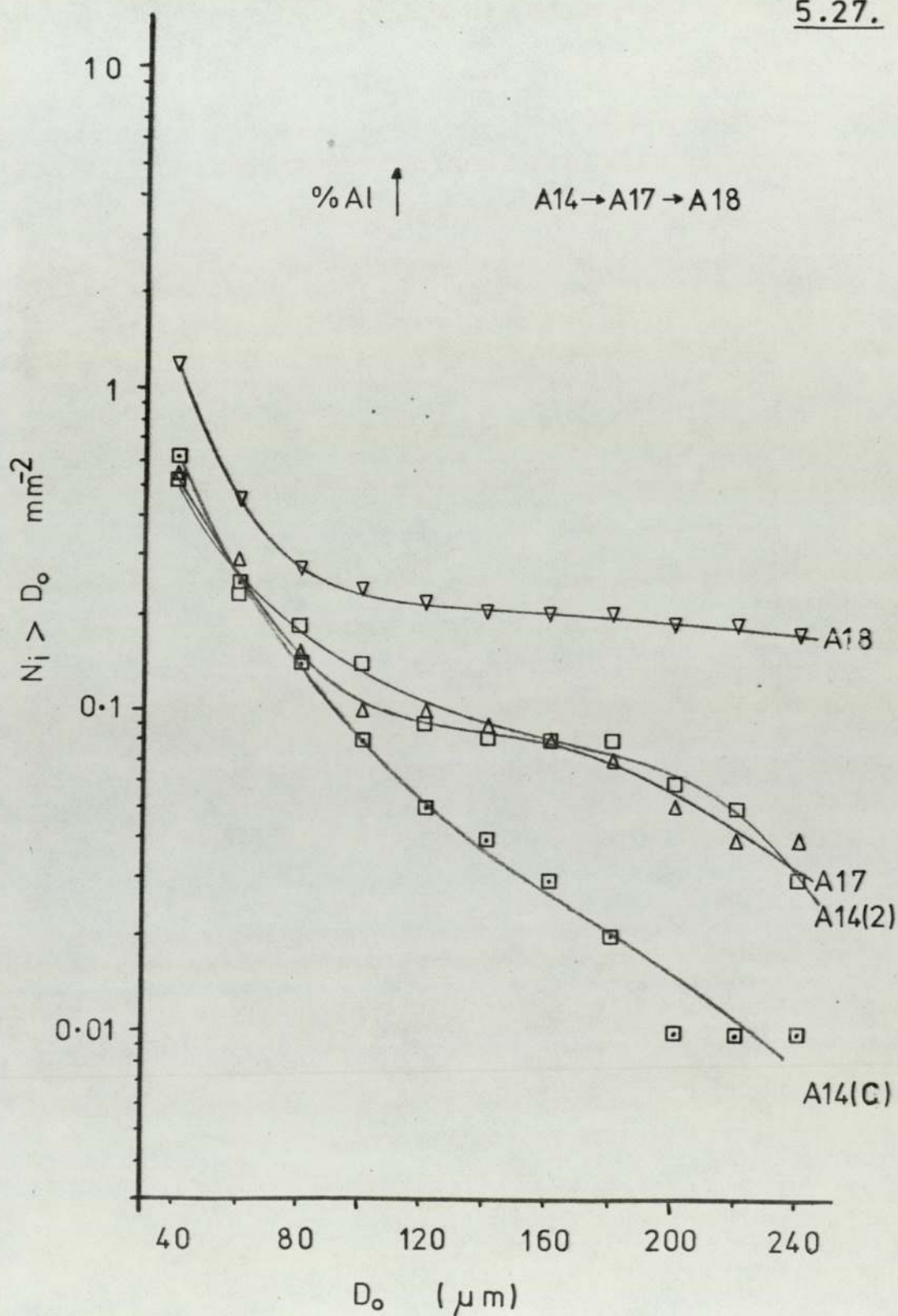
5.25.



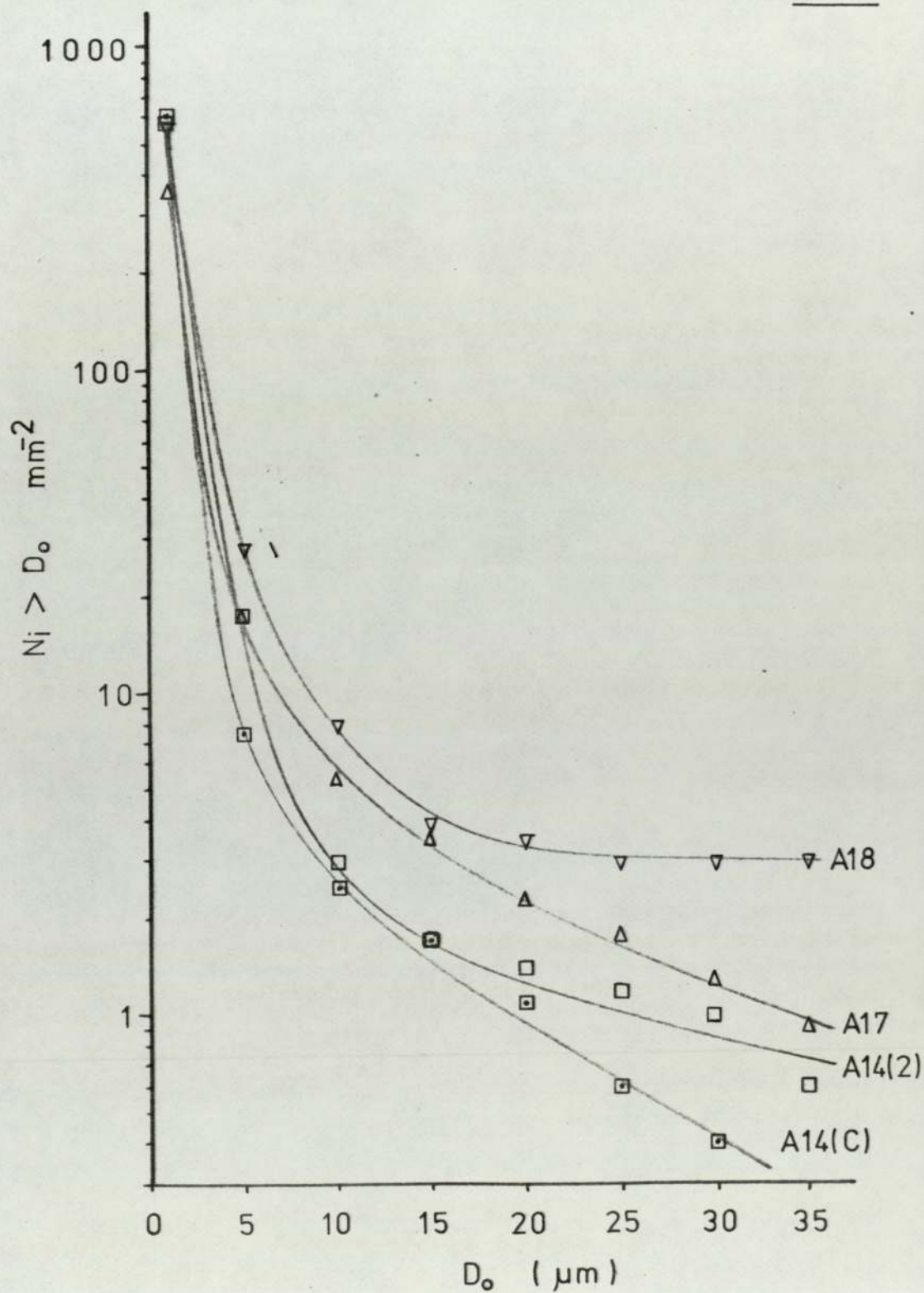
5.26.



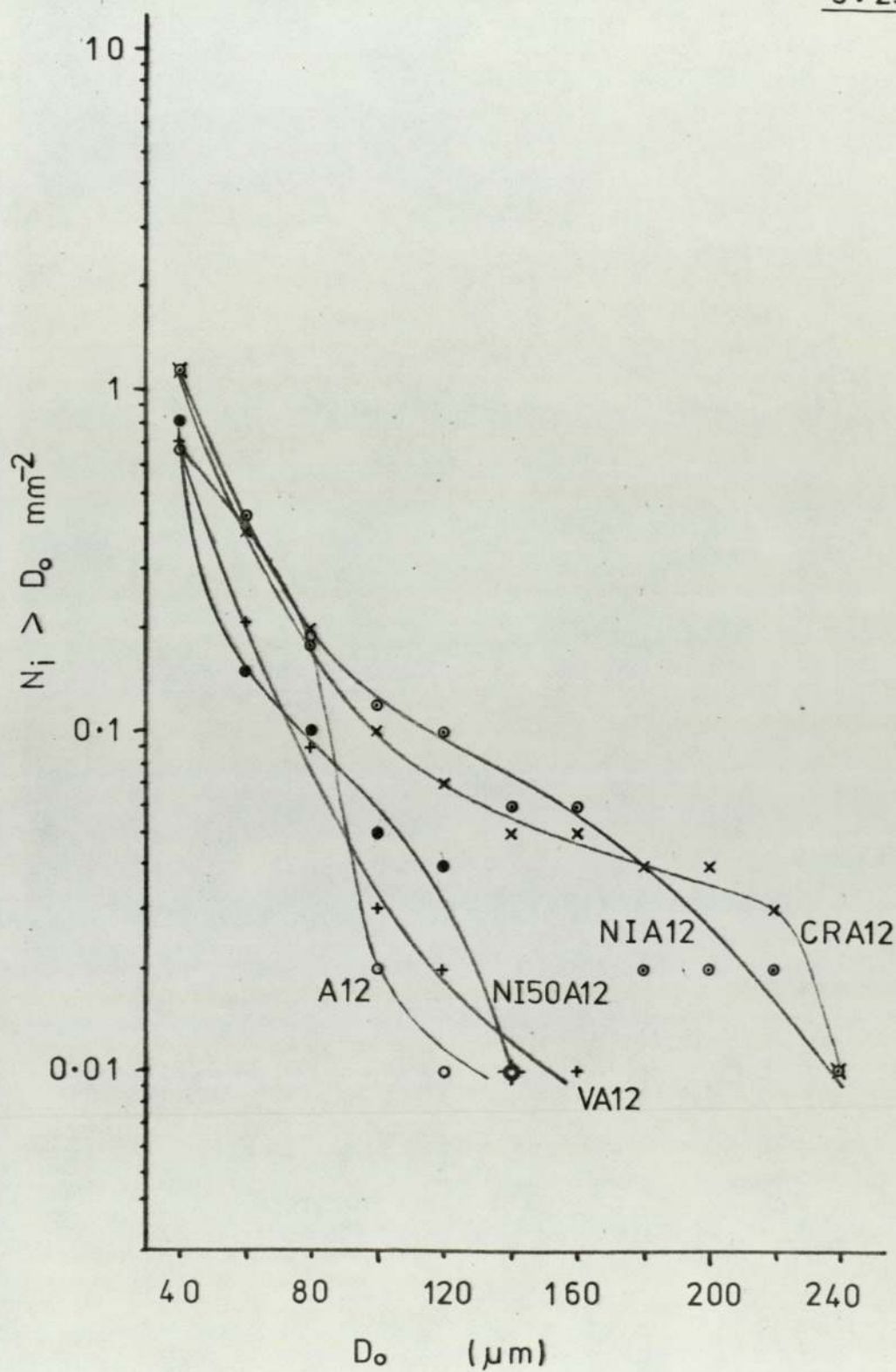
5.27.



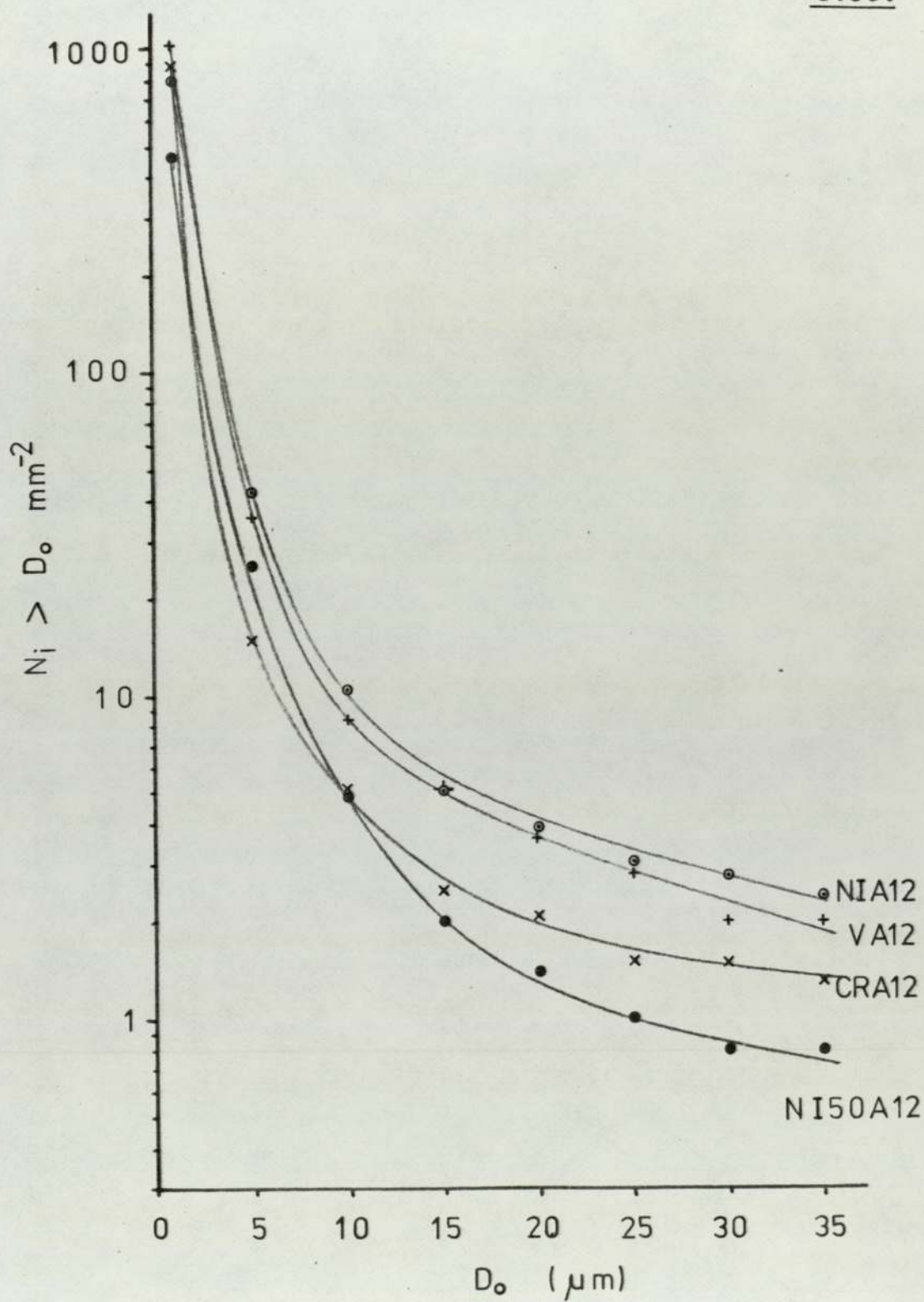
5.28.



5.29.



5.30.



and δ was an expression related to Stokes law.

In present work melt A4 which had been deoxidised with silicon showed a linear relationship of the type above (figure 5.21.) but even then there was visual evidence of agglomeration (plate 4.2.) and an attempt at coalescence. (which was limited by the high viscosity of the oxides in SiO₂ rich prods.) Melt A3 which had been deoxidised by manganese also (inclusions ~ 97% MnO ~ 3% FeO) showed a form which tended to be linear, but again coalescence would be unlikely because of the high melting point of manganese oxide.

The results for the oxides which were fluid at the experimental temperature show a marked deviation from linearity at inclusion diameters greater than 10 μ m, thus indicating that coalescence took place. It would be expected that if coalescence occurred then the total number of inclusions present would decrease as schematically indicated in figure 5.20.a

Figures 5.20. to 5.30. show the influence of increased manganese in the products upon coalescence in the fluid region of the MnO - SiO₂ - Al₂O₃ system at various levels of aluminium added.

Melts A3 - A8 (Aluminium Free).

Figures 5.21. and 5.22. show the effect for melts containing no aluminium where the products with higher manganese

contents are seen to have undergone more coalescence. This may be related to the liquidus temperatures of the various product compositions, where A6 can be seen to have a higher liquidus temperature (figure 4.2.⁴⁵⁵). This would seem to fit the logical suggestion of Lindon (9) whereby the amount of product coalescence increased as the product liquidus temperature was lowered. However, there does seem to be a slight discrepancy between melts A7 and A8 on the basis of liquidus temperatures in the MnO - Al₂O₃ - SiO₂ system (figure 4.2.^{at 55}) where A8 was seen to coalesce to a lesser extent than A7. It must be remembered, however, that the mean analyses quoted can only be regarded as a guide, and in addition melt A7 products contain a slightly higher FeO content, which is likely to lead to a decreased liquidus temperature.

Melts A9, A10, A11 and A13X
(0.01% Aluminium addition)

Again with figures 5.²³/₂₄ there seems to be some discrepancy with respect to coalescence on the basis of liquidus temperatures. Melt A9, in which the product compositions were in a low temperature liquidus region, appeared to have coalesced to a less extent than the products with the higher liquidus temperatures. (i.e. melts A10 (~1250°C) and A13X (~1400°C)). Melt A11 was not included in this comparison, since the curve produced was very dependent upon one result (figure 5.23).

However, melts Al0 and Al1 had similar product compositions, and for lower 'observed inclusion diameters (Do)' figure 5.24, the results were comparable. The results of figures 5.23, and 5.24, again show that the higher the MnO content of the product the greater the amount of coalescence.

Melts Al2 - Al6 (0.02% Aluminium
addition).

Figure 4.3. shows that the mean compositions of melts Al2, Al3, Al4, Al5 and Al6 are all in the low liquidus regions of the MnO - SiO₂ - Al₂O₃ diagram. However, the indication was that inclusions richer in MnO (melts Al4, Al5) had coalesced to a greater extent than those richer in SiO₂ (i.e. melts Al2 and Al6) Figure 5.25.,26.

Melts Al4(2), Al4(C), Al7, Al8
(constant (Mn%) addition - - variable
Si%)
aluminium content)

Figures 5.^{.27.}28. show the influence of aluminium addition, for a constant manganese and silicon addition to the melt, upon the degree of observed coalescence. Increasing the aluminium content of the deoxidant addition has increased the level of Al₂O₃ in the product and also the degree of coalescence. Although melts Al4(2), Al4(C) and Al7 have mean product compositions in the low

liquidus region and would be expected to coalesce well, the highest level of coalescence was observed in melt Al8, which had a mean liquidus temperature of approximately 1550°C. A high liquidus temperature, as for melt Al8 would be expected to inhibit coalescence since it was near the temperature of the melt at deoxidation. However, it must be emphasized that inclusions observed in melt Al8 were not glassy homogeneous phases, but consisted of Al₂O₃ rich particles (approaching the Al₂O₃ composition) within a glassy siliceous matrix. Plate 5.2 . From microprobe analysis (Appendix 4.1) the matrix has a composition of approximately 20 - 25% Al₂O₃, which is in the low liquidus temperature region of the MnO - SiO₂ - Al₂O₃ diagram (figure 5.31.). Hence it may be the case that the low liquidus matrix was a contributory controlling feature with regard to the coalescence of melt Al8.

A further interesting feature of melt Al8 was that there were a number of very large inclusions in excess of 250 μm and numerous small inclusions (< 20 μm). However, there were very few inclusions within the range 20 - 250 μm. It was also noticed that these very large inclusions often occurred in proximity to each other. (e.g. as in plate 4.11.). The inference is therefore, that groups of alumina particles may have approached each other due to interfacial surface tension effects and become enveloped in a siliceous matrix. (It must be noted that the Al8 deoxidant additive was a Mn - Si - Al alloy plus free aluminium as an admixed powder. Pickering has stated that the practice of

PLATE 5.2

X RAY PHOTOGRAPHS OF A HETROGENEOUS
INCLUSION FROM MELT A18 AS CAST

X1000

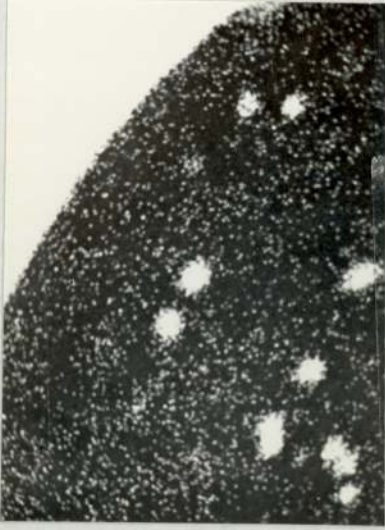
5.2a Fe X-RAY

5.2b Mn X-RAY

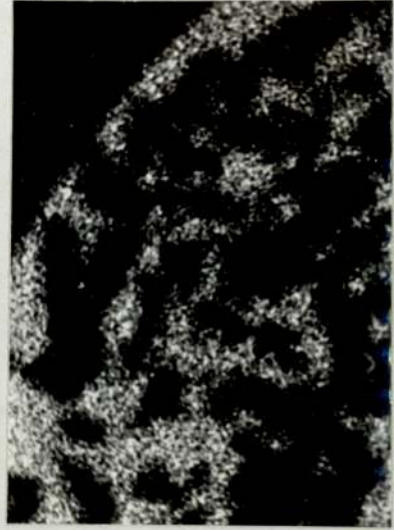
5.2c Si X-RAY

5.2d Al X-RAY

5.2



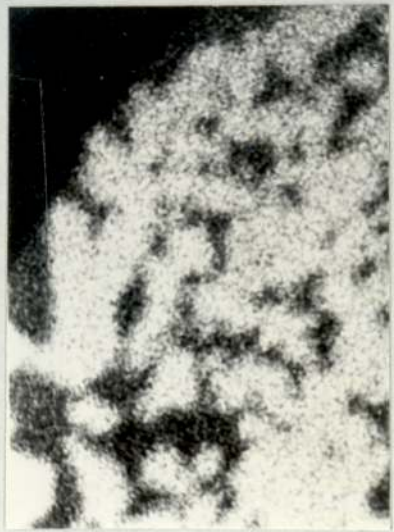
a



b

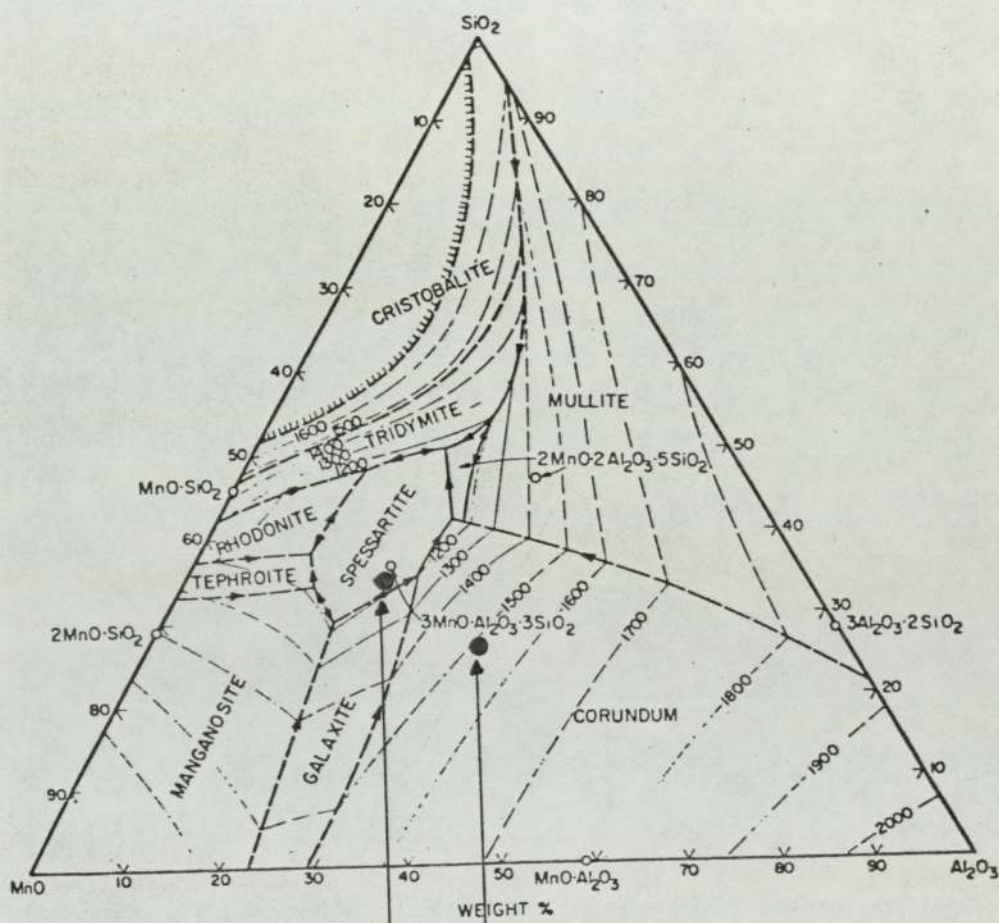


c



d

5.31



Matrix
composition

Mean inclusion analysis
for Melt Al8.

making simultaneous additions of Si and Al may lead to the formation of regions of widely different deoxidant concentration. It would therefore seem that such a condition may have existed for the case of Mn - Si - Al alloy and Al added simultaneously).

Melts NI50Al2, NIA12, CRA12 and VA12 (0.02% Aluminium + alloying elements).

With regard to the melts containing alloying additions, with the exception of NI50Al2, the deoxidation products which resulted were of similar composition to melts A12 and A16. From figures 5.29, 5.30, it would seem that the inclusions have coalesced to a slightly greater extent than observed in melt A12, particularly in melts NIA12 and CRA12. Although there are no obvious reasons why this should have occurred, it may be that the presence of these alloying elements influenced the surface properties of the oxide particles, and/or broke up the silicate network, and caused the oxides to become more fluid. Melt NI50Al2 cannot be included in the above comparisons since it had a higher silica content in the inclusions, and therefore a higher liquidus temperature and presumably a lower value of interfacial tension.

5.1.3.2

Summary of the results for inclusion
composition and its effect upon
coalescence.

It would appear ^{from} form the pseudoquantitative data tables 4.6. — 8.) represented in figures 5.21. — 5.30. that the composition of the deoxidation products influenced the size range of inclusions within the solidified bars. It would seem that the degree of coalescence of the deoxidation products was encouraged by

- i. A low liquidus temperature.
- ii. An increased level of MnO in the oxide.
- iii. High Al_2O_3 content (i.e. Al8)

A low liquidus temperature is likely to produce a deoxidation product of low viscosity at the temperature of deoxidation. The presence of a highly fluid product is expected to enable coalescence to occur. (An effect noted by Herty and Fitterer (64)). The reason why an increase in the level of MnO would aid coalescence may be attributed to

The effect of interfacial tension.

The role of surface phenomenon on the formation of inclusion clusters was widely investigated (71) and it has been established that products of low interfacial tension are likely to coalesce.

Göhler investigated the surface tension (210) of $MnO - SiO_2 - Al_2O_3$ slags at 1600°C and has indicated values in the range $0.3Jm^{-2}$ (300 dyne cm^{-1}) to $0.5Jm^{-2}$.

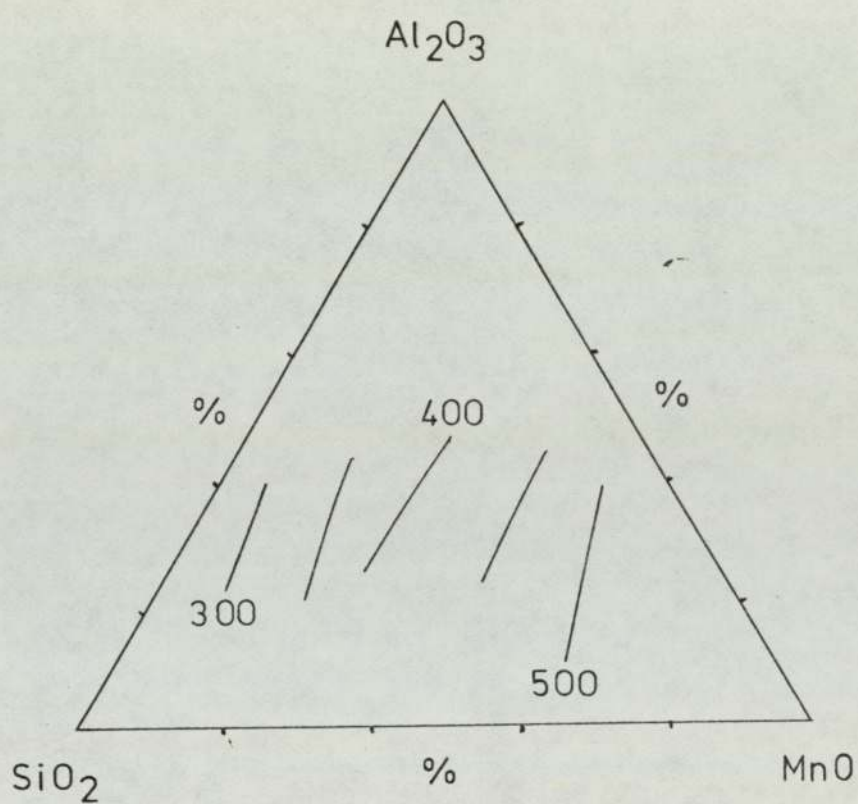
These results are indicated in figure 5.32. Assuming that the surface tension (γ_m) of iron at 1600°C and 0.01% oxygen is approximately 1.5Jm^{-2} (71) the values of interfacial tension (γ_{om}) are in the region of 1.2Jm^{-2} at 10% MnO and 1.0Jm^{-2} at 60%MnO. In comparison the values of γ_{om} for silica and alumina at 0.1% oxygen are 1.5 and 1.9Jm^{-2} respectively. These values for γ_{om} between 1.0 and 1.2 agree quite well with the results of Lindon (9) table 5.4. who obtained values in the range 1.03Jm^{-2} to 1.18Jm^{-2} calculated using Antonovs rule

$$\gamma_{om} = \gamma_m - \gamma_o$$

Table 5.4.

Composition			Interfacial energy γ_{om} (Jm^{-2})
MnOFeO	SiO ₂	Al ₂ O ₃	
35	53	12	1.05
44	46	10	1.04
52	45	3	1.03
22	61	17	1.10
30	39	31	1.10
26	29	45	1.18

Thus from the results of these workers an increase in the level of MnO in the oxide product would lower the interfacial tension and enhance coalescence.

5-32

Surface tension (dyn.cm^{-1}) of $\text{MnO-SiO}_2\text{-Al}_2\text{O}_3$ slags at 1600°C . (After Göhler)

The breaking up of the silica glass network.

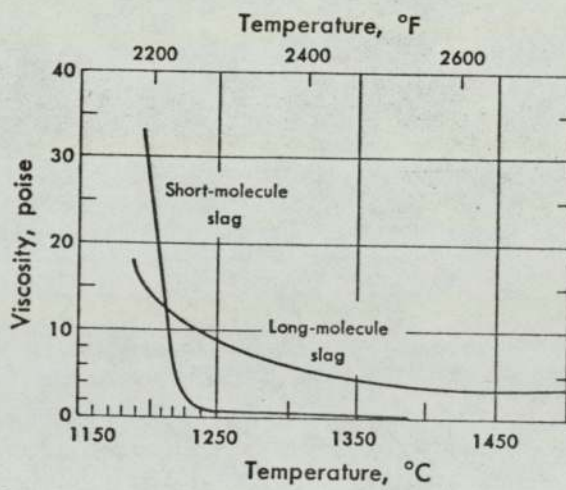
The viscosity of molten silica is very high because the Si - O network is strong, and produces a long molecule slag (18). However, the addition of a basic metal oxide reduces its viscosity by breaking down the Si - O network. As more of the oxide is added the Si - O structure is broken down still further. Fig. 5.33.

The presence of metal oxides with a strong metal oxygen attraction do not break the Si - O structure, but become part of the network itself. Table 5.5. shows which oxides are network breakers and which are network formers (after Dietzel (211) and Elliott et al (18)).

If it is assumed the oxide MnO behaves in a similar manner to CaO then the viscosity of MnO - SiO₂ - Al₂O₃ slags may show similar features to the CaO - SiO₂ - Al₂O₃ system. (Figure 5.34. after Kozakevitch and Urbain) where it can be seen that an increase in CaO leads to a lowering of viscosity up to the molecular configuration of 2CaO - SiO₂. On this premise an increase in MnO content of inclusions will lower the viscosity and therefore aid coalescence. However, it must be pointed out that the presence of too much MnO will result in a product with a high liquidus temperature. Thus in this instance coalescence will be inhibited, as is the case for pure MnO.

5.33

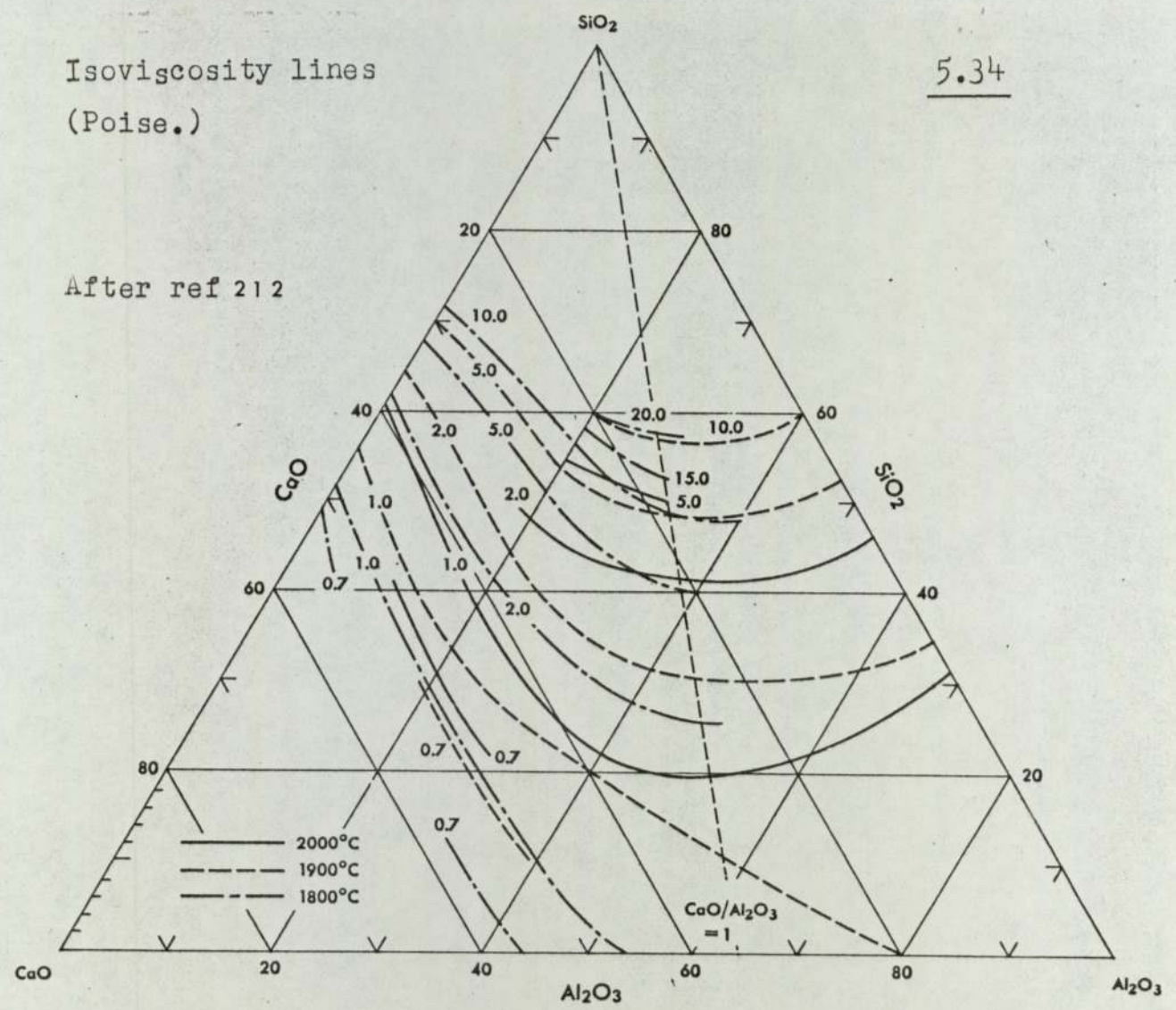
Viscosities of Long-Molecule and Short-Molecule Slags.



Isoviscosity lines
(Poise.)

5.34

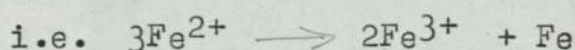
After ref 212



5.2.

Heat TreatmentMelt A7 (Mean composition %:3.5FeO, 60.9MnO, 0.3Al₂O₃, 35.3SiO₂)

The mean composition of inclusions contained within melt A7 lay within the (Rhodonite + Tephroite) region of the SiO₂ - MnO diagram (figure 4.2.). These are the equilibrium phases at heat treatment temperatures of 900 and 1100°C. However, the precipitate sizes were mainly in the region 2 - 3 μm and below, which therefore precluded microprobe analysis. The granular appearance of the inclusions did suggest that a mixture of phases may have been present (plates 4.44. & 45. section 4). Very fine white globular areas were occasionally noted with the precipitating phases, and these may have been metallic iron precipitated due to the oxidation of iron from the ferrous to ferric state, as suggested by Robinson (202).



Heat treatment of melt A7 at 1300°C, which was above the liquidus temperature for this composition should have resulted in glassy type inclusions. However, large inclusions were found containing very fine precipitates, which may have resulted from the slow cooling of the samples in the vacuum heat treatment furnace. These precipitates may have nucleated but had insufficient time to grow. The presence of what appeared to be a reaction rim (as in figure 4.44.) cannot readily be explained at a temperature of 1300°C where the

product is fluid unless the sample was in a cold spot in the furnace.

Melt All (Mean composition %: 1.8FeO,
58.2 MnO, 6.2Al₂O₃, 33.8SiO₂)

Melt All which was in a similar region of the MnO - SiO₂ - Al₂O₃ diagram as A7 (figure 4.2. ^{and 5.5}) behaved in a similar manner. However, with samples heat treated at 1300°C there was no evidence to suggest a reaction rim. Some of the large inclusions were again observed to contain precipitates possibly due to slow cooling as for A7.

The samples which had been heat treated at 900 and 1100°C did show the presence of MnS cusps, particularly noticeable with the smaller inclusion sizes (plate 4.46.) Although the sulphur level in the melt was low i.e. approximately 0.005/0.007%, sulphur was present with small inclusions (Section 5.1.2.3). However, there were no signs of MnS cusps observed in the as cast state.

It would therefore seem that the sulphur which has been observed to envelope smaller inclusions (183) migrates to specific sites on the periphery of the inclusions upon heat treatment. It can in fact be seen in plate 4.57. that the presence of these MnS precipitates occurs adjacent to areas rich in Mn.

Melts Al4 and Al5 (mean compositions%
1.8FeO, 47.1MnO, 15.2Al₂O₃, 39.9SiO₂
and 0.9FeO, 49.4MnO, 12.1Al₂O₃,
37.6SiO₂ respectively).

Both melts Al4 and Al5 contained inclusions of similar composition within the MnO - SiO₂ - Al₂O₃ system and were in a region of low liquidus temperature. (i.e. ~ 1200°C) At a heat treatment temperature of 1300°C precipitations would not be expected to take place. However, as with other samples heat treated at this temperature, precipitations was again observed in the large inclusions. This was presumed to be attributable to the slow cooling from the heat treatment temperature.

Heat treatment at lower temperatures resulted in fewer observable glassy inclusions, the presence of MnS cusps and in some instances evidence of matrix inclusion reaction (plate 4.52.) The precipitates, which were of sizes big enough to analyse were found to be Rhodonite in block or lath forms (plates 4.62-.65. and Appendix 4.3) of compositions 49 - 52% MnO, 46 - 47% SiO₂ with Al₂O₃ and FeO levels of less than 1%.

Melts Al2 and Al3 (Mean compositions%

2.5FeO, 32.1MnO, 14.3Al₂O₃, 51.1SiO₂ and 2.0FeO, 40.6MnO, 9.5Al₂O₃ and 47.9SiO₂ respectively).

As with the other samples precipitation was observed at all three heat treatment temperatures, but it was also evident that the number of inclusions showing precipitation was less. This may be due to these melts containing inclusions of higher SiO₂ content. A higher SiO₂ content would infer a higher viscosity and therefore less molecular mobility. Where precipitation did occur the precipitated phases were observed to be (both for Al2 and Al3) either; SiO₂ which precipitated as dark laths (plate 4.59.) and was probably Tridymite, or as a mixture of SiO₂ and Rhodonite (plates 4.59.-.61.) where the SiO₂ has formed in a morphology which is more consistent with Cristobalite (79). Plate 4.36. which is taken from a sample of Al2 rolled at 800°C (where precipitation had occurred) does in fact show this Cristobalite type morphology slightly better.

The tridymite was analysed as a phase containing approximately 93%SiO₂, 4%Al₂O₃, 2%MnO and 1%FeO. This was seemingly in agreement with other workers. e.g. Kiessling and Lange (79) who found tridymite to contain SiO₂ with traces of Al₂O₃, and doubted whether tridymite was a pure SiO₂ phase.

General Observation. (5.2.1)

From the investigations on heat treated samples it appeared that as the time at heat treatment temperature

increased there were fewer glassy inclusions observed, which was to be expected on the basis of a nucleation and growth phenomenon. However, one observation which cannot readily be explained was that the small inclusions did not precipitate even after long heat treatment times. This may possibly be attributable to the variation in composition at small inclusion sizes, or possible surface reactions involving Mn and S being preferred.

5.2.2.

Developments of the heat treatment programme.

As a result of the random behaviour of inclusions observed for the vacuum heat treated specimens, and the possible problems associated with slow cooling, a heat treatment programme was developed to ensure rapid cooling.

From the earlier heat treatment study it was known that melt Al⁴ contained inclusions showing precipitations, particularly noticeable at 900 and 1100°C. after one hour at temperature.

On this basis samples taken from melts Al⁴(2) and Al⁴C (which were of similar composition to Al⁴) were encapsulated in glass prior to heat treatment (to prevent oxidation). Heat treatment at 1050°C. for times at temperature of 0, 5, 10, 20, 40 and 80 minutes was followed by quenching immediately after removal from the furnace. It had been hoped that by this method a relationship of the form

$$\frac{V_t}{V_0} = 1 - e^{-kt^n}$$

could be established.

However, quantitative assessment was prevented by the unpredictable behaviour of the inclusions, and the samples from the various heat treatment times were virtually indistinguishable. Even the sample which was removed from the furnace as soon as it reached temperature showed inclusions in the various stages of precipitation. It was at this stage that any attempt at quantitative precipitation analysis was abandoned.

From these heat treatment experiments, it was concluded, on the basis of precipitation at zero minutes at temperature, that precipitation occurred during the time the samples were heating up to the temperature of heat treatment.

This is considered an important criterion when heating samples up to the temperature required for subsequent rolling.

As a result of this observation and its potentially important effect upon the deformation of inclusions upon hot rolling, further qualitative heat treatments were performed. Again using samples from melt Al₄C, these were heated in the furnace used for rolling at 820°, 920° and 1020°C. Samples were removed and quenched as soon as they had reached temperature, and after one hour at temperature. All of the samples showed a large number of inclusions containing precipitates, no difference being observed between the various samples. Plate 4.56. shows the typical Rhodonite precipitations encountered in all cases.

5.3 Inclusion Deformation

5.3.1 The behaviour of inclusion phases which did not plastically or fluidly deform at the hot rolling temperatures.

The behavioural characteristics of inclusions at the hot rolling temperatures were categorised in table 4.10. Before discussing the behaviour of the deformable inclusions, which could be quantitatively investigated, this short section will be concerned with the non-deformable and brittle inclusions.

Rolling at low temperatures generally resulted in the non deformation or brittle behaviour of inclusions, although actual behaviour was governed by individual inclusion properties of the various melts. It was generally observed that the glassy inclusions remained undeformed, as did a large majority of those containing precipitated phases.

Often associated with these non-deformable inclusions were voids at the inclusion/matrix interface (plates 4.14. and 4.15.), where contact between the inclusion and matrix was not maintained during the rolling process due to lack of adhesion (119). It was generally the case that these voids were not noticeable except in association with the larger inclusions. This was not unexpected since there is smearing of the matrix during polishing, and it is necessary to employ a repeated etch/polish technique to reveal the phenomenon more clearly especially around the smaller inclusions.

When the inclusions were not rigid they had the tendency to crack, shear and disseminate as was shown in plates 4.16.-23. section 4.8. It must be added that in the present work this phenomenon was not encountered with the glassy inclusions, but only with those which showed signs of precipitation. Presumably this was due to precipitates at the inclusion surface acting as stress concentrators and therefore inducing fracture. It may also be possible that internal cracks were present in inclusions containing precipitates, due to volume changes as precipitation occurred.

It was also noticeable that the matrix protruded into the regions where the inclusions had cracked and separated (plates 4.17.-21.). It was assumed that the matrix was forced into these voids and fissures by the action of hydrostatic stresses developed during the deformation process (35).

A further factor which emerged during the course of this investigation was that the highest incidence of brittle fractures were observed in the region of 800 - 900°C (table 5.6. figure 5.35.). Although brittle fracture may occur due to reasons outlined earlier, this type of fracture may be highlighted at temperatures within the ferrite/austenite transformation region. i.e. Approximately 850 - 900°C for the level of carbon present in these melts.

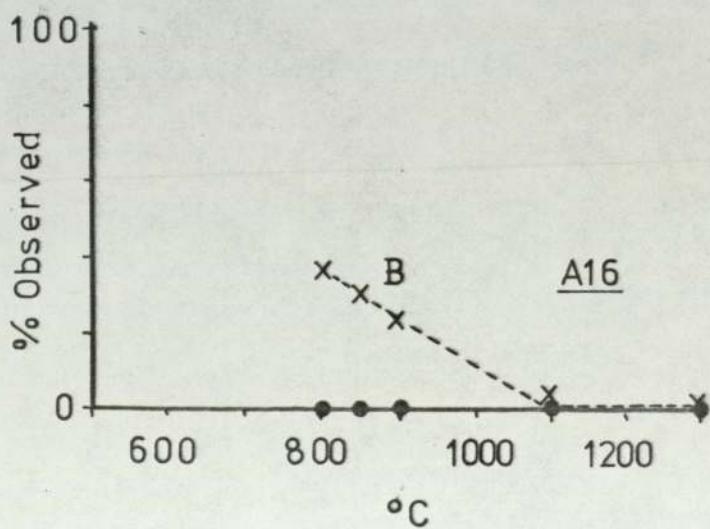
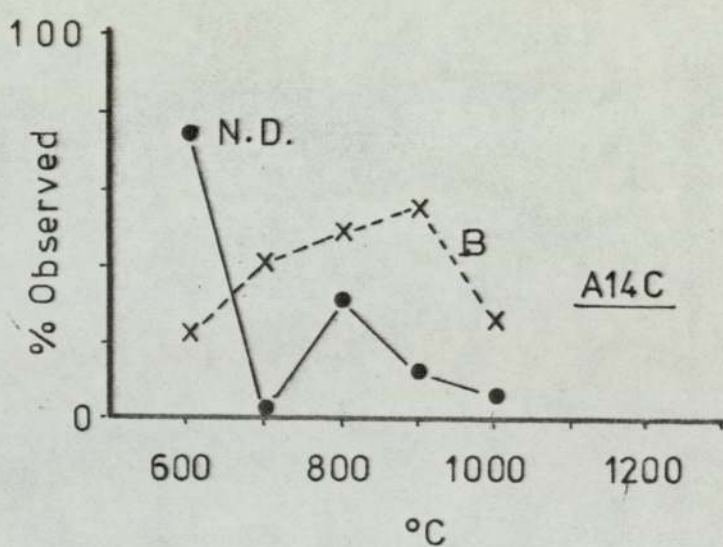
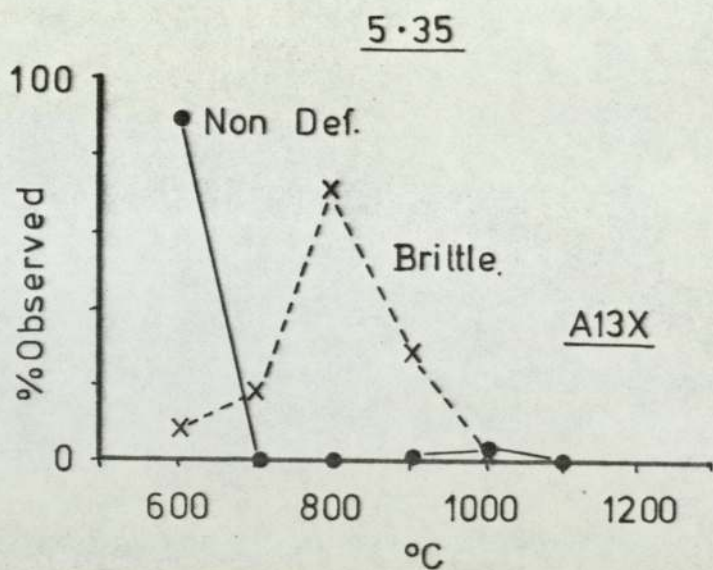
Inclusions when rolled at these temperatures may be bounded by areas of ferrite and austenite. Since there is a difference in the flow stress values for

Table 5.6

Deformation characteristics at various temperatures
for inclusions with $\sqrt{ab} > 10 \mu\text{m}$

Melt	R_T	ϵ_m	ND	DEFORMED.		BRITT (1-4)
				(1-2)	(3-4)	
Al3X	600	1.12	89	2	0	9
	700	1.12	0	82	0	18
	800	1.13	0	29	0	71
	900	1.13	1	51	20	28
	1000	1.13	3	91	5	1
Al4C	600	1.12	74	4	0	22
	700	1.12	2	58	0	40
	800	1.13	30	22	0	48
	900	1.13	12	33	0	55
	1000	1.13	5	40	30	25
Al6	800	1.16	0	64	0	36
	850	1.16	0	70	0	30
	900	1.13	0	68	8	24
	1100	1.17	0	86	10	4
	1300	1.13	0	56	44	0

N = 100



these phases, it would seem likely that a less than uniform stress situation exists around the inclusion. This stress and strain imbalance when acting upon an inclusion, particularly one containing precipitates, would possibly enhance the fracture and propagation of cracks through the inclusions.

5.3.1.1. Plastic or fluid inclusion deformation

Preliminary qualitative experiments showed that there were problems associated with the measurement of inclusion strains at various matrix strains. The largest matrix strain used i.e. 2.3 (90% reduction in height) resulted in highly strained inclusions, numbers of which showed bending, folding and often a high incidence of fracture. A further complication at this reduction was related to inclusion aspect ratio measurement. Although the inclusion major axes were easy to measure at X1000 magnification the measurement of the minor axes, which were often in the region of 2 μ m, would result in a high degree of error.

The lowest matrix strain used i.e. 0.69 (50% reduction) did not have this problem of measurement to the extent encountered in the 2.3 matrix strain samples. However, the main trouble at this strain was the difficulty in determining which of the small inclusions had deformed, and which had not.

A compromise situation of 1.2 matrix strain (i.e. 70% reduction) was eventually employed as the standard to which the matrix would be deformed. Hence all measurements were made at a nominal 1.2 matrix strain.

From these early investigations it was noted that there was a variation in inclusion strain throughout the thickness (height) of the rolled section. (which is discussed later in section 5.3.6.3). However, the central third portion appeared to give consistent

results, and the criterion that all inclusion measurements should be within the central third region was established.

5.3.1.2. Representation of inclusion size.

It soon became apparent during these investigations that inclusion relative plasticity was influenced by inclusion size. (Discussed later in section 5.3.5). As a measure of the original inclusion size for deformed inclusions, the square root of the product of major (a) and minor (b) axes was used when measurements were made on the (XY) plane :- figure 5.36.

The use of \sqrt{ab} as a measure of size is based upon the assumption that the inclusions deformed in a manner as described by plane strain, i.e. that there was no sideways spread. In addition constancy of volume was assumed.

Then :

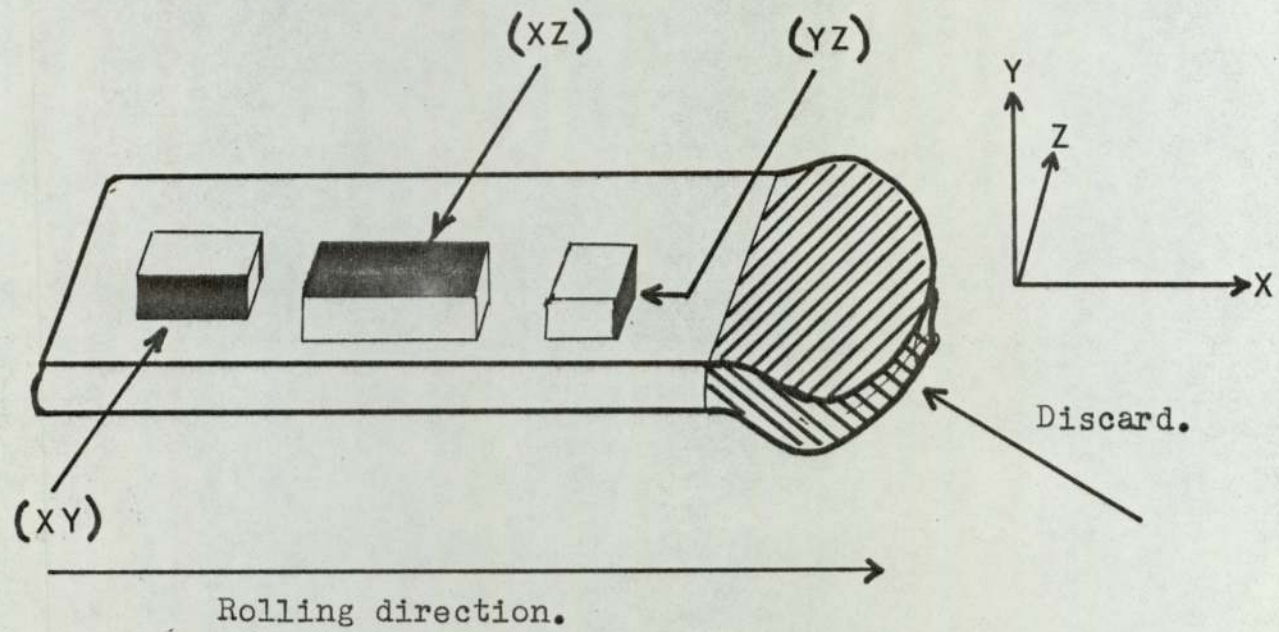
Volume of sphere = Volume of ellipsoid.

$$\frac{\pi D_0^3}{6} = \frac{\pi D_0 ab}{6}$$

$$D_0 = \sqrt{ab}$$

The plotting of relative plasticity index (\mathcal{D}) versus inclusion size defined as \sqrt{ab} results in a series of lines dependent upon the magnitude of the major and minor axes. This occurs because both terms

Fig. 5.36: Sectioning of rolled samples.



contain a and b.

viz:

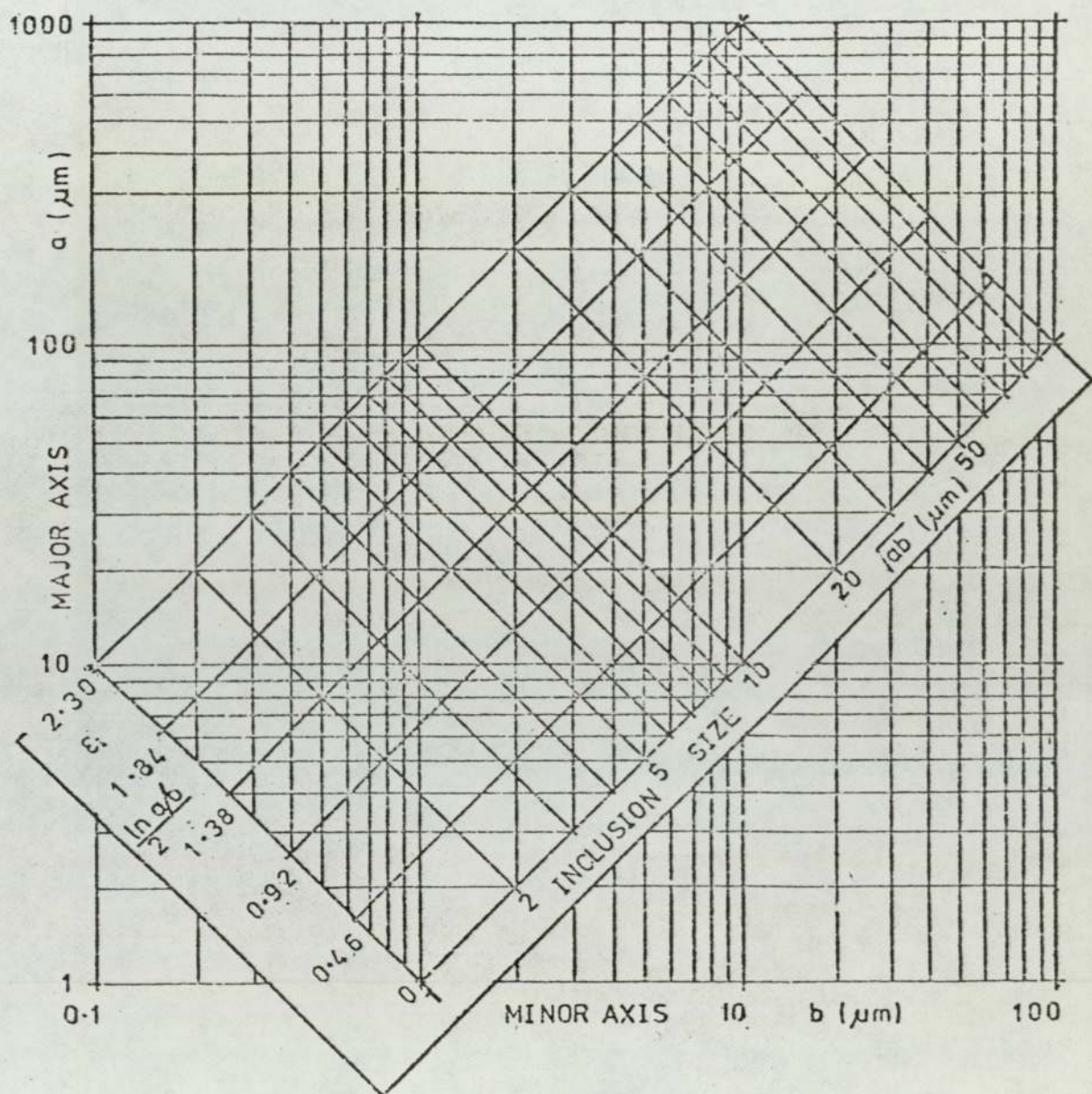
$$D_0 = \sqrt{ab}$$

$$\nu = \frac{l}{2\epsilon_m} \cdot \ln \frac{a}{b}$$

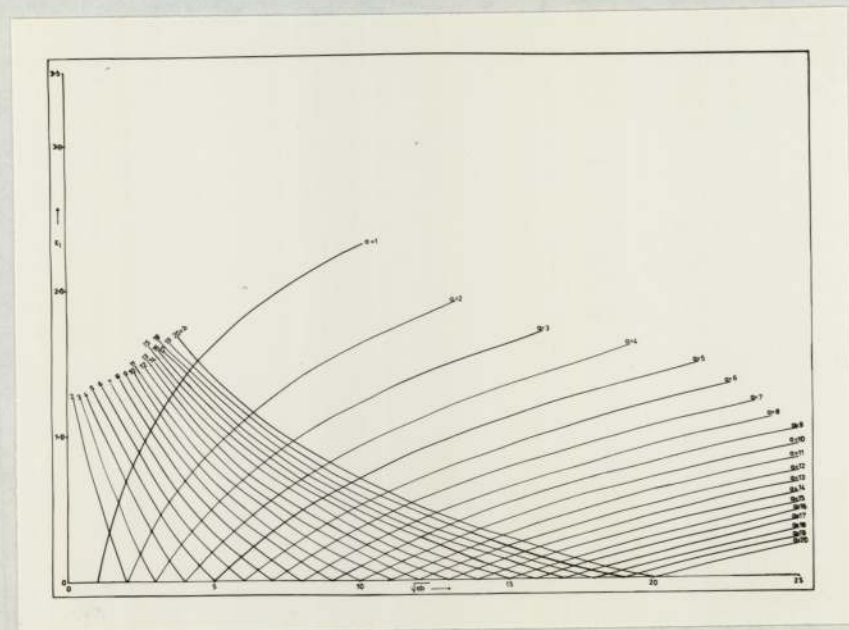
Figure 5.37 shows the dependency of ϵ_i (or ν) upon a and b values, and figure 5.38 shows the distortion when plotting ϵ_i (or ν) versus \sqrt{ab} . This latter figure indicates that small errors in measurement at small sizes may give an apparent size relationship. However, the presence of a large number of small inclusions, as is the case, will lessen the total error.

The plotting of ϵ_i (or ν) versus \sqrt{ab} , (as was the case for all measurements on the (XY) plane) does mean that the measured values of a and b may be simply determined for any point on the graph. This is particularly the case if it is recognised that measurements of a and b were made to the nearest half micron.

5-37



5.38



5.3.2. The effect of hot rolling upon inclusion deformation characteristics.

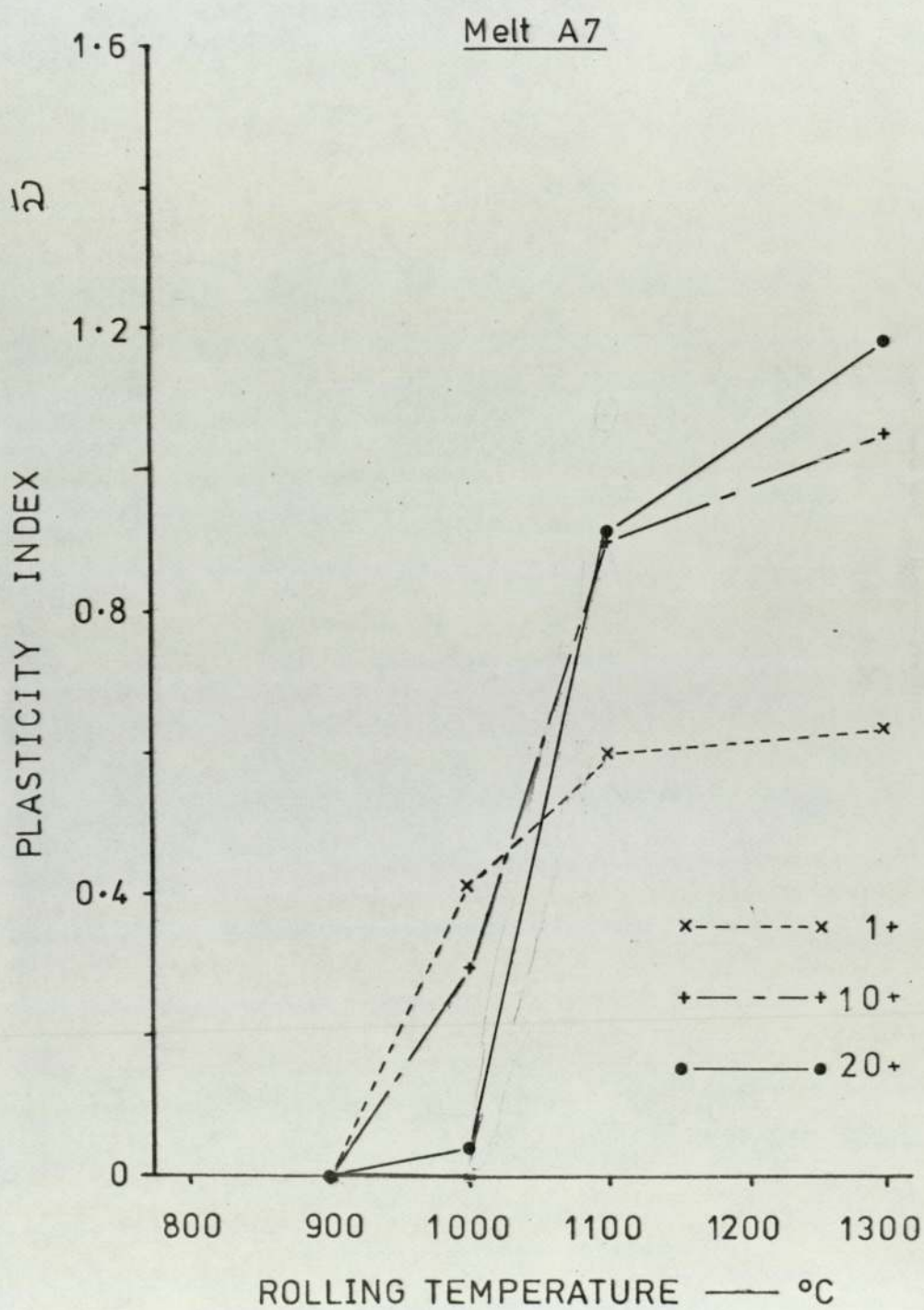
The behaviour of the inclusion phases at the hot rolling temperatures were categorised and reported upon in section 4.8 . The marked variability of deformation was indicated in plates 4.14. to 4.35. and it was seen that the presence of precipitation could effectively stop deformation even at high (i.e. 2.3) matrix strains. Plate 4.36.

5.3.3. The variation in inclusion plasticity index with temperature.

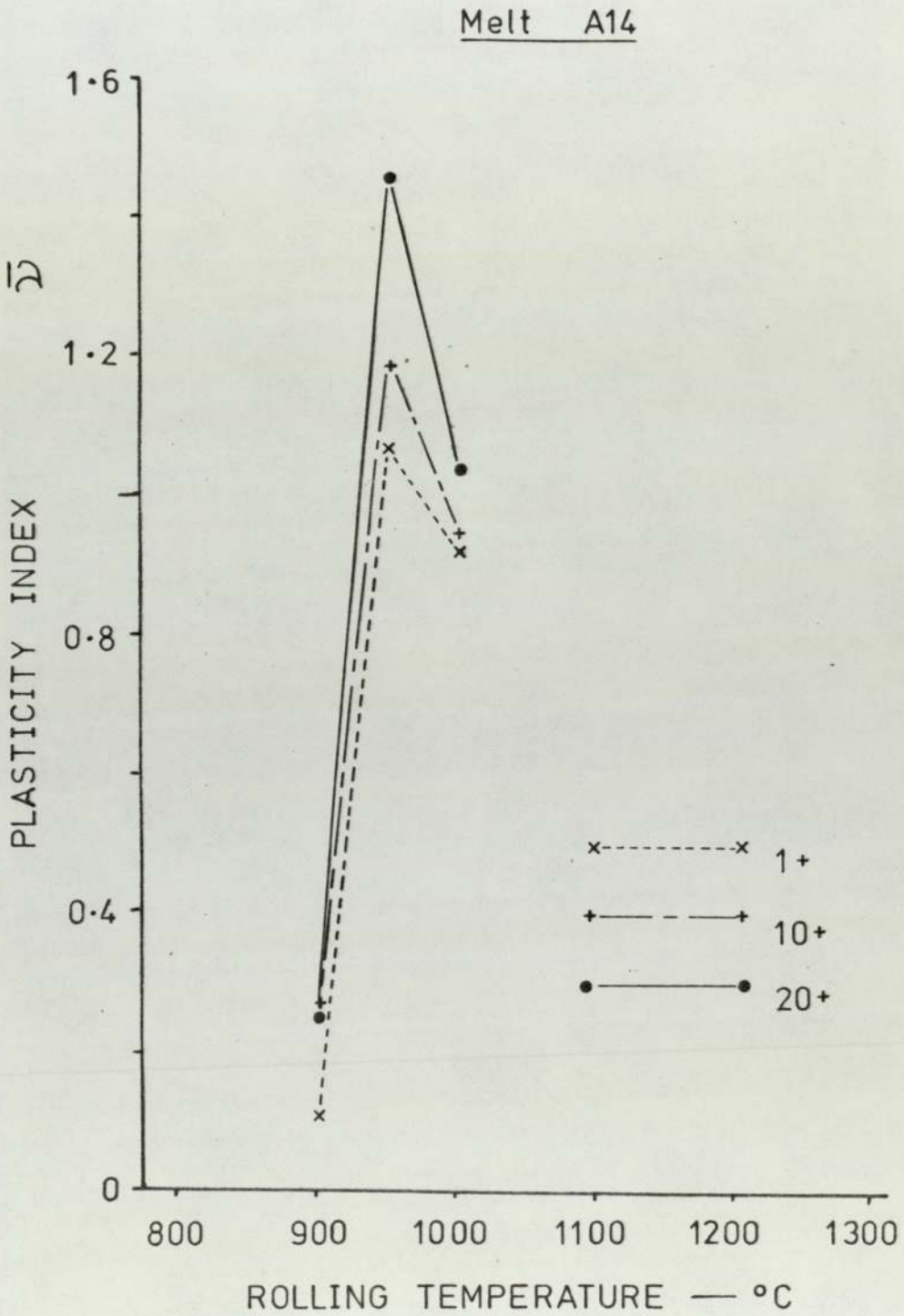
The variation in the mean relative plasticity index (ρ) with temperature was presented in table 4.9. and is shown graphically in figures 5.39. to 5.53 . It may be seen in general that there was a sharp transition from non deformable to deformable behaviour over a narrow range of temperature. This was in agreement with numerous workers (35, 94, 102) who have studied the deformation of silicate inclusions over a range of temperatures. However, due to the limited amount of material available it was not possible to determine the precise transition temperatures. Bearing this fact in mind figures 5.39. to 5.53. give a guide to the transition temperatures at different inclusion compositions.

It has been known for some time (79) that glassy inclusions may precipitate phases upon heat treatment (as

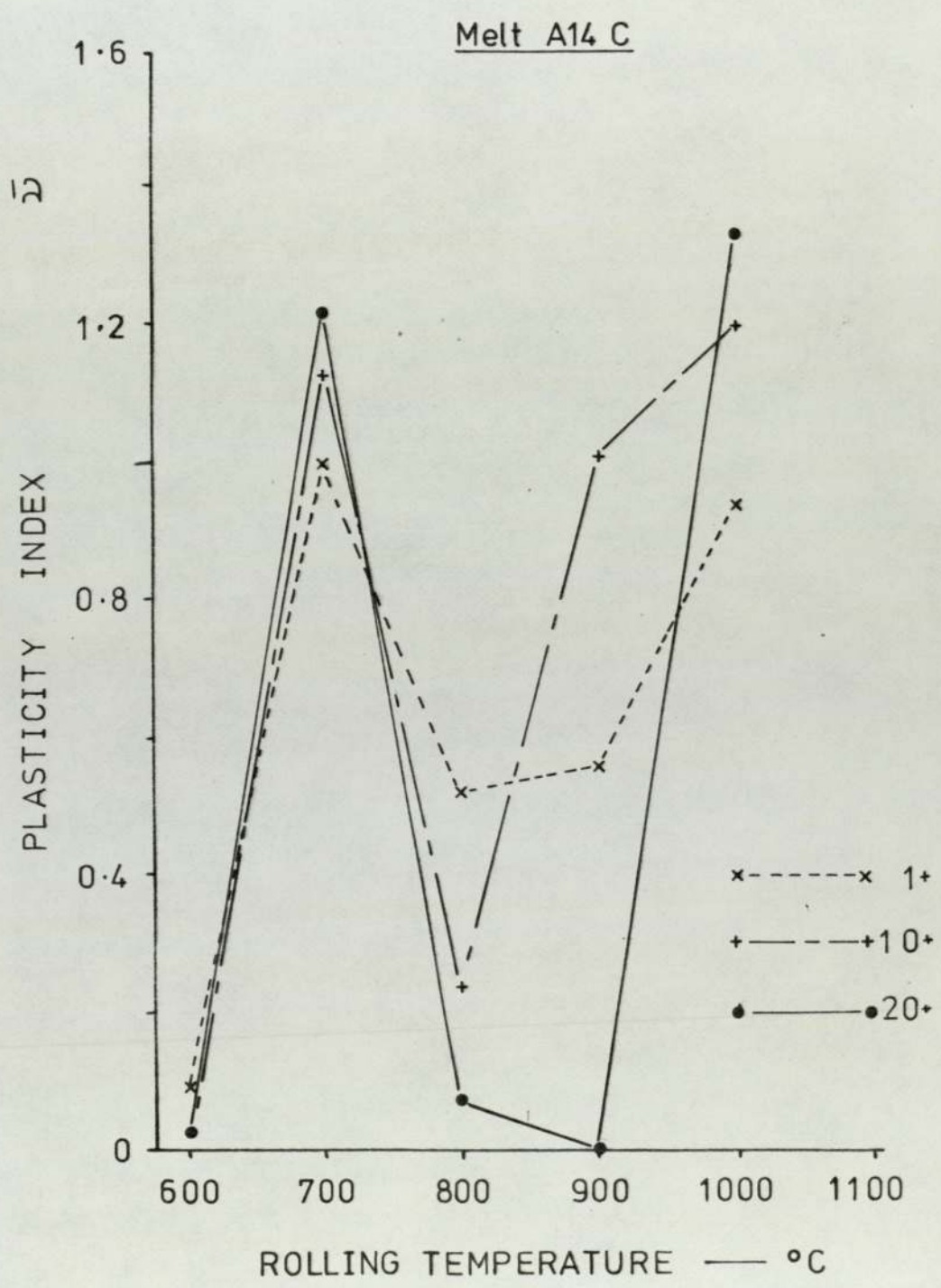
5.39.



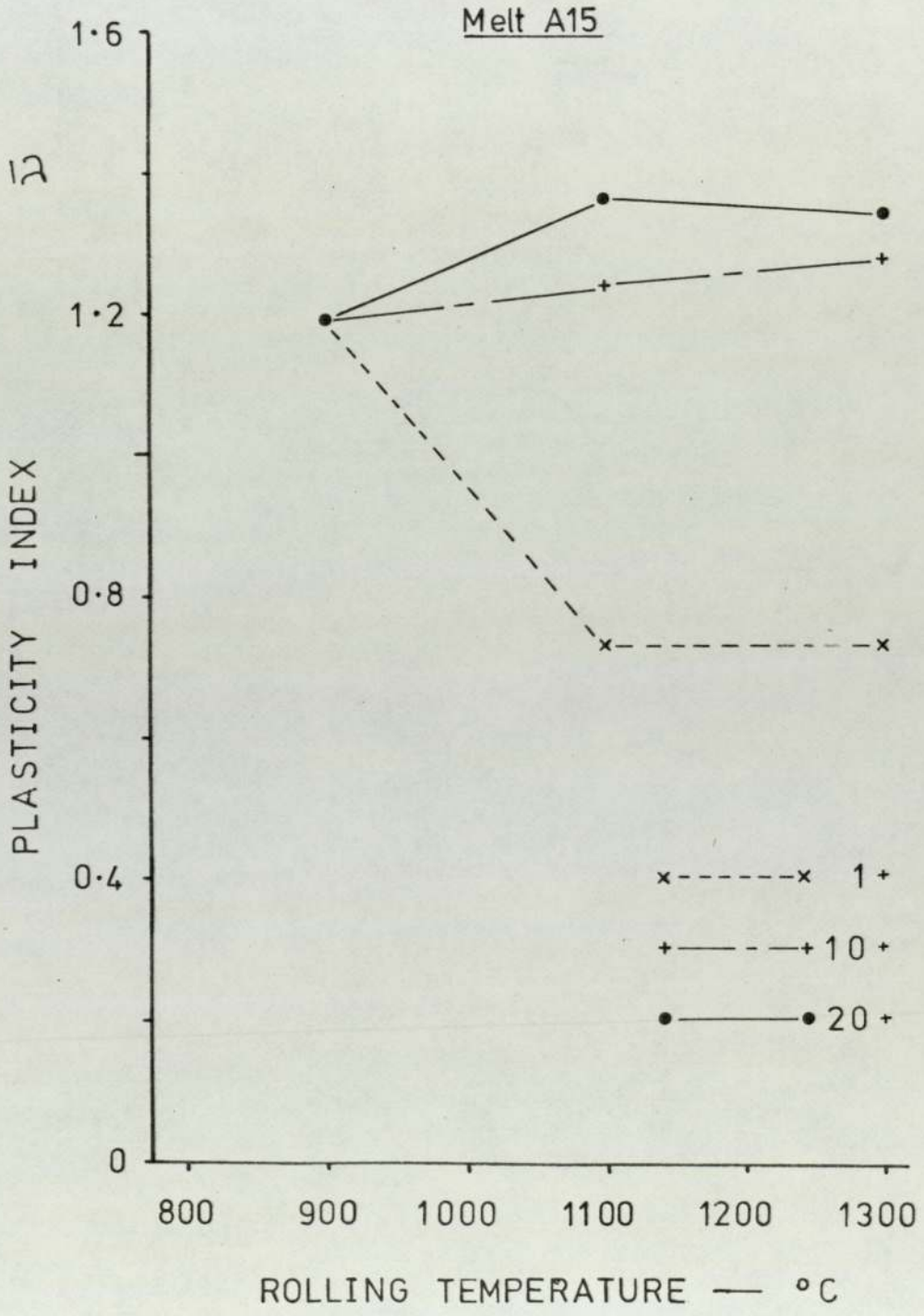
5.40.



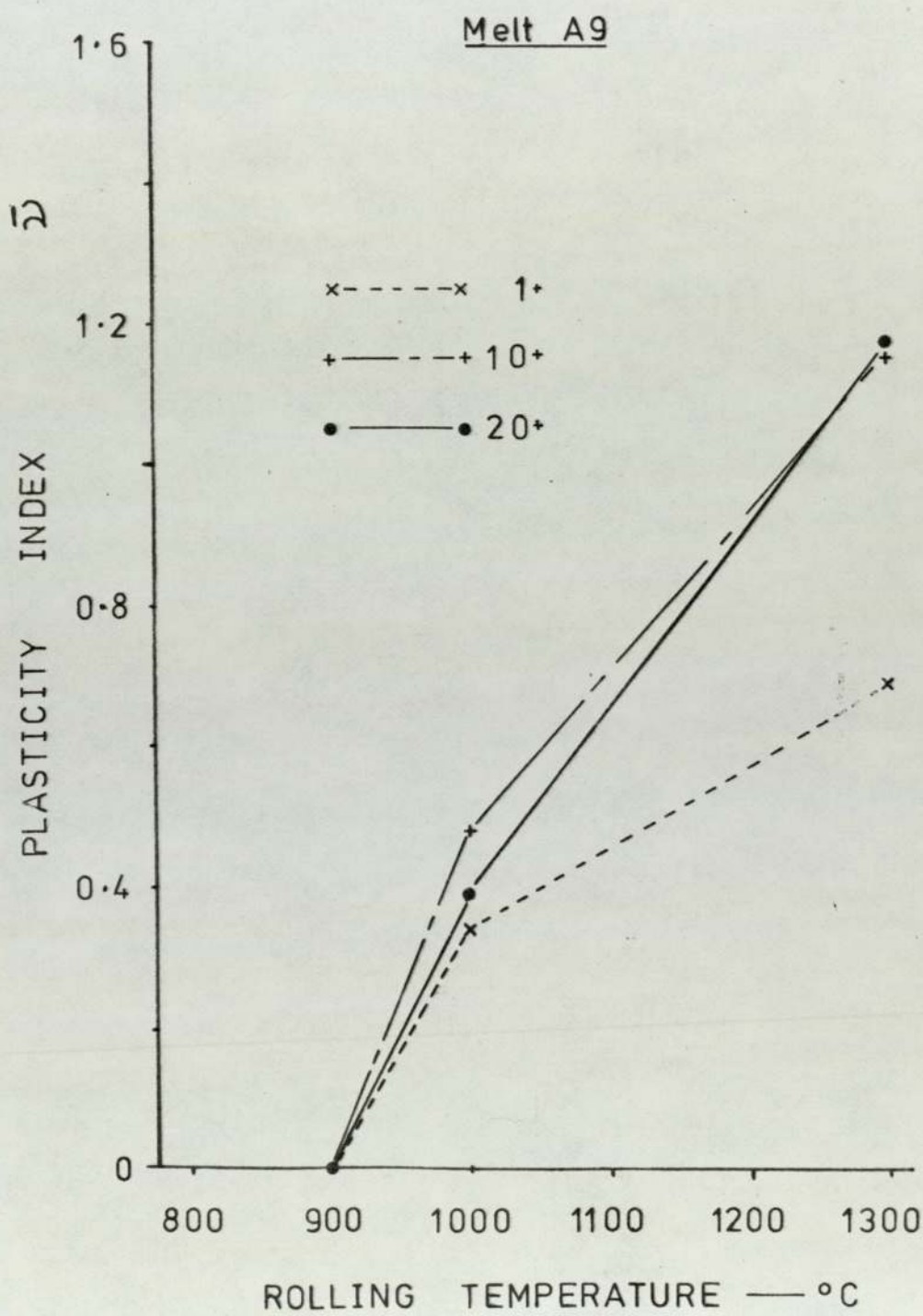
5.41.



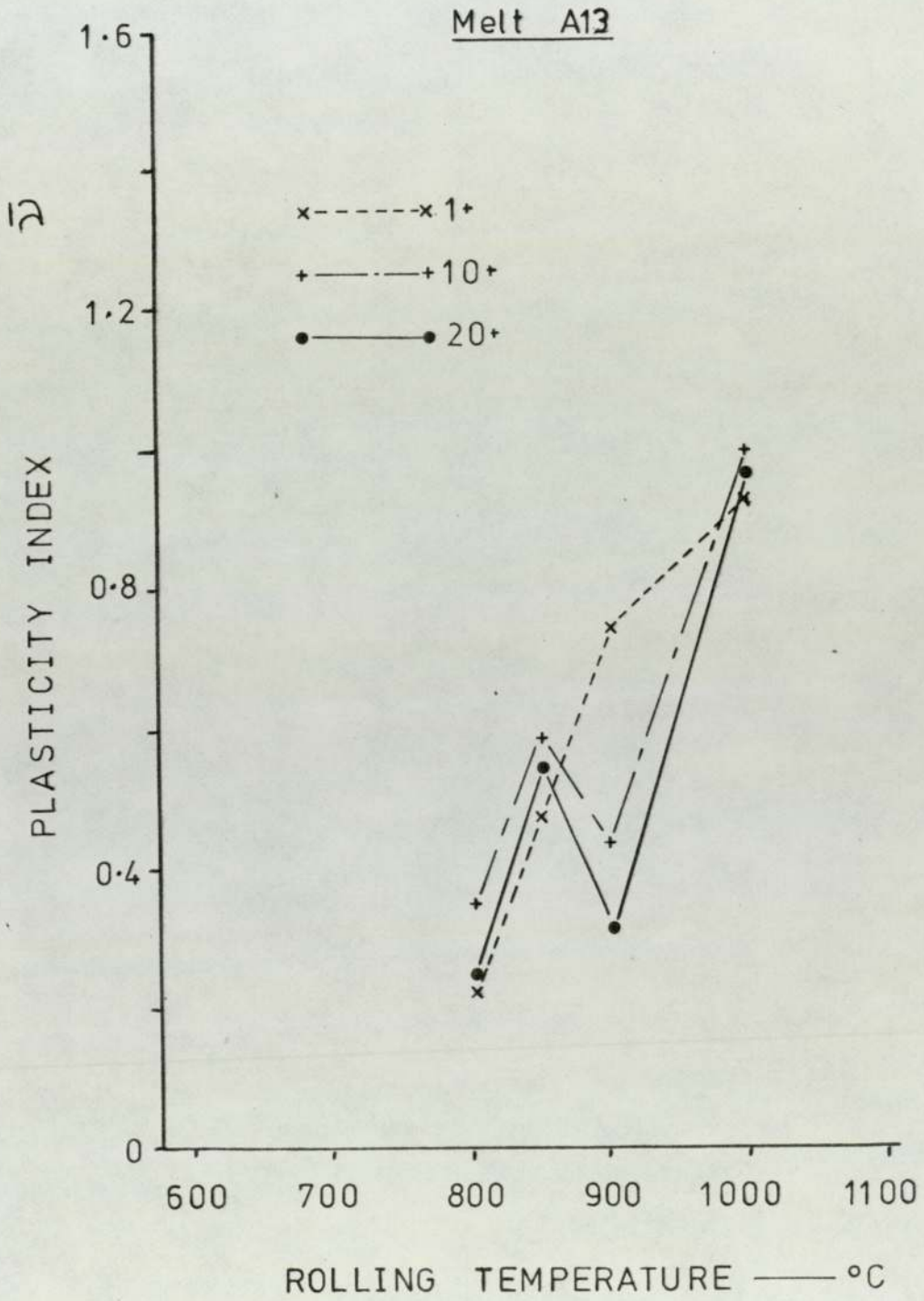
5.42.



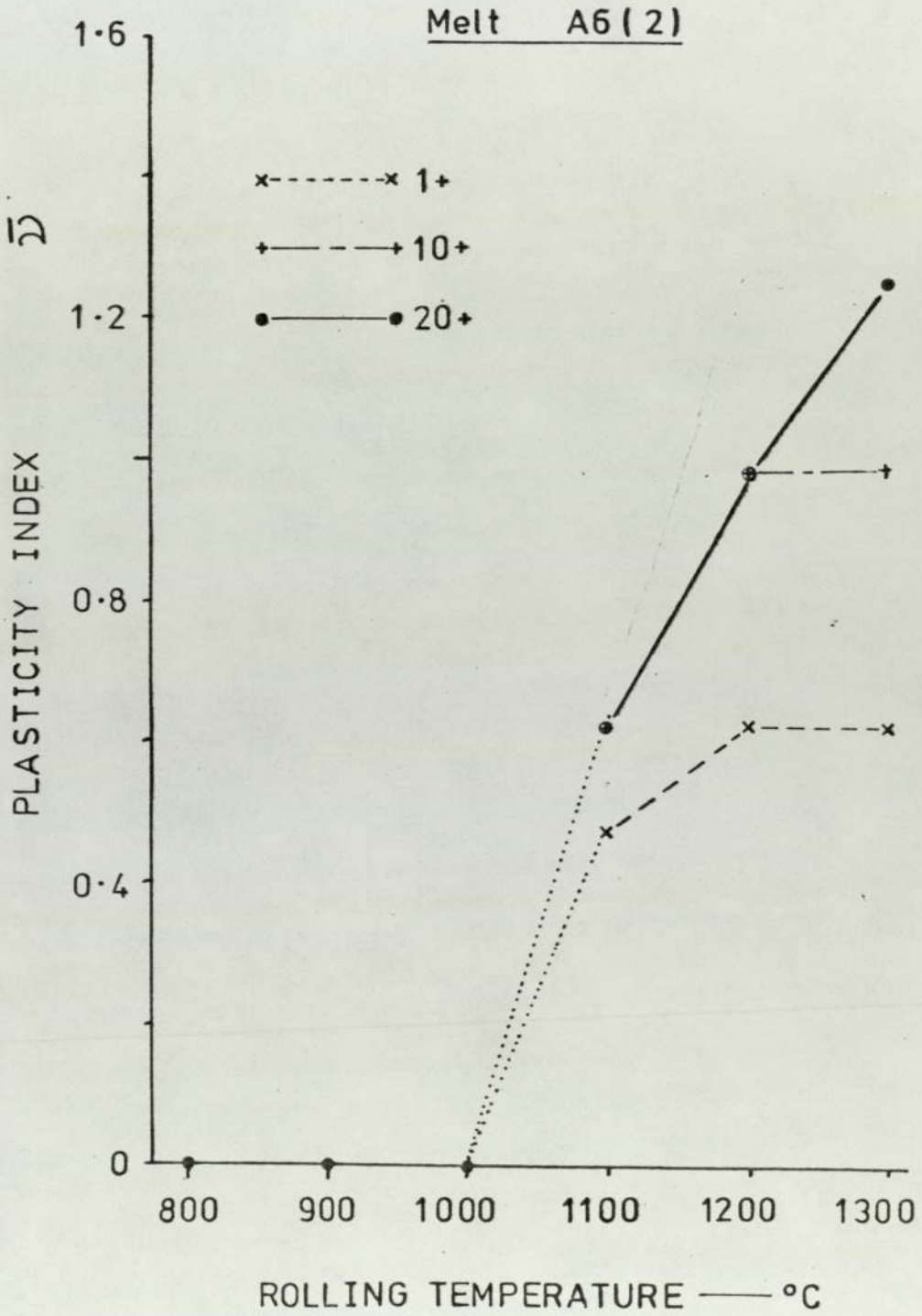
5.43.



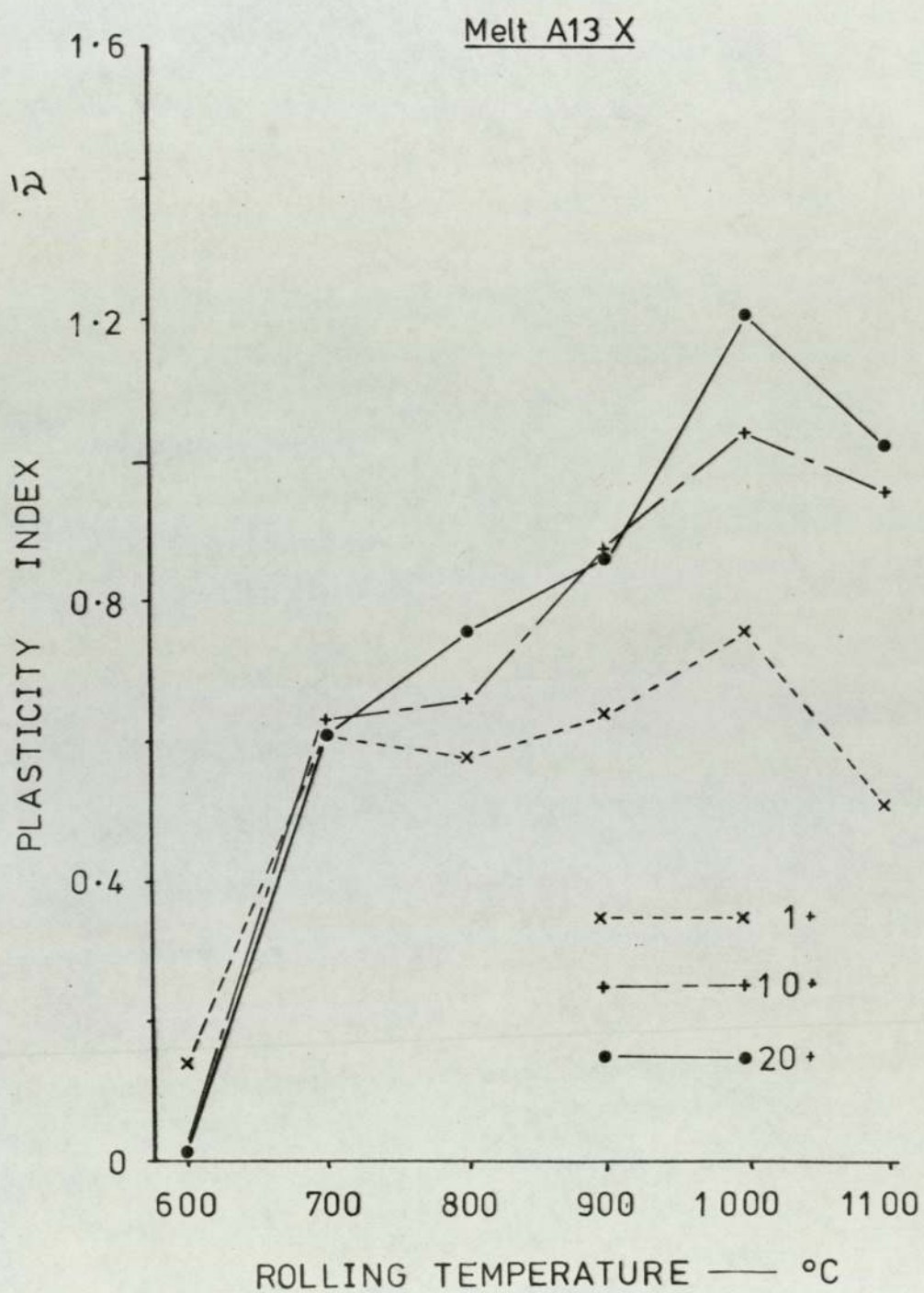
5.44.



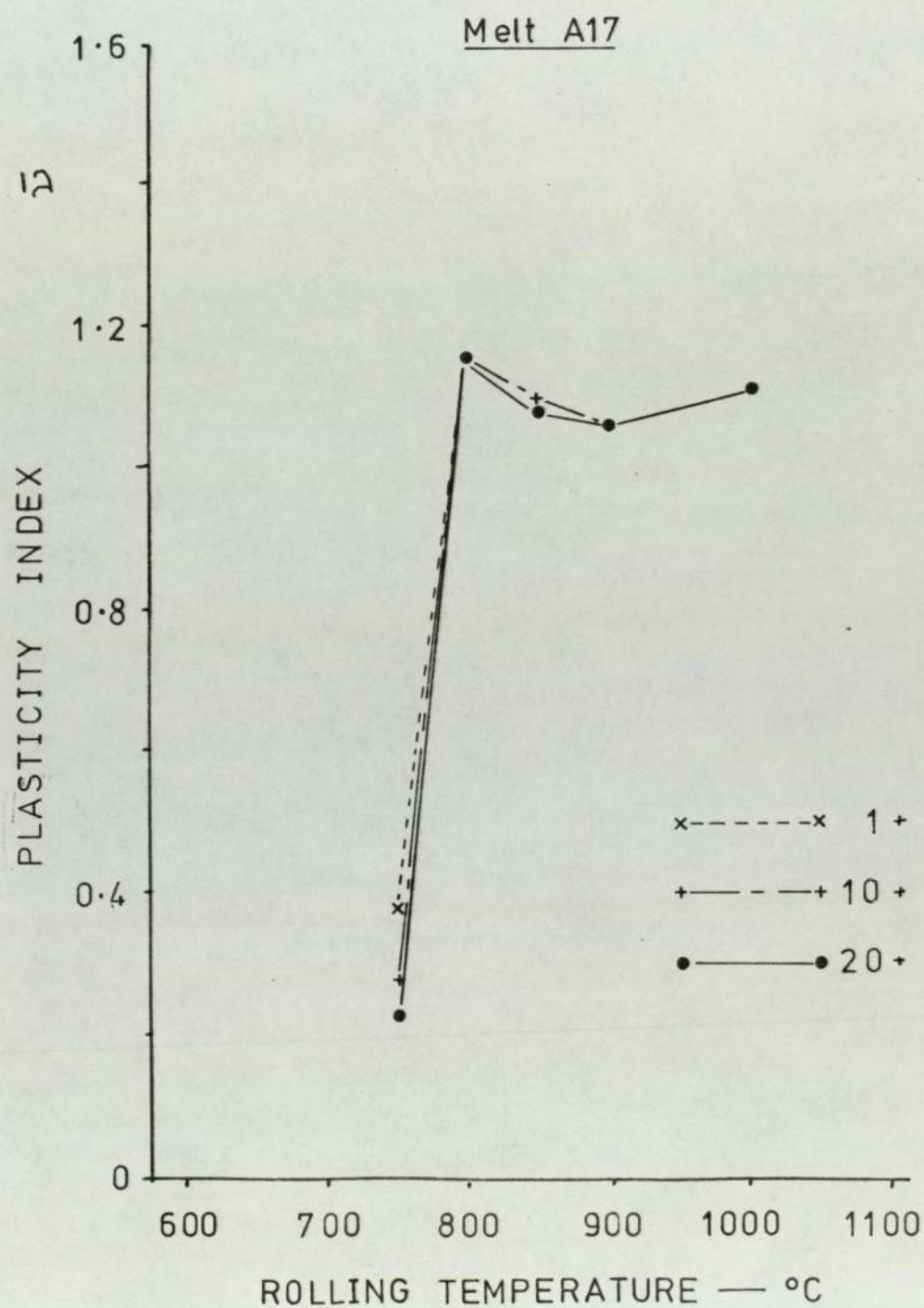
5.45.



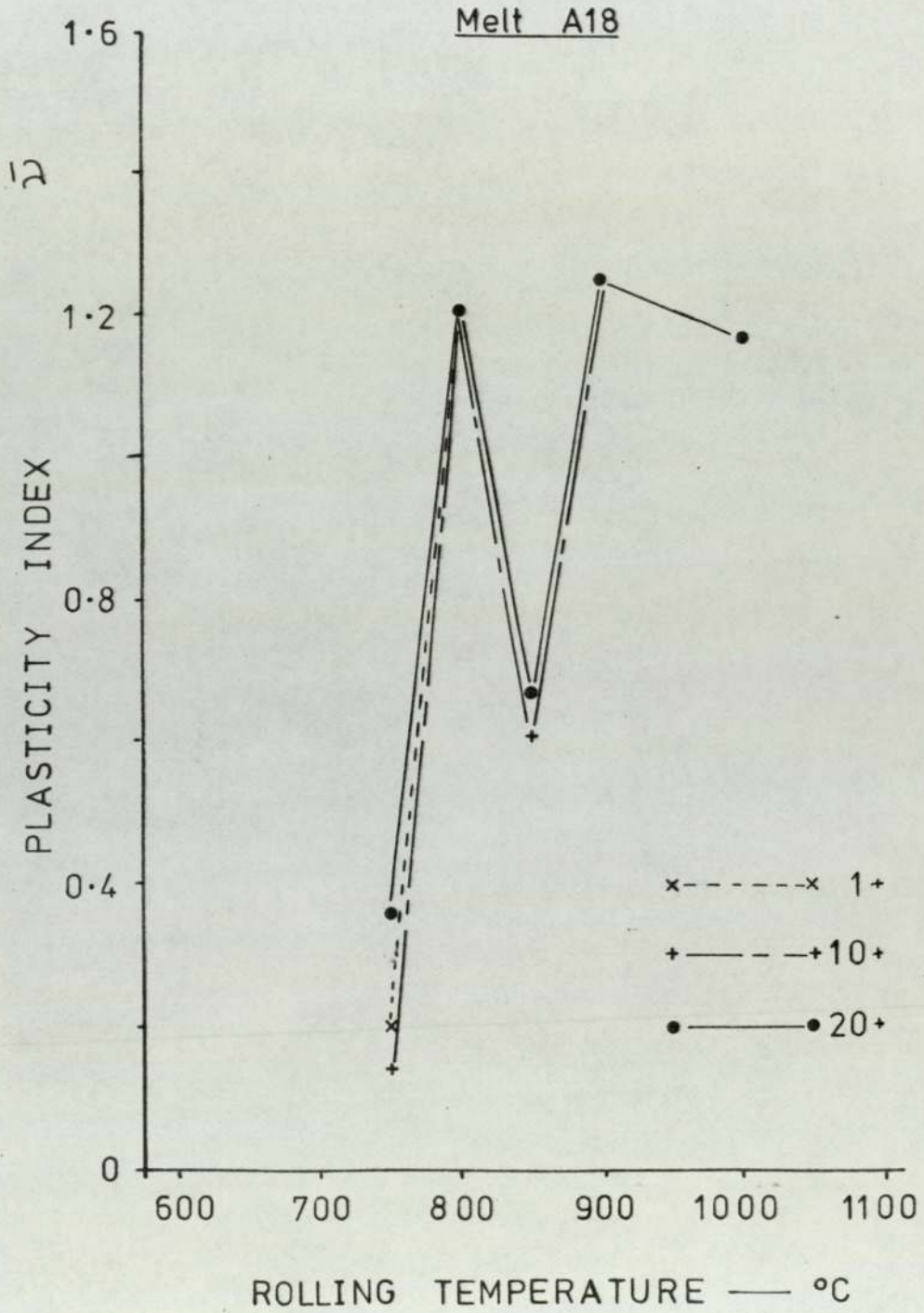
5.46.



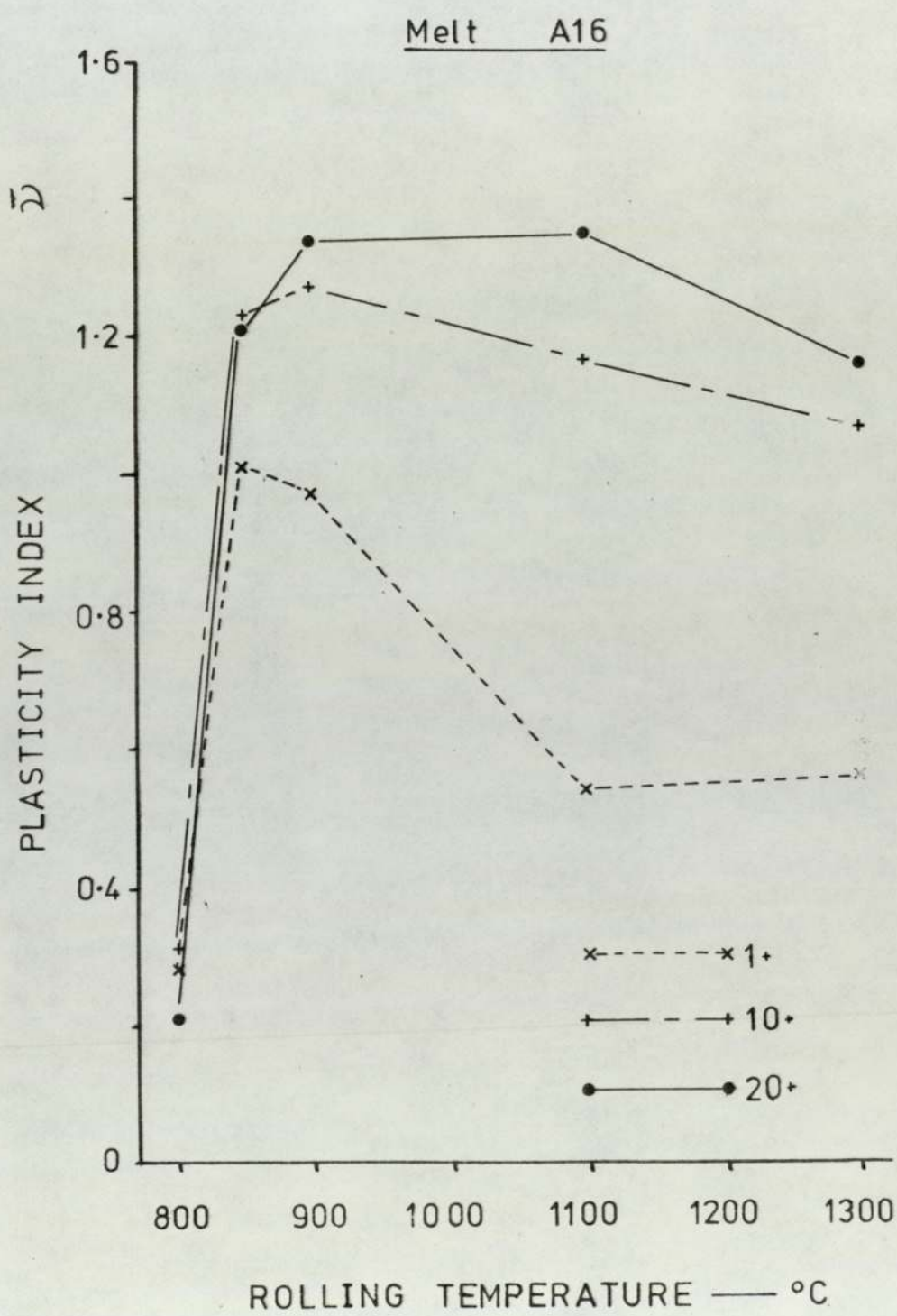
5.47.



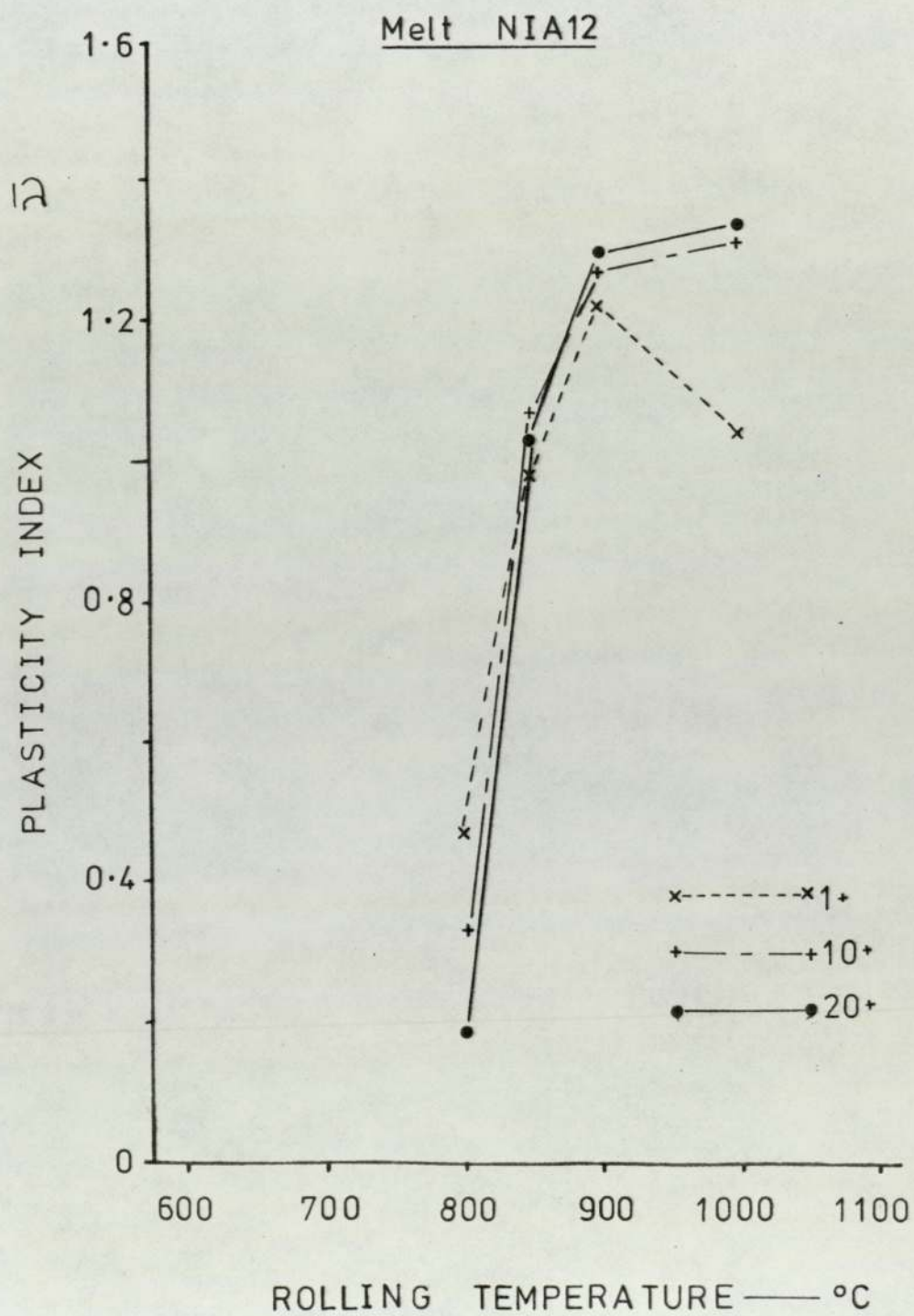
5.48.



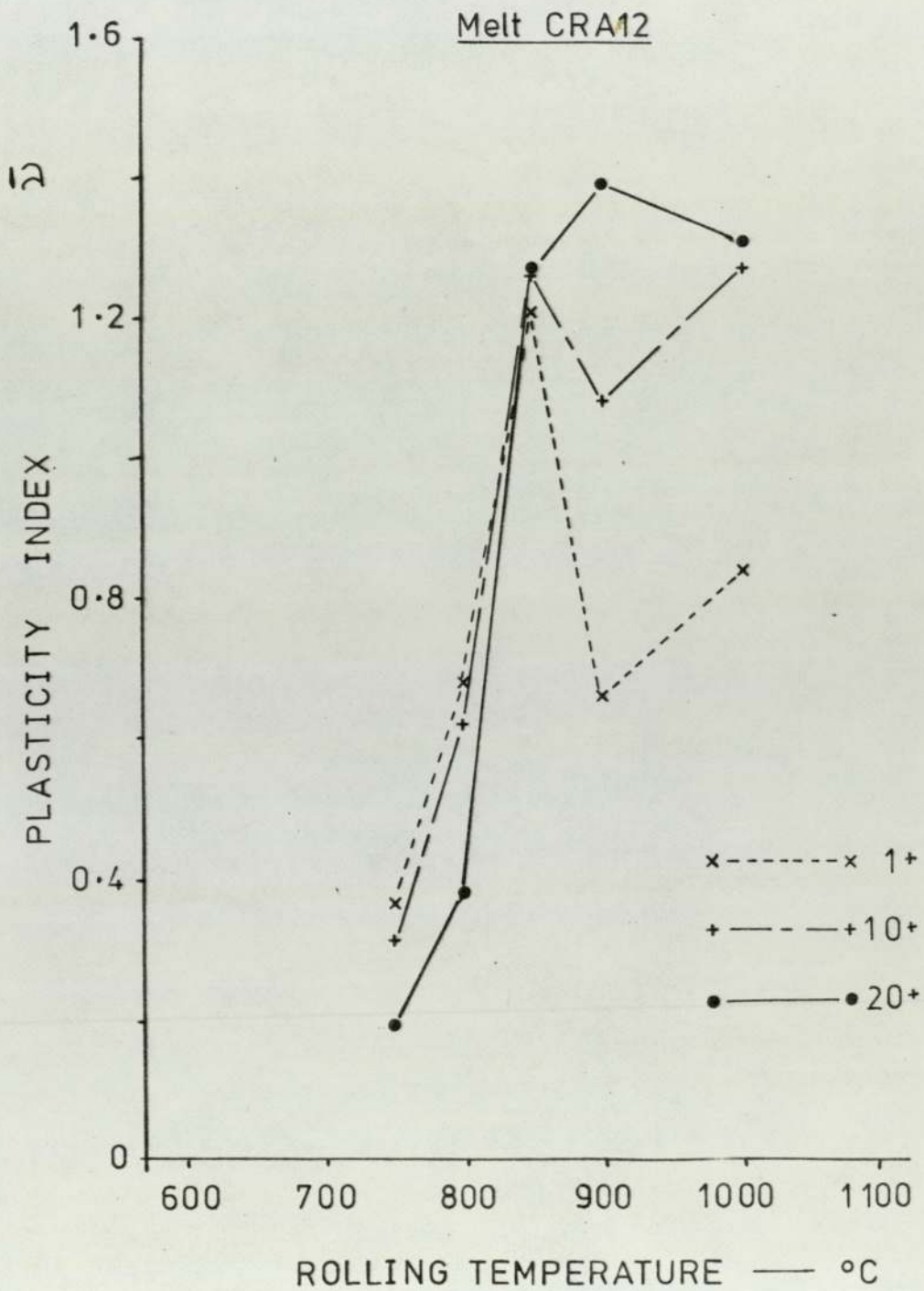
5.49.



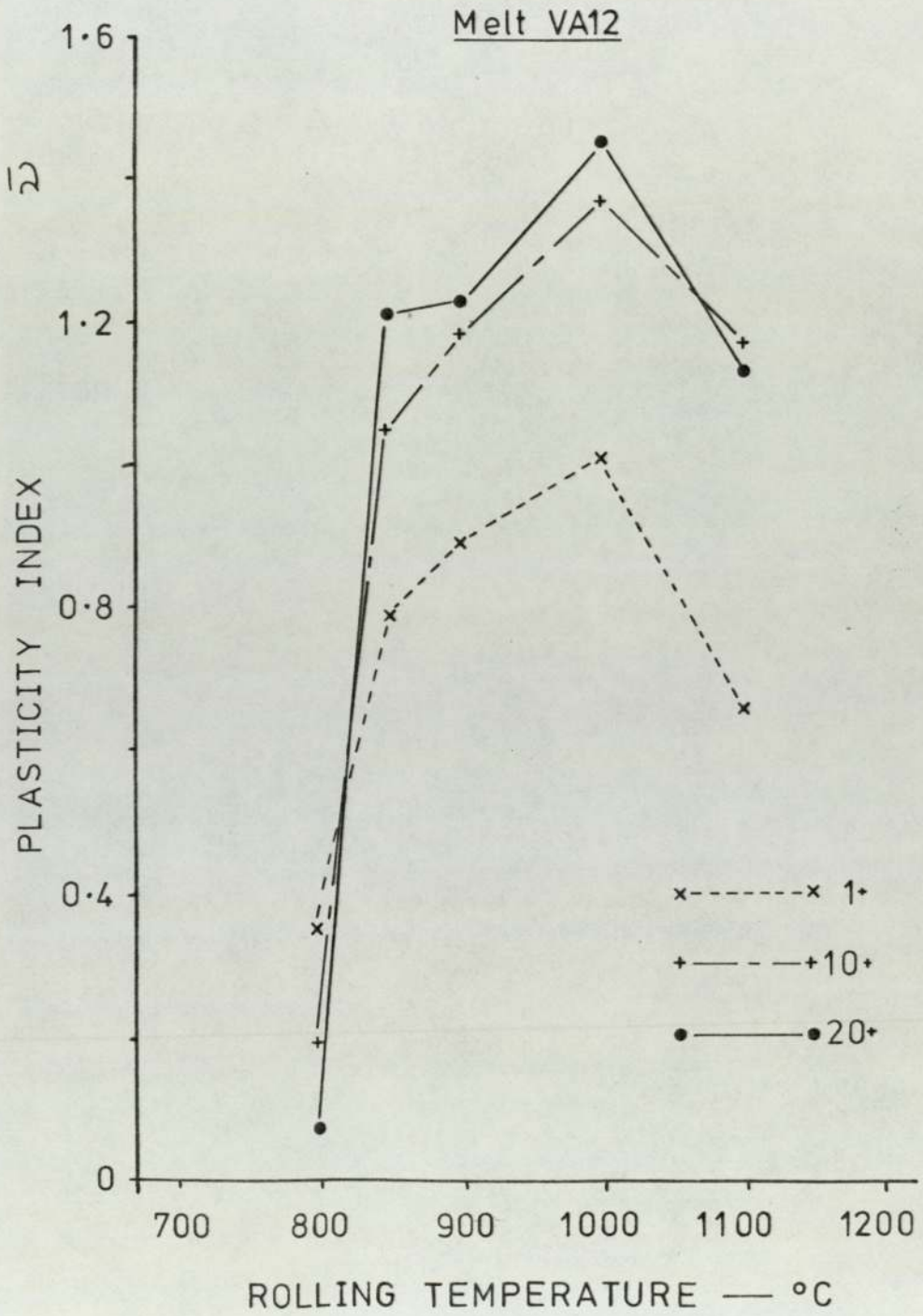
5.50.



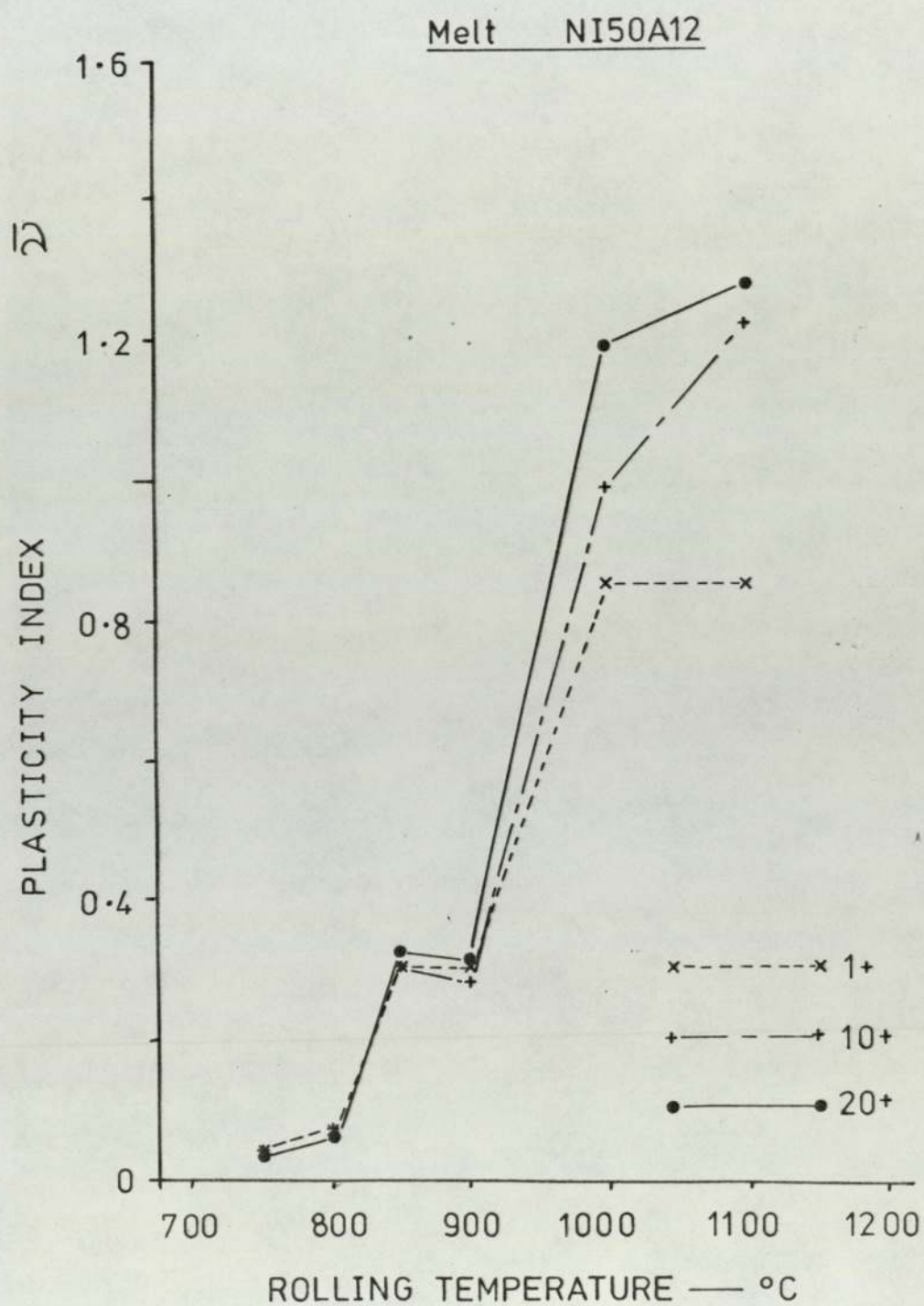
5.51.



5.52.



5.53.



was shown earlier) and hot working. Knowing that precipitation did occur this part of the discussion is broken into several sections, and will relate to inclusions greater than 20 μm in equivalent or observed diameters viz; (designated by the symbol 20+)

Group 1. - Those inclusions which precipitated Rhodonite.

This group was sub-divided into three sections.

(1a) - Inclusions with greater than 55%MnO and an alumina content in the region of or less than 5%. i.e. melts A7, A8, A10 and A11.

(1b) - Inclusions with approximately 50% Mn and an alumina content 10 - 15%. i.e. melts A14, A14C and A15.

(1c) - Inclusions which were richer in silica than groups (1a) and (1b) and which precipitated, SiO_2 , in addition to or in place of the Rhodonite. i.e. melts A9, A12 and A13.

Group 2. - Those inclusions which contained silica in the form of cristobalite in the 'as cast' and deformed conditions. i.e. melts A6 and A13X

Group 3. - Inclusions which contained alumina precipitates within silicate matrices both in the 'as cast' and deformed conditions. i.e. melts A17 and A18.

Group 4. - Inclusions which were glassy in the 'as cast' and deformed conditions i.e. melts A16, NIA12,

CRAl2, VAl2 and NI50Al2.

Group (1a) : melts A7, A8, A10 and A11.

Referring to figure 5.39, which was for melt A7, it can be seen that there was a small amount of deformation at a rolling temperature of 1000°C . This indicated that the transition temperature for these inclusions lay between 1000 and 1100°C , which was some 100°C or more below the solidus temperature for this composition shown in the MnO - SiO₂ phase diagram. (figure 4.2.). If the transition temperature for this melt was that of the solidus temperature, as is the case for crystalline inclusions (35), then there was a marked deviation from what was to be expected.

However, melt A7 contained inclusions which in some instances had approximately 17% FeO present and in addition only a few inclusions were observed to have deformed. It may therefore have been that the inclusions which had deformed were those rich in FeO. Unfortunately no microprobe analyses were performed on the deformed inclusions at 1100°C , which could have confirmed this. The presence of upto 17% FeO may however, mean that the solidus temperature was somewhat closer to the observed transition temperature, and been within the experimental error in the measurement of temperature. A further complication may have been the excess temperature derived from work done on the matrix, in which case the inclusions may have been deformed above the expected rolling

temperature.

Although not observed during the inclusion strain measurement of melt A8 at 1000°C, there were some deformed inclusions present which were later analysed on the microprobe analyser (Appendix 4.2). These analyses showed that some inclusions were extensively deformed and had low levels of FeO present i.e. less than 3%. Although melts A7 and A8 contained inclusions of similar compositions a number of deformed inclusions of A8 appeared to be glassy in nature, and as such were not directly comparable.

Melts A10 and A11 which had inclusions of compositions in the vicinity of melts A7 and A8 (figure 4.3.) showed very little deformation at 1000°C. Again at this temperature the large inclusions contained precipitates. At a rolling temperature of 1300°C which was above the solidus temperatures for all melts A7, A8, A10 and A11 there was extensive inclusion deformation.

It should be recognised that these melts contained inclusions which precipitated apparently at random. Therefore it may be that these inclusions which showed precipitation during microscopic examination and were of a highly deformed nature at rolling temperatures, below the solidus, may not have contained precipitates on every occasion when they were hot rolled. Precipitation may have occurred during the repeated heating and cooling dictated by the rolling programme, or even during the rolling, as has been reported. (79)

Robinson (35) has reported that if crystallisation

of an inclusion occurs it may become fractured upon subsequent hot rolling. However, this type of behaviour was not noted.

Group (1b) : Melts Al4, Al4(C) and Al5.

The deformability of inclusions from melt Al4 is shown in figure 5.40. , where it can be seen that there was a rapid increase in the value of mean plasticity index (\bar{y}) over the temperature range 900 to 1000°C. This was thought initially to be the non-deformable/deformable transition temperature for inclusions of melt Al4. However, a further experiment on melt Al4(C) which contained inclusions of similar composition dispelled this belief. As with melt Al4, Al4(C) showed a sharp non-deformable/deformable transition temperature when the rolling temperature was increased from 900 - 1000°C. Very little deformation of the inclusions was observed at 800°C. However, rolling at an even lower temperature of 700°C showed that extensive deformation occurred and even at a rolling temperature of 600°C limited inclusion deformation was observed. (Fig. 5.41.)

An explanation for this phenomenon may be based upon the formation of precipitates within the inclusion phases. At the rolling temperatures of 600°C and 700°C all the inclusions were of a glassy nature, and it is conceivable that the transition temperature of the silicate glass occurred within this temperature range. (A phenomenon which is discussed again in section group (4)). At temperatures in the rolling range from 800° -

1000°C precipitation was known to occur. These precipitates, which were analysed as rhodonite, appeared to be of a blocky nature as shown in plate 4.63. At 800°C and 900°C very little if any deformation was observed, and a large proportion of brittle inclusions were found. Table 5.6. especially at 900°C.

The precipitation of rhodonite would effectively change the composition of the siliceous matrix, and the suspension of particles within the matrix would change the effective viscosity of the inclusion. Above 900°C it would appear that the inclusions, which now contained a dispersed phase, reached a critical temperature where they became effectively fluid and readily deformed. The presence of blocky precipitates, appeared to have very little effect on the inclusion deformability once the inclusion was fluid (as is observed in the stereoscan photograph of a highly deformed inclusion from melt Al4 plate 4.41.).

Melt Al5, which again had inclusions of similar composition to melt Al4, showed that above 900°C extensive deformation occurred with these inclusions containing precipitates. There was some discrepancy between melt Al4 and Al5 at 900°C where it was seen that a large number of inclusions in melt Al5 were deformable. This appeared to be due to a larger number of inclusions in melt Al5 which had remained glassy, and as such were highly deformable. (Fig. 5.42.)

Group (1c) : melts A9, A12 and A13.

Melt A9 contained inclusions which readily precipitated upon rolling at 900°C and 1000°C. No visible deformation was observed at 900°C and the main characteristic at this temperature was the fracture and dissemination of these inclusions.

At 1000°C there was limited deformation, which may have indicated that there was a non-deformable/deformable transition temperature in this region (figure 5.43.). However, this may have been another case where at lower temperatures extensive deformation occurred (as in melt A14(C)). Therefore a transition temperature in the range 900 - 1000°C for this melt should be regarded with some degree of scepticism. At a rolling temperature of 1300°C extensive inclusion deformation was again observed.

Melts A12 and A13 both showed extensive precipitation within the large inclusions when rolled in the temperature range 800 - 1000°C, the smaller inclusions remained glassy as was seen in plate 4.37. From figure 5.44, the indication was that there may be a transition temperature in the region 800 - 900°C although it was again the case that the large inclusions which had deformed were both glassy, and contained precipitates. It may be noted from figure 5.44. that there appeared to be a kink in the plasticity index (ν) versus rolling temperature curve at 900°C. This may have been due to the point at 850°C being derived from two results, or

a phenomenon which occurs at 900°C which has not been discussed up to the present. The reason for a limited number of results at 850°C was a high incidence of inclusions which behaved in a brittle manner.

Group (2) : melts A6(2) and Al3X.

Both these melts contained inclusions which had silica precipitates present in the form of cristobalite as was indicated in figure 4.44. . These precipitates were present in the as cast and deformed inclusions, and deformation at the highest rolling temperatures employed showed no evidence of the re-solution of the silica particles. In addition there appeared to be no indication of excessive precipitation at any of the rolling temperatures. These inclusions appeared to behave in a similar manner to the glassy inclusions which will be discussed in section group (4).

Unfortunately it was not possible to obtain the transition temperature of the inclusion from melt A6(2) although it may be seen in figure 5.45. that it appears to be in the region of 1100°C . This indicated that the transition temperature was probably viscosity controlled, as was the case for glassy inclusions.

Melt Al3X, which contained inclusions of compositions within the $\text{FeO} - \text{MnO} - \text{SiO}_2 - \text{Al}_2\text{O}_3$ system, showed that a transition from non-deformable to deformable behaviour occurred in the region of $600 - 700^{\circ}\text{C}$ (figure 5.46.). This temperature is well below any solidus temperature

in this system. Again this indicated that the transformation temperature was controlled by the viscosity of the silicate phase in which the silica precipitates had formed. It also seems apparent from figure 5.46. that the range of temperature over which the inclusions have gone from being non-deformable to their maximum plasticity was somewhat extensive i.e. 400°C . This was significantly at variance to what was observed with the glassy inclusions of group (4).

Group (3) : Melts A17 and A18.

Both these melts contained inclusions in which alumina particles were present within a siliceous matrix. During deformation above 750°C these inclusions were observed to deform into an elongated form, which was often very angular in appearance, although the inclusions remained intact. Plates 441. & 441a. show these angular inclusions in situ in the steel matrix, which was deeply etched to reveal the inclusions.

Although it may appear that there was a transition temperature in the region of $750 - 800^{\circ}\text{C}$. Figures 5.47. and 5.48. this may be due to the siliceous matrix being of low viscosity and moving in sympathy with the alumina particles. Although deformation was not carried out at lower temperatures, where the siliceous matrix was non-deformable, fracture and dissemination may have been expected to occur. At the rolling temperatures inclusions contained within melts A17 and A18 showed a

wide scatter in plasticity indices

Group (4) : Melts Al6, NIA12, VA12, CRA12 and NI50A12

Inclusions from the above melts were found to be the only ones in these investigations which showed no signs of precipitate within the 'as cast' or deformed states. There was one exception, and this was melt VA12 which had been rolled at 1000°C. It was observed that on two occasions a deformed inclusion contained precipitates of the $MnO - Al_2O_3 - V_2O_5$ type. (plate 5.3.) However, these precipitates were thought to be of exogenous origin.

Melts Al6, NIA12, VA12 and CRA12, which contained inclusions of very similar composition, showed a rapid change in inclusion plasticity index ($\bar{\nu}$) over the temperature interval 800 - 850°C (figures 5.49. -5.52.). Melt NI50A12 which contained inclusions richer in silica, and presumable therefore had higher viscosity at the same temperatures than the other melts, showed a transition temperature in the range 850 - 950°C. (5.53)

5.3.3.1. Factors which influence the non-deformable/deformable transition curve.

Viscosity (5.3.3.1.1.)

Initially confining the discussion to the non-deformable/deformable transition for glassy inclusions, it was seen that the transition temperature varied with composition. i.e. melts Al4, Al6, NIA12, CRA12, VA12 and NI50A12. These transition temperatures were found

PLATE 5.3

X RAY PHOTOGRAPHS OF A DEFORMED
INCLUSION FROM MELT VA12

ROLLED AT 1000°C.

$$m = 1.14$$

X1000

SHOWS THE PRESENCE OF A $\text{MnO-Al}_2\text{O}_3\text{-V}_2\text{O}_5$
TYPE PRECIPITATE BELIEVED TO BE OF
EXOGENOUS ORIGIN

5.3a V - X RAY

5.3b Si-X RAY

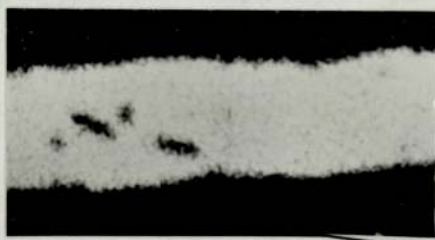
5.3c Mn-X RAY

5.3d Al-XRAY

5.3.



a.



b.



c.



d.

to occur at temperatures well below the estimated equilibrium solidus temperatures. This observation was in agreement with other workers (35,102) and is apparently due to the rapid change in silicate viscosity over a narrow temperature range. Robinson (35) has recently suggested that the transition from rigid to fluid behaviour occurs at a temperature where the viscosity of the inclusion falls to a value equal to one quarter of the shear yield strength of the steel divided by the strain rate at which the deformation occurs.

Ekerot and Klevebring (213) suggested that for glassy silicates containing between 5 and 15% Al_2O_3 the transition temperature was related to the amount of silica present. It was added that as the level of silica increased so the transition temperature would be higher since the viscosity of the silicate would have increased.

Although sparse, the results obtained for glassy silicates in this investigation indicated that this seemed to be the case. (i.e. Table 5.7 and figure 5.54.).

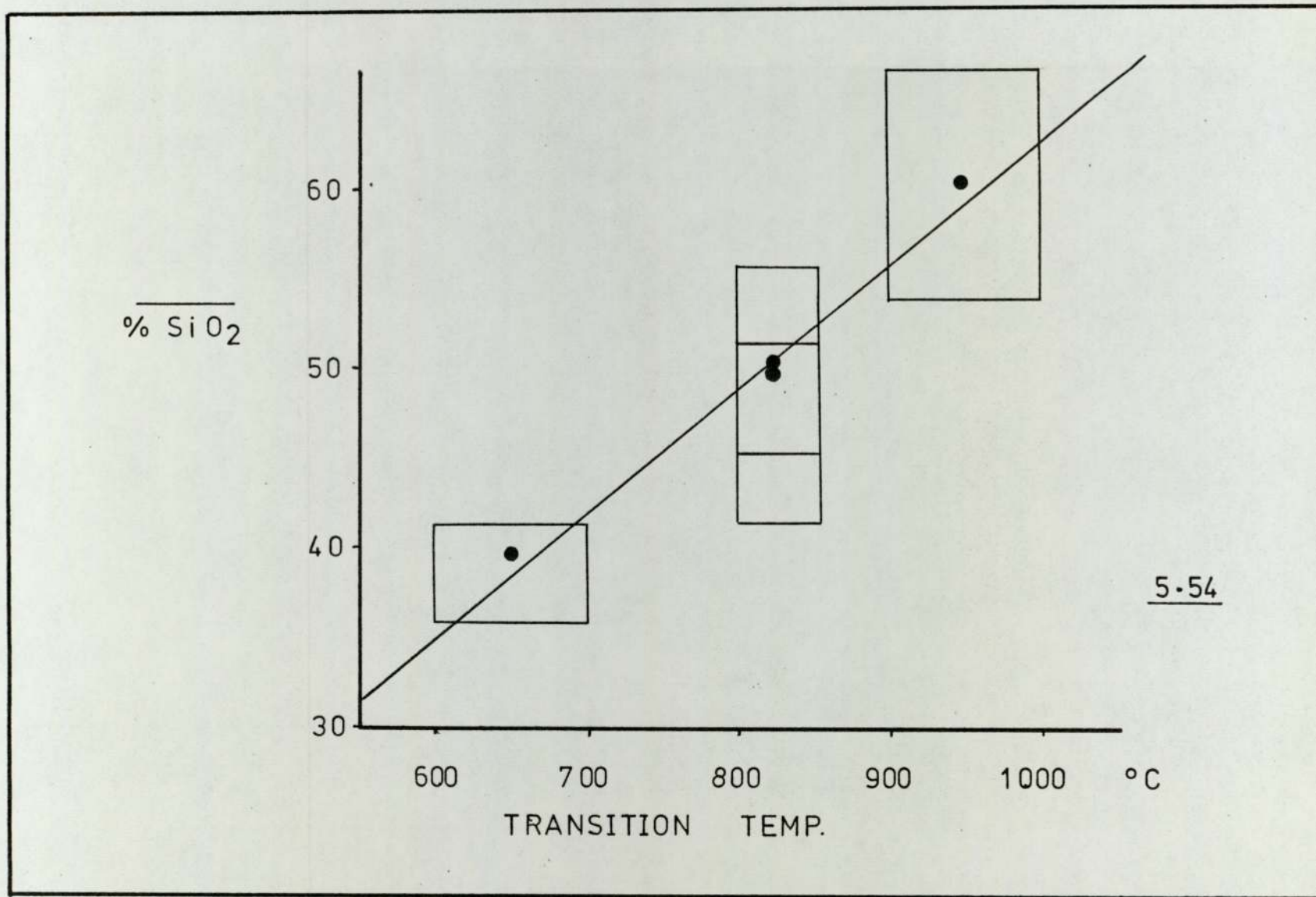


Table 5.7.

Melt	%SiO ₂	Range%	Transition Temp °C
Al4C	39.3	36.4-41.2	600 - 700°
Al6	49.5	45.5-52.3	800 - 850°
CRA12	50.3	41.2-56.5	800 - 850°
NI50A12	60.1	53.2-65.5	900 - 1000°

Precipitation. (5.3.3.1.2.)

Figures 5.45. - .46. indicated that for glassy inclusions which contained a dispersed second phase i.e. cristobalite, as in melts A6(2) and Al3X the transition from non-deformable to maximum deformable behaviour was less marked. The reason why this occurred was not obvious, although a reason may be that the presence of precipitates prevents good viscous flow within the deformable inclusions.

A similar situation may have existed for melts Al2 and Al3 (figure 5.44.) where the presence of cristobalite, and rhodonite laths presented obstacles to fluid flow.

5.3.3.2. Inclusion deformation above the transition temperature.

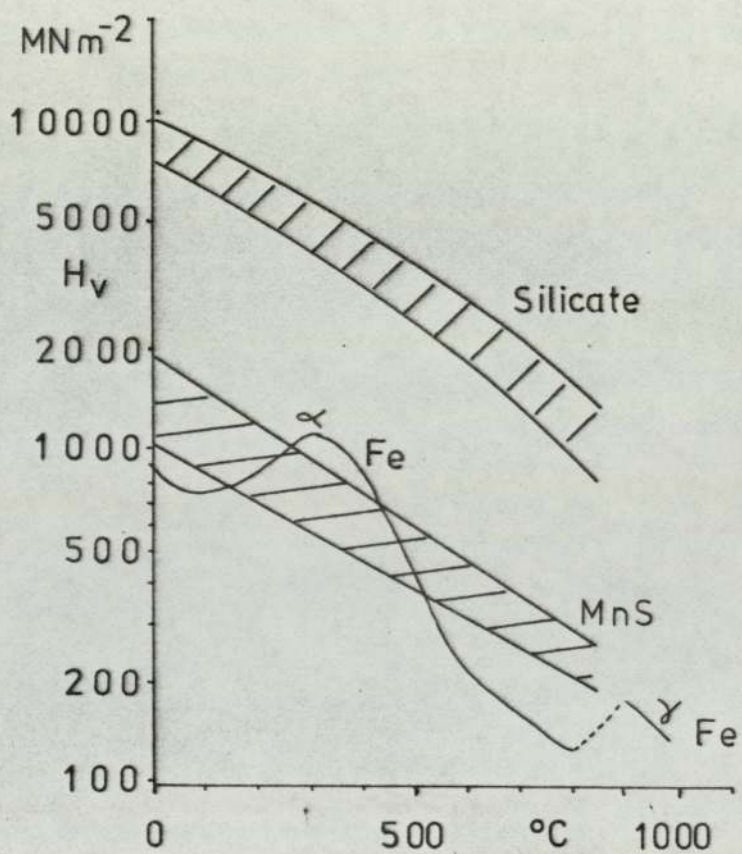
At temperatures in excess of the transition temperature, those inclusions which showed a sharp transition also indicated that there was a fall in plasticity

index as the rolling temperature was increased. e.g. melts Al4, Al6, CRA12 and VA12 and it was often observed that a peak in the relative plasticity indices occurred at the 900 - 1000°C rolling temperatures. Other workers (102) have previously reported such occurrences although no explanation was proposed. Robinson (35) has suggested that this fall in plasticity index was due to inclusion viscosity changes relative to the steel matrix. He suggested that above the transformation temperature an increase in temperature did little to effectively lower the inclusion glass viscosity. However, the yield strength of the steel matrix would reduce rapidly and the net result would be an increase in the relative strength of the inclusion and matrix. Therefore, this should lead to a decreased value of plasticity index, as detailed in section 2.2.

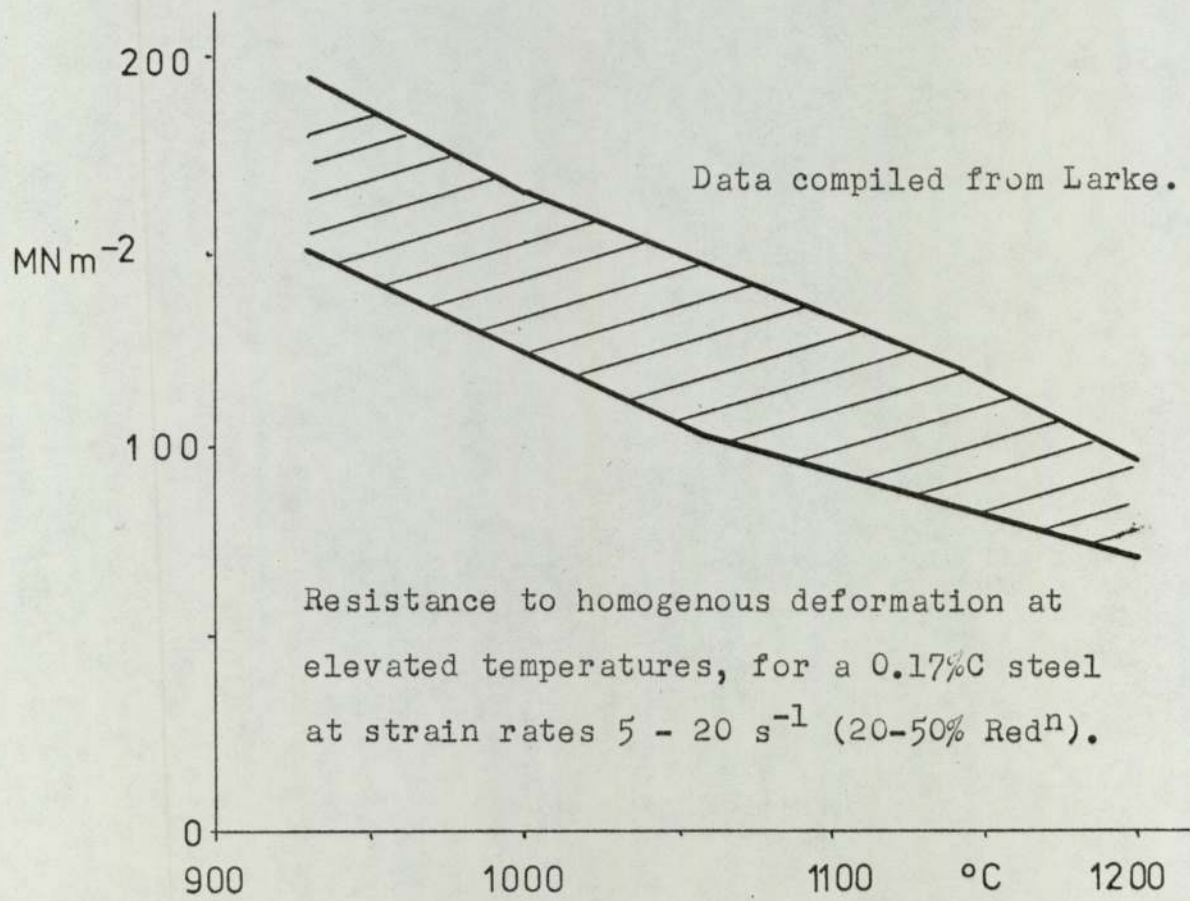
This argument does not appear to be realistic in the light of data relating to the hardness/or strength values for the matrix and silicate inclusions. Presented in figure 5.55, from reference (109) A simple calculation on the basis of such data indicated that the values of relative flow stress i.e. (σ_i/σ_m) above the transition temperature are so low as to have little effect upon the maximum value of plasticity index (ν). Appendix 5.1

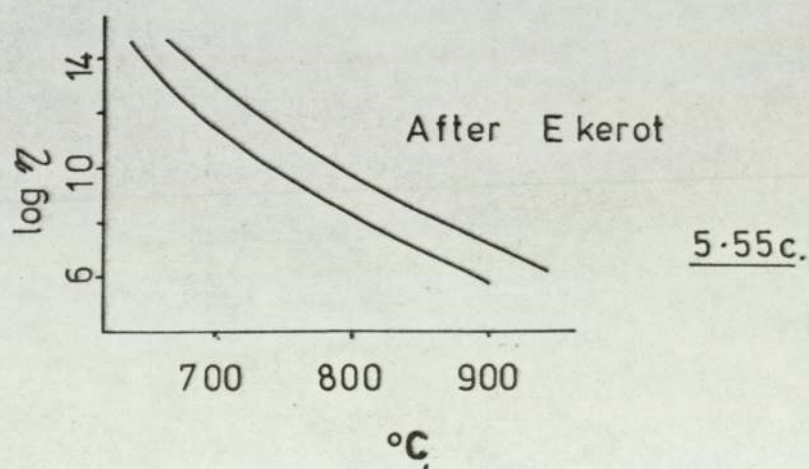
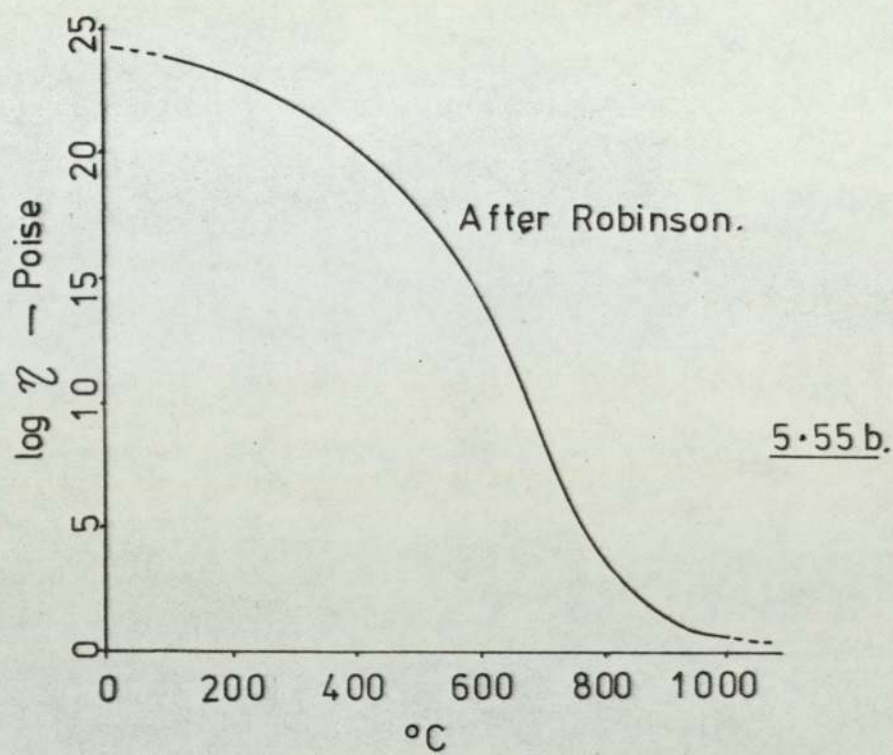
It was initially thought that the peak in plasticity index observed in the region of 900°C was due to the phase change from α ferrite to γ austenite. At the α/γ transformation temperature in the region of 900°C the austenite phase is approximately twice as hard as the

5.55



5.55 (a)





ferrite (figure 5.55.). This would give a sharp decrease in the value of plasticity index. This behaviour has been observed for MnS (109) where the change in the MnS flow stress is less drastic. However, due to the rapid change in flow stress for the silicate glasses such an effect is questionable.

Other possible explanations for this fall in plasticity index after the initial peak may be:

- (i) - The onset of internal fluid flow, whereby a proportion of the energy available for deformation is used up
- (ii) - At these higher temperatures, where the inclusions deformed in a fully fluid manner, these inclusions may break up and disperse (plate 4.35.). If this was the case, smaller inclusions of lower aspect ratio should be produced which would give a lower value of plasticity index. (Discussed further in Section 5.3.5.1.4)
- (iii)- At the higher rolling temperatures, where there is inter-pass reheating, there may be spheroidisation of the inclusions. Again this would produce a lower level of measured plasticity index. (Discussed in section 5.3.5). It would also seem reasonable that the effect of spheroidisation of inclusions would be more pronounced at low matrix strains where the inclusion deformation would be least.

5.3.4. The variation in inclusion
plasticity index with composition.

It was stated earlier in section 5.1.2 and shown in figure 5.7. to 5.15. , that there were compositional variations present for inclusions in any given melt. Hence, in any given section of material taken for strain measurement, it was probable that inclusions of different compositions were present. It was also evident that sections taken from the various positions in the as cast bar contained inclusions of slightly differing compositions (Figure 5.4.). The possibility existed that the measurement of inclusion non-deformable/deformable transformation temperatures by virtue of their compositional differences.

In order to overcome some of these difficulties the compositions of actual deformed inclusions were determined by microprobe analysis. (Appendix 4.2). The compositions and plasticity indices measured on the microprobe analyser (for inclusions greater than 10 μm) were plotted on plasticity - composition diagrams at various rolling temperatures (figures 5.56. to 5.62.). These diagrams indicated which inclusion compositions were deformable at any given temperature.

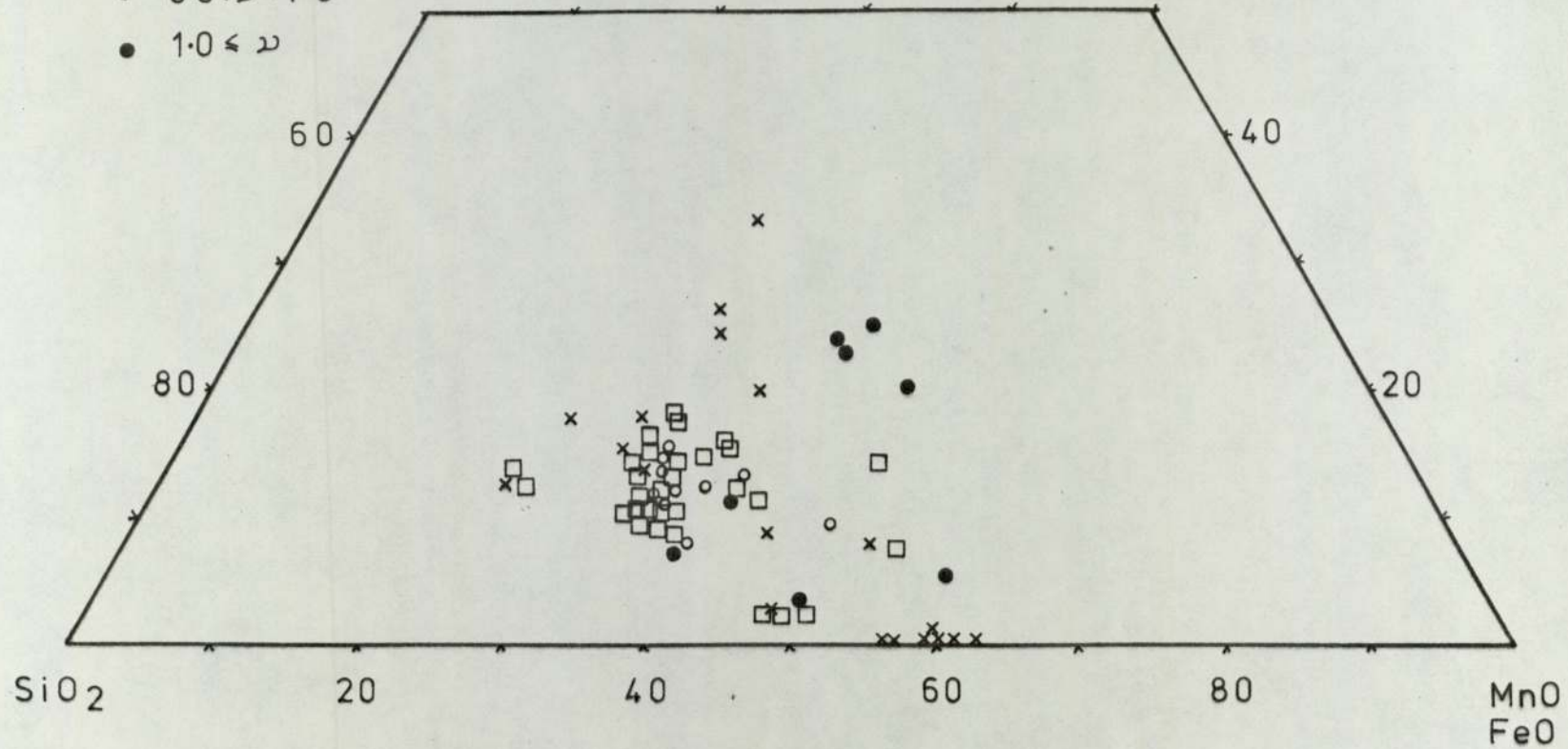
These diagrams are also indicative of precipitation affecting inclusion plasticity, which occurred during the time prior to rolling and reheating. In these diagrams all soaking (30minutes) and reheating times (\sim 10minutes) were constant up to the total matrix strain at which

5. 56.

Rolling
temperature.
800°C

- x $\nu < 0.1$
- $0.1 \leq \nu < 0.5$
- $0.5 \leq \nu < 1.0$
- $1.0 \leq \nu$

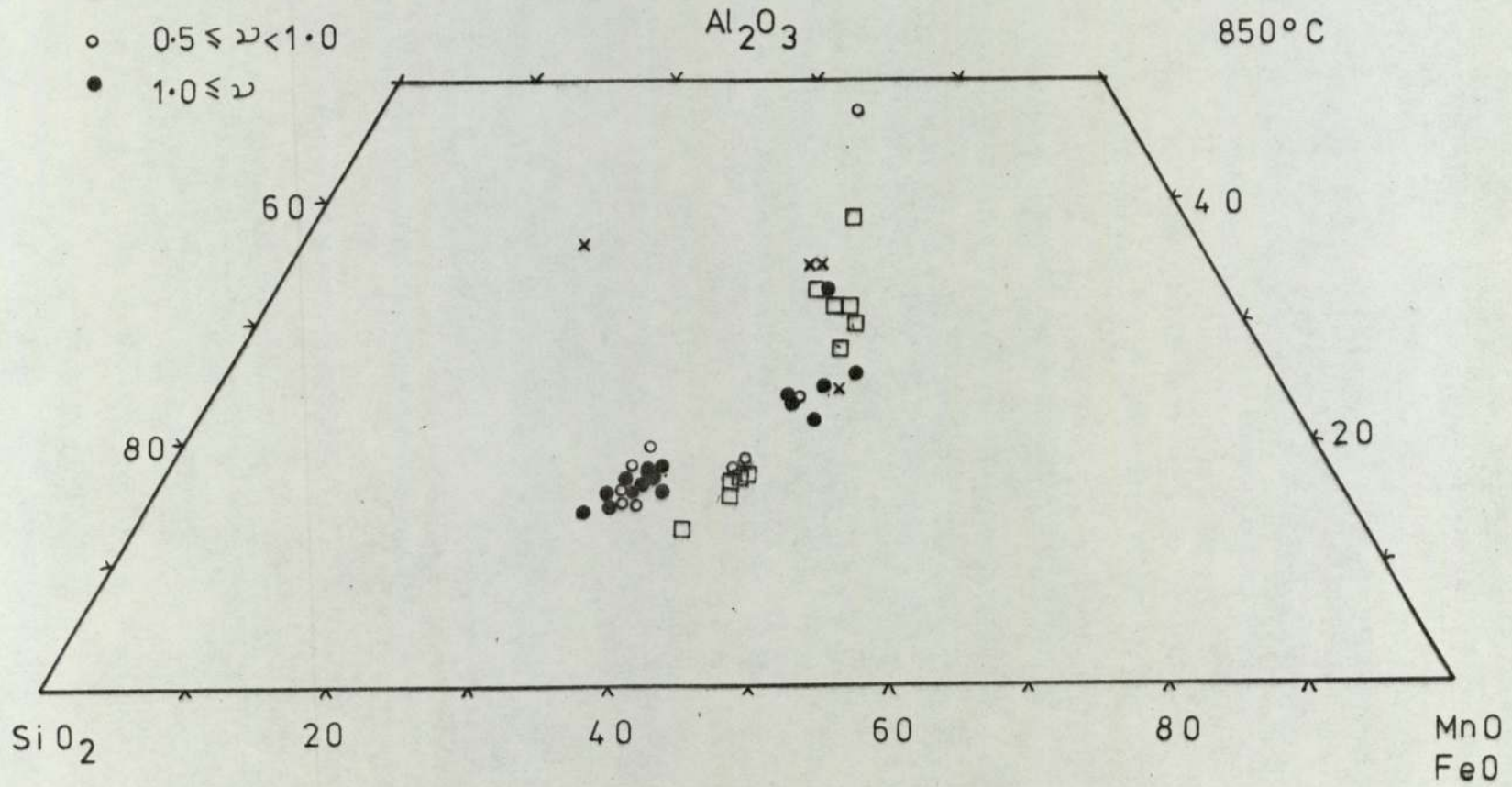
Al₂O₃



5.57.

Rolling
temperature
850°C

- x $\nu \leq 0.1$
- $0.1 \leq \nu < 0.5$
- $0.5 \leq \nu < 1.0$
- $1.0 \leq \nu$

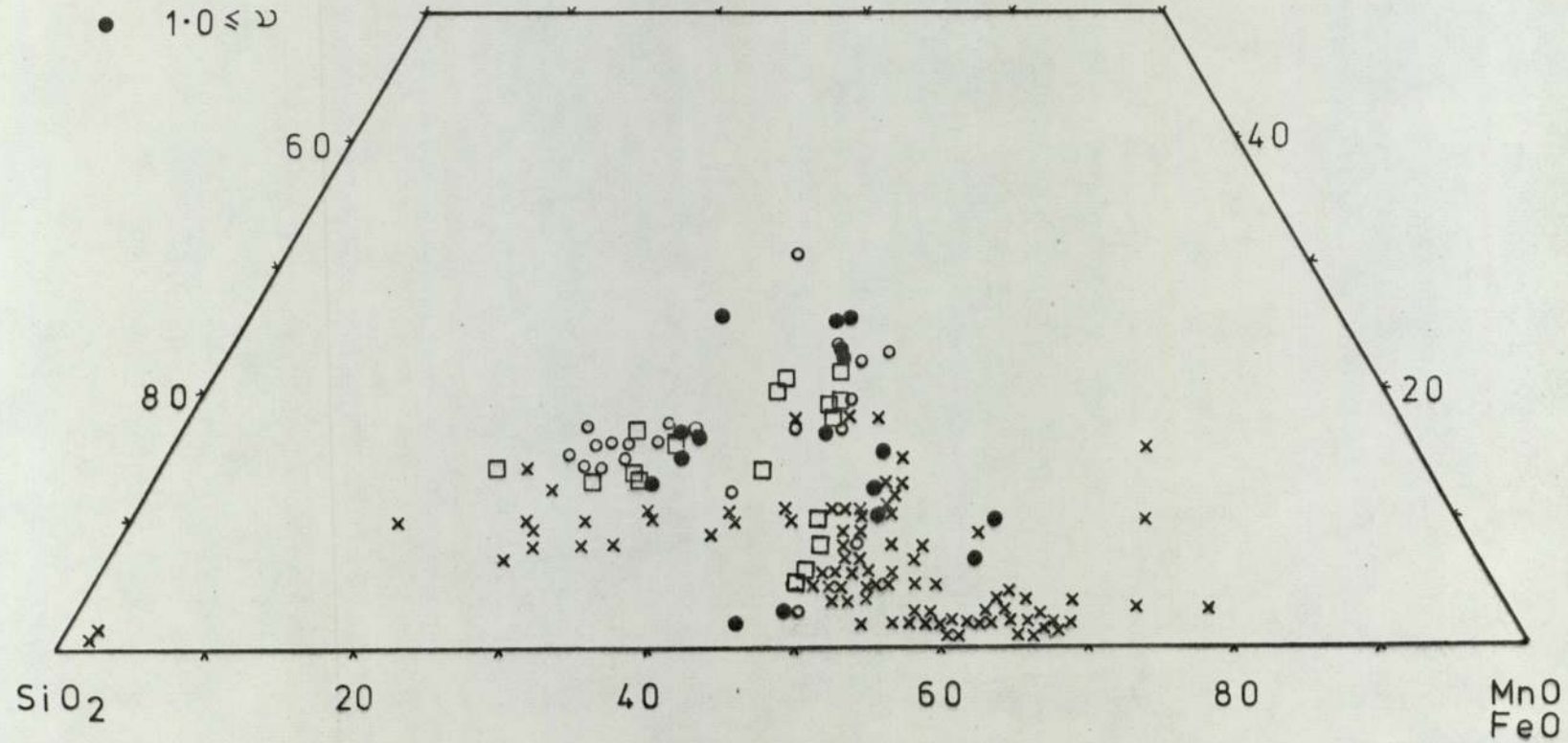


5.58.

Rolling
temperature.
900°C

- x $\nu < 0.1$
- $0.1 \leq \nu < 0.5$
- $0.5 \leq \nu < 1.0$
- $1.0 \leq \nu$

Al₂O₃

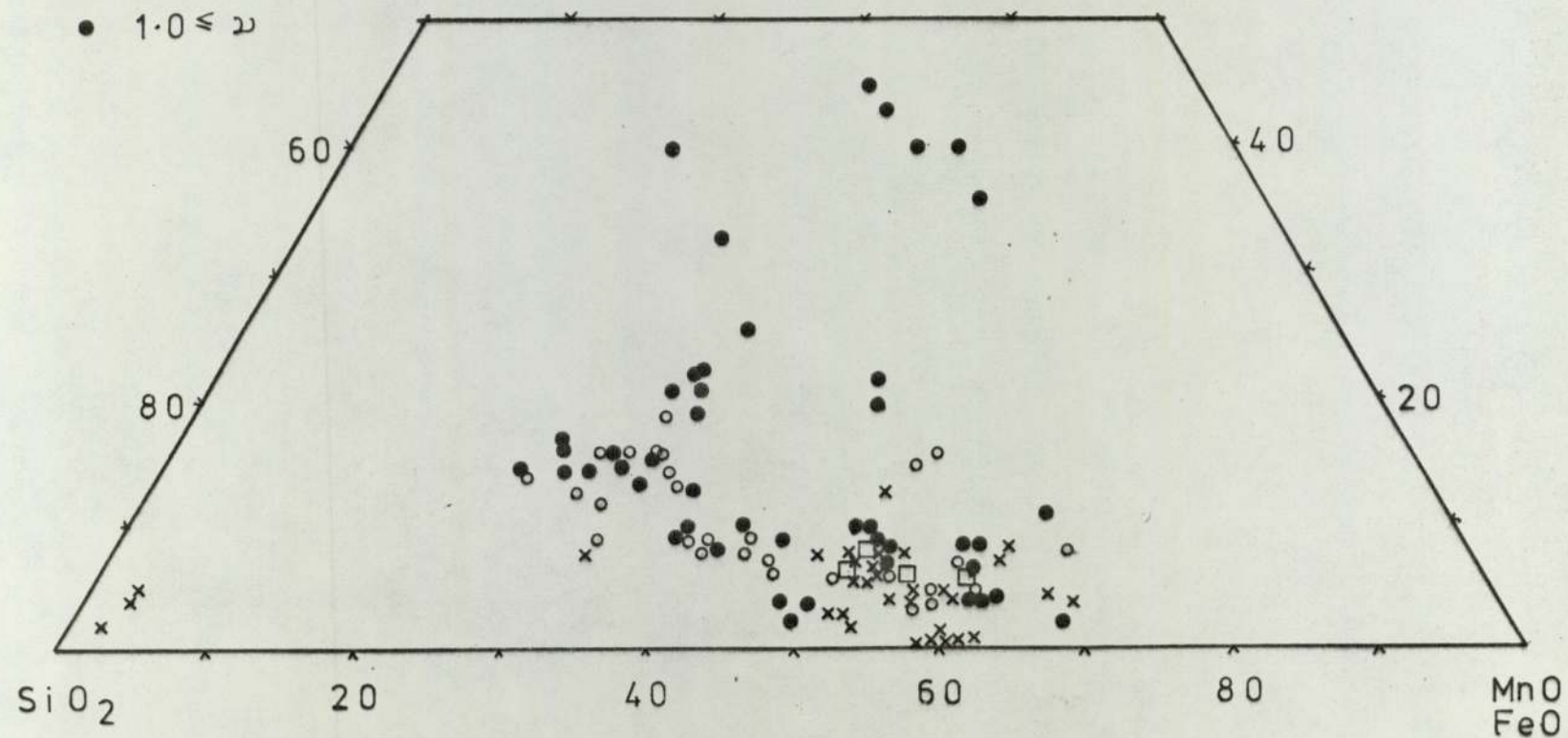


5.59.

Rolling
temperature
1000°C

- x $\nu < 0.1$
- $0.1 \leq \nu < 0.5$
- $0.5 \leq \nu < 1.0$
- $1.0 \leq \nu$

Al₂O₃

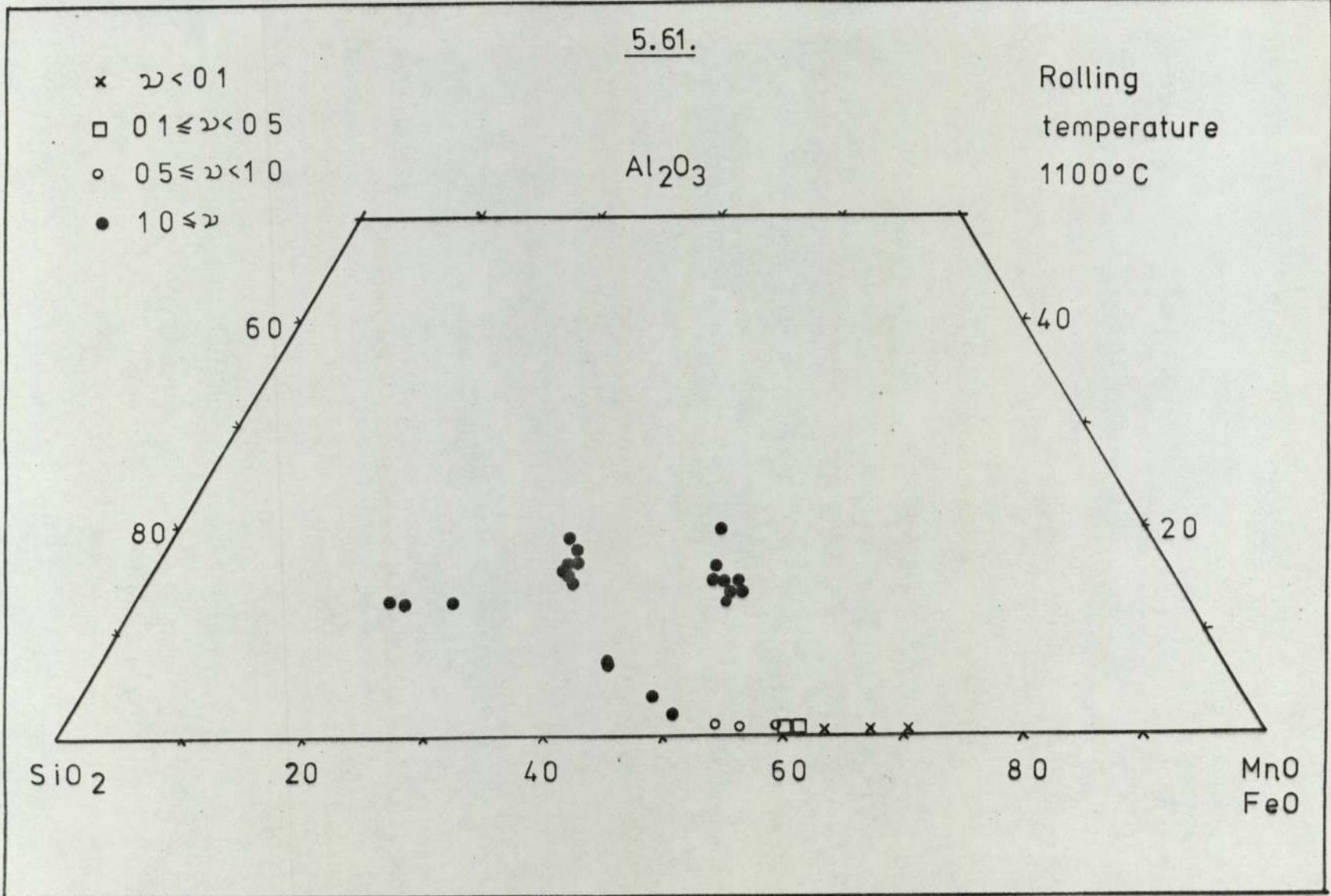


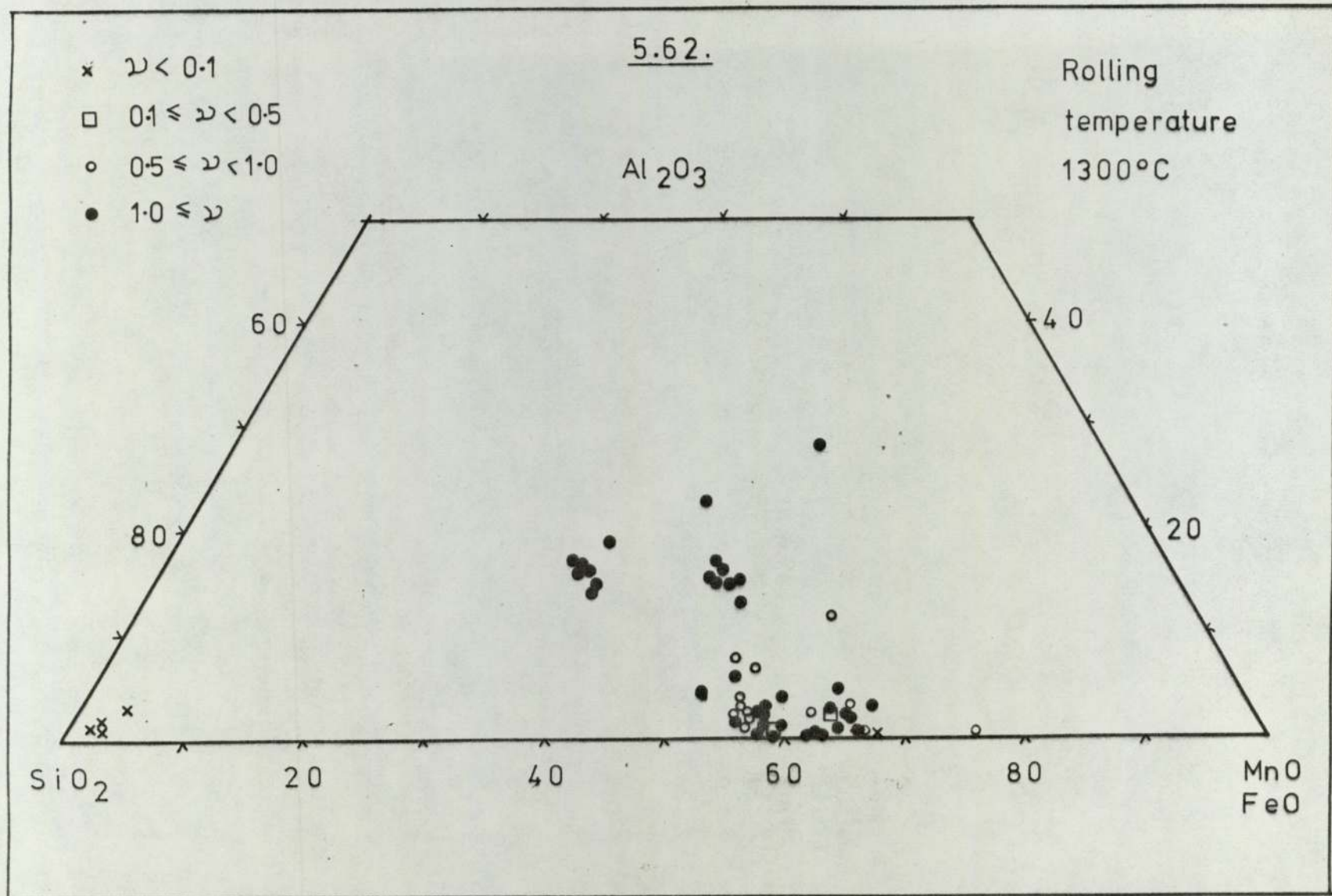
5.61.

Rolling
temperature
1100°C

- x $\nu < 0.1$
- $0.1 \leq \nu < 0.5$
- $0.5 \leq \nu < 1.0$
- $1.0 \leq \nu$

Al₂O₃





these diagrams were produced i.e. $\epsilon_m = 1.2$ (70% total reduction in height).

Rolling temperature 800°C (Fig. 5.56)

Figure 5.56. indicated that there was some deformation although variable, due to precipitation effects, in and around the region of 50% SiO_2 - 15% Al_2O_3 . At Al_2O_3 contents greater than 20% little deformation was evident except for some inclusions of lower silica content. These inclusions were those containing Al_2O_3 in glassy silicate matrix. Inclusions at approximately 40% SiO_2 on the binary (SiO_2 - FeOMnO) edge exhibited no deformation.

Rolling Temperature 850°C (Fig 5.57)

Inclusions of high deformability were shown in the region of 50% SiO_2 - 20% Al_2O_3 . Again the inclusions richer in Al_2O_3 and less rich in SiO_2 were observed to be deformable.

Rolling Temperature 900°C (Fig 5.58.)

This figure indicated that above approximately 15% Al_2O_3 the inclusions in the range 30 - 60% SiO_2 were deformable. Those inclusions which contained less than 15% Al_2O_3 in the range of compositions investigated showed only isolated inclusions which had deformed. It was the general case that these other inclusions had

precipitated second phases which prevented their deformation.

Rolling temperature 1000°C (Fig 5.59.)

Again it may be seen in this figure that inclusions with compositions within the 40% SiO₂ - 5% Al₂O₃ region are not deformable, whereas elsewhere in the low liquidus region of the diagram inclusion deformation is extensive. The inclusions of high alumina content are also seen to be highly deformable, although as pointed out earlier these inclusions had siliceous matrices within the low melting point region of the MnOFeO - SiO₂ - Al₂O₃ diagram. (Fig. 5.60.)

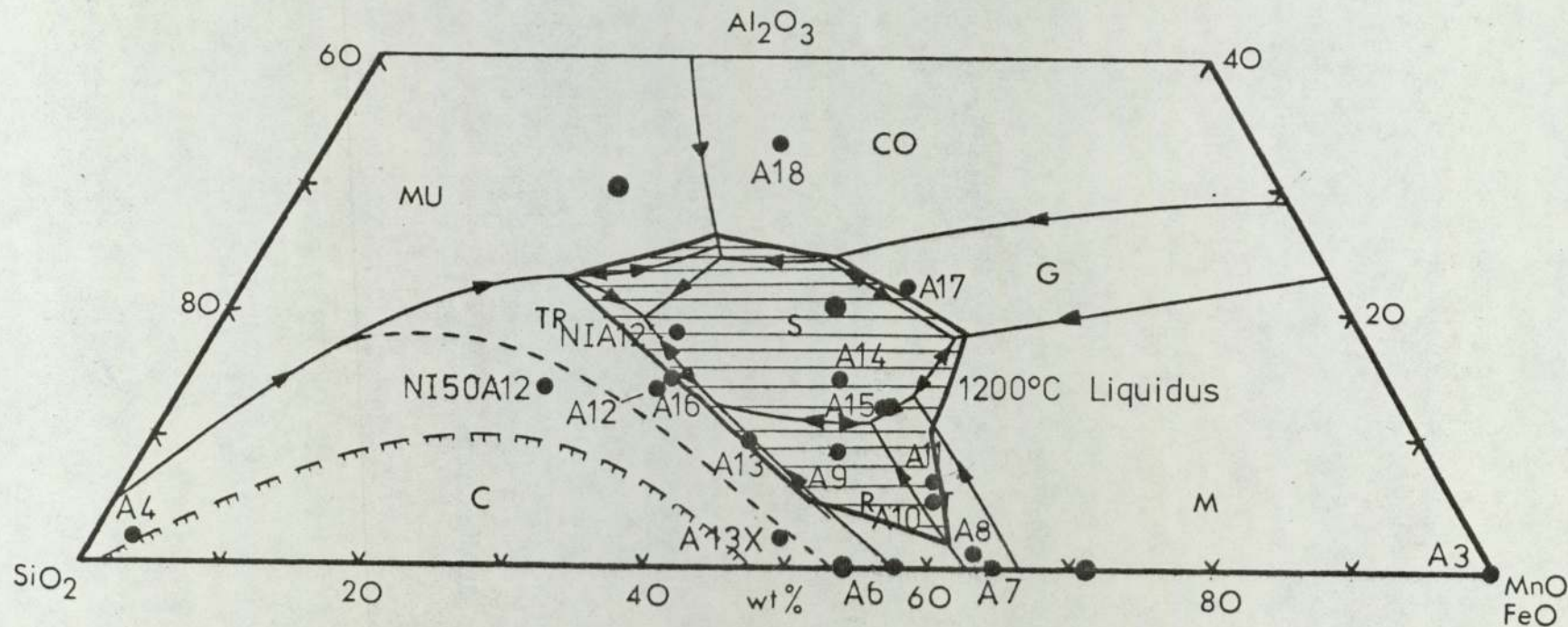
Rolling temperatures 1100° and 1300°C (Figures 5.61. & .5.62.)

From these figures it was fairly evident that almost all the inclusions within the range of compositions indicated, were of a highly deformable nature. However, with reference to figure 5.61. those inclusions containing no alumina and with silica contents less than 40% were reluctant to deform at 1100°C although at 1300°C even these inclusions were observed to deform

From the plasticity index - composition diagrams the compositions at which non-deformable/deformable transitions occurred at various temperatures were summarised in figure 5.63. . This schematic

Fig. 5-60

MEAN AS CAST INCLUSION COMPOSITIONS.



Estimated Non Deformable / Deformable
inclusion compositions at various
rolling temperatures.

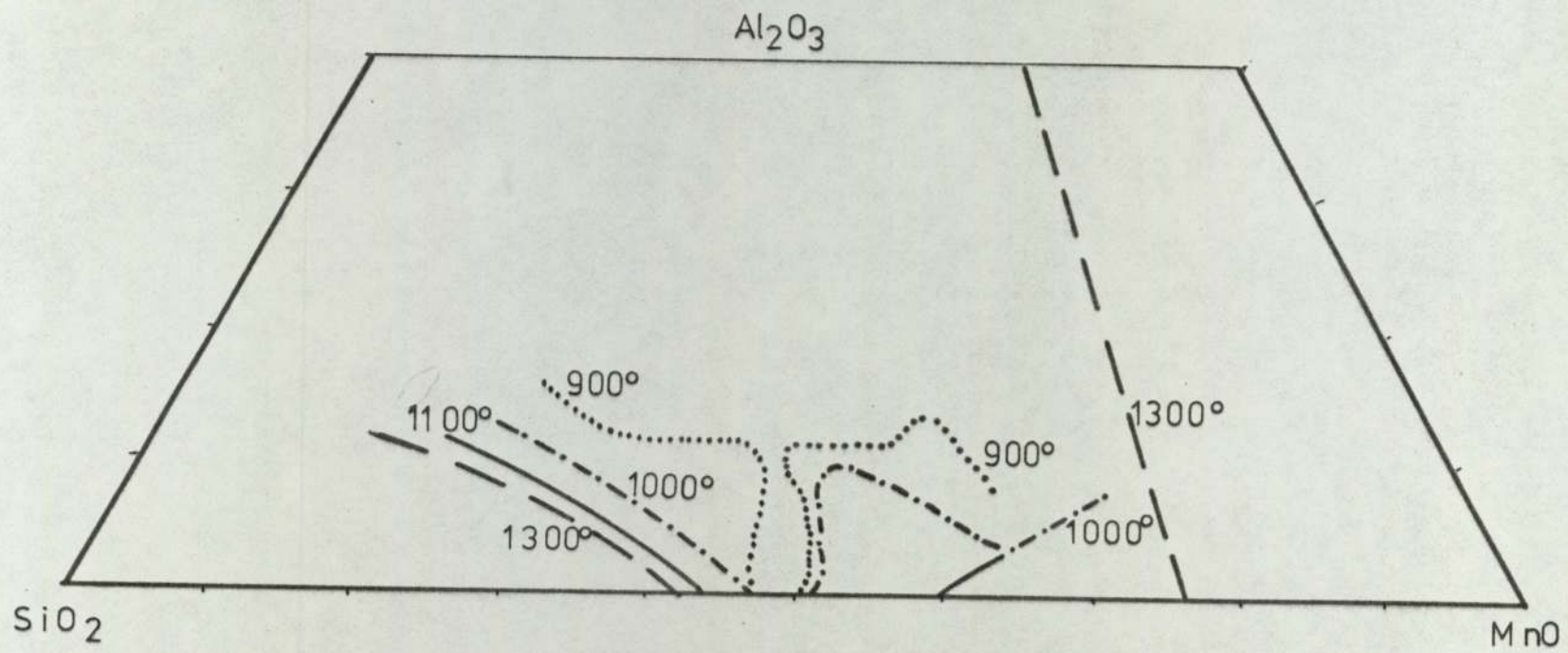


illustration was for temperatures of 900°C and above, where there are enough results to estimate the transition. This figure must only be regarded as a guide, since the results it contains are specific to the soaking and reheating times and temperatures of very low carbon steel/iron relevant to this project.

From this figure it appeared that as the rolling temperature increased the non - deformable/deformable transition temperature moved towards the binary SiO_2 - MnFeO edge of the diagram. This was not to be unexpected since the liquidus and presumably the solidus temperatures increase towards the binary edge. The noticeable feature of this diagram was that the inclusions in the 40% silica - low alumina contents, were reluctant to deform except at the highest rolling temperatures. i.e. those compositions at which precipitation readily occurred.

5.3.5. The variation in inclusion plasticity index with size.

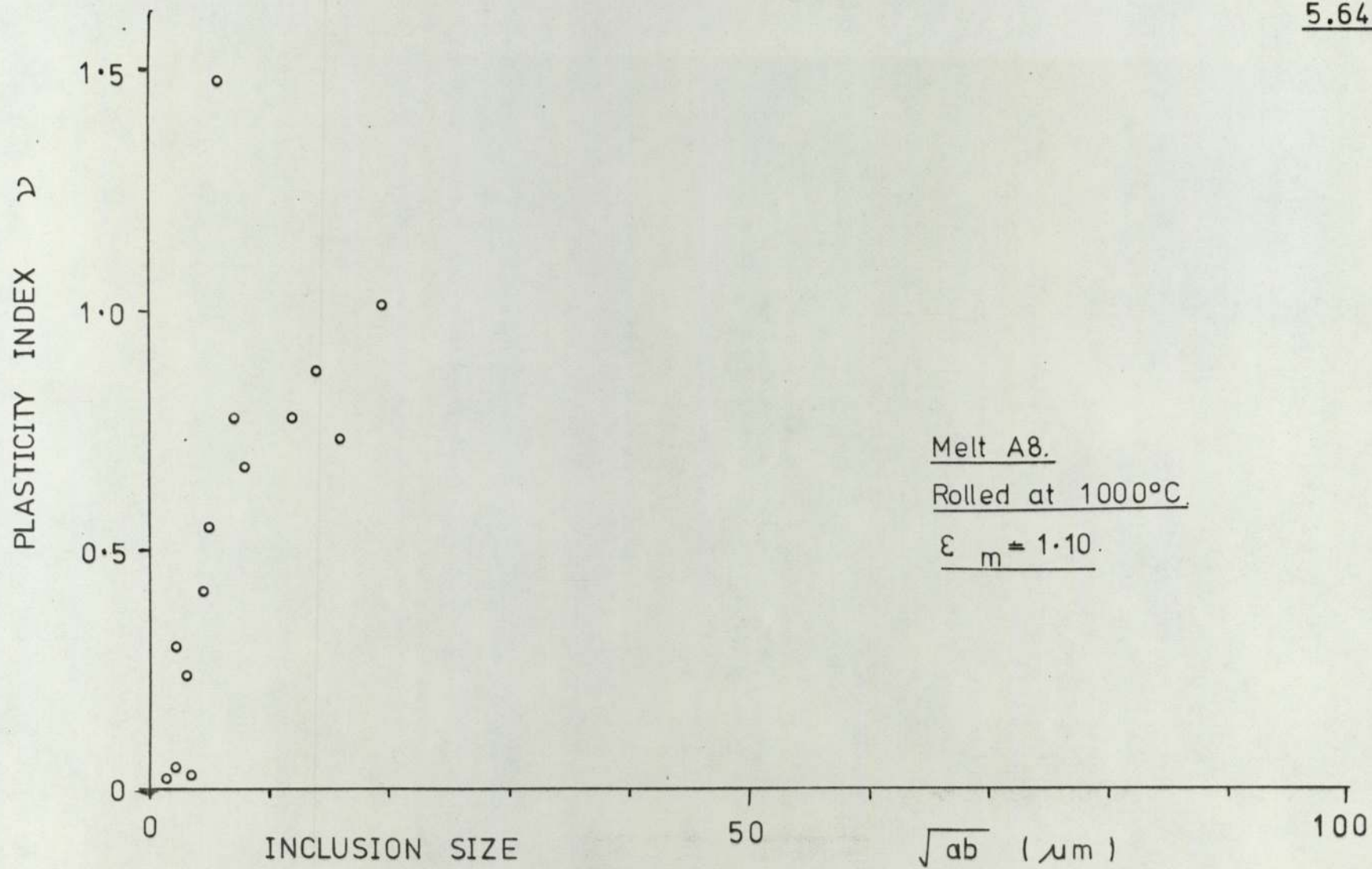
Table 4.9 and figures 5.40. to 5.53. showed that the mean plasticity indices of inclusions ($\bar{\nu}$) were seen to vary with the range of inclusion sizes incorporated in the assessment of these indices. For example it was seen (figure 5.39.) that the mean plasticity index ($\bar{\nu}$) for melt A7 varied with size range i.e. $> 1 \mu\text{m}$, $> 10 \mu\text{m}$ and $> 20 \mu\text{m}$ (\sqrt{ab} values).

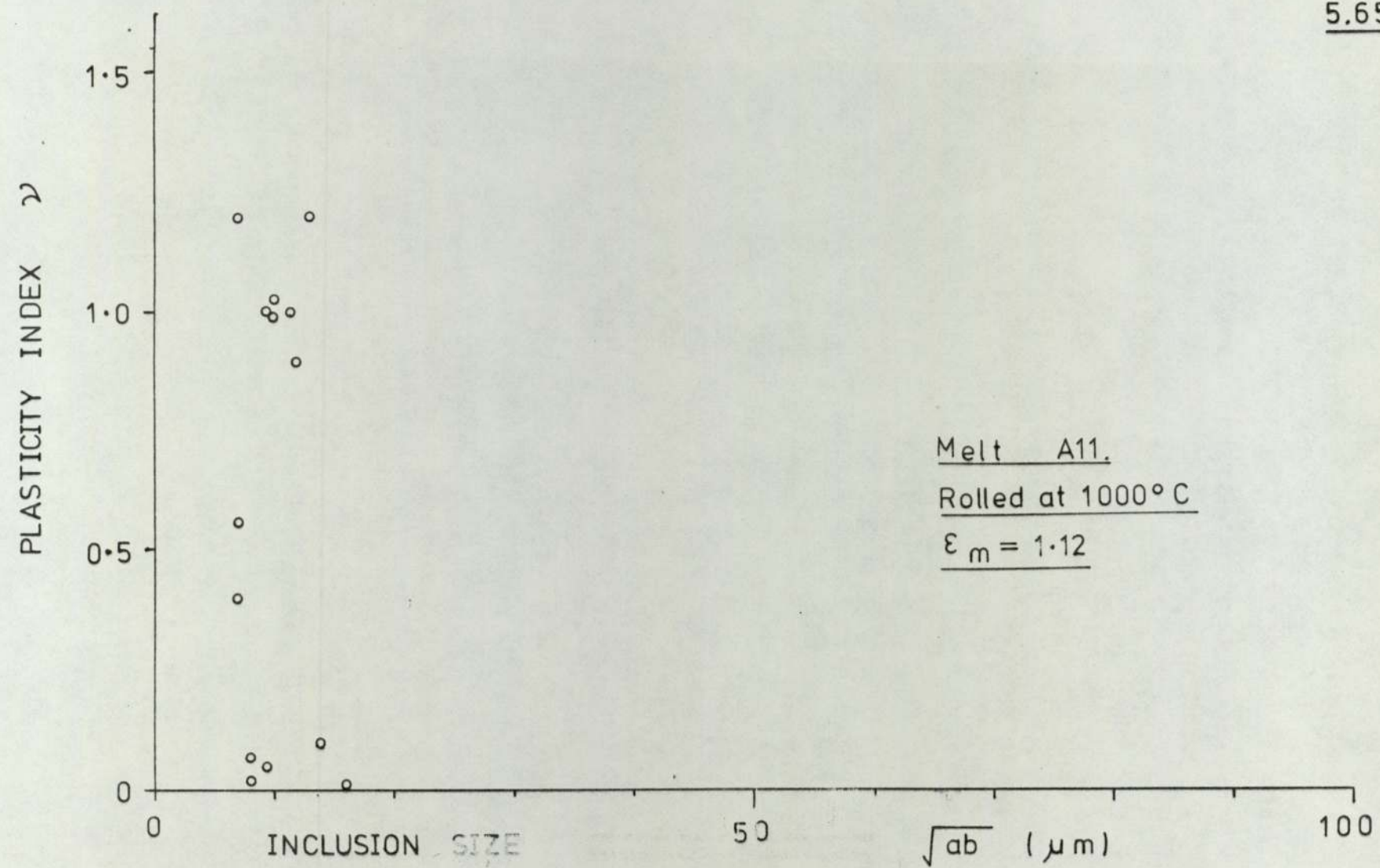
Looking now at the inclusion size (\sqrt{ab}) versus inclusion plasticity index ($\bar{\nu}$) graphs produced from observations of inclusion strains on the (XY) plane, the influence of the inclusion size upon plasticity indices is seen. Again as with section 5.3.3 this variation may be assessed in the various groups which refer to the precipitation characteristics of the inclusions.

Group (1) : inclusions which precipitated rhodonite.

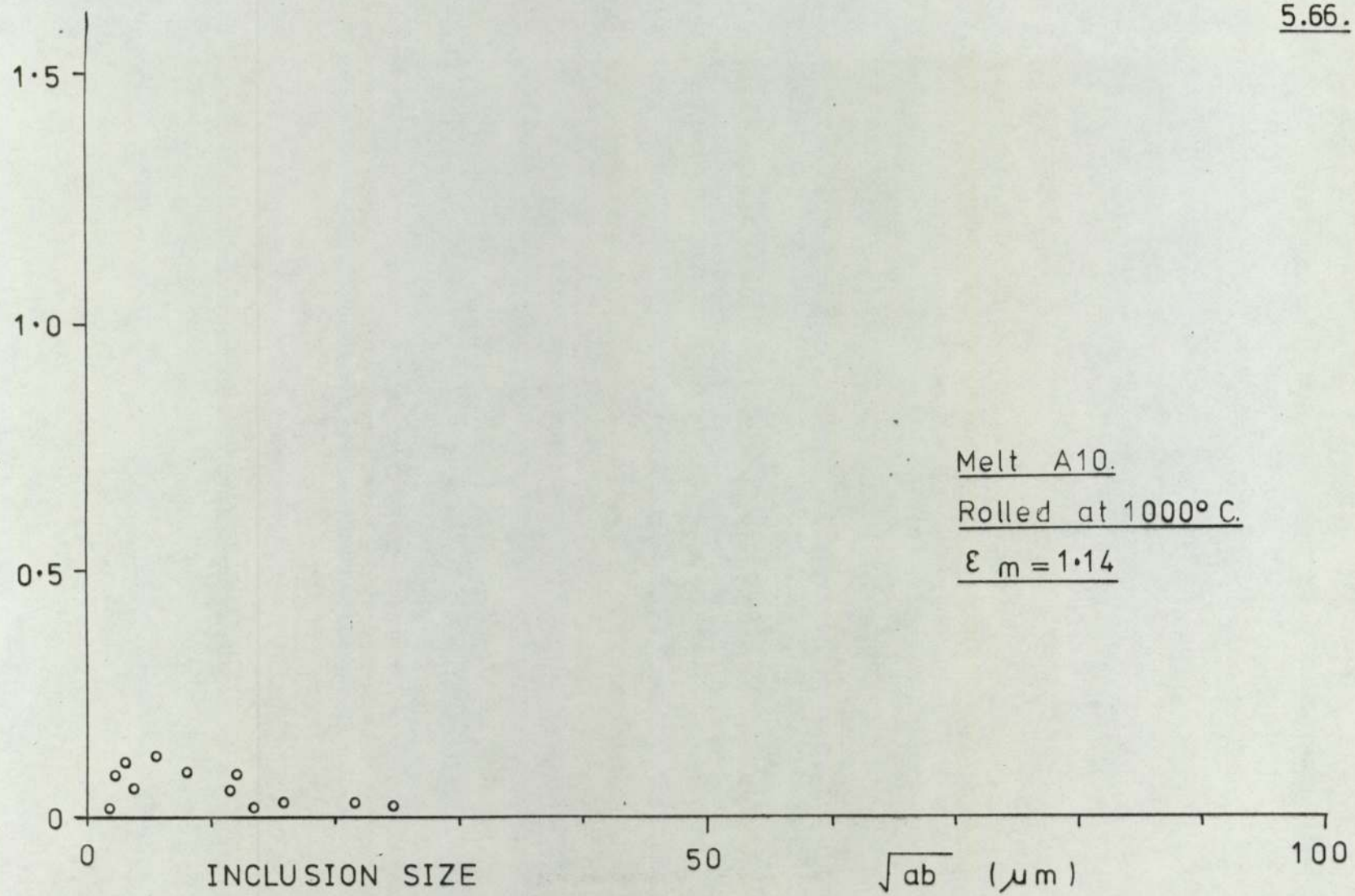
Group (1a) : melts A7, A8, A10 and A11 (Figures 5.64. to 5.70.).

Figures for melts A8, A10 and A11 (i.e. Figures 5.64. to 5.66.) showed that only the smaller ^{glassy} inclusions had deformed. In the cases of A8 and A11, these deformed inclusions were those which had not precipitated a second phase i.e. glassy inclusions. The larger



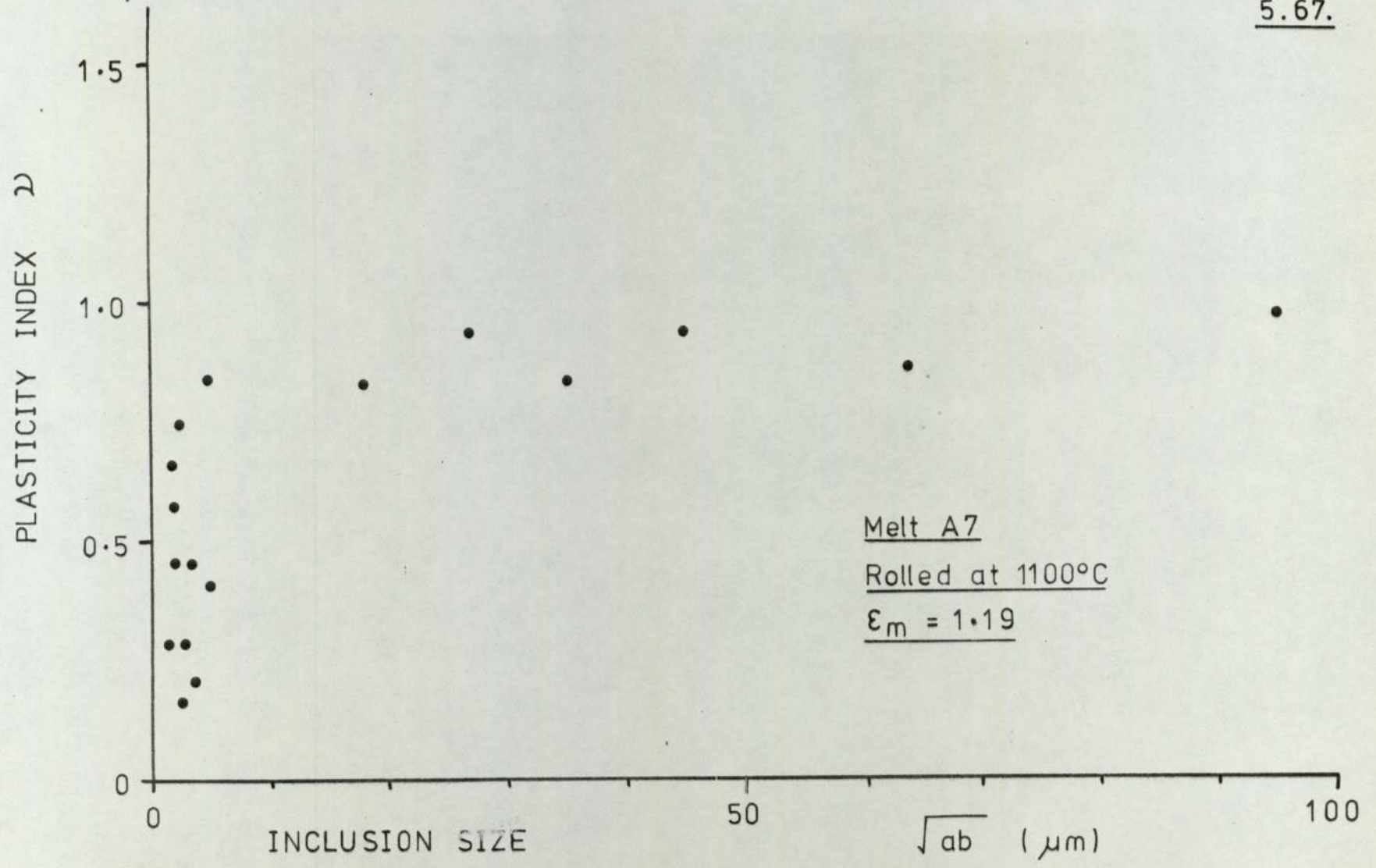


PLASTICITY INDEX ν



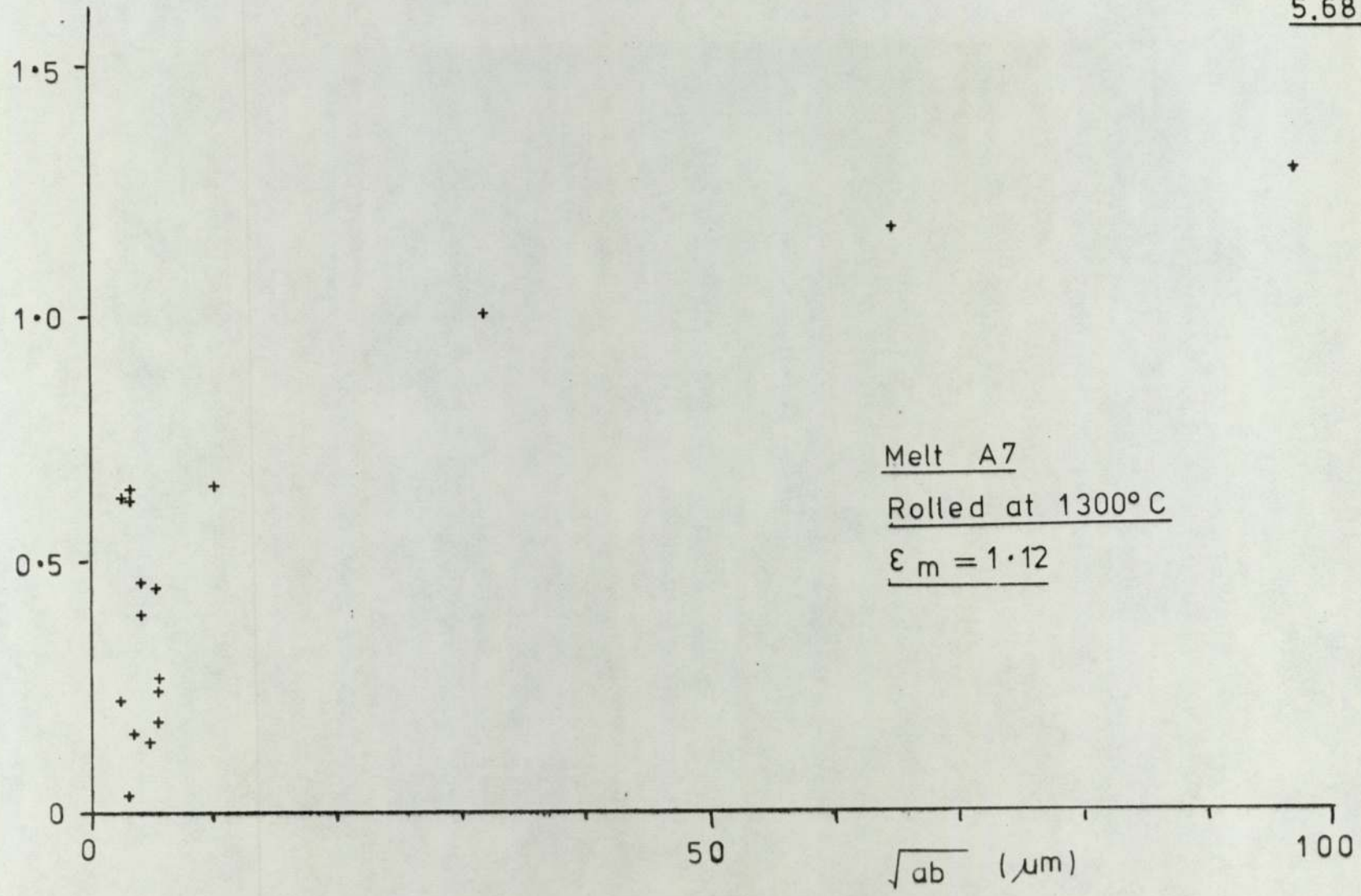
Melt A10.
Rolled at 1000° C.
 $\epsilon_m = 1.14$

5.67.

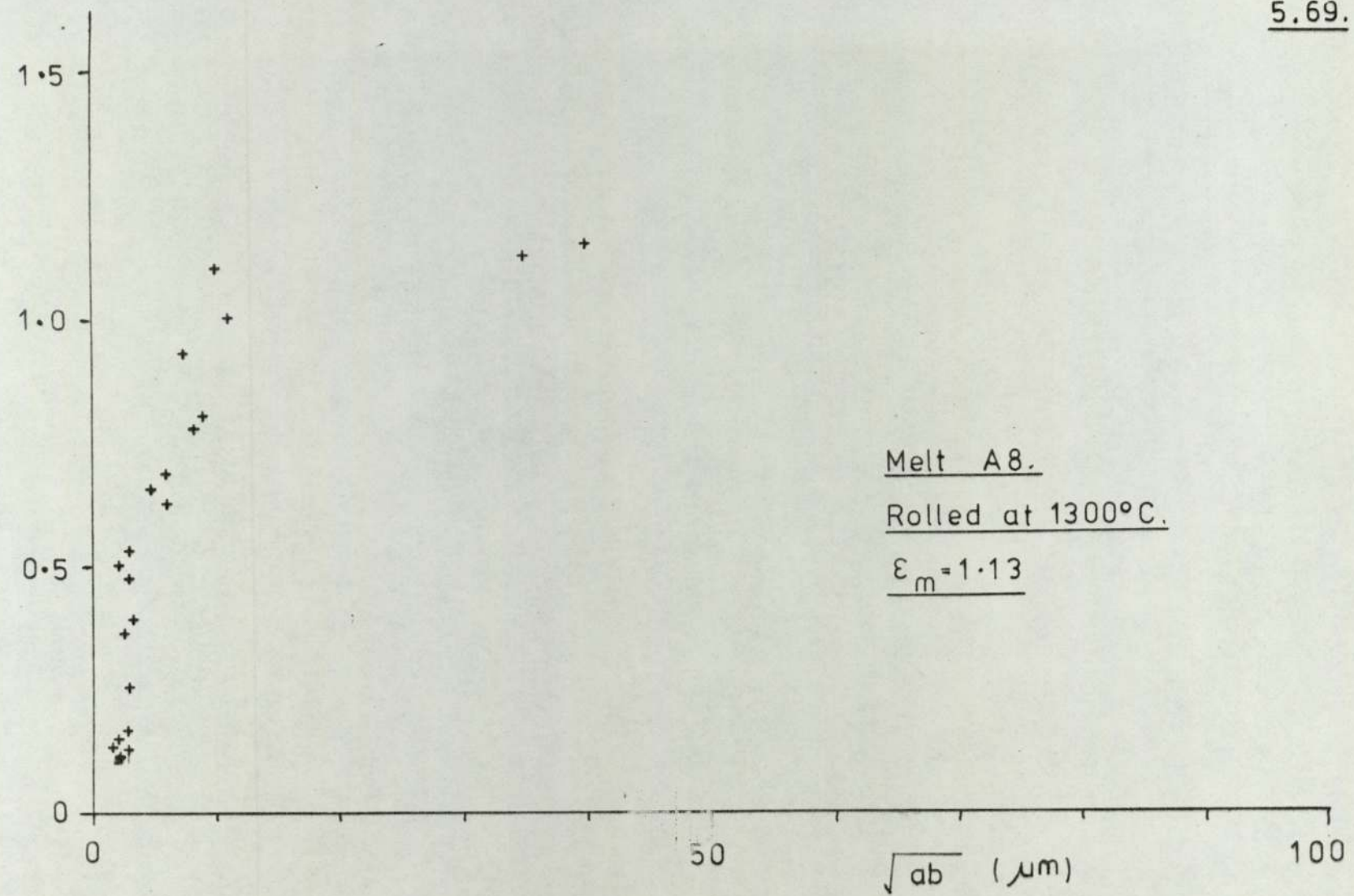


5.68.

PLASTICITY INDEX ρ



PLASTICITY INDEX ρ



PLASTICITY INDEX γ

1.5
1.0
0.5
0

0

50

100

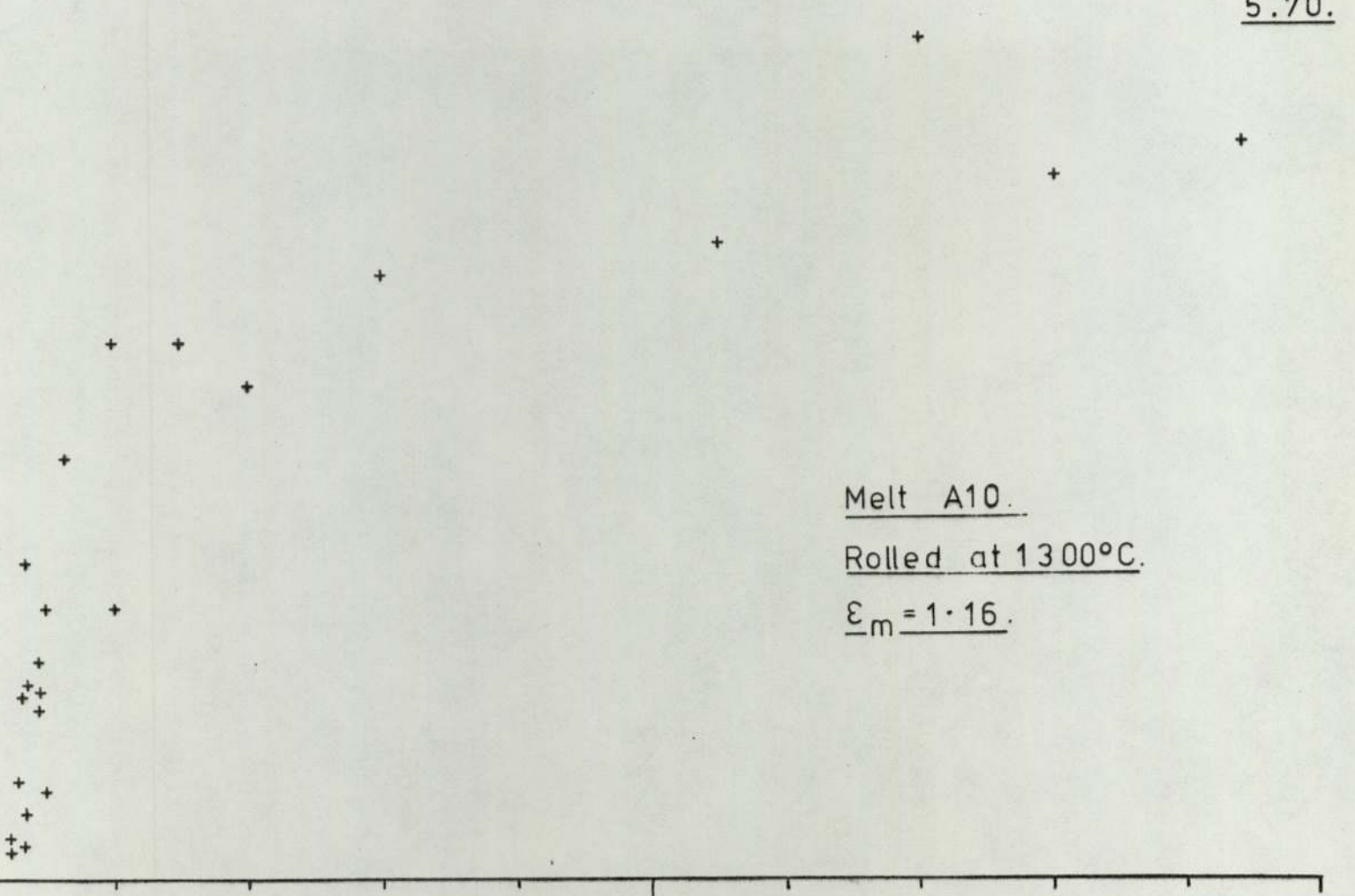
\sqrt{ab} (μm)

5.70.

Melt A10.

Rolled at 1300°C.

$\epsilon_m = 1.16.$



5.71.

PLASTICITY INDEX ρ

1.5

1.0

0.5

0

50

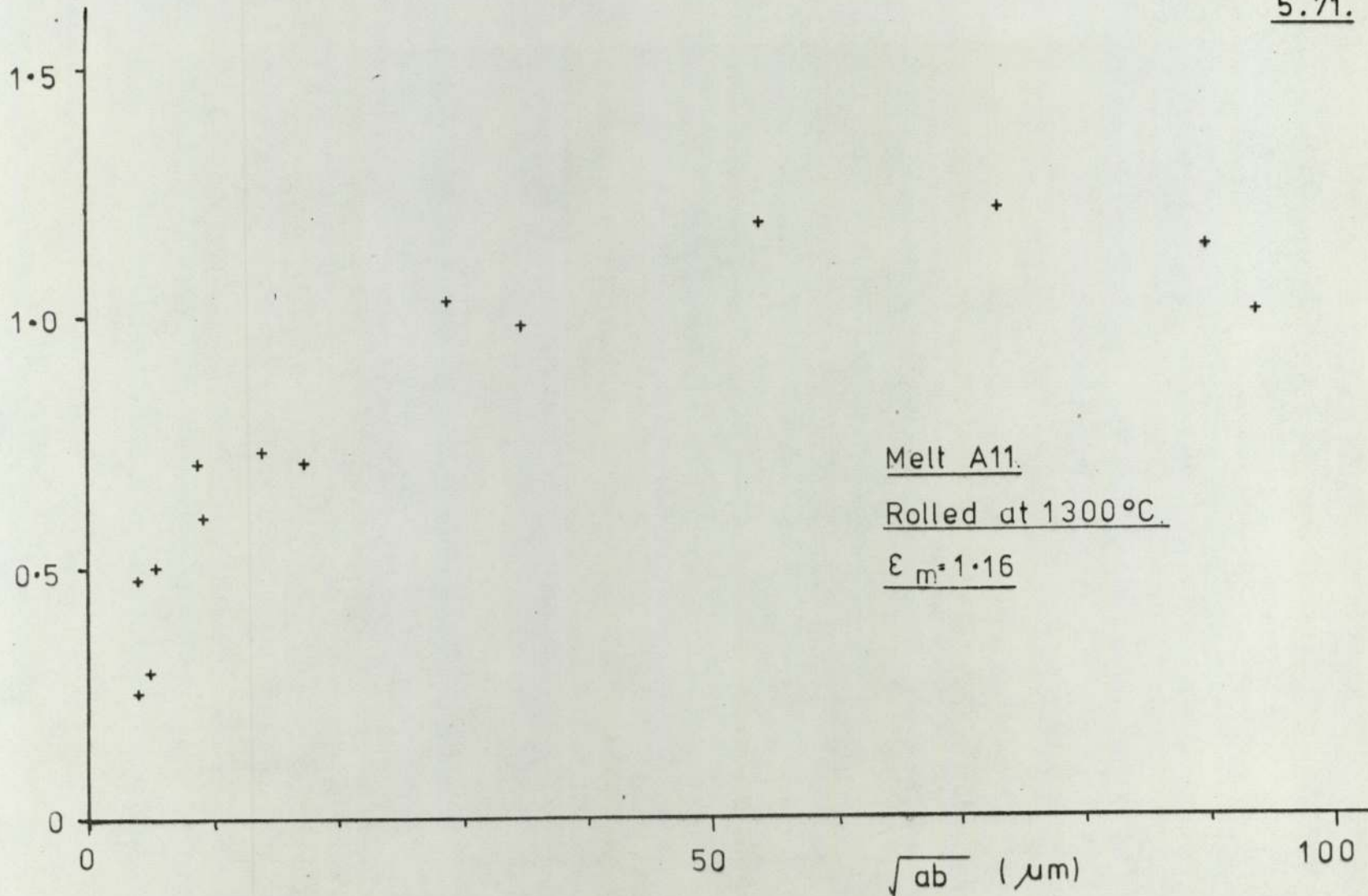
100

Melt A11.

Rolled at 1300°C.

$\epsilon_m = 1.16$

\sqrt{ab} (μm)



inclusions which contained precipitated phases had fractured disseminated or not deformed so precluding measurement. It was observed that below approximately 1 - 2 μm no inclusions had deformed. The glassy inclusions of melt A8 gave indications that the plasticity index (ρ) increased as the inclusion size increased.

Melt A7 rolled at 1100°C (Figure 5 .67.) showed that there was a rapid increase in plasticity index with size upto approximately 10 μm , but above this size the index remained constant. Figures 5 .68. to 5.71. show the size relationship at the highest rolling temperature of 1300°C where all the inclusions had deformed. Above approximately 2 μm the inclusions showed a sudden increase in plasticity index up to 20 μm , above which there was a gradual increase in the index with increase in size.

Group (1b) : melts Al4, Al4C and Al5 (Figures 5 .72. to 5.83.)

Figure 5.72. showed that the glassy inclusions of melt Al4C when rolled at 700°C deformed readily above 5 μm . The smaller inclusions were reluctant to deform, indicated by the number of deformable inclusions. (Table 4. II). At 800°C where the presence of precipitates within the inclusions were observed, it was found that they were reluctant to deform plastically (figure 5 .73.). Only a few of the small glassy

5.72.

PLASTICITY INDEX ρ

1.5
1.0
0.5
0

INCLUSION SIZE

50

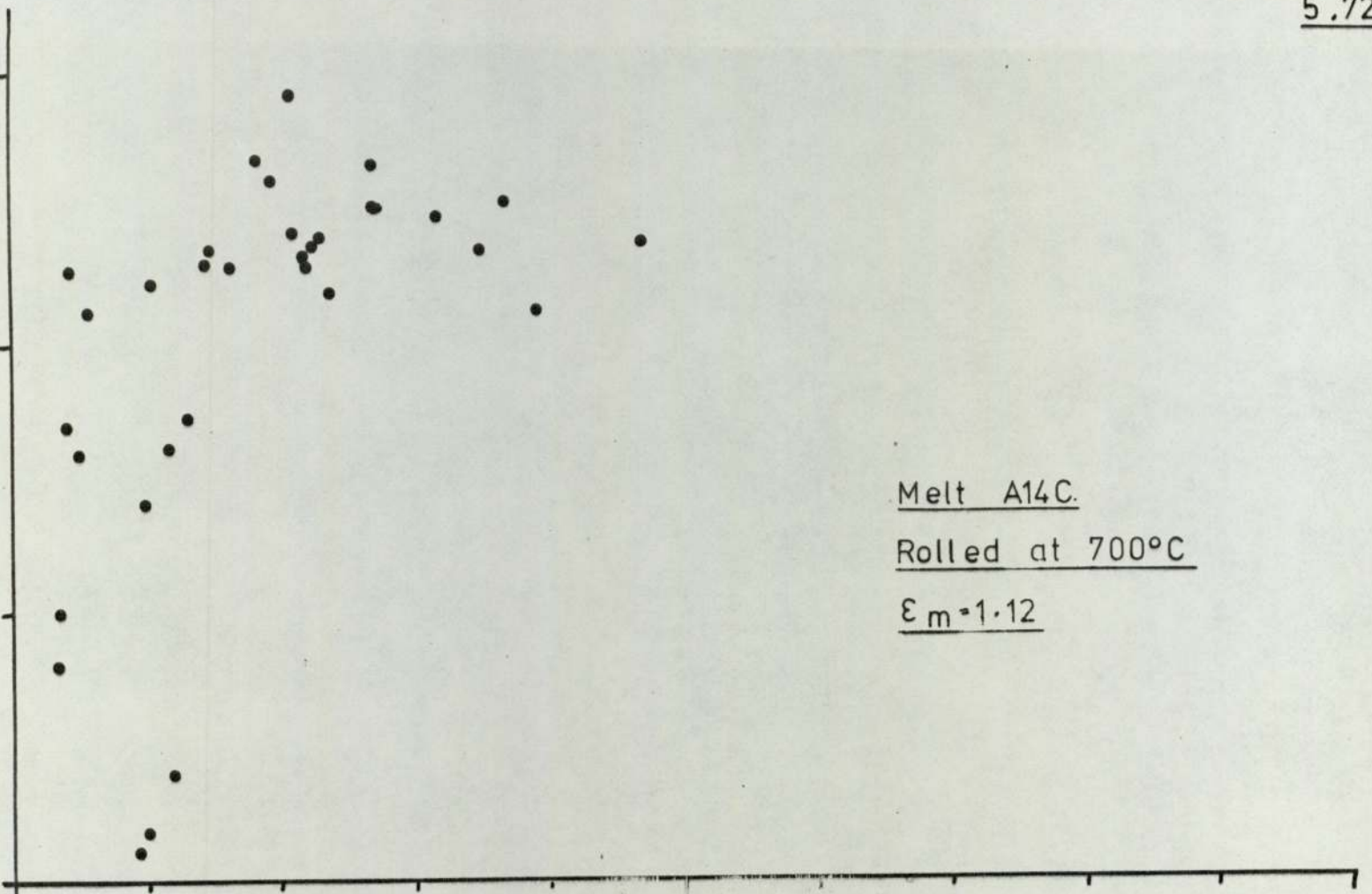
\sqrt{ab} (μm)

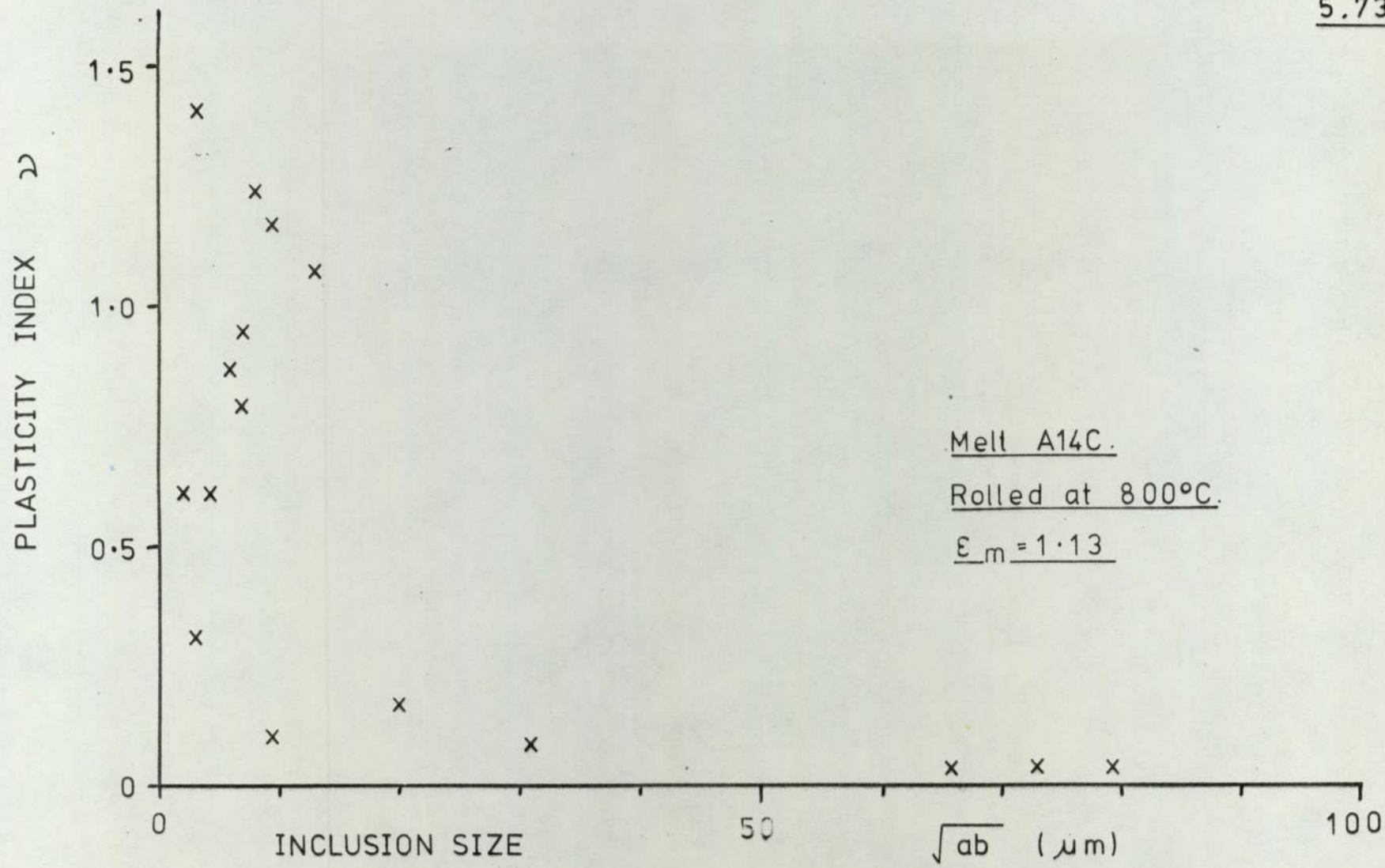
100

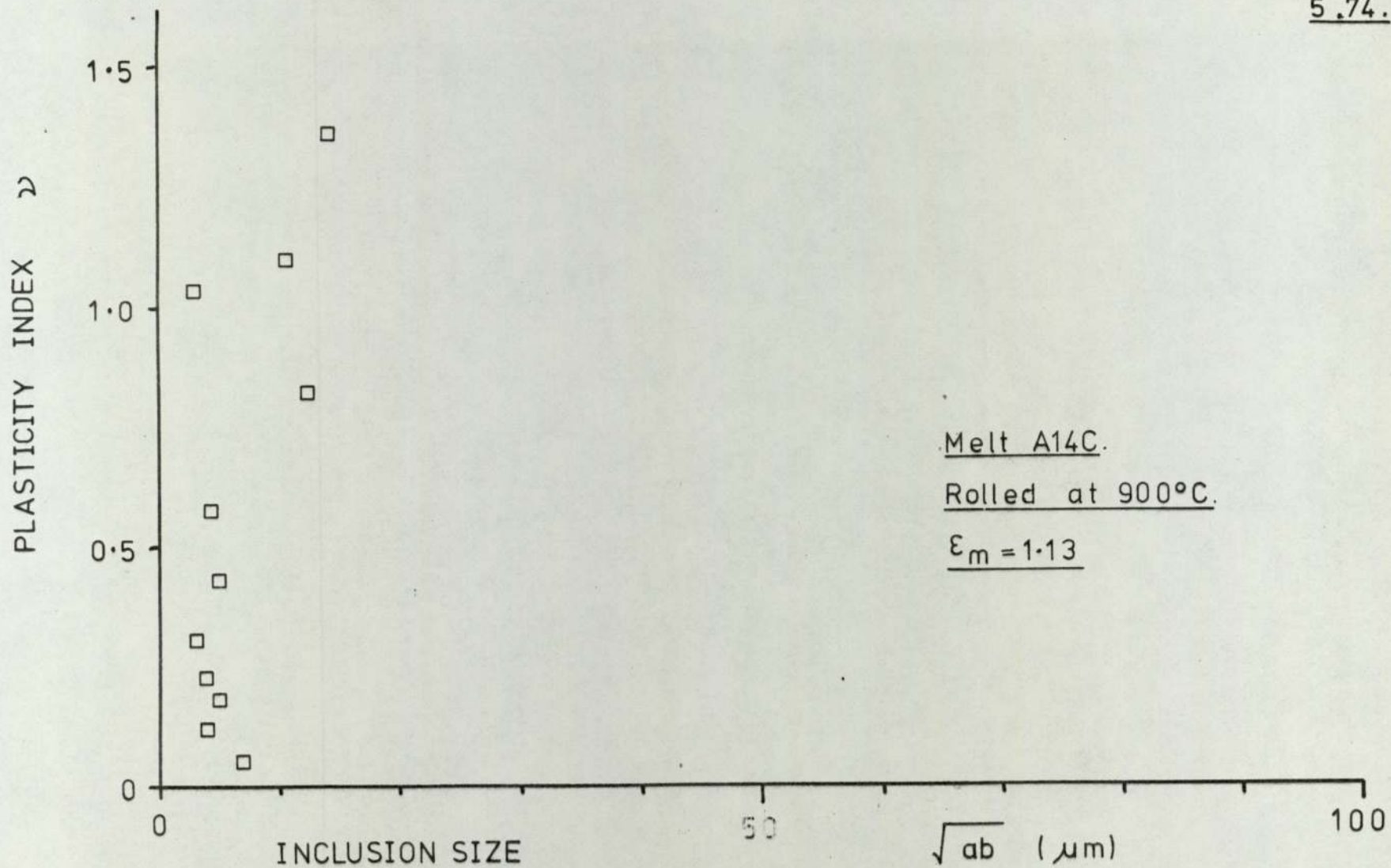
Melt A14C.

Rolled at 700°C

$\epsilon_m = 1.12$







5.75.

PLASTICITY INDEX ν

1.5

1.0

0.5

0

Melt A14

Rolled at 900°C

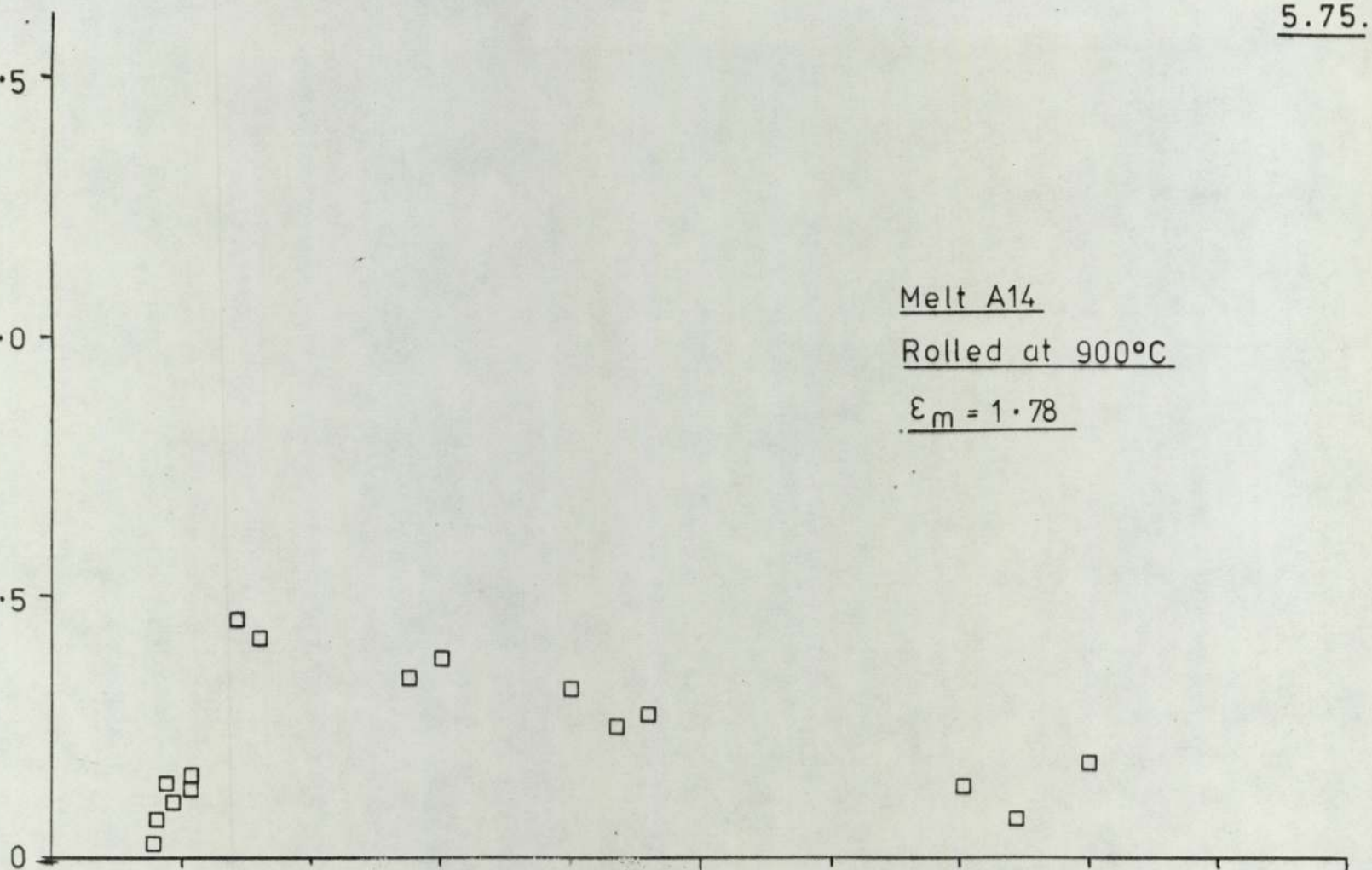
$\epsilon_m = 1.78$

INCLUSION SIZE

50

\sqrt{ab} (μm)

100



5.76.

PLASTICITY INDEX ν

1.5

1.0

0.5

0

INCLUSION SIZE

50

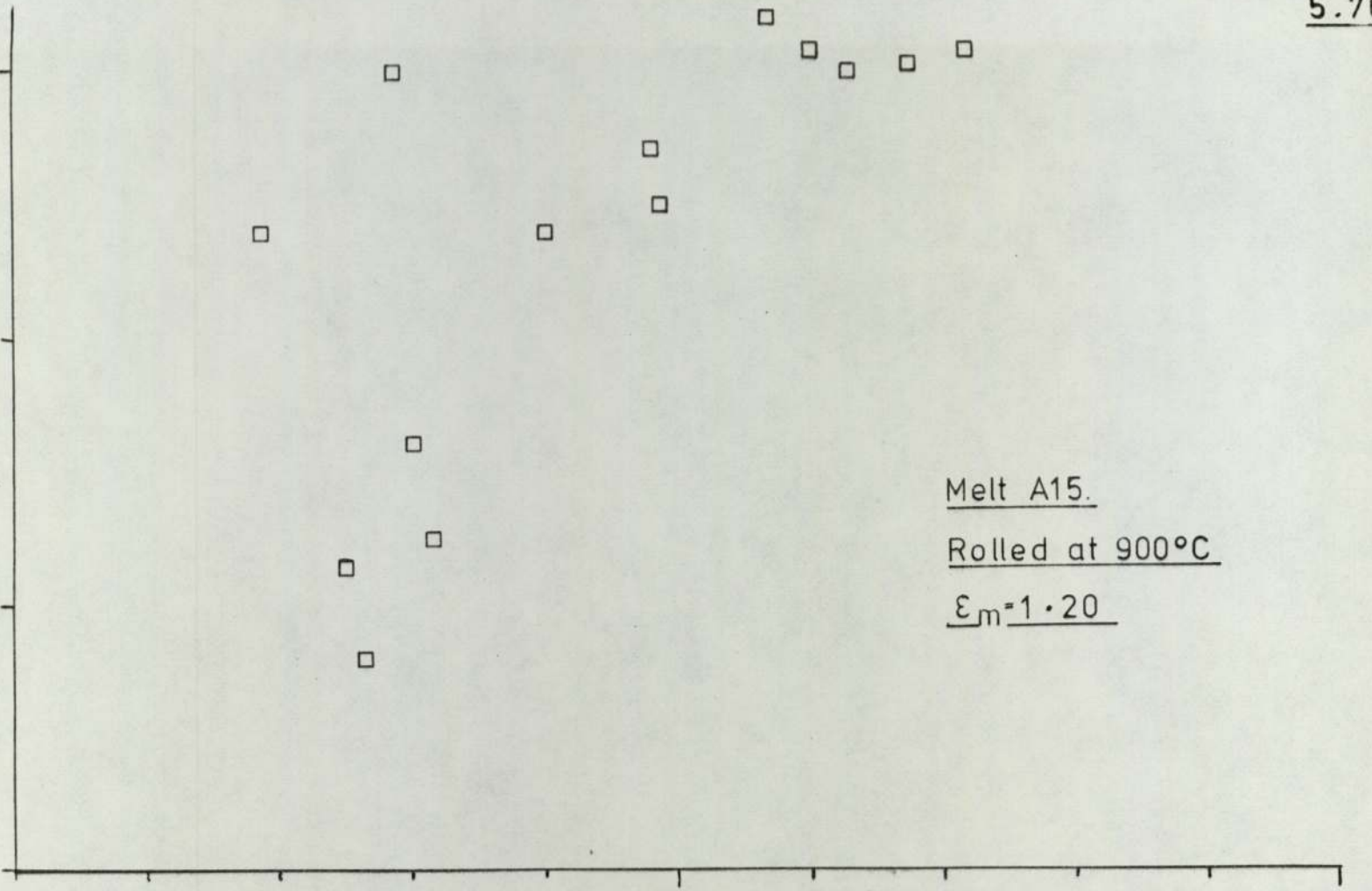
\sqrt{ab} (μm)

100

Melt A15.

Rolled at 900°C

$\epsilon_m = 1.20$



5.77.

PLASTICITY INDEX γ

1.5

1.0

0.5

0

INCLUSION SIZE

50

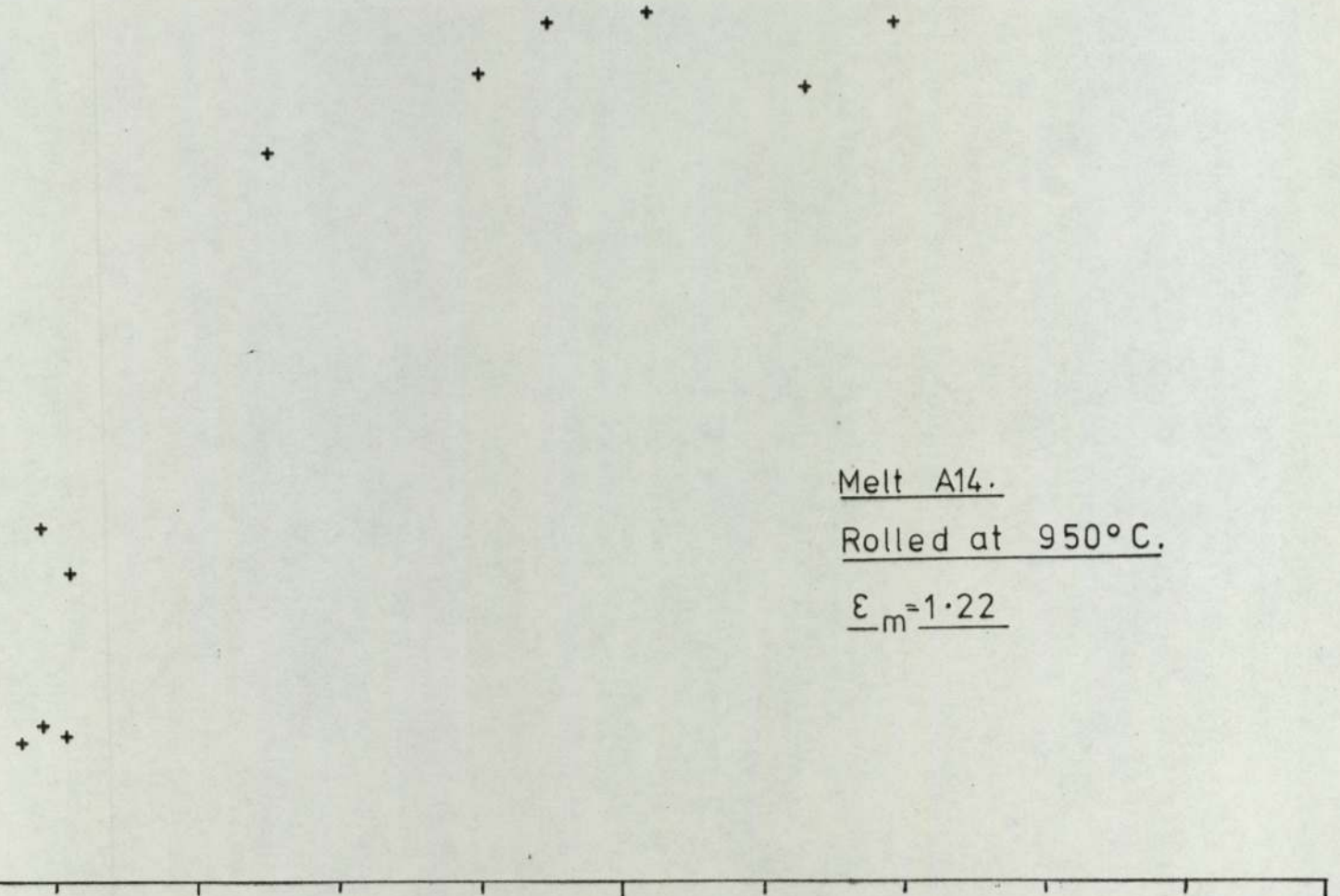
\sqrt{ab} (μm)

100

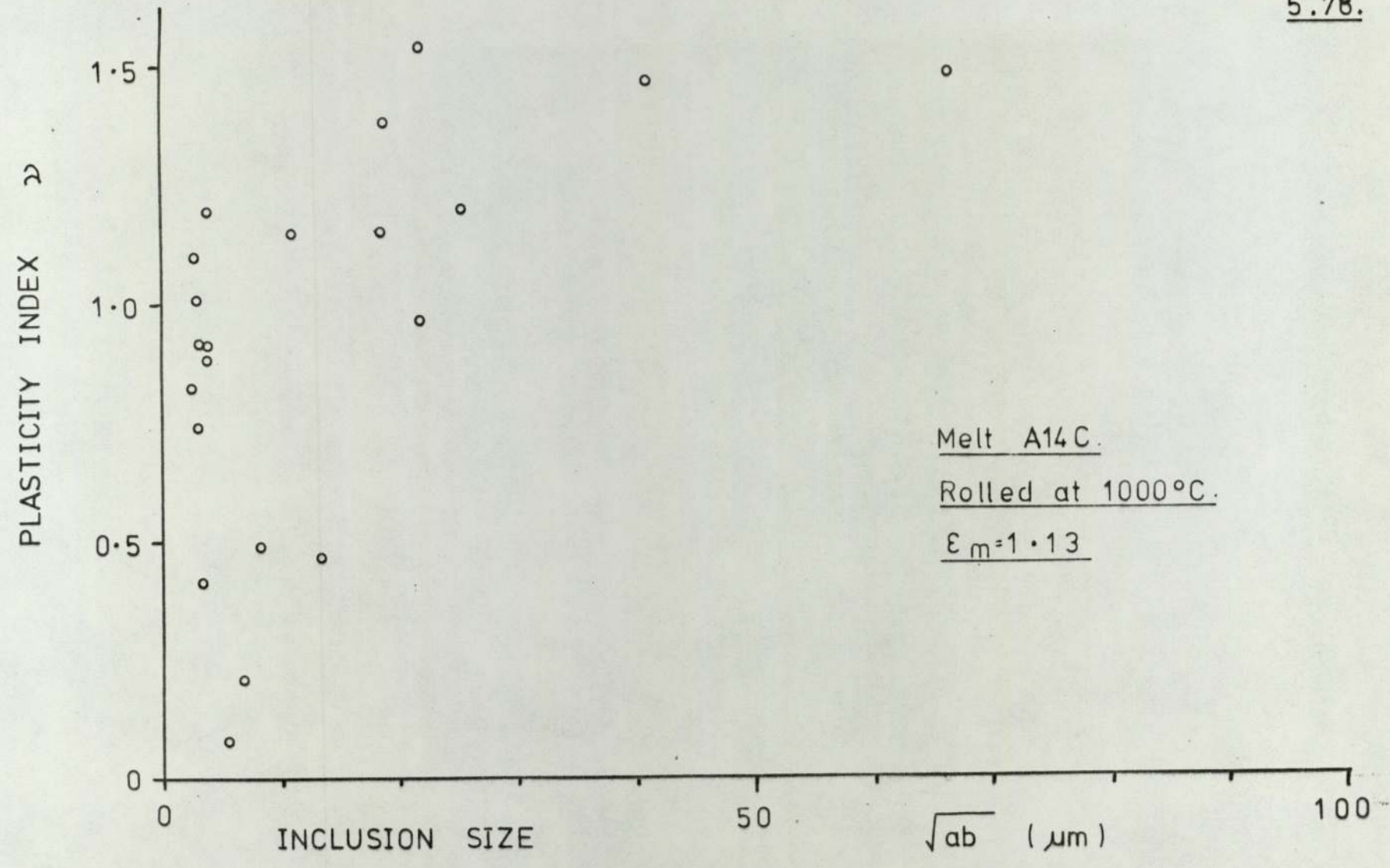
Melt A14.

Rolled at 950°C.

$\epsilon_m = 1.22$



5.78.



5.79.

PLASTICITY INDEX ρ

1.5

1.0

0.5

0

0

50

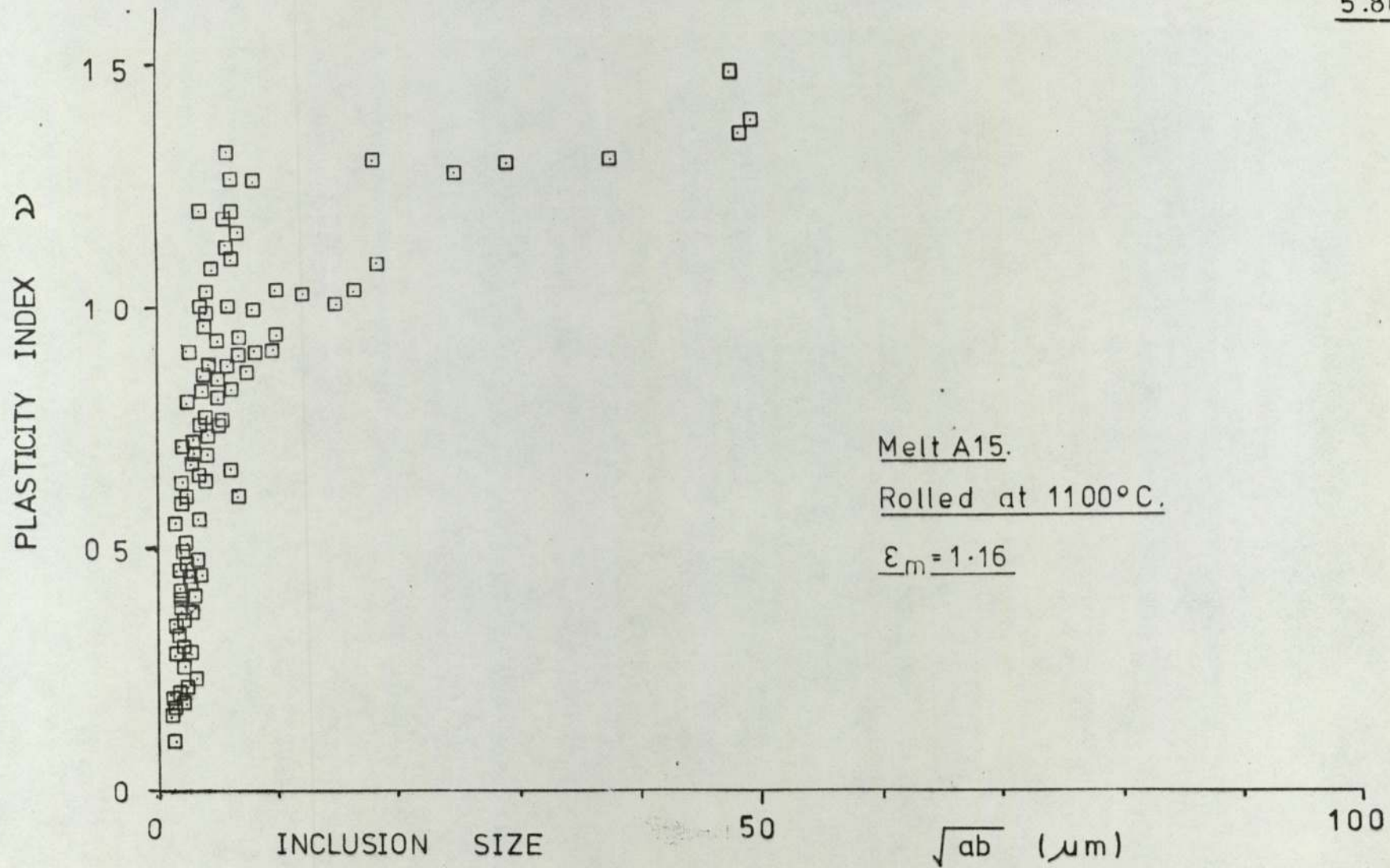
100

Melt A14.

Rolled at 1000°C

$\epsilon_m = 1.09$

\sqrt{ab} (μm)



5.81.

PLASTICITY INDEX ρ

1.5
1.0
0.5
0

0

50

100

Melt A15

Rolled at 1300°C

$\epsilon_m = 1.11$

\sqrt{ab} (μm)

inclusions deformed and the small opaque inclusions remained undeformed. Again at 900°C this trend was obvious (figure 5.74.) and the large inclusions either, deformed or fractured in a brittle manner. Melts Al₄, which was of similar composition to Al₄C, showed a slightly different behaviour pattern (Figure 5.75.). Both glassy and precipitated inclusions deformed only a limited amount, and the small inclusions showed very little if any deformation. An interesting point to note with melt Al₄ at 900°C was that inclusion deformability appeared to decrease with increase in inclusion size above 10 μm where these inclusions contained precipitate phases.

Melt Al₅, deformed at 900°C, showed a totally different character (Figure 5.76.) although of comparable composition, and was similar in its plasticity index - size relationship to melt Al₄ deformed at 950°C (figure 5.77.). Again the small inclusions were not readily deformable and it appeared that there was a rapid increase in deformability above 20 μm.

At a rolling temperature of 1000°C and above melts Al₄, Al₄C and Al₅ (Figures 5.78. to 5.81.) all showed an increased number of small deformable inclusions although again below approximately 1 - 2 μm there were no deformable inclusions. There was a rapid increase in inclusion plasticity upto about 10 μm, above which the inclusions were highly deformable.

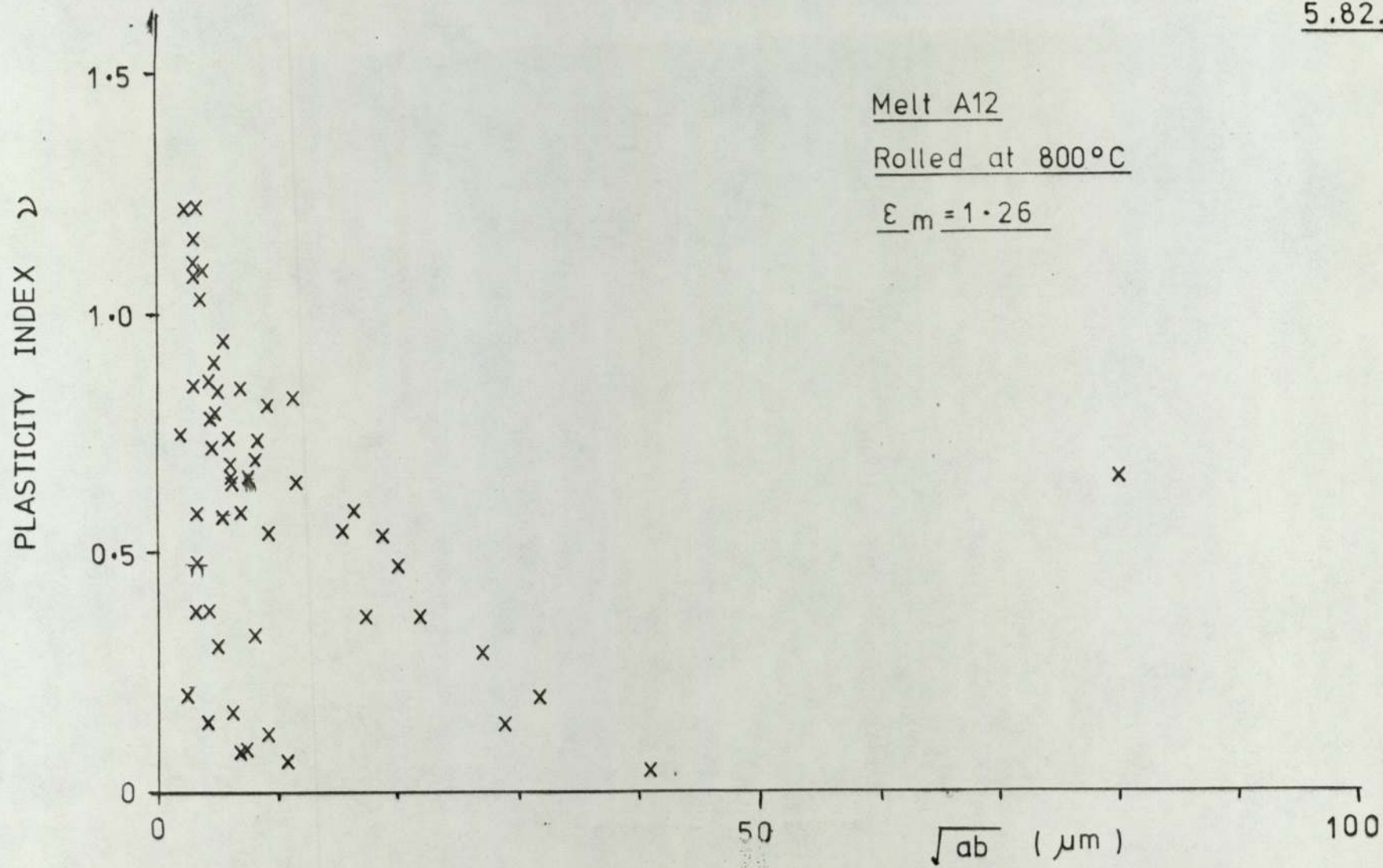
Group (1C) : melts A9, A12 and A13.

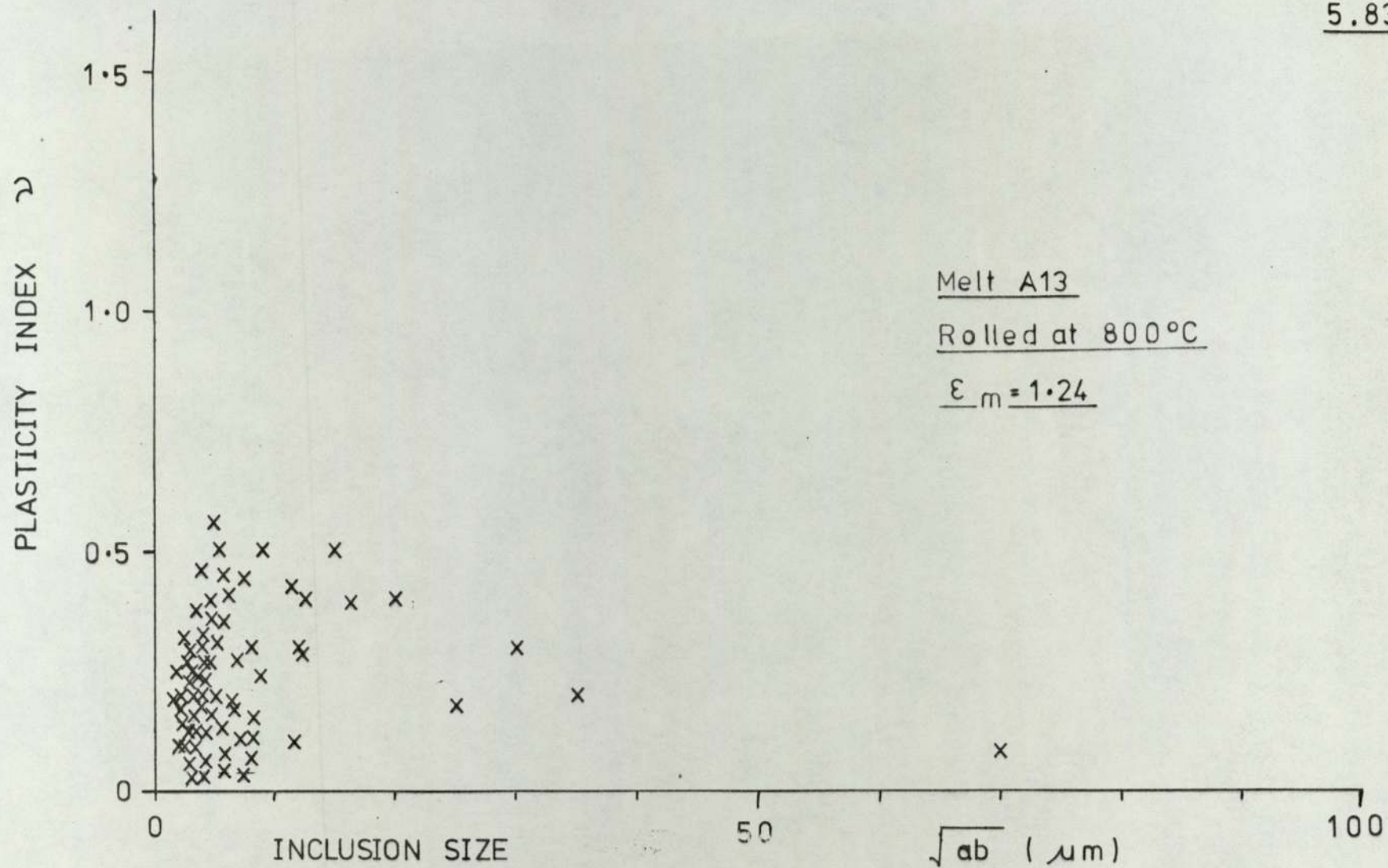
As with the melts of group (1b) rolled in the region of 900°C , melts A12 and A13 (Figures 5.82. - 5.86.) showed a similar plasticity index - size relationships. The small glassy inclusions above 1 - 2 μm in size were less deformable as the size increased. In the case of melts A12 and A13 these contained both glassy and precipitated inclusions. Thus, this fall off in plasticity index with size may not just be a precipitation effect, as was thought for melt A14, but a compositional or heating effect as is discussed later.

Melt A9 rolled at 1000°C (Figure 5.87.) again showed the difference in behaviour of the glassy phases and those containing precipitates within the glass. The glassy inclusions showed a rapid increase in plasticity index with size upto approximately 10 μm above which they appeared to be well deformed. Those inclusions containing precipitate phases and which were deformable showed low levels of inclusion deformation, although it appeared that the value of plasticity index increased with size for these inclusions. Although this latter statement is very dependant upon the result for the 90 μm inclusion.

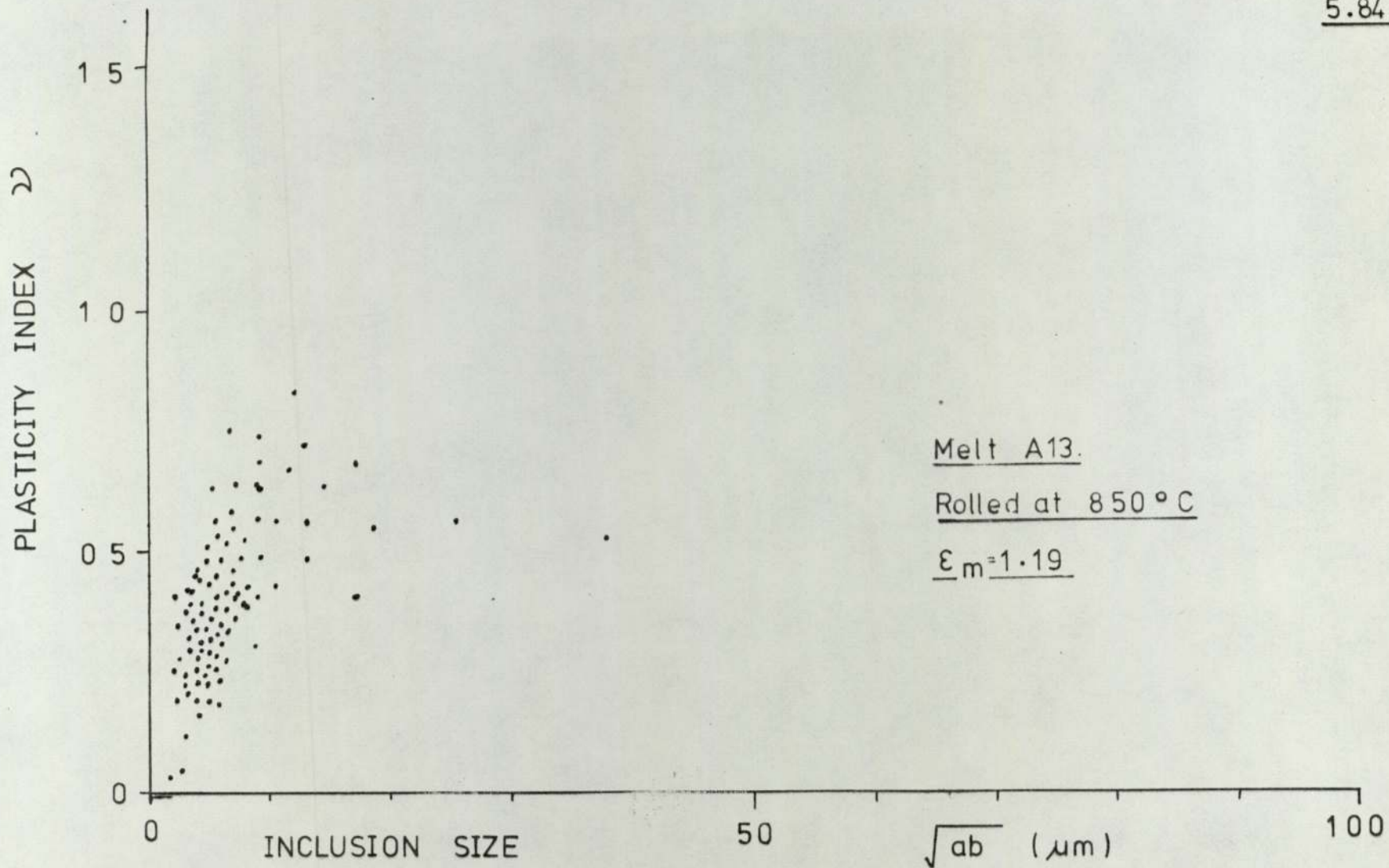
At a rolling temperature of 1000°C (Figures 5.88. and 5.89.) it was again seen that the glassy inclusions were highly deformable, whereas those containing precipitates showed less deformability. At the highest rolling temperature i.e. 1300°C . the inclusion

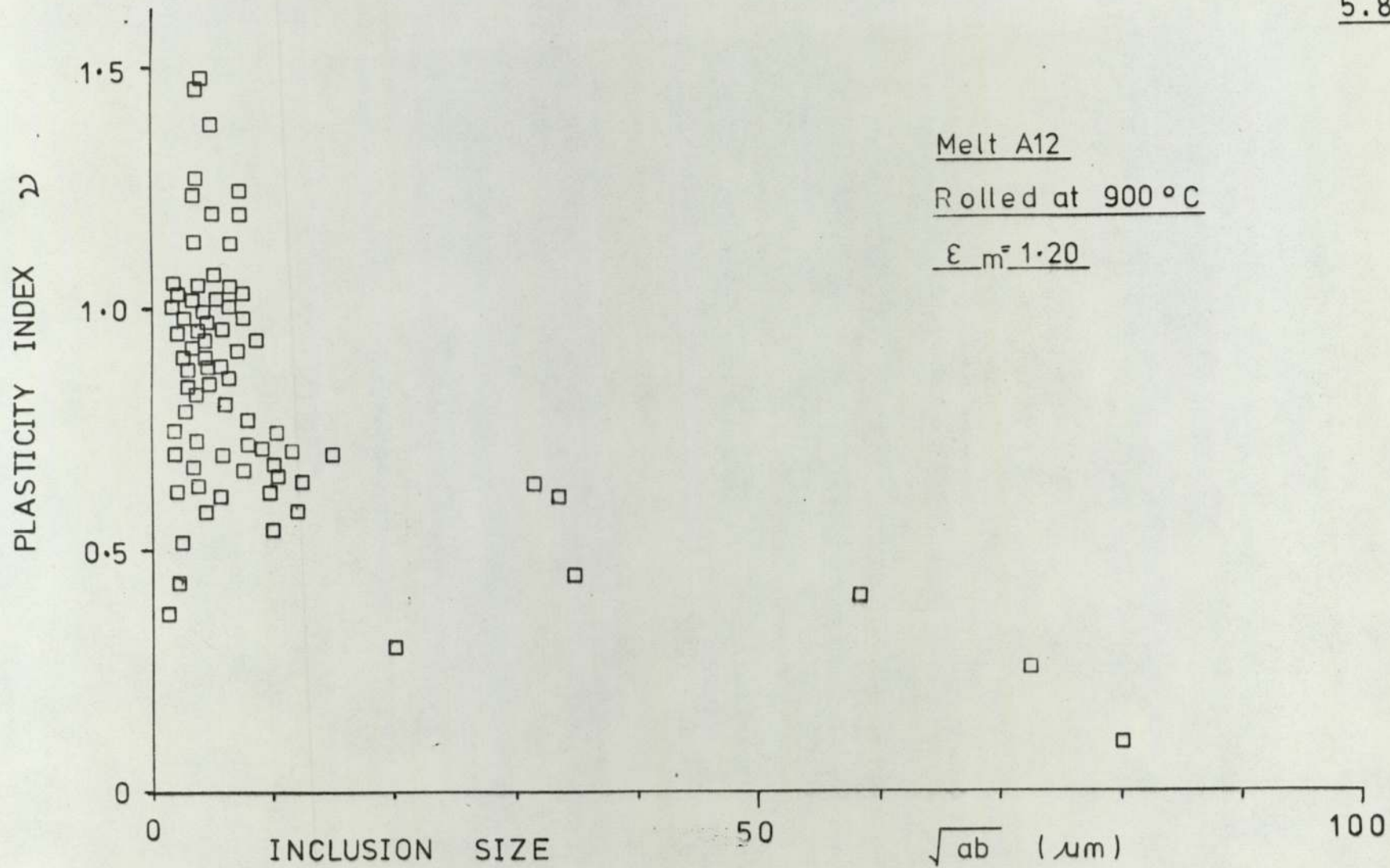
5.82.

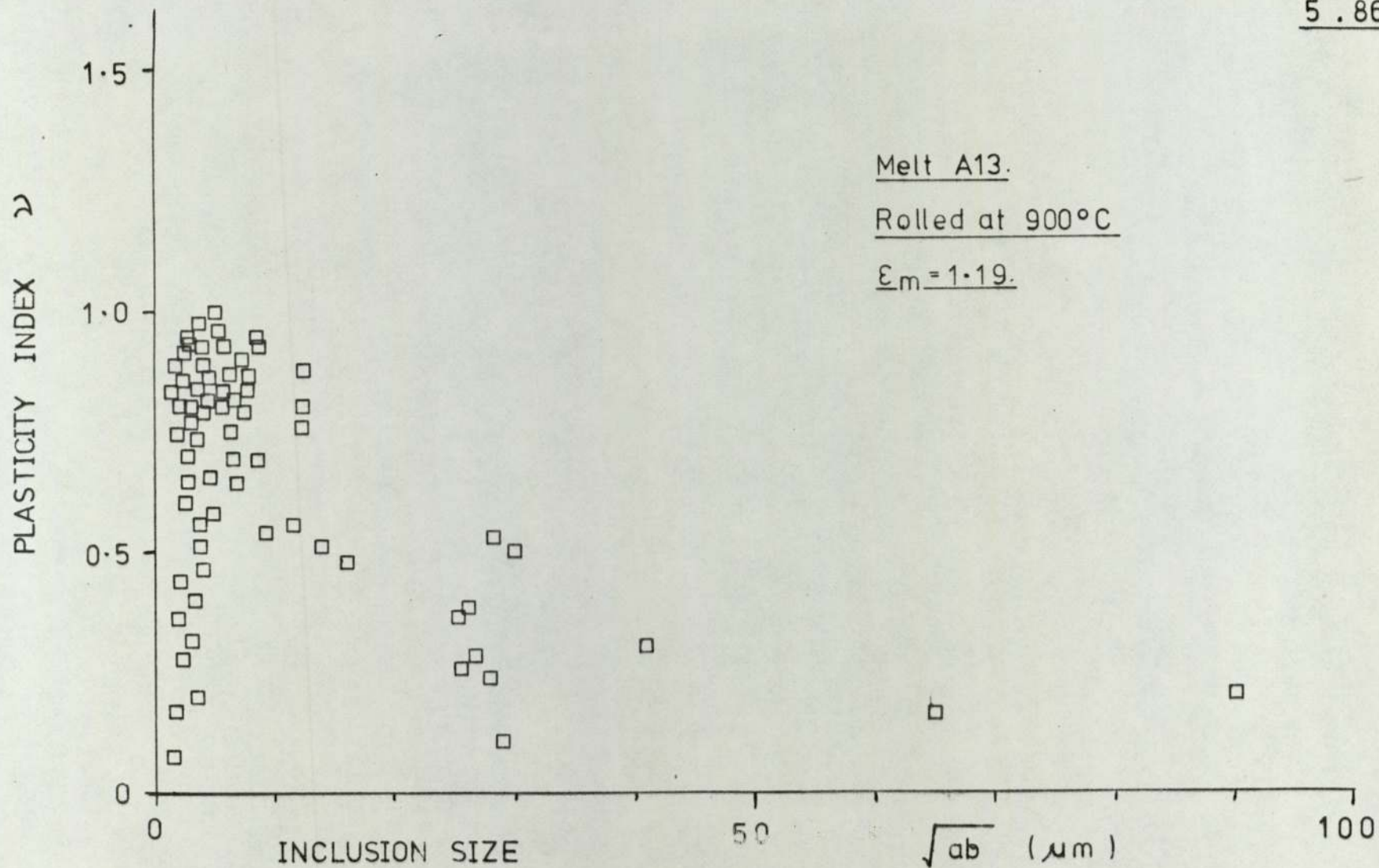




5.84.







5.87.

PLASTICITY INDEX ρ

Melt A9
Rolled at 1000°C
 $\epsilon_m = 1.11$

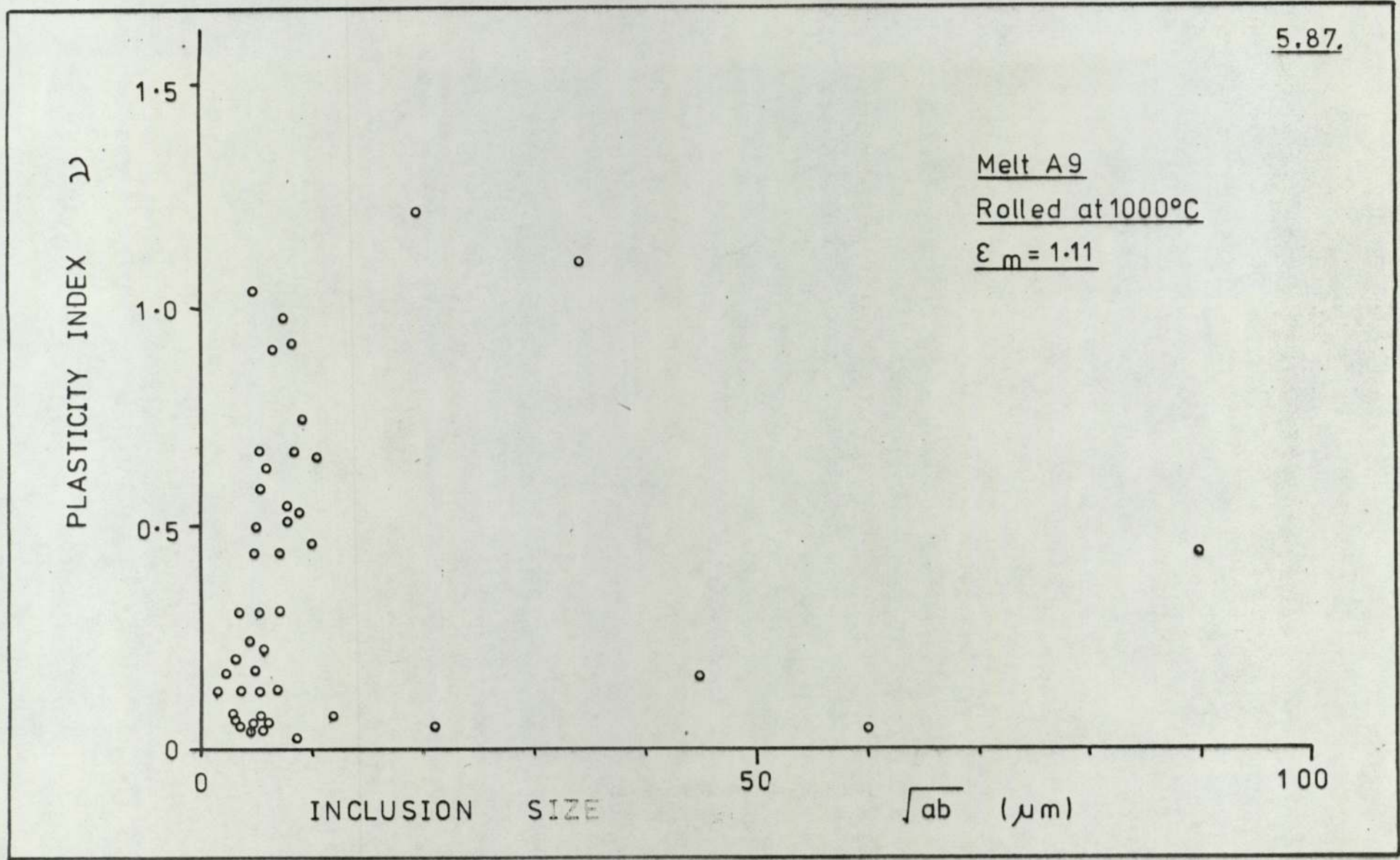
1.5
1.0
0.5
0

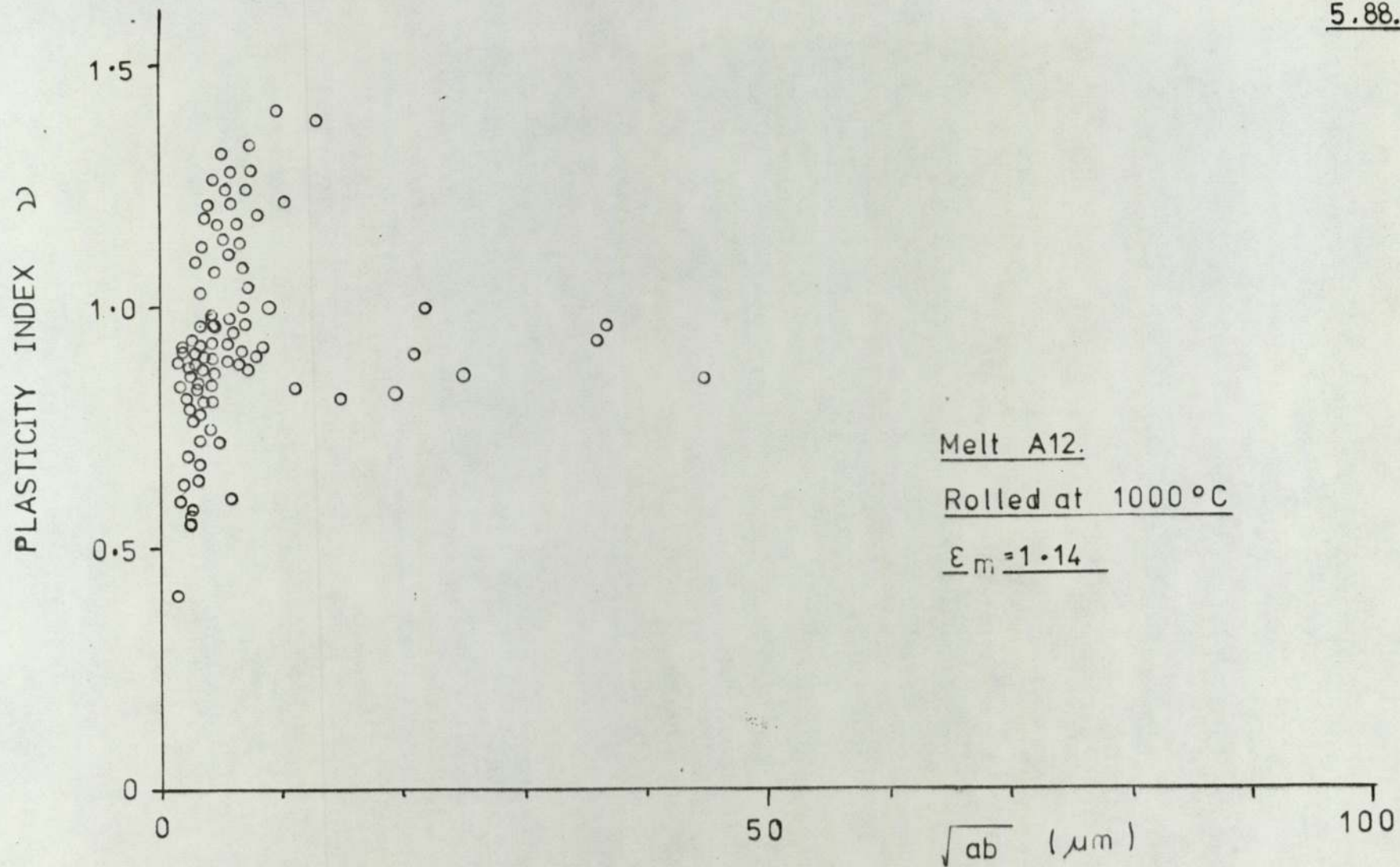
INCLUSION SIZE

50

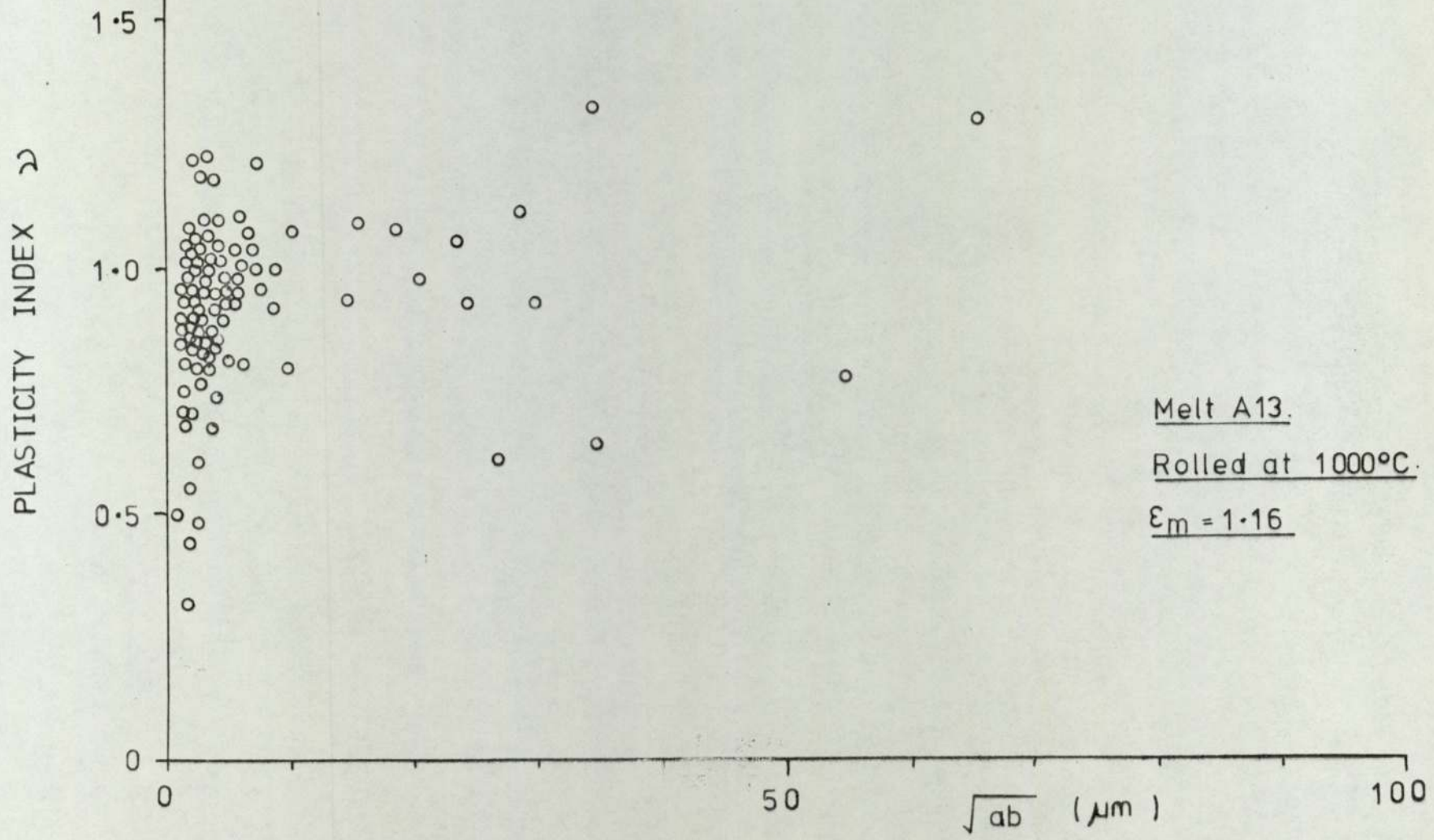
\sqrt{ab} (μm)

100





5.89.



plasticity index - size relationship was similar to the other melts at this temperature. (i.e. Figure 5.90.).

Group (2) : melts A6(2) and Al3X.

These melts contained inclusions which consisted of a silicate matrix in which particles of cristobalite were present. Hot rolling of these inclusions had no apparent effect upon the size and number of cristobalite particles within the inclusions. Below approximately 10 μm the inclusions appeared to be of a glassy nature, both in the as cast and deformed conditions.

Unlike the previous groups these melts need to be considered in isolation, since they had different inclusion non-deformable/deformable transition temperatures.

Figure 5.91. shows the plasticity index - size relationship for melt A6(2) deformed at 1100^oC, where it appears that two relationships have developed. The first shows a rapid increase in deformability with size for the small inclusion sizes, which is assumed to be the relationship for the glassy inclusions. The second is the more gradual increase in deformability with size and the rapid cut off at 60 μm size which is for the cristobalite containing inclusions. It would seem logical for the inclusions which contain the precipitates to have a lower deformability since the presence of the particles would impede fluid/viscous flow. However, the apparent fall in deformability at around 60 μm

5.90.

PLASTICITY INDEX γ

1.5

1.0

0.5

0

50

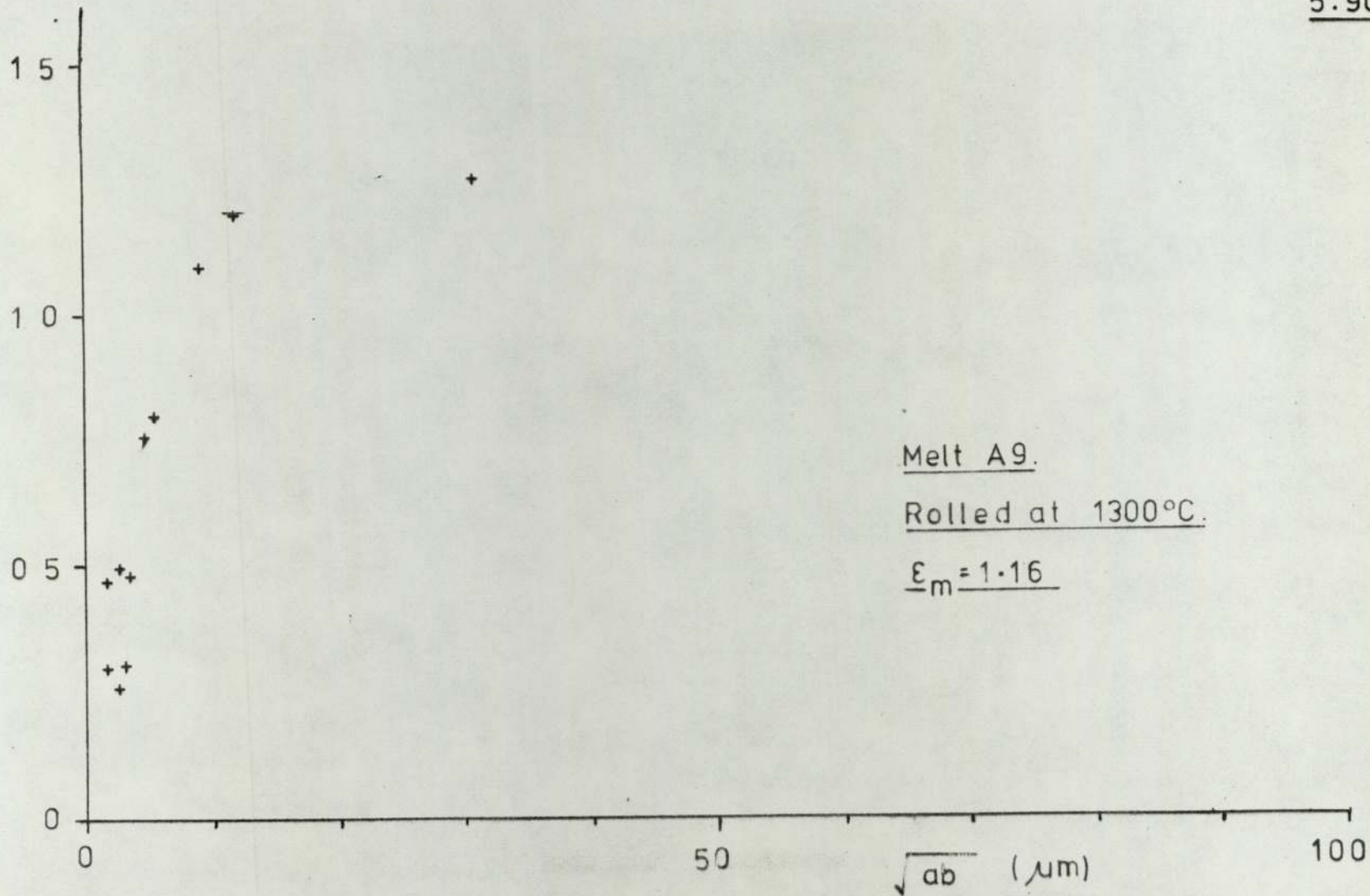
100

Melt A9.

Rolled at 1300°C.

$\epsilon_m = 1.16$

\sqrt{ab} (μm)



PLASTICITY INDEX γ

Melt A6 (2).

Rolled at 1100°C

$\epsilon_m = 1.16$

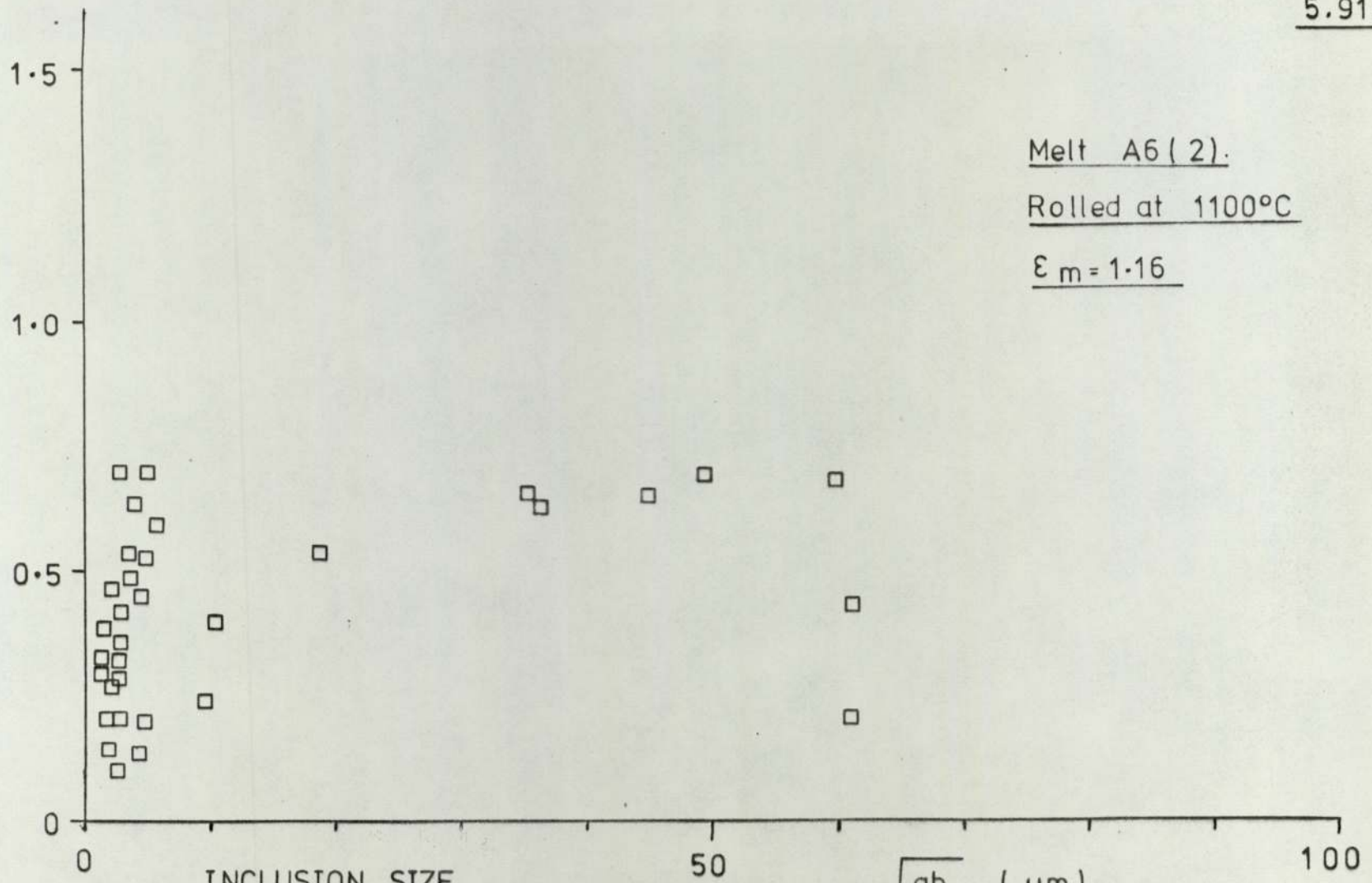
1.5
1.0
0.5
0

INCLUSION SIZE

50

\sqrt{ab} (μm)

100



cannot be accounted for, and it was assumed for convenience that they were spurious results.

Melt A6(2) rolled at 1200°C (Figure 5.92.) again showed a rapid increase in deformability index with size for the glassy inclusions. Those inclusions which contained the cristobalite phase, (i.e. the larger inclusions) showed a marked variation in deformability possibly attributable to the distribution, size and number of precipitates within the inclusions.

Figure 5.93. and 5.94. show that at the rolling temperature of 1300°C all the inclusions greater than $10\ \mu\text{m}$ were highly deformable, although it may be seen in figure 5.93. that there is a dip in plasticity index at approximately $30\ \mu\text{m}$. This dip may be due to inclusions breaking up and hence being measured as two or more inclusions of smaller aspect ratio, and smaller size. A similar explanation may be used to account for the slightly lower plasticity index in figure 5.94.

Figure 5.95. showed that at a rolling temperature of 700°C the inclusions of melt Al3X deformed to an appreciable extent although again it may be seen that the small inclusions were the least deformable. However, rolling at 800°C showed that two sets of plasticity (5.96) index - size relationships were established. These relationships can seemingly be explained by the number of precipitates within the inclusions. With reference to the photographs (in section 4 :8) of melt Al3X plates 4 .29. , it was seen that the inclusions containing a small number of cristobalite precipitates (figure 4.29.)

PLASTICITY INDEX γ

1.5
1.0
0.5
0

INCLUSION SIZE

50

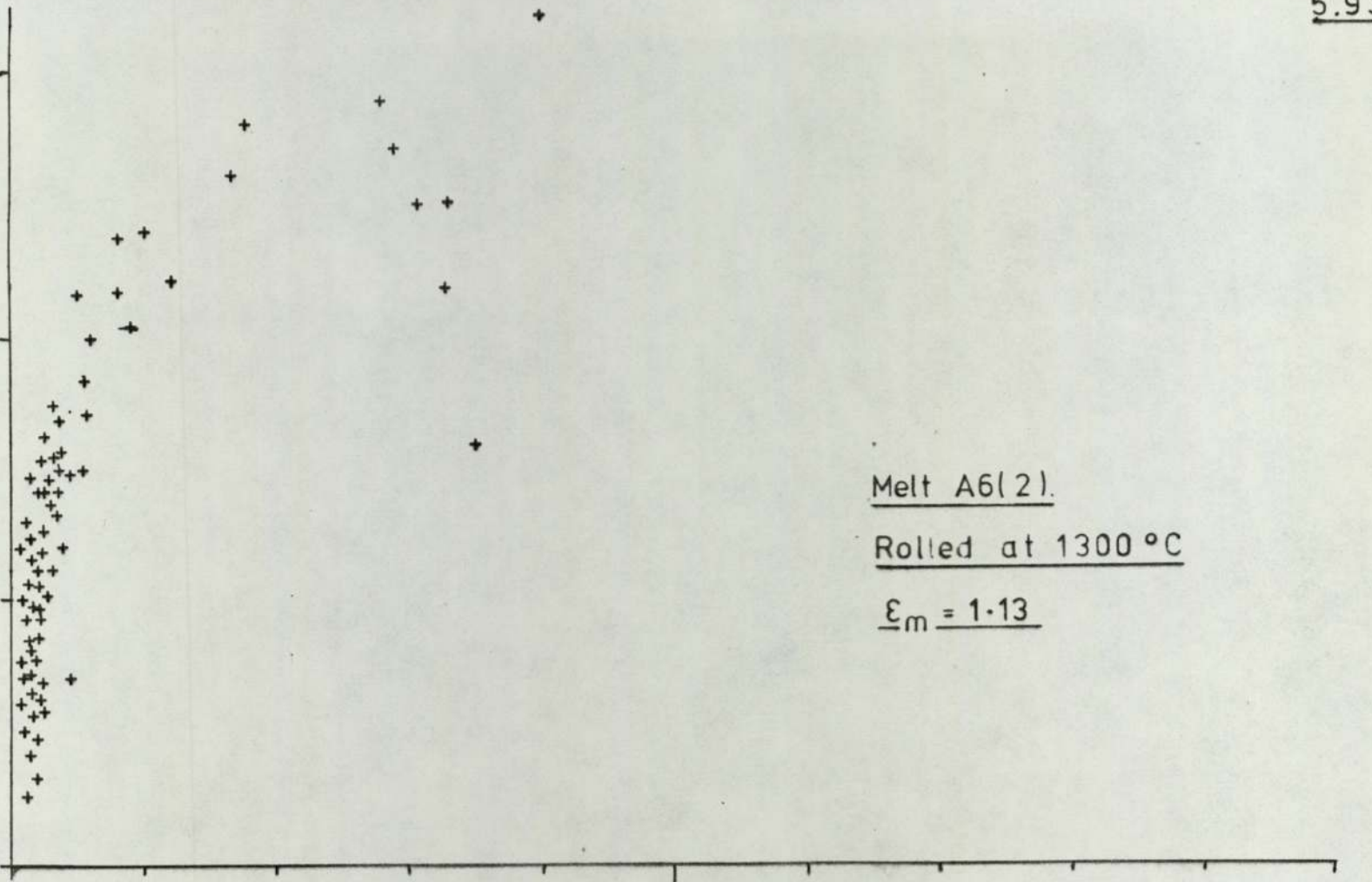
\sqrt{ab} (μm)

100

Melt A6(2).

Rolled at 1300 °C

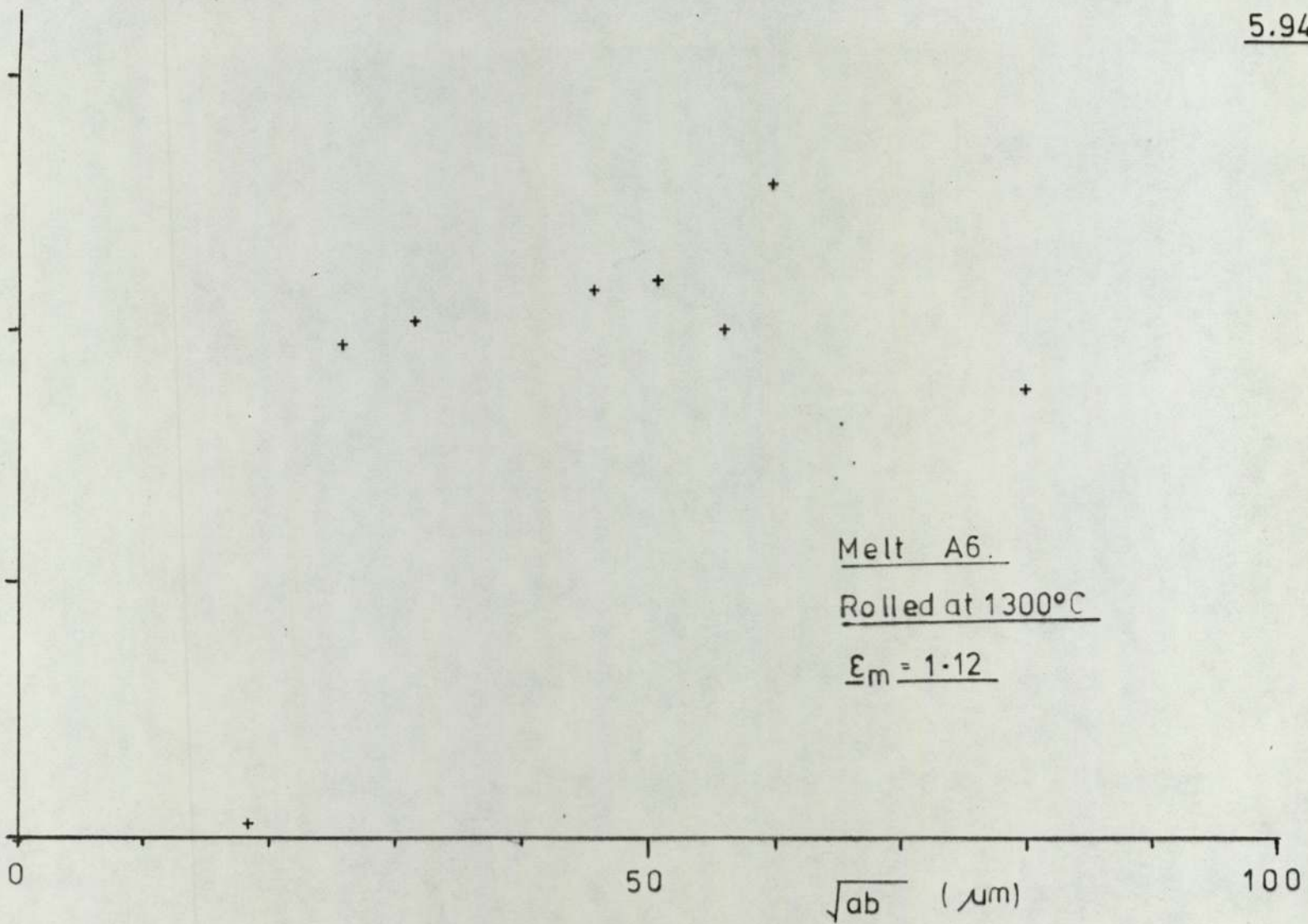
$\epsilon_m = 1.13$



5.94.

PLASTICITY INDEX ρ

1.5
1.0
0.5
0



Melt A6.

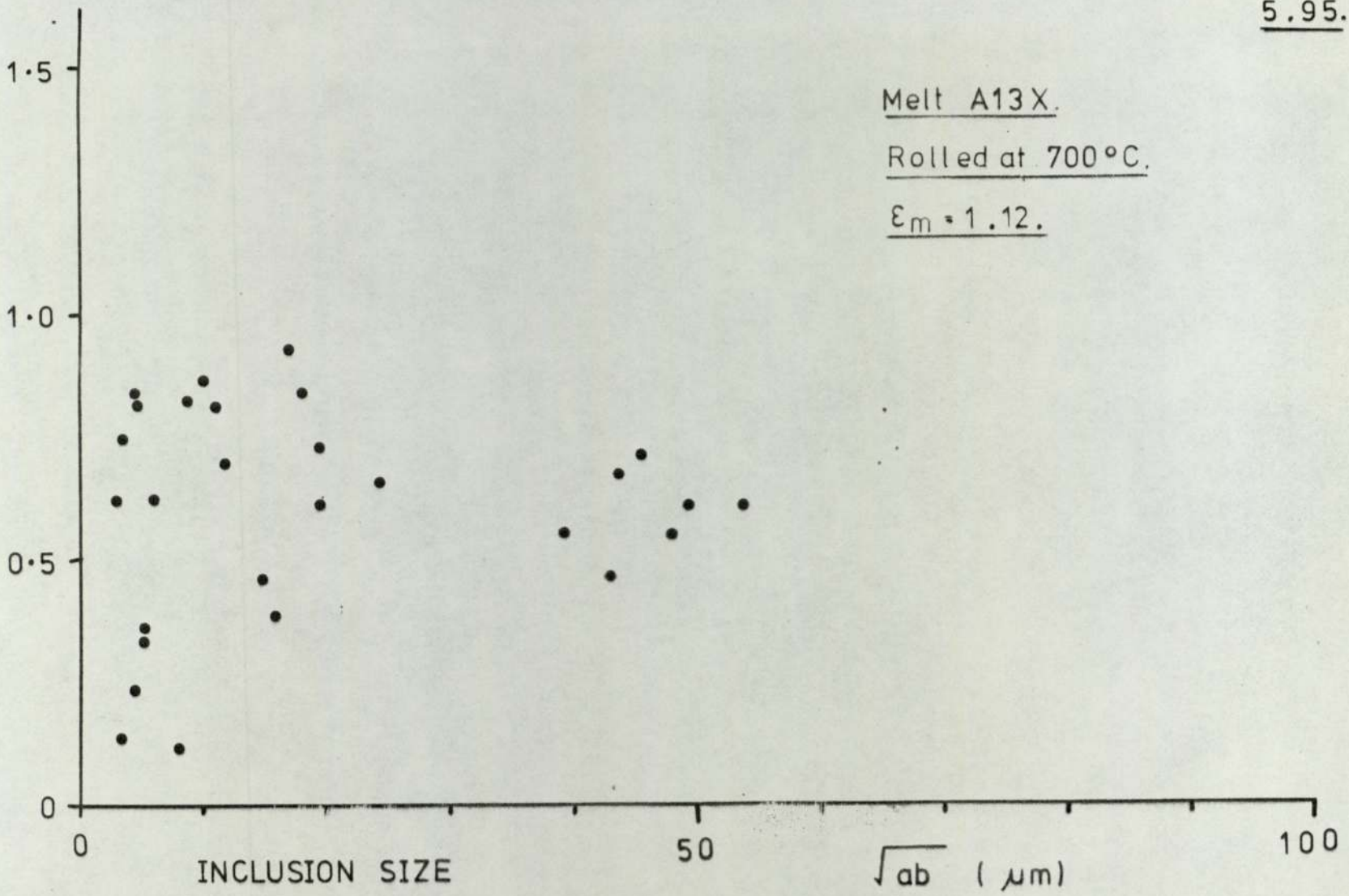
Rolled at 1300°C

$\epsilon_m = 1.12$

5.95.

PLASTICITY INDEX ρ

Melt A13X.
Rolled at 700°C.
 $\epsilon_m = 1.12.$



behaved in a similar manner to the glassy inclusions and have deformed well in excess of the larger inclusions which contain a larger number of precipitates, (figure 4.32.). Again it was presumed that the larger number of precipitates within the larger inclusions effectively strengthen these inclusions and therefore make them less deformable.

Figure 5.97. indicated that at 900°C these large inclusions had deformed, and that there was an apparent steady increase in the plasticity index with increase in size. It was also clear that only a few small inclusions had deformed, for reasons discussed later in section 5.3.5.4.

Figure 5.98. indicated that on rolling at 1000°C the small inclusions in melt A13X were again deformable. It was also evident that the larger inclusions had deformed to a greater extent than at 900°C . At the higher rolling temperature of 1100°C it was noticed that there appeared to be fewer large inclusions (figure 5.99.), although the scatter of the results was substantially less than at 1000°C .

Group (3) : melts A17 and A18

Melts A17 and A18 when rolled at 750°C indicated that the small glassy inclusions were deformable, but only limited, if any, plastic deformation of the large inclusions took place. (figures 5.100. and 5.101.). Above 750°C the results indicated that there was a

PLASTICITY INDEX \mathcal{D}

1.5

1.0

0.5

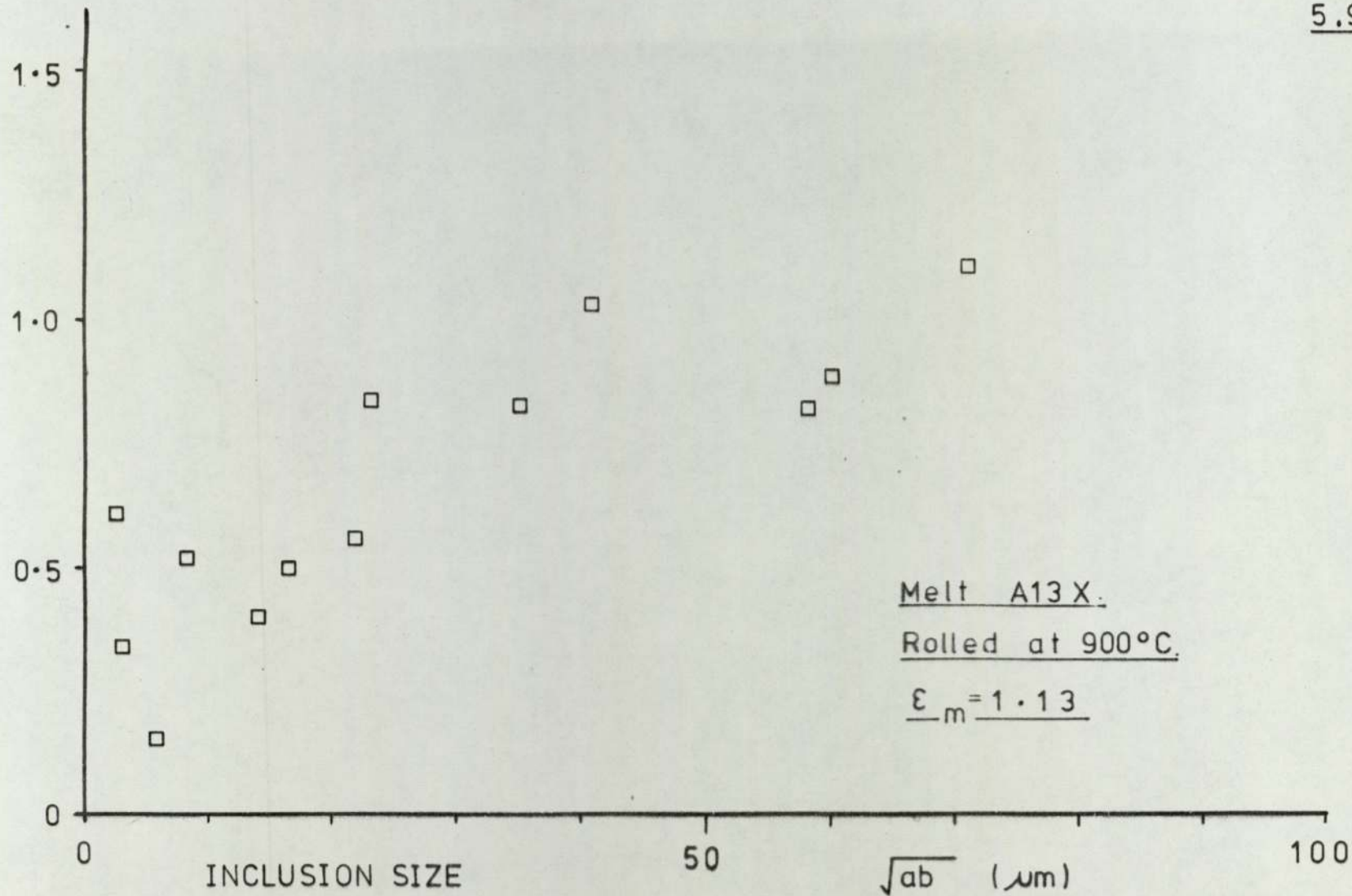
0

INCLUSION SIZE

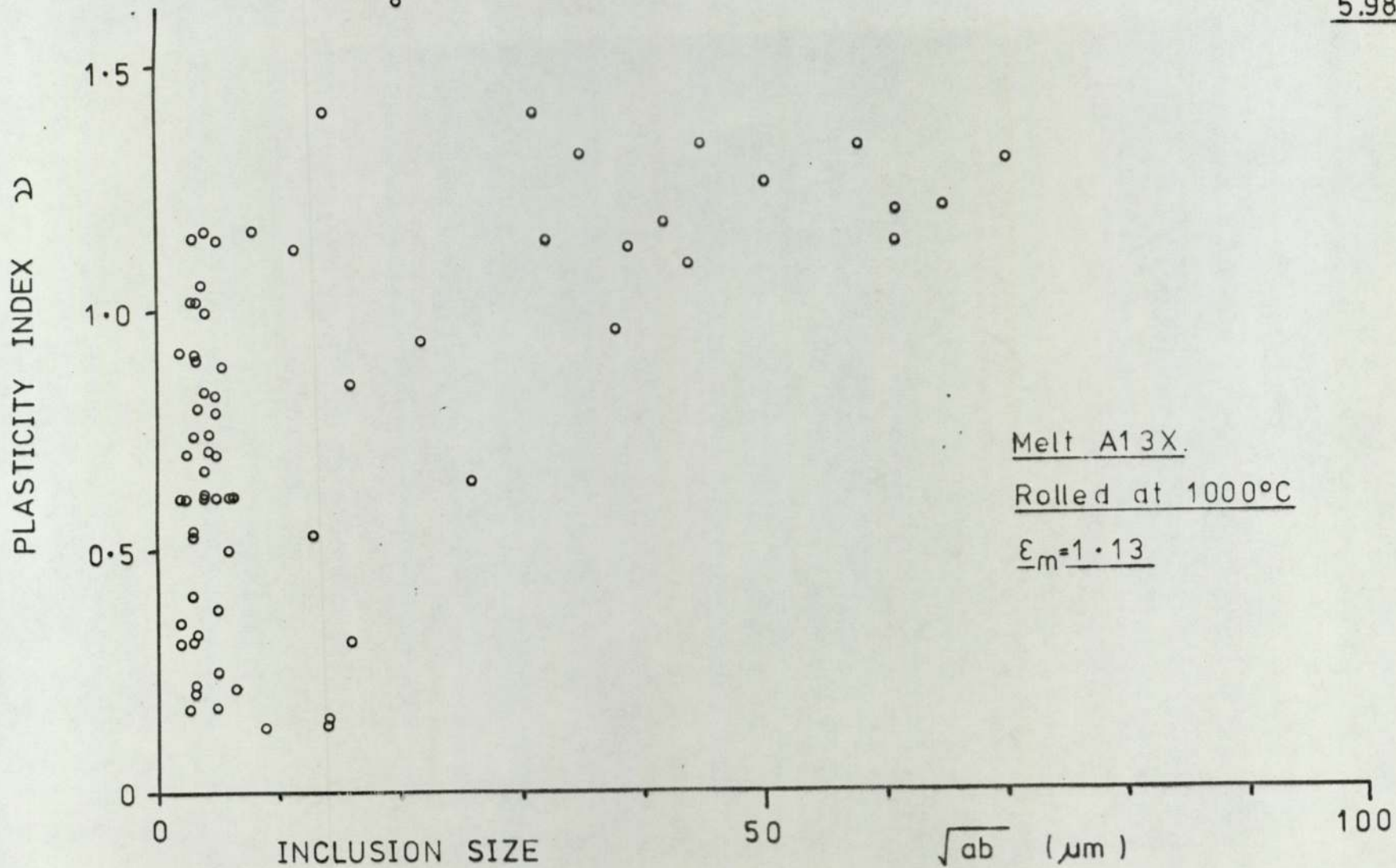
50

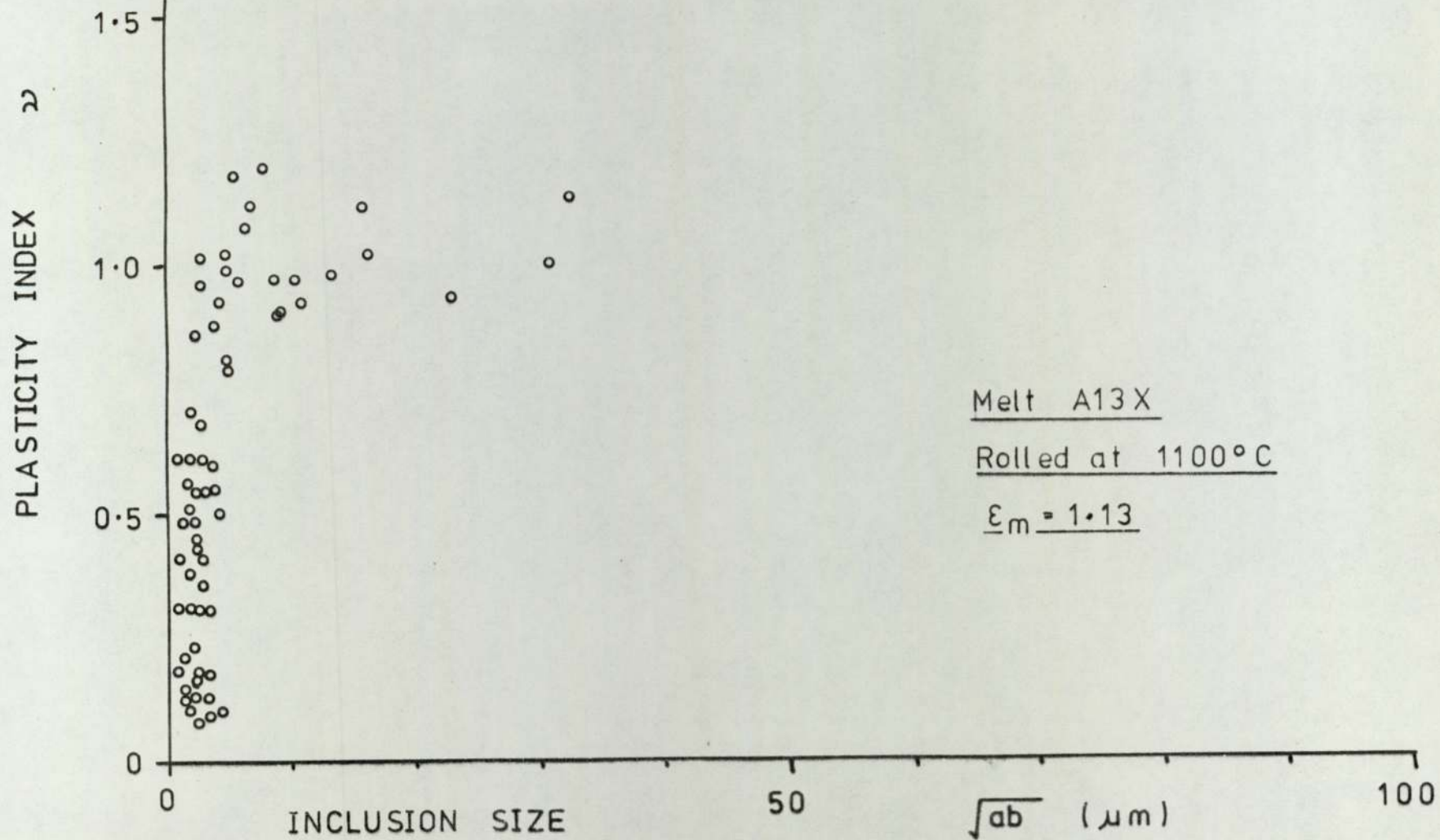
 \sqrt{ab} (μm)

100

Melt A13 X.Rolled at 900°C. $\epsilon_m = 1.13$ 

5.98.





5.100.

PLASTICITY INDEX ρ

Melt A17
Rolled at 750°C
 $\epsilon_m = 1.15$

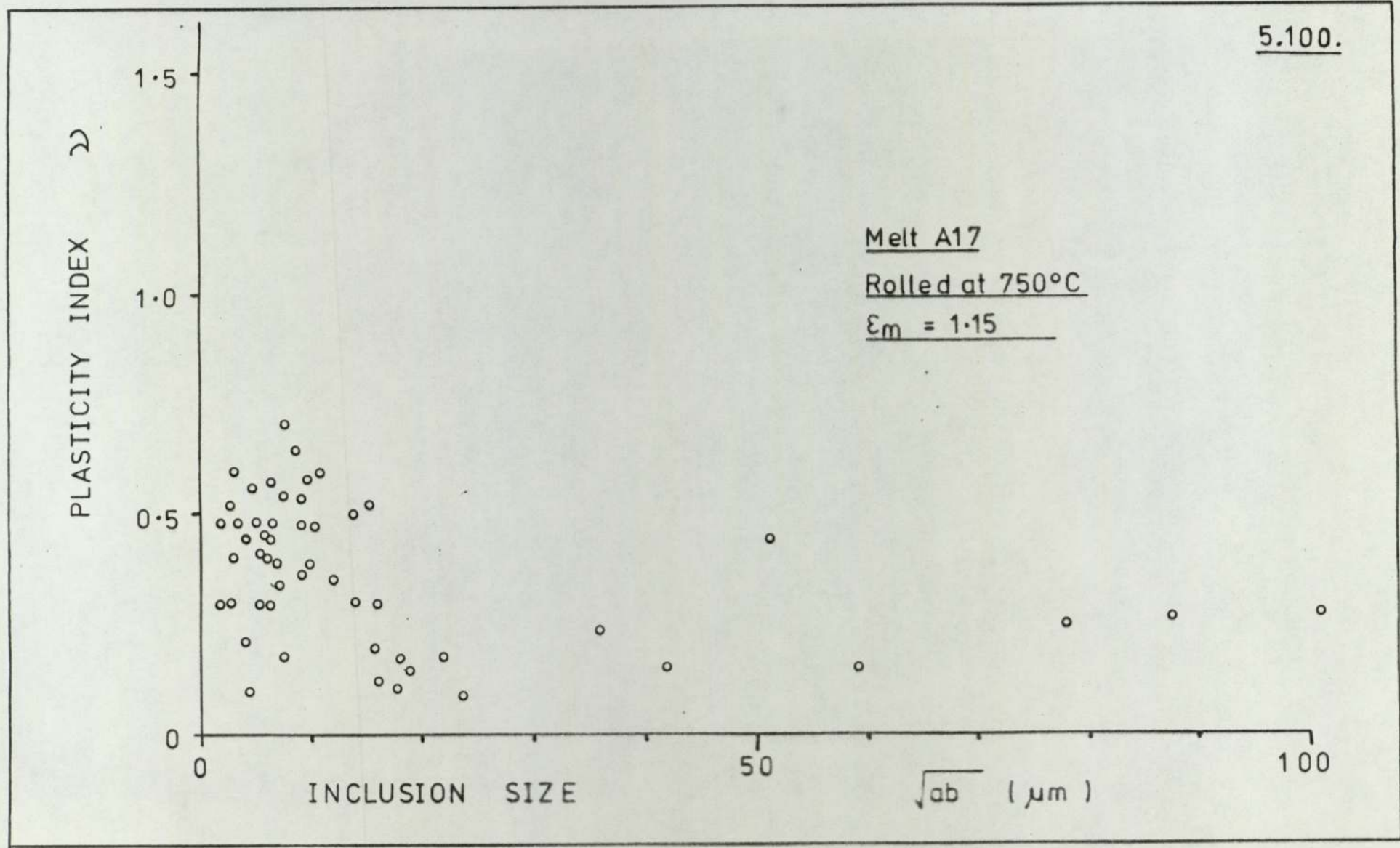
1.5
1.0
0.5
0

INCLUSION SIZE

50

\sqrt{ab} (μm)

100



5.101.

PLASTICITY INDEX ρ

1.5
1.0
0.5
0

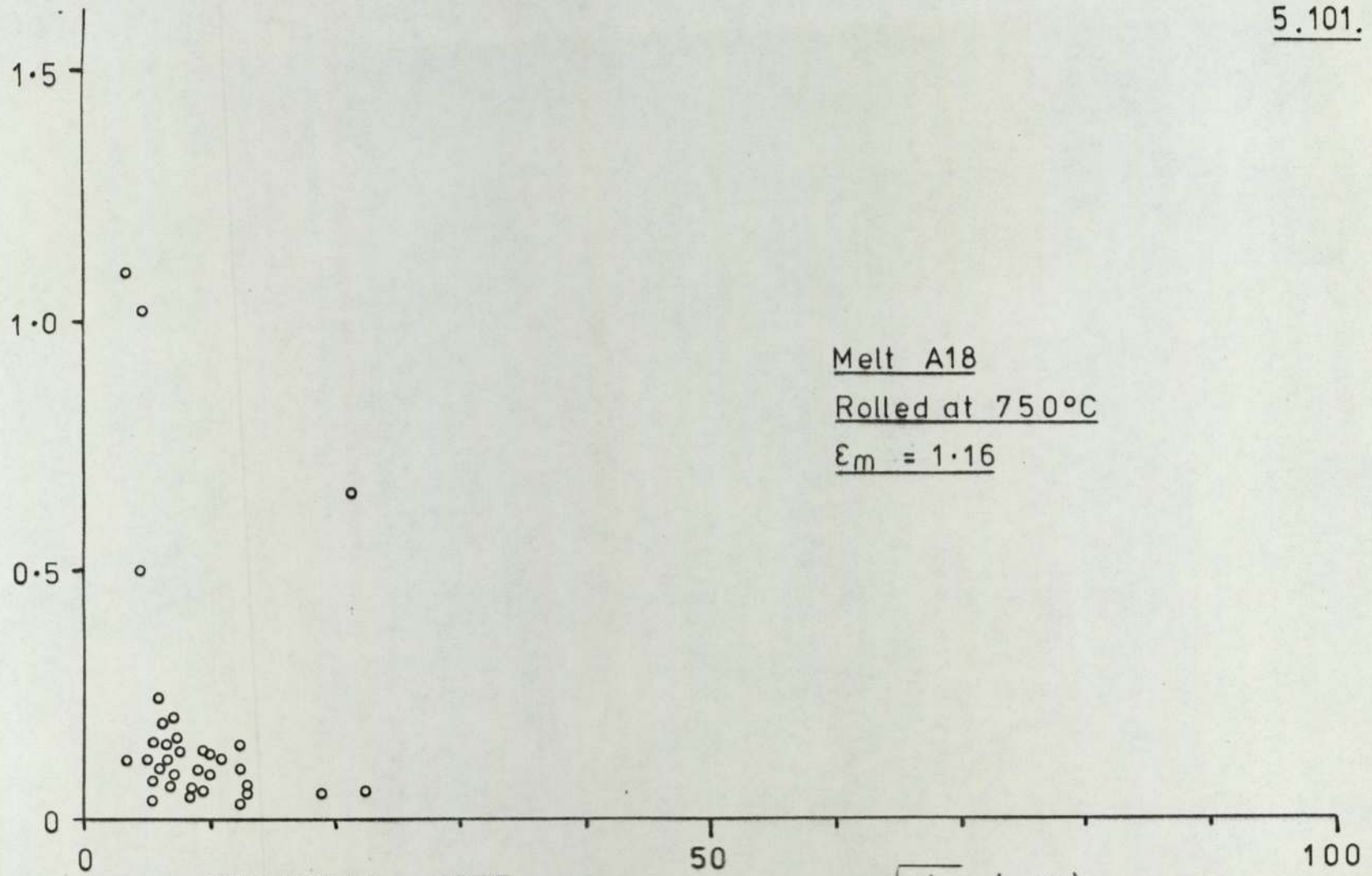
Melt A18
Rolled at 750°C
 $\epsilon_m = 1.16$

INCLUSION SIZE

50

\sqrt{ab} (μm)

100

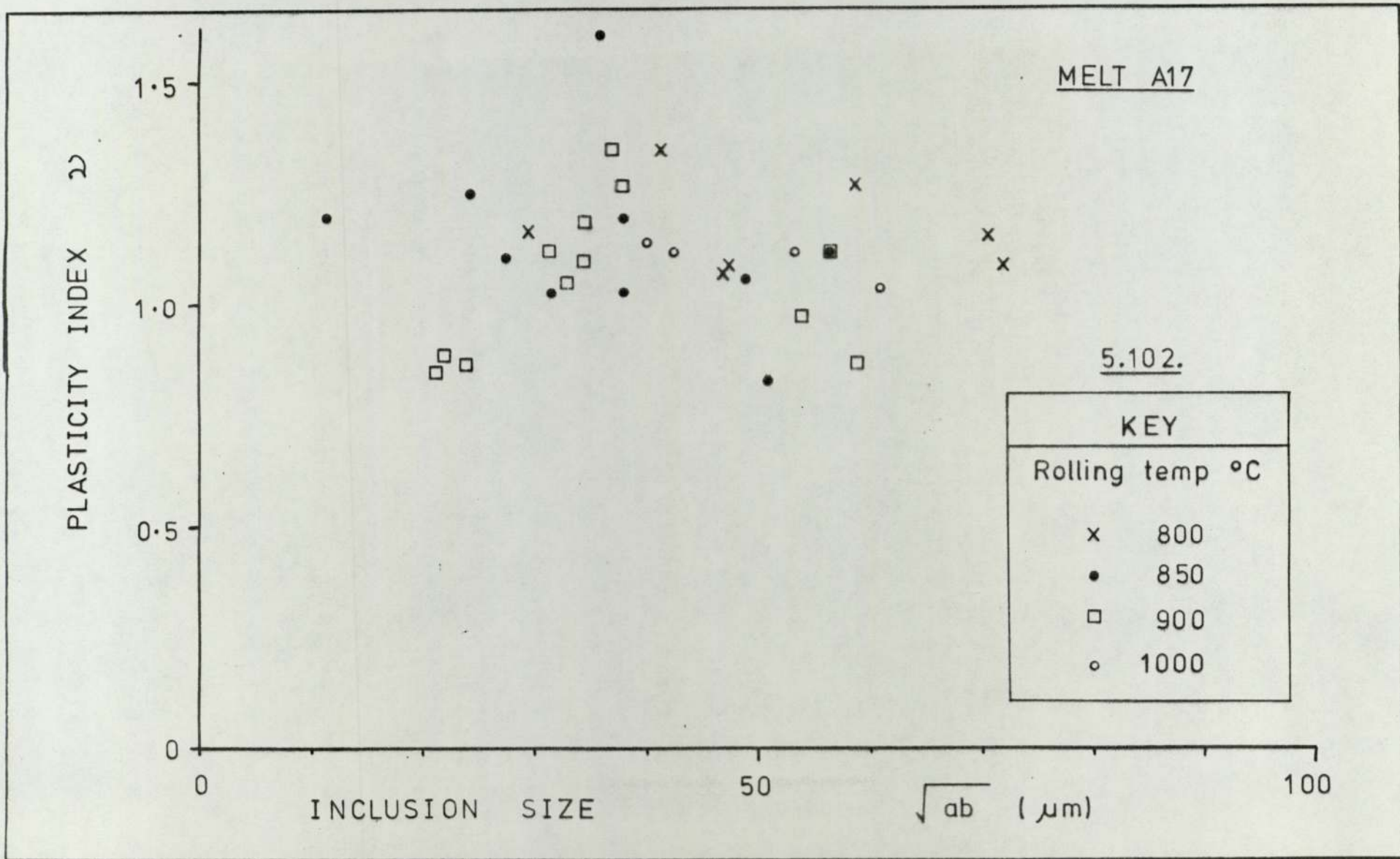


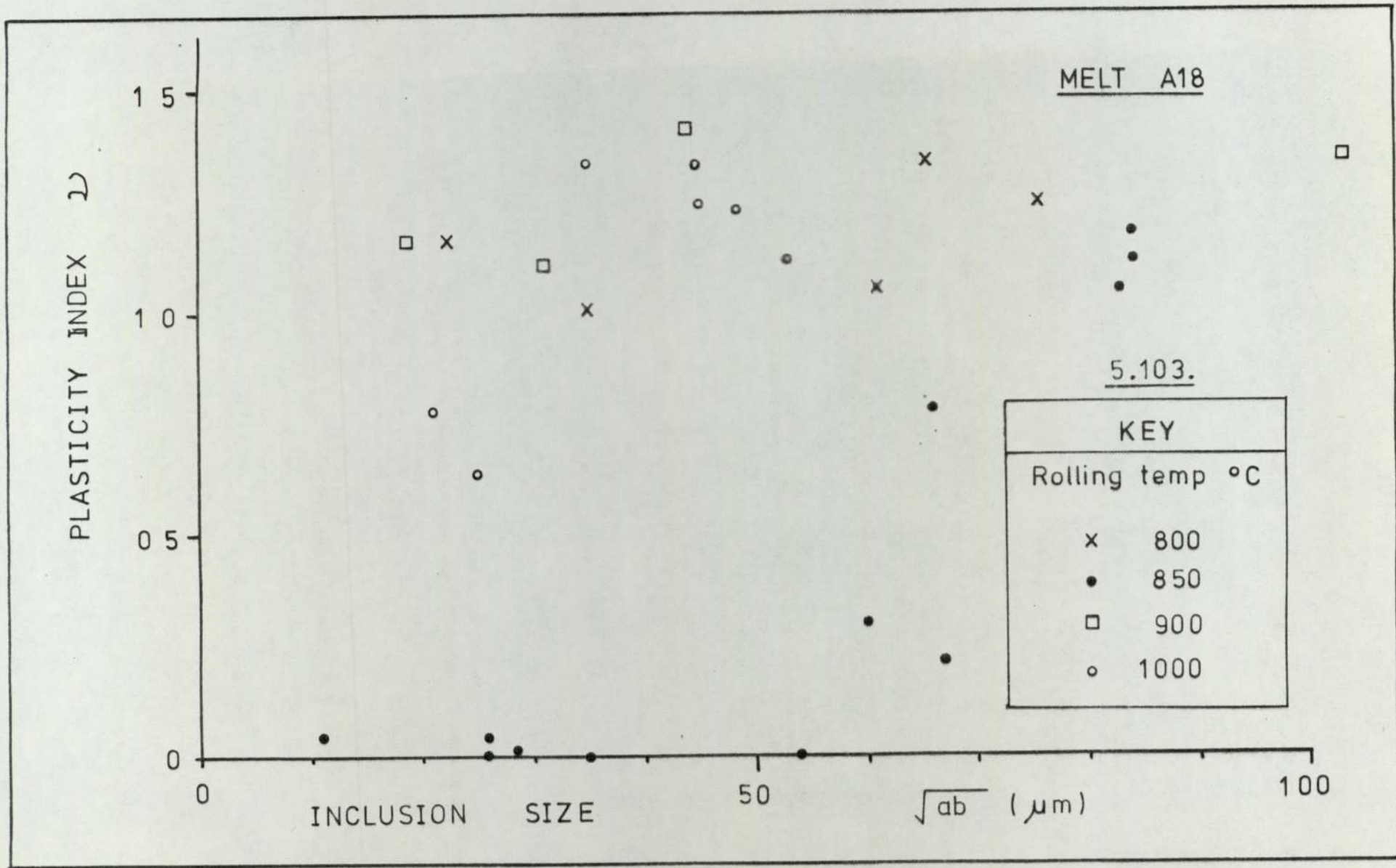
large variation in deformability and no size relationship could be established. (Figures 5.102. & 5.103.)

Group (4) : Al6, NIA12, CRA12, VA12 and NI50A12.

The group (4) inclusions were the easiest to assess ^{the} plasticity index - size relationships for, since there were no problems with precipitates masking any size effect. This group was split into two sections, the first being comprised of melts Al6, NIA12, CRA12 and VA12 which had similar inclusion compositions. In this group there was a matrix phase change encountered upon increasing the rolling temperature i.e. The ferrite/austenite phase change. However, melt NI50A12 had an austenitic matrix at all rolling temperatures, thus avoiding any problems with respect to inclusion plasticity on passing through the (ferrite plus austenite) phase region into the austenite phase region.

Figure 5.104. indicated that when melt CRA12 was rolled at 750°C there was a rapid increase in plasticity index with size from approximately 2 μm to 8 μm , but above this value there appeared to be a decrease in plasticity index with increase in size. This relationship was again emphasised by melts Al6, NIA12, CRA12 and VA12 at 800°C (Figures 5.105. to 5.108.). However, no such relationship was evident at 850°C (figures 5.109. to 5.112.). The relationship at this temperature was essentially one of a rapid increase





5.104.

PLASTICITY INDEX ρ

1.5
1.0
0.5
0

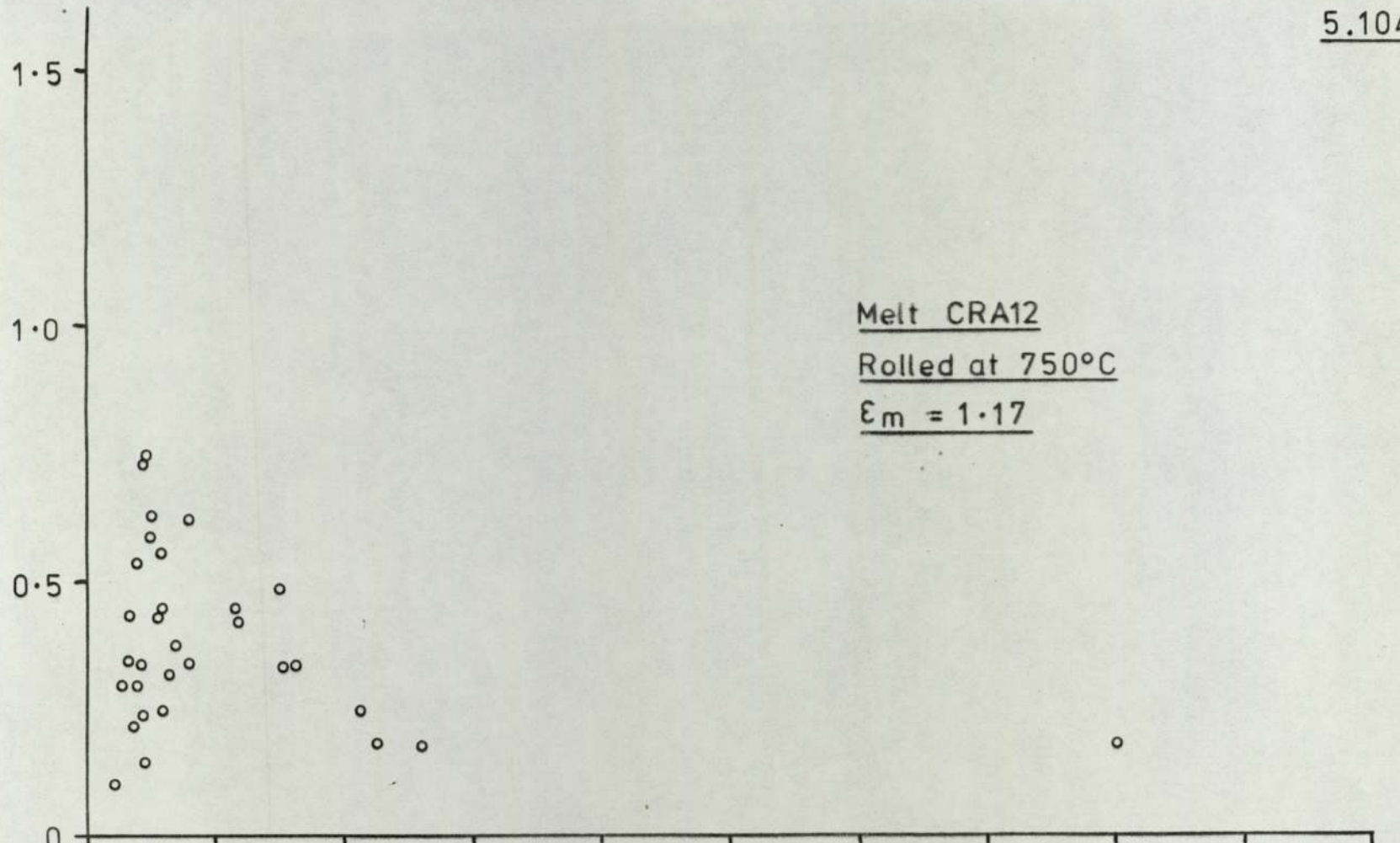
INCLUSION SIZE

50

\sqrt{ab} (μm)

100

Melt CRA12
Rolled at 750°C
 $\epsilon_m = 1.17$



PLASTICITY INDEX ρ

1.5

1.0

0.5

0

Melt A16.

Rolled at 800°C

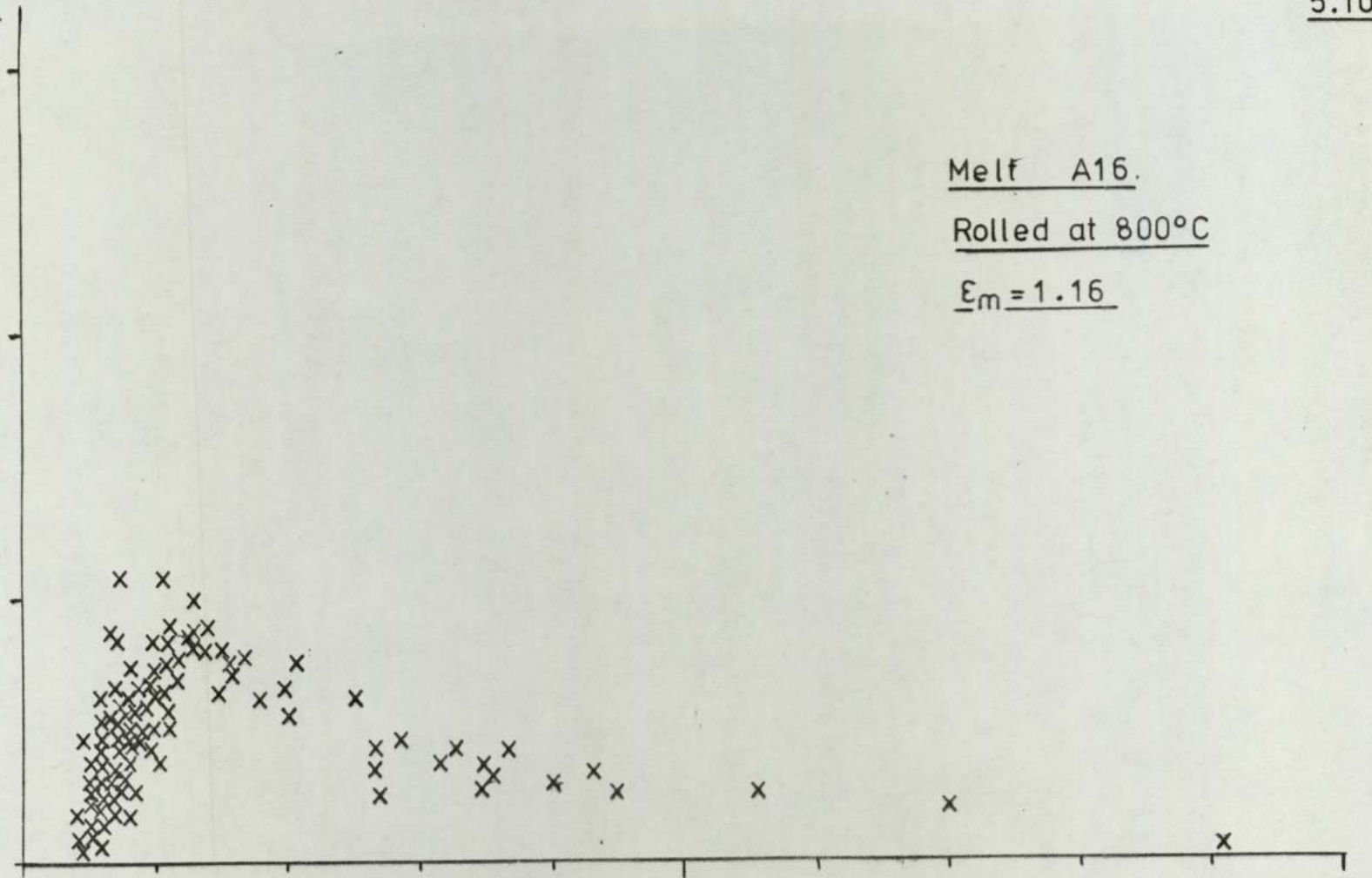
$\epsilon_m = 1.16$

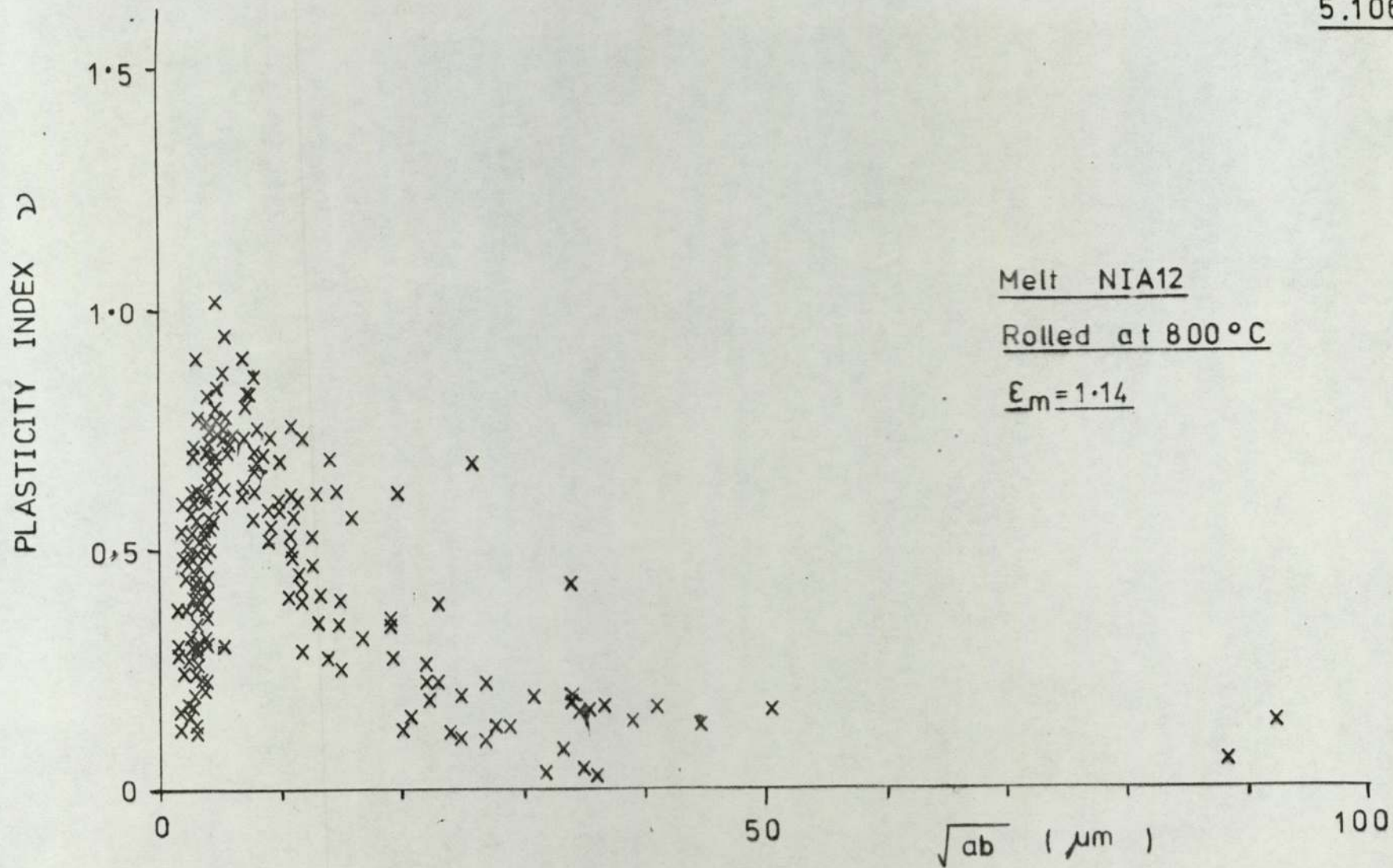
INCLUSION SIZE

50

\sqrt{ab} (μm)

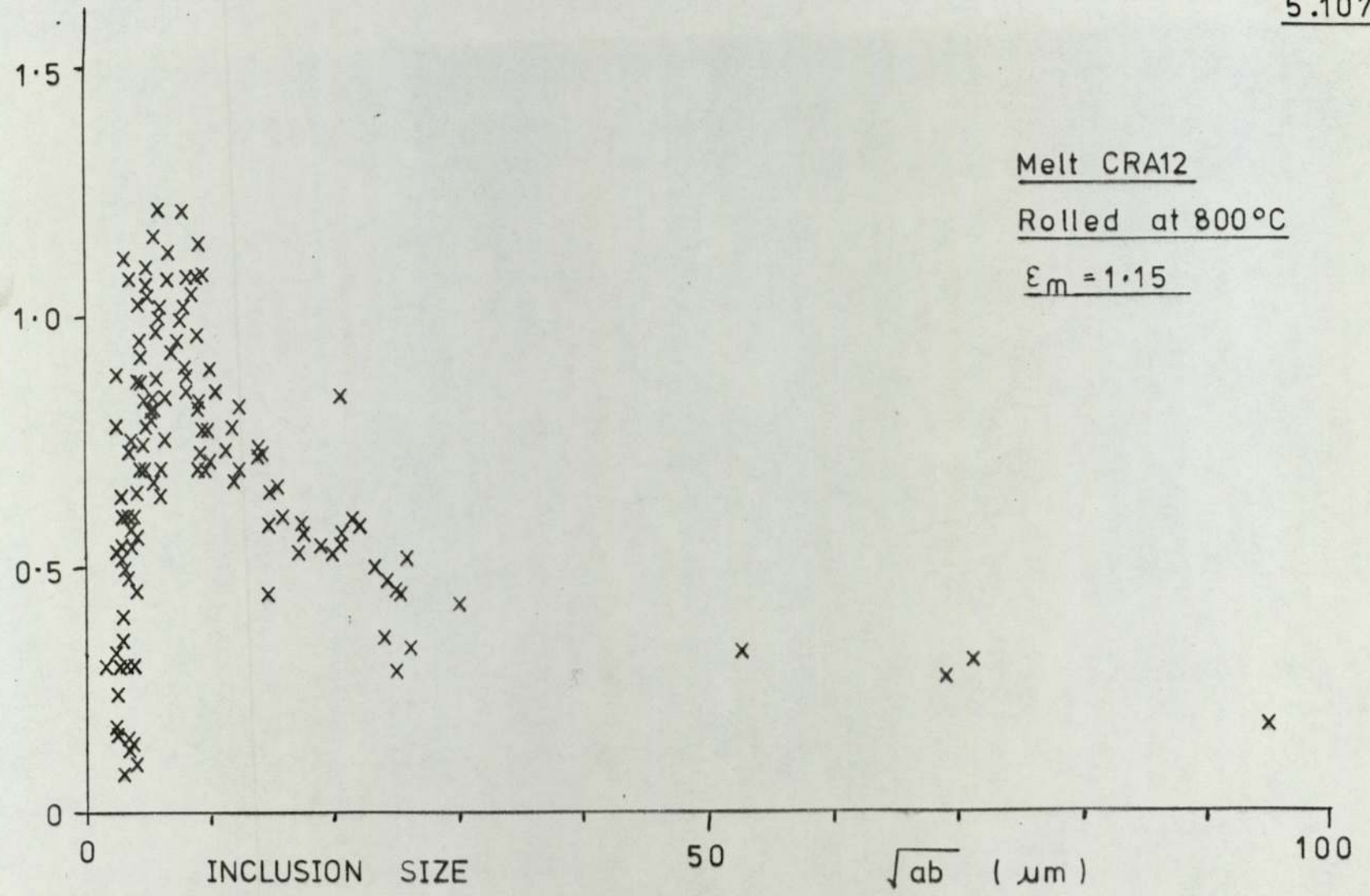
100

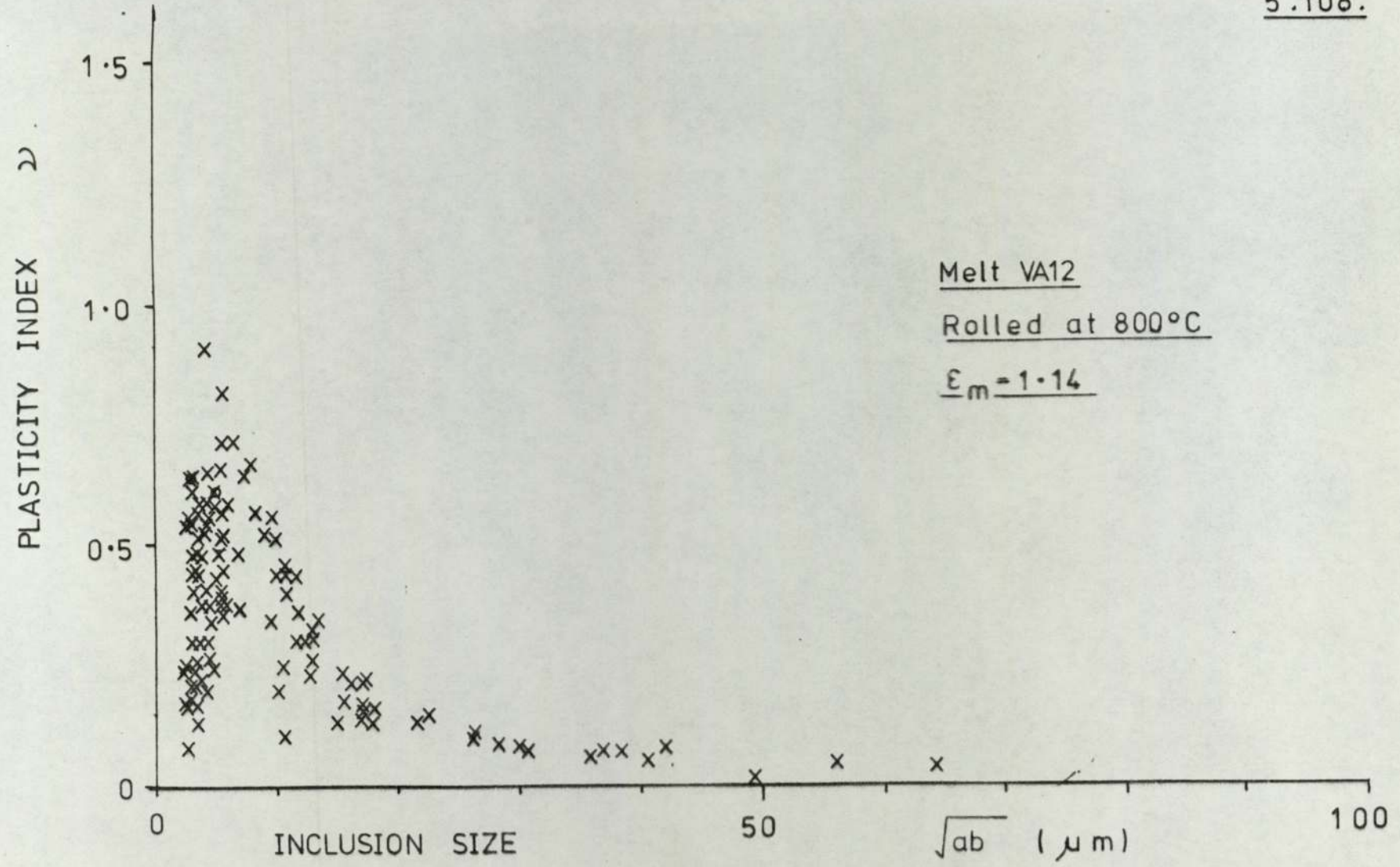




PLASTICITY INDEX ν

Melt CRA12
Rolled at 800°C
 $\epsilon_m = 1.15$





5.109.

PLASTICITY INDEX ρ

1.5
1.0
0.5
0

0

50

\sqrt{ab} (μm)

100

Melt A16.

Rolled at 850°C

$\epsilon_m = 1.16$

5.110.

PLASTICITY INDEX γ

1.5
1.0
0.5
0

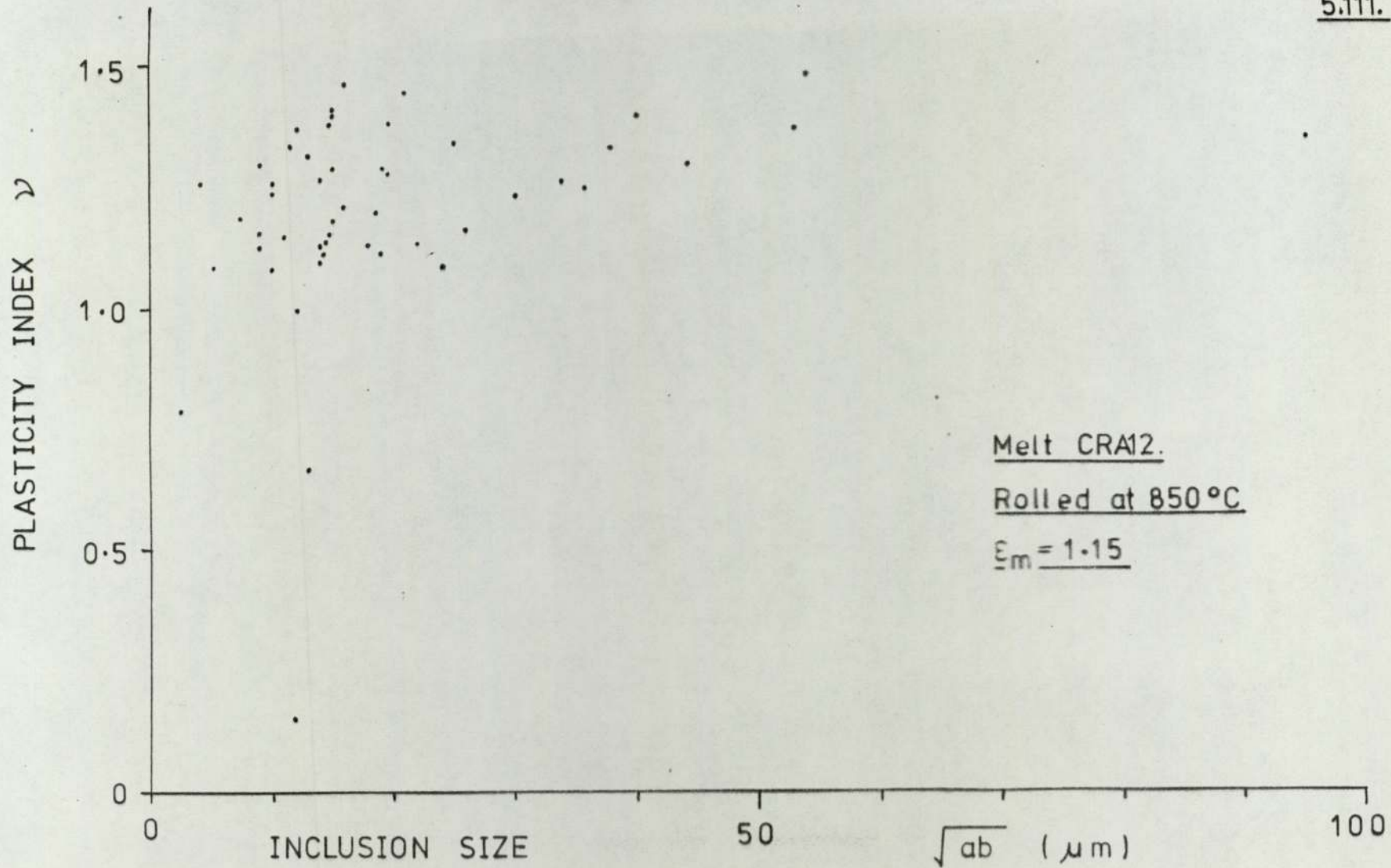
Melt NIA12
Rolled at 850°C
 $\epsilon_m = 1.12$

50

\sqrt{ab} (μm)

100

5.111.



5.112.

PLASTICITY INDEX ρ

1.5
1.0
0.5
0

INCLUSION SIZE

50

\sqrt{ab} (μm)

100

Melt VA12.

Rolled at 850 °C.

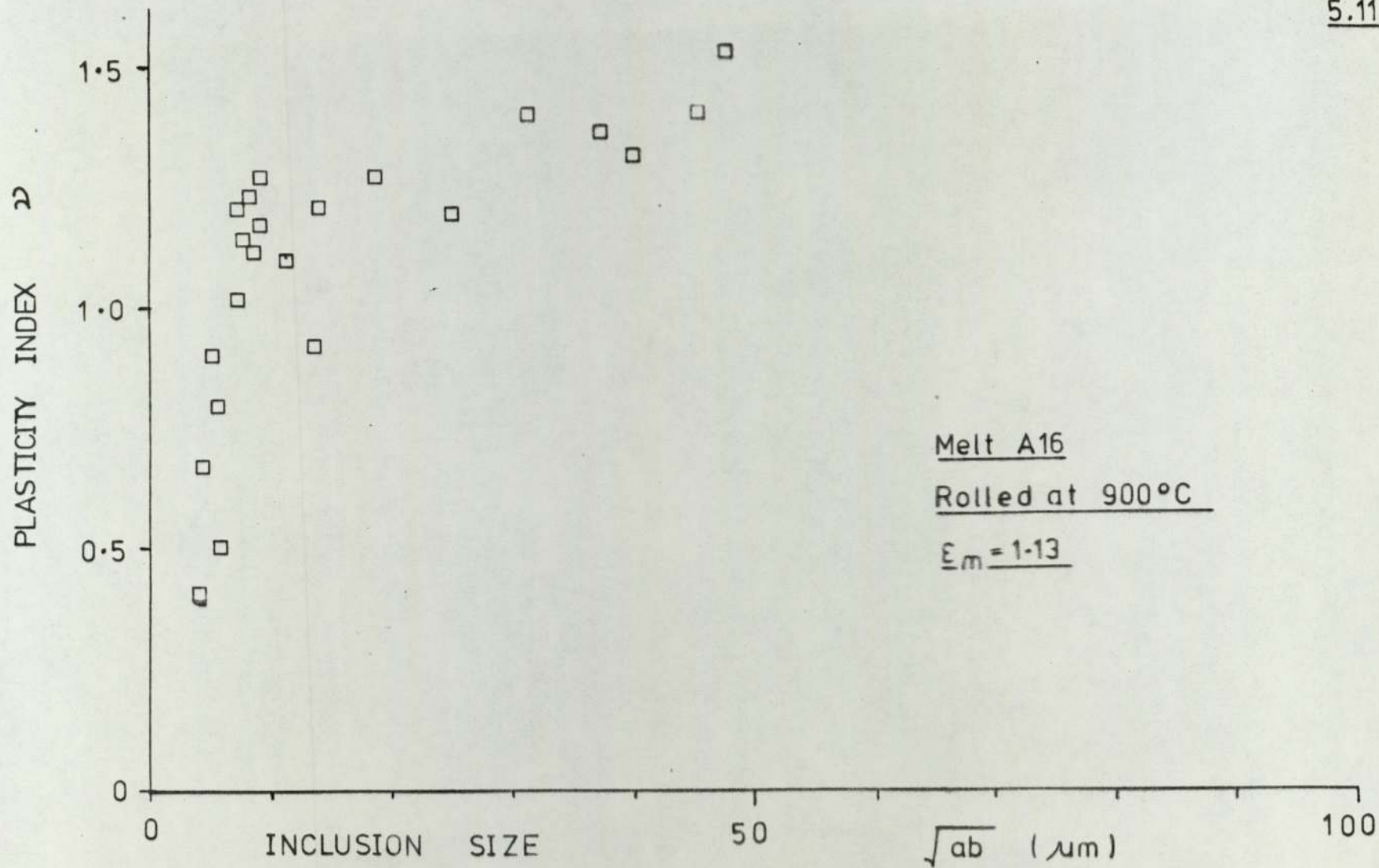
$\epsilon_m = 1.15$

in plasticity index over the range 2 - 10 μm , and a flattening out of the relationship with increased inclusion size. Similar relationships were also established at temperatures upto 1300 $^{\circ}\text{C}$ (figures 5.113. to 5.122.). However, at the higher rolling temperatures it did appear that the smaller inclusions exhibited slightly less plasticity, which may be accounted for by the break up and/or spheroidisation of the inclusions at these temperatures.

The inclusions of melt NI50Al2 did not show the same type of relationships as observed for melts Al6, NIA12, CRA12 or VA12. At the lower rolling temperatures i.e. 750 $^{\circ}\text{C}$ (figure 5.123.) and 800 $^{\circ}\text{C}$ (figure 5.124.) there appeared to be very little deformation over the entire size range. At 850 $^{\circ}\text{C}$ (figure 5.125.) an inclusion plasticity - size relationship generally appeared, whereby the larger inclusions exhibited greater deformability. There are however, a few apparently small inclusions which exhibited higher ('out of character') values of plasticity index, although these may be explained by an inclusion sectioning phenomenon. At 900 $^{\circ}\text{C}$ (figure 5.126.) there appeared to be an increase in plasticity index as size increased although there was a degree of scatter associated with the results. Once again there are two results which seem out of character, and these may also be due to the same sectioning phenomenon.

At 1000 $^{\circ}\text{C}$ (figure 5.127.) the plasticity index - size relationship was comparable with those obtained

5.113.



5.114.

PLASTICITY INDEX ν

1.5
1.0
0.5
0

0

50

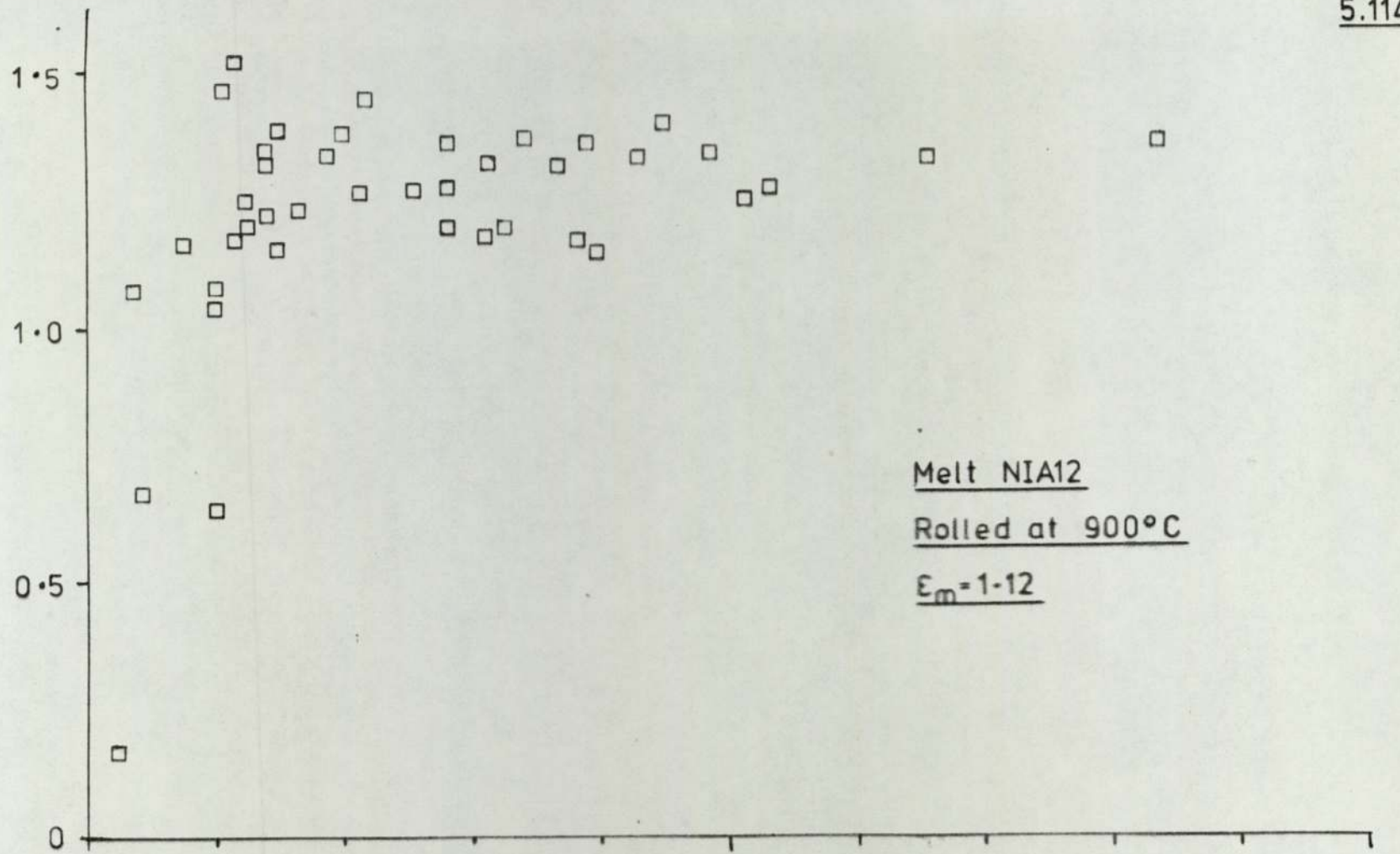
100

Melt NIA12

Rolled at 900°C

$\epsilon_m = 1-12$

\sqrt{ab} (μm)



5.115.

PLASTICITY INDEX γ .

1.5
1.0
0.5
0

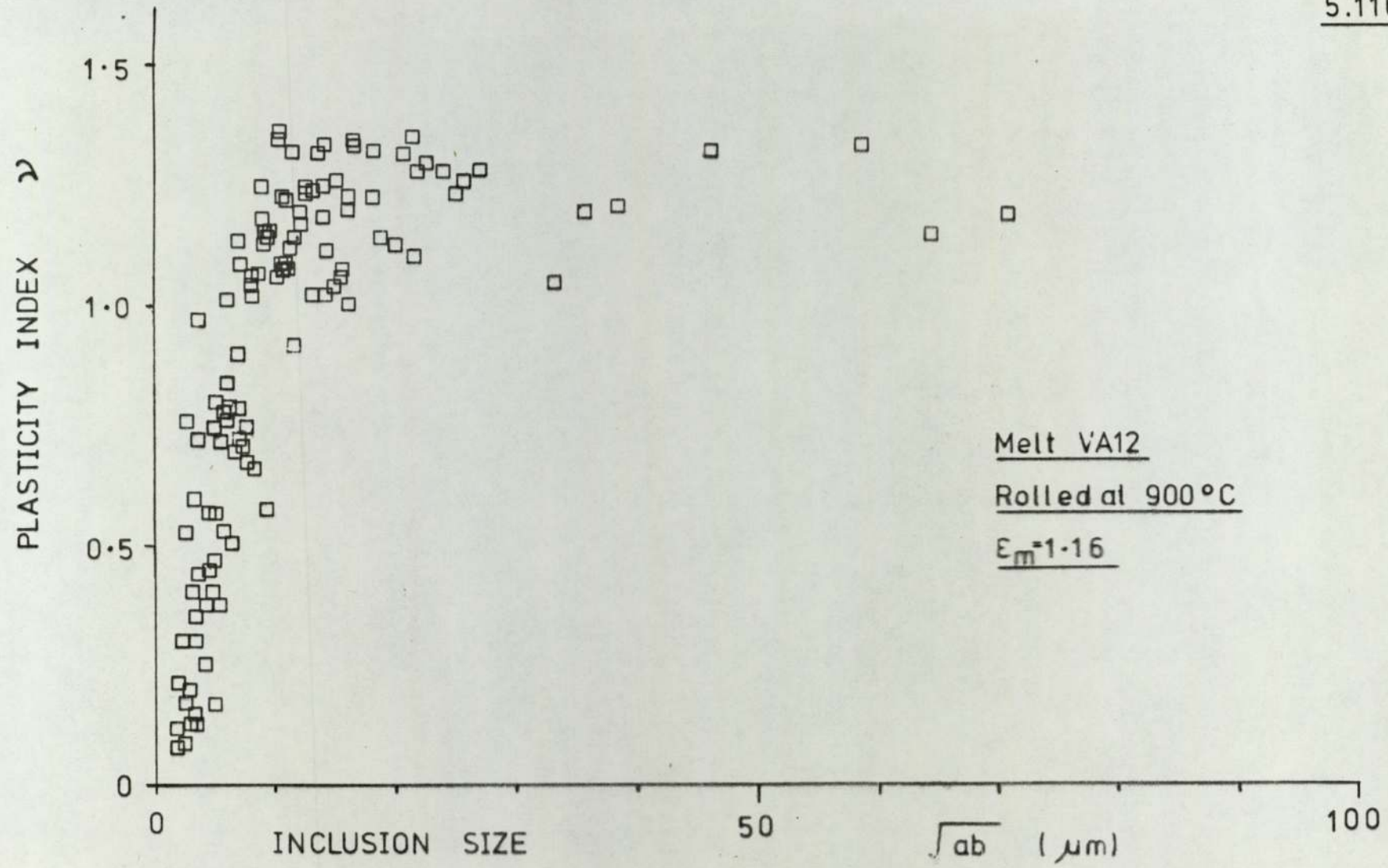
INCLUSION SIZE

50

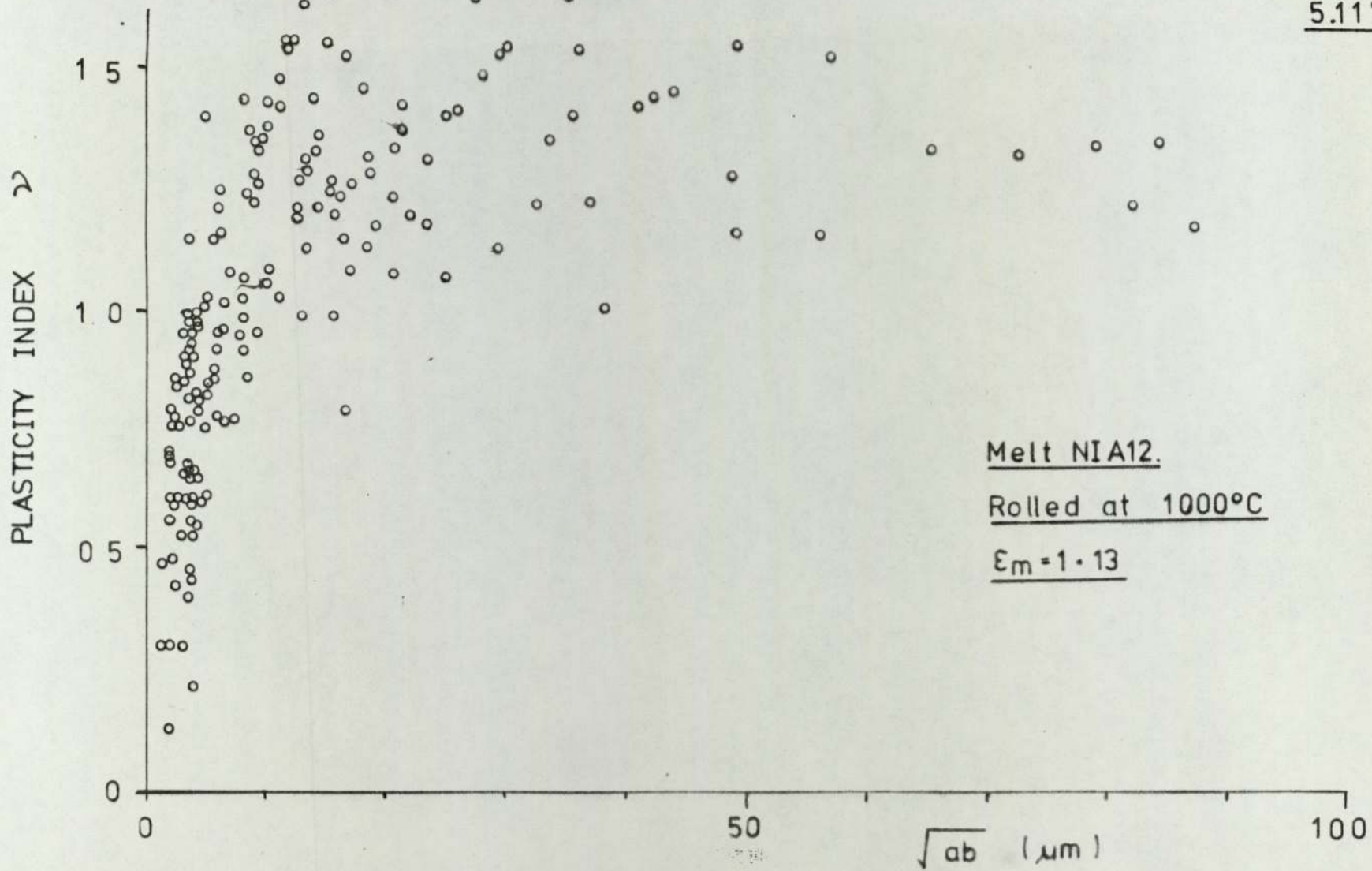
\sqrt{ab} (μm)

100

Melt CRA12
Rolled at 900°C
 $\epsilon_m = 1.16$



5.117.



5.118.

PLASTICITY INDEX γ

1.5
1.0
0.5
0

INCLUSION SIZE

50

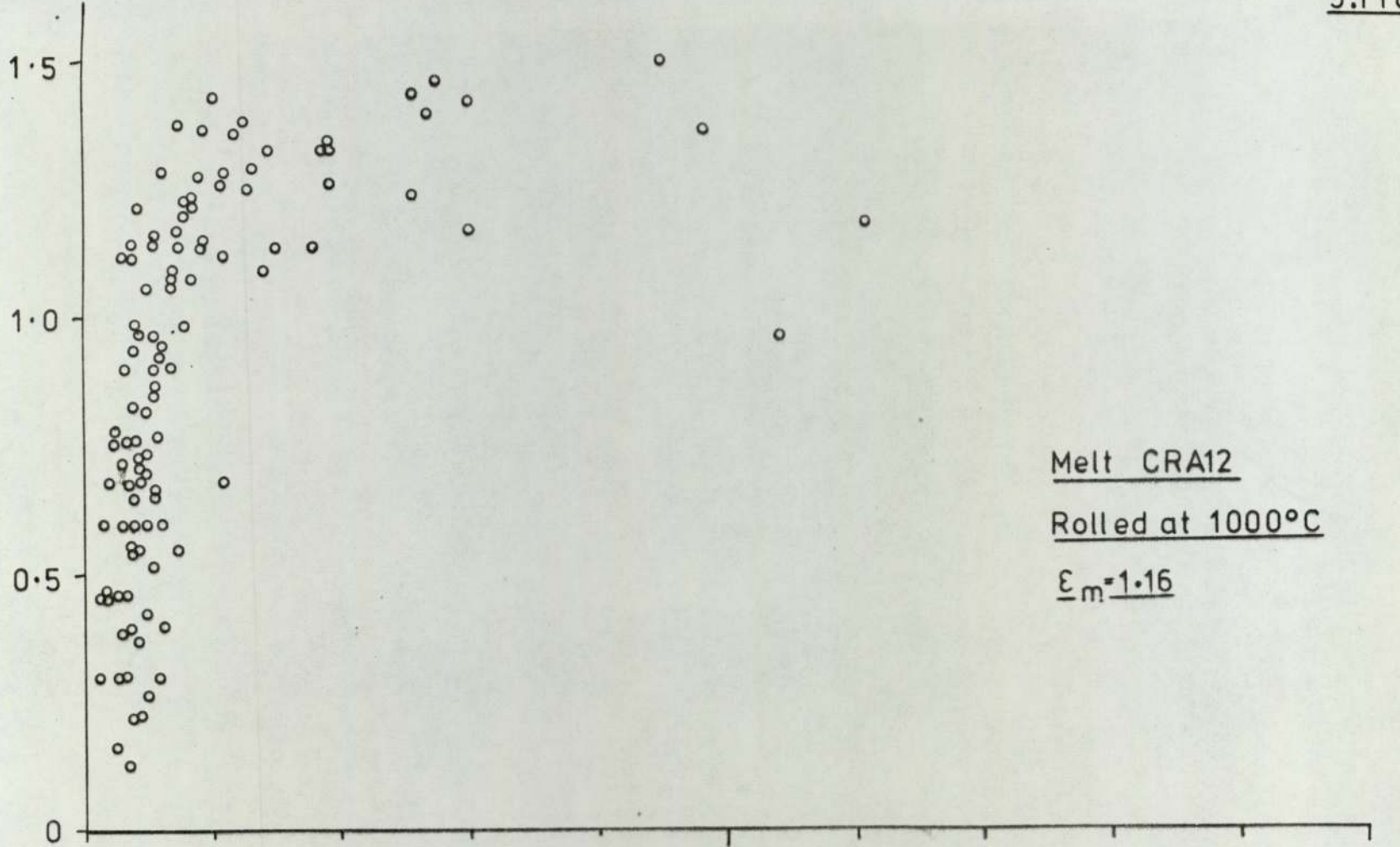
\sqrt{ab} (μm)

100

Melt CRA12

Rolled at 1000°C

$\epsilon_m = 1.16$



5.119.

PLASTICITY INDEX γ

1.5
1.0
0.5
0

INCLUSION SIZE

50

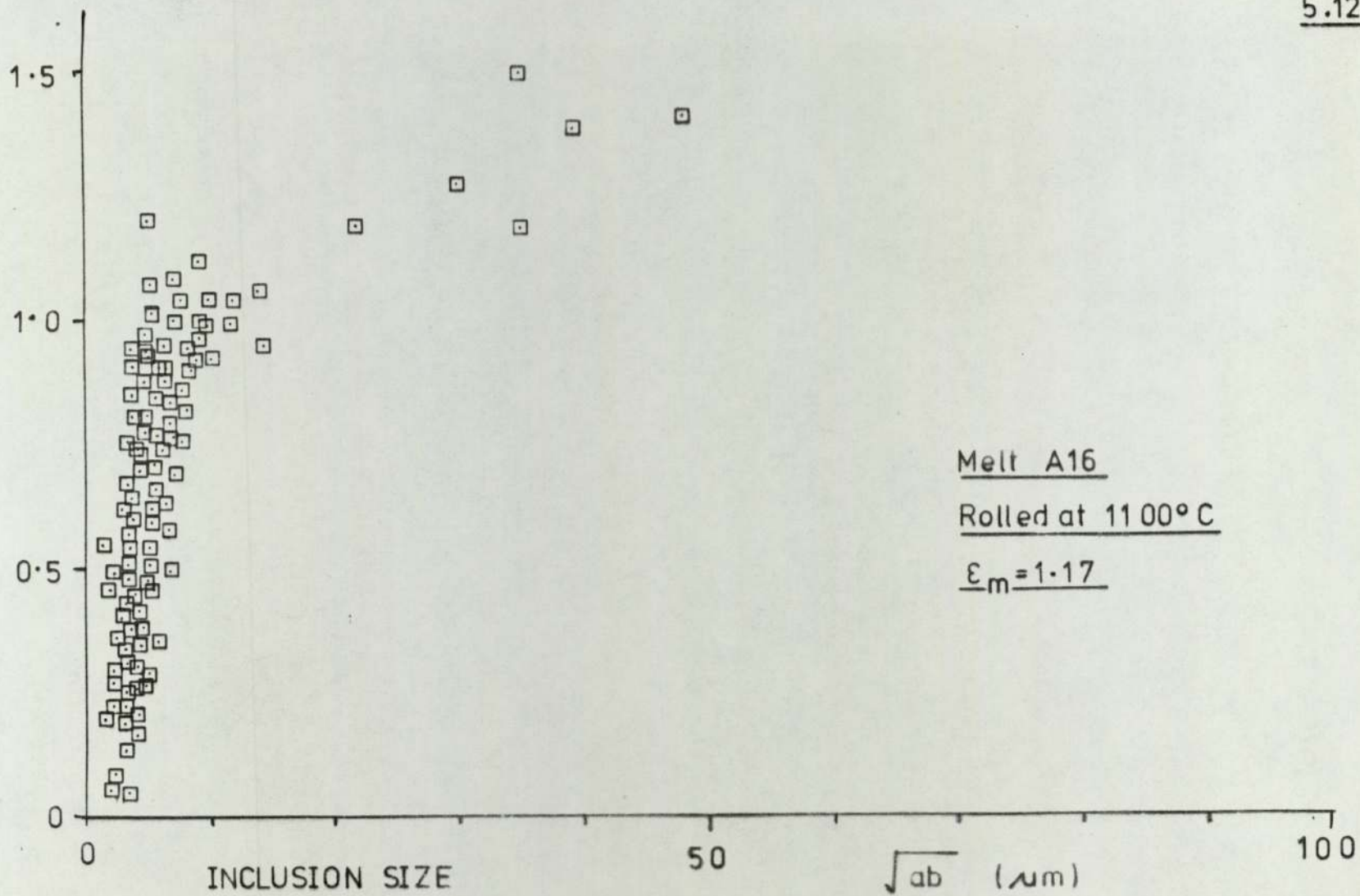
\sqrt{ab} (μm)

100

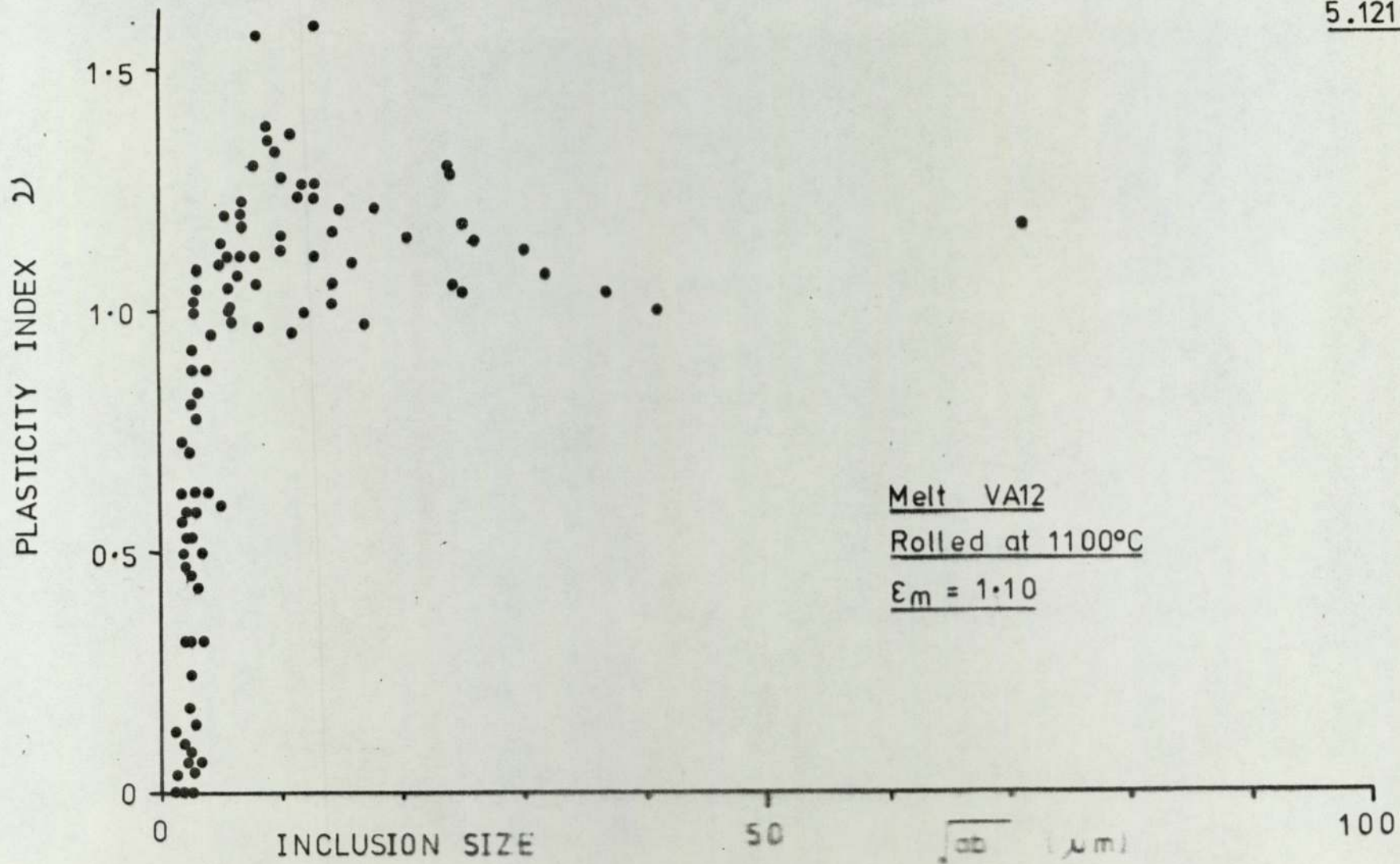
Melt VA12

Rolled at 1000°C

$\epsilon_m = 1.14$

PLASTICITY INDEX ρ 

5.121.



PLASTICITY INDEX ρ

1.5
1.0
0.5
0

Melt A16
Rolled at 1300°C
 $\epsilon_m = 1.13$

50

\sqrt{ab} (μm)

100

5.123.

PLASTICITY INDEX ν

1.5

1.0

0.5

0

0

50

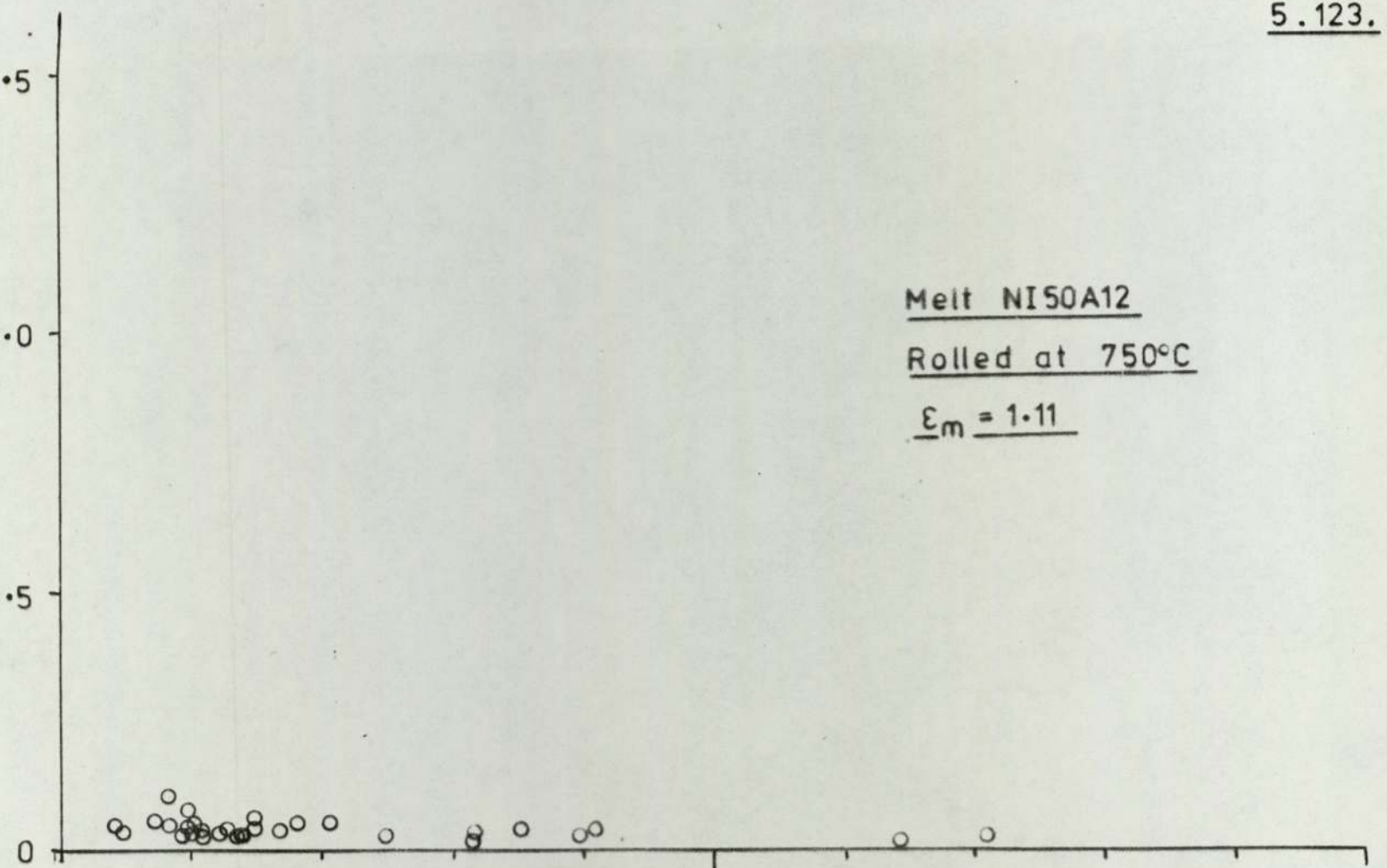
100

Melt NI50A12

Rolled at 750°C

$\epsilon_m = 1.11$

\sqrt{ab} (μm)



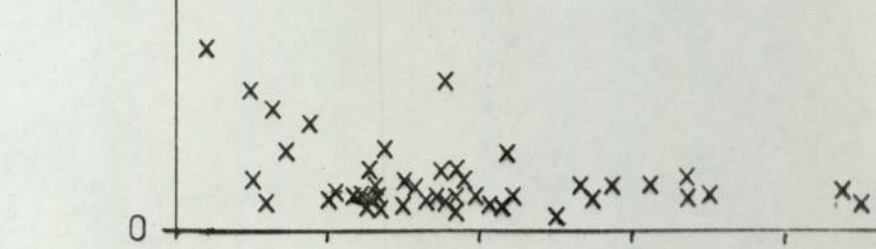
5.124.

PLASTICITY INDEX γ

1.5
1.0
0.5
0

Melt NI50A12
Rolled at 800°C
 $\bar{\epsilon}_m = 1.12$

0 50 \sqrt{ab} (μm) 100



5.125.

PLASTICITY INDEX ρ

1.5

1.0

0.5

0

0

50

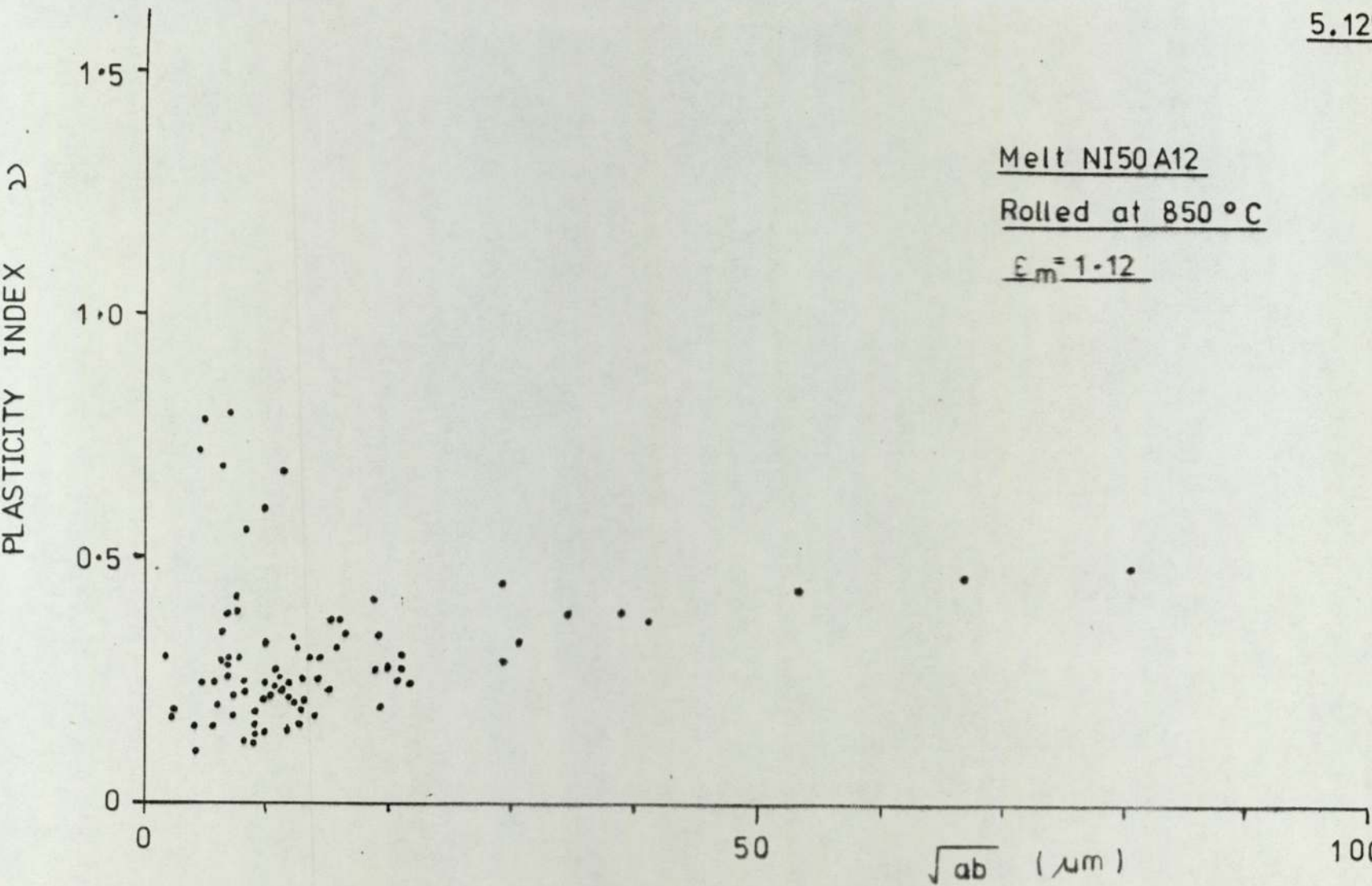
\sqrt{ab} (μm)

100

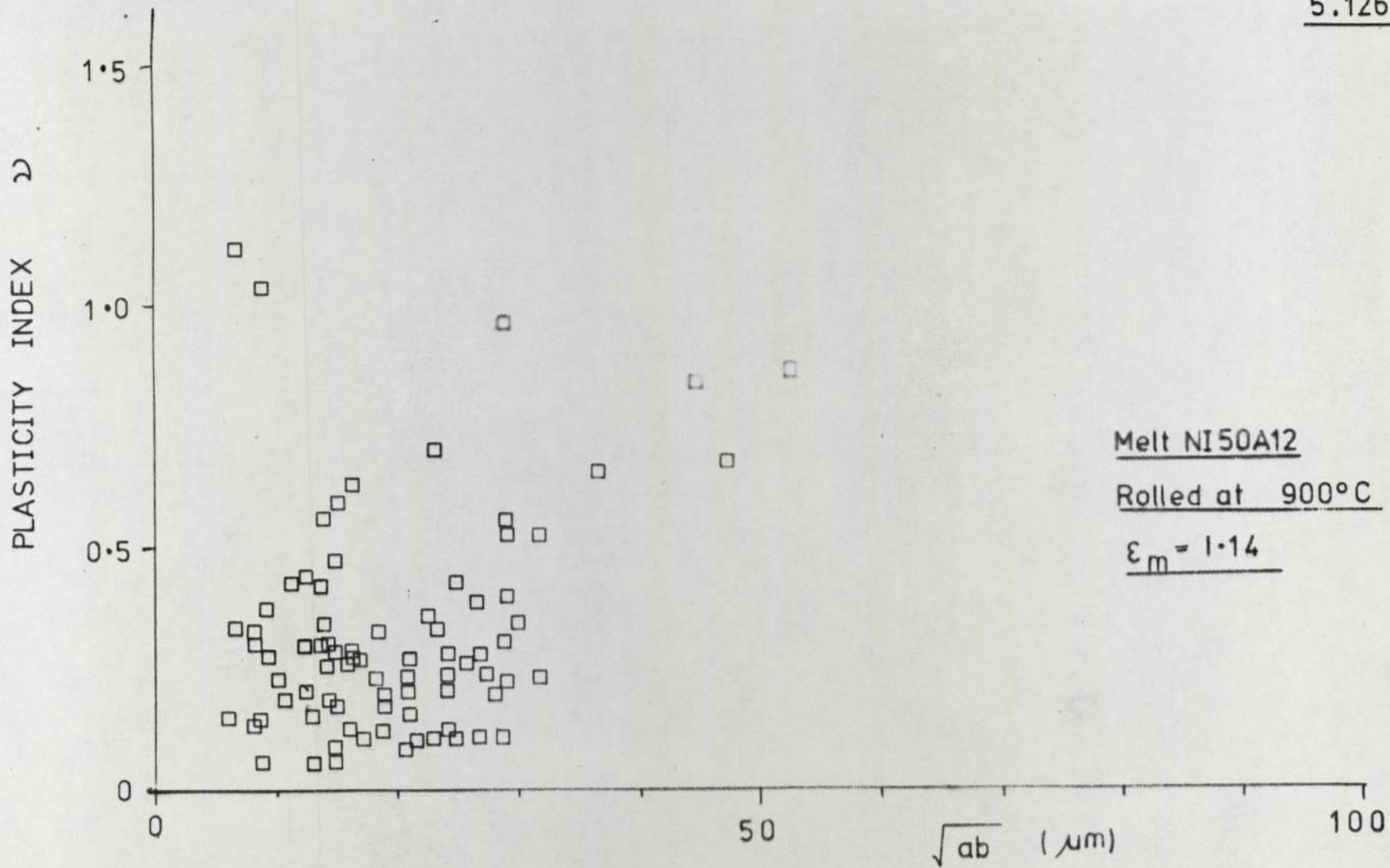
Melt NI50A12

Rolled at 850 °C

$\epsilon_m = 1.12$



5.126.



5.127.

PLASTICITY INDEX γ

1.5
1.0
0.5
0

0

50

100

Melt NI50A12

Rolled at 1000°C

$\epsilon_m = 1.13$

\sqrt{ab} (μm)

for melts Al6 etc. This relationship was again observed at 1100°C (figure 5.128.). However, it may be seen by comparing figures 5.127. and 5.128. that the general features of the curve at 1100°C have moved towards the deformation of smaller inclusions (i.e. 5 μm \rightarrow 3 μm) closer to the ordinate axis. This deformation at smaller sizes may be due to a compositional difference between large and small inclusions as has been observed (figure 5.12,) or perhaps it was an intrinsic property of inclusion size.

5.3.5.1. Summary of the general features of plasticity index versus size relationships, and the factors which influence them.

From the preceding results it may be seen that the variation in inclusion plasticity index with size is not simple and numerous factors seem to influence the behaviour pattern. It may be these factors which have led to the observations (92) that inclusion plasticity may in some instances increase with size, and in others decrease with size. Initially the factors which affect inclusions in general will be discussed followed later by the factors which influence the plasticity index - size relationships of the inclusions containing precipitates.

5.128.

PLASTICITY INDEX ρ

1.5
1.0
0.5
0

INCLUSION SIZE

50

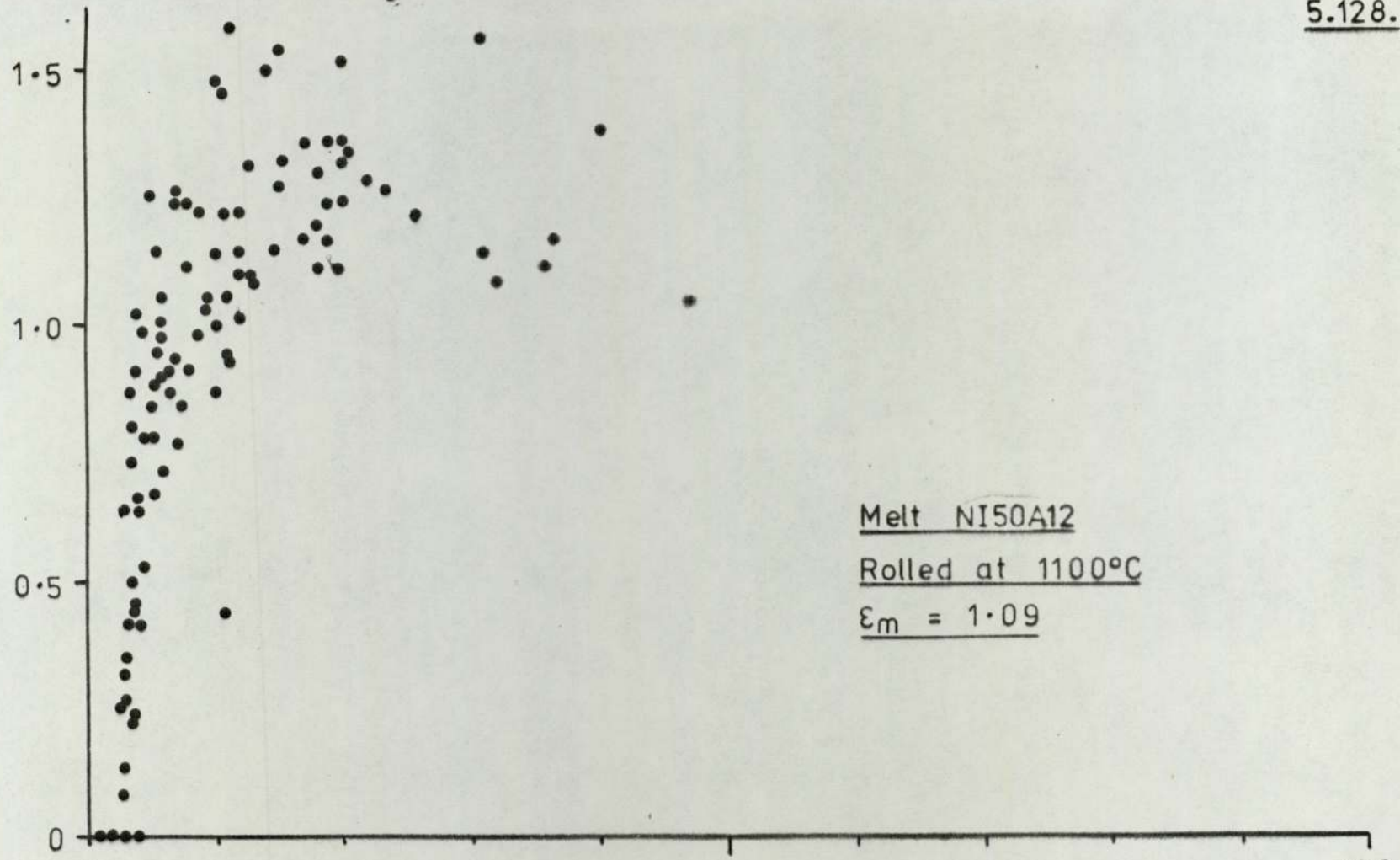
\sqrt{ab} (μm)

100

Melt NI50A12

Rolled at 1100°C

$\epsilon_m = 1.09$



5.3.5.1.1.

Inclusion composition.

It has been established that there was a variation in inclusion composition with size (section 5.1.2.) for any specific melt. Taking those melts which contained glassy inclusions at all rolling temperatures, table 5.8. shows that the smaller inclusions were richer on average in silica and less rich in alumina.

Table 5.8.

	10 μm inclusions		40 μm inclusions	
	% SiO_2	% Al_2O_3	% SiO_2	% Al_2O_3
A16	52	10	48	15
NIA12	54	10	48	19
CRA12	56	10	48	16
VA12	53	13	48	18
NI50A12	66	10	62	13

On the basis that the small inclusions were richer in silica it might be expected that these inclusions would have a slightly higher viscosity, and as such would be more difficult to deform at a given temperature. Only melt NI50A12 would appear to confirm such a behaviour. Here it was seen that the larger inclusions were the more deformable (figures 5.123. to 5.128.) and at higher temperatures the smaller inclusions sizes were

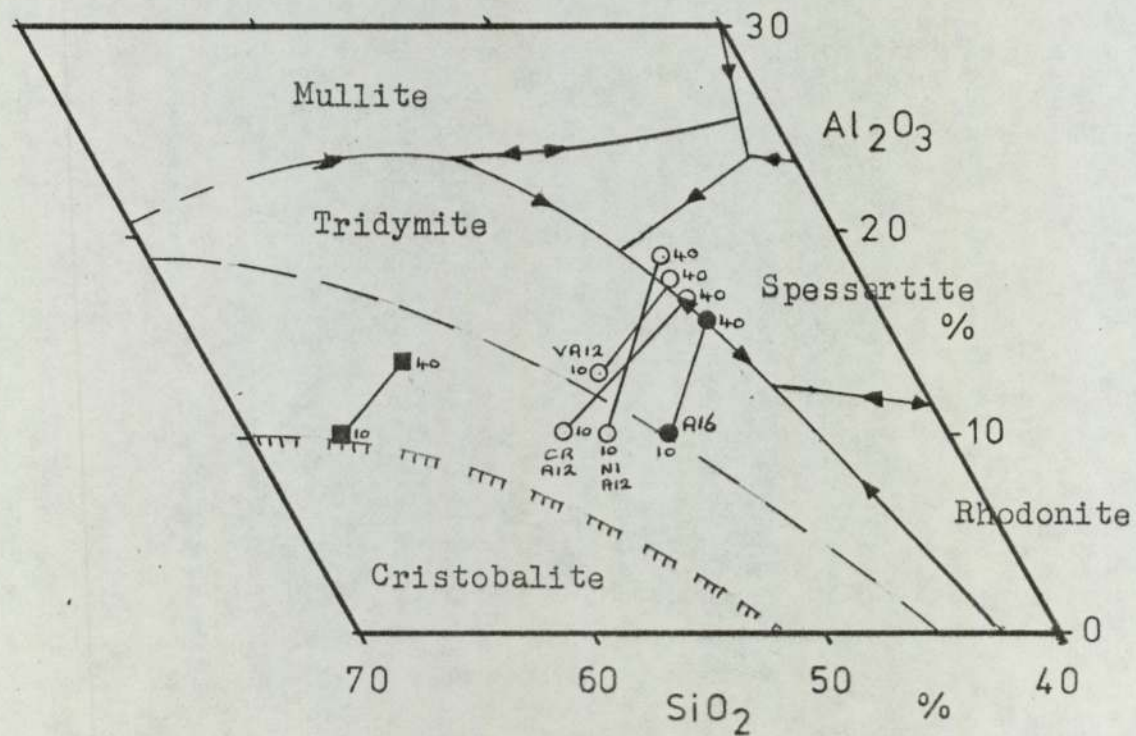
seen to deform.

The other melts i.e. Al6, NIA12, CRA12 and VA12 showed that at temperatures which were below the α/γ phase change, (which would complicate the situation) it was the smaller inclusions (greater than $5 \mu\text{m}$) which deformed the most (figures 5.104. to 5.108.). This would appear to represent a contradiction to any proposed viscosity phenomenon. Figure 5.129. indicated that the inclusion compositions expressed in table 5.8 cross a eutectic trough in the $\text{MnO} - \text{SiO}_2 - \text{Al}_2\text{O}_3$ diagram.

At first this was thought to be a possible explanation to the peak in the plasticity index - size figures. However, the work of other authors (35,102) has expressed that it is not the liquidus or solidus temperatures which influence the deformability of glasses, but the glass viscosity.

Again with respect to composition it was thought that these smaller inclusions may have contained manganese sulphide, or even have been MnS. However, although it was established that the presence of sulphur in the inclusion phases increased with a decrease in size (section 5.1.2.3) this increase was only detectable at sizes below $5 \mu\text{m}$. Since it was known that MnS inclusions become progressively more deformable at lower temperatures (109) the presence of deformable small inclusions at even lower rolling temperatures would have indicated that MnS inclusions were probably there. However, at these lower temperatures

Variation of inclusion composition with size
for the glassy inclusions of melts Al₆Ni₅OAl₂, NI-CR-V-(Al₂)



5.129

small inclusions were found to be non-deformable. Since it appeared that compositional differences could not account for this plasticity index peak, a theory based upon another variable has to be developed.

5.3.5.1.2. Adiabatic heating effects.

Since there is a temperature rise associated with the rolling process (103) it would be expected that this temperature rise would be passed onto the inclusions and in particular to those inclusions of small volume. In the case of the large inclusions it was probable that the temperature rise was transmitted to the surface layers only. It would also seem reasonable that this effect would be more noticeable at the foot of the transition curve, since a small change in temperature would cause a rapid change in viscosity.

If it was assumed that the apparent flow stress of the inclusion is given by:

$$\sigma_A = \eta \dot{\epsilon}$$

and that the rolling temperature was such that the viscosity of the inclusions was at $10^{7.5} \text{ Nm}^{-2}\text{S}$ (i.e. $10^{8.5}$ Poise) and the strain rate 20S^{-1} then:

$$\sigma_A \sim 20 \times 10^{7.5} \text{ Nm}^{-2}$$

Similarly if we assume that the matrix strength σ_m was 200MNm^{-2} (126)

$$\text{then } \frac{\sigma_{Ai}}{\sigma_m} = \frac{20 \times 10^{7.5}}{200 \times 10^6} = 3$$

If however the small inclusions are effectively at a temperature 10°C higher than the value of η may have dropped to a value of $10^7 \text{ Nm}^{-2}\text{s}$, in which case

$$\frac{\sigma_{ai}}{\sigma_m} = 1$$

Using a relationship of the type proposed by Gove and Charles (109) i.e.

$$\nu = 2 - \left(\frac{\sigma_i}{\sigma_m}\right) \quad 0 \leq \nu \leq 2$$

then the larger inclusions would not be deformable, whereas the smaller ones would have a plasticity index of unity.

5.3.5.1.3.

The ferrite to austenite

transformation.

It was mentioned earlier that in some of the plasticity index - size diagrams there was a noticeable lack of small deformable inclusions at rolling temperatures around $850 - 900^{\circ}\text{C}$. From table 4.11 and figures 5.130. and 5.131. it may be seen that the number of deformable inclusions in the range $1 - 20 \mu\text{m}$ was dependent upon the rolling temperature. These figures indicated that there was a dip in the number of deformable inclusions in the range $850 - 900^{\circ}\text{C}$, which is thought to be due to the ferrite - austenite phase transformation. The region $850 - 900^{\circ}\text{C}$ may be seen to be the ferrite plus austenite region of the iron-

Fig. 5.130

Variation in number of deformable inclusions with rolling temperature.

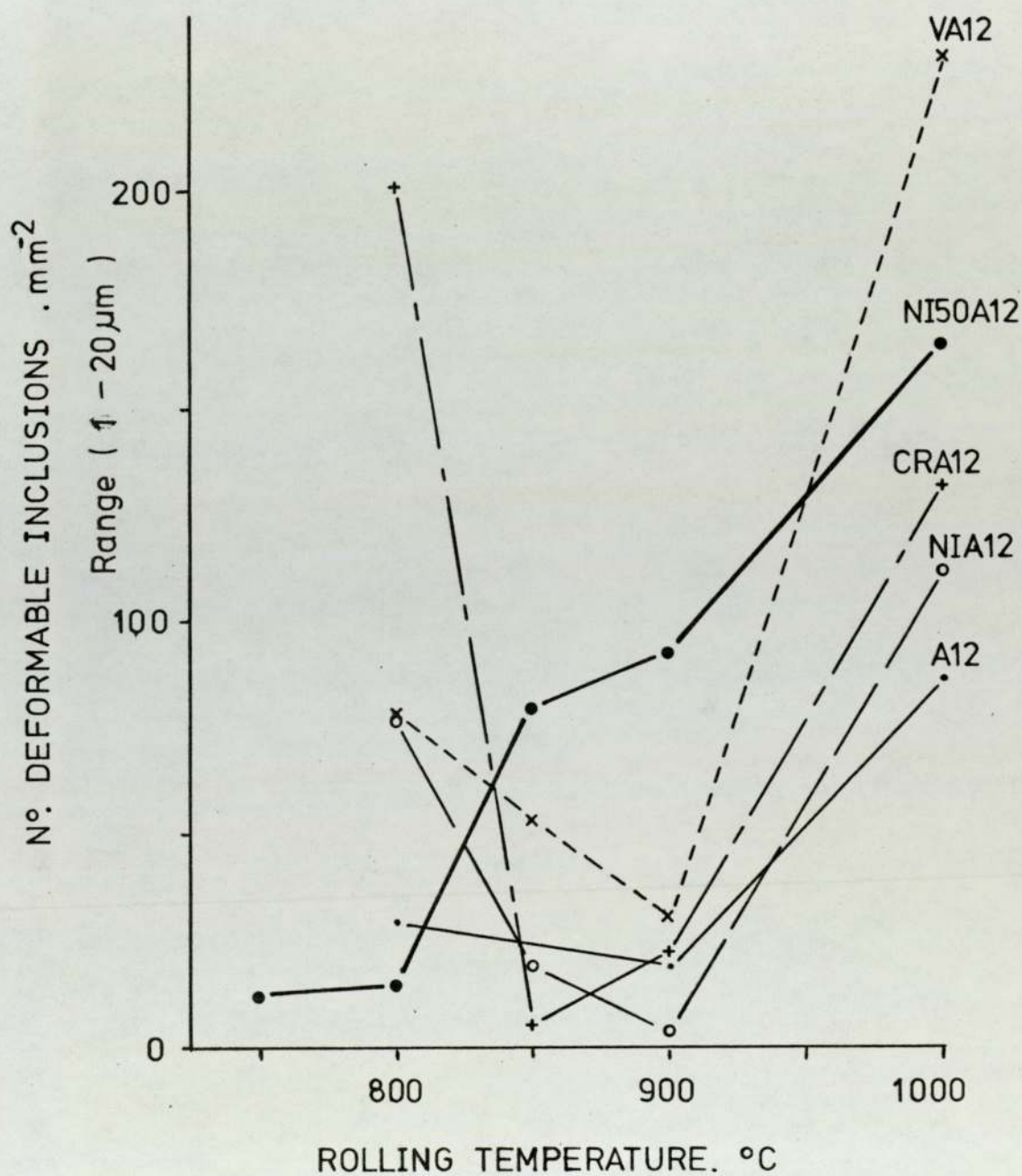
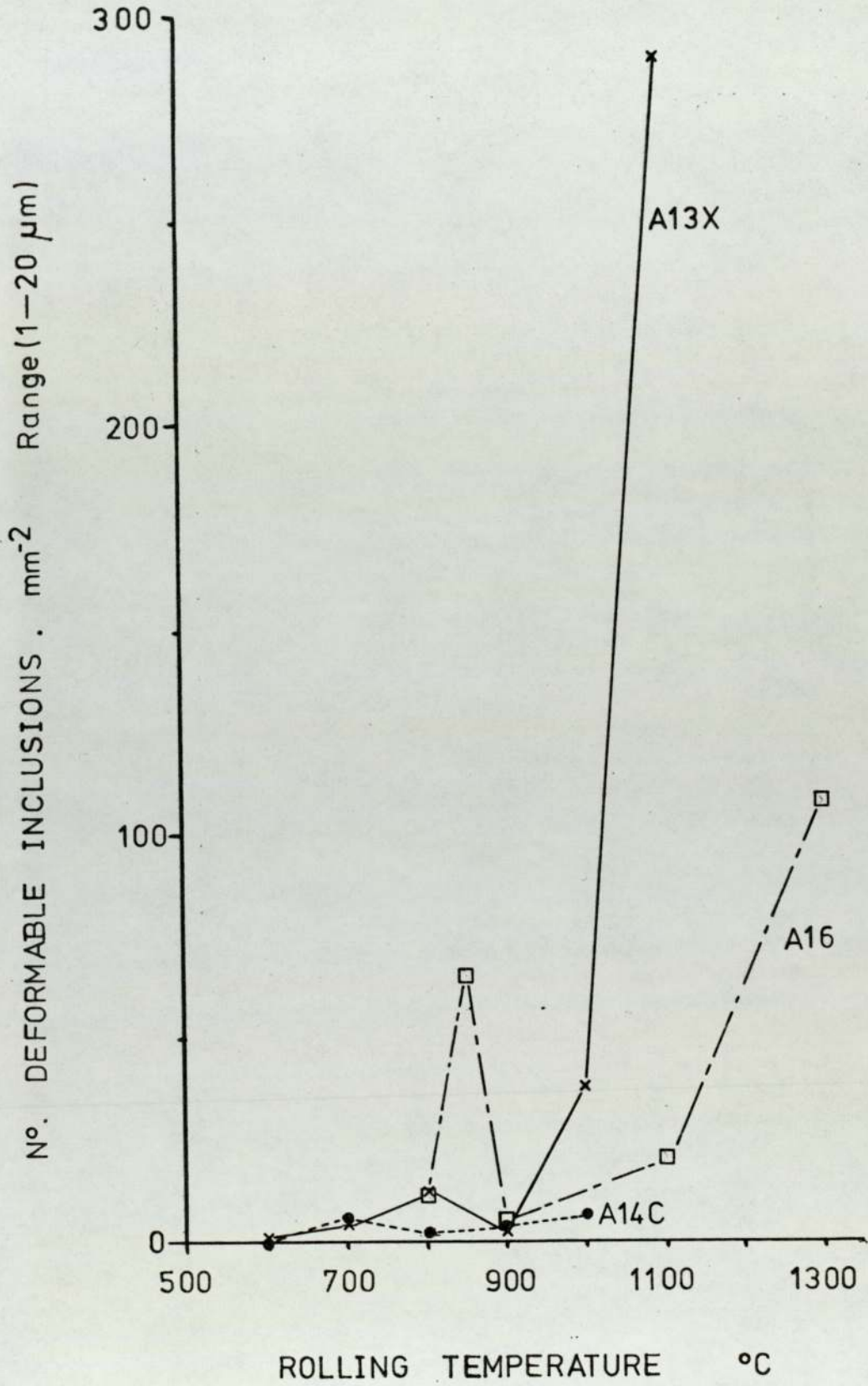
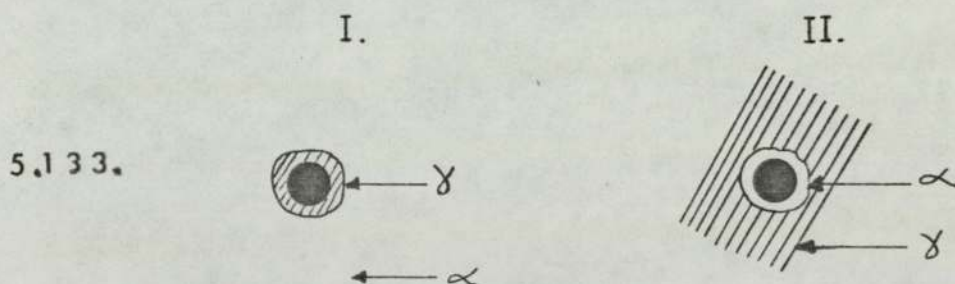


Fig. 5-131



carbon equilibrium diagram at the 0.005% to 0.01% C (figure 5.132.) used in these experiments.

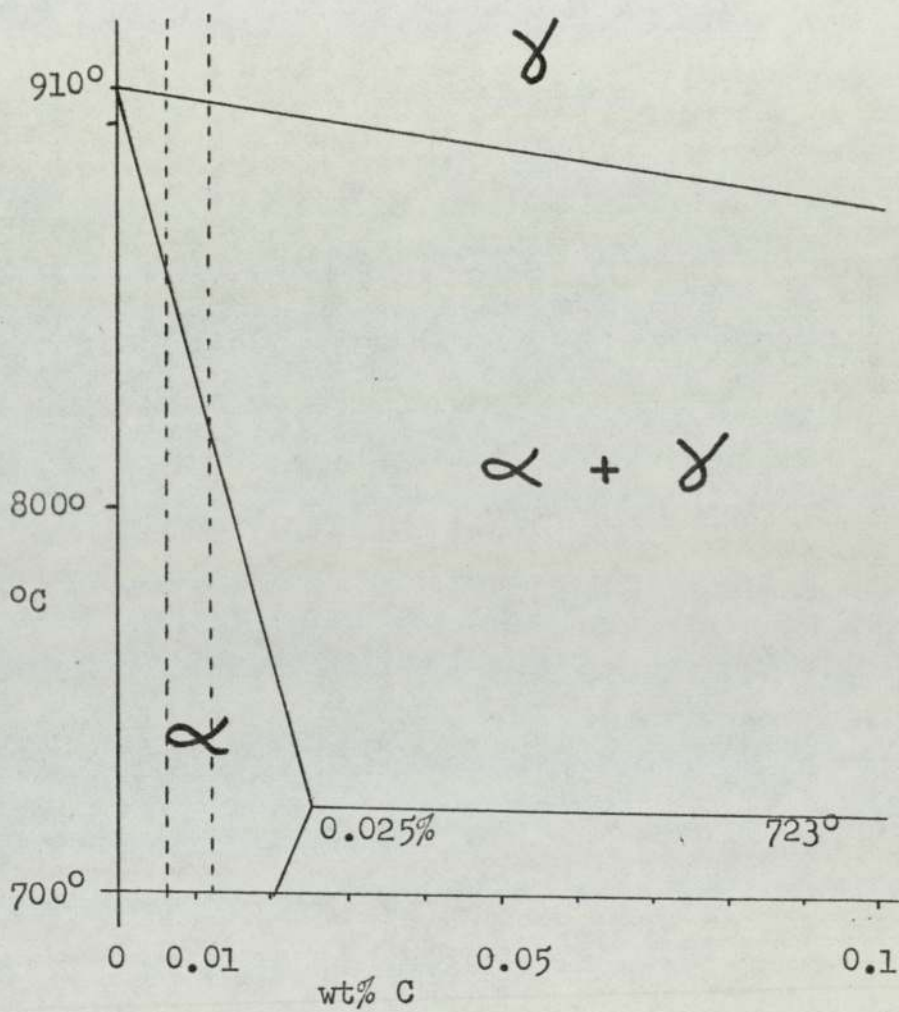
It has previously been shown that inclusions act as preferential nucleation sites for the precipitation of a second phase (107). Since the inclusions in these melts were rolled in and around the ferrite/austenite range it may be expected that either ferrite (α) or austenite (γ) nucleated and grew around the inclusions. The small inclusions may have effectively been enveloped by the precipitated material. i.e.



The possible influence of this envelope of material upon the inclusion deformation must therefore be assessed.

Case I

If an austenite envelope developed around an inclusion then the inclusion would be protected from deformation by the presence of a hard shell which resisted deformation. At the ferrite/austenite transition temperature the austenite is approximately twice as hard as the

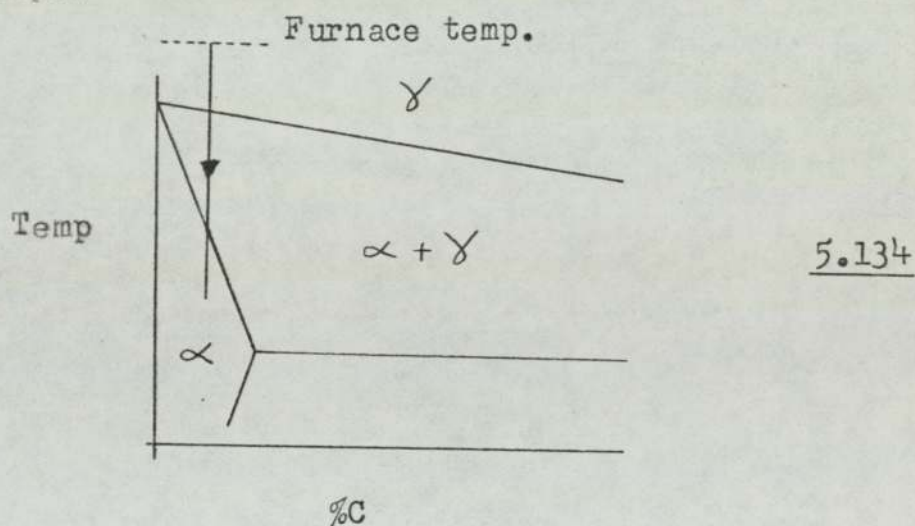
5.132

Part of the Fe - C equilibrium diagram
at the 0.01% level of carbon present in
this work.

ferrite. From the work of other authors (¹⁰⁹/₁₁₂), when the ratio of the inclusion (or second phase) strength is twice that of the matrix there is very little deformation of the inclusion of second phase.

Case II

If there is a ferrite envelope around the inclusion which is the more likely case since the material was cooling from the furnace to the rolling temperature, then the inclusion is surrounded by a soft ferritic envelope.



The ratio of the flow stresses ($\frac{\sigma_{\alpha}}{\sigma_{\gamma}}$) is approximately 0.5 and as such would infer that the ferrite envelope would deform more easily. There is now a situation where both the envelope and inclusion have the ability to deform. Whether or not the inclusion deforms is more complicated and will depend upon the transfer of stress to the inclusion, and the ratio of the inclusion to ferrite strengths. However, the bulk of the evidence from the present work suggests that in

the transformation zone the number of deformed inclusions decreased. In order to test whether or not it was the α/δ transformation which caused the fall in the number of deformable inclusions, a melt was cast which contained inclusions that were in a fully austenitic matrix at all rolling temperatures. This cast was a 50%Fe - 50%Ni alloy, and from the results contained in figure 5.130. it may be seen that there was an increase in the number of deformable inclusions as the rolling temperature was increased. No dip in the results occurred in the region 850 - 900°C.

It may be further noted that the melts which contained the alloying additions (i.e. melts NI50Al2, NIA12 CRA12 and VA12) had a greater number of deformable inclusions than were present in the unalloyed melts i.e. melts Al2 and Al6 which contained inclusions of similar composition. This may be attributed to these alloying elements strengthening the matrix.

It may also be seen from figure 5.131. that inclusion composition influenced the number of deformable inclusions. Melts Al3X and Al6 appeared to contain more deformable inclusions than melt Al4C at temperatures above 700°C. This was assumed to be due to the precipitation of second phases within the inclusions. Although precipitation would not be detected in the small inclusions of melt Al4C they often showed signs of opaqueness. This opaqueness may have been due to fine irresolvable precipitates.

5.3.5.1.4.

The break up of large inclusions.

As was suggested earlier, one of the reasons why the plasticity index at high temperatures and large inclusion drops, may be due to the break up of these larger inclusions.

Plate 4.35, shows what appears to be a large fluid inclusion breaking up into several smaller fragments. If by some chance this break up occurs at rolling passes prior to the one at which inclusion measurements were made, then there may be a large distance separating them. If this is the case then these inclusions may not be recognised as being the disseminated parts of larger inclusions, and may be measured as inclusions in their own right. At high magnifications i.e. X1000 this error may easily occur. (A case for the metallographer always firstly examining his specimens at low magnifications).

An example of the influence an inclusion breaking up upon the plasticity index - size effect is shown below i.e.

Assuming that plane strain occurs, and an inclusion which if it did not break up would have a plasticity index of $\nu = 1.5$ at a matrix strain $\epsilon_m = 1.2$ then inclusion strain is given by

$$\epsilon_i = \nu \epsilon_m$$

$$\therefore \epsilon_i = 1.8$$

Now under plane strain conditions

$$\epsilon_i = \frac{1}{2} \ln \frac{a}{b}$$

where a and b are the major and minor axes respectively

$$\left(\frac{a}{b}\right) = e^{2\epsilon_i} = e^{3.6}$$

$$\left(\frac{a}{b}\right) = 36.6$$

Again assuming plane strain

$$\epsilon_i = \ln \frac{a}{D}$$

where D is the original diameter and is also equal to \sqrt{ab}

Assuming that the original diameter was $100 \mu\text{m}$ then

$$a = 100 e^{\epsilon_i}$$

i.e. $a = 100 \times 6.05 = 605 \mu\text{m}$

If $a = 605 \mu\text{m}$ and $\left(\frac{a}{b}\right) = 36.6$

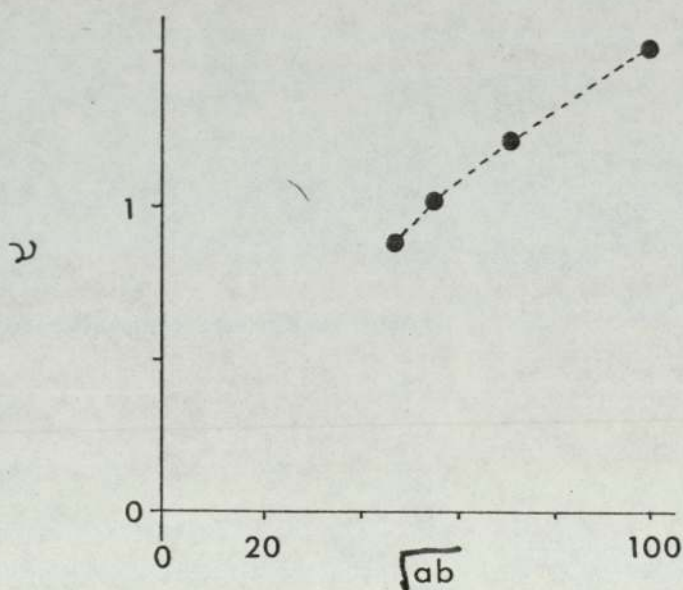
the minor axis $b = 16.5 \mu\text{m}$

Now if we assume that it broke into three parts of length $\frac{a}{2}$, $\frac{3a}{10}$ and $\frac{a}{5}$ then the resultant apparent sizes and plasticity indices are given below.

Table 5.9.

Major axis	$\frac{a}{2}$	$\frac{3a}{10}$	$\frac{a}{5}$	a
\sqrt{ab}	71 μm	55 μm	45 μm	100
ϵ_i	1.45	1.20	1.00	1.8
ν	1.21	1.00	0.83	1.5

These figures indicate that as the size of the inclusions increase so does the plasticity index viz figure 5.135.



However, it is probable that the value of relative plasticity index would be higher, since the ends where the breaks occurred would develop sharper features and become more streamlined.

5.3.5.1.5. inclusions.

The spheroidisation of deformed

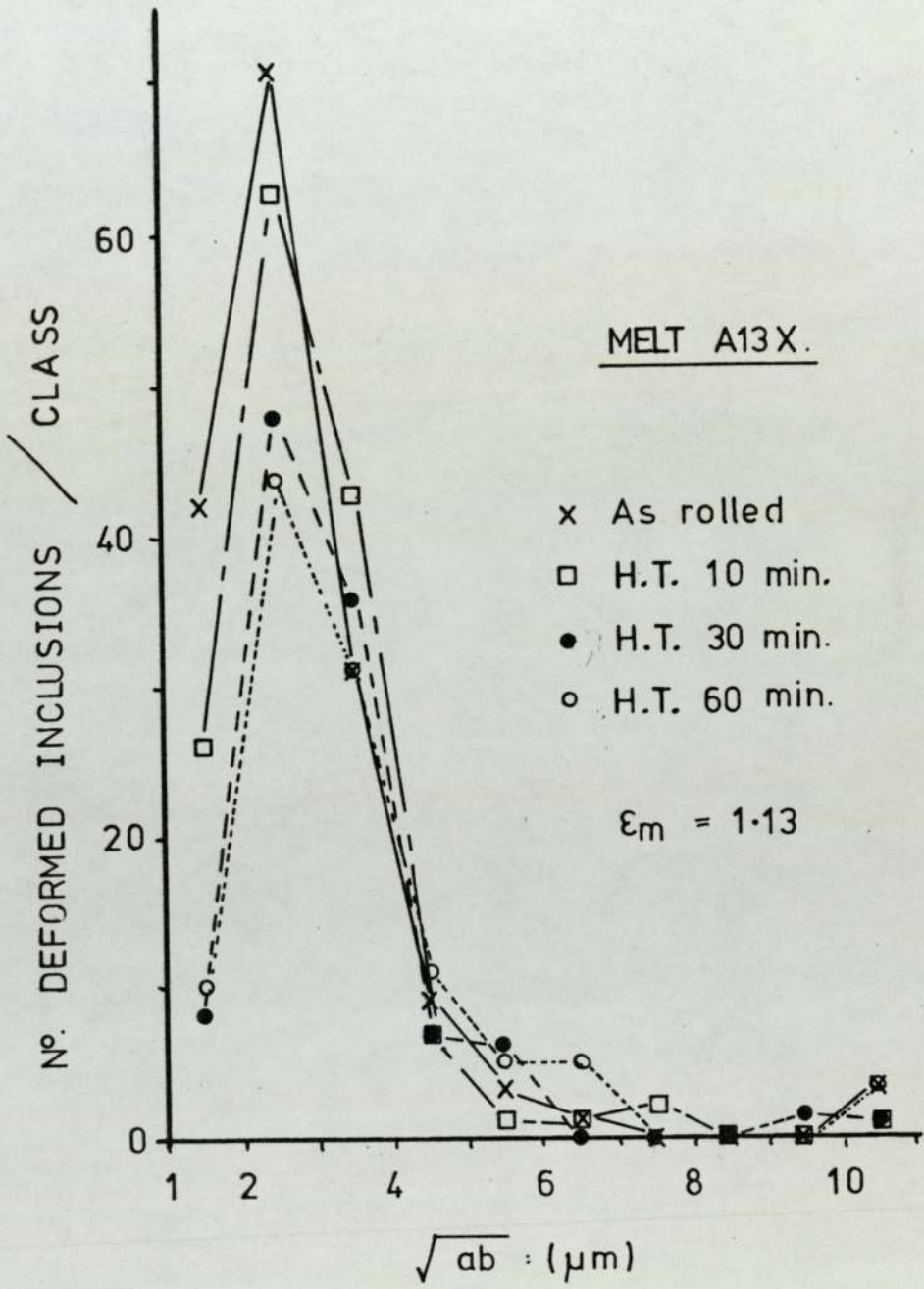
For the case of inclusions being deformed at the higher rolling temperatures, it was felt that the spheroidisation of inclusions would have an effect upon the plasticity index - size relationship, and possibly upon the mean value of plasticity index \bar{p} quoted. In order to test this hypothesis samples containing deformed inclusions were heat treated, and plasticity indices measured.

Figures 5.136. to 5.140. and tables 5.10. to 5.13. show the influence of soaking temperature upon the number of deformed inclusions contained within various size ranges, and also upon the inclusion plasticity index. Melt Al3X, which had been rolled at 1100°C, and melt CRA12 rolled at 800°C which contained a large number of deformed inclusions, were heat treated at 1050°C for 10, 30 and 60 minutes.

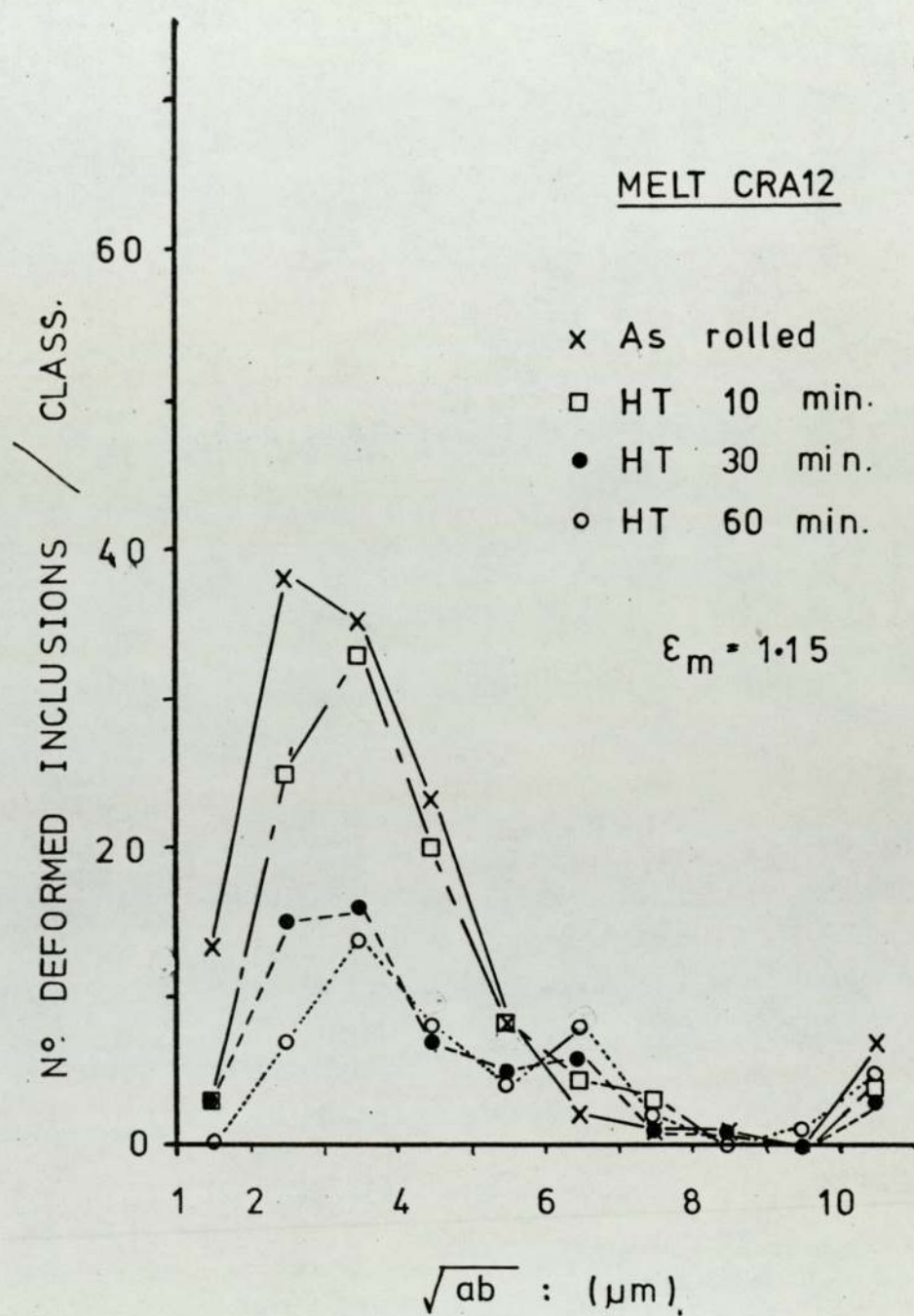
From both sets of data it may be seen that for inclusions less than 5 μm in diameter the number of deformed inclusions apparently decreased as the time at the soaking temperature increased. The greatest effect was seen for the small inclusion sizes (figures 5.136. and 5.137.). This effect was to be expected, since the small inclusions have the highest surface area to volume ratio, and will therefore tend to spheroidise in the shortest time.

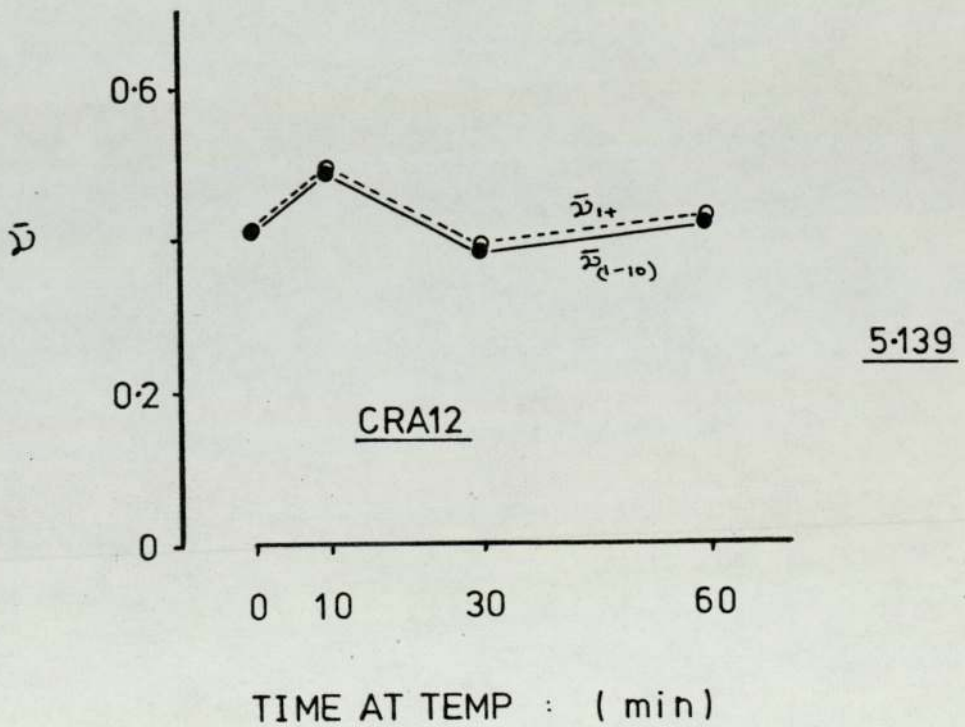
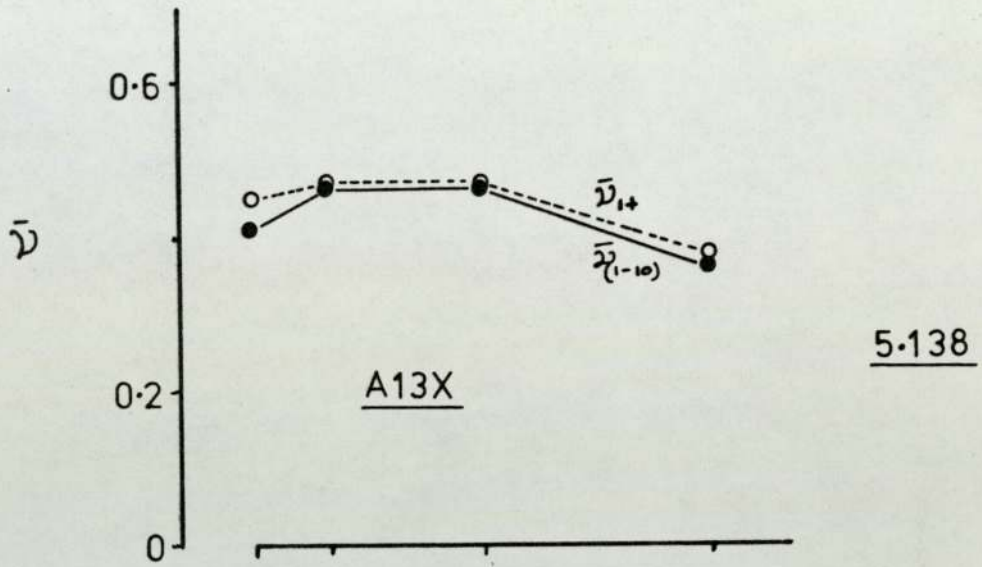
The influence of soaking temperature upon the

5-136



5-137





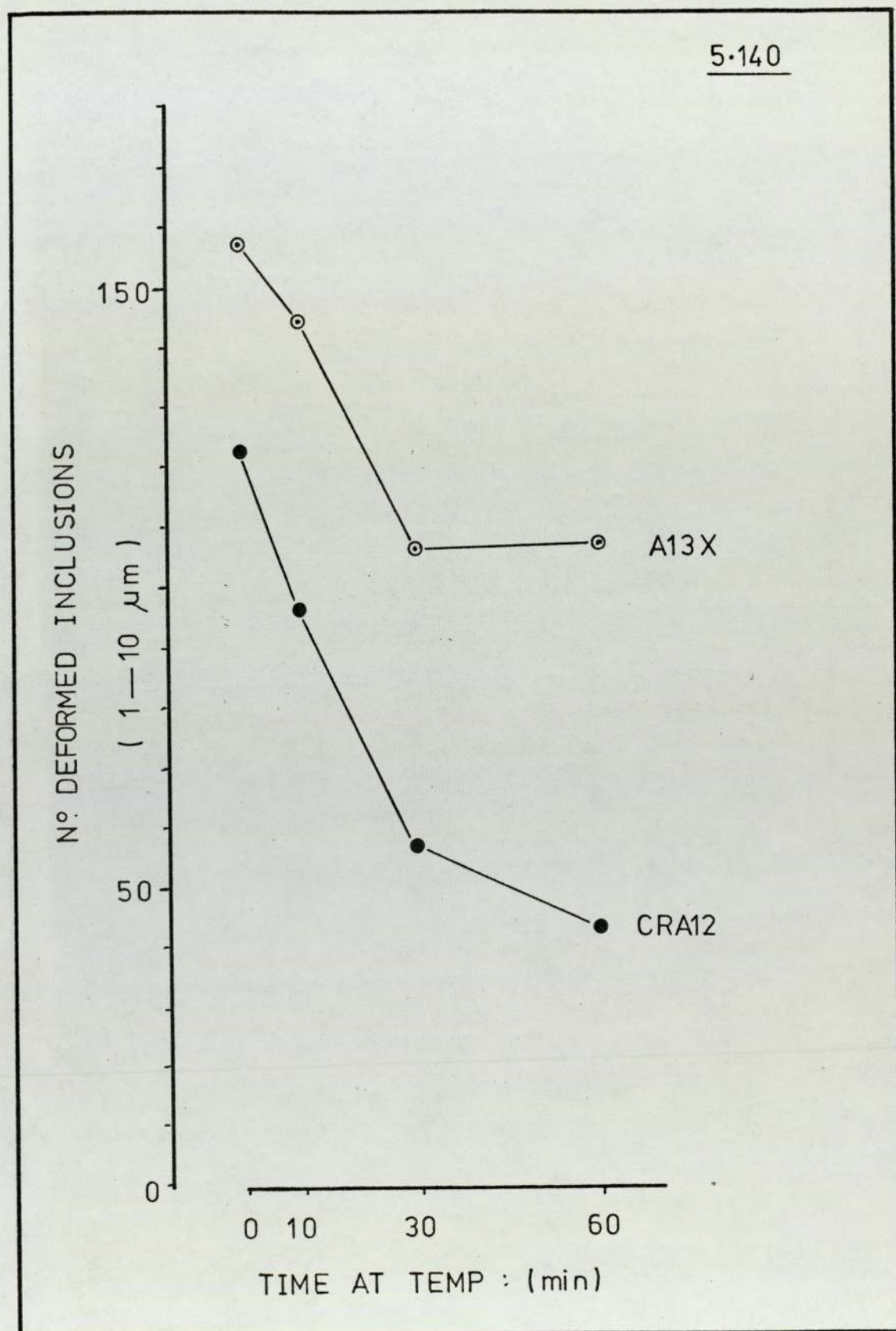


Table 5.10

Number of deformed inclusions within the various size groups for heat treated samples.

Melt A13X

$\sqrt{\text{ab}}$	AR	AR +10 mins	AR +30 mins	AR +60 mins
1 μm 2	42	26	8	10
2 3	71	63	48	44
3 4	31	43	36	31
4 5	9	7	7	11
5 6	3	1	6	5
6 7	1	1	-	5
7 8	-	2	6	6
8 9	-	-	-	-
9 10	-	-	1	1
10	3	1	1	3
$N_{DI}(\text{Total})$	160	144	107	110

AR = As Rolled

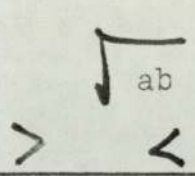
A13X (R_t 1100°C). H.T. at 1050°C.

$\epsilon_m = 1.13$

Table 5.11

Number of deformed inclusions within the various size groups for heat treated samples.

Melt CRA12

>		AR	AR +10 mins	AR +30 mins	AR +60 mins
		1	2	13	3
2	3	38	25	15	7
3	4	35	33	16	14
4	5	23	20	7	8
5	6	8	8	5	4
6	7	2	4	6	8
7	8	1	3	1	2
8	9	1	-	1	-
9	10	-	-	-	1
10		7	4	3	4
N _{DI} (Total)		128	100	57	48

AR = As Rolled

CRA12 (R_t 800°C). HT at 1050°C.

$\epsilon_m = 1.15$

Plasticity Data for Rolled and Heat Treated Samples.

A13X

	\sqrt{ab} (μm)	\bar{D}	S.D.	S.E.	N_{DI}
AR	$\sqrt{ab} > 1$	0.449	0.283	0.022	160
	$\sqrt{ab(1-10)}$	0.414	-	-	157
AR+ 10min	> 1	0.471	0.292	0.024	144
	1-10	0.465	-	-	143
AR+ 30min	> 1	0.468	0.299	0.028	107
	1-10	0.464	-	-	106
AR+ 60min	> 1	0.303	0.317	0.030	110
	1-10	0.362	-	-	107

Table 5.12

Plasticity Data for Rolled and Heat Treated Samples.

CRA12

	\sqrt{ab} (um)	\bar{u}	S.D.	S.E.	N_{DI}
AR	> 1	0.416	0.234	0.021	128
	1-10	0.413	-	-	121
AR+ 10min	> 1	0.495	0.272	0.027	100
	1-10	0.488	-	-	96
AR+ 30min	> 1	0.392	0.235	0.031	57
	1-10	0.386	-	-	54
AR+ 60min	> 1	0.433	0.233	0.034	48
	1-10	0.421	-	-	44

Table 5.13

plasticity index of inclusions within the size range 1 - 10 μm i.e. $\mathcal{V}(1 \rightarrow 10)$ appeared to be little affected. However, it does seem that initially the value of $\mathcal{V}(1-10)$ increased but then fell with progressive soaking time. This effect may be explained on the basis of the inclusion strain prior to soaking at the heat treatment temperature. i.e. the smallest inclusions were the least deformed, and as such would spheroidise the quickest. The larger inclusions had been deformed to a greater extent, and this fact in conjunction with them having a lower surface area to volume ratio would mean that they would take a longer time to spheroidise. Since there would now be fewer slightly deformed inclusions the net effect would be to push up the apparent inclusion plasticity index. Further heat treatment would tend to spheroidise the remaining well deformed inclusions. This would then lead to a lowering of the inclusion aspect ratios and as such a lower value of $\mathcal{V}(1 \rightarrow 10)$.

In the case of samples which are repeatedly reheated prior to rolling the effect of spheroidisation would be to highlight the lower deformability of inclusions of small size. This was one of the factors which possibly aided the phenomenon of a large number of apparently non-deformable small inclusions.

5.3.5.1.6.

Sectioning problems.

One of the problems encountered in the measurement of inclusion sizes was that of the sectioning probability as has been shown by Segal and Charles (125). It must be recognised that any observed inclusions size may be less than the size of the actual inclusion. This fact inevitably leads to experimental scatter in polished sections.

It was observed on several occasions (figures 5.125. and .126.) that there were points on the plasticity index - size diagrams which were out of character i.e. some apparently small inclusions had plasticity indices which were in excess of the rest of the population of small inclusions.

If we take the case of a triaxial ellipsoid, whatever the distance from the mid plane, any section parallel to that plane will have the same aspect ratio. Therefore, if a large well deformed inclusion was sectioned towards its periphery, the observed section was that of a small highly deformed inclusion. An even more exceptional case is if the part of the inclusion sectioned is in a region of ogee topology. In this case the observed ellipse has a higher value of aspect ratio than is encountered when the inclusion is sectioned towards its mid plane.

5.3.5.1.7. Surface energy criterion.

Baker and Charles (107) proposed that the energy required to create a new interface was a contributory factor as to why inclusion relative plasticity was observed (101) to decrease with a decrease in inclusion size.

The energy required to create a new interface (E_{INT}) may be taken as the product of the change in surface area (S.A.) and the interfacial energy (γ).

i.e.

$$E_{INT} = \gamma [S.A._{(DEF)} - S.A._{(ORIG)}]$$

Assuming that plane strain conditions are operative and there is no change in inclusion volume two cases may be considered.

- I) Cubic inclusions deformed to a parallelepiped (as with the model of Baker and Charles)
- II) Sphere deformed to a triaxial ellipsoid.

Case (I)

If we consider case (I) where a cubic inclusion of side (D) is deformed to a parallelepiped of sides (a) - major, (b) - minor and (D) - intermediate,

then:

$$\text{Volume} = D^3 = abD$$

$$\therefore D^2 = ab$$

and the aspect ratio $\lambda = \frac{a}{b}$

$$\lambda = \frac{a}{b} = \frac{a^2}{D^2} = \frac{D^2}{b^2} = e^{2\varepsilon_i} \quad *$$

* Assuming that under plane strain conditions inclusion strain, ε_i , may be given by

$$\varepsilon_i = \frac{1}{2} \ln \lambda$$

The surface areas of the original and deformed inclusions are:

$$\text{S.A. (orig)} = 6D^2$$

$$\text{S.A. (Def)} = 2Da + 2Db + 2ab$$

∴ The change in surface area is given by

$$\Delta(\text{S.A.}) = \left[2D^2 \left(\frac{D}{b} + \frac{D}{a} + 1 \right) \right] - 6D^2$$

$$\text{i.e.} \quad = D^2 \left[2 \left(\lambda^{1/2} + \lambda^{-1/2} + 1 \right) - 6 \right]$$

$$\text{or} \quad \Delta(\text{S.A.}) = D^2 \left[2 \left(e^{\varepsilon_i} + e^{-\varepsilon_i} + 1 \right) - 6 \right]$$

Since

$$\cosh \varepsilon_i = \frac{1}{2} \left[e^{\varepsilon_i} + e^{-\varepsilon_i} \right]$$

this expression for $\Delta(\text{S.A.})$ may be written as

$$\Delta(\text{S.A.}) = 4D^2 \left(\cosh \varepsilon_i - 1 \right)$$

Therefore $E_{INT} = 4\gamma D^2 (\cosh \epsilon_i - 1)$

and in terms of relating the expression to unit inclusion volume D^3

$$\left(\frac{E_{INT}}{V_i} \right) = \frac{4\gamma}{D} (\cosh \epsilon_i - 1)$$

Case (II).

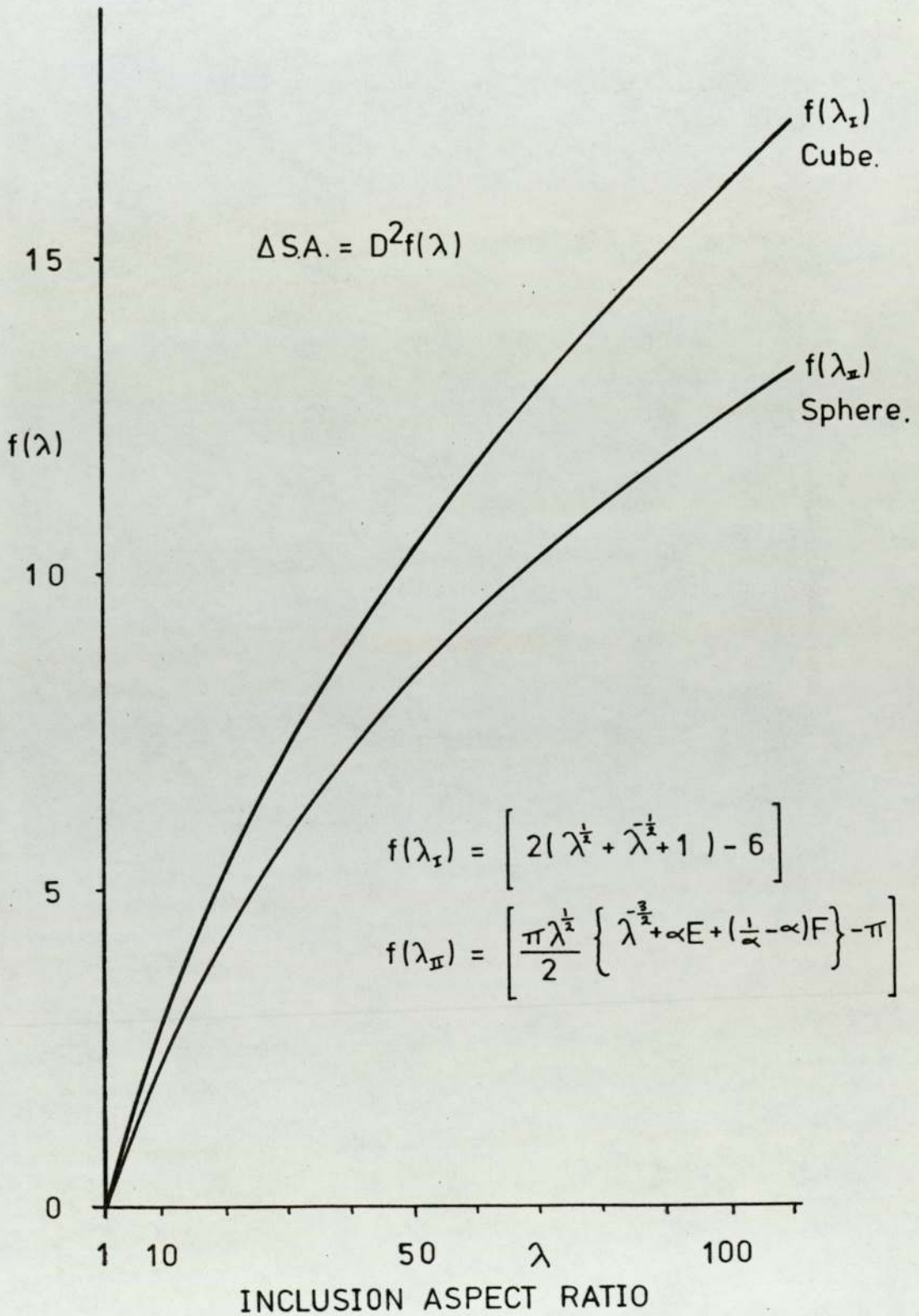
The consideration of a spherical inclusion deforming to a triaxial plane strain ellipsoid (i.e. one axis remains constant) involves a complex mathematical analysis (214) requiring the use of elliptic integrals. (215). Although complex, a solution has been evolved (216) enabling a graphical representation to be produced (figure 5.141.). The results from this analysis have indicated that the change in surface area approximates to 0.8 times the value obtained for a cubic inclusion.

$$\Delta(S.A.) = D^2 f(\lambda)$$

$$f(\lambda_{II}) \approx 0.8 f(\lambda_I)$$

Fig. 5.141

Change in inclusion surface area with aspect ratio.



The interfacial energy is thus

$$E_{INT.} = 3.2 \gamma D^2 (\cosh \epsilon_i - 1)$$

and again in terms of interfacial energy per unit volume of inclusion ($\frac{\pi D^3}{6}$)

$$\left(\frac{E_{INT.}}{V_i} \right) = 19.2 \frac{\gamma}{\pi D} (\cosh \epsilon_i - 1)$$

which is approximately

$$\left(\frac{E_{INT.}}{V_i} \right) \approx \frac{6\gamma}{D} (\cosh \epsilon_i - 1)$$

Thus it may be seen that the value of surface energy for the sphere is approximately 50% greater than that for the cube (case (I)) model.

Robinson (35) has recently performed a similar exercise which relates the rate of change of surface energy per unit volume ($\frac{\dot{E}}{V_i}$) (for the cubic model) to inclusion strain (ϵ_i) and strain rate ($\dot{\epsilon}_i$).

i.e.

$$\left(\frac{\dot{E}_{INT.}}{V_i} \right) = 4 \frac{\gamma}{D} \dot{\epsilon}_i \sinh \epsilon_i$$

It can however be shown simply that the equation derived by Robinson (35) and the equation for case (I) (i.e. the cubic inclusion) are comparable.

viz
$$\left(\frac{\dot{E}}{V} \right) = \frac{d \left(\frac{E}{V} \right)}{dt}$$

i.e.
$$\left(\frac{\dot{E}}{V} \right) = \frac{d \left(\frac{E}{V} \right)}{d \epsilon_i} \cdot \frac{d \epsilon_i}{dt}$$

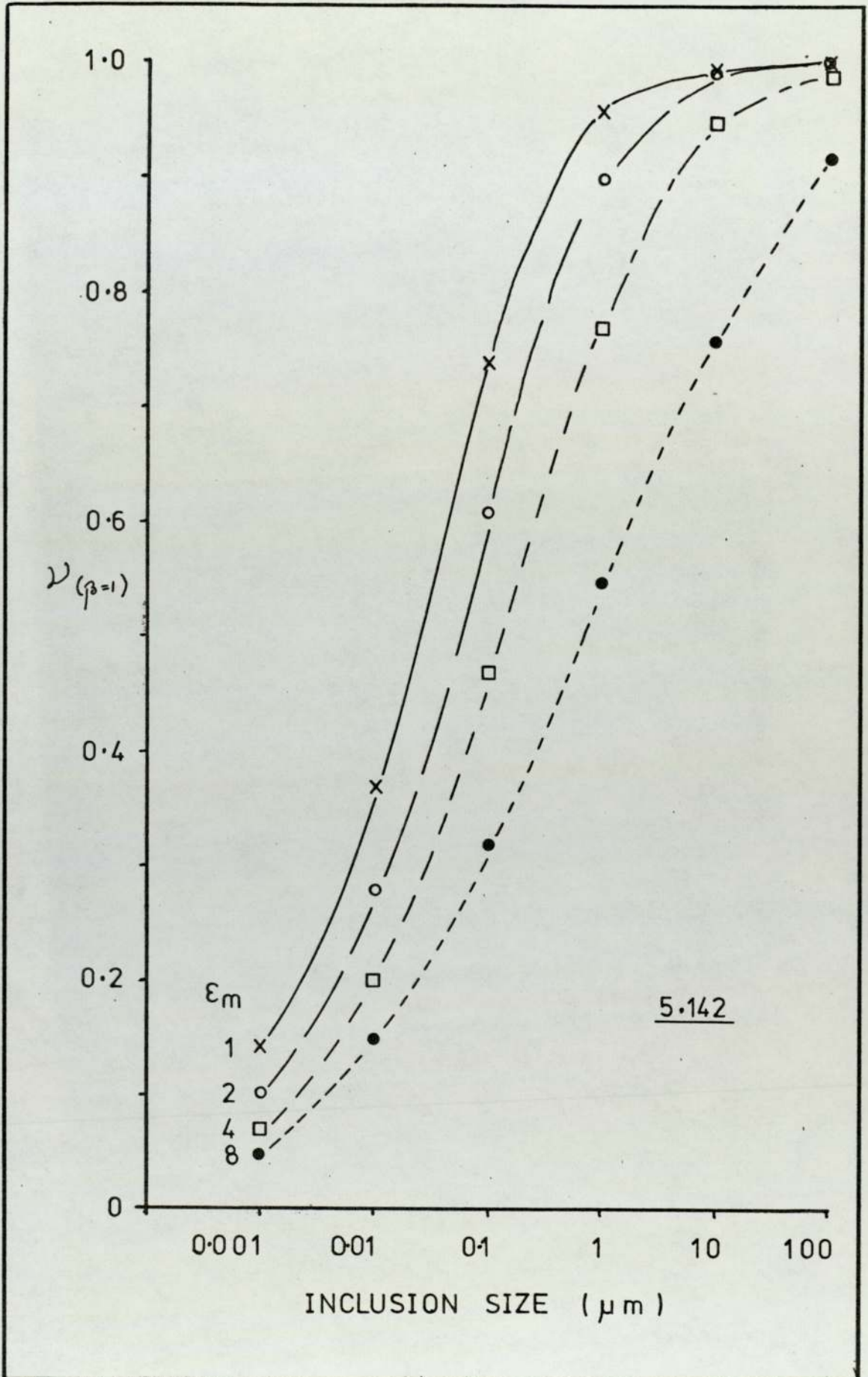
now
$$\frac{d \epsilon_i}{dt} = \dot{\epsilon}_i$$

and
$$\left(\frac{E}{V} \right) = \frac{4\gamma}{D} (\cosh \epsilon_i - 1)$$

$$\therefore \left(\frac{\dot{E}}{V} \right) = \frac{d}{d \epsilon_i} \left[\frac{4\gamma}{D} (\cosh \epsilon_i - 1) \right] \dot{\epsilon}_i$$

i.e.
$$\underline{\left(\frac{\dot{E}}{V} \right) = \frac{4\gamma}{D} (\sinh \epsilon_i) \dot{\epsilon}_i}$$

The present work, and that of other workers has indicated that the size at which inclusions do not deform is in the region of 1 - 2 μm , for silicate inclusions (103), FeO (35), and MnS (125). However, from a study of the energy associated with the increase in surface area, the surface energy effect is only noticeable at very small inclusion sizes and large reductions, as indicated by figure 5.142. (which is based on the calculation in Appendix. 5.2).



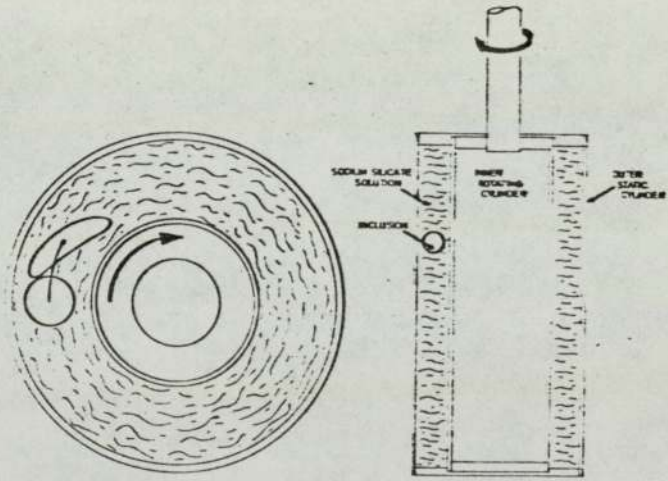
This seems to suggest that the surface energy criterion was not the major effect, but will be a contributory factor which will possibly enhance other factors.

5.3.5.1.8. Effective stresses acting upon the inclusion.

One of the factors which has not yet been discussed is the level of effective deformation stress that the inclusions see. Pickering (100) proposed that one of the reasons which may account for the non deformation of small inclusions was that they may tend to rotate within the matrix rather than deform, a view which is held by other workers (35). Robinson developed a model system based upon two concentric cylinders the inner one of which rotated (figure 5.143.). Contained between the cylinders was a sodium silicate solution, into which he injected particles of similar density and viscosity. Upon rotation of the cylinders he found that the large inclusions deformed to the shapes found in the real system. The small inclusions however remained non-deformable, and apparently rotated within the imposed shear gradient, thus supporting the suggestion of Pickering.

From work carried out in this investigation, it appeared that large inclusions began to deform before the smaller ones, and upon increased straining of the matrix the smaller inclusions progressively became

5 • 143



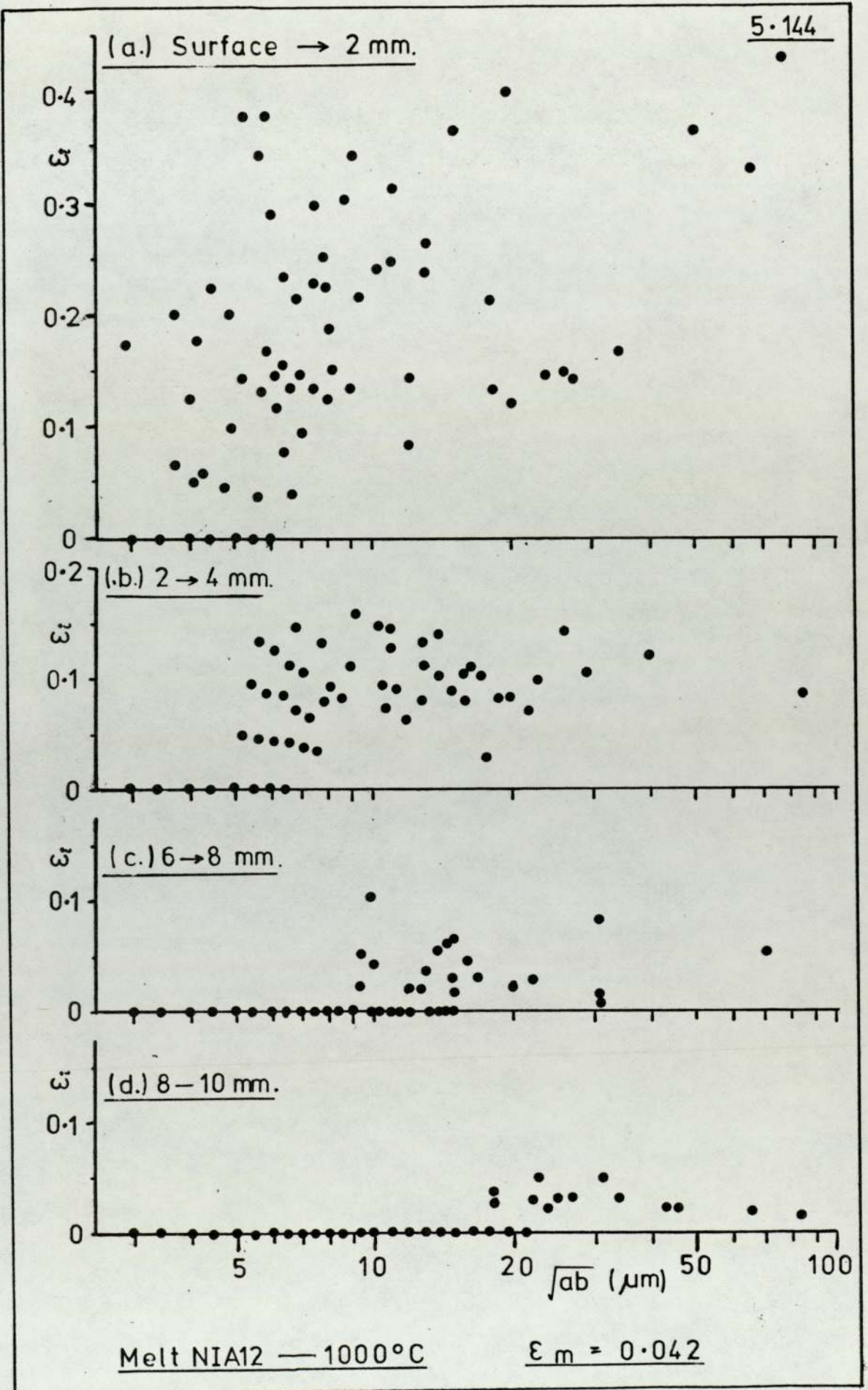
deformed. (figure 5.144.). Melt NiAl₂ was rolled at a temperature of 1000°C to a matrix height strain of 0.042 (i.e. 4% reduction). Inclusion strains were measured at various heights within the deformed bars (section 5.3.6.2), and it was found that the greatest inclusion strain had occurred in the outer layers. Since the matrix strains within the various regions in the bar were not known, the smallest size of observable deformed inclusions were plotted against the mean inclusion strain for the region measured.

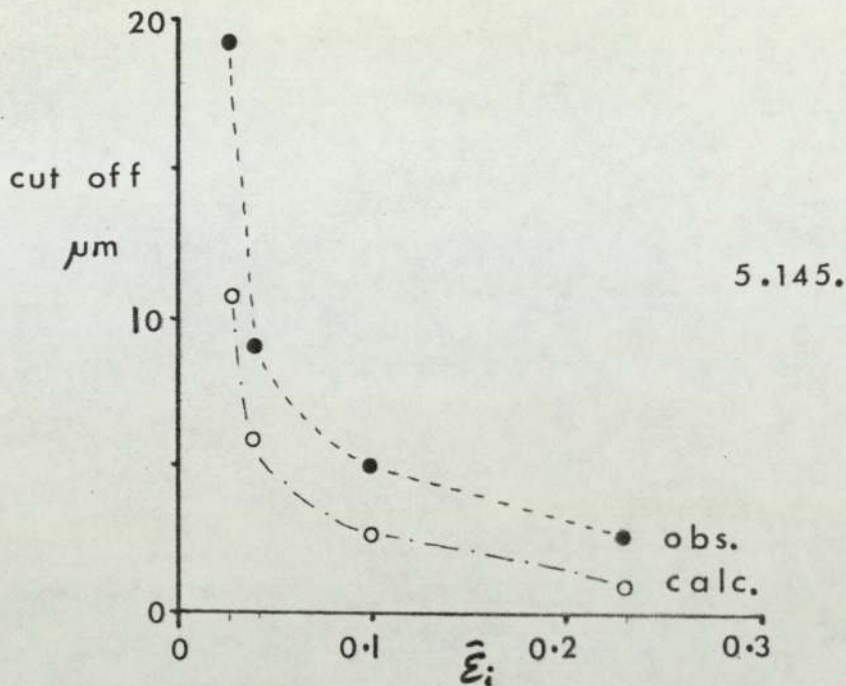
Table 5.14. and figure 5.145.

Table 5.14.

Melt NiAl₂ rolled at 1000°C $\epsilon_m = 0.042$.

Distance from the top surface	$\bar{\epsilon}_i$	D _{min} observed	Calculated D _{min}
0 - 2 mm	0.23	2.5 μm	1.07 μm
2 - 4 mm	0.10	5.0 μm	2.70 μm
6 - 8 mm	0.04	9.0 μm	6.24 μm
8 -10 mm	0.03	19.0 μm	11.20 μm





It was felt that this size effect might have been due to operator error in measurement. Although this may have occurred to some degree, the indications were that the cut off sizes were in excess of the minimum measurable sizes of the deformed inclusions.

If the deformation of an inclusion was dependent upon the degree of stress/strain that it ~~saw~~^{experienced}, then it might be expected that in regions where the matrix had strained the most, the stress levels would be highest due to work hardening. In addition there would be more slip systems operating and therefore an increased probability of smaller inclusions being intersected and/or influenced within these regions. One might therefore be tempted to suggest that the inclusions of progressively smaller sizes would be persuaded to deform as the degree of matrix strain was increased.

5.3.5.1.9. Deviation from plane strain.

A major assumption in this work has been that of plane strain deformation. However, as will be discussed later this was not the case, and lateral spread occurred to some degree. The effect of lateral spread on inclusion measurements parallel to the major and minor axis would be to effectively lower the apparent inclusion strain (plasticity) and also the inclusion size.

5.3.6. The variation of the inclusion plasticity index with the degree of matrix reduction.

The results from tables 5.15. → .19. which are presented in figures 5.146 - .147 indicate that the value of inclusion plasticity index was not constant with increasing matrix strain. The value of plasticity index may be seen to have rapidly increased with increase in strain initially and reached a peak, at approximately $0.8 \epsilon_m$. Beyond this strain the value of the plasticity index was seen to decrease with increased strain.

This observation was seemingly in disagreement with other data published (35), which suggested that there was a maximum value of plasticity index as the degree of matrix reduction tended towards zero. However, the difference encountered in the present project is believed to be due to the geometry of the samples for rolling, and the inhomogeneous deformation of the matrix (discussed in section 5.3.6.2).

Presenting these results in a slightly different way i.e. plotting inclusion strain versus matrix strain (figure 5.147.) it was shown that for very low strains no inclusion deformation was encountered. This was rapidly followed by a region where the inclusion strain - matrix strain diagram showed a linear relationship upto a matrix strain of approximately $0.8 \epsilon_m$. Above this strain value the inclusions showed resistance to deformation as the matrix strain

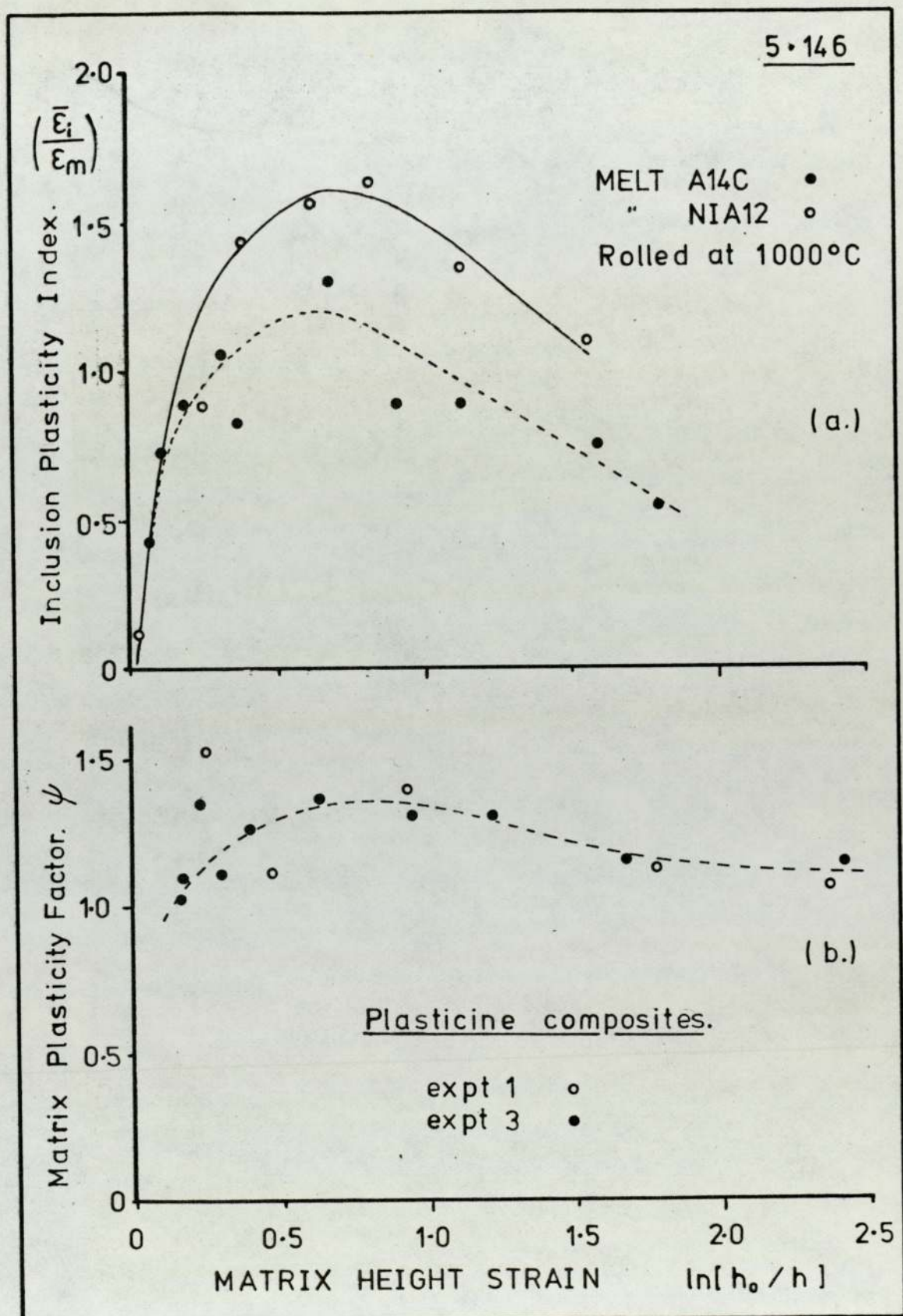
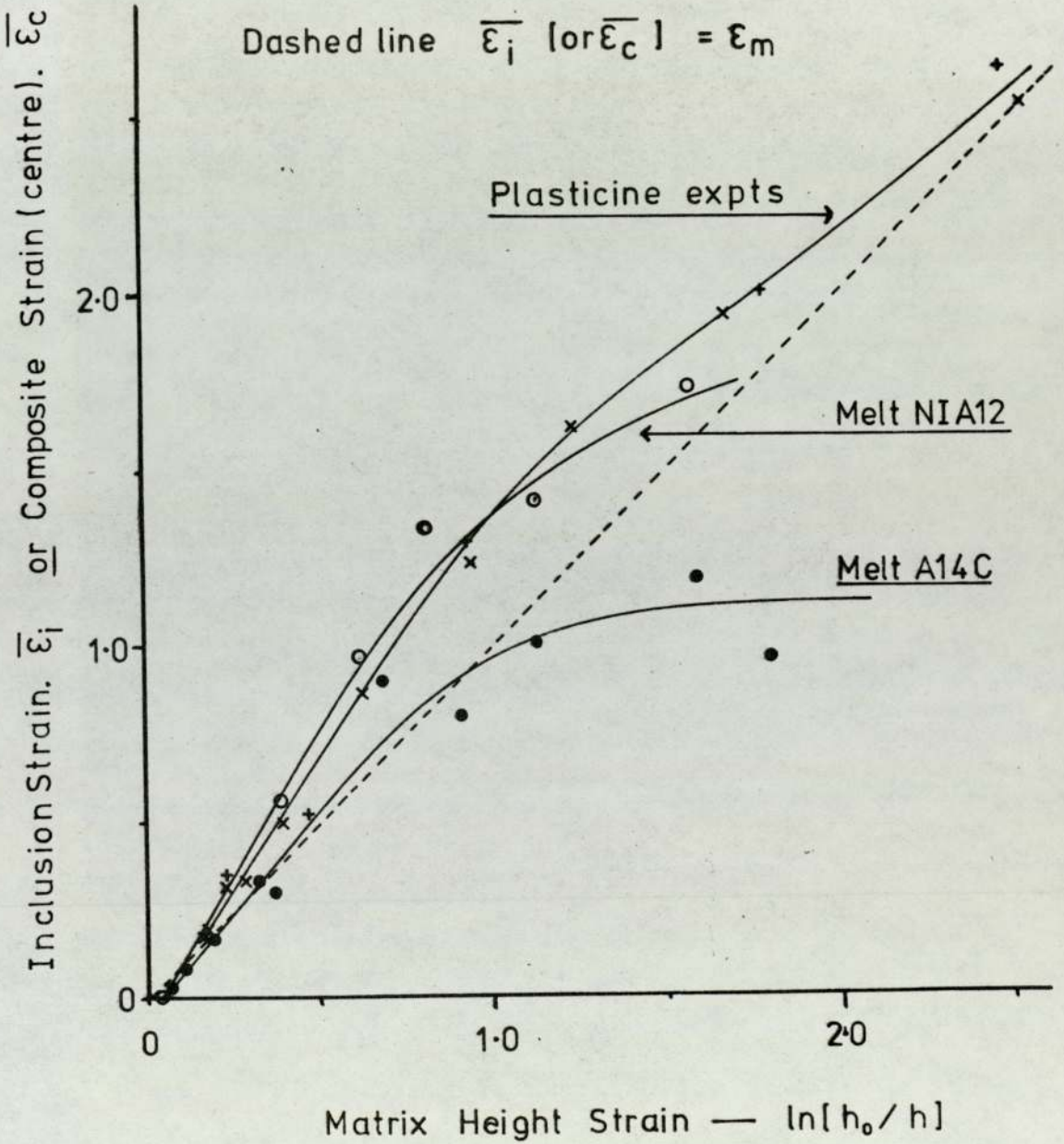


Fig. 5.147



Melt NIA12 Rolled at 1000°C

Table 5.15

ϵ_m	Top			Bottom			Centre			$\Delta\epsilon$	\bar{y}_{10+}		
	$\bar{\epsilon}_i$	$\sigma_{\bar{\epsilon}_i}$	n_L	$\bar{\epsilon}_i$	$\sigma_{\bar{\epsilon}_i}$	n_L	$\bar{\epsilon}_i$	$\sigma_{\bar{\epsilon}_i}$	n_L		\bar{y}_{10+}	$\sigma_{\bar{y}}$	n_L
0.04	0.10	-	16	-	-	-	0.005	-	9	- 0.10	0.12	-	9
0.39	0.57	0.04	11	0.47	0.02	11	0.56	0.01	11	0.04	1.43	0.03	11
0.62	0.76	0.06	9	0.78	0.06	9	0.97	0.02	8	0.20	1.56	0.03	8
0.82	1.15	0.04	7	1.02	0.05	6	1.34	0.04	7	0.26	1.63	0.05	7
1.13	1.57	0.10	5	1.41	0.06	5	1.53	0.05	5	0.04	1.35	0.05	5
1.57	1.57	0.05	4	1.60	0.06	4	1.73	0.04	5	0.14	1.10	0.03	5

Table 5.16

Melt Al4(2) Rolled at 1000°C

ϵ_m	top			bottom			central			$\Delta\epsilon_i$			
	$\bar{\epsilon}_i$	$\sigma_{\bar{\epsilon}_i}$	n_L	$\bar{\epsilon}_i$	$\sigma_{\bar{\epsilon}_i}$	n_L	$\bar{\epsilon}_i$	$\sigma_{\bar{\epsilon}_i}$	n_L		$\bar{\nu}_{10+}$	$\sigma_{\bar{\nu}}$	n_L
0.07	0.10	0.02	8	0.12	0.03	8	0.03	0.02	8	-0.08	0.43	0.29	8
0.11	0.09	0.02	8	0.10	0.03	8	0.08	0.02	7	-0.02	0.73	0.18	7
0.19	0.07	0.03	7	0.15	0.03	7	0.17	0.03	7	0.06	0.89	0.15	7
0.32	0.28	0.03	6	0.19	0.09	6	0.34	0.05	7	0.11	1.06	0.15	7

Table 5.17

<u>Melt N1A12 Rolled at 1000°C.</u>				
ϵ_m	$\bar{\epsilon}_i$ central $\frac{1}{3}$	$\Delta\epsilon_i$	$\bar{\nu}_{10+}$	n_i
0.04	0.005	—	0.12	135
0.39	0.56	0.09	1.44	81
0.62	0.97	0.21	1.56	92
0.82	1.33	0.25	1.64	55
1.13	1.52	—	1.34	77
1.56	1.72	0.14	1.11	38
<u>Melt A14 Rolled at 1000°C.</u>				
ϵ_m	$\bar{\epsilon}_i$	$\Delta\epsilon_i$	$\bar{\nu}_{10+}$	n_i
0.07	0.03	-0.08	0.38	24
0.11	0.09	-0.02	0.78	59
0.19	0.16	0.06	0.87	21
0.32	0.37	0.11	1.15	42
0.37	0.30	—	0.32	13
0.69	0.90	—	1.30	19
0.91	0.80	—	0.88	6
1.13	1.01	—	0.89	22
1.59	1.19	—	0.75	14
1.79	0.96	—	0.54	7
2.03	0.81	—	0.40	1
2.24	1.52	—	0.68	1

Plasticine experiment 1

Table 5.18

ϵ_m	Top			Bottom			Centre			$\Delta\epsilon_L$	Plasticity factor		
	$\bar{\epsilon}_L$	$\sigma_{\bar{\epsilon}_L}$	n	$\bar{\epsilon}_L$	$\sigma_{\bar{\epsilon}_L}$	n	$\bar{\epsilon}_L$	$\sigma_{\bar{\epsilon}_L}$	n		$\bar{\psi}$	$\sigma_{\bar{\psi}}$	n
0.23	0.18	0.06	4	0.19	0.06	4	0.35	0.01	5	0.17	1.52	0.04	5
0.47	0.38	0.07	4	0.43	0.03	4	0.52	0.02	5	0.12	1.11	0.04	5
0.93	0.88	0.15	4	0.75	0.14	4	1.29	0.04	5	0.48	1.39	0.04	5
1.78	1.62	0.13	4	1.47	0.13	4	2.00	0.05	5	0.46	1.12	0.03	5
2.47	2.35	0.15	4	2.02	0.05	4	2.63	0.07	5	0.45	1.06	0.03	5
<u>Plasticine experiment 2</u>													
0.15	0.13	0.12	2	0.04	0.04	2	0.23	0.04	3	0.15	1.53	0.27	3
0.22	0.10	0.06	2	0.20	0.08	2	0.26	0.02	3	0.11	1.18	0.09	3
0.38	0.22	0.19	2	0.25	0.01	2	0.41	0.05	3	0.18	1.08	0.13	3
0.67	0.49	0.11	2	0.57	0.06	2	0.83	0.01	3	0.30	1.24	0.01	3
1.10	1.04	0.02	2	0.97	0.11	2	1.30	0.02	3	0.30	1.18	0.02	3
1.69	1.68	0.14	2	1.66	0.20	2	2.02	0.11	3	0.35	1.19	0.07	3
2.36	2.08	0.21	2	2.14	0.39	2	2.76	0.07	3	0.51	1.16	0.03	3

ϵ_m	Top			Bottom			Centre			$\Delta\epsilon_L$	Plasticity factor		
	$\bar{\epsilon}_L$	$\bar{\sigma}_{\epsilon_L}$	n	$\bar{\epsilon}_L$	$\bar{\sigma}_{\epsilon_L}$	n	$\bar{\epsilon}_L$	$\bar{\sigma}_{\epsilon_L}$	n		$\bar{\psi}$	σ_ψ	n
0.166	0.19	0.04	6	0.14	0.03	6	0.17	0.02	5	0.01	1.02	0.12	5
0.173	0.16	0.04	6	0.09	0.03	6	0.19	0.03	5	0.07	1.10	0.17	5
0.230	0.21	0.03	6	0.19	0.04	6	0.31	0.02	5	0.11	1.35	0.09	5
0.297	0.30	0.05	6	0.22	0.03	6	0.33	0.02	5	0.07	1.11	0.07	5
0.396	0.44	0.08	6	0.29	0.06	6	0.50	0.01	5	0.14	1.26	0.03	5
0.632	0.61	0.08	6	0.52	0.08	6	0.86	0.03	5	0.30	1.36	0.05	5
0.947	0.95	0.13	6	0.82	0.10	6	1.23	0.03	5	0.35	1.30	0.03	5
1.237	1.20	0.15	6	1.09	0.15	6	1.61	0.04	5	0.47	1.30	0.03	5
1.677	1.67	0.07	6	1.66	0.13	6	1.93	0.07	5	0.27	1.15	0.04	5
2.535	2.17	0.14	6	2.15	0.14	6	2.53	0.07	5	0.37	1.16	0.03	5

increased, showed by a flattening of the graph .
(figure 5 .147.).

Numerous reasons have been put forward to explain this phenomenon (Section 2. 2.4.3), however, before seeking a mechanistic approach it was worthwhile examining the results of a model system. In this case the matrix strains were measured in the regions where inclusion measurements were made in the real system, and compared to the overall matrix strain. i.e. ψ

Tables 5.17-:19 and figure 5 .146: .147: show the results obtained from experiments using rolled plasticine composites (detailed in section 3.) of the same initial height as used in the real system. The results plotted in figure 5 .147. show the mean strain in the central one third of the composite versus the overall matrix strain. Again it may be observed that there was a linear portion to the curve upto a matrix strain of approximately 1.2. Beyond this value there was a tendency towards the flattening of the curve, although not to the extent as shown by the inclusions within the real system. An interesting feature with the composite results was that in all instances the mean central composite strain was in excess of the matrix height strain value even though the matrix was of the homogeneous material.

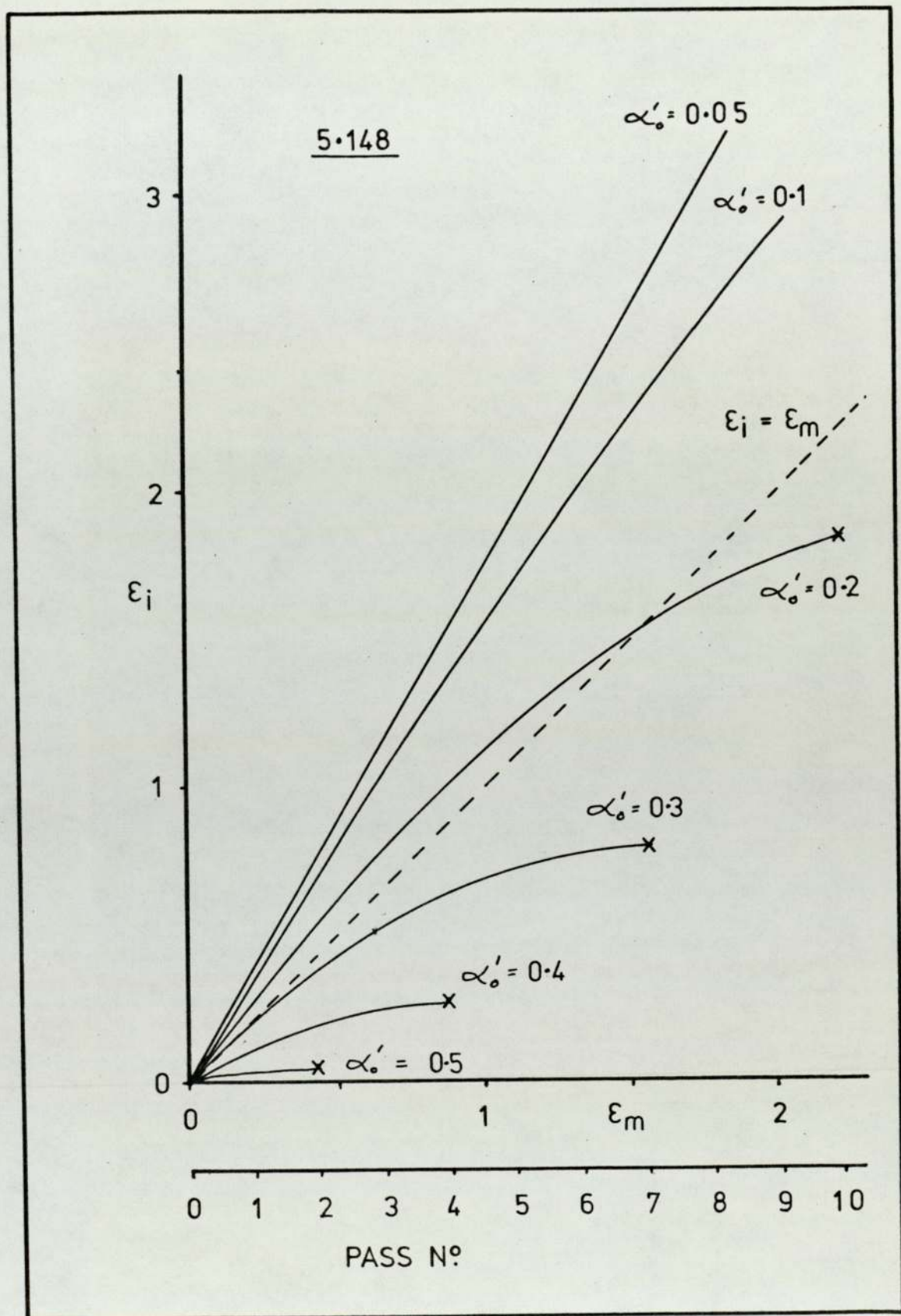
The indication from these results was that inhomogeneous deformation of the matrix took place. This result has serious implications when referring to the deformation of inclusions measured in the central

region of the hot rolled samples. However, bearing this in mind, the inhomogeneity of deformation does not account for the fall off in inclusion strain with increased matrix strain. Hence, mechanistic approaches must be looked into.

The two casts used in the investigation of inclusion strain versus matrix strain were NIA12 and Al₄C rolled at 1000°C. This rolling temperature was well in excess of the non-deformable/deformable transition temperature (Section 5.3.3). Cast NIA12 contained glassy inclusions at the rolling temperature whereas Al₄C there were precipitate phases within the inclusions which would tend to increase their apparent flow stress. From figure 5.146. it may be seen that at all matrix strains the inclusions of melt NIA12 (greater than 10 μm in size) have been more deformable than those of Al₄C thus fitting the hypothesis.

Although numerous mechanisms may be cited (Section 2.2.4) for the fall in the ratio of inclusion strain to matrix strain as the degree of matrix strain increases, this type of behaviour may be predicted on the basis of strain rate. Figure 5.148. shows the theoretical variation in inclusion strain with matrix strain for various values of apparent inclusion to matrix flow stress ratios α_0 for the experimental work in this project.

In the hot rolling process the mean deformation rate (strain /rate) increases as the ingoing thickness decreases for a constant reduction per pass, roll



velocity, and roll diameter (126).

i.e.

$$\dot{\epsilon} = v_r \ln\left(\frac{h_1}{h_2}\right) \sqrt{\frac{2}{D(h_1 - h_2)}}$$

where

$\dot{\epsilon}$ = mean strain rate (s^{-1})

v_r = peripheral roll velocity (ms^{-1})

D = roll diameter (m)

h_1 = entry thickness (m)

h_2 = exit thickness (m)

The work of Alder and Phillips (217) showed that the resistance to homogeneous deformation was dependent upon the strain rate. This resistance may be equated as

$$\sigma = \sigma_0 \dot{\epsilon}^n$$

where σ_0 is the level of stress when $\dot{\epsilon}$ is unity

n is the strain rate sensitivity index.

From their work on a 0.17% Carbon steel deformed at temperatures in the range 930 - 1200°C and reductions of 10 to 50% the value of n was in the region of 0.1 (table 5.20.).

Table 5.20.

Temperature °C	Values of n at percentage reductions in height per pass of:		
	10%	20%	50%
930	0.088	0.084	0.105
1000	0.108	0.100	0.122
1060	0.112	0.107	0.155
1135	0.123	0.129	0.198
1200	0.116	0.122	0.196

Thus at 1000°C rolling temperature the deformation stress of the steel matrix may be given as

$$\sigma_m = \sigma_{m_0} \dot{\epsilon}^{0.1}$$

Assuming that inclusions within the matrix behave as Newtonian fluids their apparent flow stress, according to Ekerot (102), may be represented by the relationship

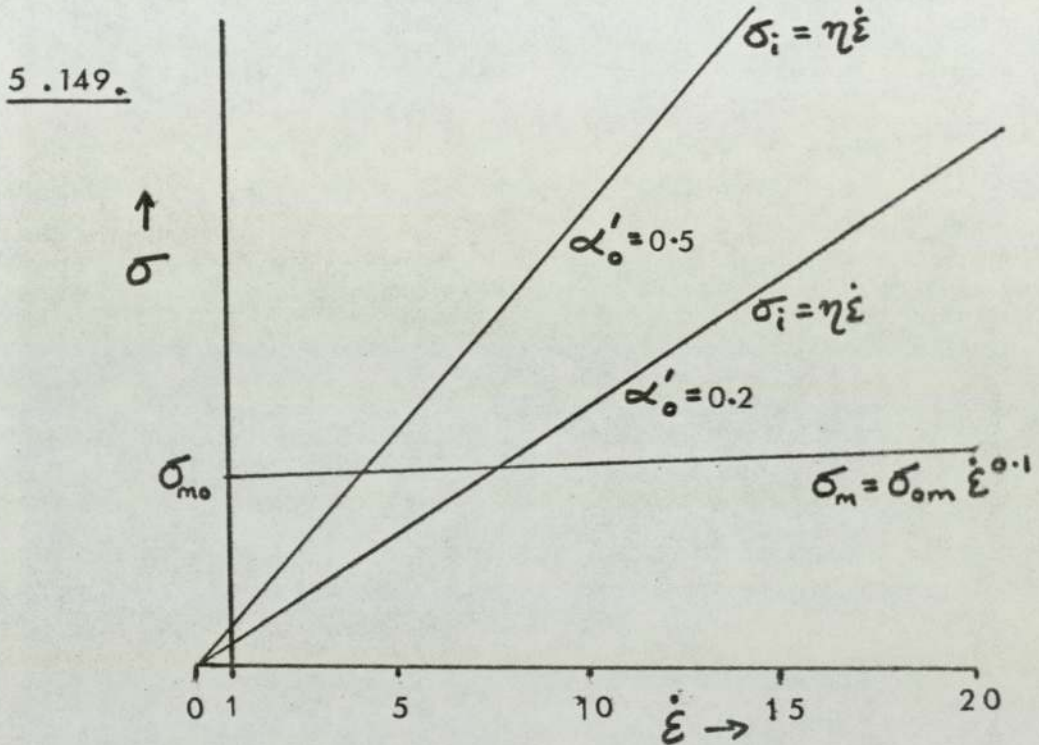
$$\sigma_i = \eta \dot{\epsilon}$$

where η is the viscosity of the inclusion.

Thus it is clear that both the matrix and inclusion phases are strain rate dependent, the inclusion phase being the more dependent. Figure 5.14 9, indicates the apparent deformation stresses at the various passes (i.e. as the total matrix strain, and strain rate

increases) for various inclusion to matrix stress ratios measured at $\dot{\epsilon} = 1$.

$$\alpha'_0 = \left(\frac{\sigma_{i0}}{\sigma_{m0}} \right)_{\dot{\epsilon}=1}$$



If α'_0 is defined as the inclusion/matrix stress ratio at $\dot{\epsilon} = 1$, α' is the value at a value of $\dot{\epsilon} > 1$. The two stress equations for the inclusion

$$\sigma_i = \eta \dot{\epsilon}$$

and the matrix

$$\sigma_m = \sigma_{om} \dot{\epsilon}^{0.1}$$

$$\therefore \left(\frac{\sigma_i}{\sigma_m} \right) = \alpha' = \frac{(\eta \dot{\epsilon})_{\dot{\epsilon}=1} \cdot \dot{\epsilon}}{\sigma_{om} \dot{\epsilon}^{0.1}}$$

N.B. $\frac{(\eta\dot{\epsilon})_{\dot{\epsilon}=1}}{\sigma_m}$ is numerically equivalent to $\frac{\eta}{\sigma_m}$ and may be regarded as the 'unit strain rate' inclusion to matrix deformation stress ratio.

$$\therefore \underline{\alpha' = \alpha'_0 \dot{\epsilon}^{0.9}}$$

It is also well known that the potential inclusion plasticity index is dependent upon the ratio of inclusion and matrix stresses. For a given constant strain rate there may be a simple relationship, as with the work of Gove and Charles (109).

e.g.

$$\nu = 2 - \alpha'$$

For the situation of multiple rolling passes, as in this work, each pass of equal matrix strain has a correspondingly different strain rate, and therefore a different value of apparent deformation stress ratio (α'). Hence, the change in inclusion strain with respect to matrix strain for a given pass is

$$\frac{\Delta \epsilon_i}{\Delta \epsilon_m} = 2 - \alpha'$$

Between two subsequent passes in the rolling process, the value of ϵ_i after the n^{th} pass may be given via

$$\epsilon_{i(n)} = (2 - \alpha') \Delta \epsilon_m + \epsilon_{i(n-1)}$$

For a 20% reduction height per pass

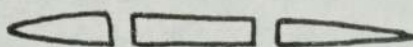
$$\Delta \epsilon_m = 0.223$$

Substituting for (α') the equation becomes

$$\epsilon_{i(n)} = \left\{ 2 - [\alpha'_0 \dot{\epsilon}^{0.9}] \right\} \Delta \epsilon_m + \epsilon_{i(n-1)}$$

Hence, the total inclusion strain after a given pass may be calculated for any value of inclusion to matrix flow stress ratio (Appendix 5:3). Thus an inclusion strain/matrix strain diagram may be compiled from such calculations i.e. figure 5.148.

From the calculations it may be seen that an inclusion ceases to deform when the matrix reduction promotes a situation where $\eta \dot{\epsilon}_{(i+1)}$ exceeds approximately $2 \sigma_{om} \dot{\epsilon}^n$ i.e. when $\alpha' \geq 2$. Such a situation may result in the characteristic fracture.



which has often been observed. This may be due to the matrix deforming and the inclusion resisting deformation. This fracture phenomenon will obviously be dependent upon the degree of adhesion between the inclusion and matrix phases, and the efficiency of stress transfer across the interface. It may be that fracture occurs when the value of deformation stress exceeds the fracture stress of the inclusion.

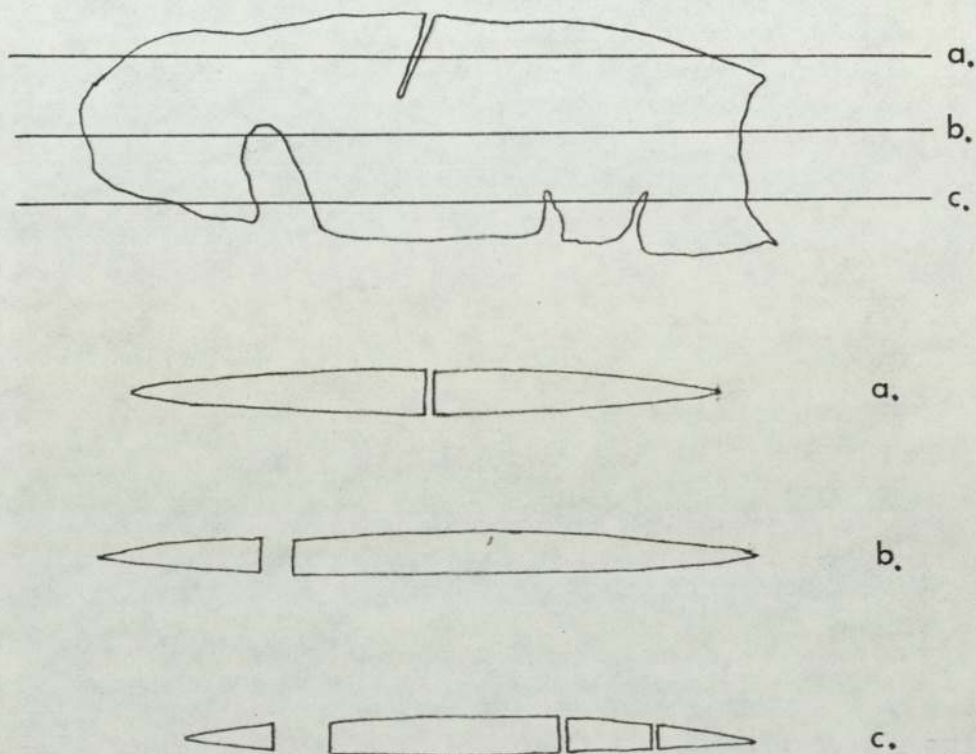
The analysis of inclusion/matrix strain on the basis of strain rate also indicated that, as the relative strength of the inclusion to matrix increased the degree to which the matrix need be strained to prevent the inclusion deforming decreased. This possibly indicated that inclusion fracture of the type indicated would occur earlier for inclusions of lower deformability.

In summary, the shape of the inclusion - matrix strain diagram may be explained in part in terms of strain rate for a multipass situation. i.e. As the matrix strain was increased, the strain rate increased, which led to an increased value of apparent inclusion to matrix stress ratio. This effectively led to the inclusions being less able to deform at the higher strain rates and therefore a flattening of the inclusion - matrix strain diagram ensued.

However, the stress and strain distributions around a deforming inclusion are complex, and such a simple fracture may not occur. It is often the case that inclusions thin in localised regions (35), analogous to the stretching of chewing gum. In addition fracture may not be uniform throughout the inclusion and fracture across an inclusion may be inhibited and the crack blunted to some degree, due to the viscous nature of silicate inclusions.

Figure 5.150. is a schematic illustration of the inclusion observed in section 4.8 which shows cracks associated with an inclusion viewed on the plane

of the major (a) and the intermediate axis (D).



5.150.

Thus the section taken at 90° to this plane may show the inclusion to be fractured, and possibly disseminated as indicated by section (C).

5.3.6.1. The effect of matrix/inclusion constraint.

The effect of matrix/inclusion constraint upon the inclusion strain/matrix strain diagram was investigated in order to assess its influence upon limiting inclusion deformation.

Using a simplified model based upon the idea of Robinson (202) it was assumed that the total work done by the matrix was consumed by the inclusion deformation and constraint.

i.e.

Work done (matrix) = work done (inclusion) + work done (constraint).

$$\sigma_m \epsilon_m = \sigma_i \epsilon_i + \frac{\sigma_m \pi (\epsilon_m - \epsilon_i) e^{2\epsilon_i}}{4}$$

Solution of ϵ_i from the above equation via Newtons method for various values of ϵ_m at a value of

$$\beta = \left(\frac{\sigma_i}{\sigma_m} \right) = 1.1$$

i.e. table 5.21

Table 5.21.

ϵ_m	ϵ_i	ν
0.001	0.00068	0.680
0.005	0.0034	0.676
0.01	0.0067	0.671
0.05	0.031	0.62
0.1	0.055	0.55
0.5	0.107	0.21
1.0	0.114	0.11
5.0	0.120	0.02

indicated that the effect of constraint would be to limit inclusion strain as the matrix strain increased and so result in a characteristic $\epsilon_i \vee \epsilon_m$ diagram. figure 5.151.

The effect of matrix/inclusion constraint upon the plasticity index/relative flow stress diagram.

Using the expression above (derived in appendix 5.4) for the simple case involving matrix, inclusion and constraint terms, values of ν were derived for a value of matrix strain (ϵ_m) tending towards zero i.e. $\epsilon_m = 0.001$. The values of ν at various inclusion/matrix stress ratios (β) were computed and are shown in table 5.22. and figure 5.152.

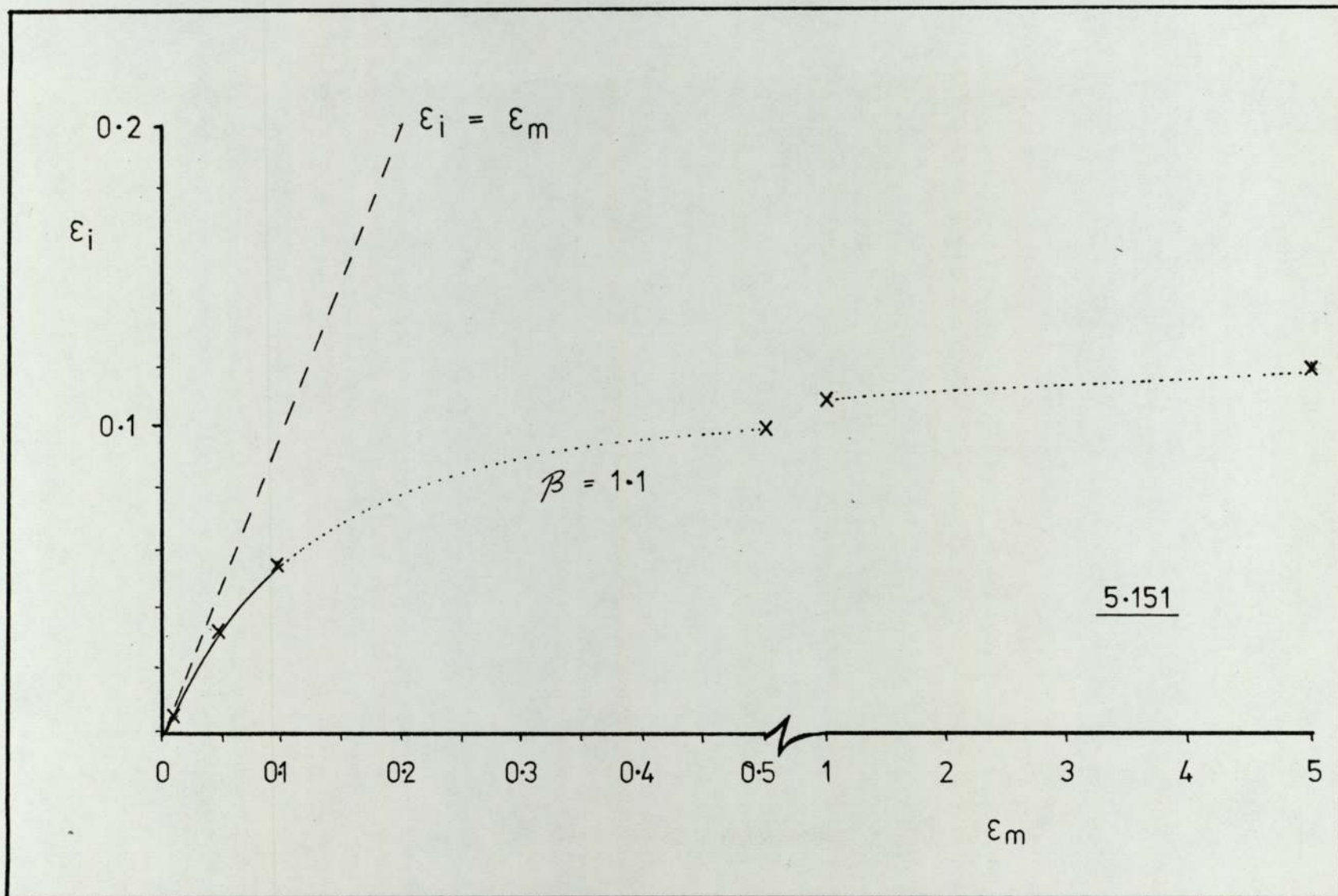
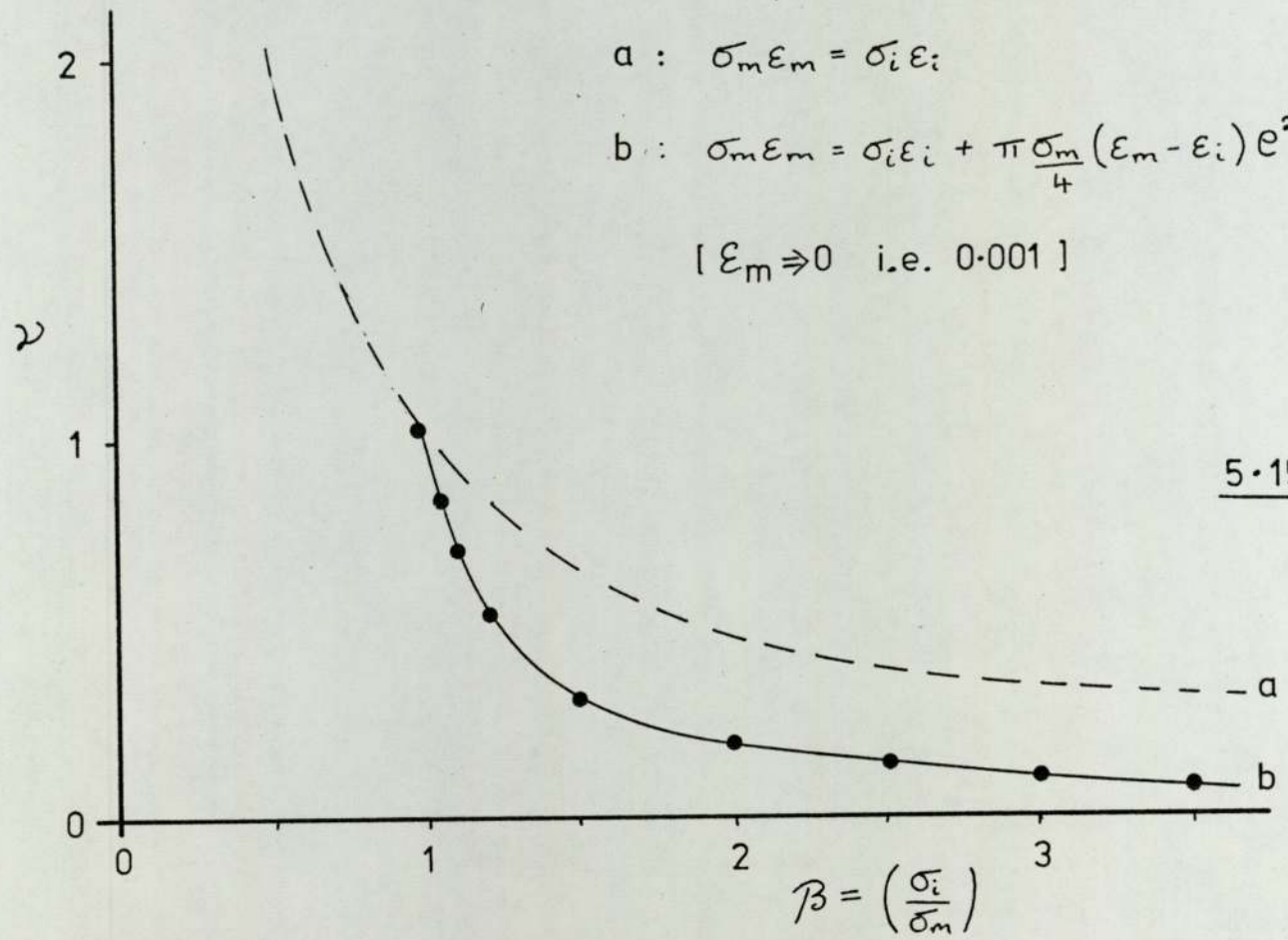


Table 5.22.

β	$\omega(\epsilon_m=0.001)$
1.000	1.000
1.001	0.995
1.005	0.977
1.01	0.955
1.05	0.810
1.1	0.680
1.2	0.517
1.3	0.416
1.4	0.349
1.5	0.300
2.0	0.177
2.5	0.125
3.0	0.097
3.5	0.079
4.0	0.068

This simple analysis indicated that the region of the original ω vs β diagram at values of $\beta > 1.0$ would be lowered towards the abscissa (β) axis. i.e. less deformation would be possible if constraint takes up an appreciable part of the energy available for deformation.

However, constraint at the matrix/inclusion interface is dependent upon the bonding between them.



5.3.6.2. Inhomogeneous deformation of the Matrix.

Since the geometry of the specimens to be rolled prevented plane strain deformation, the variation in the deformation patterns of the rolled samples were investigated. From tables 5.23. - .35. and figures 5.153. it was observed that inclusion strains were not constant throughout the height (thickness) of the deformed samples. The mean inclusion strains at various heights varied as a function of the degree of matrix strain.

Observations and measurements did show that for small deformations the regions of highest strain were at the top and bottom surfaces. As the degree of deformation was increased the areas of highest inclusion strain were seen to be in the central region of the section (figure 5 ^{.153.}_{.15%}).

However, as with all real systems, factors are in evidence to complicate the measurement of inhomogeneous deformation. Since the samples were hot rolled, there was a natural (Newtonian) cooling of the sample surfaces. In addition there were imposed temperature gradients due to roll chilling effects. Hence there was a non uniform temperature distribution through the sample. In the case of the deformation of silicate inclusions surface chilling would tend to reduce the deformability of inclusions in the surface region, and accentuate the strain differences when the material deforms more at the

Table 5.23
Melt Al4(2) Rolled at 1000°C
Matrix strain $\epsilon_m = 0.065$ (0.07)

x(mm)	n_i	$\bar{\epsilon}_i$	S_{ϵ_i}	S.E.	\bar{x}
0.0	6	0.11	0.09	0.04	1.57
1.0	4	0.09	0.12	0.06	1.28
2.0					
3.0	4	0.08	0.11	0.01	1.14
4.0	1	0.10			1.43
5.0	1	0.05			0.71
6.0					
7.0	2	0.08	0.00	0.00	1.14
8.0	2	0.09	0.01	0.01	1.28
9.0	2	0.07	0.00	0.00	1.00
10.0	3	0.07	0.03	0.02	1.00
11.0	5	0.00	0.00	0.00	0.00
12.0	3	0.00	0.00	0.00	0.00
13.0	1	0.00			0.00
14.0	4	0.00	0.00	0.00	0.00
15.0	1	0.00			0.00
16.0	3	0.00	0.00	0.00	0.00
17.0	2	0.09	0.05	0.04	1.28
18.0	2	0.07	0.03	0.02	1.00
19.0	2	0.15	0.03	0.02	2.14
20.0	1	0.19			2.71
21.0	1	0.21			3.00
22.0	3	0.11	0.01	0.00	1.57
23.0	4	0.13	0.03	0.01	1.86

Table 5.24
Melt Al4 (2) Rolled at 1000°C
Matrix strain $\epsilon_m = 0.105 (0.11)$

x(mm)	n _i	$\bar{\epsilon}_i$	S_{ϵ_i}	S.E.	\bar{y}
0.0	3	0.17	0.03	0.02	1.55
1.0	4	0.10	0.04	0.02	0.91
2.0					
3.0	3	0.12	0.11	0.06	1.09
4.0	1	0.10			0.91
5.0	4	0.07	0.03	0.02	0.64
6.0	4	0.09	0.03	0.02	0.82
7.0	2	0.07	0.01	0.01	0.64
8.0	3	0.05	0.02	0.01	0.45
9.0	2	0.04	0.03	0.02	0.27
10.0	1	0.03			0.27
11.0	4	0.07	0.05	0.02	0.64
12.0	7	0.10	0.04	0.02	0.91
13.0	4	0.11	0.06	0.03	1.00
14.0	3	0.17	0.07	0.04	1.55
15.0	2	0.08	0.01	0.01	0.73
16.0	5	0.09	0.04	0.04	0.82
17.0	1	0.19			1.73
18.0	1	0.08			0.73
19.0					
20.0					
21.0	2	0.18	0.04	0.03	1.64
22.0	3	0.17	0.01	0.01	1.55

Table 5.25

Melt Al₄ (2) Rolled at 1000°CMatrix strain $\bar{\epsilon}_m = 0.188$ (0.19)

x(mm)	n _i	$\bar{\epsilon}_i$	S_{ϵ_i}	S.E.	$\bar{\epsilon}$
0.0					
1.0					
2.0	1	0.11			0.58
3.0	1	0.06			0.32
4.0	1	0.22			1.15
5.0	1	0.04			0.21
6.0	3	0.09	0.07	0.04	0.47
7.0	1	0.13			0.68
8.0	2	0.20	0.01	0.01	1.05
9.0	3	0.22	0.05	0.03	1.15
10.0	2	0.31	0.06	0.04	1.63
11.0	1	0.10			0.53
12.0	2	0.08	0.02	0.01	0.42
13.0	1	0.14			0.74
14.0	2	0.24	0.18	0.12	1.26
15.0	1	0.21			1.11
16.0	1	0.20			1.05
17.0	1	0.14			0.74
18.0	1	0.11			0.58
19.0	1	0.13			0.68
20.0					

Table 5.26

Melt Al₄ (2) Rolled at 1000°CMatrix strain $\epsilon_m = 0.316$ (0.32)

x(mm)	n _i	$\bar{\epsilon}_i$	S_{ϵ_i}	S.E.	\bar{y}
0.0	2	0.24	0.26	0.19	0.76
1.0	3	0.26	0.12	0.07	0.81
2.0	3	0.29	0.09	0.05	0.91
3.0	2	0.25	0.13	0.09	0.80
4.0	1	0.41			1.28
5.0	2	0.27	0.33	0.24	0.84
6.0	6	0.39	0.18	0.07	1.22
7.0	5	0.38	0.20	0.09	1.19
8.0	4	0.30	0.15	0.07	0.94
9.0	3	0.55	0.23	0.14	1.72
10.0	3	0.37	0.15	0.09	1.16
11.0	2	0.20	0.22	0.16	0.63
12.0	2	0.19	0.04	0.03	0.59
13.0	1	0.20			0.63
14.0					
15.0	2	0.46	0.07	0.05	1.44
16.0	2	0.45	0.09	0.07	1.41
17.0					
18.0					
19.0					

Table 5.27

Melt NIA12 Rolled at 1000°C.Matrix strain $\epsilon_m = 0.042$

x(mm)	n_i	$\bar{\epsilon}_i$	S_{ϵ_i}	S.E. $\bar{\epsilon}_i$	\bar{y}
0.0	4	0.26	< 0.01	< 0.01	6.29
0.5	6	0.18	"	"	4.31
1.0	4	0.24	"	"	5.64
1.5	4	0.28	"	"	6.57
2.0	5	0.12	"	"	2.88
2.5	5	0.11	"	"	2.55
3.0	6	0.10	"	"	2.28
3.5	11	0.08	"	"	1.88
4.0	6	0.06	"	"	1.47
4.5	9	0.05	"	"	1.28
5.0	7	0.06	"	"	1.33
5.5	13	0.06	"	"	1.45
6.0	9	0.02	"	"	0.54
6.5	9	0.02	"	"	0.54
7.0	10	0.02	"	"	0.47
7.5	6	0.01	"	"	0.26
8.0	11	0.01	"	"	0.14
8.5	10	0.01	"	"	0.24
9.0	11	0.02	"	"	0.36
9.5	11	0.01	"	"	0.12
10.0	7	0.00	"	"	0.00
10.5	7	0.00	"	"	0.00
11.0	2	0.00	"	"	0.00
11.5	12	0.00	"	"	0.00
12.0	15	0.00	"	"	0.00

Table 5.27 (cont.)

$x(\text{mm})$	n_i	$\bar{\epsilon}_i$	S_{ϵ_i}	S.E.	\bar{y}
12.5	10	0.00	0.00	0.00	0.00
13.0	7	0.00	"	"	0.00
13.5	14	0.00	"	"	0.05
14.0	11	0.01	"	"	0.10
14.5	12	0.00	"	"	0.02

Table 5.28

Melt NIA12 Rolled at 1000°CMatrix Strain $\epsilon_m = 0.385$

x(mm)	n _i	$\bar{\epsilon}_i$	S_{ϵ_i}	S.E.	\bar{y}
0.0	10	0.33	0.08	0.03	0.85
0.5	10	0.43	0.12	0.04	1.12
1.0	13	0.52	0.08	0.02	1.36
1.5	7	0.51	0.07	0.03	1.33
2.0	7	0.68	0.07	0.03	1.75
2.5	4	0.66	0.04	0.02	1.72
3.0	6	0.61	0.09	0.04	1.59
3.5	5	0.75	0.08	0.04	1.96
4.0	10	0.59	0.12	0.04	1.54
4.5	4	0.65	0.02	0.01	1.67
5.0	9	0.59	0.10	0.03	1.52
5.5	5	0.55	0.07	0.03	1.44
6.0	5	0.54	0.14	0.06	1.41
6.5	11	0.55	0.11	0.03	1.42
7.0	6	0.56	0.16	0.07	1.46
7.5	8	0.60	0.12	0.04	1.57
8.0	15	0.56	0.10	0.03	1.46
8.5	9	0.54	0.14	0.05	1.41
9.0	8	0.61	0.05	0.02	1.57
9.5	6	0.59	0.11	0.04	1.55
10.0	4	0.51	0.10	0.05	1.32
10.5	4	0.59	0.10	0.05	1.59
11.0	5	0.47	0.11	0.05	1.23

Table 5.28 (cont)

$x(\text{mm})$	n_i	$\bar{\epsilon}_i$	S_{ϵ_i}	S.E.	\bar{y}
11.5	10	0.51	0.07	0.02	1.33
12.0	9	0.53	0.14	0.05	1.39
12.5	13	0.54	0.07	0.02	1.40
13.0	11	0.57	0.06	0.02	1.49
13.5	10	0.47	0.08	0.03	1.21
14.0	10	0.52	0.05	0.01	1.34
14.5	11	0.47	0.07	0.02	1.21
15.0	10	0.45	0.08	0.03	1.17
15.5	10	0.36	0.07	0.02	0.96
16.0	8	0.33	0.07	0.02	0.86

Table 5.29

Melt NIA12 Rolled at 1000°CMatrix strain $\epsilon_m = 0.622$

x(mm)	n_i	$\bar{\epsilon}_i$	S_{ϵ_i}	S.E.	\bar{y}
0.0	11	0.45	0.07	0.02	0.73
0.5	6	0.49	0.10	0.04	0.79
1.0	10	0.61	0.10	0.03	0.98
1.5	11	0.82	0.10	0.03	1.32
2.0	12	0.89	0.12	0.04	1.42
2.5	9	0.87	0.08	0.03	1.40
3.0	10	0.86	0.09	0.03	1.39
3.5	11	0.91	0.09	0.03	1.46
4.0	11	0.90	0.09	0.03	1.45
4.5	11	0.98	0.13	0.04	1.58
5.0	13	1.01	0.13	0.04	1.62
5.5	11	0.87	0.10	0.03	1.39
6.0	10	1.04	0.25	0.08	1.68
6.5	9	0.93	0.13	0.04	1.49
7.0	10	0.94	0.11	0.04	1.52
7.5	9	1.03	0.12	0.04	1.66
8.0	10	0.96	0.14	0.05	1.54
8.5	9	0.85	0.15	0.05	1.37
9.0	11	0.92	0.15	0.04	1.47
9.5	11	0.91	0.13	0.04	1.46
10.0	10	0.93	0.16	0.05	1.50
10.5	9	0.90			1.44

Table 5.29 (cont.)

$x(\text{mm})$	n_i	$\bar{\epsilon}_i$	S_{ϵ_i}	S.E.	\bar{y}
11.0	10	0.87			1.40
11.5	11	0.67			1.08
12.0	9	0.46			0.74
12.5	8	0.47			0.76

Table 5.30
Melt NIA12 Rolled at 1000°C
Matrix strain $\epsilon_m = 0.817$

x(mm)	n_i	$\bar{\epsilon}_i$	S_{ϵ_i}	S.E.	\bar{y}
0.0	4	1.05	0.07	0.04	1.28
0.5	2	1.08	0.03	0.02	1.32
1.0	3	1.07	0.11	0.06	1.31
1.5	7	1.16	0.16	0.06	1.42
2.0	5	1.15	0.12	0.05	1.41
2.5	4	1.31	0.27	0.13	1.60
3.0	4	1.25	0.19	0.09	1.52
3.5	7	1.36	0.11	0.04	1.67
4.0	13	1.36	0.14	0.04	1.66
4.5	5	1.37	0.18	0.08	1.67
5.0	10	1.44	0.17	0.05	1.77
5.5	9	1.44	0.21	0.07	1.76
6.0	8	1.23	0.25	0.09	1.51
6.5	3	1.14	0.24	0.14	1.40
7.0	7	1.24	0.12	0.05	1.52
7.5	5	1.01	0.20	0.09	1.24
8.0	2	0.95	0.08	0.06	1.17
8.5	5	1.03	0.11	0.05	1.26
9.0	4	0.91	0.08	0.04	1.14
9.5	2	0.97	0.04	0.03	1.18
10.0		No Data			

Table 5.31

Melt NIA12 Rolled at 1000°CMatrix strain $\epsilon_m = 1.131$

x(mm)	n _i	$\bar{\epsilon}_i$	S_{ϵ_i}	S.E.	\bar{x}
0.0	13	1.91	0.17	0.05	1.68
0.5	14	1.36	0.22	0.06	1.20
1.0	9	1.42	0.18	0.06	1.25
1.5	13	1.58	0.19	0.05	1.40
2.0	11	1.58	0.20	0.06	1.40
2.5	18	1.59	0.16	0.04	1.41
3.0	17	1.52	0.23	0.05	1.34
3.5	13	1.55	0.23	0.06	1.37
4.0	12	1.52	0.22	0.06	1.35
4.5	17	1.45	0.32	0.08	1.28
5.0	14	1.58	0.27	0.07	1.37
5.5	13	1.45	0.14	0.04	1.28
6.0	14	1.48	0.16	0.04	1.31
6.5	11	1.28	0.11	0.03	1.13
7.0	9	1.29	0.21	0.07	1.14

Table 5.32

Melt NIA12 Rolled at 1000°CMatrix strain $\epsilon_m = 1.566$

x(mm)	n _i	$\bar{\epsilon}_i$	S_{ϵ_i}	S.E.	$\bar{\mu}$
0.0	11	1.49	0.21	0.06	0.95
0.5	11	1.51	0.39	0.11	0.96
1.0	9	1.57	0.21	0.07	1.02
1.5	10	1.71	0.25	0.08	1.09
2.0	8	1.71	0.34	0.12	1.09
2.5	7	1.76	0.22	0.08	1.12
3.0	15	1.65	0.19	0.05	1.06
3.5	20	1.74	0.27	0.06	1.11
4.0	9	1.68	0.23	0.08	1.07
4.5	11	1.45	0.37	0.11	0.93
5.0	4	1.54	0.09	0.04	0.99

Table 5.33

Plasticine experiment (1)

Ligament.	$\epsilon_m = 0.23$		$\epsilon_m = 0.47$		$\epsilon_m = 0.93$		$\epsilon_m = 1.78$		$\epsilon_m = 2.47$	
	$\bar{\epsilon}_L$	$\bar{\psi}$	$\bar{\epsilon}_L$	$\bar{\psi}$	$\bar{\epsilon}_L$	$\bar{\psi}$	$\bar{\epsilon}_L$	$\bar{\psi}$	$\bar{\epsilon}_L$	$\bar{\psi}$
1	0.16	0.69	0.24	0.69	0.54	0.58	1.57	0.88	2.07	0.84
2	0.02	0.08	0.28	0.59	0.74	0.80	1.28	0.72	2.12	0.86
3	0.27	1.17	0.54	1.14	1.12	1.20	1.85	1.04	2.74	1.11
4	0.27	1.19	0.47	1.01	1.13	1.21	1.76	0.99	2.37	0.96
5	0.35	1.50	0.51	1.08	1.30	1.40	2.05	1.15	2.69	1.09
6	0.34	1.48	0.47	1.01	1.16	1.25	1.99	1.12	2.57	1.04
7	0.37	1.61	0.58	1.23	1.43	1.54	2.08	1.17	2.87	1.16
8	0.30	1.31	0.52	1.10	1.24	1.33	1.80	1.01	2.44	0.99
9	0.37	1.60	0.54	1.16	1.31	1.41	2.06	1.16	2.54	1.03
10	0.25	1.09	0.49	1.04	1.02	1.10	1.71	0.96	2.12	0.86
11	0.32	1.38	0.48	1.03	0.96	1.03	1.67	0.94	2.02	0.82
12	0.12	0.50	0.39	0.82	0.56	0.60	1.32	0.74	2.03	0.82
13	0.07	0.30	0.35	0.75	0.46	0.49	1.17	0.66	1.90	0.77

Table 5.34

Plasticine Experiment (2)

Ligament	$\epsilon_m = 0.15$		$\epsilon_m = 0.22$		$\epsilon_m = 0.38$		$\epsilon_m = 0.67$		$\epsilon_m = 1.10$		$\epsilon_m = 1.69$		$\epsilon_m = 2.36$	
	$\bar{\epsilon}_L$	$\bar{\psi}$	$\bar{\epsilon}_L$	$\bar{\psi}$	$\bar{\epsilon}_L$	$\bar{\psi}$	$\bar{\epsilon}_L$	$\bar{\psi}$	$\bar{\epsilon}_L$	$\bar{\psi}$	$\bar{\epsilon}_L$	$\bar{\psi}$	$\bar{\epsilon}_L$	$\bar{\psi}$
1	0.01	0.10	0.04	0.18	0.03	0.09	0.38	0.56	1.02	0.93	1.54	0.91	1.86	0.79
2	0.25	1.67	0.15	0.67	0.41	1.09	0.60	0.89	1.06	0.96	1.81	1.07	2.29	0.97
3	0.32	2.15	0.27	1.27	0.44	1.15	0.85	1.27	1.34	1.22	1.98	1.17	2.67	1.13
4	0.20	1.32	0.22	0.98	0.32	0.85	0.81	1.21	1.26	1.15	1.84	1.10	2.90	1.23
5	0.18	1.20	0.29	1.30	0.47	1.25	0.82	1.23	1.29	1.17	2.23	1.32	2.71	1.15
6	0.08	0.53	0.28	1.27	0.25	0.67	0.63	0.95	1.07	0.97	1.86	1.10	2.53	1.07
7	0.00	0.00	0.12	0.53	0.24	0.64	0.50	0.75	0.86	0.78	1.45	0.86	1.75	0.74

$$\bar{\psi} = \frac{\bar{\epsilon}_L}{\epsilon_m}$$

Table 5.35
Plasticine Experiment (3)

Ligament	Matrix strain values (ϵ_m)							
	0.166		0.173		0.230		0.297	
	$\bar{\epsilon}_L$	$\bar{\psi}$	$\bar{\epsilon}_L$	$\bar{\psi}$	$\bar{\epsilon}_L$	$\bar{\psi}$	$\bar{\epsilon}_L$	$\bar{\psi}$
1	0.00	0.00	0.00	0.00	0.17	0.75	0.09	0.30
2	0.06	0.38	0.07	0.41	0.12	0.53	0.23	0.78
3	0.18	1.08	0.21	1.23	0.21	0.89	0.39	1.32
4	0.20	1.21	0.18	1.03	0.22	0.97	0.32	1.07
5	0.28	1.70	0.27	1.55	0.29	1.27	0.39	1.32
6	0.22	1.32	0.24	1.38	0.27	1.19	0.39	1.31
7	0.19	1.16	0.27	1.53	0.35	1.53	0.35	1.17
8	0.11	0.66	0.18	1.05	0.25	1.11	0.27	0.91
9	0.16	0.98	0.14	0.82	0.32	1.40	0.36	1.22
10	0.18	1.08	0.22	1.26	0.33	1.44	0.33	1.12
11	0.19	1.16	0.14	0.80	0.31	1.36	0.33	1.10
12	0.15	0.88	0.11	0.63	0.26	1.15	0.27	0.92
13	0.16	0.98	0.19	1.07	0.27	1.17	0.30	1.02
14	0.17	1.00	0.09	0.50	0.25	1.09	0.21	0.71
15	0.17	1.03	0.15	0.87	0.25	1.07	0.21	0.72
16	0.16	0.98	0.00	0.00	0.12	0.53	0.12	0.40
17	0.00	0.00	0.00	0.00	0.01	0.05	0.20	0.68

Table 5.35 (cont.)

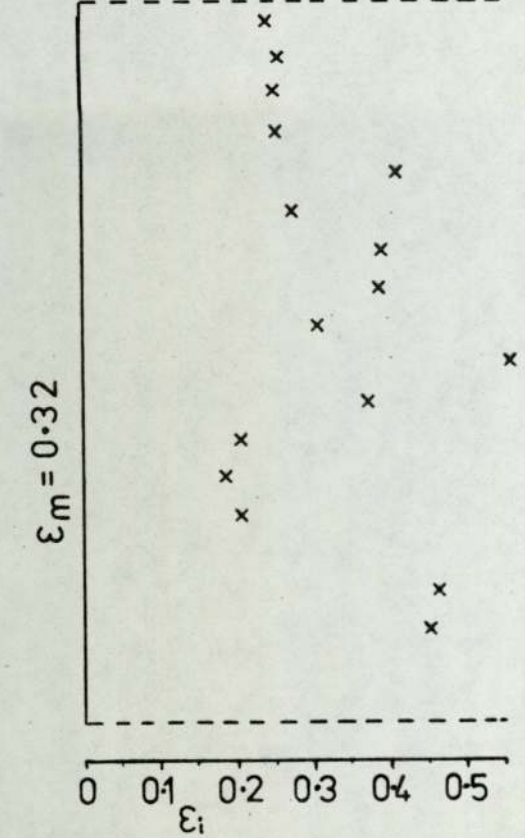
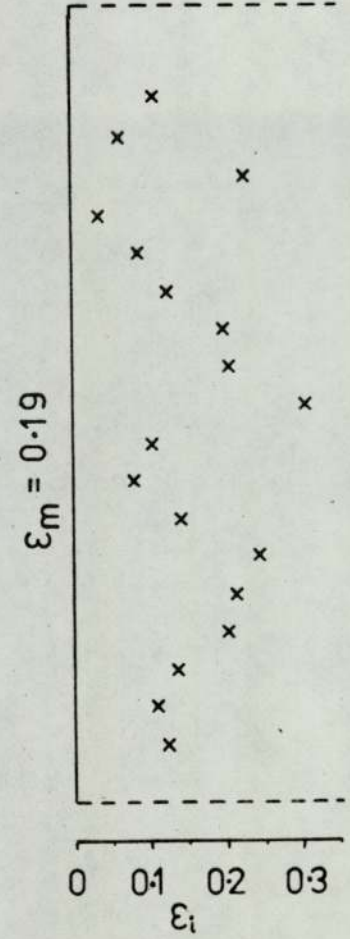
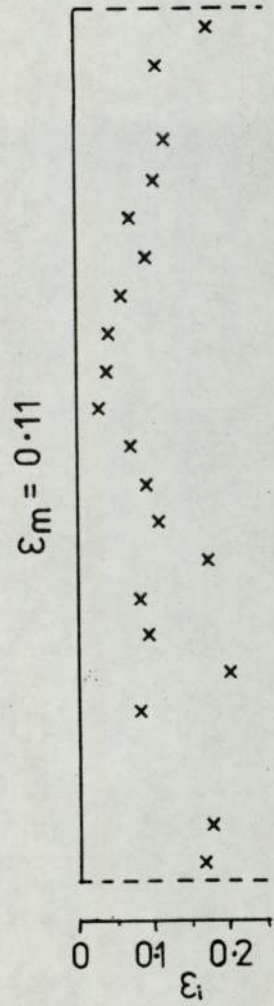
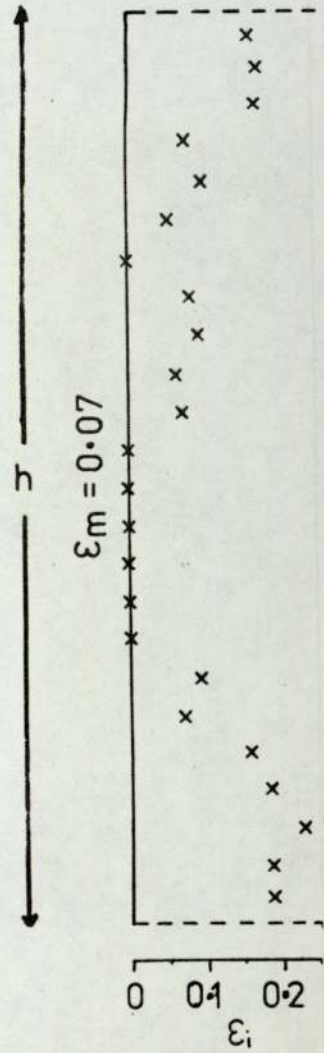
Plasticine experiment (3)

Ligament	Matrix strain values (\mathcal{E}_m)					
	0.396		0.632		0.947	
	$\bar{\mathcal{E}}_L$	$\bar{\psi}$	$\bar{\mathcal{E}}_L$	$\bar{\psi}$	$\bar{\mathcal{E}}_L$	$\bar{\psi}$
1	0.19	0.47	0.34	0.53	0.52	0.55
2	0.30	0.75	0.44	0.69	0.61	0.65
3	0.50	1.26	0.64	1.02	0.97	1.03
4	0.37	0.93	0.67	1.06	1.19	1.26
5	0.77	1.96	0.82	1.30	1.22	1.28
6	0.48	1.20	0.77	1.23	1.16	1.22
7	0.50	1.27	0.93	1.46	1.28	1.35
8	0.48	1.22	0.91	1.44	1.17	1.23
9	0.54	1.37	0.81	1.29	1.30	1.38
10	0.49	1.23	0.86	1.37	1.19	1.26
11	0.50	1.26	0.81	1.28	1.22	1.28
12	0.44	1.10	0.77	1.23	1.11	1.18
13	0.40	1.01	0.71	1.12	1.05	1.11
14	0.37	0.93	0.55	0.87	0.89	0.94
15	0.27	0.69	0.48	0.76	0.76	0.80
16	0.19	0.47	0.40	0.63	0.59	0.62
17	0.07	0.19	0.23	0.37	0.53	0.56

Table 5.35 (cont.)

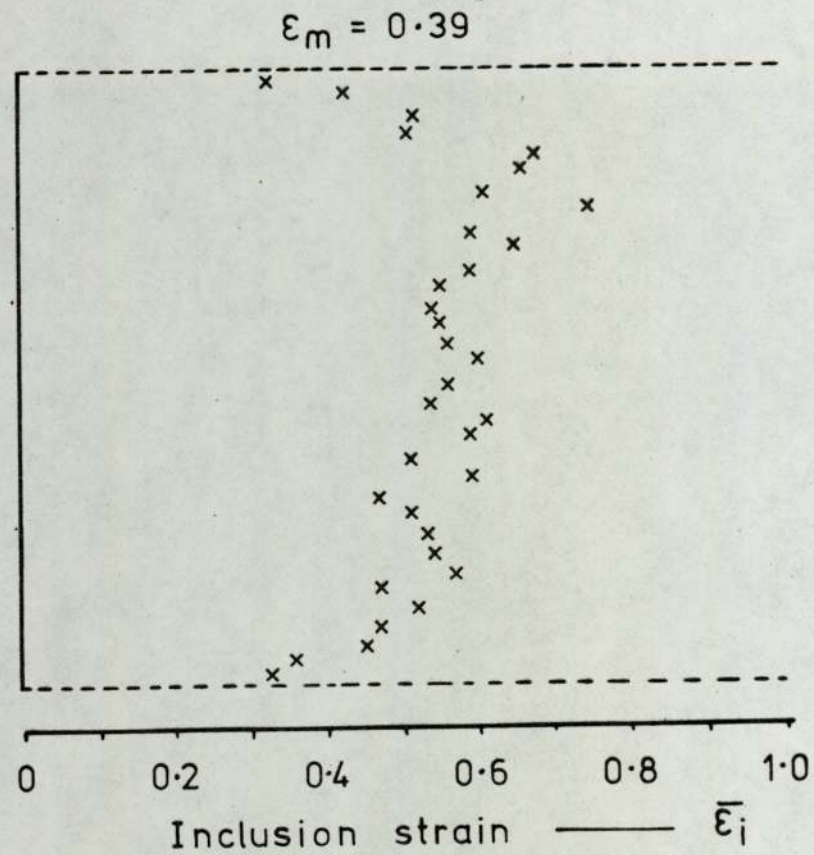
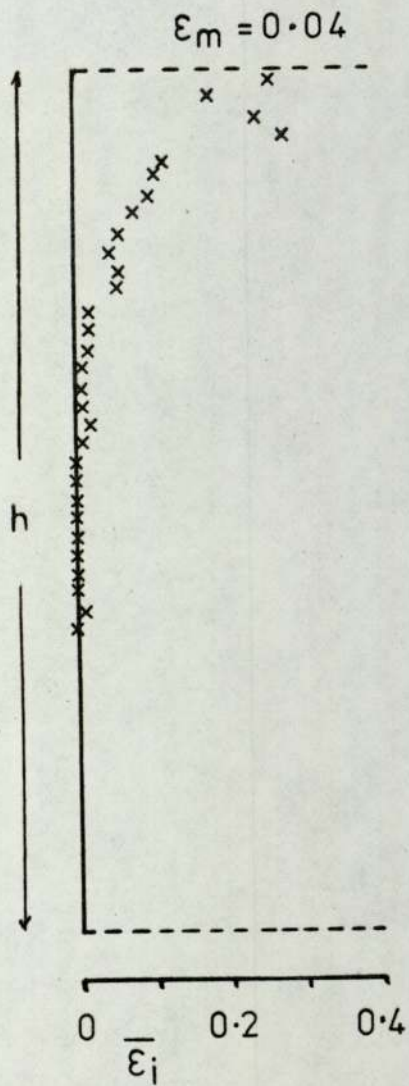
Plasticine Experiment (3)

Ligament	Matrix strain values (ϵ_m)					
	1.237		1.677		2.535	
	$\bar{\epsilon}_L$	$\bar{\psi}$	$\bar{\epsilon}_L$	$\bar{\psi}$	$\bar{\epsilon}_L$	$\bar{\psi}$
1	0.63	0.50	1.68	1.00	2.02	0.80
2	0.88	0.70	1.37	0.82	2.17	0.86
3	1.30	1.04	1.70	1.02	1.59	0.63
4	1.36	1.08	1.61	0.96	2.30	0.91
5	1.57	1.25	1.86	1.12	2.50	0.99
6	1.45	1.15	1.78	1.06	2.42	0.95
7	1.76	1.40	2.00	1.19	2.74	1.08
8	1.54	1.23	1.90	1.13	2.42	0.95
9	1.65	1.31	2.14	1.27	2.54	1.00
10	1.56	1.24	1.70	1.02	2.34	0.90
11	1.54	1.23	1.92	1.15	2.59	1.02
12	1.39	1.10	1.65	0.98	2.46	0.97
13	1.45	1.15	1.70	1.06	2.42	0.95
14	1.25	1.00	1.66	0.99	2.34	0.92
15	1.09	0.89	1.42	0.84	2.17	0.86
16	0.77	0.61	1.32	0.80	1.83	0.72
17	0.56	0.45	2.24	1.33	1.65	0.65

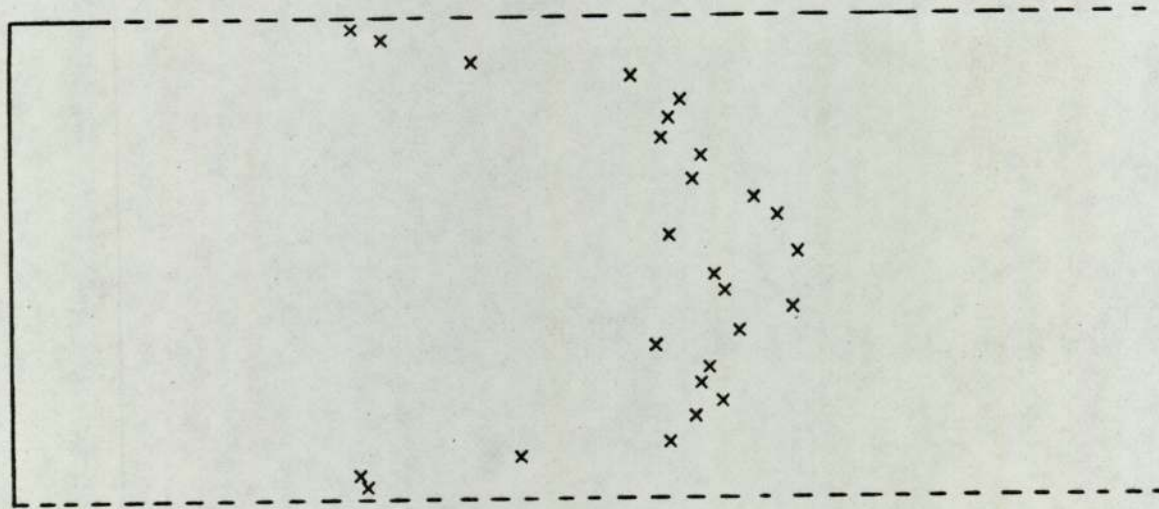


5.153

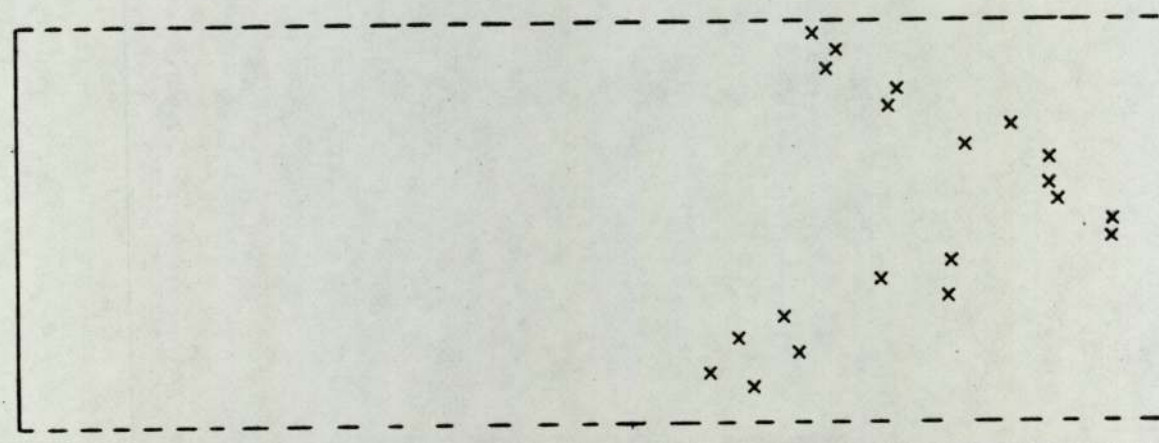
Variation in inclusion strain (ϵ_i), throughout the thickness of rolled samples (1000°C), at various matrix strains (ϵ_m).



Variation in inclusion strain ($\bar{\epsilon}_i$), throughout the thickness (height) of rolled samples (1000°C), at various matrix strains (ϵ_m). MELT NIA12.

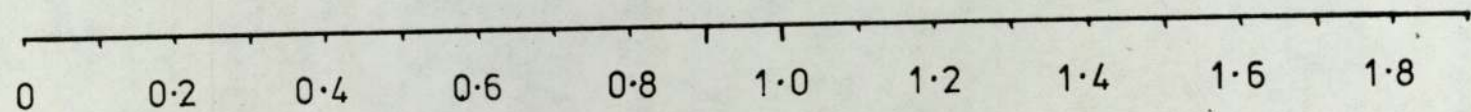
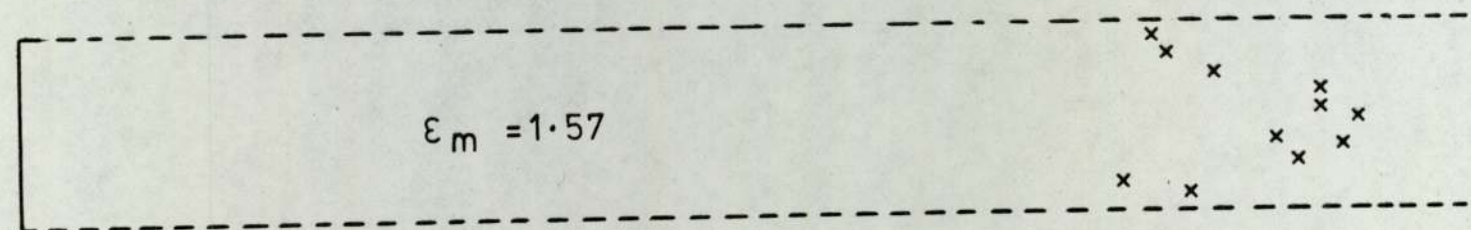
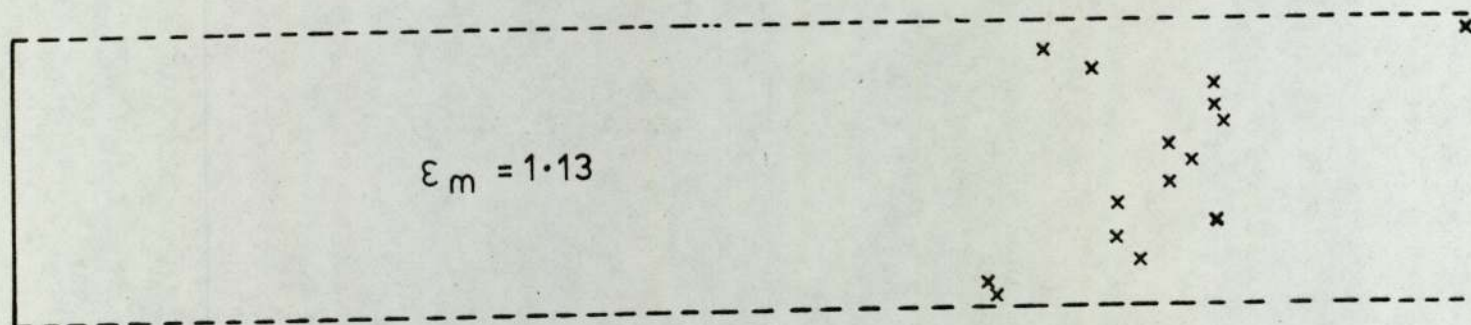


$\epsilon_m = 0.62$

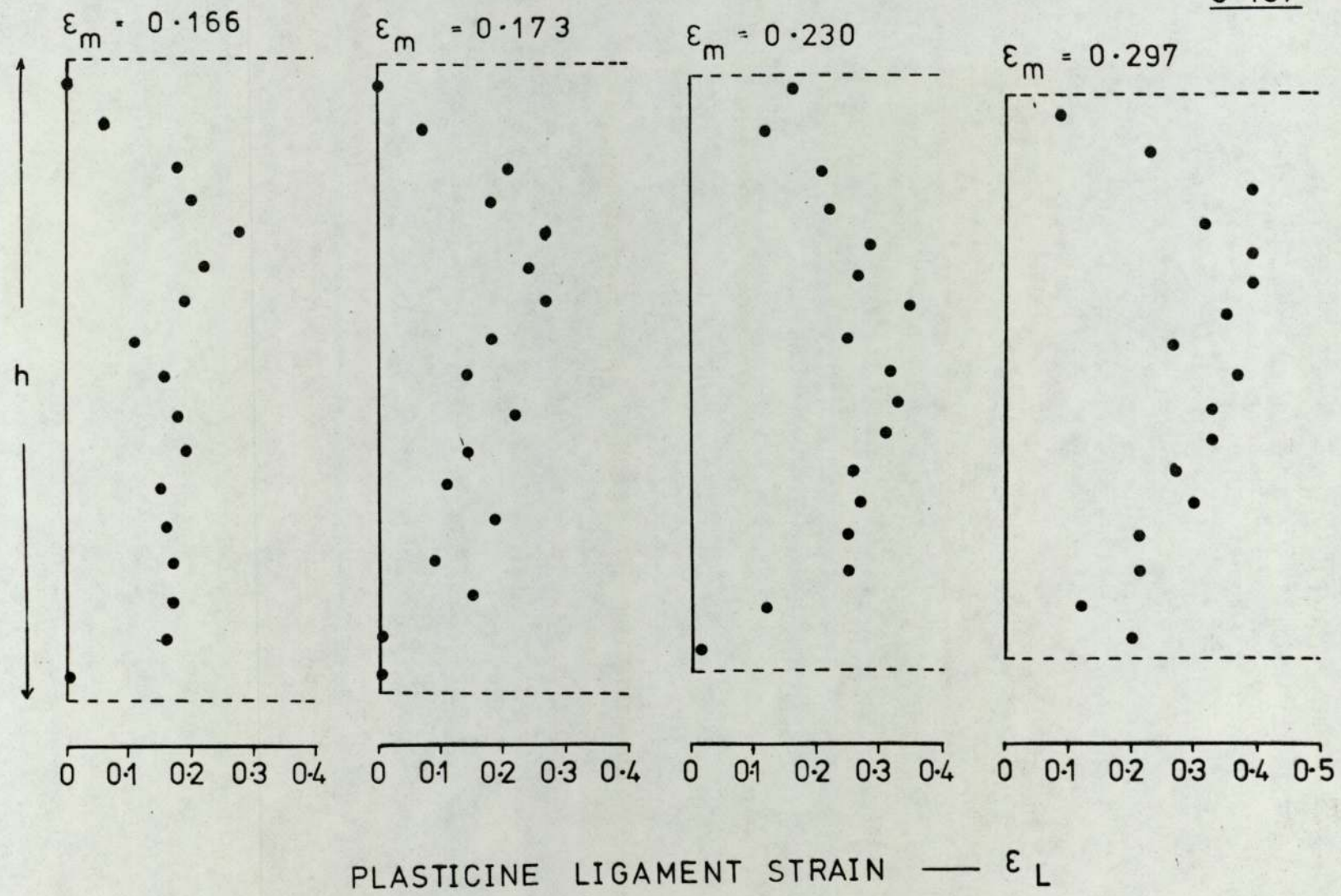


$\epsilon_m = 0.82$

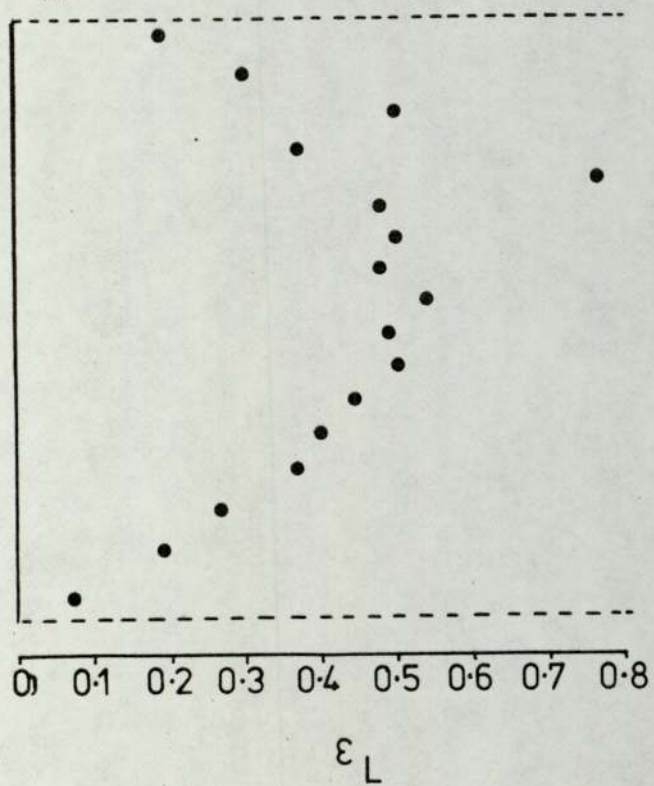
0 0.2 0.4 0.6 0.8 1.0 1.2 1.4
Inclusion strain — $\bar{\epsilon}_i$



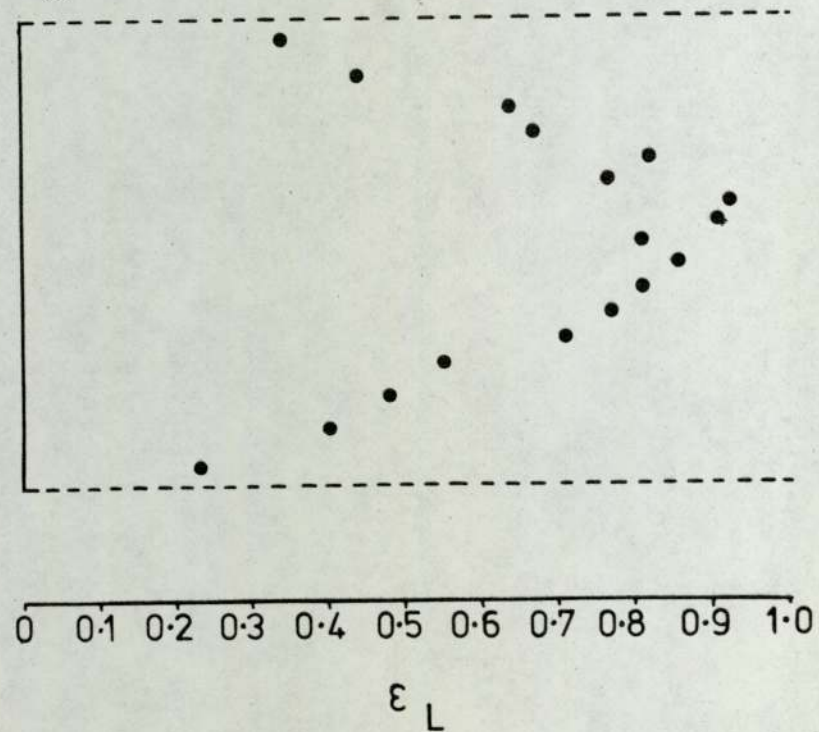
Inclusion strain — $\bar{\epsilon}_i$



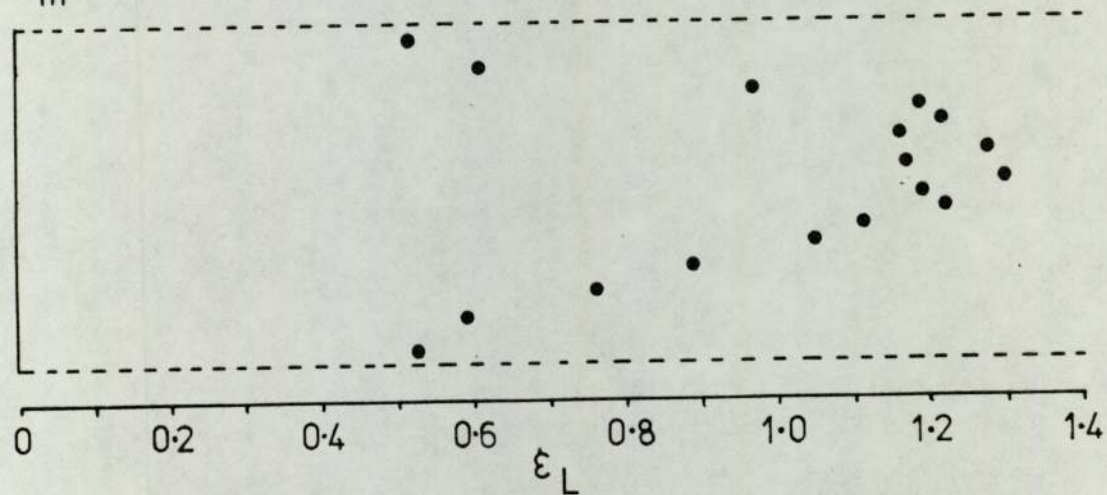
$$\epsilon_m = 0.396$$



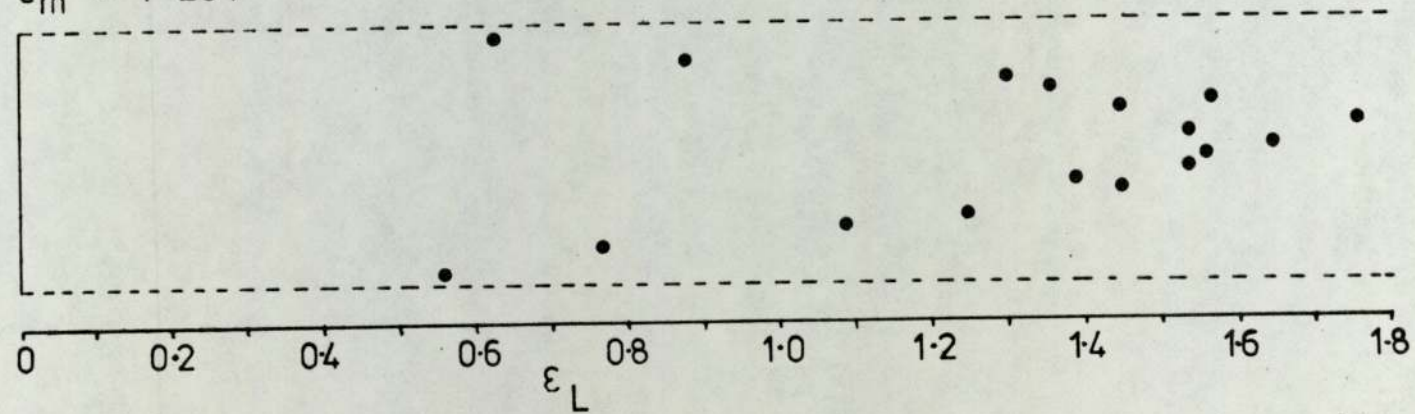
$$\epsilon_m = 0.632$$



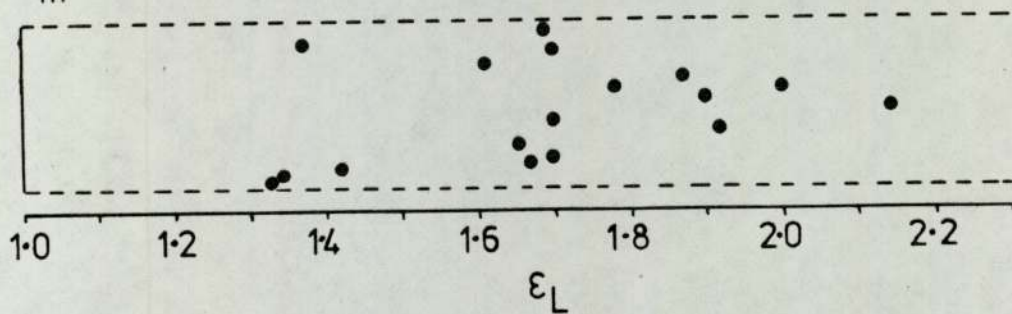
$$\epsilon_m = 0.947$$



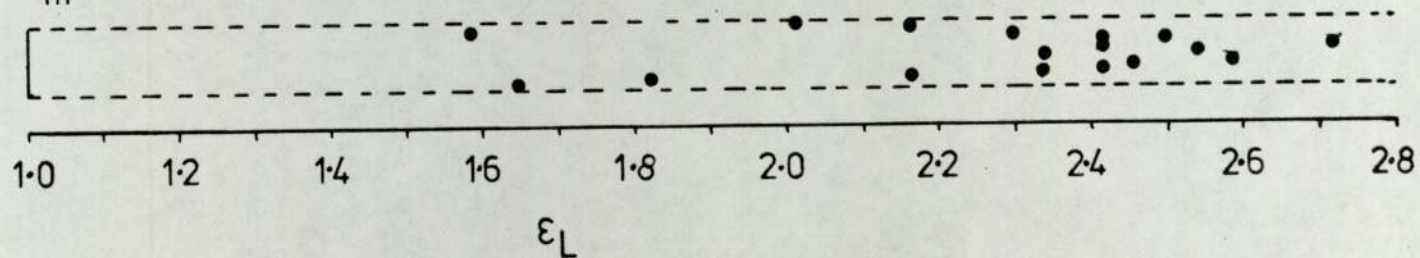
$$\epsilon_m = 1.237$$



$$\epsilon_m = 1.677$$



$$\epsilon_m = 2.535$$



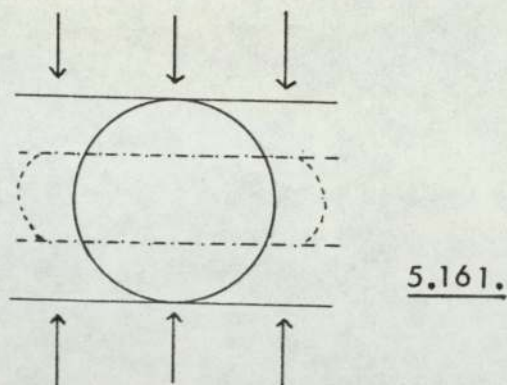
5.160

centre. However, if the major strain was at the surface the effect would be attenuated.

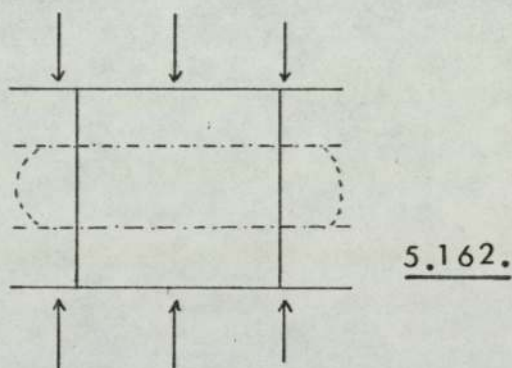
Since the cooling effect was seen as a potential complicating factor, the matrix deformation was investigated using a composite plasticine model system. The results of the plasticine models rolled at room temperature (22°C) were considered to simulate the conditions in hot rolled steels of uniform temperature gradient. In addition the work hardening index of plasticine at room temperature, which has been assessed as approximately 0.2 (114) is in the range encountered with steels at hot working temperatures

The actual results obtained (table 5.35 and figures 5.157, 5.160) showed that there was a slight discrepancy with respect to the actual inclusion - steel system. This discrepancy was that in the model system at low matrix deformations no pronounced surface strains were encountered. However, at increased matrix strains the central regions of the plasticine composites deformed in excess of the surface layers as with the real system.

Returning to the matrix deformation at low matrix strains, these discrepancies in surface strains encountered with the model and real systems may be attributable to the geometry of the specimens used. In the case of the steel samples a round bar was rolled into a strip viz.



However, in the model systems the initial shape of the composite was a bar of square cross section, equal in height to the diameter of the round steel bar. This was again rolled into strip form.



By simple observation of the initial geometries it may be deduced that the deformation at the surface of the round bar will be greater due to the lack of material preventing lateral widthways spread.

An interesting phenomenon of both the plasticine and steel experiments was the strain disparity between the centre and surface regions of rolled samples at the various matrix reductions. A value of strain disparity $\Delta\epsilon$ defined as the difference between the mean strain in the central $\frac{1}{3}$ rd region of the sample and the mean strains of the top and bottom $\frac{1}{3}$ rds of the

samples.

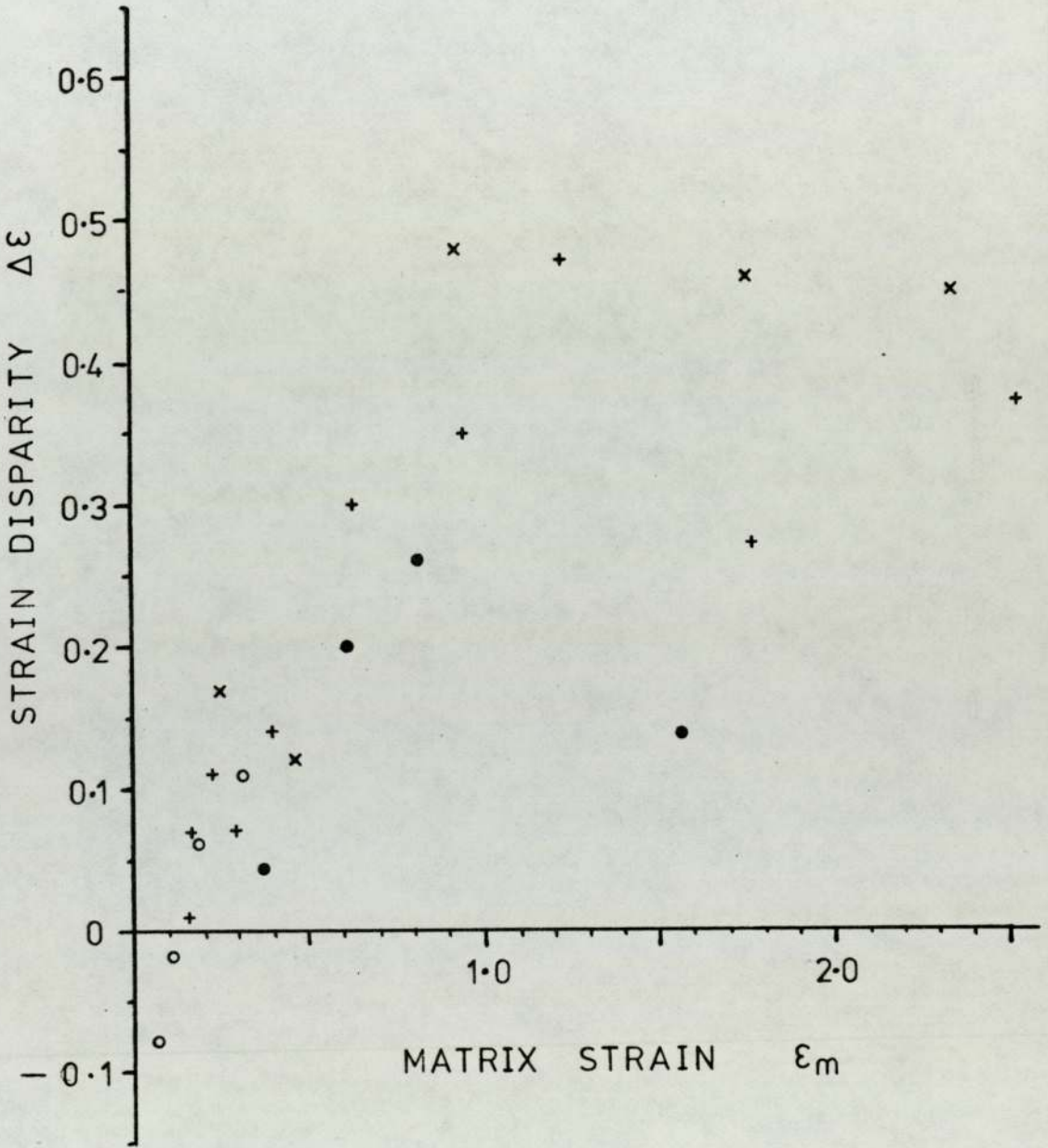
i.e

$$\Delta \epsilon = \bar{\epsilon}_c - \left[\frac{\bar{\epsilon}_T + \bar{\epsilon}_B}{2} \right]$$

In this way non symmetrical deformation about the centre of the specimen in the horizontal rolling plane was eliminated by the grouping of the top and bottom sections.

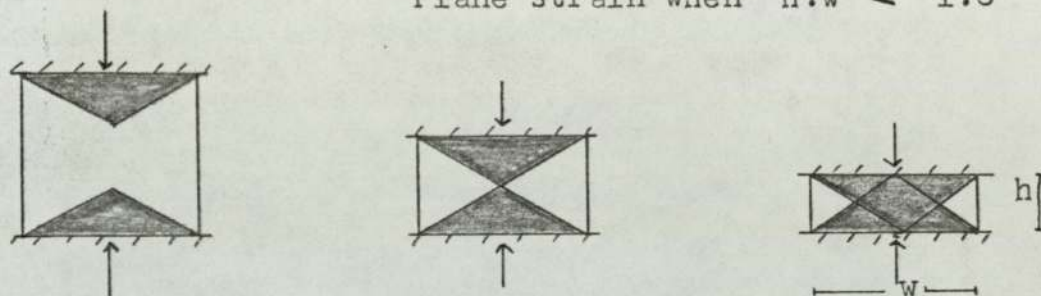
From the results compiled in tables 5.24. and figure 5.163. it may be seen that for both the plasticine and steel specimens the value of $\Delta \epsilon$ was linearly variable with the mean matrix strain $\bar{\epsilon}_m$ upto approximately $\bar{\epsilon}_m = 0.8$. As the matrix strain was increased beyond a value of (0.8 to 1.0) there was a deviation from linearity, as was observed for the inclusion (composite)/matrix strain diagram figure 5.146.^{146.} section 5.3.6. From figure 5.163. it may be seen that at these higher matrix strains upto 2.5 the value of $\Delta \epsilon$ appeared to reach a plateau for the (+, x) plasticine models, whereas the suggestion for the steel-inclusion sample was a decrease in strain disparity. However, there was only limited data available for the steel-inclusions sample.

In the early stages of deformation, it would be expected that constraint would prevent large degrees of strain in the surface regions and most of the deformation would occur in the central region. As the degree of matrix strain increased it may be that the

5.163

central region work hardened to an extent such that it was as easy, or easier for the surface layers to deform. At these higher strains conditions would be tending towards a more of a plane strain situation, and there would be overlapping of the zones of constraint due to the roll faces. viz in an idealised situation.

5.164.

Plane strain when $h:w < 1:6$ 

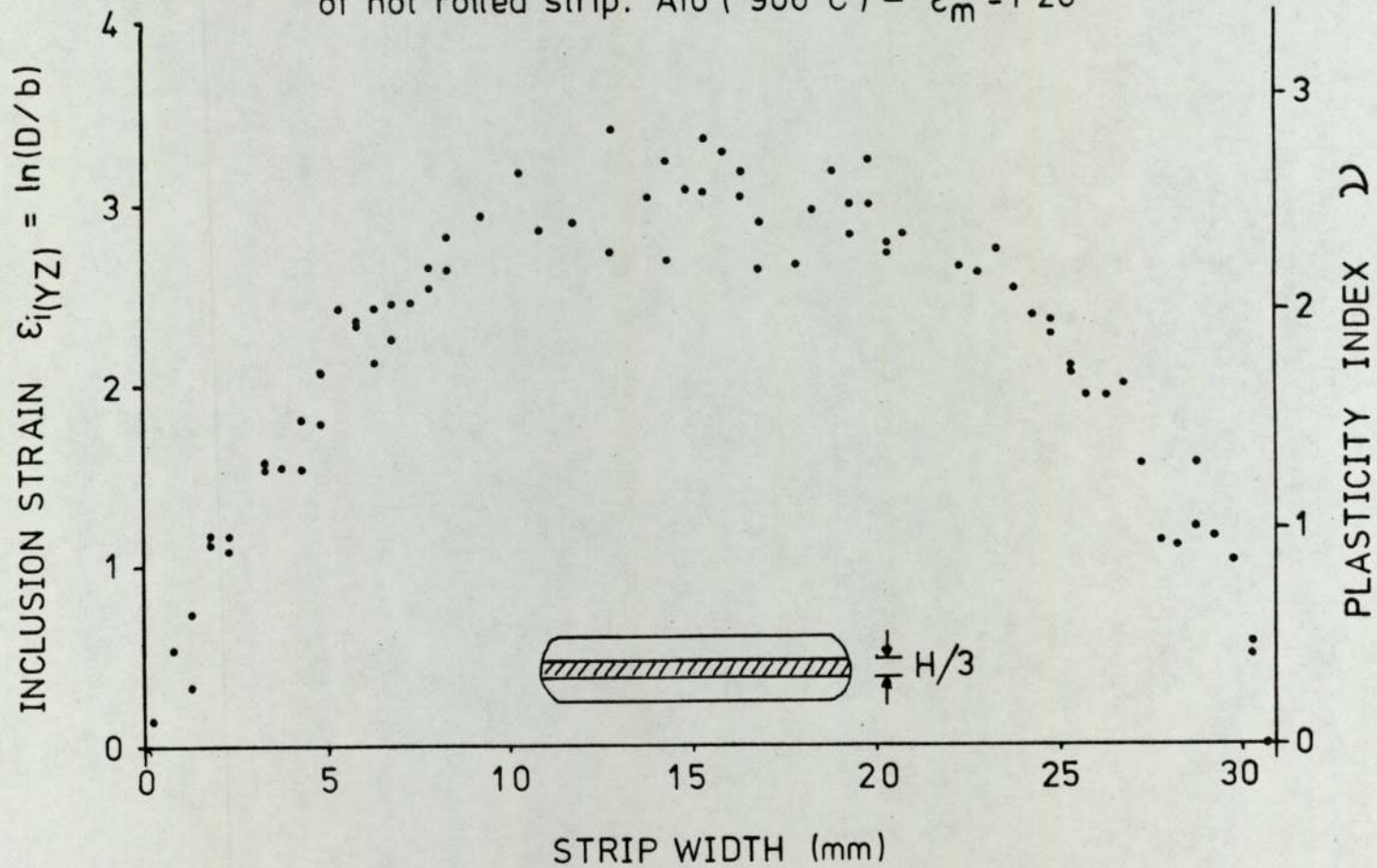
In order for $\Delta\epsilon$ to decrease at higher reductions it would seem necessary that the deformation takes place mainly at the surface. However, if inclusions are being used to ascertain the degree of matrix deformation it must be emphasized that inclusions become more reluctant to deform as the matrix strain is increased. (section 5.3.6)

5.3.6.3. Variation in inclusion strain
across specimen width.

Figure 5.165. shows the variation in inclusion strain across the width of the specimen as measured on the (YZ) plane, for inclusions greater than 10 μm (in order to avoid complications due to size.) It can be seen that in the mid $\frac{1}{3}$ rd section of the width that inclusion strain is reasonably constant (providing that measurement is not made outside the mid $\frac{1}{3}$ rd section in the through height (thickness) direction). This is a necessary restriction because of the non homogeneous deformation pattern throughout the height (thickness) direction.

This fact does aid the experimental side of the investigations whereby if the sample is sectioned on the (XY) plane slightly away from the mid width there appears to be negligible error in the measurements of inclusion strain.

Variation in inclusion strain across the width
of hot rolled strip. A16 (900°C) - $\epsilon_m = 1.20$



5.3.7.

The measurement of matrix strain.

The use of the equation.

$$\epsilon_m = \ln \frac{h_o}{h_f}$$

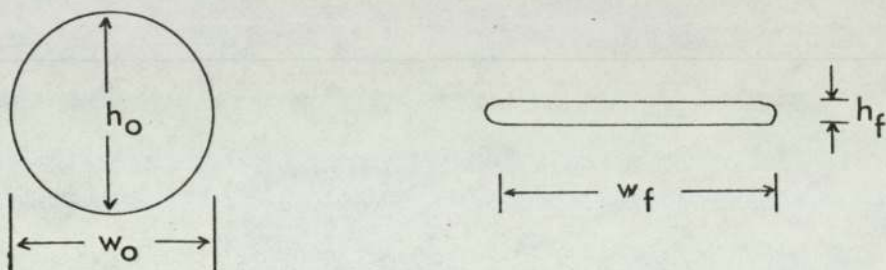
(where ϵ_m is the matrix strain, and h_o and h_f are the initial and final heights (thickness) of the sample).

which is for plane strain deformation has been used throughout this work. Had the condition of plane strain been met the use of

$$\epsilon_m = \ln \frac{A_o}{A_f}$$

would have been just as valid.

However, in these experiments, the condition of plane strain was not met due to the starting geometry of the samples. The initial shape of the material was of a circular bar, which was deformed into a flat strip viz : figure 5.166.



As may be seen from figure 5.166 a matrix strain based upon the equation $\epsilon_m = \ln \frac{A_o}{A_f}$ involves the

measurement of A_f , which was not easily determined by simple means. The measurement of h_o and h_f was, however, relatively straight forward.

Reeves (21) has investigated the relationship between the apparent area ($h_f w_f$) and the true area (by Archimedes principle) for various reductions of a bar initially 24mm in diameter. His results have been plotted (figure 5.167.) and it may be seen that there is an approximately linear relationship between 30% and 90% reduction in height.

In order to observe the differences in the value of matrix strain via the various formulae, values of w_h were obtained at various reductions for melt NIA12 rolled at 1000°C (table 5.36.). Figure 5.168. was a plot of these results.

These results indicated that there was a large discrepancy in the values of ϵ_m . It may also be observed that the value of ϵ_m via area measurements was substantially lower than the value of ϵ_m via height measurements. Therefore, had the former value of ϵ_m been used in the measurements of inclusion plasticity index, the values of ν would have been higher. However, it must be remembered that in the rolling process the height strain is the only independent variable and therefore it would seem logical to refer to matrix strains in terms of the height true strain.

$$\ln \frac{h_o}{h_f}$$

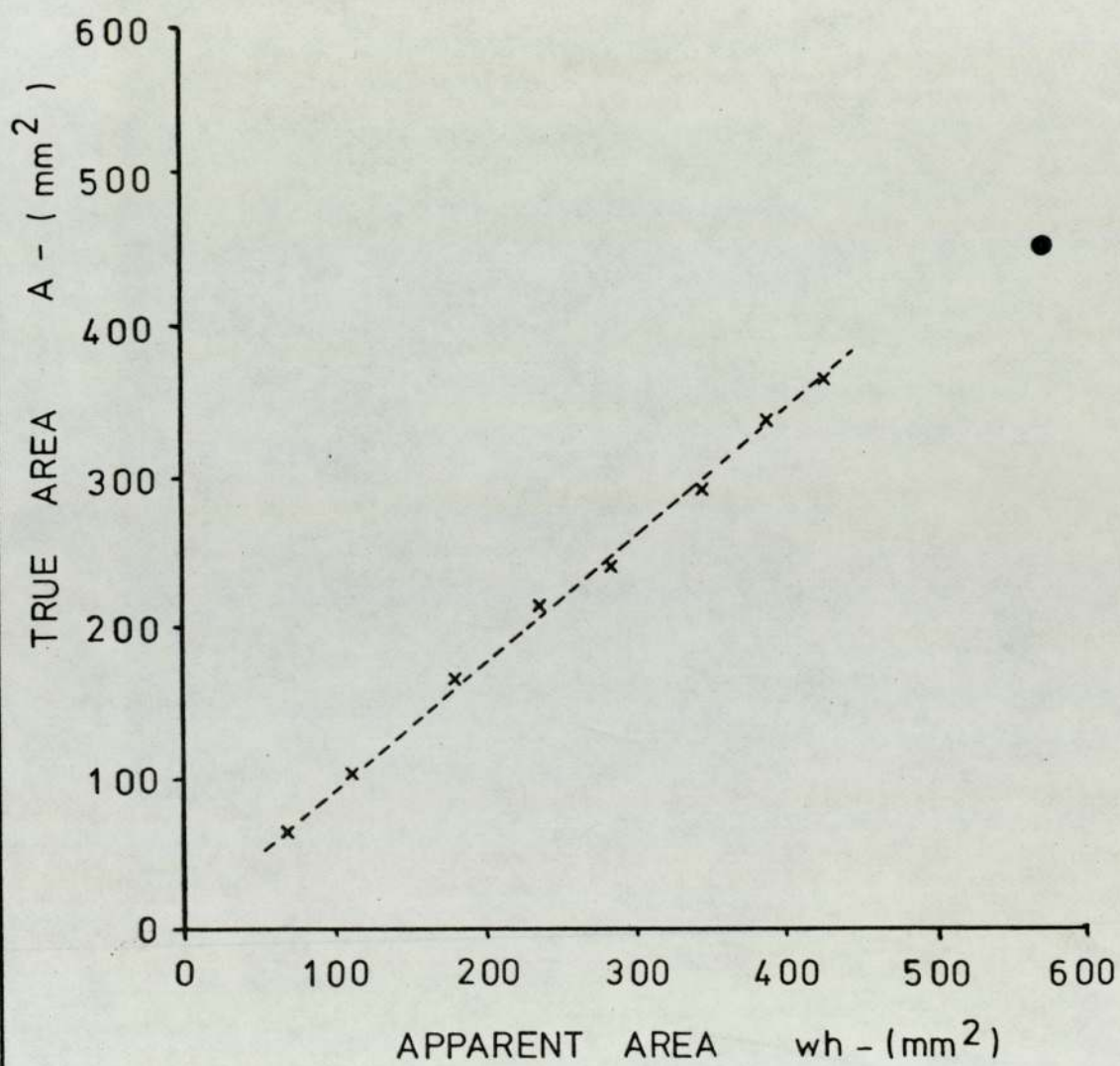
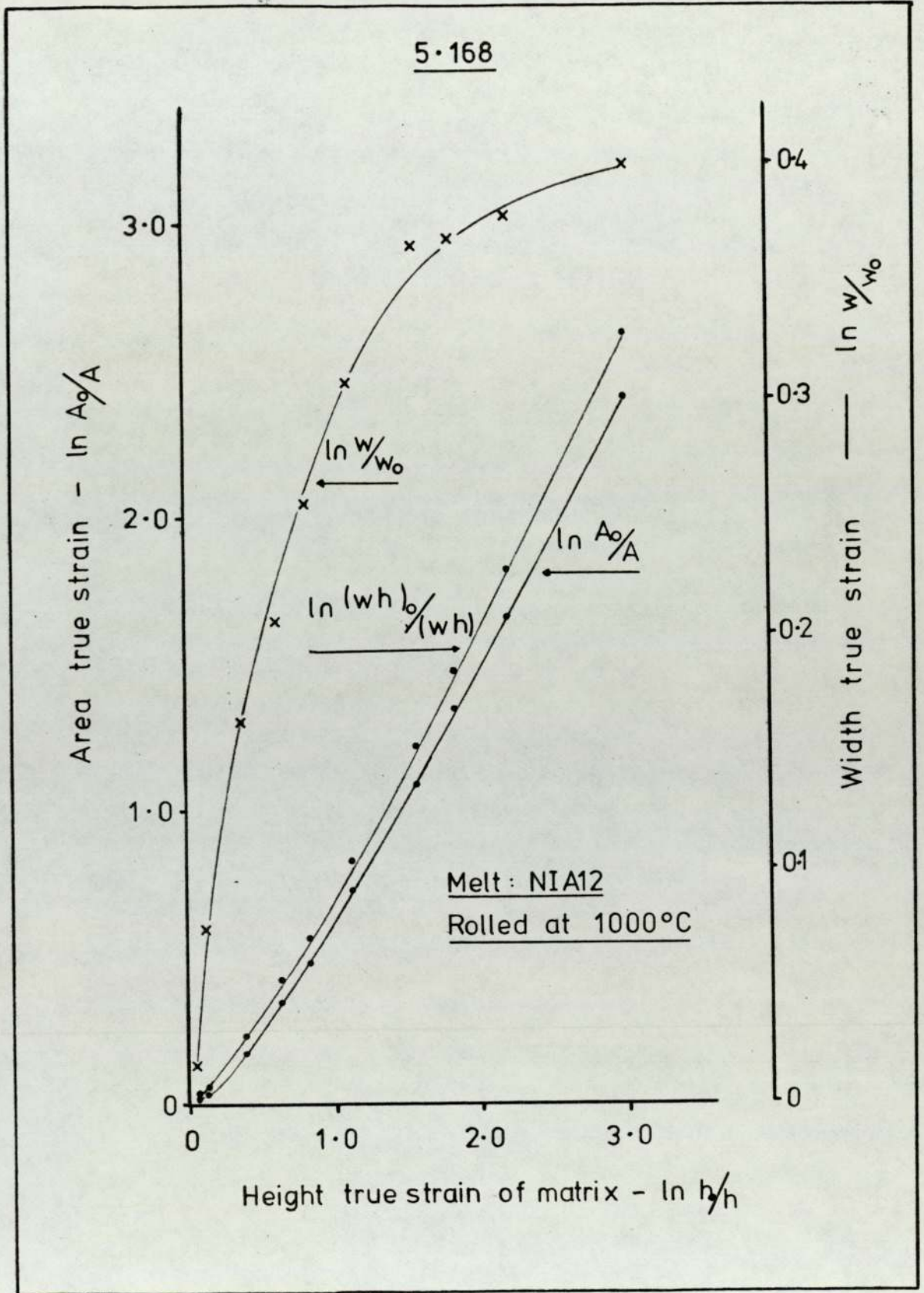
5.167

Table 5.36

MELT NIA12 ROLLING TEMPERATURE 1000°C

Sample	$\%Rd_h^n$	h(mm)	w(mm)	wh(mm ²)	A(mm ²)	$\ln \frac{h_0}{h}$	$\ln \frac{W}{W_0}$	$\ln \left(\frac{wh}{wh_0} \right)$	$\ln \frac{A_0}{A}$
0	-	23.70	23.70	562	441	-	-	-	-
1	4.0	22.75	24.07	548	435	0.042	0.015	0.025	0.014
2	10.5	21.20	25.50	541	430	0.111	0.073	0.038	0.025
3	31.9	16.13	27.87	450	375	0.385	0.162	0.222	0.162
4	46.3	12.72	29.2	371	315	0.622	0.209	0.415	0.336
5	55.8	10.47	30.7	321	275	0.817	0.259	0.560	0.472
6	67.7	7.65	32.2	246	215	1.131	0.306	0.826	0.718
7	79.1	4.95	33.9	168	150	1.566	0.358	1.207	1.078
8	84.1	3.76	34.2	129	115	1.841	0.367	1.471	1.344
9	88.7	2.66	34.6	92	85	2.187	0.378	1.809	1.646
10	95.1	1.17	35.3	41	40	3.008	0.398	2.617	2.400



5.3.8. The deformation of inclusions
within the roll throat.

As was mentioned in section 5.3.6.2 inclusion deformation varied throughout the height of the rolled sample. This deformation pattern was of course, dependent upon the rolling technique and the geometries of mill and sample. However, since the mode of matrix deformation in this project was by rolling, a guide to the deformation of inclusions present within the material in the region of the roll throat would enable a clearer picture of inclusion deformation to be established. Thus a sample of material was stopped in the roll throat, such that the maximum matrix height strain was 0.88 at 1050°. This higher strain of 0.88 compared to the normal 0.2 was used in order to accentuate the deformation pattern. However, it must be remembered that by doing this, conditions in the roll throat differ from those normally encountered (e.g. different strain rate). This technique was thus only intended to be a qualitative study of inclusion deformation in the roll throat. Plates 5.4. to 5.6. show the geometry of the rolling specimen after removing it from the roll throat.

Figure 5.169. shows inclusion strain throughout the roll throat, and indicated that initially as the material entered the rolls deformation was at the surface. As the material progressed through the rolls there was a change over in deformation patterns, and the



5.4.



5.5.



5.6.

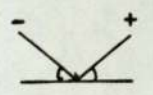
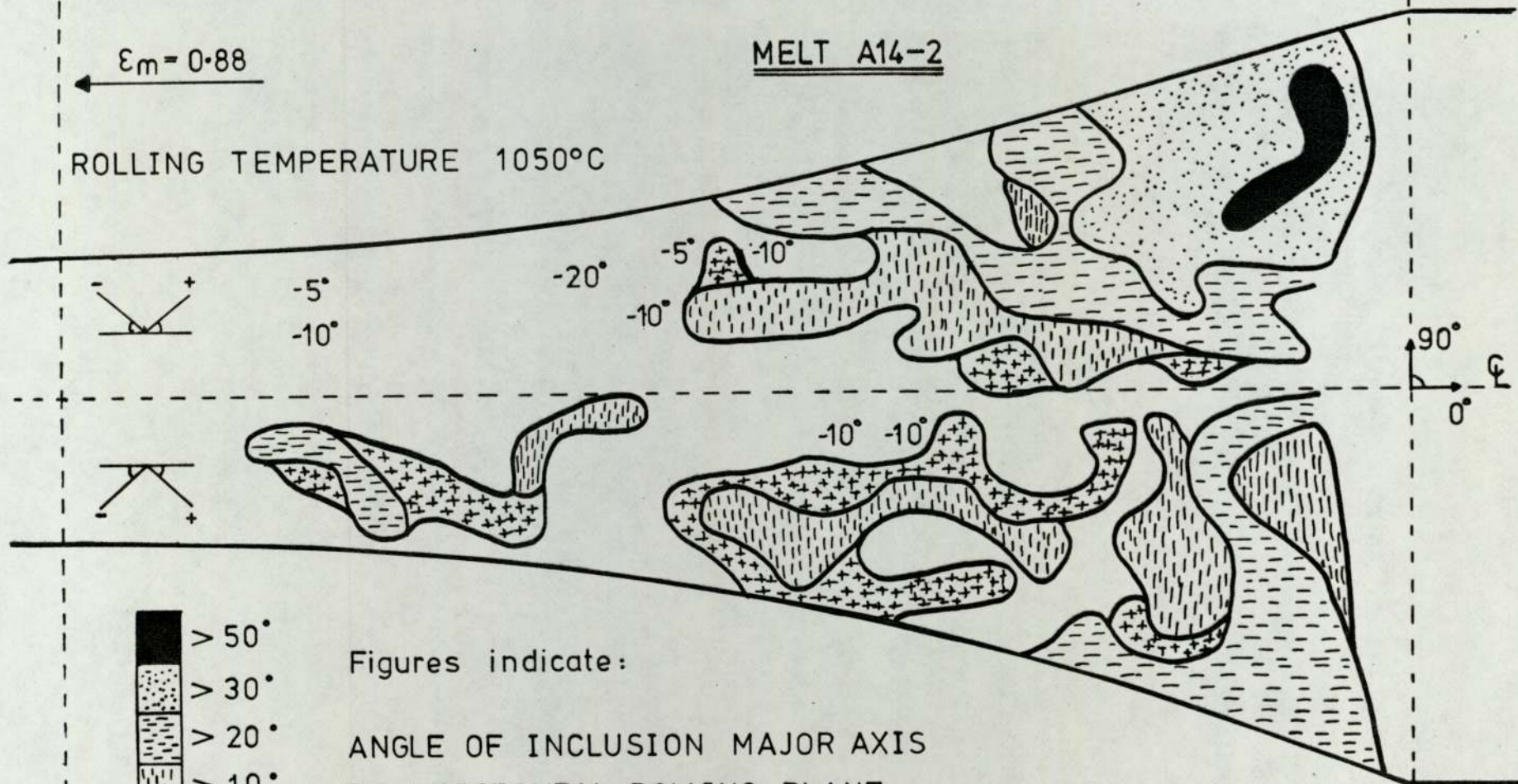
5-169

$\epsilon_m = 0$

$\epsilon_m = 0.88$

MELT A14-2

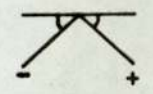
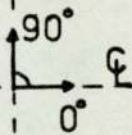
ROLLING TEMPERATURE 1050°C







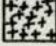
-5°
-10°

-20°

-5°
-10°



-10° -10°

-  > 50°
-  > 30°
-  > 20°
-  > 10°
-  > 5°

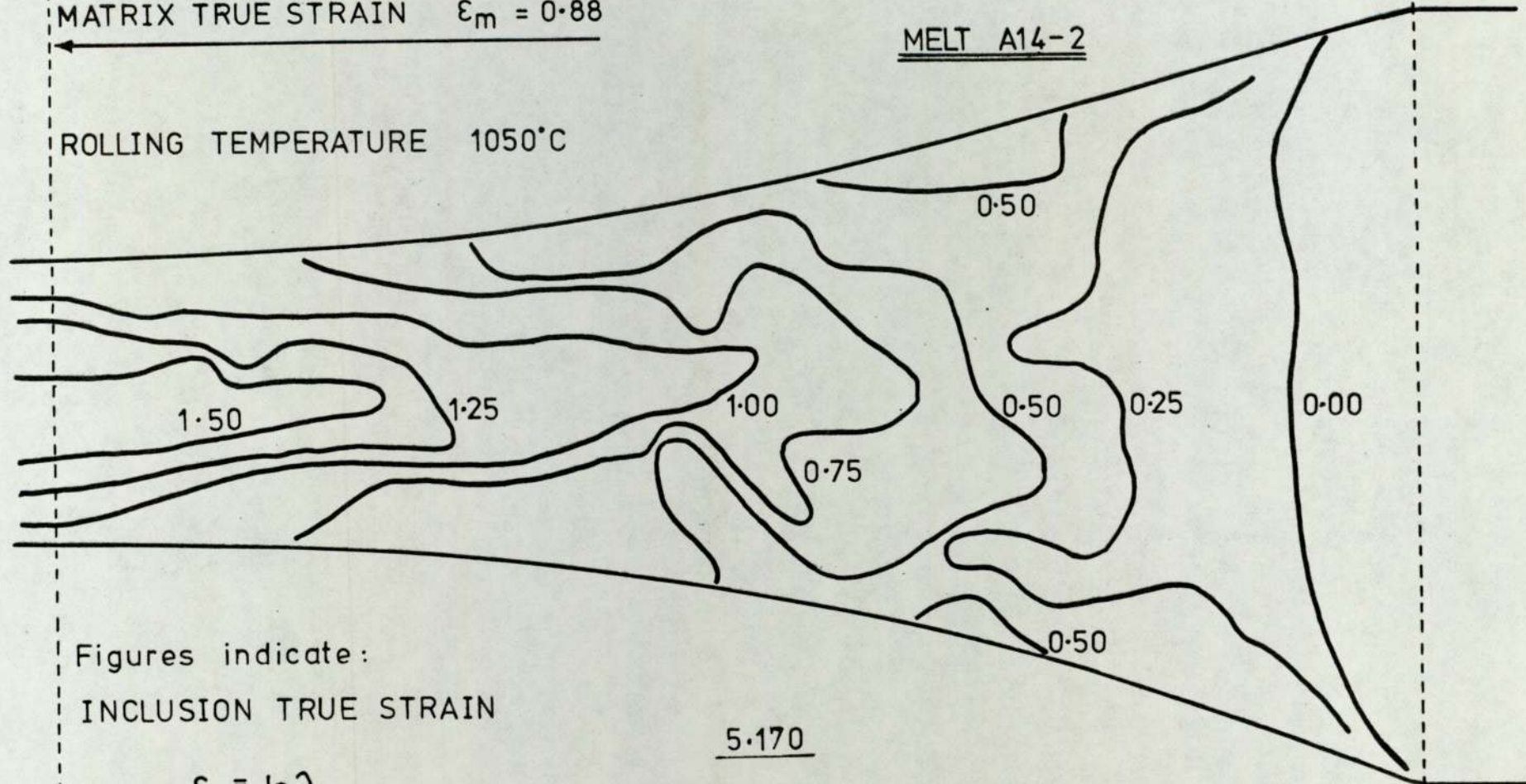
Figures indicate:
ANGLE OF INCLUSION MAJOR AXIS
TO HORIZONTAL ROLLING PLANE.

MATRIX TRUE STRAIN $\epsilon_m = 0.88$

ROLLING TEMPERATURE 1050°C

MELT A14-2

$\epsilon_m = 0$



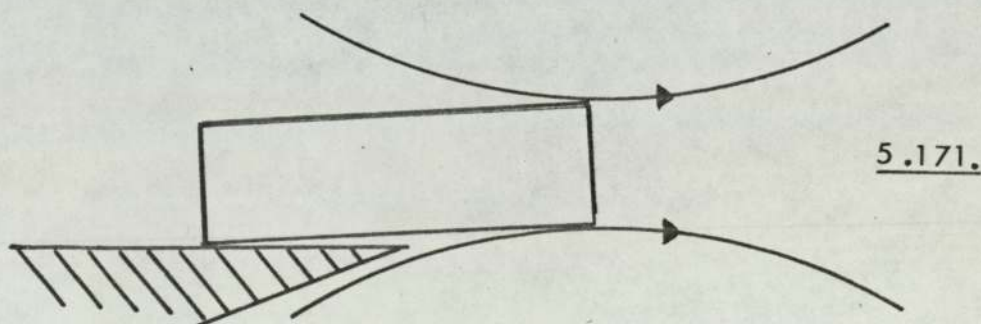
Figures indicate:
INCLUSION TRUE STRAIN

$$\epsilon_i = \frac{\ln \lambda}{2}$$

5.170

material in the central region of the mid plane section had deformed the most. However, there do appear to be some abnormalities concerning figure 5 .169. , where it may be seen that inclusions in the surface regions have a greater value of strain earlier on in the rolling process than later on. This effect may however be due to a sparseness of results encountered in these regions.

As a further guide to the deformation of inclusions within the roll throat figure 5 .170. shows the orientation of the inclusion major axis to the horizontal rolling plane. From this figure it may be observed that there was non symmetrical deformation about the horizontal rolling plane. This asymmetry was due to one surface of the material entering the rolls slightly before the other, as a result of the slight difference in height between the entry guide and the bottom roll i.e.

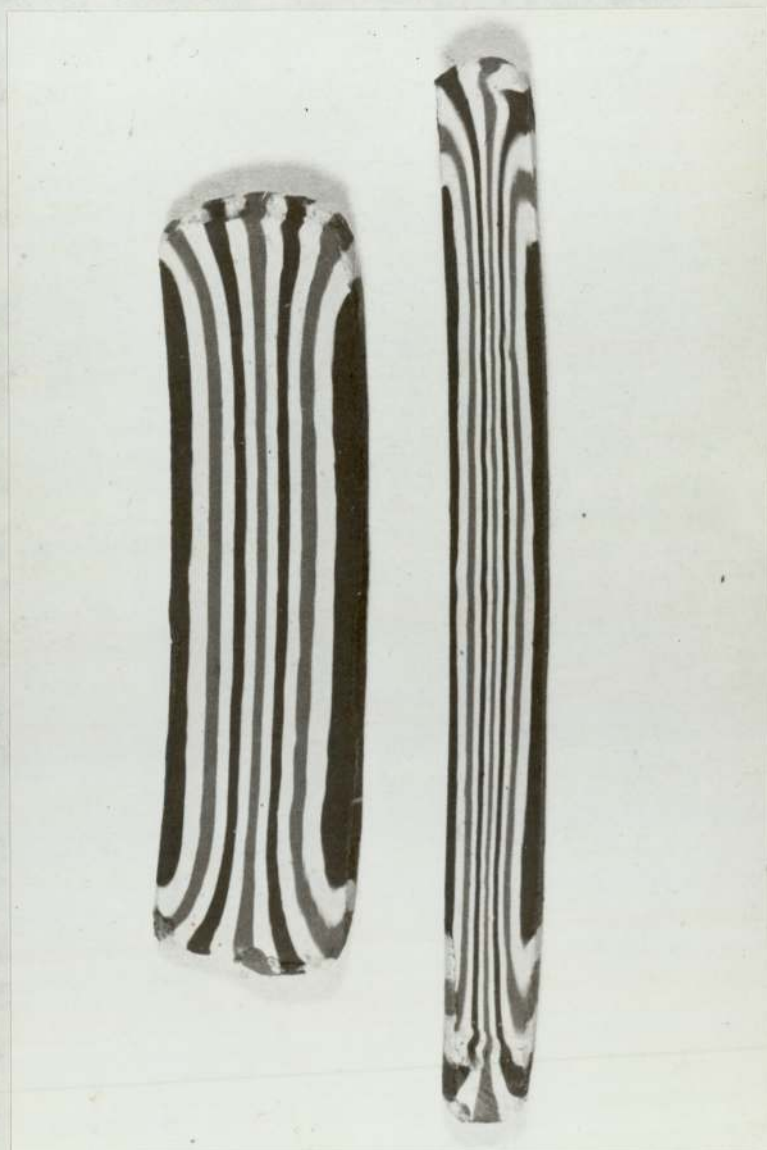


This shearing effect has also been shown with rolled plasticine models, after several passes, where the deformation of top and bottom surfaces are compared i.e. plates 5.7. to 5.9.

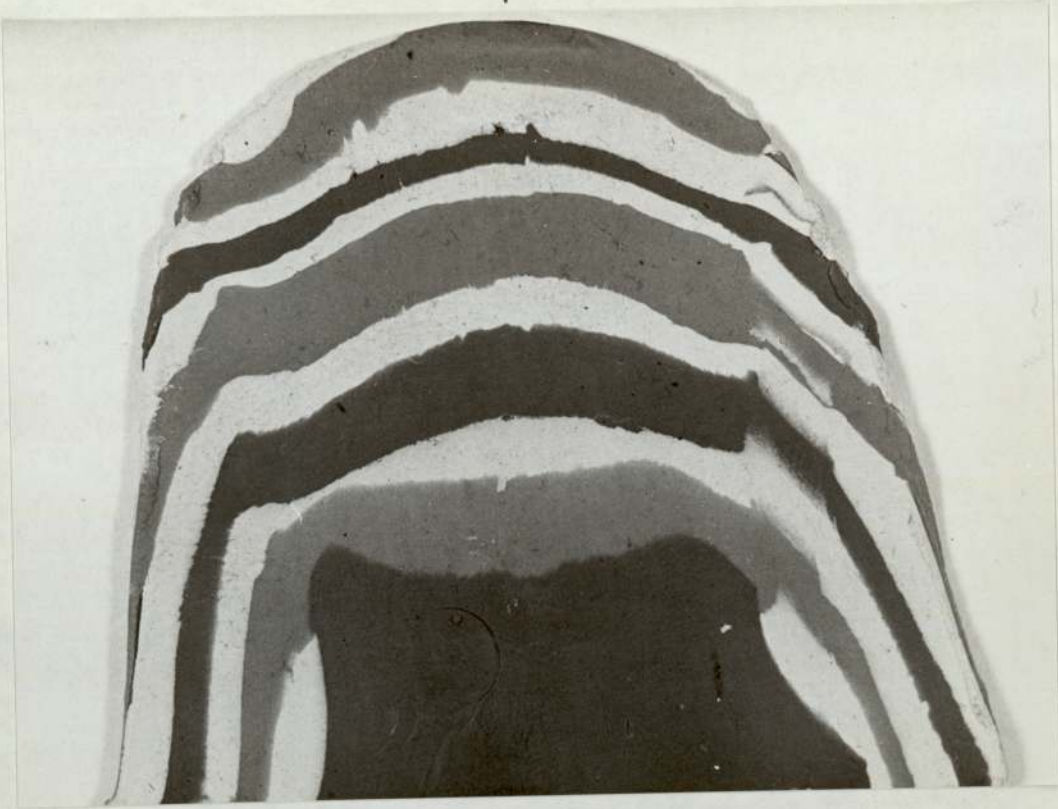
T

5.7

B



T



5.8.

B



5.9.

3.9. The variation in inclusion plasticity index with the plane of measurement.

Throughout this project it has been assumed that plane strain conditions existed in the areas of the rolled samples where inclusion strain measurements were made. Although this was an incorrect assumption it did enable an investigation into inclusion plasticity to be carried out in a straightforward manner.

The strain of the inclusions was measured on the (XY) plane figure 5.172. using the relationship

$$\epsilon'_{y(XY)} = \frac{1}{2} \ln \frac{a}{b} \quad - \text{ Assuming plane strain.}$$

If plane strain conditions had been operative it is known that values of strain measured on the other orthogonal planes would have been of equal magnitude to that of the (XY) plane.

i.e.

$$\epsilon'_{y(XZ)} = \epsilon'_{y(YZ)} = \epsilon'_{y(XY)}$$

$$\ln \left(\frac{a}{D_0} \right) \quad \ln \left(\frac{D_0}{b} \right) \quad \frac{1}{2} \ln \left(\frac{a}{b} \right)$$

Measurements of inclusion strains (for melts Al6 and VA12) on the planes (XZ) and (YZ) were made, assuming that plane strain conditions were operative and therefore assuming that

$$\epsilon'_{y(XZ)} = \ln \left(\frac{a}{D_0} \right)$$

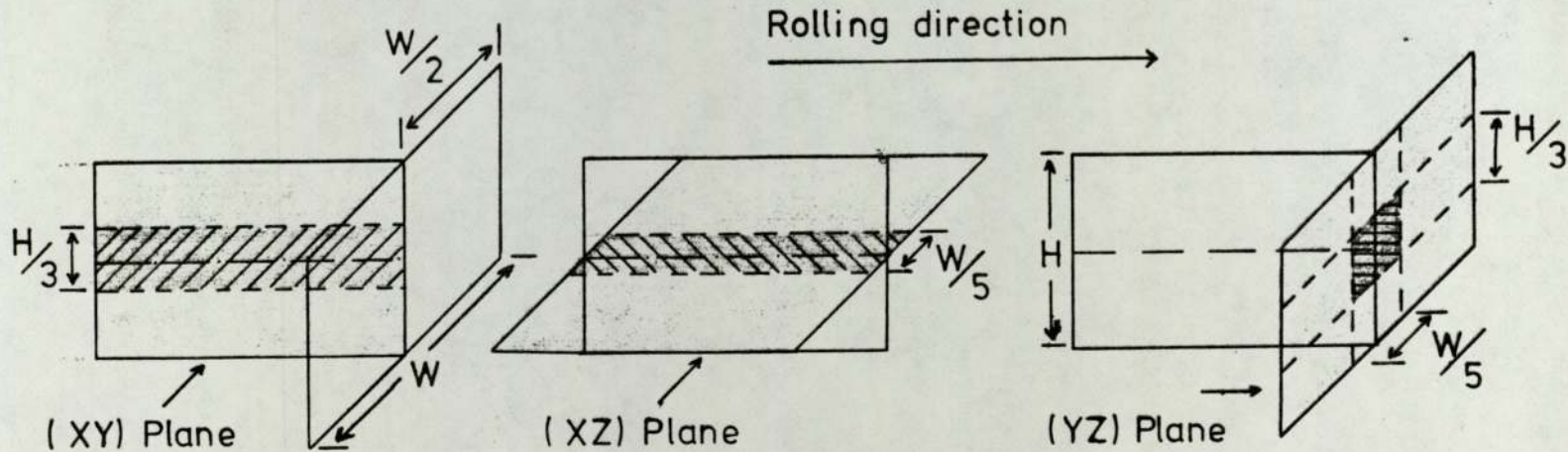
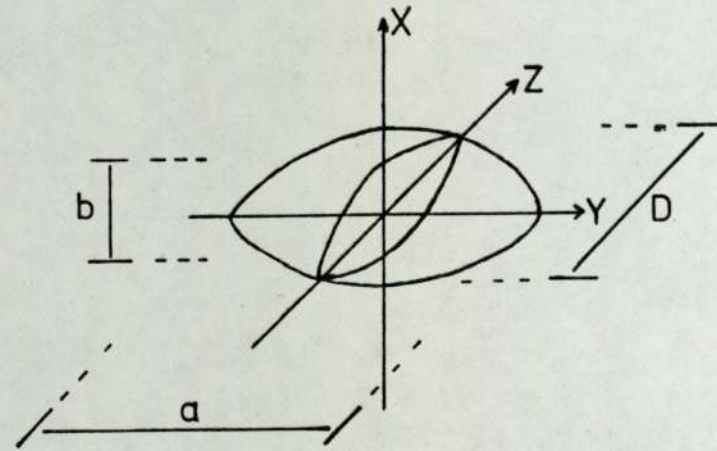
Fig. 5-172

Measurement of inclusion strain.

$$\epsilon_{i(XY)} = \frac{1}{2} \ln(a/b)$$

$$\epsilon_{i(XZ)} = \ln(a/D)$$

$$\epsilon_{i(YZ)} = \ln(D/b)$$



and
$$\epsilon'_y(YZ) = \ln\left(\frac{D_0}{b}\right)$$

From the results obtained for melt Al6 (table 5.37.) it became obvious that the measured inclusion strains were distinctly different on each of the section planes. Furthermore the values of inclusion strain lay either side of the value for the strain on the (XY) plane.

i.e.
$$\epsilon'_{y(XZ)} < \epsilon'_{y(XY)} < \epsilon'_{y(YZ)}$$

It was also noticeable that the value of $\epsilon'_{y(XY)}$ lay almost intermediate between $\epsilon'_{y(XZ)}$ and $\epsilon'_{y(YZ)}$ figure 5.173.

An analysis of the non plane strain situation (Appendix 5.5) indicated that this phenomenon was to be expected and it was shown that if the measurements of inclusion strain on the various planes had assumed the plane strain condition then

$$\epsilon'_{y(XY)} = \frac{\epsilon'_{y(XZ)} + \epsilon'_{y(YZ)}}{2}$$

The value $\epsilon'_{y(XY)}^{\text{THEORY}}$ was derived from the measurements of $\epsilon'_{y(XZ)}$ and $\epsilon'_{y(YZ)}$ and it was found that it compared favourably with the measured value of $\epsilon'_{y(XY)}$ (table 5.26.³⁷ and figure 5.173.)

The analysis shown in appendix 5.5 also indicated that the width strain ϵ_z of the inclusions could be determined from measurements on the various planes.

Table 5.37

Mean inclusion strain and plasticity values measured on various planes,
for melt Al6 at rolling temperatures 800 - 1300°C.

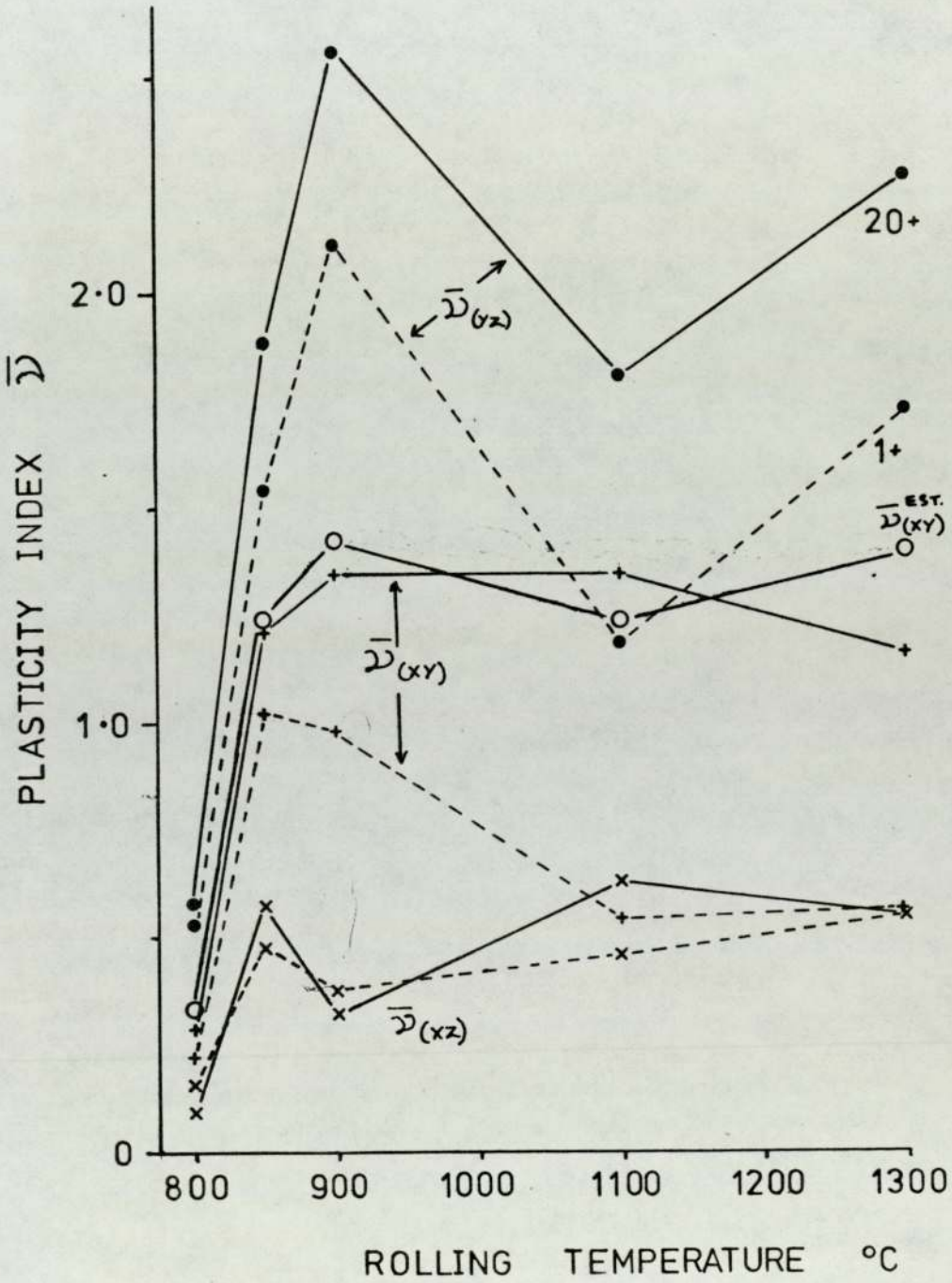
Rolling Temp °C	Matrix Strain	Plane	No. Def Inclns.			$\bar{\epsilon}_i$			\bar{D}		
			1+	10+	20+	1+	10+	20+	1+	10+	20+
800	1.16	(XZ)	41	16	8	0.19	0.14	0.10	0.16	0.12	0.09
		(YZ)	62	31	11	0.61	0.75	0.67	0.53	0.65	0.58
		(XY)	140	51	19	0.32	0.36	0.24	0.28	0.31	0.21
		(D)*	-	-	-	0.41	0.44	0.38	0.35	0.38	0.33
850	1.16	(XZ)	13	10	7	0.55	0.63	0.68	0.47	0.54	0.59
		(YZ)	64	37	22	1.78	2.20	2.18	1.54	1.90	1.88
		(XY)	180	50	18	1.17	1.43	1.40	1.01	1.23	1.21
		(D)*	-	-	-	1.17	1.41	1.44	1.01	1.22	1.24

$$(D)^* = \left[\frac{(XZ) + (YZ)}{2} \right]$$

Table 5.37 (cont.)

Rolling Temp °C	Matrix Strain	Plane	No. Def Inclns			$\bar{\epsilon}_i$			$\bar{\nu}$		
			1+	10+ (μm)	20+	1+	10+ (μm)	20+	1+	10+ (μm)	20+
900	1.13	(XZ)	22	6	1	0.42	0.35	0.36	0.37	0.31	0.32
		(YZ)	64	55	23	2.38	2.56	2.89	2.11	2.27	2.56
		(XY)	37	10	7	1.09	1.44	1.51	0.97	1.27	1.34
		(D)	-	-	-	1.40	1.46	1.63	1.24	1.29	1.44
1100	1.17	(XZ)	20	3	1	0.54	0.96	0.74	0.46	0.82	0.63
		(YZ)	47	7	4	1.38	2.09	2.12	1.18	1.79	1.81
		(XY)	98	11	6	0.63	1.37	1.52	0.54	1.17	1.35
		(D)	-	-	-	0.95	1.53	1.42	0.82	1.31	1.22
1300	1.13	(XZ)	34	8	1	0.62	0.61	0.62	0.55	0.54	0.55
		(YZ)	64	40	25	1.95	2.41	2.57	1.73	2.13	2.27
		(XY)	155	42	25	0.63	1.21	1.31	0.56	1.07	1.16
		(D)	-	-	-	1.29	1.51	1.60	1.14	1.34	1.41

5.173



$$\epsilon_z = \frac{2}{3} \left[\epsilon'_y(yz) - \epsilon'_y(xy) \right] \quad (i)$$

$$\epsilon_z = \frac{2}{3} \left[\epsilon'_y(xy) - \epsilon'_y(xz) \right] \quad (ii)$$

$$\epsilon_z = \frac{1}{3} \left[\epsilon'_y(yz) - \epsilon'_y(xz) \right] \quad (iii)$$

Calculations of ϵ_z via equation (i) was preferred since the measurement of inclusion strains was much easier on the (YZ) and (XY) planes. Strains in the (XZ) plane were difficult to measure for two reasons,

a) Slight deviations from the horizontal polishing plane leads to erroneous $\lambda_{(xz)}$ values

b) When the inclusions were well deformed into plates (i.e. higher temperatures.) they had the tendency to fall out from the polished surface.

Values of ϵ_z calculated via the above equations (table 5.38) showed that for a given temperature of rolling these values were of similar magnitude.

As may be shown the value of $\epsilon'_y(xy)$ is only equal to ϵ_y under plane strain conditions.

i.e.

$$\frac{1}{2} \ln \frac{a}{b} = \ln \frac{D_0}{b}$$

If for any other value of $\epsilon'_y(xy)$ there is some associated widthways spread then the following

Inclusion width strain at various temps ($\epsilon_m = 1.2$ approx.)

Table 5.38

ϵ_z defined as	Rolling Temp °C					Inclusion Size
	800	850	900	1100	1300	
$= \frac{2}{3} [\epsilon'_{y(YZ)} - \epsilon'_{y(XY)}]$	0.26	0.51	0.75	0.48	0.81	10 μm +
	0.29	0.52	0.92	0.40	0.84	20 μm +
$= \frac{2}{3} [\epsilon'_{y(XY)} - \epsilon'_{y(XZ)}]$	0.15	0.53	0.73	0.27	0.40	10 μm +
	0.09	0.48	0.76	0.53	0.46	20 μm +
$= \frac{1}{3} [\epsilon'_{y(YZ)} - \epsilon'_{y(XZ)}]$	0.20	0.52	0.74	0.75	0.60	10 μm +
	0.19	0.50	0.84	0.46	0.65	20 μm +

relationship holds

$$\epsilon'_y(xy) = \epsilon_y - \frac{\epsilon_z}{2}$$

$$\therefore \epsilon_y = \epsilon'_y(xy) + \frac{\epsilon_z}{2}$$

The value of inclusion plasticity index for the plane strain condition \mathcal{W}_{PE} is given by

$$\mathcal{W}_{PE} = \frac{\epsilon_y}{\epsilon_{my}}$$

where ϵ_{my} is the matrix strain in the y direction

However, if non plane strain conditions are operative \mathcal{W}_{PE} may be estimated if ϵ_z is known i.e.

$$\mathcal{W}_{PE} = \frac{\epsilon_y}{\epsilon_{my}} = \frac{\left[\epsilon'_y(xy) + \frac{\epsilon_z}{2} \right]}{\epsilon_{my}}$$

However, ϵ_z may be substituted for (Appendix 5.5) and the estimate of \mathcal{W}_{PE} may be determined via

$$\mathcal{W}_{PE} = \frac{2\epsilon'_y(xy) + \epsilon'_y(yz)}{3\epsilon_{my}} \quad (iv)$$

$$\mathcal{W}_{PE} = \frac{4\epsilon'_y(xy) - \epsilon'_y(xz)}{3\epsilon_{my}} \quad (v)$$

$$\mathcal{V}_{P_{\epsilon}} = \frac{2\epsilon'_y(yz) + \epsilon'_y(xz)}{3\epsilon_m} \quad (vi)$$

Again the determination of $\mathcal{V}_{P_{\epsilon}}$ via equation (iv) is preferred for the same reasons associated with the measurement of $\epsilon(xz)$

Strain analyses using the preferred equations

$$\epsilon_z = \frac{2}{3} \left[\epsilon'_y(yz) - \epsilon'_y(xy) \right]$$

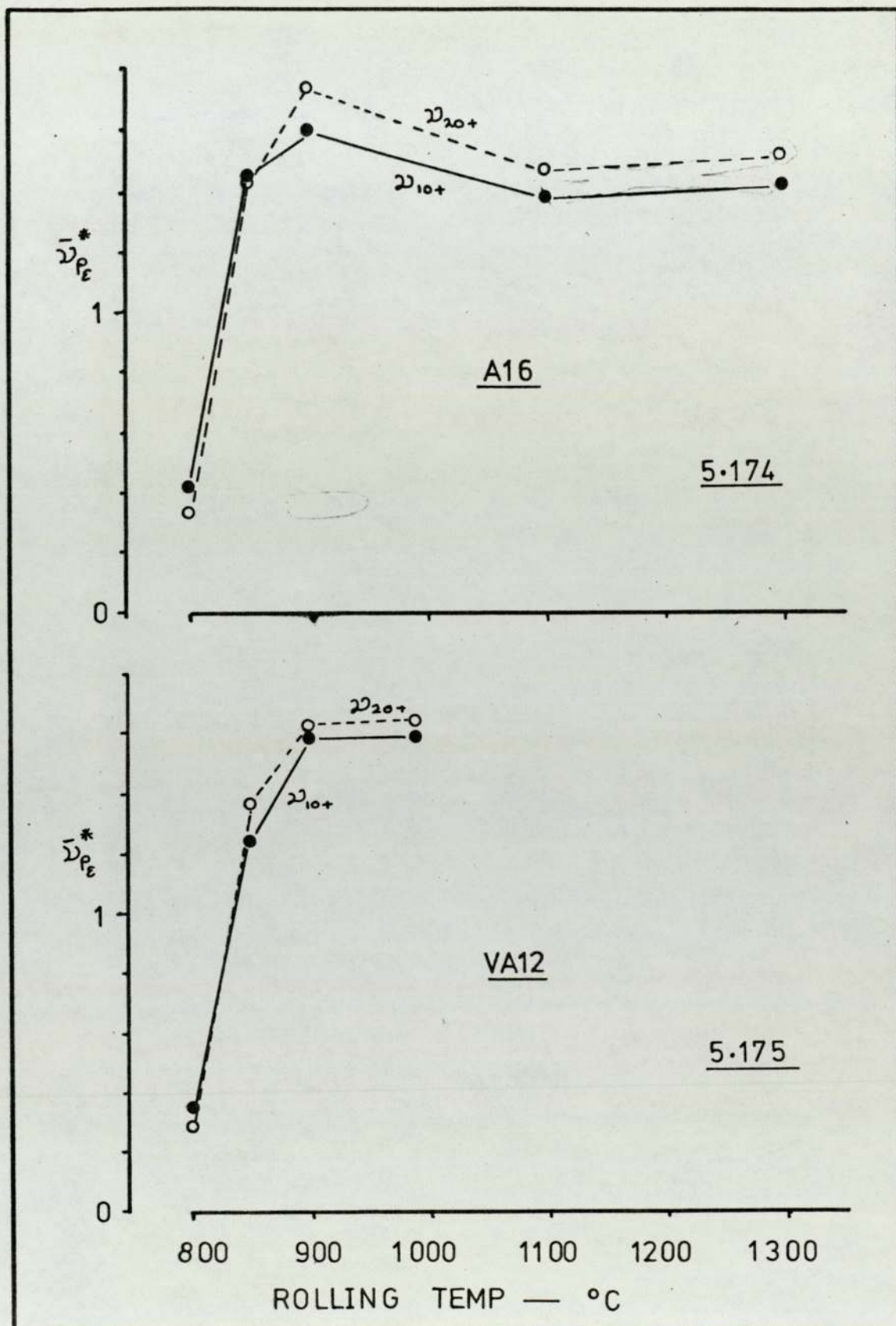
$$\epsilon_{P_{\epsilon}} = \frac{2\epsilon'_y(xy) + \epsilon'_y(yz)}{3}$$

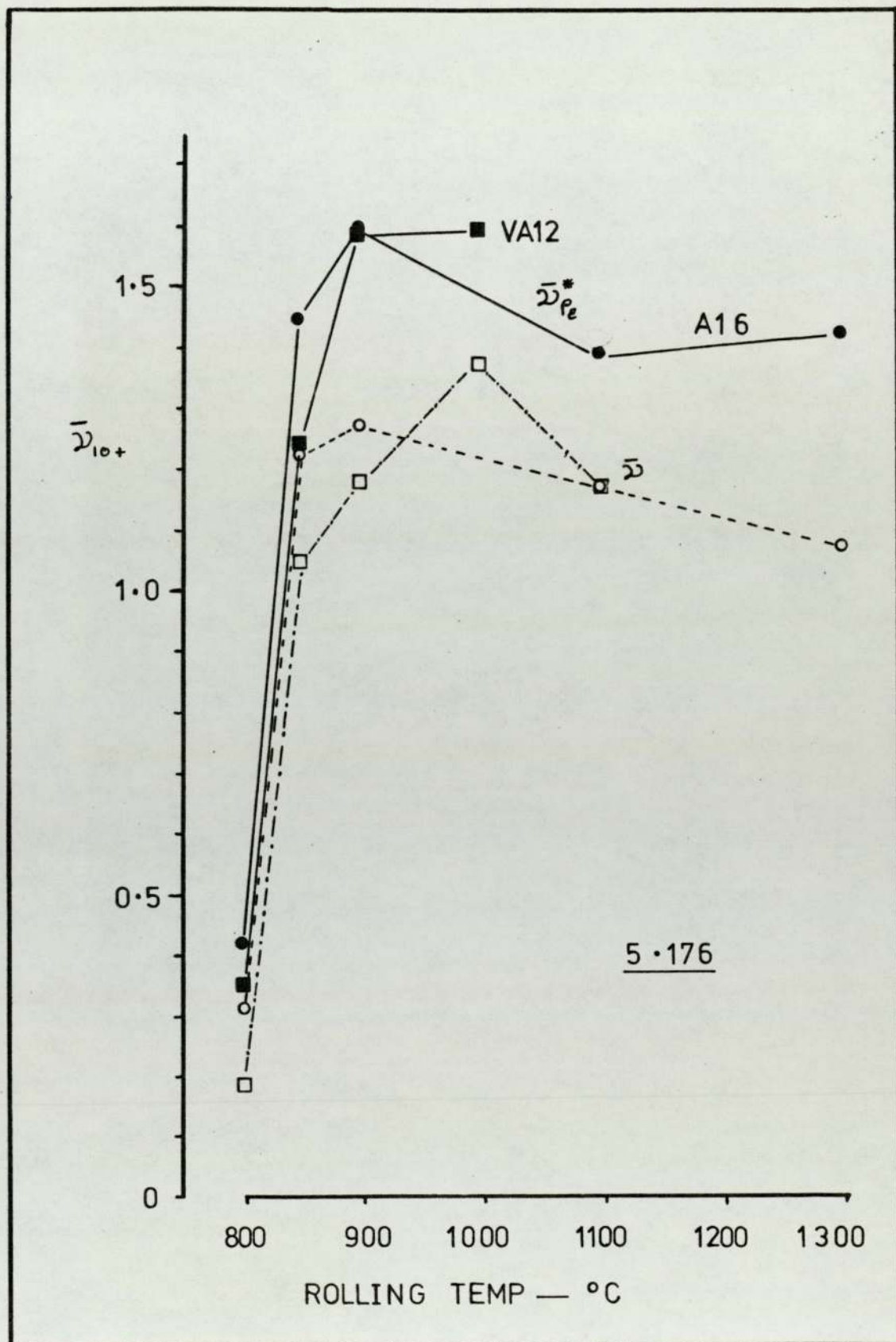
are shown for melts Al6 and VA12 over a range of temperatures (Tables 5.39. and 5.40. , Figures 5.174. and 5.175.).

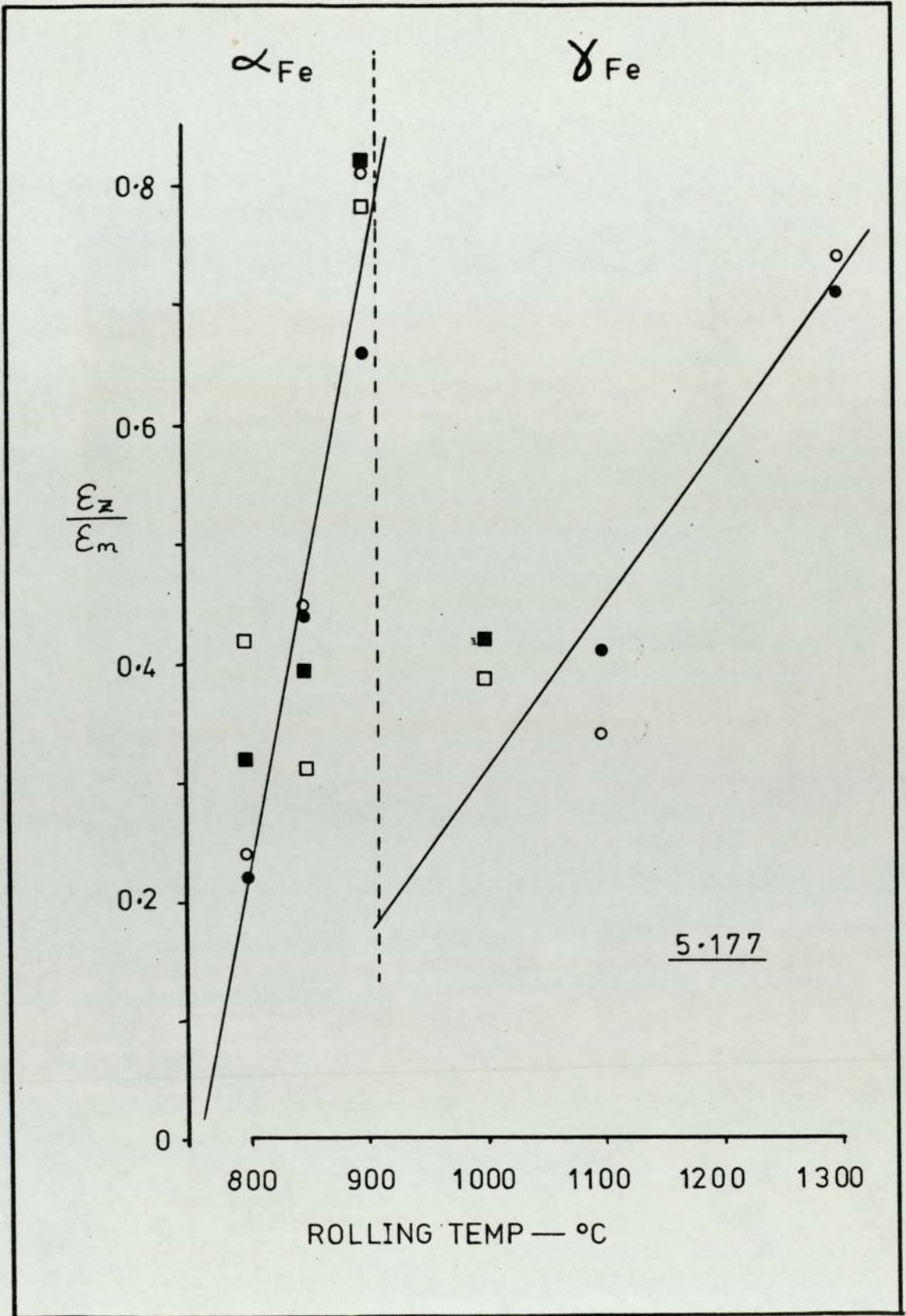
From figure 5.176. it may be observed that $\mathcal{V}_{P_{\epsilon}}$ is greater than $\mathcal{V}_{(xy)}$. It may also be observed that in the case of melt Al6 there is a noticeable peak in the plane strain plasticity index at a rolling temperature of 900°C. Figure 5.177. which shows data from both melts indicated that there was a kink in the widthways strain in the region of 900°C which corresponds to the ferrite/austenite phase change in pure iron. It would therefore appear that the maximum widthways strain in

$\Sigma_m =$	Rolling Temp. °C	Size Range	$\epsilon'_{\gamma}(XY)$ n	$\epsilon'_{\gamma}(YZ)$ n	Σ_Z	ϵ_{Z/ϵ_m}	$\epsilon_{P\epsilon}^*$	$\nu_{P\epsilon}^*$
1.16	800	10+	0.36 51	0.75 31	0.26	0.22	0.49	0.42
		20+	0.24 19	0.67 11	0.29	0.25	0.38	0.33
1.16	850	10+	1.43 50	2.20 37	0.51	0.44	1.68	1.45
		20+	1.40 18	2.18 22	0.52	0.45	1.66	1.43
1.13	900	10+	1.44 10	2.56 55	0.75	0.66	1.81	1.60
		20+	1.51 7	2.89 23	0.92	0.81	1.97	1.74
1.17	1100	10+	1.37 11	2.09 7	0.48	0.41	1.61	1.38
		20+	1.52 6	2.12 4	0.40	0.34	1.72	1.47
1.13	1300	10+	1.21 42	2.41 40	0.80	0.71	1.61	1.42
		20+	1.31 25	2.57 25	0.84	0.74	1.73	1.53

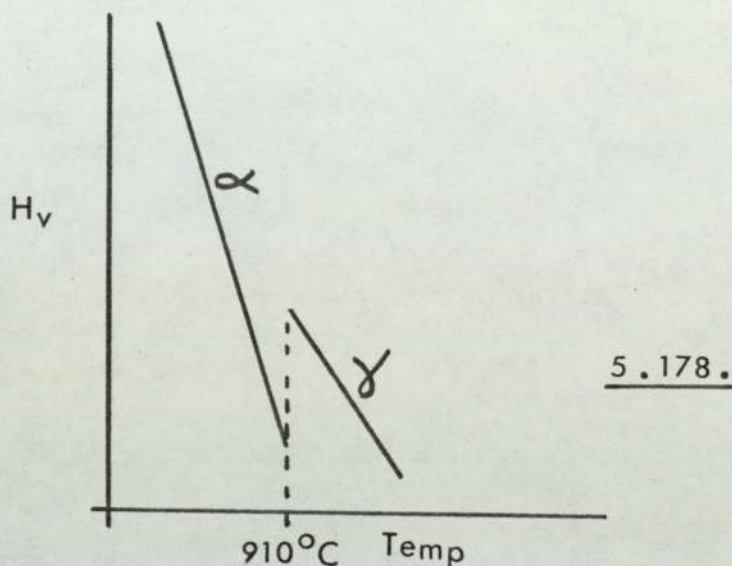
$\epsilon_m =$	Rolling Temp. °C	Size Range	$\Sigma \gamma'_{(XY)}$ n	$\Sigma \gamma'_{(YZ)}$ n	ΣZ	ϵ_Z / ϵ_m	ϵ_{PE}^*	ν_{PE}^*		
1.14	800	10+	0.22	39	0.77	26	0.37	0.32	0.40	0.35
		20+	0.08	15	0.82	15	0.49	0.43	0.33	0.29
1.15	850	10+	1.21	58	1.89	24	0.45	0.39	1.43	1.24
		20+	1.43	19	1.93	23	0.36	0.31	1.57	1.36
1.16	900	10+	1.37	47	2.79	17	0.95	0.82	1.84	1.58
		20+	1.43	17	2.79	17	0.91	0.78	1.88	1.62
1.14	1000	10+	1.56	21	2.31	12	0.50	0.44	1.81	1.59
		20+	1.65	14	2.31	12	0.44	0.39	1.87	1.64
1.10	1100	10+	1.29	36						
		20+	1.24	12						







the inclusions is encountered when the matrix is in its softest condition. i.e. ferrite just below the α/δ transition temperature.

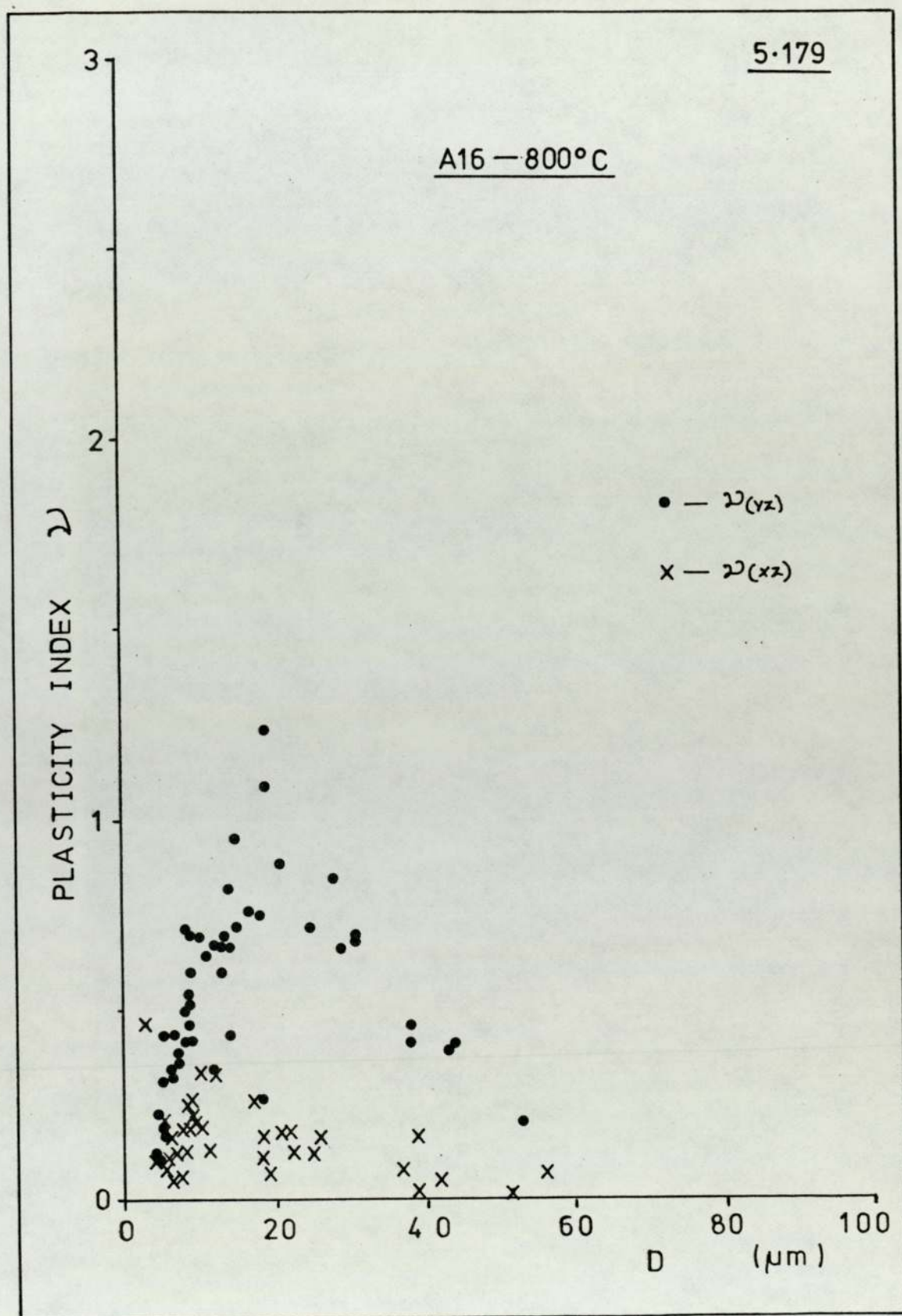


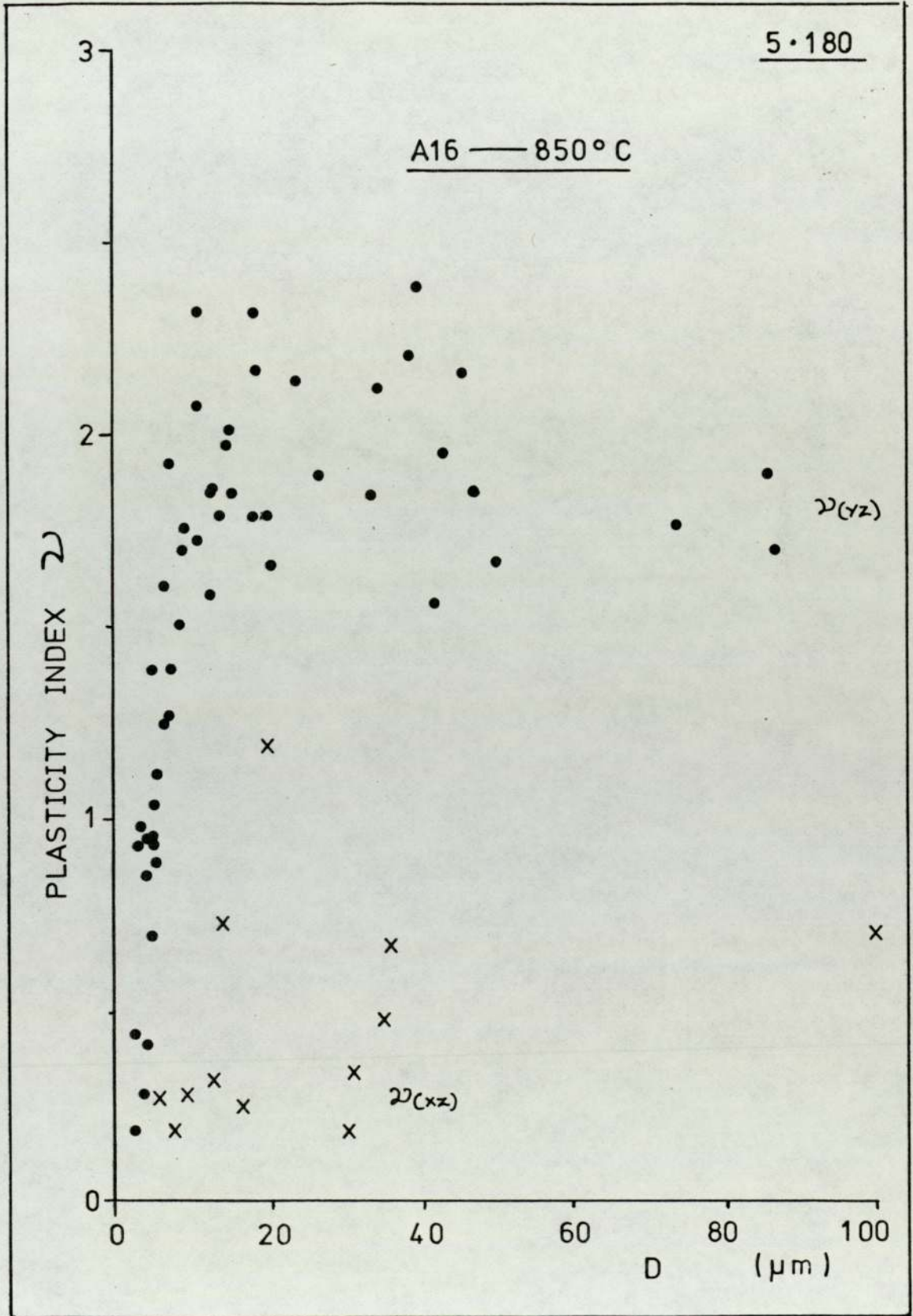
At temperatures above the α/δ transition, widthways spread appears to increase with increase in temperature i.e. with the softening of the matrix.

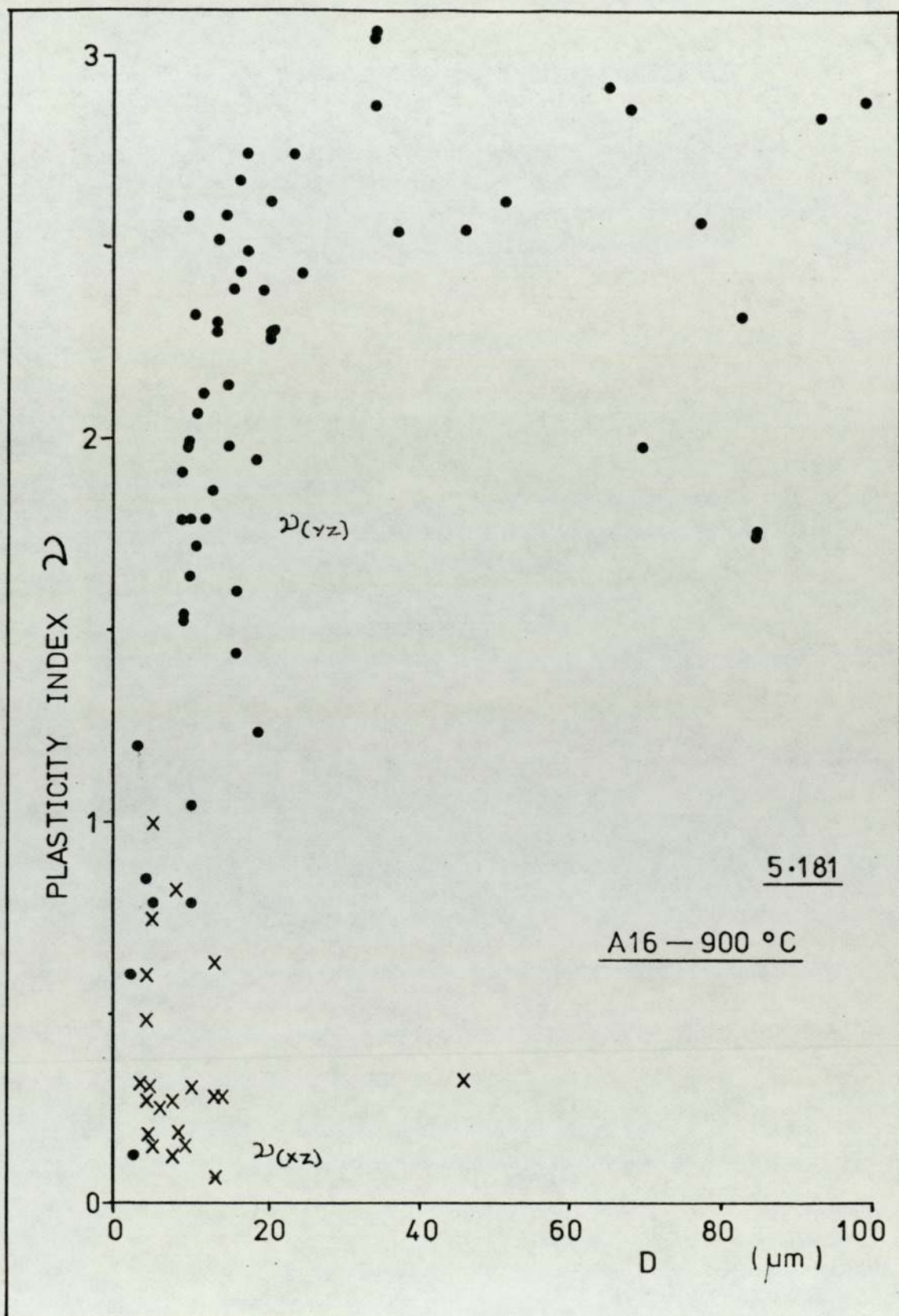
5.3.9.1. The variation of plasticity index with size for measurements on the (XZ) and (YZ) planes.

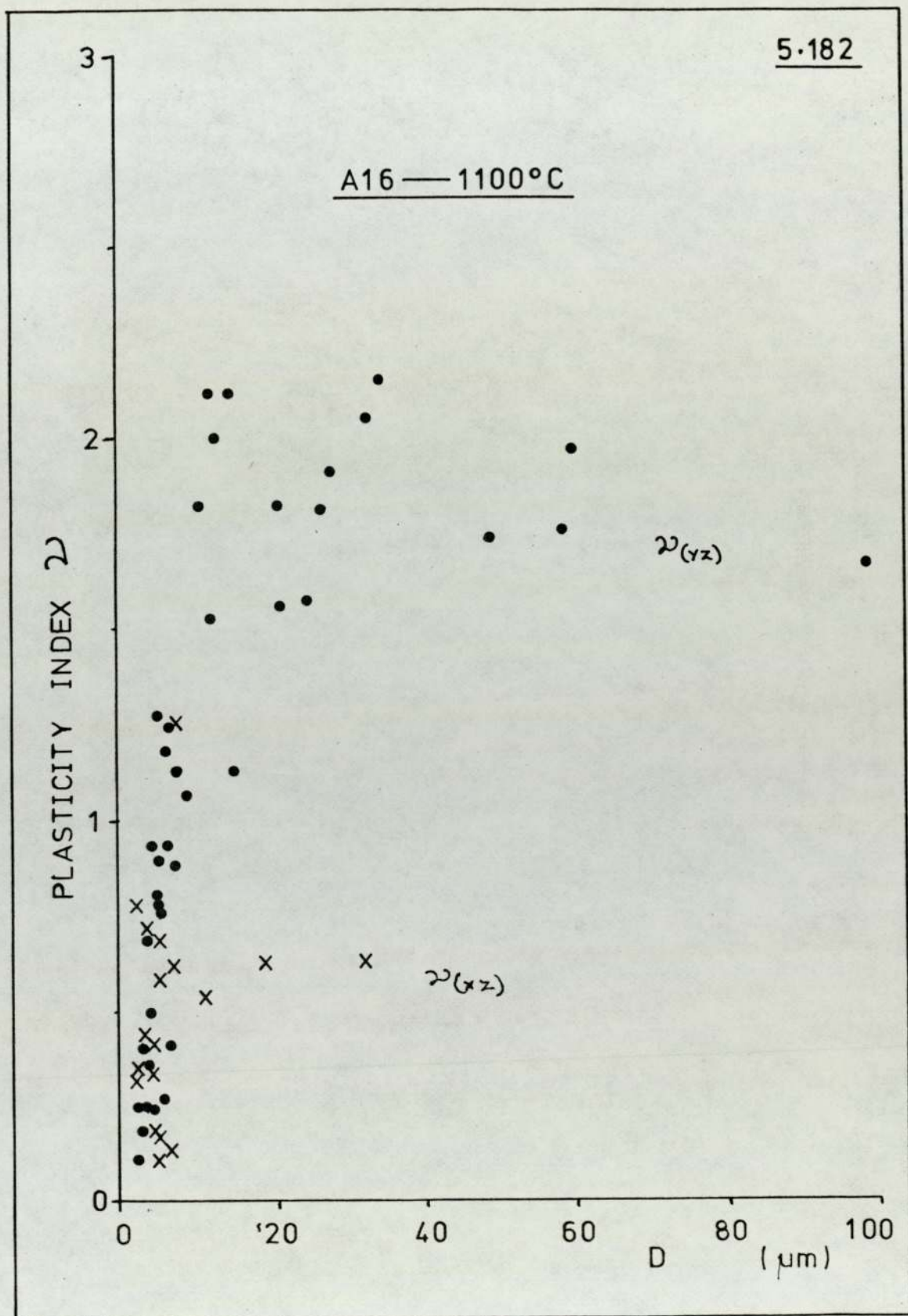
Plasticity index measurements for the various inclusion sizes have been plotted for melt Al6 at various rolling temperatures. Figures 5.179. to 5.183. Values of plasticity index for plane (YZ) show similar variations with size to those encountered for the (XY) plane (figure 5.105.)

i.e. At 800°C. there is a peak in the plasticity index at around 20 μm and a non deformable inclusion cut of size of around 5 μm . At higher temperatures there is a rapid increase in $\psi_{(YZ)}$ with size over the range









2 - 20 μm followed by a levelling out of the values of $\nu(YZ)$ at greater sizes.

Results are shown for plasticity index measurements on plane (XZ) ^{and} do not indicate any size relationship, there being a large degree of scatter associated with these points. At the higher rolling temperatures, i.e. greater than 900°C there are very few results for the larger inclusion sizes due to the polishing problems associated with the (XZ) plane mentioned earlier.

If the sizes at which the maximum plasticity indices occurred observed on the (XY) and (YZ) planes, are compared it is seen that there is a discrepancy (figures 5.105. and 5.179.).

i.e. Approximately 12 μm for the (XY) plane and 20 μm for the (YZ) plane.

However, the value of 12 μm for the (XY) plane was computed by $\sqrt{\text{major} \times \text{minor}}$ observed axes, whereas the value of 20 μm was the intermediate (D) axis measured on the (YZ) plane as the largest axis.

It must be remembered that plane strain deformation was not observed, and that at 800°C a lateral inclusion strain (ϵ_z) of approximately 0.28 occurred (table 5.38) i.e.

$$\epsilon_z = 0.28 = \ln \frac{D}{D_0}$$

where D_0 is the original inclusion size

$$\therefore D_0 = \frac{D}{e^{0.28}} = \frac{D}{1.32}$$

$$\text{i.e. } D_o = \frac{20}{1.32}$$

$$\text{thus } \underline{D_o \sim 15 \mu\text{m}}$$

Similarly a calculation may be performed for the \sqrt{ab} size observed.

From constancy of volume

$$abD = D_o^3$$

$$\text{Also } D = 1.32 D_o$$

$$\therefore \sqrt{ab} = \sqrt{\frac{D_o^2}{1.32}}$$

$$\begin{aligned} \text{i.e. } D_o &= \sqrt{1.32} \times \sqrt{ab} \\ &= \sqrt{1.32} \times 12 \end{aligned}$$

Thus

$$\underline{D_o \sim 14 \mu\text{m}}$$

From these simple calculations it appears that the maximum plasticity index occurred at an initial inclusion size of approximately 14 - 15 μm diameter, for melts Al6 at 800^o C. The discrepancy between values of 12 μm on the (XY) plane and 20 μm on the (YZ) plane was a result of non plane strain deformation.

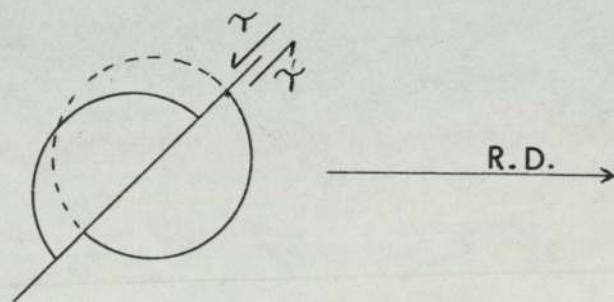
5.3.10. Some possible mechanisms of inclusion deformation.

The deformation of an inclusion embedded in a matrix is governed by matrix stresses and strains imposed by the mode of deformation. The plastic deformation of the matrix is by slip on suitably orientated slip planes, and the maximum shear stress acting is at 45° to the principal stress.

Thus if a siliceous inclusion is cut by a slip plane which is at 45° to the principal applied stress, it will have a tendency to shear along this slip plane unless the inclusion is of sufficient strength to resist deformation. Shear in a brittle inclusion was shown in figure 4.23. where it was seen to be at $\sim 45^{\circ}$ to the rolling direction.

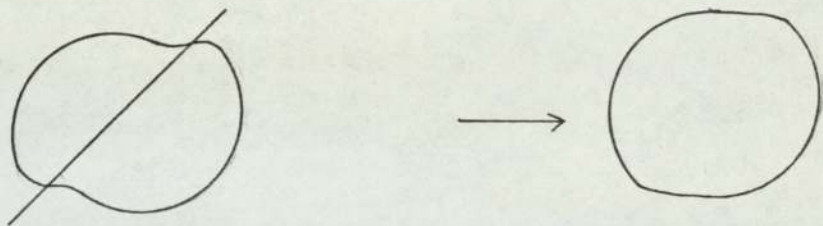
If the inclusion has the ability to deform plastically then again the inclusion may be sheared viz :

5.184.



However, since siliceous inclusions are of a viscous nature the asperities produced will tend to be smoothed by surface tension effects, this smoothing out effect being aided by a lower viscosity (e.g. by an increase in the temperature of deformation).

5.185.



This effect was apparently observed in Plate 5.102

Since metals are crystalline, deformation takes place when critical shear stresses are generated on the more favourable crystallographic slip planes. The most important slip systems in iron are

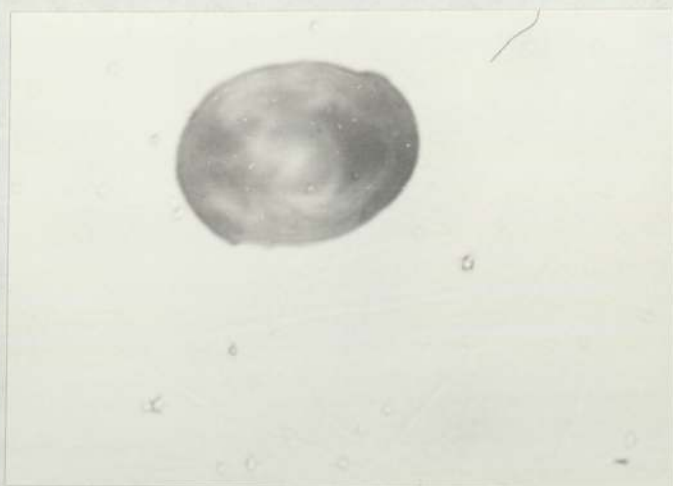
$\{111\} \langle 110 \rangle$ for f.c.c. austenite

$\{110\} \langle 111 \rangle$ for b.c.c. ferrite (although the slip plane is not well defined (218)).

Slip will preferentially occur on one of these slip systems until the stresses on other slip systems reach a critical value and begin shearing. Thus the shear deformation may move from one slip system to another.

Plate 5.11 indicates the slip lines adjacent to inclusions on a $\{111\}$ austenite plane (indicated by the etching phenomenon whereby it may be seen that the major slip directions are parallel to the sides of the triangular etch phenomenon, i.e. at 60° to each other. It may also be observed that some slip lines change direction, these changes in direction appearing parallel to the sides of the etch phenomenon. i.e. slip has changed direction within the $\{111\} \langle 110 \rangle$ family of slip directions.

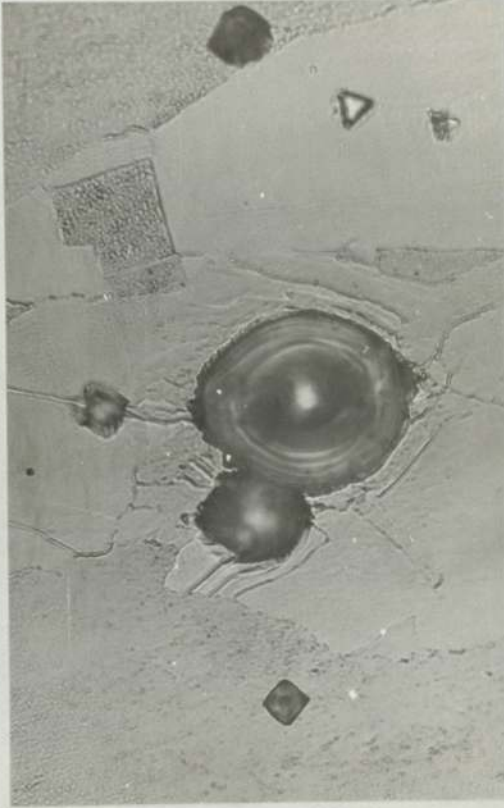
Plate 5.12 shows an inclusion which appeared to have been sheared on two planes, as indicated. One of



5. 10.



5. 12.



5. 11.

these planes appeared to be in the region of 45° to the rolling direction, and the other approximately 60° to the first. Slip planes at these angles could possibly be accounted for if the polished section showed a $\{111\}$ type plane, these two sheared regions would then be parallel to $\langle 110 \rangle$ directions (i.e. the favoured slip directions) the first of these directions being inclined at the critical shear stress angle of 45° .

Referring back to plate 5.11 (a) it may be observed that the distances between the slip lines appear to be in the region of $2-5 \mu\text{m}$. If this distance happens to be the minimum value encountered during the deformation process, then this may give a lead as to why the smaller inclusions are reluctant to deform.

Inclusions which are of diameters less than the interslip plane spacing may not be intersected by a slip plane, therefore, they are situated in a shear strain gradient. This situation may be analogous to the model of Robinson (35) who studied the deformation of immiscible viscous globules within a viscous liquid of the same density within a shear gradient. Thus a small inclusion within this shear gradient may effectively rotate rather than deform. Shear stresses on a slip plane may not therefore impinge directly upon an inclusion. It could be considered, that since these shear stresses are not impinging upon the interface, decohesion of the interface may be avoided. Therefore, this may be an attributable factor as to why conical voids are not found around silicate inclusions less than approximately $2-3 \mu\text{m}$ in diameter (116).

5.4 Practical implications.

In order to prevent the formation of blowholes in steels it is essential that the oxygen activity in the melt be lowered to a value such that the carbon-oxygen reaction does not take place. To achieve this end, commercially, solid deoxidation products become entrapped within the steel.

The use of aluminium, although an excellent deoxidant may lead to products being present which are deleterious in such fields as wire and tube manufacture. They may also lead to a deterioration in mechanical properties of steels for critical application where mechanical properties are of prime importance.

The use of manganese-silicon-aluminium deoxidation techniques prevents the formation of harmful alumina particles. The size and separation rates of these complex deoxidation products are however dependent upon the composition of the inclusions present. The choice of a suitable deoxidant alloying technique may enable the steelmaker to tailor inclusion characteristics to the needs of the processor.

A knowledge of inclusion behaviour during heat treatment and soaking prior to deformation processes may be beneficial. Use may be made of internal inclusion precipitations, in controlling their deformability during the actual deformation process. Thus a potentially harmful highly plastic inclusion may be rendered less harmful by internal precipitation reactions impairing

inclusion deformability.

Studies of inclusion characteristics during processing, and the parameters which influence their behaviour may give valuable insight in how to use or render them less harmful in the final product.

5.4.1 Machinability.

It has been shown that within the $(\text{FeMn})\text{O}-\text{SiO}_2-\text{Al}_2\text{O}_3$ system there are numerous compositions of inclusions which have low softening temperatures. It was pointed out in section 2.3 that low melting point silicates may be beneficial at high cutting temperatures where they behave in a similar manner to MnS at lower temperatures.

From this project it was seen that inclusion softening temperatures may be as low as 700°C within the stated system. It may be the case that some of these inclusions with low softening temperatures may be effective under conditions where MnS inclusions have been traditionally used.

It must though be pointed out that inclusions with low softening temperatures are of a glassy nature and the presence of precipitates within such inclusions leads to a higher apparent softening temperature. It is with this fact in mind one must choose compositions carefully since some of these inclusions readily nucleate precipitates within the glassy matrix, often noticeable even when heat treated for short periods of time.

5.4.2 Surface quality of rolled products.

An area where non-deformable inclusions may cause problems is in the production of rolled strip. The presence of these inclusions may impair surface quality particularly if the strip is intended to be polished. Furthermore, if the rolled strip is to be the substrate for a plating process, surface blemishes may cause lack of adhesion with the plating, resulting in flaking and corrosion. Thus an inclusion composition may be chosen for its fluidity if the product is not for constructional purposes.

5.4.3. Implications to mechanical properties.

It has previously been established that inclusion type, size, shape and processing influences the mechanical properties of the final product. By researching into the behaviour of inclusions during deformation processes it may well be the case that for any given inclusion composition, a steel processing schedule may be derived, such that the presence of these inclusions may be turned to an advantage, or at least restrict the harmful influence of inclusions to an acceptable level.

Conclusions

6.1 Part I of discussion

(i) Over the range of compositions encountered in this project it appeared that as the Mn:Si ratio increased then there was a corresponding increase in the MnO:SiO₂ ratio of the inclusion products ($> 10 \mu\text{m}$) for values of Mn/Si < 3 . Above this value the MnO:SiO₂ ratio appeared asymptotic at a value of approximately 1.75.

(ii) Inclusion compositions were observed to vary with the position from which samples were taken from the 'as cast' bar. This variation was attributed to experimental technique, solution of the deoxidant and product formation. The inclusions from the topmost section of the bar were found to be richest in alumina.

(iii) Inclusion composition was found to vary with inclusion size. It was generally observed that the smaller inclusions were less rich in alumina, but with a corresponding increase in the silica and/or manganese oxide levels.

In melts containing MnO-SiO₂ deoxidation products there was very little evidence of compositional variation.

(iv) Although there was less than 0.01% sulphur in the cast steels, it was observed that below 5 μm diameter inclusions showed an increased amount of sulphur present over the larger inclusions. However, no evidence of MnS or duplex oxide/sulphide inclusions were observed in the 'as cast' state.

(v) Inclusion size distributions reported * in terms of the number of inclusions greater than a given inclusion diameter (per unit area), indicated that inclusion agglomeration and coalescence had occurred to a marked extent. Evidence indicated that within the area of inclusion compositions covered, the greatest amount of coalescence was found within the low liquidus region of the $\text{MnO-SiO}_2\text{-Al}_2\text{O}_3$ diagram.

Coalescence appeared to be encouraged by

- a) A low liquidus temperature.
- b) An increase in the level of MnO in the oxide product.
- c) An increase in the Al_2O_3 content in the product.

Part II of discussion.

(i) As time at the heat treatment temperature increased fewer glassy inclusions were observed.

(ii) Heat treatment at 900° , 1100° and 1300°C (for a given time at temperature) showed that the largest precipitates were observed at 1100°C .

(iii) Quantitative studies were hampered by the apparently random variation in precipitation behaviour.

(iv) In general the smaller inclusions appeared to remain glassy for longer periods than their larger counterparts.

(v) The more siliceous inclusions appeared more resistant to heat treatment induced precipitation than

those richer in manganese oxide.

(vi) Inclusions susceptible to precipitation were often found to precipitate during soaking at temperatures prior to rolling.

(vii) Heat treatment appeared to promote sulphur rich areas at the peripheries of the inclusions, particularly in the vicinity of Mn rich precipitates.

Part III of discussion.

(i) During this investigation inclusions have been observed to exhibit rigid, brittle, plastic and fluid behaviour.

(ii) Rigid glassy inclusions remained intact at low rolling temperatures, whereas inclusions containing precipitates often fractured.

(iii) Often associated with large non-deformable inclusions were voids at the matrix~~in~~inclusion interface in the rolling direction.

(iv) Where large inclusions had cracked and fractured it was observed that the matrix had been forced into these fissures.

(v) The greatest incidence of brittle fracture was observed when rolling was performed in the 800°-900°C. region

(vi) The mean relative plasticity index (ρ) was generally seen to rise rapidly over a narrow temperature range.

(vii) The transition from non-deformable to

deformable behaviour often occurred at temperatures more than 200°C . below the estimated liquidus/solidus temperatures.

(viii) The presence of precipitates within glassy inclusions limited the extent of inclusion deformation in comparison to glassy inclusions of the same composition.

(ix) For glassy inclusions containing between 5 and 15% Al_2O_3 the non-deformable/deformable transition temperature increased as the silica content of the inclusions increased.

(x) At temperatures in excess of the transition temperature, those inclusions which showed a sharp transition curve also showed a fall in the value of $\bar{\nu}$ with temperature.

(xi) The highest peak values of $\bar{\nu}$ were observed in the range 900° - 1000°C .

(xii) At temperatures well in excess of the transition temperature inclusions appeared to break up in a fluid manner.

(xiii) Values of $\bar{\nu}$ for constant matrix reduction were plotted for individual inclusions of measured compositions. It was observed that the most deformable inclusions lay within the low liquidus region of the $\text{MnO-SiO}_2\text{-Al}_2\text{O}_3$ diagram.

(xiv) Values of $\bar{\nu}$ were found to be dependent upon the size range of inclusions included within the statistical analysis.

$$\text{i.e. } \mathcal{V}_{(1+)} \neq \mathcal{V}_{(10+)} \neq \mathcal{V}_{(20+)}$$

Inclusion size has been measured via the use of \sqrt{ab} where a and b have the major and minor axes of the deformed inclusion.

(xv) Inclusion deformation increased with inclusion size for glassy inclusions, although at temperatures at the foot of the transformation curve a peak in the plasticity index - size relationship occurred.

(xvi) There appeared to be a critical size of inclusion below which inclusions would not deform. In this work this critical size was at an observed inclusion diameter of approximately 1 - 2 μm .

(xvii) Over the rolling temperature range of 850° - 900° the number of deformable inclusions (over the size range 1-20 μm) reached a trough value.

(xviii) An increase in \mathcal{V} with size for the larger inclusions at rolling temperatures in excess of the transition temperature may be accounted for by the break up of fluid inclusions.

(xix) Spheroidisation of small deformed inclusions may occur upon reheating and thus enhance the plasticity index - size relationship.

(xx) From limited data it appeared that large inclusions deformed before the small ones.

(xxi) Inclusion, and plasticine model systems indicated that inclusion strain fell relative to matrix strain as matrix strain was increased.

(xxii) An explanation to the above phenomenon has been proposed on the basis of non homogeneous deformation of the matrix.

(xxiii) A theoretical analysis has shown that a fall in plasticity index with increased matrix strain may be explained by the influence of strain rate during a multipass rolling programme.

(xxiv) Inclusion strains have been seen to vary significantly through the thickness of a sample stopped within the roll throat.

(xxv) It has been shown that the values of relative plasticity index have a different value depending upon which orthogonal planes the inclusion strains were measured.

(xxvi) Equations have been developed to relate measured inclusion strains to a plane strain deformation condition.

6.2 Suggestions for further work.

(1) During the course of this work inclusion size has been measured using the \sqrt{ab} criterion, determined optically. However, optical examination is restricted to a maximum of approximately X1000 magnification due to problems of resolution making the measurement of \mathcal{E}_i for small inclusions difficult.

The use of the scanning electron microscope would lead to a more effective technique since its resolution is much improved. However, the problems of image foreshortening and calibration at various magnifications would need to be overcome.

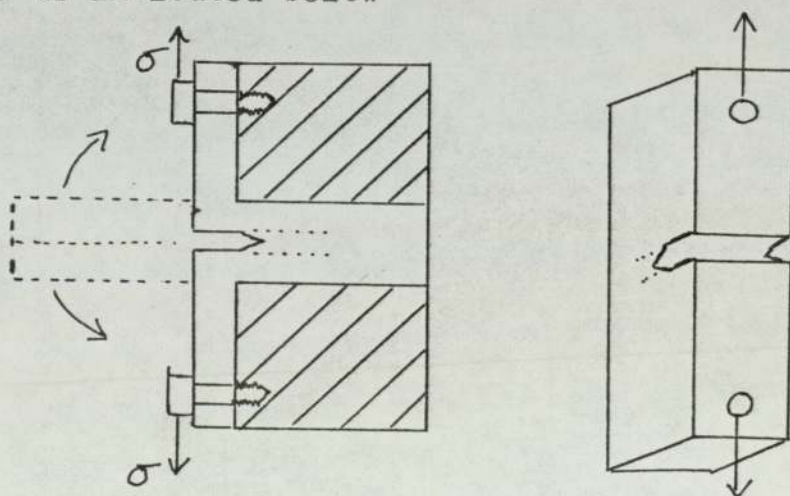
In addition it may be possible to develop a quantitative E.D.P.X. system such that inclusion compositions could be determined at the same time. Since the measurement of \mathcal{E}_i and \sqrt{ab} values is tedious it may be well worth utilising a computer punch tape unit to ease the situation. The use of a suitable computer programme would enable ρ versus \sqrt{ab} graphs to be produced directly and also generate the statistical data.

(2) One of the factors which influences inclusion deformability and which has not received attention is strain rate. As has been shown, strain rate will influence deformability, but only limited work has been performed on investigating the influence of various degrees of strain rate upon the value of relative plasticity index. Strain rate may be investigated either by rolling or by Camm plastometry. The latter being preferred.

(3) Inclusion plasticity could be investigated with reference to the h/w ratio of the material rolled, since it is known that this will vary the deformation pattern of the matrix.

(4) Measurement of ν should be performed on the 3 orthogonal planes and the validity of the equations generated in section 5.3 could be tested. Obtaining a value of ν from the two most suitable planes would give a better indication of the true plasticity parameters.

(5) The influence of the effect of inclusion deformability could be investigated with respect to material toughness. i.e. C.O.D. tests could be performed on S.T. rolled samples. This may be accomplished by the welding or silver soldering of extension pieces, or perhaps by a modified T tear test piece as indicated below



The fracture mechanics aspect of this type of design would need to be investigated.

(6) The use of a hot torsion bar technique may enable inclusion plasticity to be investigated whereby a variety of γ (shear strain) values may be encompassed with one specimen i.e. from investigating from surface to centre.

Also by applying the same strain in the opposite direction to the same γ value an insight into inclusion deformation may be obtained.

(7) The standard method of investigating the relationship between inclusions and metals has been to measure the inclusion strains within a metal matrix. A 'negative' approach may allow further information to be gleaned i.e. Investigate the deformation of metal wires or spheroidal metal powders within glass matrices deformed at high temperatures.

(8) The use of model inclusion/matrix systems should be investigated further and correlated with real systems in a near exact geometries as used in inclusion/metal systems.

(9) It may be of interest to examine the machinability of steels containing low melting point inclusions as observed in this project and compare them with the MnS containing steels usually used at the lower machining temperatures.

(10) Inclusion precipitation should be looked at in a quantitative manner at the various heat treatment temperatures and nucleation and growth studies performed upon typical inclusion compositions.

(11) An examination into the deformation characteristics of commonly found exogenous inclusions could be performed (e.g. simulate 'launder' deposit pick up). In addition the behaviour of reoxidation products could be looked into.

ACKNOWLEDGEMENTS.

The author wishes to thank his supervisor Dr. J.C. Billington for all the encouragement and helpful advice during the course of this work.

Thanks are also due to the members of the academic and technical staff of the Department of Metallurgy and Materials. However, specific acknowledgements are made to the following: Mr. G. Reeves, Mr. D. Webb and Mr. R. Howells, whose co-operation was gratefully appreciated, and finally to my colleague Mr. J. C. B. Asante. for the numerous impromptu dicussions.

APPENDICES

Appendix 3.1

Calculation of deoxidation alloy composition.
i.e. Alloy DA12.

Appendix 3.2

Calculated deoxidation alloy compositions.

Appendix 3.3

Calculation of Fe_2O_3 addition.

Appendix 3.1CALCULATION OF DEOXIDATION ALLOY COMPOSITIONe.g. ALLOY DA12

Aimed for deoxidation product 35%MnO, 45%SiO₂, 20% Al₂O₃

- Assumptions:
- i) 100% utilisation of deoxidation elements
 - ii) Initial oxygen level of 0.09 wt%
 - iii) Final " " " 0.005 wt%

DATA.

Activity $a_{\text{MnO}} = 0.05$

$a_{\text{SiO}_2} = 0.35$

Equilibrium constants $K_{\text{MnO}} = 1.97 \times 10^1$

at 1600°C.

$K_{\text{SiO}_2} = 4.17 \times 10^4$

$K_{\text{Al}_2\text{O}_3} = 1.5 \times 10^{14}$

Oxygen combined as MnO (%) = $35 \times 16/71 = 7.887 \%$

" " " SiO₂ " = $45 \times 32/60 = 24.000 \%$

" " " Al₂O₃ " = $20 \times 48/102 = 9.412 \%$

Total Oxygen in product = 41.299%

Fraction of total oxygen combined as MnO	=	0.1910
" " " " " "	SiO ₂	= 0.5811
" " " " " "	Al ₂ O ₃	= 0.2279
		<u>1.0000</u>

Available oxygen for deoxidation is (0.09 - 0.005)%
i.e. 0.085wt%. This will be distributed between MnO,
SiO₂ and Al₂O₃ thus

$$\begin{aligned} \text{As MnO} &= 0.085 \times 0.1910 = 0.01623 \% \\ \text{" SiO}_2 &= 0.085 \times 0.5811 = 0.04939 \% \\ \text{" Al}_2\text{O}_3 &= 0.085 \times 0.2279 = 0.01937 \% \end{aligned}$$

Stoichiometric requirements for Mn, Si and Al in
products are:

$$\begin{aligned} \text{Mn} &= 0.01623 \times 55/16 = 0.0558 \text{ wt } \% \\ \text{Si} &= 0.04939 \times 28/32 = 0.0432 \text{ wt } \% \\ \text{Al} &= 0.01937 \times 54/48 = 0.0218 \text{ wt } \% \end{aligned}$$

The manganese and silicon required for equilibrium
purposes can be obtained from

$$K_{XO} = \frac{\%XO}{\%X \times \%O}$$

the equilibrium amount of aluminium being negligible
i.e. $< 10^{-4}$ wt% at 1600°C (1873K)

For manganese in equilibrium

$$K_{\text{MnO}} = \frac{Q_{\text{MnO}}}{\% \text{Mn} \times \% \text{O}}$$

$$\% \text{Mn} = \frac{0.05}{19.7 \times 0.005} = 0.508 \text{ wt\%}$$

For silicon in equilibrium

$$K_{\text{SiO}_2} = \frac{Q_{\text{SiO}_2}}{\% \text{Si} \times \% \text{O}^2}$$

$$\% \text{Si} = \frac{0.35}{4.17 \times 10^4 \times (0.005)^2} = 0.336 \text{ wt\%}$$

Hence for a 100gm melt the total required amounts of deoxidising elements are as follows

	stoichiometric		equilibrium	
Mn	0.056	+	0.508	= 0.564 gm
Si	0.043	+	0.336	= 0.379 gm
Al	0.022	+	0.000	= <u>0.022 gm</u>
				= <u>0.965 gm</u>

Thus the total weight of the Mn-Si-Al deoxidant required is 0.965% of the charge weight.

Composition of deoxidation alloy is as follows

58.45% Mn, 39.27% Si, 2.28% Al.

Appendix 3.2

CALCULATED DEOXIDATION ALLOY COMPOSITIONS

Deox Alloy	Elem	Oxide Prod.	α_{xo} (1600C)	Stoich wt%	Eqm. 1600C wt%	Total wt%	Comp ⁿ wt%
DA6	Mn	55	0.18	0.099	1.827	1.928	73.31
	Si	45	0.68	0.049	0.653	0.702	26.69
	Al	-	-	-	-	-	-
						2.630	
DA7	Mn	60	0.27	0.113	2.744	2.857	85.92
	Si	40	0.44	0.046	0.423	0.468	14.08
	Al	-	-	-	-	-	-
						3.325	
DA8	Mn	65	0.42	0.129	4.267	4.395	90.80
	Si	35	0.28	0.042	0.403	0.445	9.20
	Al	-	-	-	-	-	-
						4.840	
DA9	Mn	45	0.12	0.076	1.219	1.295	76.67
	Si	45	0.35	0.046	0.336	0.382	22.62
	Al	10	-	0.012	-	0.012	0.71
						1.689	

Deox Alloy	Elem	Oxide Prod.	α_{xo} (1600°C)	Stoich wt%	Egm 1600C wt%	Total wt%	Comp ⁿ wt%
DA10	Mn	50	0.14	0.088	1.423	1.511	83.67
	Si	40	0.25	0.043	0.240	0.283	15.67
	Al	10	-	0.012	-	0.012	0.64
						<u>1.806</u>	
DA11	Mn	55	0.19	0.101	1.931	2.032	91.24
	Si	35	0.15	0.038	0.144	0.182	8.17
	Al	10	-	0.013	-	0.013	0.58
						<u>2.227</u>	
DA12	Mn	35	0.05	0.056	0.508	0.564	58.45
	Si	45	0.35	0.043	0.336	0.379	39.27
	Al	20	-	0.022	-	0.022	2.28
						<u>0.965</u>	
DA13	Mn	40	0.07	0.066	0.711	0.777	71.94
	Si	40	0.25	0.040	0.240	0.280	25.93
	Al	20	-	0.023	-	0.023	2.13
						<u>1.080</u>	
DA14	Mn	45	0.11	0.077	1.118	1.195	85.41
	Si	35	0.15	0.036	0.144	0.180	12.87
	Al	20	-	0.024	-	0.024	1.72
						<u>1.399</u>	

Deox Alloy	Elem	Oxide Prod.	A_{xO} (1600C)	Stoich wt%	Egm. 1600C wt%	Total wt%	Comp ⁿ wt%
DA15 *	Mn	40	-	-	-	1.571	81.46
	Si	35	-	-	-	0.325	16.88
	Al	25	-	-	-	0.032	1.66
						<u>1.928</u>	
DA16 *	Mn	35	-	-	-	0.639	51.3
	Si	40	-	-	-	0.463	46.4
	Al	25	-	-	-	0.027	2.28
						<u>1.129</u>	
DA17 †	Mn	-	-	-	-	1.195	-
	Si	-	-	-	-	0.180	-
	Al	40	-	-	-	0.046	-
						<u>1.421</u>	
DA18 †	Mn	-	-	-	-	1.195	-
	Si	-	-	-	-	0.180	-
	Al	60	-	-	-	0.066	-
						<u>1.441</u>	

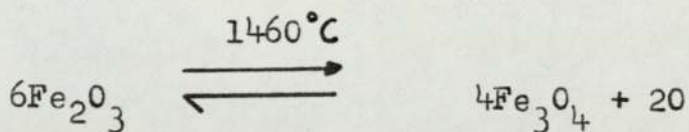
* Blended Deoxidants

† DA14 + extra Al addition

Appendix 3.3

CALCULATION OF Fe₂O₃ ADDITION

Assuming the following reaction



If the initial oxygen content of the electrolytic iron is 0.06wt% and the required level is 0.09wt% then the amount of oxygen to be added is 0.03wt%.

Allowing for the reduction of Fe₂O₃

$$\frac{(3 \times 16) \times 6}{(4 \times 16) \times 4} = \frac{18}{16}$$

Equivalent O as Fe₂O₃

$$= 0.03\% \times \frac{18}{16} = 0.03375\%$$

Now 48 gms O \equiv 160 gms Fe₂O₃

\therefore 1 gm O \equiv 3.33 gms Fe₂O₃

Hence % addition of Fe₂O₃ = 0.1124%

\therefore In a charge of 1.5kg of electrolytic iron, the

Fe₂O₃ addition = 1.69 gms.

Appendix 4.1As cast inclusion analyses. %.Symbols.

XO Data in the first columns refers to the computed inclusion compositions.

XO' in the data columns refers to the 100% rationalised data.

D(μm) is the observed inclusion size.

Accuracy of results.

MnO' , Al₂O₃' , and SiO₂' data is no better than to the nearest percentage.

FeO' is \pm 100%

Melt A3

Fe_2O_3	MnO	Al_2O_3	SiO_2	FeO'	MnO'	$\text{Al}_2\text{O}_3'$	SiO_2'	D(μm)
33.9	71.1	-	-	30.0	70.0	-	-	7
11.4	91.0	-	-	10.1	89.9	-	-	7
7.5	95.8	-	-	6.6	93.4	-	-	8
3.8	96.2	-	-	3.4	96.6	-	-	11
4.0	96.2	-	-	3.6	96.4	-	-	15
4.1	94.2	-	-	3.8	96.2	-	-	23
4.0	94.8	-	-	3.7	96.3	-	-	10
4.5	95.9	-	-	4.1	95.9	-	-	10
3.9	96.4	-	-	3.5	96.5	-	-	15
4.2	96.4	-	-	3.8	96.2	-	-	16
22.2	85.0	-	-	19.0	81.0	-	-	6

Melt A4

Fe_2O_3	MnO	Al_2O_3	SiO_2	FeO'	MnO'	$\text{Al}_2\text{O}_3'$	SiO_2'	D(μm)
2.3	-	3.2	95.5	2.0	-	3.2	94.8	20
2.5	-	2.1	97.0	2.2	-	2.1	95.7	32
2.8	-	1.3	97.1	2.5	-	1.3	96.2	12
2.4	-	3.0	96.2	2.1	-	3.0	94.9	14
2.8	-	1.9	97.1	2.5	-	1.9	95.7	26
2.5	-	2.7	95.7	2.2	-	2.7	95.1	8
2.4	-	1.3	96.1	2.2	-	1.3	96.5	15
2.8	-	2.0	95.8	2.5	-	2.0	95.5	32
2.0	-	2.1	96.0	1.8	-	2.1	96.1	-
2.3	-	2.1	96.9	2.0	-	2.1	95.9	-
2.2	-	2.4	95.7	2.0	-	2.4	95.6	-
2.1	-	2.1	96.1	1.9	-	2.1	96.0	-

Melt A6

Fe_2O_3	MnO	Al_2O_3	SiO_2	FeO'	MnO'	$\text{Al}_2\text{O}_3'$	SiO_2'	D(μm)
0.4	53.4	0.2	29.1	0.4	64.3	0.3	35.0	-
1.5	50.3	0.2	44.4	1.4	52.3	0.2	46.1	-
0.9	53.8	0.4	42.0	0.8	55.5	0.4	43.3	-
1.2	52.3	0.2	42.6	1.1	54.4	0.2	44.3	-
1.2	53.3	0.3	41.6	1.1	55.4	0.3	43.2	-
2.7	44.4	0.4	37.4	2.9	52.5	0.5	44.2	-
1.6	53.3	0.2	38.8	1.5	56.9	0.2	41.4	-
1.7	52.0	0.2	42.6	1.6	54.0	0.2	44.2	-
1.2	53.2	0.2	42.3	1.1	55.0	0.2	43.7	-
2.0	50.0	0.2	44.3	1.9	51.9	0.2	46.0	-
0.9	54.7	0.3	42.7	0.8	55.5	0.3	43.4	-
2.8	52.7	0.1	41.9	2.6	54.2	0.1	43.1	-
2.0	57.6	0.4	37.8	1.8	59.0	0.4	38.7	92
2.3	53.7	0.2	40.0	2.2	56.0	0.2	41.7	21

Melt A6 (cont.)

Fe_2O_3	MnO	Al_2O_3	SiO_2	FeO'	MnO'	$\text{Al}_2\text{O}_3'$	SiO_2'	D(μm)
1.7	57.5	0.1	39.5	1.6	58.3	0.1	40.1	23
2.0	54.8	0.3	40.1	1.9	56.5	0.3	41.3	116
3.4	57.3	0.1	41.0	3.0	56.5	0.1	40.4	55
0.1	57.3	0.2	41.3	0.1	57.9	0.2	41.8	-
0.1	50.1	0.1	38.8	0.1	56.2	0.1	43.6	-

Melt A6 (2)

Fe_2O_3	MnO	Al_2O_3	SiO_2	FeO'	MnO'	$\text{Al}_2\text{O}_3'$	SiO_2'	D(μm)
13.0	51.0	0.6	41.5	11.1	48.7	0.6	39.6	10
2.0	58.4	0.3	43.0	1.7	56.4	0.3	41.5	30
2.0	51.2	0.4	42.9	1.9	53.0	0.4	44.5	15
8.0	54.6	0.2	41.4	7.0	52.8	0.2	40.0	40
5.0	55.1	0.2	37.0	4.7	56.9	0.2	38.2	6
3.0	56.9	0.1	38.0	2.8	58.2	0.1	38.9	9
1.0	56.2	2.8	43.2	0.9	54.5	2.7	41.9	33
2.0	56.0	0.5	38.9	1.8	57.6	0.5	40.0	11
0.0	56.1	0.1	43.4	0.0	56.3	0.1	43.6	77
0.8	56.3	0.0	41.3	0.8	57.3	0.0	41.9	41
4.9	54.7	0.2	37.2	4.6	56.7	0.2	38.6	5
19.8	44.1	1.0	28.6	19.5	48.1	1.1	31.3	4
2.0	42.1	0.8	38.7	2.2	50.5	0.9	46.4	59
2.3	39.8	0.3	41.8	2.4	47.5	0.4	49.7	27

Melt A7

Fe_2O_3	MnO	Al_2O_3	SiO_2	FeO	MnO	Al_2O_3	SiO_2	D(μm)
18.6	52.7	0.3	30.8	16.7	52.4	0.3	30.6	16
5.8	58.8	0.3	31.9	5.4	61.1	0.3	33.2	35
3.9	61.2	0.1	35.2	3.5	61.2	0.1	35.2	50
3.7	61.3	0.5	36.9	3.3	60.1	0.5	36.2	89
10.8	54.7	0.2	34.7	9.8	55.1	0.2	34.9	21
7.8	58.5	0.3	32.0	7.2	59.8	0.3	32.7	12
1.2	63.9	0.3	37.3	1.0	62.3	0.3	36.4	-
0.8	62.7	0.4	36.7	0.7	62.4	0.4	36.5	-
1.0	60.2	0.6	37.4	0.9	60.8	0.6	37.7	-
0.8	62.3	0.5	37.9	0.7	61.4	0.5	37.4	-
1.3	67.0	0.4	30.4	1.2	67.7	0.4	30.7	-
0.1	62.1	0.2	37.9	0.1	61.9	0.2	37.8	-
1.3	62.0	0.3	36.7	1.2	61.9	0.3	36.6	-
0.9	64.6	0.2	36.9	0.8	63.0	0.2	36.0	-
1.5	63.2	0.4	36.3	1.3	62.4	0.4	35.9	-

Melt A8

Fe_2O_3	MnO	Al_2O_3	SiO_2	FeO'	MnO'	$\text{Al}_2\text{O}_3'$	SiO_2'	D(μm)
1.0	63.5	0.2	36.3	0.9	62.9	0.2	36.0	-
1.6	63.0	1.6	37.4	1.4	60.9	1.5	36.2	-
0.6	64.1	1.1	37.7	0.5	62.0	1.1	36.4	-
0.5	66.1	1.0	34.8	0.4	64.6	1.0	34.0	-
1.6	65.4	0.8	36.6	1.4	62.7	0.8	35.1	-
0.8	57.2	0.8	44.2	0.7	55.6	0.8	42.9	-
1.7	60.0	2.0	40.6	1.5	57.7	1.9	38.9	-
2.0	63.8	1.2	37.7	1.7	61.0	1.2	36.1	-
1.5	60.5	1.5	40.0	1.3	58.5	1.5	38.7	-
1.3	61.6	1.2	39.1	1.1	59.8	1.2	37.9	-
1.3	62.8	1.8	36.9	1.1	61.2	1.8	35.9	-
1.6	61.7	1.6	38.2	1.4	59.9	1.6	37.1	-

Melt A9

Fe_2O_3	MnO	Al_2O_3	SiO_2	FeO'	MnO'	$\text{Al}_2\text{O}_3'$	SiO_2'	D(μm)
0.6	53.7	3.9	44.3	0.5	52.5	3.8	43.2	130
0.7	51.2	2.4	44.4	0.6	52.0	2.4	45.0	230
0.5	49.7	6.4	44.9	0.5	49.0	6.3	44.2	-
0.6	56.0	5.0	39.3	0.5	55.6	5.0	38.9	-
0.4	53.7	3.8	42.5	0.3	53.5	3.8	42.4	-
0.7	41.1	18.9	42.3	0.6	39.9	18.4	41.1	-
0.4	47.6	11.3	40.4	0.4	47.7	11.3	40.5	-
0.7	52.7	5.4	41.0	0.6	52.9	5.4	41.1	-
0.5	51.1	4.8	43.2	0.5	51.3	4.9	43.3	-
0.4	50.1	6.5	44.0	0.4	49.6	6.4	43.6	-
0.7	50.2	6.8	41.0	0.7	50.9	6.9	41.5	-
0.3	47.7	9.6	41.6	0.2	48.1	9.7	42.0	-
2.1	39.1	19.0	40.2	1.9	39.0	19.0	40.1	56
2.7	53.3	6.1	41.5	2.4	51.6	5.9	40.1	13
1.8	41.7	18.8	41.5	1.6	40.2	18.1	40.1	27

Melt A9 (cont.)

Fe_2O_3	MnO	Al_2O_3	SiO_2	FeO'	MnO'	$\text{Al}_2\text{O}_3'$	SiO_2'	D(μm)
3.6	47.4	10.9	41.1	3.2	46.2	10.6	40.0	27
2.5	42.9	9.9	41.0	2.3	44.7	10.3	42.7	-
2.4	43.5	10.9	39.7	2.2	45.2	11.3	41.2	-
2.4	44.4	12.2	40.9	2.2	44.6	12.2	41.0	-
2.5	47.9	8.4	40.9	2.3	48.1	8.5	41.1	-
1.3	46.7	11.7	40.9	1.2	46.5	11.7	40.7	-
0.8	44.4	10.4	40.1	0.7	46.4	10.9	41.9	-
1.0	45.1	9.9	40.7	0.9	46.7	10.3	42.1	-
2.4	46.7	14.8	35.9	2.2	46.9	14.9	36.1	-
2.8	48.9	6.9	39.9	2.6	49.8	7.0	40.6	-
1.3	54.4	5.0	39.8	1.2	54.2	5.0	39.7	-
1.0	50.8	2.1	44.8	0.9	51.5	2.1	45.4	-

Melt AlO

Fe_2O_3	MnO	Al_2O_3	SiO_2	FeO'	MnO'	$\text{Al}_2\text{O}_3'$	SiO_2'	D(μm)
1.8	66.4	61.3	33.0	1.5	61.9	5.9	30.8	-
2.6	65.8	2.1	38.1	2.2	60.7	2.0	35.2	-
2.3	50.7	3.2	34.0	2.3	55.7	3.5	38.5	-
2.2	66.3	4.9	34.2	1.8	61.7	4.6	31.9	-
2.2	50.2	3.5	34.4	2.2	55.7	3.9	38.2	-
2.1	57.6	2.7	34.7	1.9	59.5	2.8	35.8	-
1.9	59.6	3.8	34.9	1.7	59.6	3.8	34.9	-
1.8	55.2	2.8	36.9	1.7	57.2	2.9	38.2	80
2.8	49.2	5.6	38.7	2.6	51.2	5.8	40.3	10
1.9	61.4	6.8	26.3	1.8	63.8	7.1	27.3	-
3.1	48.7	8.4	34.5	3.0	51.6	8.9	36.6	30
2.9	57.9	1.9	35.0	2.7	59.4	2.0	35.9	-
2.0	63.1	9.7	29.4	1.7	60.7	9.3	28.3	35
3.2	53.8	3.2	37.3	3.0	55.4	3.3	38.4	-
3.6	51.5	1.3	39.2	3.4	54.1	1.4	41.2	-

Melt A10 (cont.)

Fe_2O_3	MnO	Al_2O_3	SiO_2	FeO '	MnO '	Al_2O_3 '	SiO_2 '	D(μm)
4.3	53.7	2.8	34.6	4.1	56.5	2.9	36.4	-
2.2	48.3	6.4	38.5	2.1	50.7	6.7	40.4	-
1.5	47.2	16.6	35.4	1.3	46.9	16.5	35.2	18

Melt All

Fe_2O_3	MnO	Al_2O_3	SiO_2	FeO	MnO	Al_2O_3	SiO_2	D(μm)
0.7	63.8	7.3	35.9	0.6	59.3	6.8	33.4	-
0.9	56.1	12.4	35.5	0.8	53.5	11.8	33.9	-
1.9	48.1	4.1	35.8	1.9	53.6	4.6	39.9	-
2.1	56.2	8.4	28.8	2.0	59.0	8.8	30.2	-
3.5	54.0	4.5	35.1	3.3	55.8	4.7	36.3	-
3.0	58.0	4.2	30.5	2.8	60.8	4.4	32.0	-
4.4	53.5	3.8	35.3	4.1	55.4	3.9	36.6	50
0.8	62.3	4.7	28.6	0.7	64.7	4.9	29.7	86
0.8	62.9	2.0	29.5	0.8	66.1	2.1	31.0	73
0.6	55.0	9.6	31.6	0.6	56.9	9.9	32.7	42
1.6	57.5	17.8	21.0	1.5	58.8	18.2	21.5	-
0.8	56.1	12.8	35.3	0.7	53.5	12.2	33.6	15
2.7	47.5	5.0	40.7	2.5	49.7	5.2	42.6	8
2.7	56.3	8.5	29.0	2.5	58.5	8.8	30.1	17
1.6	53.1	5.1	34.8	1.5	56.2	5.4	36.9	-

Melt All (cont.)

Fe ₂ O ₃	MnO	Al ₂ O ₃	SiO ₂	FeO'	MnO'	Al ₂ O ₃ '	SiO ₂ '	D(μm)
2.5	58.7	5.0	31.0	2.3	60.6	5.2	32.0	-
2.4	55.1	4.5	33.9	2.3	57.6	4.7	35.4	-
1.1	65.3	4.5	31.2	1.0	64.0	4.4	30.6	80
1.1	55.3	4.5	36.2	1.0	57.0	4.6	37.3	80
1.7	55.5	6.3	41.0	1.5	53.2	6.0	39.3	10
3.5	55.4	1.5	43.7	3.0	53.4	1.5	42.1	10
2.9	63.9	2.5	33.4	2.6	62.4	2.4	32.6	20
3.3	61.2	1.2	35.6	3.0	60.6	1.2	35.3	15

Melt Al2

Fe_2O_3	MnO	Al_2O_3	SiO_2	FeO'	MnO'	$\text{Al}_2\text{O}_3'$	SiO_2'	D(μm)
1.7	28.7	13.1	52.7	1.6	29.9	13.6	54.9	-
0.8	32.2	15.2	42.7	0.8	35.5	16.7	47.0	-
2.0	34.3	10.8	41.4	2.0	38.8	12.2	46.9	-
1.8	32.5	20.2	41.5	1.7	33.9	21.1	43.3	-
2.7	31.4	12.6	55.8	2.4	30.7	12.3	54.6	60
2.4	29.9	16.2	53.1	2.1	29.5	16.0	52.4	30
3.1	27.7	16.5	55.3	2.7	27.1	16.1	54.1	10
8.5	24.9	14.5	51.5	7.8	25.3	14.7	52.3	10
2.6	28.3	17.6	51.4	2.4	28.4	17.7	51.7	15
2.0	25.2	13.7	57.8	1.8	25.6	13.9	58.7	12
2.2	25.4	13.4	56.2	2.0	26.2	13.8	58.0	40
1.2	36.1	11.1	50.3	1.1	36.6	11.3	51.0	100
1.6	37.5	9.7	51.3	1.4	37.5	9.7	51.3	20
1.9	27.2	15.1	56.7	1.7	27.0	15.0	56.3	35
1.5	29.9	12.2	57.8	1.3	29.5	12.1	57.1	55

Melt A12 (cont.,)

Fe_2O_3	MnO	Al_2O_3	SiO_2	FeO'	MnO'	$\text{Al}_2\text{O}_3'$	SiO_2'	D(μm)
5.6	28.0	13.4	49.3	5.3	29.3	14.0	51.5	10
2.7	29.7	14.3	49.8	2.5	30.9	14.9	51.8	10
2.9	29.7	16.1	47.8	2.7	30.9	16.7	49.7	15
9.1	27.1	12.8	47.5	8.6	28.4	13.4	49.7	15
5.0	27.8	13.5	48.9	4.8	29.4	14.3	51.6	10
5.6	28.1	13.5	49.2	5.3	29.3	14.1	51.3	-
2.7	29.7	14.4	49.7	2.5	30.9	15.0	51.6	-
1.7	28.7	13.1	52.2	1.6	30.0	13.7	54.6	-
1.8	32.5	20.2	41.5	1.7	33.9	21.1	43.3	97
2.9	29.7	16.2	47.7	2.7	30.9	16.8	49.6	80
9.1	27.2	12.9	47.5	8.6	28.4	13.5	49.6	4
5.0	27.8	13.6	48.8	4.8	29.4	14.4	51.5	7
5.6	28.0	13.4	49.3	5.3	29.3	14.0	51.5	6
2.6	28.5	14.7	49.8	2.5	29.9	15.4	52.2	75
2.7	30.4	12.9	55.3	2.4	30.1	12.8	54.7	60

Melt Al2 (cont.)

Fe_2O_3	MnO	Al_2O_3	SiO_2	FeO'	MnO'	$\text{Al}_2\text{O}_3'$	SiO_2'	D(μm)
1.9	28.5	8.5	65.9	1.6	27.2	8.1	63.0	75
1.0	32.3	11.8	39.3	1.1	38.3	14.0	46.6	10
2.1	25.1	12.3	40.1	2.1	39.3	13.8	44.9	10
1.9	33.4	12.5	40.9	1.9	37.7	14.1	46.2	15
2.3	37.5	10.2	40.7	2.3	41.5	11.3	45.0	15
1.3	35.6	12.3	41.8	1.3	37.8	13.8	47.0	10
1.4	39.1	10.2	42.3	1.4	42.1	11.0	45.5	18
1.1	35.1	14.2	41.1	1.1	38.4	15.5	45.0	75
0.8	29.1	10.3	52.3	0.8	31.5	11.1	56.6	35
2.6	30.6	18.2	47.3	2.4	31.1	18.5	48.1	34
4.7	30.3	16.4	47.9	4.3	30.7	16.6	48.5	18
2.6	31.3	11.9	52.3	2.4	32.0	12.2	53.4	15

Melt Al3.

Fe_2O_3	MnO	Al_2O_3	SiO_2	FeO'	MnO'	$\text{Al}_2\text{O}_3'$	SiO_2'	D(μm)
2.4	37.2	14.9	46.2	2.2	37.0	14.8	46.0	40
2.9	36.3	8.1	49.8	2.7	37.5	8.4	51.4	10
4.8	45.3	6.4	44.4	4.3	45.1	6.4	44.2	70
2.4	45.7	5.9	45.5	2.2	56.0	5.9	45.8	80
2.6	29.9	15.7	51.2	2.4	30.2	15.9	51.6	25
2.9	37.3	9.5	49.9	2.6	37.6	9.6	50.2	35
2.3	42.9	9.5	44.2	2.1	43.5	9.6	44.8	60
2.8	37.9	8.6	49.8	2.6	38.4	8.7	50.4	-
4.3	40.7	9.7	44.7	3.9	41.1	9.8	45.2	160
2.8	39.8	9.2	50.2	2.5	39.1	9.0	49.4	-
2.6	39.6	9.5	47.1	2.4	40.2	9.6	47.8	50
4.3	41.0	9.3	43.7	4.0	41.9	9.5	44.6	-
3.2	39.6	9.9	46.7	2.9	40.0	10.0	47.1	65
1.4	40.9	8.2	45.4	1.3	42.7	8.6	47.4	37
0.7	40.3	10.1	49.4	0.6	40.1	10.1	49.2	35

Melt A13 (cont.)

Fe_2O_3	MnO	Al_2O_3	SiO_2	FeO'	MnO'	$\text{Al}_2\text{O}_3'$	SiO_2'	D(μm)
1.1	40.9	10.4	49.0	1.0	40.4	10.3	48.4	-
1.0	40.0	14.5	44.0	0.9	40.2	14.6	44.3	-
0.7	40.1	5.2	54.1	0.6	40.1	5.2	54.0	-
1.4	40.7	10.5	48.6	1.2	40.3	10.4	48.1	-
0.6	40.9	10.0	48.5	0.8	41.0	10.0	48.6	-
0.7	40.7	9.3	50.6	0.6	40.2	9.2	50.0	-
0.8	40.0	3.2	55.9	0.7	40.1	3.2	56.0	-

Melt AL3X

Fe_2O_3	MnO	Al_2O_3	SiO_2	FeO'	MnO'	$\text{Al}_2\text{O}_3'$	SiO_2'	D(μm)
9.0	37.0	3.9	48.7	8.3	37.8	4.0	49.8	80
9.3	34.7	4.2	51.1	8.5	35.3	4.2	52.0	40
8.9	44.1	2.1	43.7	8.2	45.0	2.2	44.6	14
7.1	42.4	3.0	47.2	6.5	42.8	3.0	47.7	14
5.1	41.2	1.7	48.7	4.8	42.8	1.8	50.6	9
8.2	41.2	3.5	48.5	7.3	41.0	3.5	48.2	21
8.2	43.4	2.1	46.0	7.4	43.9	2.1	46.5	68

Melt Al4

Fe_2O_3	MnO	Al_2O_3	SiO_2	FeO'	MnO'	$\text{Al}_2\text{O}_3'$	SiO_2'	D(μm)
2.0	55.1	15.7	27.9	1.8	54.8	15.6	27.8	120
3.3	45.4	13.7	36.6	3.0	46.0	13.9	47.1	15
3.3	43.2	17.1	33.8	3.1	44.5	17.6	34.8	15
2.7	46.2	12.4	37.6	2.5	46.8	12.6	38.2	15
2.7	46.2	12.4	37.6	2.5	46.8	12.6	38.2	15
0.9	44.4	16.8	34.5	0.8	46.0	17.4	35.8	40
0.7	49.6	7.1	39.2	0.7	51.4	7.4	40.6	140
2.4	49.1	6.0	40.4	2.2	50.3	6.1	41.4	35
2.4	43.0	17.5	34.1	2.2	44.4	18.1	35.2	35
2.5	44.5	21.2	30.8	2.3	45.1	21.5	31.2	35
2.5	45.8	14.4	35.6	2.3	46.7	14.7	36.3	20
2.5	48.1	17.2	33.8	2.2	47.5	17.0	33.3	17
2.7	42.8	18.0	36.0	2.5	43.1	18.1	36.3	15
2.6	44.4	16.5	35.2	2.4	45.1	16.8	35.8	20

Melt Al4 (cont.)

Fe ₂ O ₃	MnO	Al ₂ O ₃	SiO ₂	FeO'	MnO'	Al ₂ O ₃ '	SiO ₂ '	D(μm)
1.8	45.9	19.8	35.8	1.6	44.5	19.2	34.7	67
1.3	51.2	13.3	37.4	1.1	49.7	12.9	36.3	41
1.6	43.5	24.6	34.2	1.4	41.9	23.7	33.0	83
2.1	48.7	15.2	37.9	1.8	46.9	14.7	36.6	46
1.5	50.9	13.2	38.1	1.3	49.2	12.8	36.8	27
1.1	50.1	13.5	38.4	1.0	48.6	13.1	37.3	24
1.3	50.5	13.7	37.7	1.1	49.0	13.3	36.6	26
1.7	49.7	14.6	37.4	1.5	48.1	14.1	36.2	31
1.6	47.8	17.3	36.8	1.4	46.3	16.7	35.6	58
1.8	47.7	18.1	37.2	1.6	45.6	17.3	35.5	63
1.4	50.4	15.9	38.6	1.2	47.5	15.0	36.4	39
1.4	49.8	14.4	37.6	1.2	48.3	14.0	36.5	33

Melt A14(2)

Fe_2O_3	MnO	Al_2O_3	SiO_2	FeO'	MnO'	$\text{Al}_2\text{O}_3'$	SiO_2'	D(μm)
2.9	53.8	6.6	37.3	2.6	53.6	6.6	37.1	50
2.4	56.9	5.1	39.2	2.1	55.0	5.0	37.9	56
2.1	56.3	5.9	39.1	1.9	54.5	5.7	37.9	73
4.9	53.1	6.5	41.7	4.2	50.2	6.1	39.5	40
2.3	57.5	5.8	39.7	2.0	54.7	5.5	37.8	80
2.5	38.2	36.0	25.5	2.2	37.4	35.3	25.0	147
3.7	60.4	2.2	37.6	3.2	58.4	2.1	36.3	10
3.1	58.0	4.8	37.4	2.7	56.3	4.7	36.2	13
2.9	58.3	4.8	38.1	2.5	56.2	4.6	36.7	14
2.2	57.1	4.1	39.0	2.0	55.9	4.0	38.1	45

Melt Al₄C

Fe ₂ O ₃	MnO	Al ₂ O ₃	SiO ₂	S	FeO'	MnO'	Al ₂ O ₃ '	SiO ₂ '	S'	D(μm)
0.7	43.1	15.5	41.4	0.02	0.6	42.8	15.4	41.2	0.02	30
0.9	50.0	10.3	40.1	0.04	0.8	49.4	10.2	39.6	0.04	17
0.7	51.0	8.0	40.4	0.13	0.6	50.9	8.0	40.4	0.13	13
0.4	51.1	8.1	40.5	0.04	0.3	51.0	8.1	40.5	0.04	15
0.3	49.0	13.0	38.2	0.01	0.3	48.8	12.9	38.0	0.01	60
0.6	51.0	9.4	39.9	0.08	0.5	50.6	9.3	39.6	0.08	14
0.9	50.1	10.1	39.9	0.06	0.8	49.6	10.0	39.6	0.05	18
1.3	50.2	9.0	40.0	0.19	1.2	49.9	8.9	39.8	0.19	-
0.7	43.1	15.4	41.4	0.15	0.6	42.8	15.3	41.1	0.15	24
0.8	49.1	10.3	39.9	0.03	0.8	49.0	10.3	39.9	0.03	-
0.7	50.0	7.5	41.5	0.59	0.6	49.8	7.5	41.4	0.59	6
1.0	50.7	8.7	40.9	0.01	0.9	50.1	8.6	40.4	0.01	-
1.1	50.4	7.7	37.6	-	1.0	52.1	8.0	38.9	-	-
1.3	50.8	11.6	37.2	-	1.2	50.4	11.5	36.9	-	-
0.9	50.1	12.8	36.5	-	0.8	50.0	12.8	36.4	-	-

Melt A15

Fe ₂ O ₃	MnO	Al ₂ O ₃	SiO ₂	FeO'	MnO'	Al ₂ O ₃ '	SiO ₂ '	D(μm)
1.9	52.1	13.4	36.1	1.6	50.5	13.0	34.9	-
1.1	51.9	17.0	34.0	1.0	44.9	16.3	32.8	-
1.4	52.6	13.6	32.2	1.3	52.1	13.6	32.3	-
1.4	52.9	7.5	40.5	1.2	51.8	7.3	39.7	17
1.2	52.0	8.1	41.3	1.0	50.7	7.9	40.3	21
0.5	49.9	10.3	41.4	0.5	48.9	10.1	40.5	35
0.5	49.9	8.1	40.0	0.4	50.7	8.3	40.6	40
0.6	51.0	8.1	40.1	0.5	51.1	8.2	40.2	36
1.3	52.0	6.2	40.6	1.2	52.0	6.2	40.6	21
8.6	48.7	4.3	36.6	8.0	50.0	4.5	37.6	6
1.6	53.0	6.2	39.9	1.4	52.7	6.2	39.7	10
0.4	51.2	8.2	40.6	0.4	51.1	8.1	40.5	35
0.7	50.0	10.3	40.0	0.6	49.5	10.2	39.6	48
0.6	50.1	10.2	39.8	0.5	49.8	10.2	39.6	96
1.6	52.2	7.3	39.9	1.4	51.7	7.3	39.6	16

Melt Al5 (cont.)

Fe ₂ O ₃	MnO	Al ₂ O ₃	SiO ₂	FeO'	MnO'	Al ₂ O ₃ '	SiO ₂ '	D(μm)
2.3	52.3	7.4	40.0	2.1	51.3	7.3	39.3	7
1.6	52.8	7.4	40.1	1.4	51.9	7.2	39.4	21
0.7	50.7	12.2	39.9	0.6	50.0	11.8	38.6	100
0.8	51.0	12.1	41.1	0.7	48.6	11.6	39.1	115
1.6	55.0	6.0	40.4	1.4	53.5	5.8	39.3	14
1.6	55.0	6.2	36.5	1.4	55.5	6.3	36.8	11
2.6	51.7	10.4	41.6	2.2	48.8	9.8	39.2	154
1.2	50.9	8.2	40.6	1.1	50.5	8.1	40.3	51
1.3	48.9	14.4	38.1	1.1	47.7	14.0	37.2	19
0.7	48.9	15.2	37.8	0.6	47.7	14.8	36.8	44
0.8	50.8	13.2	37.9	0.7	49.5	12.9	36.9	105
0.6	49.4	15.3	38.4	0.5	47.7	14.8	37.1	45
0.7	46.1	22.3	34.4	0.6	44.6	21.6	33.3	68
0.4	48.0	15.3	37.2	0.4	47.6	15.2	36.9	65
0.2	49.0	13.0	38.0	0.2	48.9	13.0	37.9	69
0.3	46.1	19.2	35.4	0.3	45.7	19.0	35.1	122

Melt A15(cont.)

Fe_2O_3	MnO	Al_2O_3	SiO_2	FeO'	MnO'	$\text{Al}_2\text{O}_3'$	SiO_2'	D(μm)
1.0	50.8	12.9	37.1	0.9	49.9	12.7	36.5	90
0.8	43.1	26.5	32.6	0.7	41.9	25.6	31.7	57
0.5	48.9	15.4	37.4	0.4	47.9	15.1	36.6	56
0.5	49.9	13.1	37.1	0.5	49.6	13.0	36.9	81
0.6	50.1	13.2	38.2	0.5	49.1	12.9	37.4	106
0.5	49.9	14.3	37.0	0.4	49.1	14.1	36.4	127
0.8	47.6	14.1	36.1	0.7	48.3	14.3	36.6	45
0.7	47.2	17.3	36.4	0.6	46.5	17.0	35.9	58
1.4	47.0	18.3	36.4	1.2	45.7	17.8	35.4	71
0.3	50.0	15.1	37.6	0.3	48.6	14.7	36.5	62
0.5	47.6	14.3	37.5	0.5	47.7	14.3	37.6	183

Melt A15 (cont.) Top section (1)

Fe ₂ O ₃	MnO	Al ₂ O ₃	SiO ₂	FeO'	MnO'	Al ₂ O ₃ '	SiO ₂ '	D(μm)
1.9	43.9	18.5	34.7	1.7	44.4	18.7	35.1	-
1.8	47.0	15.7	34.2	1.6	47.7	15.9	34.7	-
2.0	42.1	20.4	35.6	1.8	42.1	20.4	35.6	-
2.0	46.1	15.4	35.2	1.8	46.8	15.6	35.7	-
1.0	43.8	22.3	33.3	0.9	43.7	22.2	33.2	-
1.8	46.8	21.4	33.4	1.6	45.3	20.7	32.4	-
2.2	42.9	14.2	34.9	2.1	45.7	15.1	37.1	-
1.0	43.1	15.5	41.4	0.9	42.7	14.9	41.5	-
1.8	42.9	15.0	41.7	1.6	42.4	14.8	41.2	-
2.0	53.2	14.6	32.6	1.8	52.0	14.3	31.9	-

Melt Al5 (cont.) Mid section (3)

Fe_2O_3	MnO	Al_2O_3	SiO_2	FeO'	MnO'	$\text{Al}_2\text{O}_3'$	SiO_2'	D(μm)
0.7	50.0	10.3	40.0	0.6	49.5	10.2	39.6	-
0.9	51.0	8.2	40.6	0.8	50.7	8.2	40.3	-
1.9	50.9	8.0	40.5	1.7	50.3	7.9	40.1	-
0.7	49.0	15.4	38.1	0.6	47.5	14.9	36.9	-
0.9	51.0	13.2	37.9	0.8	49.6	12.8	36.8	-
1.1	48.9	15.3	38.3	0.9	47.3	14.8	37.0	-
1.8	48.0	15.3	37.3	1.6	47.0	14.9	36.5	-
1.2	48.8	13.3	38.0	1.1	48.2	13.1	37.6	-
1.0	50.9	13.4	37.3	0.9	49.7	13.1	36.4	-
1.8	48.9	15.5	37.4	1.6	47.3	15.0	36.2	-

Melt A15 (cont.) Bottom Section (5)

Fe_2O_3	MnO	Al_2O_3	SiO_2	FeO'	MnO'	$\text{Al}_2\text{O}_3'$	SiO_2'	D(μm)
0.6	51.0	9.4	39.9	0.5	50.6	9.3	39.6	-
1.7	50.0	9.2	40.7	1.5	49.3	9.1	40.1	-
0.7	51.0	10.3	39.5	0.6	50.3	10.2	38.9	-
1.8	49.9	10.7	40.9	1.6	48.4	10.4	39.7	-
1.8	50.0	10.1	40.0	1.6	49.2	9.9	39.3	-
1.8	49.9	9.0	39.8	1.6	49.7	9.0	39.7	-
2.1	51.1	12.2	41.3	1.8	48.0	11.5	38.8	-
1.7	49.2	14.4	36.2	1.5	48.6	14.2	35.7	-
1.8	49.8	10.3	39.9	1.6	49.0	10.1	39.3	-
1.8	50.0	13.4	37.1	1.6	49.0	13.1	36.3	-

Melt Al6

Fe_2O_3	MnO	Al_2O_3	SiO_2	FeO'	MnO'	$\text{Al}_2\text{O}_3'$	SiO_2'	D(μm)
3.0	34.2	16.5	51.0	2.6	32.8	15.8	48.9	41
27.3	33.0	8.6	48.3	21.5	28.8	7.5	42.2	5
11.0	32.7	9.7	53.3	9.4	31.0	9.2	50.5	6
3.8	34.0	11.3	55.0	3.3	32.8	10.9	53.0	10
3.0	33.4	15.9	50.9	2.6	32.5	15.5	49.5	32
3.2	34.8	12.1	53.9	2.8	33.6	11.7	52.0	13
5.2	33.7	11.9	53.8	4.5	32.4	11.4	51.7	12
2.9	33.6	14.1	52.9	2.5	32.6	13.7	51.2	18
2.4	33.1	17.3	49.7	2.1	32.4	16.9	48.6	30
2.8	34.4	17.5	49.5	2.4	33.1	16.8	47.6	44
2.4	35.0	17.2	48.6	2.1	34.0	16.7	47.2	113
2.8	33.9	19.9	47.0	2.4	32.8	19.3	45.5	35
2.4	34.0	16.7	49.1	2.1	33.4	16.4	48.2	70
2.3	33.8	15.4	50.5	2.0	33.2	15.1	49.6	82
2.2	33.5	16.8	49.8	1.9	32.8	16.5	48.8	78

Melt Al6 (cont.)

Fe_2O_3	MnO	Al_2O_3	SiO_2	FeO'	MnO'	$\text{Al}_2\text{O}_3'$	SiO_2'	D(μm)
2.2	33.5	16.8	49.8	1.9	32.8	16.5	48.8	78
2.1	33.8	17.5	49.3	1.8	33.0	17.1	48.1	60
2.1	34.2	16.5	49.8	1.9	33.4	16.1	48.6	78
2.6	34.5	16.4	49.6	2.3	33.6	15.9	48.2	33
2.8	34.3	12.4	54.0	2.4	33.2	12.0	52.3	11
2.3	34.0	17.4	49.6	2.0	33.0	16.9	48.1	72
2.7	34.5	13.7	52.0	2.4	33.6	13.4	50.7	12
2.7	33.4	14.8	52.2	2.4	32.5	14.4	50.8	18
3.8	30.1	9.3	48.3	3.8	33.0	10.2	53.0	8
2.8	35.4	12.5	52.8	2.4	34.3	12.1	51.2	10
2.8	34.8	12.8	53.2	2.4	33.7	12.4	51.5	12
14.8	32.2	9.6	49.2	12.8	30.9	9.2	47.2	6
2.4	33.4	16.2	49.6	2.1	33.0	16.0	48.9	21
2.7	34.2	16.6	49.8	2.4	33.2	16.1	48.3	57
2.1	34.2	15.9	50.3	1.9	33.4	15.5	49.2	39

Melt A18

Fe_2O_3	MnO	Al_2O_3	SiO_2	FeO'	MnO'	$\text{Al}_2\text{O}_3'$	SiO_2'	D(μm)
2.1	39.0	34.2	27.6	1.8	38.0	33.3	26.8	100
2.5	38.2	36.0	25.5	2.2	37.5	35.3	25.0	62
1.6	40.8	31.8	29.3	1.4	39.5	30.8	28.3	44
2.6	43.5	25.1	32.1	2.3	42.2	24.4	31.1	60
1.4	42.8	28.1	31.2	1.2	41.4	27.1	30.2	126
1.4	42.6	29.0	30.4	1.2	41.2	28.1	29.5	65
2.6	41.3	29.6	30.1	2.2	40.0	28.7	29.1	17
2.4	41.3	30.2	30.2	2.1	39.8	29.1	29.1	16
3.0	43.8	24.8	32.9	2.6	42.1	23.8	31.5	11
2.9	41.7	28.4	31.0	2.5	40.2	27.4	29.9	5
2.4	40.9	31.6	29.0	2.1	39.4	30.5	28.0	21
1.3	41.4	30.7	29.6	1.1	40.2	29.9	28.8	57
1.5	39.0	35.3	26.7	1.3	38.1	34.5	26.1	69
2.2	39.8	33.1	27.7	2.0	38.7	32.3	27.0	13
3.2	42.7	27.2	30.7	2.8	41.3	26.2	29.7	9
2.4	36.4	41.9	24.1	2.1	34.8	40.1	23.0	22

Melt 18 (cont.)

Fe_2O_3	MnO	Al_2O_3	SiO_2	FeO'	MnO'	$\text{Al}_2\text{O}_3'$	SiO_2'	D(μm)
1.4	34.4	38.8	21.4	1.3	35.9	40.5	23.3	72
2.1	35.0	47.0	22.7	1.8	32.8	44.1	21.3	29
2.3	38.3	39.7	26.7	1.9	35.9	37.2	25.0	14
2.7	35.0	52.5	24.7	2.1	30.6	45.8	21.5	34
3.1	38.5	36.8	29.1	2.6	35.9	34.4	27.2	8
9.8	37.8	31.1	29.0	8.3	35.4	29.1	27.2	4
3.0	38.7	36.3	29.2	2.5	36.2	33.9	27.3	10
2.1	36.0	44.4	23.6	1.8	34.0	41.9	22.3	20
3.0	38.5	37.8	28.1	2.5	36.0	35.3	26.2	15
2.2	35.4	45.9	22.6	1.8	33.5	43.4	21.3	20
4.1	37.6	36.1	29.8	3.4	35.1	33.7	27.8	6
37.7	28.5	27.4	21.7	30.4	25.6	24.5	19.5	3
2.5	9.3	85.3	7.7	2.2	8.9	81.6	7.3	8
-	-	100.0	-	-	-	100.0	-	14
2.3	41.3	29.3	46.3	1.8	34.7	24.6	38.9	32

Melt Al8(cont.)

Fe ₂ O ₃	MnO	Al ₂ O ₃	SiO ₂	FeO'	MnO'	Al ₂ O ₃ '	SiO ₂ '	D(μm)
1.9	36.0	42.3	23.2	1.6	34.9	41.0	22.5	29
1.6	42.8	27.0	31.7	1.4	41.6	26.2	30.8	306
1.5	42.0	28.7	31.1	1.3	40.7	27.8	30.1	192
1.3	42.4	28.3	30.8	1.1	41.3	27.6	30.0	140
1.0	18.6	50.4	9.0	1.1	23.6	63.9	11.4	260
0.8	6.5	82.0	2.9	0.8	7.0	89.0	3.1	260
1.7	17.0	58.8	10.4	1.8	19.4	67.0	11.8	260 (mean)
40.8	23.0	35.5	16.0	33.0	20.7	31.9	14.4	260 Fe rich
0.6	14.6	68.5	10.6	0.6	15.5	72.7	11.2	260 Al rich
1.8	37.5	21.0	27.4	1.9	42.8	24.0	33.3	290 matrix
48.0	26.6	23.0	20.1	38.3	23.6	20.3	17.8	290 Fe rich
-	-	100.0	-	-	-	100.0	-	290 Al rich
1.3	14.8	79.8	11.2	1.1	13.8	74.6	10.5	50 Al rich
1.8	48.1	21.0	34.3	1.5	45.8	20.0	32.7	50 matrix
1.5	9.9	84.2	7.6	1.3	9.6	81.7	7.4	28 Al rich
1.5	47.2	23.8	34.8	1.3	44.1	22.2	32.5	28 matrix

Melt NIA12

Fe_2O_3	MnO	Al_2O_3	SiO_2	FeO'	MnO'	$\text{Al}_2\text{O}_3'$	SiO_2'	D(μm)
2.9	30.7	18.2	47.3	2.6	31.1	18.4	47.9	34
5.3	30.3	16.4	47.8	4.8	30.5	16.5	48.2	18
2.9	31.3	11.9	52.3	2.7	31.9	12.1	53.3	15
2.6	31.6	13.2	50.9	2.4	32.2	13.5	51.9	24
1.8	29.9	25.6	41.1	1.7	30.4	26.1	41.8	57
1.9	30.5	20.4	46.8	1.7	30.7	20.5	47.1	53
9.6	27.8	9.1	52.3	8.8	28.4	9.3	53.5	11
2.2	31.4	14.4	49.4	2.0	32.3	14.8	50.8	22
2.2	30.0	13.1	51.4	2.0	31.1	13.6	53.2	23
2.5	30.4	18.3	47.0	2.3	31.0	18.7	48.0	77
1.7	30.4	23.1	42.6	1.6	31.1	23.7	43.6	94
1.8	30.5	19.5	47.6	1.6	30.7	19.7	48.0	62
2.0	29.7	23.3	42.9	1.8	30.4	23.9	43.9	98
1.8	30.7	18.8	46.7	1.7	31.4	19.2	47.7	64

Melt N1A12 (cont.)

Fe_2O_3	MnO	Al_2O_3	SiO_2	FeO'	MnO'	$\text{Al}_2\text{O}_3'$	SiO_2'	D(μm)
1.8	29.5	26.8	42.8	1.6	29.3	26.7	42.5	57
1.8	30.1	19.8	48.0	1.6	30.2	19.9	48.2	52
2.2	30.5	18.5	48.9	2.0	30.5	18.8	48.8	60
2.1	30.8	18.8	47.9	1.9	31.0	18.9	48.2	44
2.0	30.7	21.3	46.1	1.8	30.7	21.3	46.2	97
2.1	30.0	19.5	47.3	1.9	30.4	19.8	47.9	70
1.9	30.0	19.4	48.2	1.7	30.2	19.3	48.5	58
1.9	30.0	20.9	46.1	1.7	30.4	21.2	46.7	113
2.0	30.8	21.0	46.0	1.8	30.9	21.1	46.2	144
1.8	30.4	21.3	46.0	1.6	30.6	21.5	46.3	82
2.2	30.4	18.2	48.9	2.0	30.6	18.3	49.2	46
1.8	30.7	20.4	47.4	1.6	30.7	20.4	47.3	100
2.2	31.0	18.0	49.3	2.0	30.9	18.0	49.2	52
2.0	31.0	20.8	46.6	1.8	30.9	20.8	46.5	122

Melt NIA12 (cont.)

Fe_2O_3	MnO	Al_2O_3	SiO_2	FeO'	MnO'	$\text{Al}_2\text{O}_3'$	SiO_2'	D(μm)
2.3	30.8	18.0	49.6	2.1	30.7	17.9	49.4	69
1.8	30.7	21.3	46.5	1.6	30.7	21.3	46.4	81
1.8	30.6	22.9	44.7	1.6	30.7	22.9	44.8	161
2.2	31.3	13.8	52.9	2.0	31.3	13.8	52.9	20
2.3	31.0	16.1	50.5	2.1	31.1	16.2	50.7	53
3.1	30.7	11.4	53.9	2.8	31.1	11.5	54.7	18
2.5	31.7	13.1	53.6	2.2	31.5	13.0	53.3	20
37.3	22.5	7.1	46.1	30.7	20.6	6.5	42.2	6
2.7	31.6	14.1	52.2	2.4	31.5	14.0	52.0	22
2.7	30.5	17.2	49.7	2.4	30.6	17.3	49.8	37
2.6	30.5	19.6	48.2	2.3	30.3	19.5	47.8	52
2.2	30.7	12.8	53.3	2.0	31.1	13.0	54.0	31
59.3	17.9	3.6	42.2	41.5	16.4	3.3	38.7	5
6.0	30.1	8.6	54.7	5.5	30.5	8.7	55.4	8

Melt NIA12

Fe_2O_3	MnO	Al_2O_3	SiO_2	NiO	S	FeO'	MnO'	$\text{Al}_2\text{O}_3'$	SiO_2'	NiO'	S'	D(μm)
1.1	29.7	16.0	52.2	0.5	0.05	1.0	29.9	16.1	52.5	0.5	0.05	21
0.9	29.8	17.5	50.0	0.4	0.15	0.8	30.2	17.7	50.7	0.4	0.15	30
2.5	29.8	12.6	54.6	0.5	0.19	2.3	29.8	12.6	54.6	0.5	0.19	15
0.9	29.9	12.6	54.1	0.4	0.09	0.8	30.5	12.9	55.3	0.4	0.09	14
0.8	29.8	9.6	57.2	0.7	0.24	0.7	30.3	9.8	58.2	0.7	0.24	12
0.9	28.4	7.3	59.5	0.5	0.37	0.8	29.3	7.5	61.4	0.5	0.38	8
5.7	26.6	6.9	60.0	0.6	0.58	5.1	26.7	6.9	60.1	0.6	0.58	6
24.5	20.0	1.9	52.5	1.4	3.52	21.8	19.7	1.9	51.6	1.4	3.47	4
3.0	25.2	3.5	52.8	1.3	3.52	3.0	28.3	3.9	59.3	1.5	3.95	5
50.2	12.1	4.9	22.4	2.2	4.76	49.4	13.2	5.3	24.5	2.4	5.20	3
95.2	8.5	3.9	20.8	2.8	6.27	66.9	6.6	3.0	16.2	2.2	4.90	2
89.1	8.4	3.8	16.5	2.4	4.88	69.0	7.2	3.3	14.2	2.1	4.20	2

Melt CRA12

Fe ₂ O ₃	MnO	Al ₂ O ₃	SiO ₂	Cr ₂ O ₃	FeO'	MnO'	Al ₂ O ₃ '	SiO ₂ '	Cr ₂ O ₃ '	D(μm)
0.4	33.3	11.8	56.0	0.5	0.3	32.6	11.6	55.0	0.5	11
0.6	33.1	21.9	50.0	0.9	0.5	31.1	20.6	47.0	0.9	62
0.7	34.5	18.3	50.7	0.6	0.6	33.0	17.4	48.5	0.6	94
0.6	34.1	18.9	50.6	0.6	0.5	32.5	18.1	48.3	0.6	86
0.6	33.6	11.7	59.5	1.6	0.5	31.4	11.0	55.7	1.5	9
0.9	33.6	23.9	46.7	0.7	0.7	31.8	22.6	41.2	0.7	78
0.5	33.7	14.3	45.4	0.9	0.4	35.5	15.1	47.9	1.0	32
1.2	34.2	17.9	46.3	0.7	1.1	34.2	17.8	46.3	0.7	41
0.7	33.6	18.5	49.3	1.1	0.6	32.6	18.0	47.8	1.0	63
1.0	33.4	14.9	52.3	1.4	0.8	32.5	14.5	50.9	1.3	26
0.7	33.7	8.8	57.3	0.9	0.6	33.3	8.7	56.5	0.9	10
0.3	34.2	16.0	49.3	1.1	0.3	33.9	15.8	48.9	1.1	52
1.1	34.1	5.2	59.1	1.6	1.0	33.8	5.1	58.5	1.6	5
0.7	33.1	16.6	50.5	0.3	0.6	32.7	16.4	49.9	0.3	65
0.3	32.0	18.1	50.4	1.4	0.2	31.3	17.7	49.3	1.4	88

Melt CRA12 (cont.)

Fe_2O_3	MnO	Al_2O_3	SiO_2	Cr_2O_3	FeO'	MnO'	$\text{Al}_2\text{O}_3'$	SiO_2'	$\text{Cr}_2\text{O}_3'$	D(μm)
0.9	33.8	16.1	51.3	0.7	0.8	32.9	15.7	49.9	0.7	44
1.0	32.7	10.0	56.8	0.4	0.9	32.5	9.9	56.4	0.4	15
0.7	33.8	14.3	54.2	0.9	0.6	32.5	13.7	52.2	0.9	20
0.6	32.1	18.9	50.4	0.6	0.5	31.3	18.4	49.2	0.6	83
0.5	32.7	14.6	46.4	0.4	0.4	34.6	15.4	49.1	0.4	24
0.3	32.6	17.1	53.6	0.5	0.3	31.4	16.4	51.5	0.4	76
0.7	32.6	13.9	55.4	0.5	0.6	31.6	13.5	53.8	0.5	26
0.3	32.0	18.1	50.4	1.1	0.2	31.4	17.8	49.5	1.1	90
0.8	33.9	16.1	52.5	0.7	0.7	32.6	15.5	50.5	0.7	20
0.6	32.9	13.4	52.2	0.6	0.5	33.1	13.4	52.4	0.6	10
0.5	32.2	16.0	51.0	1.0	0.4	32.0	15.9	50.7	1.0	26
0.7	34.9	12.7	52.2	0.7	0.6	34.5	12.5	51.6	0.7	15

Melt VA12

Fe_2O_3	MnO	Al_2O_3	SiO_2	V_2O_5	S	FeO'	MnO'	$\text{Al}_2\text{O}_3'$	SiO_2'	$\text{V}_2\text{O}_5'$	S'	D(μm)
0.6	31.5	16.7	49.8	0.7	0.00	0.5	31.7	16.8	50.2	0.7	0.00	34
0.6	31.8	15.2	51.3	0.5	0.01	0.5	32.0	15.3	51.6	0.5	0.01	17
0.7	31.4	12.8	56.2	0.8	0.40	0.6	30.7	12.5	55.0	0.8	0.39	9
1.4	30.9	8.9	59.7	1.1	2.40	1.2	29.6	8.6	57.3	1.1	2.30	5
14.4	23.2	5.7	41.9	1.9	1.10	14.9	26.7	6.6	48.3	2.2	1.26	4
0.6	31.5	15.9	50.9	0.7	0.01	0.5	31.6	16.0	51.1	0.7	0.01	26
0.8	31.6	25.7	43.5	0.9	0.01	0.7	30.9	25.1	42.5	0.9	0.01	97
0.9	31.9	26.2	42.6	0.7	0.01	0.8	31.2	25.6	41.7	0.7	0.01	103
0.8	31.4	24.7	44.2	1.5	0.01	0.7	30.6	24.1	43.1	1.5	0.01	81
0.5	32.9	14.3	51.4	0.7	0.04	0.5	33.0	14.3	51.5	0.7	0.04	12
0.6	31.0	32.8	39.4	0.8	0.01	0.5	29.7	31.4	37.7	0.8	0.01	137
0.3	32.3	16.8	47.1	0.5	0.03	0.3	33.3	17.3	48.6	0.5	0.03	11

Melt NI50Al2

Fe_2O_3	MnO	Al_2O_3	SiO_2	NiO	FeO'	MnO'	$\text{Al}_2\text{O}_3'$	SiO_2'	NiO'	D(μm)
29.9	12.7	8.2	46.2	0.5	28.5	13.4	8.7	48.9	0.5	7
1.3	20.7	13.0	64.3	0.5	1.2	20.8	13.0	64.5	0.5	26
1.3	24.1	13.9	60.8	0.5	1.2	24.0	13.8	60.5	0.5	46
1.3	24.1	15.1	58.4	0.5	1.2	24.3	15.2	58.8	0.5	62
1.3	21.8	13.5	61.3	0.5	1.2	22.2	13.7	62.4	0.5	42
1.3	23.4	16.5	55.5	0.3	1.2	24.2	17.0	57.3	0.3	58
1.3	21.1	12.8	62.5	0.8	1.2	21.5	13.0	63.5	0.8	32
1.3	21.1	13.8	61.4	0.9	1.2	21.5	14.0	62.4	0.9	27
1.3	23.0	16.1	55.8	0.5	1.2	23.8	16.7	57.8	0.5	85
1.3	21.8	14.5	60.0	0.6	1.2	22.2	14.8	61.2	0.6	60
1.3	24.7	15.6	57.5	0.5	1.2	24.8	15.6	57.8	0.5	65
1.3	20.8	12.4	64.5	0.6	1.2	20.9	12.5	64.8	0.6	26
1.3	25.3	17.7	55.0	0.5	1.2	25.4	17.5	55.2	0.5	70
1.3	23.5	14.5	59.5	0.4	1.2	23.7	14.6	60.1	0.4	56
1.3	24.9	16.0	56.9	0.3	1.2	25.1	16.1	57.3	0.3	88

Melt NI50Al2 (cont.)

Fe_2O_3	MnO	Al_2O_3	SiO_2	NiO	FeO'	MnO'	$\text{Al}_2\text{O}_3'$	SiO_2'	NiO'	D(μm)
2.0	21.5	13.8	50.0	0.5	1.8	22.0	14.1	61.5	0.5	62
2.0	22.0	13.7	59.4	0.5	1.8	22.6	14.1	61.0	0.5	34
2.0	23.7	15.6	55.2	0.5	1.8	24.5	16.1	57.0	0.5	51
2.0	22.8	13.1	59.3	0.5	1.8	23.4	13.4	60.8	0.5	30
2.0	22.4	13.1	60.3	0.5	1.8	22.8	13.4	61.5	0.5	36
2.0	21.7	13.1	59.7	0.5	1.9	22.4	13.5	61.7	0.5	40
2.0	20.9	13.4	60.8	0.5	1.9	21.5	13.8	62.4	0.5	28
2.0	23.3	15.0	54.7	0.5	1.9	24.5	15.7	57.4	0.5	35
2.0	22.3	13.7	58.9	0.5	1.9	22.9	14.1	60.6	0.5	30
2.0	20.8	13.8	60.5	0.5	1.9	21.4	14.2	62.1	0.5	51
2.0	20.7	12.8	61.1	0.5	1.9	21.4	13.2	63.1	0.5	27
2.0	25.1	17.6	54.0	0.5	1.8	25.4	17.8	54.6	0.5	97
2.0	25.3	17.1	53.5	0.5	1.8	25.8	17.4	54.5	0.5	57
2.0	19.2	10.0	59.7	0.5	2.0	21.0	11.0	65.5	0.6	12
2.0	19.9	12.6	62.3	0.5	1.9	20.5	13.0	64.2	0.5	49

Melt NI50Al2 (cont.)

Fe_2O_3	MnO	Al_2O_3	SiO_2	NiO	FeO'	MnO'	$\text{Al}_2\text{O}_3'$	SiO_2'	NiO'	D(μm)
1.3	24.9	15.3	57.0	0.5	1.2	25.2	15.5	57.7	0.5	60
1.3	24.3	15.0	58.4	0.5	1.2	24.5	15.1	58.7	0.5	50
1.3	20.9	13.2	63.3	0.5	1.2	21.1	13.3	63.4	0.5	36
1.3	22.5	14.7	60.0	0.5	1.2	22.8	14.9	60.7	0.5	66
1.3	23.7	15.4	57.6	0.5	1.2	24.1	15.7	58.6	0.5	30
1.3	23.2	13.9	60.2	0.5	1.2	23.4	14.0	60.8	0.5	30
1.3	21.5	14.1	61.8	0.5	1.2	21.7	14.2	62.4	0.5	58
1.3	24.4	16.5	55.9	0.5	1.2	24.8	16.7	56.8	0.5	164
1.3	24.9	17.6	54.0	0.5	1.2	25.4	17.9	55.0	0.5	108
1.3	24.1	16.1	57.1	0.5	1.2	24.4	16.3	57.7	0.5	32
1.3	21.1	13.1	62.8	0.5	1.2	21.4	13.3	63.7	0.5	25
1.3	24.5	14.5	58.4	0.5	1.2	24.7	14.6	58.9	0.5	47
1.3	22.6	14.0	60.6	0.5	1.2	22.9	14.2	61.3	0.5	38
1.3	24.7	16.7	56.1	0.5	1.2	24.9	16.5	56.6	0.5	56
1.3	24.0	16.3	56.8	0.5	1.2	24.3	16.5	57.5	0.5	41

Melt NI50Al2 (cont.)

Fe_2O_3	MnO	Al_2O_3	SiO_2	NiO	FeO'	MnO'	$\text{Al}_2\text{O}_3'$	SiO_2'	NiO'	D(μm)
2.0	25.1	18.2	51.9	0.5	1.9	25.7	18.7	53.2	0.5	81
2.0	23.5	13.2	58.8	0.5	1.8	24.0	13.5	60.1	0.5	35
2.0	22.3	12.6	60.3	0.5	1.9	22.9	12.9	61.8	0.5	45
2.0	20.7	13.3	60.8	0.5	1.9	21.3	13.7	62.6	0.5	41
2.0	22.8	12.9	59.8	0.5	1.8	23.3	13.2	61.1	0.5	32
2.0	21.5	11.7	61.6	0.5	1.9	22.1	12.1	63.5	0.5	31

Appendix 4.2Analysis of deformed inclusions. %.Symbols.

XO Data - Computed composition.

XO' Data - Rationalised to 100%.

\sqrt{ab} - Inclusion size computed via the square root of the product of the major and minor observed axes. (μm).

ω - Inclusion 'Relative plasticity index' as measured when in the microprobe analyser.

Accuracy of results.

XO' Data to the nearest percentage.

FeO' \pm 100%

ω to the nearest decimal place.

Melt A3

Rolling Temp °C	Fe ₂ O ₃	MnO	Al ₂ O ₃	SiO ₂	FeO'	MnO'	Al ₂ O ₃ '	SiO ₂ '	\sqrt{ab}	γ
900	3.7	97.2	-	-	3.3	96.7	-	-	9	0.0
	4.9	96.2	-	-	4.4	95.6	-	-	7	0.0
	1.6	97.1	-	-	1.5	98.5	-	-	13	0.0
	17.7	88.5	-	-	15.2	84.8	-	-	5	0.0
1100	8.2	90.1	-	-	7.6	92.4	-	-	8	0.0
	11.3	84.5	-	-	10.7	89.3	-	-	6	0.0
	3.1	96.7	-	-	2.8	97.2	-	-	15	0.0
	3.2	97.5	-	-	2.9	97.1	-	-	21	0.0
	2.9	95.2	-	-	2.7	97.3	-	-	8	0.0
1300	3.8	96.6	-	-	3.4	96.6	-	-	12	0.0
	14.0	95.8	-	-	11.6	96.6	-	-	12	0.0
	14.0	86.9	-	-	12.7	87.3	-	-	6	0.0
	9.1	94.6	-	-	8.0	92.0	-	-	8	0.0

Melt A4

Rolling temp ^o C	Fe ₂ O ₃	MnO	Al ₂ O ₃	SiO ₂	FeO'	MnO'	Al ₂ O ₃ '	SiO ₂ '	\sqrt{ab}	ν
900	2.2	-	1.3	97.2	2.0	-	1.3	96.7	-	0.0
	2.1	-	1.9	96.4	1.9	-	1.9	96.2	-	0.0
	2.2	-	2.0	95.6	2.0	-	2.0	96.0	-	0.0
1000	2.5	-	4.9	93.3	2.2	-	4.9	92.9	10	0.0
	2.0	-	2.3	96.4	1.8	-	2.3	95.9	15	0.0
	3.2	-	4.2	92.8	2.9	-	4.2	92.9	20	0.0
1300	2.0	-	4.3	96.9	1.8	-	1.3	96.9	20	0.0
	1.5	-	2.3	96.6	1.3	-	2.3	96.4	14	0.0
	2.5	-	1.0	97.0	2.2	-	1.0	96.8	17	0.0
	3.4	-	3.6	96.5	3.0	-	3.5	93.5	15	0.0

Melt A6

Rolling Temp °C	Fe ₂ O ₃	MnO	Al ₂ O ₃	SiO ₂	FeO'	MnO'	Al ₂ O ₃ '	SiO ₂ '	\sqrt{ab}	ν
800	1.1	58.6	0.5	39.2	1.0	59.0	0.5	39.5	-	0.0
	1.2	53.3	0.8	43.1	1.1	54.2	0.8	43.9	-	0.0
	1.6	56.2	0.3	41.1	1.5	56.7	0.3	41.5	-	0.0
	1.2	55.1	0.5	38.8	1.1	57.7	0.5	40.6	-	0.0
	1.3	60.5	0.6	37.4	1.2	60.7	0.6	37.5	-	0.0
900	1.6	56.6	1.9	35.8	1.5	59.1	2.0	37.4	-	0.0
	2.2	55.3	2.0	36.7	2.1	57.6	2.1	38.2	-	0.0
	1.2	56.1	2.1	37.2	1.1	58.1	2.2	38.6	-	0.0
	0.8	57.4	1.9	39.9	0.7	57.5	1.9	39.8	-	0.0
	40.6	22.9	2.9	16.4	46.4	29.1	3.9	20.8	-	0.0
	2.3	55.3	2.1	40.4	2.1	55.4	2.1	40.5	-	0.0
	1.2	56.2	2.1	36.5	1.1	58.6	2.2	38.1	-	0.0
	1.2	53.3	2.0	39.5	1.1	55.6	2.1	41.2	-	0.0
	1.5	56.3	2.1	36.0	1.4	58.8	2.2	37.6	-	0.0

Melt A6 (cont.)

Rolling Temp °C	Fe ₂ O ₃	MnO	Al ₂ O ₃	SiO ₂	FeO'	MnO'	Al ₂ O ₃ '	SiO ₂ '	\sqrt{ab}	ν
900 (cont.)	1.5	55.4	2.1	37.1	1.4	57.7	2.2	38.7	-	0.0
	2.5	55.2	2.1	36.3	2.4	57.6	2.2	37.9	-	0.0
	1.6	55.4	2.1	37.0	1.5	57.7	2.2	38.6	-	0.0
	2.8	52.0	2.2	39.1	2.6	54.3	2.3	40.8	-	0.0
	1.7	54.0	2.2	38.2	1.6	56.3	2.3	39.8	-	0.0
	1.4	58.4	2.1	34.2	1.3	60.9	2.2	35.6	-	0.0
	1.4	53.4	2.1	39.1	1.3	55.7	2.2	40.8	-	0.0
	2.4	54.8	2.1	36.8	2.3	57.2	2.2	38.4	-	0.0
1000	1.9	57.8	1.0	39.1	1.7	58.0	1.0	39.3	-	0.0
	0.9	57.0	0.2	41.7	0.8	57.2	0.2	41.8	-	0.0
	1.0	56.9	0.4	38.8	0.9	59.0	0.4	39.7	-	0.0
	4.0	56.5	0.9	35.3	3.7	58.7	0.9	36.7	15	0.0
	3.0	56.9	0.6	38.7	2.7	57.5	0.6	39.1	-	0.0
	2.0	56.9	1.3	38.0	1.8	58.1	1.3	38.8	-	0.0

Melt A6 (cont.)

Rolling Temp °C	Fe ₂ O ₃	MnO	Al ₂ O ₃	SiO ₂	FeO'	MnO'	Al ₂ O ₃ '	SiO ₂ '	\sqrt{ab}	γ
1000	3.2	57.5	0.5	37.4	2.9	58.5	0.5	38.1	-	0.0
(cont.)	1.0	58.1	0.5	39.3	0.9	58.8	0.5	39.8	-	0.0
1300	3.1	56.5	0.2	41.1	2.8	56.2	0.2	40.9	46	0.9
	5.9	55.9	0.1	41.2	5.2	54.7	0.1	40.2	31	1.2
	3.9	54.3	0.1	39.4	3.6	55.8	0.1	40.5	28	1.1
	2.9	56.1	0.1	39.5	2.7	57.1	0.1	40.2	27	1.1
	4.0	57.0	0.3	41.5	3.5	55.7	0.3	40.5	53	1.1

Melt A6 (2)

Rolling Temp °C	Fe ₂ O ₃	MnO	Al ₂ O ₃	SiO ₂	FeO'	MnO'	Al ₂ O ₃ '	SiO ₂ '	\sqrt{ab}	D
800	2.0	56.4	0.8	39.8	1.8	57.1	0.8	40.3	9	0.0
	1.9	52.2	0.7	42.9	1.8	53.5	0.7	44.0	54	0.0
	2.0	56.5	1.2	39.5	1.8	57.1	1.2	39.9	17	0.0
	2.6	54.3	0.3	39.1	2.4	56.5	0.3	40.7	14	0.0
	5.0	56.6	0.4	39.9	4.4	55.8	0.4	39.3	32	0.0
1100	1.4	51.0	1.0	43.7	1.3	52.6	1.0	45.1	45	0.6
	3.0	53.7	0.9	37.4	2.9	56.7	1.0	39.5	71	0.3
	1.9	52.3	0.8	41.7	1.8	54.2	0.8	43.2	52	0.6
	2.1	56.5	0.6	38.5	1.9	58.0	0.6	39.5	43	0.5
	4.1	57.0	0.9	38.3	3.7	57.1	0.9	38.3	62	0.2
1200	2.0	52.3	0.4	42.7	1.9	53.8	0.4	43.9	44	1.0
	0.8	53.3	0.9	43.3	0.7	54.3	0.9	44.1	72	1.1
	1.2	52.4	0.8	42.8	1.1	54.0	0.8	44.1	31	1.1

Melt A6 (2) (cont.)

Rolling Temp °C	Fe ₂ O ₃	MnO	Al ₂ O ₃	SiO ₂	FeO'	MnO'	Al ₂ O ₃ '	SiO ₂ '	\sqrt{ab}	D
1300	0.9	56.5	1.0	41.9	0.8	56.4	1.0	41.8	28	1.2
	3.1	54.3	0.5	40.0	2.9	55.6	0.5	41.0	31	1.3
	2.0	53.7	0.7	40.5	1.9	55.5	0.7	41.9	42	1.6
	4.5	54.1	0.8	39.5	4.1	54.9	0.8	40.2	36	1.2

Melt A7

Rolling Temp °C	Fe ₂ O ₃	MnO	Al ₂ O ₃	SiO ₂	Fe'	Mn'	Al ₂ O ₃ '	SiO ₂ '	\sqrt{ab}	γ
900	0.9	60.9	2.2	35.7	0.8	61.1	2.2	35.8	-	0.0
	1.1	60.5	2.2	39.4	1.0	58.7	2.1	38.2	-	0.0
	2.0	65.3	0.3	31.2	1.8	66.2	0.3	31.6	-	0.0
	0.9	60.6	3.1	33.4	0.8	61.9	3.2	34.1	-	0.0
	0.8	60.9	2.2	34.0	0.7	62.3	2.2	34.8	-	0.0
	0.9	62.9	2.2	32.0	0.8	64.2	2.3	32.7	-	0.0
	1.0	63.3	2.3	31.5	0.9	61.9	2.3	34.9	-	0.0
	1.2	58.9	2.3	35.7	1.1	60.1	2.4	36.4	-	0.0
	1.6	61.2	2.2	33.0	1.5	62.6	2.2	33.7	-	0.0
	1.0	60.5	2.2	34.3	0.9	61.8	2.3	35.0	-	0.0
	1.1	60.2	3.3	33.5	1.0	61.4	3.4	34.2	-	0.0
1100	2.8	60.6	0.5	36.4	2.5	60.6	0.5	36.4	50	0.0
	8.6	60.6	0.3	32.5	7.6	59.9	0.3	32.1	16	0.0
	13.5	59.8	0.1	29.4	12.0	58.9	0.1	29.0	9	0.0

Melt A7 (cont.)

Rolling Temp °C	Fe ₂ O ₃	MnO	Al ₂ O ₃	SiO ₂	FeO'	MnO'	Al ₂ O ₃ '	SiO ₂ '	\sqrt{ab}	γ
1300	3.6	61.3	0.1	37.8	3.2	59.8	0.1	36.9	65	1.2
	4.0	60.5	0.5	39.0	3.5	58.4	0.5	37.6	89	1.3
	3.1	59.6	0.4	38.7	2.8	58.7	0.4	38.1	57	1.2
	4.0	50.9	0.1	38.7	3.9	54.6	0.1	41.5	54	1.1
	2.9	61.1	0.3	37.4	2.6	60.3	0.3	36.9	77	1.1

Melt 48

Rolling Temp °C	Fe ₂ O ₃	MnO	Al ₂ O ₃	SiO ₂	FeO	MnO	Al ₂ O ₃	SiO ₂	\sqrt{ab}	ν
900	1.1	65.0	2.6	32.7	1.0	64.2	2.6	32.3	-	0.0
	1.1	63.9	2.6	29.6	1.0	65.8	2.7	30.5	-	0.0
	1.0	61.5	3.1	35.7	0.9	60.8	3.1	25.3	-	0.0
	1.1	64.0	2.6	32.5	1.0	63.9	2.6	32.5	-	0.0
	1.1	62.5	4.3	34.5	1.0	61.1	4.2	33.7	-	0.0
	1.9	63.1	15.1	17.4	1.8	64.8	15.5	17.9	-	0.0
	1.8	62.7	2.5	35.3	1.6	61.4	2.5	34.6	-	0.0
	1.6	62.3	2.5	37.8	1.4	59.9	2.4	36.3	-	0.0
	1.0	63.7	0.7	33.2	0.9	64.7	0.7	33.7	60	0.0
	1.2	64.1	1.6	35.1	1.1	62.9	1.6	34.5	80	0.0
	1.3	59.4	1.8	33.1	1.2	62.2	1.9	34.7	80	0.0
	1.3	63.9	2.9	34.9	1.1	62.1	2.8	33.9	100	0.0
	1.0	61.5	2.0	32.7	0.9	63.3	2.1	33.7	60	0.0
	1.6	63.9	4.7	33.0	1.4	62.0	4.6	32.0	80	0.0

Melt A8 (cont.)

Rolling Temp °C	Fe ₂ O ₃	MnO	Al ₂ O ₃	SiO ₂	FeO	MnO	Al ₂ O ₃	SiO ₂	\sqrt{ab}	D
900	1.6	63.3	4.7	34.2	1.4	61.1	4.5	33.0	40	0.0
	2.7	62.9	4.0	33.2	2.4	61.3	3.9	32.4	80	0.0
	1.7	63.2	2.9	35.0	1.5	61.6	2.2	34.1	80	0.0
	1.3	63.0	2.9	34.8	1.1	61.8	2.8	34.2	80	0.0
1000	2.7	66.0	8.4	29.0	2.3	62.4	7.9	27.4	-	0.9
	1.2	58.0	6.2	35.4	1.1	57.6	6.2	35.2	41	0.7
	3.1	55.5	4.3	38.1	2.8	55.1	4.3	37.8	53	0.8
	2.0	56.8	3.3	37.9	1.8	56.9	3.3	38.0	25	0.5
1300	3.1	62.1	0.3	34.5	2.8	62.3	0.3	34.6	38	1.0
	7.7	64.8	0.2	34.8	6.5	60.7	0.2	32.6	27	1.2
	4.0	65.4	0.3	34.3	3.5	63.1	0.3	33.1	13	0.7
	49.8	61.0	0.2	34.2	31.9	43.5	0.1	24.4	15	0.8
	4.4	65.1	0.2	34.2	3.8	62.9	0.2	33.1	26	1.2
	54.8	2.2	34.3	31.5	42.0	1.9	29.2	26.9	27	0.0

Melt A9

Rolling Temp °C	Fe ₂ O ₃	MnO	Al ₂ O ₃	SiO ₂	FeO'	MnO'	Al ₂ O ₃ '	SiO ₂ '	\sqrt{ab}	ν
900	0.7	51.3	6.9	44.5	0.6	49.7	6.7	43.1	220	0.0
	0.9	56.1	5.1	39.4	0.8	55.3	5.0	38.9	100	0.0
	0.8	54.7	4.8	43.1	0.7	52.9	4.7	41.7	150	0.0
	0.8	53.7	3.8	44.2	0.7	52.4	3.7	43.2	180	0.0
	2.2	41.2	19.1	42.3	1.9	39.4	18.3	40.5	50	0.0
	2.8	45.1	11.3	40.5	2.5	45.4	11.4	40.7	30	0.0
	1.0	52.3	5.6	43.9	0.9	50.9	5.5	42.8	50	0.0
	2.1	50.0	9.4	42.3	1.8	48.3	9.1	40.8	120	0.0
	1.0	51.7	5.4	45.2	0.9	50.1	5.2	43.8	65	0.0
	1.0	51.3	4.5	43.9	0.9	51.0	4.5	43.6	-	0.0
	1.0	51.0	4.8	43.2	0.9	51.1	4.8	43.2	-	0.0
	2.1	48.6	6.5	44.1	1.9	48.1	6.4	43.6	45	0.0
	2.8	44.2	10.6	41.3	2.6	44.8	10.8	41.9	15	0.0
	2.8	44.1	11.0	40.8	2.6	44.8	11.2	41.5	10	0.0
	2.8	46.5	7.1	42.5	2.6	47.2	7.2	43.1	20	0.0

Melt 49 (cont.)

Rolling Temp °C	Fe ₂ O ₃	MnO	Al ₂ O ₃	SiO ₂	FeO'	MnO'	Al ₂ O ₃ '	SiO ₂ '	\sqrt{ab}	ν
900	2.8	46.2	9.7	41.8	2.5	46.1	9.7	41.7	20	0.0
(cont.)	5.6	45.8	6.9	41.1	5.1	46.3	7.0	41.6	10	0.0
	1.0	52.6	5.1	43.1	0.9	51.7	5.0	42.4	80	0.0
	1.9	48.0	8.0	42.6	1.7	47.9	8.0	42.5	30	0.0
	2.1	49.4	6.9	43.1	1.9	48.8	6.8	42.6	40	0.0
	2.0	46.5	8.6	42.4	1.8	46.8	8.7	42.7	25	0.0
	3.0	46.9	10.0	40.0	2.7	47.1	10.0	40.2	15	0.0
1000	1.0	48.3	3.2	43.3	0.9	50.5	3.3	45.2	-	0.0
	2.9	45.9	8.3	41.3	2.7	46.8	8.5	42.1	-	0.0
	2.9	49.9	5.9	40.7	2.6	50.3	6.0	41.1	-	0.0
	1.0	51.0	2.5	44.3	0.9	51.7	2.5	44.9	-	0.0
	2.0	48.4	3.0	46.0	1.8	48.8	3.0	46.4	-	0.0
	2.9	48.7	8.4	40.6	2.6	48.5	8.4	40.5	-	0.0
	1.0	51.4	6.3	40.9	0.9	51.7	6.3	41.1	-	0.0

Melt A9 (cont.)

Rolling Temp °C	Fe ₂ O ₃	MnO	Al ₂ O ₃	SiO ₂	FeO'	MnO'	Al ₂ O ₃ '	SiO ₂ '	\sqrt{ab}	ν
1000	3.0	50.1	4.1	39.3	2.8	52.1	4.3	40.9	-	0.0
(cont.)	0.9	48.7	5.3	42.0	0.8	50.3	5.5	43.4	-	0.0
	1.9	48.4	7.5	41.2	1.7	49.0	7.6	41.7	-	0.0
	3.2	48.0	5.7	43.4	2.9	48.0	5.7	43.4	-	0.1
1300	5.3	54.1	3.4	42.1	4.6	51.8	3.3	40.4	20	1.5
	3.8	51.0	5.9	42.3	3.3	49.7	5.8	41.2	35	1.3
	1.8	49.5	3.0	41.0	1.7	52.0	3.2	43.1	58	1.3
	1.2	50.1	3.5	39.3	1.2	53.3	3.7	41.8	71	0.9
	1.8	55.1	3.7	37.3	1.7	56.4	3.8	38.2	54	1.3
	11.5	52.9	2.5	37.7	10.0	51.1	2.4	36.4	14	0.9
	4.7	48.8	7.9	40.8	4.2	48.0	7.8	40.1	122	0.8
	1.9	41.2	3.7	37.3	2.0	49.1	4.4	44.6	23	1.2

Melt A10

Rolling Temp °C	Fe ₂ O ₃	MnO	Al ₂ O ₃	SiO ₂	FeO'	MnO'	Al ₂ O ₃ '	SiO ₂ '	\sqrt{ab}	ν
900	2.0	44.8	18.2	35.3	1.8	44.8	18.2	35.3	20	0.0
	2.1	56.7	4.5	37.9	1.9	56.1	4.5	37.5	25	0.0
	2.7	59.3	1.4	39.1	2.4	58.0	1.4	38.3	40	0.0
	3.2	53.3	3.0	37.9	3.0	54.9	3.1	39.0	35	0.0
	3.3	53.4	2.0	39.6	3.0	54.5	2.0	40.4	10	0.0
	1.2	55.5	2.8	40.0	1.1	55.9	2.8	40.3	75	0.0
	2.5	52.7	2.8	41.8	2.3	52.9	2.8	42.0	15.	0.0
	1.7	55.1	2.5	39.3	1.6	56.0	2.5	39.9	10	0.0
	2.5	53.1	2.6	39.2	2.3	54.7	2.7	40.4	35	0.0
	2.5	52.9	2.7	38.9	2.3	54.7	2.8	40.2	-	0.0
	2.0	56.2	2.4	39.1	1.8	56.5	2.4	39.3	-	0.0
	1.9	62.4	1.3	31.1	1.8	64.7	1.4	32.2	-	0.0
	2.3	54.8	2.6	38.9	2.1	55.7	2.6	39.5	-	0.0
	2.8	44.8	7.6	35.4	2.8	49.6	8.4	39.2	40	0.0
	1.8	57.4	1.3	37.9	1.7	58.4	1.3	38.6	80	0.0

Melt AlC (cont.)

Rolling Temp °C	Fe ₂ O ₃	MnO	Al ₂ O ₃	SiO ₂	FeO	MnO	Al ₂ O ₃	SiO ₂	\sqrt{ab}	ν
900	1.8	59.3	3.8	40.0	1.6	56.6	3.6	38.2	60	0.0
(cont.)	1.3	52.7	2.0	37.6	1.3	56.4	2.1	40.2	15	0.0
	3.7	52.7	2.0	40.1	3.4	53.7	2.0	40.9	15	0.0
	1.9	55.0	2.0	40.0	1.7	55.7	2.0	40.5	150	0.0
	2.8	51.8	1.7	41.5	2.6	53.1	1.7	42.6	70	0.0
	0.8	55.5	1.8	32.1	0.8	61.6	2.0	35.6	-	0.0
	2.7	65.0	1.7	31.9	2.4	64.3	1.7	31.6	-	0.0
	3.0	53.8	2.0	40.0	2.7	54.6	2.0	40.6	-	0.0
1000	2.9	55.8	4.4	37.7	2.6	55.5	4.4	37.5	24	0.0
	3.0	53.2	3.7	39.5	2.7	53.7	3.7	39.9	12	0.0
	1.9	55.6	8.8	41.0	1.6	51.9	8.2	38.3	11	0.0
	2.0	61.4	4.4	40.5	1.7	56.8	4.1	37.5	60	0.0
	1.9	50.3	5.2	41.9	1.7	50.8	5.2	42.3	15	0.0
	1.0	53.7	6.6	39.6	0.9	51.1	6.5	39.3	11	0.1
	2.9	51.2	3.6	39.1	2.7	53.1	3.7	40.5	12	0.2

Melt A10 (cont.)

Rolling Temp °C	Fe ₂ O ₃	MnO	Al ₂ O ₃	SiO ₂	FeO'	MnO'	Al ₂ O ₃ '	SiO ₂ '	\sqrt{ab}	ν
1300	2.6	55.2	2.0	43.7	2.3	53.5	1.9	42.3	24	0.5
	2.7	57.4	2.6	43.6	2.3	54.1	2.5	41.1	42	1.2
	4.0	54.8	8.2	41.6	3.3	50.7	7.6	38.5	23	0.7
	2.4	53.8	2.7	45.6	2.1	52.6	2.6	42.6	48	0.7
	2.0	51.0	2.0	39.2	1.9	54.3	2.1	41.7	115	0.9
	1.9	54.1	0.8	41.9	1.7	54.9	0.8	42.5	59	0.5
	2.6	54.0	4.4	43.6	2.2	51.8	4.2	41.8	37	0.7
	3.3	58.7	2.3	43.9	2.8	54.4	2.1	40.7	57	1.1
	6.5	56.4	3.0	35.3	5.8	56.1	3.0	35.1	7	0.3
	8.2	54.9	1.9	43.7	6.8	50.9	1.8	40.5	9	0.4

Melt All

Rolling Temp °C	Fe ₂ O ₃	MnO	Al ₂ O ₃	SiO ₂	FeO'	MnO'	Al ₂ O ₃ '	SiO ₂ '	\sqrt{ab}	γ
900	1.6	64.4	1.5	31.1	1.5	65.4	1.5	31.6	40	0.0
	1.4	65.6	3.9	29.8	1.3	65.2	3.9	29.6	80	0.0
	3.2	58.8	2.5	35.1	2.9	59.2	2.5	35.4	60	0.0
	2.8	58.5	2.4	34.9	2.6	59.5	2.4	35.5	15	0.0
	1.3	61.0	2.1	34.6	1.2	61.7	2.1	35.0	15	0.0
	2.1	62.4	2.4	30.9	1.9	63.9	2.5	31.7	150	0.0
	2.4	62.8	2.5	34.8	2.1	61.4	2.4	34.0	70	0.0
	2.0	61.4	2.4	35.0	1.8	61.0	2.4	34.8	-	0.0
	2.0	54.1	8.8	31.7	1.9	56.1	9.1	32.9	40	0.0
	1.3	60.9	2.1	30.7	1.2	64.2	2.2	32.4	150	0.0
	2.1	61.9	2.5	33.3	1.9	62.2	2.5	33.4	-	0.0
1000	2.6	64.3	4.8	31.1	2.3	62.7	4.7	30.3	22	0.0
	3.0	58.7	7.6	33.6	2.6	57.2	7.4	32.7	50	0.0
	2.3	58.6	8.5	31.5	2.1	58.2	8.4	31.3	38	0.0

Melt All (cont.)

Rolling Temp °C	Fe ₂ O ₃	MnO	Al ₂ O ₃	SiO ₂	FeO'	MnO'	Al ₂ O ₃ '	SiO ₂ '	\sqrt{ab}	ν
1000	2.2	65.8	3.7	28.5	2.0	65.6	3.7	28.5	65	0.0
(cont.)	2.2	56.0	6.2	41.0	1.9	53.2	5.9	39.0	8	0.0
	4.9	45.0	5.5	43.6	4.5	45.7	5.6	44.3	11	0.9
	0.8	56.5	6.1	35.0	0.7	57.5	6.2	35.6	11	0.1
	1.7	57.4	6.6	35.2	1.5	57.0	6.6	34.9	11	0.6
	2.9	56.2	8.7	35.4	2.5	54.6	8.5	34.4	23	1.2
1300	8.9	58.8	2.8	32.0	7.9	57.9	2.8	31.5	19	1.0
	3.7	60.7	0.2	30.3	3.5	64.2	0.2	32.1	22	0.0
	5.9	53.4	12.2	31.1	5.2	52.4	12.0	30.5	14	0.7
	4.3	59.1	4.8	34.0	3.8	58.1	4.7	33.4	40	1.0
	4.6	64.3	2.5	35.8	3.9	60.2	2.3	33.5	27	1.1
	6.4	63.8	2.4	35.9	5.3	59.2	2.2	33.3	29	1.4
	2.3	0.0	104.3	0.3	1.9	0.0	97.8	0.3	70	0.0
	2.1	62.9	3.2	36.1	1.8	60.4	3.1	34.7	30	1.1
	5.6	63.9	3.5	36.1	4.6	58.9	3.2	33.3	8	0.8

Melt A12

Rolling Temp °C	Fe ₂ O ₃	MnO	Al ₂ O ₃	SiO ₂	FeO'	MnO'	Al ₂ O ₃ '	SiO ₂ '	\sqrt{ab}	ν
800	3.1	45.1	9.3	43.2	2.8	44.9	9.3	43.0	19	0.6
	1.8	33.9	14.4	44.1	1.7	36.1	15.3	46.9	17	0.4
	2.9	37.0	12.9	46.5	2.6	37.4	13.0	47.0	17	0.8
	2.2	38.6	7.6	44.1	2.2	41.8	8.2	47.8	16	1.4
	2.6	40.0	11.3	47.5	2.3	39.6	11.2	47.0	9	0.3
	2.8	31.4	8.5	56.7	2.5	31.7	8.6	57.2	10	0.0
	2.7	34.1	20.1	41.1	2.5	34.9	20.7	42.0	12	0.0
	2.3	19.1	15.9	50.1	2.4	21.9	18.2	57.5	38	0.0
	2.4	49.1	3.0	53.3	2.0	45.7	2.8	49.6	30	0.0
	0.9	26.2	7.3	39.5	1.1	35.5	9.9	53.5	140	0.0
	3.1	37.7	11.2	49.3	2.8	37.3	11.1	48.8	24	1.4
	2.7	40.9	9.2	56.1	2.2	37.7	8.5	51.6	29	1.0
	1.7	26.7	15.4	45.2	1.7	30.1	17.3	50.9	40	0.0
	3.1	35.6	15.3	52.2	2.6	33.6	14.5	49.3	8	0.3

Melt A12 (cont.)

Rolling Temp °C	Fe ₂ O ₃	MnO	Al ₂ O ₃	SiO ₂	FeO'	MnO'	Al ₂ O ₃ '	SiO ₂ '	\sqrt{ab}	ν
800	5.2	35.6	16.8	50.8	4.3	33.0	15.6	47.1	9	0.3
	6.6	37.1	7.9	61.9	5.3	32.9	7.0	54.9	11	1.0
	3.6	40.8	12.9	52.6	3.0	37.3	11.8	48.0	6	0.2
	3.1	33.0	12.4	55.0	2.7	31.7	11.9	53.7	-	0.0
	2.1	31.2	13.3	54.9	1.9	30.8	13.1	54.2	-	0.0
	2.0	31.1	17.0	51.4	1.8	30.7	16.8	50.7	-	0.0
	2.5	26.9	15.1	53.3	2.3	27.6	15.5	54.6	-	0.0
	2.1	30.1	16.2	48.5	2.0	31.1	16.8	50.2	-	0.0
	3.4	30.9	12.9	53.6	3.0	30.8	12.8	53.4	-	0.0
	2.4	32.2	17.7	50.7	2.1	31.3	17.2	49.3	-	0.0
	3.9	30.2	16.0	48.3	3.6	30.8	16.3	49.3	-	0.0
	2.1	38.3	9.1	50.8	1.9	38.3	9.1	50.8	-	0.0
	3.9	26.9	9.7	57.6	3.6	27.5	9.9	58.9	-	0.0
	3.3	46.1	7.3	42.8	3.0	46.5	7.4	43.2	-	0.0

Melt Al2 (cont.)

Rolling Temp °C	Fe ₂ O ₃	MnO	Al ₂ O ₃	SiO ₂	FeO'	MnO'	Al ₂ O ₃ '	SiO ₂ '	\sqrt{ab}	ψ
900	1.8	26.0	7.2	67.9	1.6	25.3	7.0	66.1	80	0.0
	1.5	26.9	12.3	59.6	1.4	26.9	12.3	59.5	20	0.0
	2.3	26.4	10.3	65.2	2.0	25.4	9.9	62.7	25	0.0
	1.7	25.4	9.5	62.6	1.5	25.7	9.6	63.2	50	0.0
	2.0	27.0	8.8	65.0	1.8	26.3	8.6	63.4	40	0.0
	1.8	26.6	9.6	63.5	1.6	26.3	9.5	62.7	50	0.0
	2.0	33.0	8.8	65.0	1.7	30.4	8.1	59.9	-	0.0
	1.4	0.1	90.6	0.0	1.4	0.1	98.5	0.0	-	0.0
	3.1	43.0	11.0	45.7	2.7	41.9	10.7	44.6	80	0.0
	1.8	37.7	10.0	46.9	1.7	39.2	10.4	48.7	60	0.0
	3.2	30.0	8.5	57.5	2.9	30.3	8.6	58.2	40	0.0
	2.3	31.2	11.0	54.6	2.1	31.6	11.1	55.2	20	0.0
	1.7	38.5	9.3	50.7	1.5	38.5	9.3	50.7	40	0.0
	2.3	15.9	10.0	71.8	2.0	15.9	10.0	72.0	15	0.0

Melt A12 (cont.)

Rolling Temp °C	Fe ₂ O ₃	MnO	Al ₂ O ₃	SiO ₂	FeO'	MnO'	Al ₂ O ₃ '	SiO ₂ '	\sqrt{ab}	ν
900	1.8	42.1	11.1	44.3	1.6	42.5	11.2	44.7	25	0.0
	2.7	37.0	9.4	50.7	2.4	37.2	9.4	50.9	20	0.0
	2.9	36.9	9.9	46.0	2.7	38.7	10.4	46.2	-	0.0
	2.5	30.7	9.6	52.0	2.4	32.5	10.2	55.0	-	0.0
	1.5	27.2	13.9	56.1	1.4	27.6	14.1	56.9	24	0.5
	3.0	30.1	17.5	49.1	2.7	30.3	17.6	49.4	11	0.8
	2.7	30.3	13.4	54.6	2.4	30.1	13.3	54.2	7	0.3
	2.6	31.0	15.9	50.5	2.4	31.1	15.9	50.6	8	0.4
	2.5	30.0	16.1	49.9	2.3	30.5	16.4	50.8	8	0.7
	2.6	27.8	15.5	52.8	2.4	28.2	15.7	53.6	9	0.5
	2.0	30.2	17.2	52.8	1.8	29.6	16.9	51.8	14	0.3
	2.0	29.9	15.9	53.1	1.8	29.7	15.8	52.8	10	0.7
	2.5	28.0	14.2	54.6	2.3	28.3	14.3	55.1	29	0.5
	2.6	27.4	16.5	56.5	2.3	26.7	16.1	55.0	13	0.7
	2.5	27.7	16.6	52.8	2.3	27.9	16.7	53.1	25	0.6

Melt A12 (cont.)

Rolling Temp °C	Fe ₂ O ₃	MnO	Al ₂ O ₃	SiO ₂	FeO'	MnO'	Al ₂ O ₃ '	SiO ₂ '	\sqrt{ab}	ν
1000	2.8	29.4	19.5	49.8	2.5	29.0	19.3	49.2	12	0.7
	1.7	27.4	11.8	55.8	1.6	28.4	12.2	27.8	20	0.8
	2.7	29.7	8.7	57.6	2.5	30.2	8.8	58.5	44	0.7
	2.1	37.2	9.1	49.8	1.9	38.0	9.3	50.8	27	0.9
	2.7	26.3	15.8	55.4	2.4	26.3	15.8	55.4	31	0.8
	2.1	27.2	15.0	50.3	2.0	28.8	15.9	53.3	57	0.7
	2.8	29.7	15.1	48.5	2.6	31.0	15.8	50.6	38	0.5
	2.8	28.1	15.9	53.7	2.5	28.0	15.9	53.6	54	1.0
	2.1	30.1	16.0	50.0	1.9	30.7	16.3	51.0	46	0.8
	2.0	39.1	8.7	50.8	1.8	38.9	8.7	50.6	65	1.0
	2.9	37.2	8.6	53.7	2.6	36.4	8.4	52.6	43	0.5
	2.0	35.1	10.1	51.4	1.8	35.7	10.3	52.2	73	1.2
	0.8	36.6	10.7	50.3	0.7	37.2	10.9	51.2	-	70.1

Melt Al3

Rolling Temp °C	Fe ₂ O ₃	MnO	Al ₂ O ₃	SiO ₂	FeO'	MnO'	Al ₂ O ₃ '	SiO ₂ '	√ab	U
800	10.0	30.2	12.1	52.0	8.7	29.2	11.7	50.3	52	0.9
	5.4	27.6	14.9	56.2	4.7	26.7	14.4	54.3	5	0.2
	3.0	31.0	14.4	54.9	2.6	30.1	14.0	53.3	18	0.5
	2.3	32.1	15.5	53.7	2.0	31.1	15.0	51.9	12	0.7
	0.6	32.1	9.3	53.7	0.6	33.6	9.7	56.2	49	0.2
	3.1	30.8	16.1	53.6	2.7	29.8	15.6	51.9	12	0.5
	2.0	33.7	12.0	52.0	1.8	33.9	12.1	52.3	15	0.6
	5.4	30.4	14.9	56.2	4.6	26.6	14.0	52.8	6	0.1
	3.0	35.4	14.4	54.1	2.5	33.2	13.5	50.8	21	0.4
	2.3	35.0	15.6	53.8	1.9	32.9	14.7	50.5	48	0.1
	0.6	35.4	9.2	53.8	0.6	35.8	9.3	54.4	9	0.4
	3.1	34.3	16.1	53.6	2.6	32.1	15.1	50.2	10	0.6
	2.1	30.1	13.5	52.3	1.9	30.8	13.8	53.5	-	0.1
	2.7	39.2	12.2	44.8	2.5	39.7	12.4	45.4	-	0.1

Melt Al3 (cont.)

Rolling. Temp °C	Fe ₂ O ₃	MnO	Al ₂ O ₃	SiO ₂	FeO'	MnO'	Al ₂ O ₃ '	SiO ₂ '	\sqrt{ab}	ψ
800	2.2	38.0	13.6	46.7	2.0	37.9	13.6	46.6	-	0.1
	2.8	34.0	10.5	50.1	2.6	35.0	10.8	51.6	-	0.1
	2.1	47.1	4.6	45.0	1.9	47.8	4.7	45.6	-	0.0
	4.3	38.7	7.8	49.2	3.9	38.9	7.8	49.4	-	0.0
	2.9	44.2	5.7	43.8	2.7	45.9	5.9	45.5	-	0.0
	1.9	49.0	7.4	45.4	1.7	47.3	7.1	43.9	-	0.0
	2.3	32.7	9.7	45.6	2.3	36.3	10.8	50.6	-	0.0
850	2.4	38.2	17.7	42.6	2.1	38.0	17.6	42.4	16	0.4
	2.3	39.7	17.3	42.4	2.1	39.1	17.0	41.8	13	0.4
	2.0	37.9	17.9	43.3	1.8	37.6	17.7	42.9	18	0.2
	2.7	37.7	17.5	43.2	2.4	37.4	17.4	42.9	10	0.4
	2.6	37.6	18.5	42.9	2.3	37.1	18.3	42.3	11	0.2
	2.3	39.0	17.9	42.1	2.1	38.6	17.7	41.7	14	0.3
	2.6	38.7	18.8	41.8	2.3	38.1	18.5	41.1	16	0.6

Melt Al3 (cont.)

Rolling Temp °C	Fe ₂ O ₃	MnO	Al ₂ O ₃	SiO ₂	FeO'	MnO'	Al ₂ O ₃ '	SiO ₂ '	√ab	μ
850	3.1	39.5	18.9	43.7	2.7	37.7	18.0	41.6	8	0.3
	3.6	39.5	17.8	45.0	3.0	37.5	16.9	42.6	8	0.2
	2.7	39.7	18.6	44.1	2.3	37.9	17.8	42.0	11	0.7
	4.0	38.8	18.3	42.1	3.5	37.7	17.8	40.9	13	0.4
	3.0	39.6	18.7	44.2	2.5	37.7	17.8	42.0	12	0.4
900	2.7	47.0	5.0	44.9	2.5	47.3	5.0	45.2	30	0.0
	3.2	45.8	5.6	44.0	2.9	46.5	5.7	44.8	-	0.0
	1.9	48.1	6.3	45.1	1.7	47.5	6.2	44.6	-	0.0
	3.7	45.1	6.2	44.7	3.4	45.4	6.2	45.0	10	0.0
	2.2	48.7	3.9	43.3	2.0	49.8	4.0	44.2	80	0.0
	1.7	40.9	11.7	45.9	1.5	40.9	11.7	45.9	100	0.0
	2.5	52.5	2.0	44.9	2.2	51.7	2.0	44.2	60	0.0
	2.5	47.5	5.9	44.7	2.2	47.3	5.9	44.5	40	0.0
	2.7	47.6	5.0	44.0	2.5	48.0	5.0	44.5	20	0.0

Melt Al3 (cont.)

Rolling Temp °C	Fe ₂ O ₃	MnO	Al ₂ O ₃	SiO ₂	FeO'	MnO'	Al ₂ O ₃ '	SiO ₂ '	\sqrt{ab}	μ
900	2.6	48.3	4.2	44.8	2.4	48.5	4.2	45.0	30	0.0
	2.5	46.7	4.8	46.8	2.2	46.4	4.8	46.5	37	0.2
	2.2	46.4	6.5	47.0	1.9	45.5	6.4	46.1	17	0.1
	2.2	37.3	13.4	42.3	2.1	38.9	14.0	45.1	25	0.2
	2.4	45.3	8.1	41.5	2.2	46.7	8.4	42.8	14	0.5
	2.8	38.3	11.7	48.4	2.5	37.9	11.6	48.0	35	0.5
	2.4	46.1	8.4	44.8	2.1	45.4	8.3	44.2	21	0.3
	2.4	45.7	9.8	42.6	2.2	45.6	9.8	42.5	19	0.2
	2.3	25.1	14.4	56.3	2.1	25.7	14.7	57.5	13	0.8
	2.8	29.6	12.4	52.7	2.6	30.5	12.8	54.2	71	0.3
	2.5	29.8	13.5	53.2	2.3	30.2	13.7	53.9	14	0.9
	1.8	26.8	13.4	55.9	1.7	27.4	13.7	57.2	32	0.4
	2.2	28.9	13.5	52.9	2.0	29.7	13.9	54.4	13	0.8
	2.0	29.2	13.5	52.7	1.9	30.0	13.9	54.2	35	0.5

Melt Al3 (cont.)

Rolling Temp °C	Fe ₂ O ₃	MnO	Al ₂ O ₃	SiO ₂	FeO'	MnO'	Al ₂ O ₃ '	SiO ₂ '	\sqrt{ab}	μ
900	2.2	48.4	6.5	47.0	1.9	46.6	6.3	45.2	-	-
	2.5	46.7	4.8	46.9	2.2	46.4	4.8	46.6	-	-
	7.2	37.3	13.4	42.3	6.5	37.5	13.5	42.5	-	-
1000	1.6	24.3	14.1	55.8	1.5	25.4	14.7	58.3	14	1.1
	1.6	29.0	15.1	53.5	1.5	29.3	15.2	54.0	14	1.1
	0.7	29.8	11.9	56.7	0.6	30.1	12.0	57.3	10	0.8
	1.7	40.4	9.3	52.4	1.5	39.0	9.0	50.6	55	0.8
	1.8	33.4	14.6	50.7	1.6	33.3	14.5	50.6	12	0.7
	2.6	34.4	9.1	51.5	2.4	35.3	9.3	52.9	21	1.0
	0.5	41.4	10.2	48.2	0.4	41.3	10.2	48.1	26	1.0
	5.1	39.8	9.2	45.9	4.6	40.0	9.2	46.1	30	1.0
	3.1	33.4	13.1	50.4	2.8	33.5	13.1	50.6	19	1.1
	2.1	33.1	13.1	50.0	1.9	33.6	13.4	51.0	31	0.9
2.0	41.1	6.2	45.4	1.9	43.5	6.6	48.0	27	0.8	

Melt A13 (cont.)

Rolling Temp °C	Fe ₂ O ₃	MnO	Al ₂ O ₃	SiO ₂	FeO'	MnO'	Al ₂ O ₃ '	SiO ₂ '	\sqrt{ab}	ν
1000	5.6	38.4	9.6	48.0	5.0	38.0	9.5	47.5	34.0	0.6
	4.7	39.3	8.0	50.3	4.2	38.6	7.9	49.4	27	0.8
	1.9	30.4	7.9	59.2	1.7	30.6	8.0	59.7	-	0.0

Melt Al3X

Rolling Temp °C	Fe ₂ O ₃	MnO	Al ₂ O ₃	SiO ₂	FeO	MnO	Al ₂ O ₃	SiO ₂	\sqrt{ab}	ν
700	8.8	35.9	4.9	50.3	8.0	36.3	5.0	50.8	16	0.6
	6.8	36.4	3.5	49.7	6.4	38.0	3.6	52.0	28	0.8
	3.8	39.3	4.1	48.7	3.6	41.1	4.3	51.0	75	0.5
	9.8	32.8	2.0	51.6	9.2	34.5	2.1	54.3	40	0.6
800	10.0	40.4	3.5	49.0	8.9	39.7	3.4	48.1	19	1.0
	5.0	42.3	0.2	47.5	4.8	44.7	0.2	50.3	113	0.5
	3.6	41.2	2.5	48.8	3.4	43.1	2.6	51.0	54	0.4
	6.7	42.1	3.3	48.0	6.1	42.3	3.3	48.3	32	0.1
900	2.0	39.8	1.9	49.1	2.0	43.0	2.0	53.0	30	1.1
	2.9	42.9	3.0	47.1	2.8	44.9	3.1	49.3	46	1.1
	7.2	39.2	3.2	46.4	6.8	41.2	3.4	48.7	15	0.8

Melt Al3X (cont.)

Rolling Temp °C	Fe ₂ O ₃	MnO	Al ₂ O ₃	SiO ₂	FeO'	MnO'	Al ₂ O ₃ '	SiO ₂ '	\sqrt{ab}	γ
1000	13.1	37.6	3.5	47.4	11.8	37.5	3.5	47.2	53	1.2
	11.7	36.2	3.8	48.0	10.7	36.8	3.8	48.7	26	1.2
	6.8	42.5	2.4	48.3	6.1	42.8	2.4	48.7	23	1.4
1100	1.8	42.3	7.7	54.5	1.5	39.8	7.3	51.4	19	1.0
	10.1	39.2	2.3	46.1	9.4	40.6	2.4	47.7	16	1.1
	4.0	54.3	2.5	38.4	3.7	54.9	2.6	38.8	37	1.0

Melt Al4

Rolling Temp °C	Fe ₂ O ₃	MnO	Al ₂ O ₃	SiO ₂	FeO'	MnO'	Al ₂ O ₃ '	SiO ₂ '	\sqrt{ab}	ν
900	1.4	44.4	18.4	37.2	1.2	43.9	18.2	36.7	200	0.0
	1.5	51.2	10.7	38.8	1.3	50.2	10.5	38.0	200	0.0
	1.3	50.6	15.3	36.2	1.1	49.0	14.8	35.1	150	0.0
	1.8	50.4	13.0	36.1	1.6	49.8	12.9	35.7	80	0.0
	1.6	50.2	12.6	35.3	1.5	50.4	12.7	35.5	60	0.0
	3.6	47.8	12.7	35.8	3.2	47.5	13.6	35.6	10	0.0
	1.8	51.8	7.8	36.9	1.7	52.8	8.0	37.6	120	0.0
	1.3	48.8	11.4	37.2	1.2	49.5	11.6	37.7	30	0.0
	1.1	51.3	6.4	38.5	1.0	52.8	6.6	39.6	60	0.0
	1.3	49.2	13.1	37.2	1.2	48.9	13.0	36.9	20	0.0
	2.6	40.9	19.6	37.5	2.3	40.8	19.5	37.4	16	0.5
	2.8	39.7	19.1	37.2	2.6	40.3	19.4	37.8	28	0.3
	2.4	42.4	16.4	37.4	2.2	43.1	16.7	38.0	36	0.5
	2.4	39.9	21.2	35.3	2.2	40.5	21.5	35.8	67	0.3

Melt Al4 (cont.)

Rolling Temp °C	Fe ₂ O ₃	MnO	Al ₂ O ₃	SiO ₂	FeO	MnO	Al ₂ O ₃	SiO ₂	\sqrt{ab}	γ
900	4.7	34.1	19.6	39.7	4.3	34.9	20.1	40.7	55	0.1
	2.5	42.9	19.2	37.8	2.2	42.0	18.8	37.0	16	0.5
	2.4	41.0	19.4	37.3	2.2	41.1	19.4	37.4	28	0.3
	1.8	41.8	16.5	37.3	1.7	43.0	17.0	38.4	42	0.3
	2.0	40.2	20.9	34.8	1.8	41.2	21.4	35.6	38	0.3
	4.7	34.0	20.0	39.0	4.4	35.0	20.6	40.1	55	0.1
	3.1	40.0	19.0	37.6	2.8	40.2	19.1	37.8	-	0.1
	3.0	42.5	19.0	38.7	2.6	41.3	18.5	37.6	-	0.1
	2.1	41.2	18.4	37.8	1.9	41.5	18.5	38.1	-	0.1
	2.8	48.2	18.1	35.4	2.4	46.2	17.4	34.0	-	0.0
	1.7	49.7	10.4	36.8	1.6	50.5	10.6	37.4	-	0.0
	1.3	49.0	14.3	37.2	1.2	48.2	14.1	36.6	-	0.0
	1.3	52.0	6.3	39.0	1.2	52.8	6.4	39.6	-	0.0
	1.5	48.8	12.7	36.4	1.4	49.2	19.8	36.7	-	0.0

Melt Al4 (cont.)

Rolling Temp °C	Fe ₂ O ₃	MnO	Al ₂ O ₃	SiO ₂	FeO	MnO	Al ₂ O ₃	SiO ₂	\sqrt{ab}	γ
900	2.1	44.0	17.8	37.4	1.9	43.5	17.6	37.0	-	0.0
	1.4	50.6	10.2	39.3	1.2	49.9	10.1	38.8	-	0.0
	0.8	49.8	13.1	35.0	0.7	50.5	13.3	35.5	-	0.0
950	1.5	46.2	15.8	32.3	1.4	48.3	16.5	33.8	63	1.0
	1.5	48.1	20.4	33.5	1.3	46.5	19.7	32.4	-	0.0
	1.6	55.9	8.0	37.8	1.4	54.2	7.8	36.7	80	0.0
	2.1	51.9	5.9	38.4	1.9	52.9	6.0	39.2	55	1.5
	2.1	40.0	21.2	34.2	1.9	41.1	21.8	35.2	50	1.5
	0.8	37.9	4.7	36.3	0.9	47.6	5.9	45.6	44	0.0
1000	2.0	49.5	15.5	34.4	1.6	48.9	15.3	34.0	39	0.9
	2.2	57.7	1.9	26.8	2.2	65.3	2.2	30.3	71	1.0
	1.3	38.0	19.2	28.6	1.4	43.7	22.1	32.9	60	1.1
	2.4	50.7	15.8	32.5	2.1	50.1	15.6	32.1	24	0.9
	1.0	36.2	10.1	28.0	1.2	48.1	13.4	37.2	40	0.0

Melt 214 (2)

Rolling Temp °C	Fe ₂ O ₃	MnO	Al ₂ O ₃	SiO ₂	Fe'	Mn'	Al ₂ O ₃ '	SiO ₂ '	\sqrt{ab}	γ
1000	2.0	58.0	4.3	33.6	1.8	59.4	4.4	34.4	29	1.3
	1.3	56.6	5.8	35.0	1.2	57.5	5.9	35.5	36	1.2
	2.1	58.4	3.2	33.8	1.9	60.0	3.3	34.8	22	1.3
	2.9	51.8	8.0	30.5	2.8	55.8	8.6	32.9	49	1.3
	6.8	50.4	10.3	25.1	6.7	54.8	11.2	27.3	18	1.4

Melt Al₄C

Rolling Temp, °C	Fe ₂ O ₃	MnO	Al ₂ O ₃	SiO ₂	FeO'	MnO'	Al ₂ O ₃ '	SiO ₂ '	\sqrt{ab}	γ
700	2.3	49.1	15.1	37.9	2.0	47.1	14.5	36.4	74	1.2
	1.4	51.2	13.1	38.4	1.2	49.3	12.6	36.9	31	1.3
	1.7	49.3	15.4	37.8	1.5	47.4	14.8	36.4	86	1.3
	1.7	45.7	21.9	34.7	1.5	44.0	21.1	33.4	38	1.2
	1.7	48.9	15.5	37.8	1.5	47.1	14.9	36.4	44	1.2
	2.1	49.3	13.6	38.5	1.8	47.7	13.2	37.3	15	0.7
800	2.9	52.7	7.4	41.0	2.5	50.8	7.1	39.5	32	0.2
	13.1	48.3	5.1	39.1	11.3	43.3	4.9	37.5	16	1.0
	1.6	51.6	8.8	41.5	1.4	49.9	8.5	40.2	93	0.0
	1.9	49.0	14.8	38.2	1.7	47.2	14.3	36.8	62	0.1

Melt 140 (cont.)

Rolling Temp °C	Fe ₂ O ₃	MnO	Al ₂ O ₃	SiO ₂	FeO'	MnO'	Al ₂ O ₃ '	SiO ₂ '	\sqrt{ab}	ν
900	1.3	50.8	10.4	41.2	1.1	49.1	10.0	39.8	37	0.0
	2.5	52.1	8.7	16.6	2.8	65.4	10.9	20.8	25	0.0
	2.4	52.1	8.7	16.6	2.7	65.5	10.9	20.9	25	0.0
1000	1.7	50.8	10.6	41.1	1.5	48.8	10.2	39.5	41	1.3
	1.6	50.7	10.6	41.5	1.4	48.6	10.2	39.8	29	1.2
	2.3	51.2	8.4	41.9	2.0	49.4	8.1	40.5	12	0.4
	3.1	53.2	6.3	41.2	2.7	51.4	6.1	39.8	16	0.9
	17.2	48.1	4.7	37.6	14.6	45.4	4.4	35.5	18	1.3
	3.0	52.5	6.5	41.8	2.6	50.7	6.3	40.4	61	1.5
	2.3	52.1	8.2	41.0	2.0	50.4	7.9	39.7	108	1.4
	2.4	50.7	8.7	41.4	2.1	49.2	8.5	40.2	63	1.4

Melt Al5

Rolling Temp °C	Fe ₂ O ₃	MnO	Al ₂ O ₃	SiO ₂	FeO	MnO	Al ₂ O ₃	SiO ₂	\sqrt{ab}	γ
900	0.6	49.0	10.3	39.9	0.5	49.1	10.3	40.0	38	0.0
	1.2	49.9	13.3	39.1	1.0	48.3	12.9	37.8	73	1.2
	1.4	49.9	12.3	37.0	1.3	49.7	12.2	36.8	60	0.0
	1.2	45.1	18.2	40.6	1.0	43.0	17.3	38.7	65.0	1.2
	1.1	42.1	18.2	42.8	1.0	40.4	17.5	41.1	42	0.9
	2.9	53.6	7.4	39.7	2.5	51.9	7.2	38.4	10	0.0
	1.9	49.8	15.2	37.4	1.6	47.8	14.6	35.9	45	1.3
	1.9	49.8	12.3	37.3	1.7	49.3	12.2	36.9	-	0.0
	1.8	53.8	5.2	41.5	1.6	52.7	5.1	40.6	16	0.0
	1.3	53.8	7.4	39.7	1.1	52.7	7.2	38.9	21+	0.0
	0.7	50.0	15.2	36.3	0.6	49.0	14.9	35.6	- +	-
	0.3	51.7	12.3	37.3	0.2	50.7	12.2	36.9	- +	-
	0.5	55.2	5.2	41.5	0.4	53.9	5.1	40.5	- +	-
	0.5	45.1	17.5	36.3	0.5	45.4	17.6	36.6	- +	-

+ Brittle Inclusions

Melt 15 (cont.)

Rolling Temp °C	Fe ₂ O ₃	MnO	Al ₂ O ₃	SiO ₂	FeO'	MnO'	Al ₂ O ₃ '	SiO ₂ '	√ab	λ
900	1.0	49.6	13.6	39.6	0.9	47.8	13.1	38.2	- +	-
	0.5	41.2	24.0	35.8	0.5	40.6	23.7	35.3	- +	-
1100	1.2	45.0	21.3	36.9	1.0	43.2	20.4	35.4	47	1.3
	1.9	49.9	15.2	37.2	1.6	48.0	14.6	35.8	30	1.5
	2.1	45.0	22.3	36.7	1.8	42.5	21.1	34.7	39	1.2
	1.9	49.8	14.3	38.1	1.7	47.9	13.8	36.7	46	1.4
	1.8	47.0	17.3	38.4	1.6	45.1	16.6	36.8	44	1.1
	1.3	49.0	15.2	37.4	1.1	47.7	14.8	36.4	79	1.6
	1.0	48.1	14.8	39.2	0.9	46.7	14.4	38.1	49	1.0
	1.9	49.8	14.3	37.4	1.7	48.3	13.9	36.2	45	1.0
	2.0	47.1	15.4	37.6	1.8	46.2	15.1	36.9	36	1.0
	1.8	48.4	13.3	39.1	1.6	47.3	13.0	38.2	17	0.8

+ Brittle Inclusions

Melt A15 (cont.)

Rolling Temp °C	Fe ₂ O ₃	MnO	Al ₂ O ₃	SiO ₂	FeO'	MnO'	Al ₂ O ₃ '	SiO ₂ '	\sqrt{ab}	γ
1300	2.2	41.1	24.1	35.9	1.9	39.9	23.4	34.8	48	1.1
	1.9	45.1	15.2	36.1	1.7	45.1	15.2	38.1	25	1.1
	1.9	45.2	15.2	38.1	1.7	45.1	15.2	38.0	46	1.0
	5.3	43.9	15.1	36.4	4.8	43.8	15.1	36.3	15	1.0
	2.0	46.1	16.4	37.8	1.8	45.2	16.1	37.0	57	1.2
	1.7	44.2	17.3	37.1	1.5	44.1	17.3	37.1	24	1.0
	3.4	46.9	13.3	37.1	3.0	46.7	13.3	37.0	18	1.3
	1.7	46.4	15.1	36.8	1.5	46.5	15.1	36.9	41	1.5

Melt Al6

Rolling Temp °C	Fe ₂ O ₃	MnO	Al ₂ O ₃	SiO ₂	FeO'	MnO'	Al ₂ O ₃ '	SiO ₂ '	√ ab	✓
800	1.5	32.5	13.3	55.5	1.3	31.7	13.0	54.0	69	0.2
	4.0	32.2	10.5	54.5	3.6	31.9	10.4	54.1	17	0.3
	3.1	32.1	10.0	54.2	2.8	32.4	10.1	54.7	17	0.5
	1.4	32.7	13.2	52.2	1.3	32.9	13.3	52.5	37	0.2
	2.5	34.2	10.5	53.6	2.3	34.0	10.4	53.3	15	0.5
	2.6	33.7	10.0	54.3	2.3	33.6	10.0	54.1	15	0.6
	6.0	29.7	7.5	49.5	5.8	32.3	8.2	53.8	16	0.4
	2.2	37.0	8.6	51.1	2.0	37.5	8.7	51.8	13	0.5
	3.3	33.2	8.2	51.1	3.1	34.8	8.6	53.5	15	0.6
	1.5	33.5	9.7	52.6	1.4	34.5	10.0	54.1	42	0.2
	1.7	33.1	12.1	52.6	1.5	33.3	12.2	52.9	37	0.3
	2.1	33.7	11.5	52.2	1.9	34.0	11.6	52.5	31	0.2
	2.5	32.1	9.7	54.4	2.3	32.6	9.8	55.3	18	0.3
	2.1	32.5	11.3	54.4	1.9	32.5	11.3	54.3	30	0.3

Melt Al6 (Cont.)

Rolling Temp °C	Fe ₂ O ₃	MnO	Al ₂ O ₃	SiO ₂	FeO'	MnO'	Al ₂ O ₃ '	SiO ₂ '	\sqrt{ab}	ρ
800	1.9	33.6	11.6	53.5	1.7	33.5	11.5	53.3	38	0.3
	2.2	32.8	11.5	54.5	1.9	32.6	11.4	54.1	35	0.3
	2.5	30.9	10.1	55.8	2.3	31.2	10.2	56.3	20	0.3
	1.6	33.2	12.9	52.0	1.4	33.4	13.0	52.2	35	0.1
850	2.3	32.8	17.4	46.3	2.1	32.6	17.3	48.0	63	1.3
	2.4	32.1	17.8	46.6	2.2	32.5	18.0	47.2	32	1.1
	1.3	32.9	17.4	47.6	1.2	33.2	17.6	48.0	55	1.2
	1.6	33.1	15.8	46.6	1.5	34.1	16.3	48.1	80	1.2
900	50.8	21.9	12.1	35.2	39.8	19.1	10.5	30.6	11	1.0
	3.3	32.7	15.1	49.7	3.0	32.6	15.0	49.5	17	1.1
	1.6	33.5	16.8	48.5	1.4	33.4	16.8	48.4	22	1.0

Melt Al6 (cont.)

Rolling Temp °C	Fe ₂ O ₃	MnO	Al ₂ O ₃	SiO ₂	FeO'	MnO'	Al ₂ O ₃ '	SiO ₂ '	\sqrt{ab}	ν
1100	2.0	32.3	16.7	49.7	1.8	32.1	16.6	49.5	60	1.0
	2.3	33.6	20.3	51.2	1.9	31.4	16.9	47.8	32	1.2
	2.2	33.2	15.6	51.2	1.9	32.6	15.3	50.2	33	1.1
	1.7	33.1	16.4	48.3	1.5	33.3	16.5	48.6	81	1.1
1300	29.5	29.8	33.1	27.1	22.8	25.6	28.4	23.3	40	1.2
	2.1	33.1	16.8	49.1	1.9	32.8	16.6	48.7	60	1.0
	2.5	32.5	16.5	48.8	2.3	32.5	16.5	48.8	46	1.0
	5.2	32.5	14.5	50.0	4.6	32.0	14.3	49.2	24	1.0
	2.1	32.7	17.0	49.4	1.9	32.4	16.8	48.9	33	1.1
	3.0	31.0	16.0	48.0	2.8	31.7	16.4	49.1	47	1.3
	2.0	36.0	16.0	50.0	1.7	34.7	15.4	48.2	18	1.0
	2.0	35.0	19.0	46.0	1.8	34.4	18.7	45.2	27	1.1

Melt A17

Rolling Temp °C	Fe ₂ O ₃	MnO	Al ₂ O ₃	SiO ₂	FeO'	MnO'	Al ₂ O ₃ '	SiO ₂ '	\sqrt{ab}	γ
800	3.4	40.1	24.5	32.2	3.1	40.1	24.5	32.3	59	1.3
	2.0	40.1	24.6	35.3	1.8	39.4	24.2	34.6	70	1.1
	2.4	40.9	23.6	35.6	2.1	40.0	23.1	34.8	30	1.2
	2.3	39.8	17.4	28.8	2.5	45.1	19.8	32.6	47	1.0
850	2.0	40.4	24.3	35.5	1.7	39.6	23.9	34.8	38	1.0
	2.0	40.2	24.6	35.4	1.8	39.4	24.1	34.7	51	0.8
	6.7	39.4	22.4	35.1	5.8	38.3	21.8	34.1	25	1.3
	92.0	15.5	8.7	14.2	68.3	12.8	7.2	11.7	12	1.2
	3.5	39.6	24.6	32.0	3.2	39.9	24.8	32.2	38	1.2
	27.0	34.0	20.5	29.4	22.5	31.4	19.0	27.2	27	1.1
	1.7	40.1	24.2	35.1	1.5	39.7	24.0	34.8	49	1.1

Melt A17 (cont.)

Rolling Temp °C	Fe ₂ O ₃	MnO	Al ₂ O ₃	SiO ₂	FeO'	MnO'	Al ₂ O ₃ '	SiO ₂ '	\sqrt{ab}	γ
900	5.5	38.5	23.0	35.0	4.9	37.9	22.7	34.5	32	1.1
	3.1	39.0	24.8	35.4	2.7	38.2	24.3	34.7	38	1.3
	2.9	39.9	8.7	31.5	3.1	48.3	10.5	38.1	35	1.1
	3.0	40.6	22.5	33.7	2.7	40.8	22.6	33.9	22	0.9
	4.3	41.5	6.0	26.4	5.0	53.4	7.7	34.0	17	1.1
	3.7	39.5	24.4	35.6	3.2	38.4	23.7	34.6	32	1.1
	2.7	41.3	23.0	31.6	2.5	41.9	23.3	32.2	21	0.9
	3.1	39.2	26.5	34.3	2.6	38.1	25.5	33.3	57	1.1
	2.8	39.1	25.9	33.2	2.5	38.8	25.7	32.9	54	1.0
	1.9	39.8	24.9	35.5	1.7	39.0	24.4	34.9	59	0.9
1000	5.6	39.5	42.5	19.7	4.7	37.0	39.8	18.5	62	1.1
	2.8	38.6	42.1	22.9	2.3	36.4	39.7	21.6	40	1.2
	2.5	42.0	19.5	33.0	2.3	43.5	20.1	34.1	53	1.1
	3.1	39.1	33.8	18.0	3.0	41.7	36.1	19.2	42	1.1

Melt Al8

Rolling Temp °C	Fe ₂ O ₃	MnO	Al ₂ O ₃	SiO ₂	FeO'	MnO'	Al ₂ O ₃ '	SiO ₂ '	\sqrt{ab}	γ
850	2.0	36.3	36.5	29.3	1.7	35.0	35.1	28.2	35	0.0
	2.2	36.8	36.4	28.0	1.9	35.4	34.9	27.8	54	0.0
	5.7	41.2	26.9	30.1	5.0	39.9	26.0	29.1	152	1.4
	3.6	38.1	32.0	28.0	3.2	37.6	31.6	27.6	27	0.1
	2.3	37.6	34.0	29.2	2.1	36.5	33.1	28.4	28	0.1
	2.8	38.5	40.9	24.1	2.4	36.3	38.6	22.7	26	0.1
	2.7	17.8	39.0	45.9	2.3	16.9	37.1	43.6	24	0.0
	2.8	38.5	33.9	29.3	2.4	37.0	32.5	28.1	87	1.1
	2.6	42.8	29.1	30.1	2.2	41.0	27.9	28.9	63	0.2
	3.4	43.9	25.9	33.0	2.9	41.4	24.5	31.2	17	0.0
	3.7	41.7	31.5	29.1	3.1	39.5	29.8	27.6	30	0.2
	1.5	34.9	50.9	19.7	1.3	32.7	47.7	18.4	72	0.6
	2.7	41.7	32.7	28.9	2.3	39.5	30.9	27.3	63	0.2
1000	2.3	34.2	45.2	23.4	2.0	32.6	43.1	22.3	38	1.3
	2.8	31.3	45.8	22.2	2.5	30.7	45.0	21.8	72	1.1

Melt CRA12

Rolling Temp °C	Fe ₂ O ₃	MnO	Al ₂ O ₃	SiO ₂	Cr ₂ O ₃	FeO	MnO'	Al ₂ O ₃ '	SiO ₂ '	Cr ₂ O ₃ '	\sqrt{ab}	γ
800	0.8	32.6	14.6	50.3	0.5	0.7	33.1	14.8	51.0	0.5	34	0.6
	0.5	32.6	14.9	50.4	0.5	0.4	33.0	15.1	51.0	0.5	37	0.3
	1.3	32.0	15.5	50.0	1.4	1.2	32.0	15.5	50.0	1.4	21	0.6
	1.4	32.0	14.1	51.0	1.0	1.3	32.2	14.2	51.3	1.0	12	0.8
	0.7	31.8	16.9	49.2	0.5	0.6	32.1	17.0	49.7	0.6	62	0.4
	0.5	32.2	14.6	50.6	0.6	0.5	32.7	14.9	51.3	0.6	124	0.2
	0.3	32.1	16.2	49.6	1.4	0.3	32.3	16.2	49.8	1.4	70	0.2
	1.3	32.8	13.7	50.6	0.9	1.2	33.1	13.9	51.0	0.9	116	0.1
	1.1	32.0	13.9	50.2	0.7	1.0	32.7	14.2	51.3	0.7	17	0.5
	0.9	31.4	14.3	50.3	0.5	0.8	32.3	14.7	51.7	0.6	53	0.2
	0.9	34.1	14.2	51.0	0.8	0.8	33.8	14.1	50.6	0.8	29	0.3
	0.5	32.1	14.5	53.1	1.3	0.4	31.6	14.3	52.3	1.3	26	0.5
	0.3	32.0	18.1	50.4	1.5	0.3	31.3	17.7	49.3	1.4	89	0.1
	0.7	32.4	15.2	52.5	1.0	0.6	31.8	15.0	51.6	1.0	20	0.3

Melt CRA12 (cont.)

Rolling Temp °C	Fe ₂ O ₃	MnO	Al ₂ O ₃	SiO ₂	Cr ₂ O ₃	FeO	MnO	Al ₂ O ₃	SiO ₂	Cr ₂ O ₃	\sqrt{ab}	γ
800	0.4	32.2	13.1	55.7	0.6	0.3	32.3	12.8	54.1	0.6	12	0.4
	0.6	32.3	18.7	50.6	1.7	0.5	31.1	18.0	48.8	1.6	45	1.4
850	1.5	32.6	21.4	49.9	1.2	1.2	30.6	20.1	46.9	1.2	53	0.6
	1.2	33.2	17.3	52.9	0.9	1.0	31.5	16.4	50.2	0.9	34	0.7
	0.9	34.0	16.1	52.5	0.2	0.8	32.8	15.5	50.7	0.2	20	0.8
	0.7	32.6	16.3	51.5	1.5	0.6	31.8	15.9	50.2	1.4	36	1.1
	1.0	31.1	18.2	48.9	0.0	0.9	31.4	18.4	49.3	0.0	87	0.9
1000	1.4	32.5	17.1	53.6	0.5	1.1	31.0	16.3	51.0	0.5	78	1.2
	1.1	32.6	14.0	55.4	0.5	0.9	31.5	13.6	53.5	0.5	28	1.4
	0.7	26.6	14.4	54.2	0.2	0.6	27.7	15.0	56.5	0.1	16	1.0
	0.7	26.4	5.6	36.4	1.1	0.9	37.6	8.0	51.9	1.6	8	0.6

Melt VA12

Rolling Temp °C	Fe ₂ O ₃	MnO	Al ₂ O ₃	SiO ₂	V ₂ O ₅	FeO	MnO	Al ₂ O ₃	SiO ₂	V ₂ O ₅	\sqrt{ab}	γ
800	1.4	28.7	33.3	34.0	0.7	1.3	29.3	34.0	34.8	0.7	72	0.1
	0.8	32.2	17.9	49.2	0.5	0.8	32.0	17.8	49.0	0.5	12	0.4
	0.7	30.2	26.9	41.0	0.7	0.7	30.4	27.0	41.2	0.7	37	0.1
	0.8	31.6	25.5	42.8	1.0	0.7	31.1	25.1	42.1	1.0	96	0.0
	0.5	31.0	27.3	41.3	1.0	0.4	30.7	27.0	40.9	1.0	85	0.0
	0.5	32.8	14.5	50.8	0.3	0.5	33.2	14.7	51.4	0.3	10	0.6
	0.5	32.5	17.7	48.5	0.2	0.5	32.7	17.8	48.8	0.2	9	0.2
	0.7	27.3	9.1	44.8	1.3	0.8	32.8	10.9	53.9	1.6	7	0.3
850	0.7	31.5	16.7	49.8	0.7	0.7	31.7	16.8	50.2	0.7	34	1.5
	1.5	32.3	16.1	50.0	0.4	1.3	32.3	16.2	49.9	0.4	42	0.6
	0.5	32.4	16.0	50.0	0.5	0.5	32.6	16.1	50.3	0.5	49	0.5
	0.7	32.6	16.6	50.1	0.5	0.6	32.5	16.5	49.9	0.5	38	0.5
	0.5	31.8	16.6	50.0	0.4	0.5	32.1	16.7	50.3	0.4	39	0.7

Melt VA12 (cont.)

Rolling Temp °C	Fe ₂ O ₃	MnO	Al ₂ O ₃	SiO ₂	V ₂ O ₅	FeO'	MnO'	Al ₂ O ₃ '	SiO ₂ '	V ₂ O ₅ '	\sqrt{ab}	λ
850	0.4	31.8	15.2	51.3	0.1	0.3	32.2	15.4	52.0	0.1	19	1.0
	0.4	29.6	14.1	53.1	0.3	0.4	30.4	14.5	54.4	0.3	18	1.1
	0.6	31.8	15.2	51.0	0.2	0.5	32.2	15.4	51.7	0.2	21	1.1
	0.5	26.6	13.1	57.2	0.5	0.4	27.2	13.4	58.5	0.5	6	0.2
	0.5	32.3	16.9	49.1	0.9	0.4	32.4	17.0	49.3	0.9	41	1.1
1000	0.4	20.4	39.4	37.2	1.1	0.4	20.7	40.0	37.8	1.1	75	1.2
	0.5	28.0	16.7	40.1	0.8	0.6	32.5	19.4	46.6	0.9	17	1.1
	0.4	29.4	18.4	43.1	0.6	0.4	32.0	20.0	46.9	0.7		
	0.5	30.5	22.4	44.7	0.7	0.5	30.9	22.7	45.2	0.8	35	1.1
	0.5	30.4	22.5	45.9	0.3	0.4	30.6	22.7	46.1	0.2		
	0.7	27.8	34.2	38.9	1.5	0.6	27.0	33.2	37.8	1.4	19	1.0
	0.7	30.2	43.0	5.1	25.1	0.6	29.0	41.4	4.9	24.2	100	1.5
	0.5	30.0	24.5	38.0	1.8	0.4	31.7	25.9	40.1	1.9		

Melt VA12 (cont.)

Rolling Temp °C	Fe ₂ O ₃	MnO	Al ₂ O ₃	SiO ₂	V ₂ O ₅	FeO	MnO	Al ₂ O ₃	SiO ₂	V ₂ O ₅	\sqrt{ab}	γ
1100	0.4	35.2	16.1	52.5	0.3	0.4	33.7	15.4	50.3	0.3	45	1.3
	0.5	32.2	16.3	51.4	1.7	0.4	31.6	16.0	50.4	1.7	47	1.1
	0.7	33.7	18.3	48.9	0.3	0.6	33.1	18.0	48.1	0.3	23	1.0

Melt N1A12

Rolling Temp °C	Fe ₂ O ₃	MnO	Al ₂ O ₃	SiO ₂	FeO	MnO	Al ₂ O ₃	SiO ₂	\sqrt{ab}	γ
900	2.6	32.1	16.2	47.1	2.4	32.9	16.5	48.2	30	1.2
	1.9	30.0	26.0	41.5	1.7	30.2	26.2	41.9	22	1.2
	2.9	30.7	13.3	53.1	2.6	30.8	13.4	53.2	23	1.3
	2.1	31.7	16.6	47.7	2.0	32.4	16.9	48.7	30	1.1
1000	1.9	31.6	21.0	45.3	1.7	31.7	21.0	45.5	25	1.3
	1.9	29.4	20.3	46.5	1.7	30.1	20.7	47.5	42	1.3
	3.6	30.1	22.2	46.2	3.2	29.5	21.6	45.5	19	1.1

Melt NI50Al2

Rolling Temp °C	Fe ₂ O ₃	MnO	Al ₂ O ₃	SiO ₂	FeO'	MnO'	Al ₂ O ₃ '	SiO ₂ '	\sqrt{ab}	β
800	1.2	22.0	13.6	61.5	1.1	22.4	13.9	62.6	47	0.1
	1.3	22.0	14.4	61.4	1.2	22.2	14.6	62.0	60	0.0
	3.4	24.2	16.9	56.9	3.0	24.0	16.7	53.3	120	0.0
	5.3	20.9	13.9	63.6	4.6	20.2	13.5	61.7	22	0.1
900	2.0	21.1	13.8	62.9	1.8	21.1	13.9	63.2	25	0.1
	1.9	23.2	13.9	60.8	1.7	23.3	13.9	61.0	63	0.0
	3.4	32.1	31.8	34.9	3.0	31.5	31.2	34.3	86	0.8
	1.9	24.8	17.4	54.0	1.8	25.3	17.7	55.2	32	0.8
1000	2.9	23.9	15.6	56.6	2.7	24.2	15.8	57.3	39	1.2
	3.4	21.3	13.8	60.6	3.1	21.5	14.0	61.4	22	1.3
	1.5	23.0	13.9	59.3	1.4	23.6	14.2	60.8	17	0.9
	2.4	23.6	16.3	55.6	2.2	24.2	16.8	56.8	43	1.4

Melt NI50A12 (cont.)

Rolling Temp °C	Fe ₂ O ₃	MnO	Al ₂ O ₃	SiO ₂	FeO'	MnO'	Al ₂ O ₃ '	SiO ₂ '	\sqrt{ab}	δ
1100	5.5	20.7	13.0	61.4	4.9	20.7	13.0	61.4	33	1.3
	1.8	20.9	13.1	65.5	1.6	20.7	13.0	64.7	55	1.2
	3.5	21.4	14.8	69.3	2.9	19.7	13.6	63.8	28	1.4

Appendix 4.3Analysis of precipitates within inclusions.Symbols.

XO, & XO' refer to compositional data as in
appendices 4.1 & 4.2

Accuracy of results.

XO' no better than $\pm 10\%$

FeO' " " " $\pm 100\%$

Analysis of precipitates within inclusions

Melt	Fe ₂ O ₃	MnO	Al ₂ O ₃	SiO ₂	FeO	MnO	Al ₂ O ₃	SiO ₂
Al2 heat treated at 1100°C for 2 hours	0.4	18.6	3.6	90.5	0.3	16.5	3.2	80.5
	2.0	41.2	4.1	50.9	1.8	42.0	4.2	51.9
Al3 heat treated at 1100°C for 2 hours	1.0	32.1	11.0	55.1	0.9	32.4	11.0	55.6
	1.0	2.6	4.0	93.1	0.9	2.6	4.0	92.5
	2.3	39.2	13.9	48.0	2.0	38.0	13.5	46.5
	2.0	36.8	4.0	45.1	2.1	42.0	4.6	51.4
Al4 heat treated at 1100°C for 2 hours	2.3	15.5	22.1	59.7	2.1	15.6	22.2	60.1
	2.0	46.1	3.4	46.6	1.8	47.1	3.5	47.6
	1.9	21.4	15.7	61.2	1.7	21.4	15.7	61.2
	2.7	36.6	8.3	49.6	2.5	37.8	8.6	51.2
	1.3	23.6	16.9	58.1	1.2	23.7	16.9	58.2
	1.3	49.3	2.4	45.3				

Analysis of precipitates within inclusions (cont.)

Melt	Fe ₂ O ₃	MnO	Al ₂ O ₃	SiO ₂	FeO	MnO	Al ₂ O ₃	SiO ₂
Al4 heat treated at 1100°C for 2 hours	1.7	22.3	16.5	59.8	1.5	22.3	16.5	59.7
	1.4	38.5	2.1	40.2	1.5	46.9	2.6	49.0
	0.9	18.9	15.9	63.2	0.8	19.1	16.1	63.7
	2.1	38.4	6.8	44.5	2.1	41.9	7.4	48.6
	0.9	23.1	17.1	58.6	0.8	23.2	17.2	58.8
	0.5	49.0	1.9	46.5	0.5	50.1	1.9	47.5
Al7 as cast	1.2	2.1	98.4	1.3	1.0	2.0	95.7	1.3
Al8 as cast Al rich	0.6	1.2	99.7	0.7	0.5	1.2	97.6	0.7
	0.6	14.6	68.5	10.6	0.6	15.5	72.7	11.2
	-	-	100.0	-	-	-	100.0	-
	1.3	14.8	79.8	11.2	1.1	13.8	74.6	10.5
	1.5	9.9	84.2	7.6	1.3	9.6	81.7	7.4

Analysis of precipitates within inclusions (cont.)

Melt	Fe_2O_3	MnO	Al_2O_3	SiO_2	FeO'	MnO'	Al_2O_3'	SiO_2'		
A18	40.8	23.0	35.5	16.0	33.0	20.7	31.9	14.4		
as cast										
Fe rich	48.0	26.6	23.0	20.1	38.3	23.6	20.3	17.8		
	Fe_2O_3	MnO	Al_2O_3	SiO_2	V_2O_5	FeO'	MnO'	Al_2O_3'	SiO_2'	V_2O_5'
VA12 rolled at 1000°C.	0.7	30.2	43.0	5.1	38.0	0.6	25.8	36.7	4.3	32.4

Appendix 5.1

Values of plasticity index based upon the variation of inclusion and matrix apparent flow stresses with temperature.

$^{\circ}\text{C}$	η [*] Poise	σ_i [☆] Nm^{-2}	σ_{Fe} [*] N m^{-2}	$\frac{\sigma_i}{\sigma_{\text{Fe}}}$	ν [☆]
600	10^{14}	2×10^{15}	2.5×10^8	8×10^6	0
650	10^{11}	2×10^{12}	2.0×10^8	1×10^4	0
700	10^8	2×10^9	1.7×10^8	1.1×10^1	0
750	10^6	2×10^7	1.4×10^8	1.4×10^{-1}	1.860
800	10^4	2×10^5	1.2×10^8	1.6×10^{-3}	1.998
850	$10^{2.5}$	$2 \times 10^{3.5}$	1.5×10^8	$1.3 \times 10^{-4.5}$	
900	$10^{1.5}$	$2 \times 10^{2.5}$	1.9×10^8	$1 \times 10^{-5.5}$	1.999
950			1.7×10^8		
1000	10^1	2×10^2	1.5×10^8		

★ From figure 5.55(b).

☆ Assumes $\sigma_i = \eta \dot{\epsilon}$ (at $\dot{\epsilon} = 20\text{s}^{-1}$)

* From figure 5.55

☆ Assumes $\nu = 2 - \left(\frac{\sigma_i}{\sigma_m}\right)$

Appendix 5.2

The dependence of inclusion plasticity index upon inclusion size on the basis of a surface energy criterion.

Assume that the work done in deforming the inclusion and overcoming the surface energy effect is equal to the work done by the matrix.

$$\text{i.e. } \sigma_m \epsilon_m = \sigma_i \epsilon_i + \frac{6\gamma}{D} (\cosh \epsilon_i - 1)$$

where γ is the surface energy (e.g. 1.5 Jm^{-2}) and D is the inclusion diameter

$$\therefore \sigma_m \epsilon_m = \sigma_i \epsilon_i + \frac{9}{D} (\cosh \epsilon_i - 1)$$

solving for ϵ_i using 'Newton's method'.

$$\begin{aligned} \epsilon_i &= \epsilon_i^* - \left[\frac{f(\epsilon_i^*)}{f'(\epsilon_i^*)} \right] \\ &= \epsilon_i - \left[\frac{\sigma_i \epsilon_i^* + \frac{9}{D} (\cosh \epsilon_i^* - 1) - \sigma_m \epsilon_m}{\sigma_i + \frac{9}{D} (\sinh \epsilon_i^*)} \right] \end{aligned}$$

let β = ratio of inclusion to matrix flow stress

$$\text{i.e. } = \sigma_i / \sigma_m$$

$$\therefore \epsilon_i = \epsilon_i^* - \left[\frac{\sigma_m (\beta \epsilon_i^* - \epsilon_m) + \frac{9}{D} (\cosh \epsilon_i^* - 1)}{\beta \sigma_m + \frac{9}{D} (\sinh \epsilon_i^*)} \right]$$

letting $\sigma_m = 100 \text{ MNm}^{-2}$

$\beta = 1$ (\dots no matrix constraint term)

Values of ϵ_i and ϵ_i/ϵ_m (i.e. ν) for various values of D (μm) and ϵ_m were calculated i.e.

	$\epsilon_m = 1$		$\epsilon_m = 2$		$\epsilon_m = 4$		$\epsilon_m = 8$	
D (μm)	ϵ_i	ν	ϵ_i	ν	ϵ_i	ν	ϵ_i	ν
0.001	0.138	0.14	0.199	0.10	0.286	0.07	0.408	0.05
0.01	0.371	0.37	0.558	0.28	0.818	0.20	1.165	0.15
0.1	0.741	0.74	1.229	0.61	1.880	0.47	2.629	0.32
1.0	0.956	0.96	1.808	0.90	3.095	0.77	4.405	0.55
10.0	0.995	0.99	1.976	0.99	3.806	0.95	6.067	0.76
100.0	0.999	1.00	1.997	1.00	3.976	0.99	7.321	0.915

Variation of ϵ_i with ϵ_m on the basis of strain rate:

$$\alpha' = \alpha'_0 \dot{\epsilon}^{0.9}$$

Appendix 5.

$$\epsilon_{i(n)} = (2 - \alpha') \Delta \epsilon_m + \epsilon_{i(n-1)}$$

$$\Delta \epsilon_m = 0.2231.$$

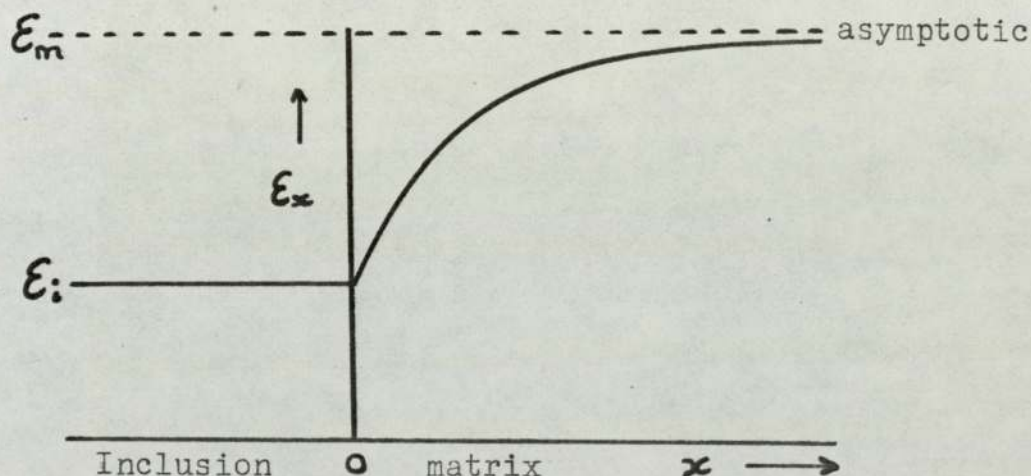
Roll pass No. (n)	Total matrix strain ϵ_m	Mean strain rate s^{-1}	$\alpha'_0 = 0.05$		$\alpha'_0 = 0.10$		$\alpha'_0 = 0.20$		$\alpha'_0 = 0.30$		$\alpha'_0 = 0.40$		$\alpha'_0 = 0.50$	
			α'	ϵ_i	α'	ϵ_i	α'	ϵ_i	α'	ϵ_i	α'	ϵ_i	α'	ϵ_i
1	0.223	4.18	0.18	0.406	0.36	0.365	0.72	0.285	1.09	0.204	1.45	0.123	1.81	0.042
2	0.446	4.65	0.20	0.808	0.40	0.722	0.80	0.553	1.20	0.383	1.60	0.213	1.99	0.044
3	0.669	5.20	0.22	1.205	0.44	1.070	0.88	0.802	1.32	0.534	1.76	0.266	2.00+	"
4	0.893	5.86	0.25	1.596	0.49	1.407	0.98	1.029	1.47	0.652	1.96	0.274	-	"
5	1.116	6.51	0.27	1.982	0.54	1.733	1.08	1.234	1.62	0.737	2.00+	"	-	"
6	1.339	7.25	0.30	2.362	0.60	2.047	1.19	1.415	1.78	0.784	"	"	-	"
7	1.563	8.09	0.33	2.735	0.66	2.347	1.31	1.568	1.97	0.791	"	"	-	"
8	1.785	9.11	0.37	3.100	0.73	2.630	1.46	1.688	2.00+	"	"	"	-	"
9	2.008	10.23	0.41	3.456	0.81	2.895	1.62	1.772	"	"	"	"	-	"
10	2.231	11.25	0.44	3.804	0.88	3.144	1.77	1.824	"	"	"	"	-	"

Appendix 5.4

Constraint at an inclusion - matrix interface.

Consider the case of an inclusion such that it is less deformable than the matrix in which it is embedded. A condition will exist such that there is constraint associated with the strain disparity.

viz.



where: ϵ_m = matrix strain at infinity

ϵ_i = inclusion strain

x = distance from the inclusion/matrix interface

An idealised approximation to the matrix strain at a distance (x) from the interface may be expressed mathematically as:

$$\epsilon_x = \epsilon_m - \left(\frac{\epsilon_m - \epsilon_i}{1 + x^2} \right)$$

Constraint energy per unit volume of matrix may be expressed as:

$$\frac{E_c}{V} = \int_0^{\infty} \sigma_m (\epsilon_m - \epsilon_x) dx$$

or:

$$\begin{aligned} \frac{E_c}{V} &= \int_0^{\infty} \sigma_m (\epsilon_m - \epsilon_i) \frac{dx}{1+x^2} \\ &= \sigma_m (\epsilon_m - \epsilon_i) \tan^{-1} [x]_0^{\infty} \\ &= \sigma_m (\epsilon_m - \epsilon_i) \frac{\pi}{2} \end{aligned}$$

$$\frac{E_c}{V} = \frac{\sigma_m \pi (\epsilon_m - \epsilon_i)}{2}$$

Constraint energy (E_c) is given by.

$$E_c = \text{Constraint energy per unit vol } x \\ \text{constrained vol of matrix}$$

i.e.

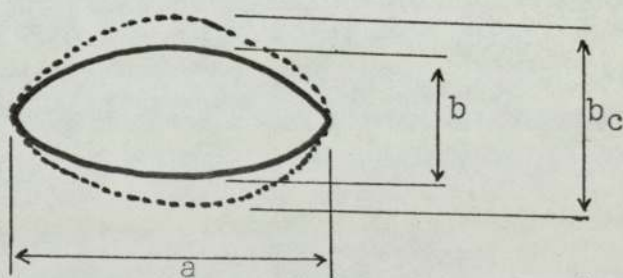
$$E_c = \frac{E_c}{V} \cdot V_c$$

Now the volume of an inclusion is given by:

$$V_i = \frac{\pi abD}{6}$$

where a = major axis, b = minor axis, D = intermediate axis

assuming that constraint (taking a simple case) is in the ab plane and in the b axis direction.



[a and D axes remain constant]

then the constrained volume around the inclusion may be given by:

$$V_c = \frac{\pi aD}{6} (b_c - b)$$

In order to simplify the developed expressions, assume that $(b_c - b)$ is related to the length of the major axis e.g. $(b_c - b) \sim a/2$

$$\text{then } V_c = \frac{\pi a^2 D}{12}$$

Thus constraint energy is given as

$$E_c = \frac{\sigma_m \pi (\epsilon_m - \epsilon_i)}{2} \times \frac{\pi a^2 D}{12}$$

Now relating this constraint energy to inclusion unit volume (i.e. E_c/V_i)

$$\frac{E_c}{V_i} = \frac{\sigma_m \pi (\epsilon_m - \epsilon_i)}{2} \times \frac{\pi a^2 D}{12} \times \frac{6}{\pi D^3}$$

$$\frac{E_c}{V_i} = \frac{\sigma_m \pi (\epsilon_m - \epsilon_i)}{4} \cdot \frac{a^2}{D^2}$$

Assuming that plane strain conditions are operative (i.e. no strain in the D axis direction)

then:

$$\epsilon_i = \ln a/D$$

$$\text{i.e. } \frac{a^2}{D^2} = e^{2\epsilon_i}$$

The equation for constraint energy per unit volume of inclusion can now be represented by

$$\frac{E_c}{V_i} = \frac{\sigma_m \pi (\epsilon_m - \epsilon_i) \rho^{2\epsilon_i}}{4}$$

Appendix 5.4(a)

Derivation of a simplified equation relating inclusion and matrix strains with deformation and constraint energies.

- Assume that (i) 100% utilisation of energy
 (ii) Energy taken up in deforming an inclusion is the sum of the deformation and constraint energies

case (a)

If the inclusion is inherently of greater deformability than the matrix, then assumption (ii) refers to deformation energy alone.

$$\therefore \text{Work done (matrix)} = \text{Work done (inclusion)}$$

$$\text{i.e. } \sigma_m \epsilon_m = \sigma_i \epsilon_i$$

$$\epsilon_i = \epsilon_m \frac{\sigma_m}{\sigma_i}$$

case (b)

If the inclusion is of lesser deformability then equating work done.

$$\sigma_m \epsilon_m = \sigma_i \epsilon_i + \frac{\sigma_m \pi (\epsilon_m - \epsilon_i) e^{2\epsilon_i}}{4}$$

or

$$0 = \sigma_i \varepsilon_i + \frac{\sigma_m \pi (\varepsilon_m - \varepsilon_i) e^{2\varepsilon_i} - \sigma_m \varepsilon_m}{4}$$

Using Newton's analysis to determine the value of ε_i from the above equation

$$\varepsilon_i = x - \frac{f(x)}{f'(x)} \quad \text{where } x \text{ is the estimated value of } \varepsilon_i$$

$$\therefore f(x) = \sigma_i x + \frac{\pi \sigma_m (\varepsilon_m - \varepsilon_x) e^{2x} - \sigma_m \varepsilon_m}{4}$$

$$f'(x) = \sigma_i + \frac{d}{dx} \left(\frac{\pi \sigma_m (\varepsilon_m - \varepsilon_x) e^{2x}}{4} \right)$$

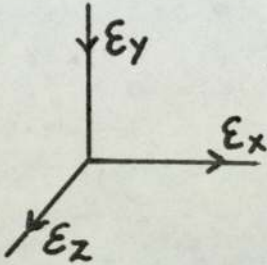
$$= \sigma_i + \frac{\pi \sigma_m e^{2x}}{4} [2(\varepsilon_m - \varepsilon_x) - 1]$$

$$\varepsilon_i \approx x - \frac{\left[\sigma_i x + \frac{\pi \sigma_m (\varepsilon_m - \varepsilon_x) e^{2x} - \sigma_m \varepsilon_m}{4} \right]}{\left[\sigma_i + \frac{\pi \sigma_m [2(\varepsilon_m - \varepsilon_x) - 1] e^{2x}}{4} \right]}$$

Appendix 5.5

Variation in ν with respect to the plane of measurement.

Consider the case of homogeneous deformation such that an applied strain ϵ_y results in the two strains ϵ_x and ϵ_z which may have values $0 \rightarrow \epsilon_y$.

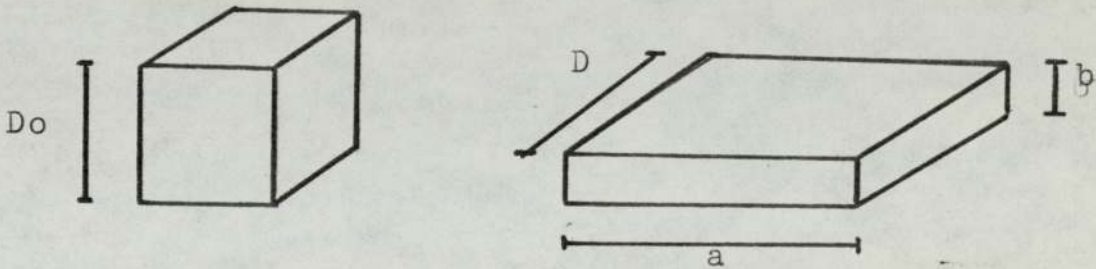


$$\text{i.e. } \epsilon_y = \epsilon_x + \epsilon_z$$

ϵ_y is the largest strain $\epsilon_z \rightarrow 0$

Now consider a block of material of volume D^3 being deformed to a parallelepiped of axial lengths a, b, D , assuming also that there is no volume change.

i.e.



$$\text{Const. vol. } D_0^3 = abD$$

True strains may now be given for each of the directions X, Y, Z as

$$\epsilon_x = \ln \frac{a}{D_0}, \quad \epsilon_z = \ln \frac{D}{D_0} \quad \text{and} \quad \epsilon_y = \ln \frac{D_0}{b}$$

$$\text{i.e.} \quad \ln \frac{a}{D_0} + \ln \frac{D}{D_0} - \ln \frac{D_0}{b} = 0$$

Considering each of the planes on which strains act

$$(XZ) \quad : \quad \epsilon_X \text{ and } \epsilon_Z : \left[\begin{array}{c} \ln \frac{a}{D_0} + \ln \frac{D}{D_0} \end{array} \right]$$

$$(YZ) \quad : \quad \epsilon_Y \text{ and } \epsilon_Z : \left[\begin{array}{c} \ln \frac{D_0}{b} + \ln \frac{D}{D_0} \end{array} \right]$$

$$(XY) \quad : \quad \epsilon_X \text{ and } \epsilon_Y : \left[\begin{array}{c} \ln \frac{a}{D_0} + \ln \frac{D_0}{b} \end{array} \right]$$

For non plane strain in terms of physical measurement D_0 cannot be found and aspect ratios involving other axial lengths can only be measured

i.e.

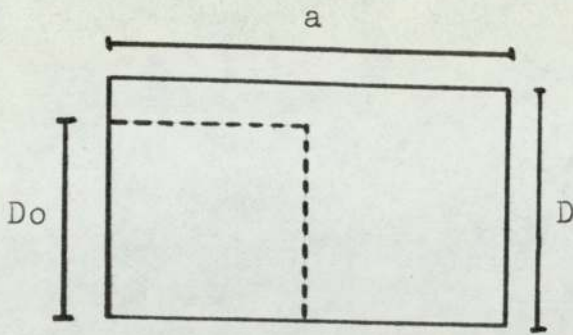
$$(XZ) \quad \text{plane} \quad \lambda_{(XZ)} = a/D$$

$$(YZ) \quad \text{plane} \quad \lambda_{(YZ)} = D/b$$

$$(XY) \quad \text{plane} \quad \lambda'_{(XY)} = a/b$$

Now consider the relationships between the quantity which can physically be measured, and the strains present on each of the planes.

(XZ) plane

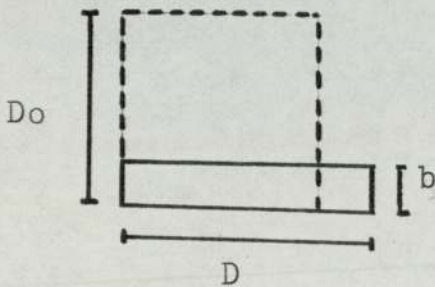


$$\ln \frac{a}{D_0} = \ln \frac{a}{D} + \ln \frac{D}{D_0}$$

i.e. $\epsilon_X = \ln \lambda_{(XZ)} + \epsilon_Z$

$$\therefore \underline{\underline{\ln \lambda_{(XZ)} = \epsilon_X - \epsilon_Z}} \quad (i)$$

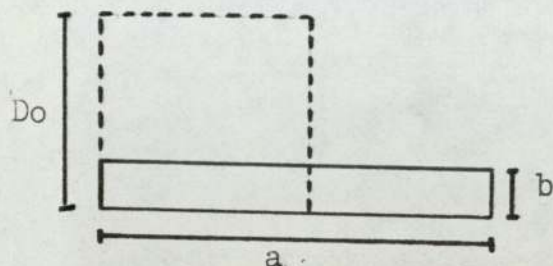
(YZ) plane



$$\ln \frac{D}{b} = \ln \frac{D_0}{b} + \ln \frac{D}{D_0}$$

$$\therefore \underline{\underline{\ln \lambda_{(YZ)} = \epsilon_Y + \epsilon_Z}} \quad (ii)$$

(XY) Plane



$$\ln \frac{a}{b} = \ln \frac{a}{Do} + \ln \frac{Do}{b}$$

$$\therefore \underline{\underline{\ln \lambda^{(XY)} = \epsilon_X + \epsilon_Y}} \quad \text{(iii)}$$

Taking the limiting case of plane strain $\epsilon_Z = 0$

$$\therefore \epsilon_X = \epsilon_Y$$

(XZ) plane

$$\ln \lambda^{(XZ)} = \epsilon_X - 0 = \epsilon_X = \epsilon_Y$$

(YZ) plane

$$\ln \lambda^{(YZ)} = \epsilon_Y + 0 = \epsilon_Y$$

(XY) plane

$$\ln \lambda^{(XY)} = \epsilon_X + \epsilon_Y = 2\epsilon_Y$$

Estimates of the strain ϵ'_Y by measurements on any of the section planes are.

$$\epsilon'_Y (XZ) = \ln \lambda (XZ) \quad (\text{iv}).$$

All equal under

$$\epsilon'_Y (YZ) = \ln \lambda (YZ) \quad (\text{v}).$$

 P_ϵ conditions.

$$\epsilon'_Y (XY) = \frac{1}{2} \ln \lambda (XY) \quad (\text{vi}).$$

These estimates are in fact the equations which are used in practice for measuring inclusion strains during rolling, where plane strain is assumed.

When inclusion strains are measured on the false assumption that plane strain exists, the resultant measured quantities termed $\epsilon'_Y ()$ may be related to the linear strains ϵ_X , ϵ_Y and ϵ_Z i.e.

$$\epsilon'_Y (XZ) = \epsilon_X - \epsilon_Z \quad (\text{vii}).$$

$$\epsilon'_Y (YZ) = \epsilon_Y + \epsilon_Z \quad (\text{viii}).$$

$$\epsilon'_{Y(XZ)} = \epsilon'_{Y(YZ)} =$$

$$\epsilon'_{Y(XY)} = \epsilon_Y \text{ in the}$$

$$\epsilon'_Y (XY) = \frac{1}{2} (\epsilon_X + \epsilon_Y) \quad (\text{ix}).$$

limiting case of P_ϵ when $\epsilon_Z = 0$ & $\epsilon_X = \epsilon_Y$

From the above equations it also follows that $\epsilon'_Y (XY)$ may be estimated from measurements of $\epsilon'_Y (XZ)$ and $\epsilon'_Y (YZ)$ i.e.

$$\epsilon'_Y (XY) = \frac{1}{2} (\epsilon_X + \epsilon_Y)$$

$$= \frac{1}{2} \left(\left[\epsilon'_{Y(XZ)} + \epsilon_Z \right] + \left[\epsilon'_{Y(YZ)} - \epsilon_Z \right] \right)$$

$$\therefore \underline{\underline{\epsilon'_Y (XY) = \frac{1}{2} (\epsilon'_{Y(XZ)} + \epsilon'_{Y(YZ)})}} \quad (\text{x}).$$

Estimation of width spread (ϵ_Z)

Taking the general case for the estimation of ϵ_Y from measurements on the (XY) plane, using the equations which assume plane strain i.e. (vi).

$$\epsilon'_{Y(XY)} = \frac{1}{2} \ln \lambda_{(XY)} = \frac{1}{2} \ln \frac{a}{b}$$

$$\text{Constant volume } D_0^3 = abD$$

$$\therefore \epsilon'_{Y(XY)} = \frac{1}{2} \ln \left(\frac{D_0^3}{Db^2} \right)$$

$$= \frac{1}{2} \ln \left(\frac{D_0}{b} \right)^2 + \frac{1}{2} \ln \frac{D_0}{D}$$

$$\text{i.e. } \underline{\underline{\epsilon'_{Y(XY)}}} = \epsilon_Y - \frac{1}{2} \epsilon_Z \quad (\text{xi})$$

Also

$$\epsilon'_{Y(XZ)} = \epsilon_X - \epsilon_Z \quad (\text{vii})$$

$$\text{but } \epsilon_X = 2 \epsilon'_{Y(XY)} - \epsilon_Y \quad \text{from eqn (ix)}$$

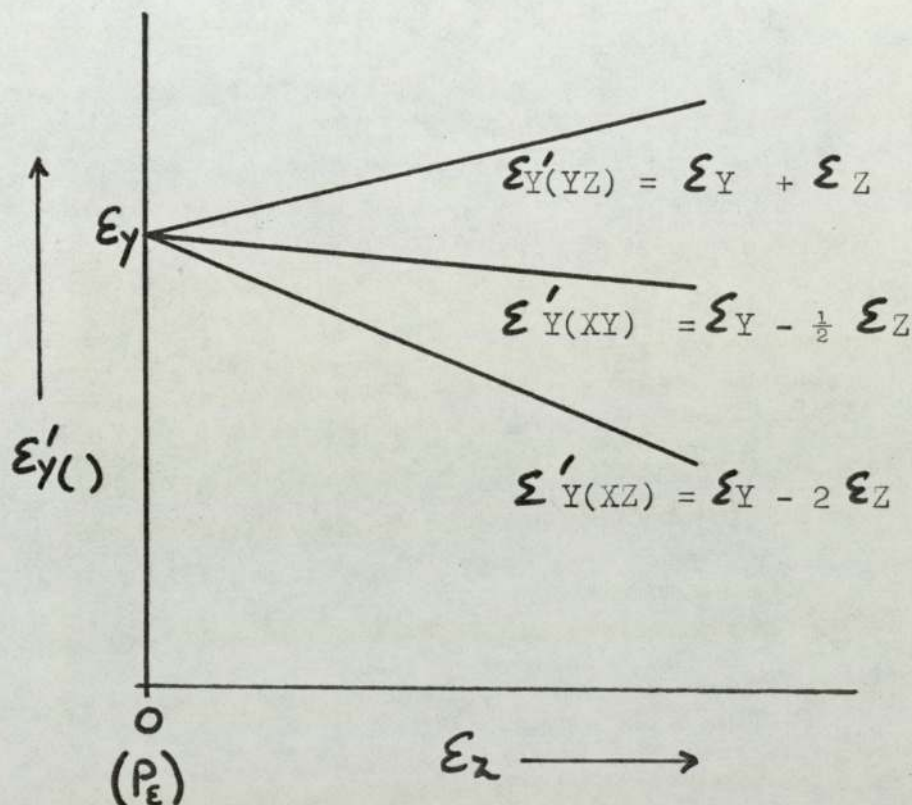
$$\therefore \epsilon'_{Y(XZ)} = 2 \epsilon'_{Y(XY)} - \epsilon_Y - \epsilon_Z$$

$$\text{and } \epsilon'_{Y(XY)} = \epsilon_Y - \frac{\epsilon_Z}{2} \quad \text{from eqn (xi)}$$

$$\therefore \epsilon'_{Y(XZ)} = 2 \left(\epsilon_Y - \frac{\epsilon_Z}{2} \right) - \epsilon_Y - \epsilon_Z$$

$$\text{i.e. } \underline{\underline{\epsilon'_{Y(XZ)}}} = \epsilon_Y - 2 \epsilon_Z \quad (\text{xii})$$

Graphically the variation of the measured estimates of ϵ_Y (ϵ'_Y) for conditions moving away from plane strain are:



from which it is observed that as ϵ_Z increases $\epsilon'_{Y(YZ)}$ increases but both $\epsilon'_{Y(XY)}$ and $\epsilon'_{Y(XZ)}$ decrease.

Estimating ϵ_Z from measurements of $\epsilon'_{Y(XY)}$ and $\epsilon'_{Y(YZ)}$

Combining eqns. (viii) and (xi)

$$\epsilon'_{Y(YZ)} - \epsilon_Z = \epsilon'_{Y(XY)} + \frac{\epsilon_Z}{2}$$

$$\therefore \epsilon_Z = \frac{2}{3} \left[\epsilon'_{Y(YZ)} - \epsilon'_{Y(XY)} \right] \quad \text{(xiii)}$$

Similarly for the planes $\epsilon'_{Y(XY)}$ and $\epsilon'_{Y(XZ)}$

Combining eqns (xii) and (xi)

$$\epsilon'_{Y(XZ)} + 2\epsilon_Z = \epsilon'_{Y(XY)} + \frac{\epsilon_Z}{2}$$

$$\therefore \underline{\underline{\epsilon_Z}} = \frac{2}{3} \left[\epsilon'_{Y(XY)} - \epsilon'_{Y(XZ)} \right] \quad \text{(xiv)}$$

and for $\epsilon'_{X(XZ)}$ and $\epsilon'_{X(YZ)}$

Combining eqns (xii) and (viii)

$$\epsilon'_{Y(XZ)} + 2\epsilon_Z = \epsilon'_{Y(YZ)} - \epsilon_Z$$

$$\therefore \underline{\underline{\epsilon_Z}} = \frac{1}{3} \left[\epsilon'_{Y(YZ)} - \epsilon'_{Y(XZ)} \right] \quad \text{(xv)}$$

Thus it can be seen clearly that by measuring any two strain estimates, the width strain ϵ_Z may be determined

Derivation of a plane strain corrected plasticity index.

From the preceding section it is obvious that measurements of ϵ'_Y () on the (XY) plane will vary and become smaller as the amount of width spread increases.

However, by making measurements either on the (XZ) or the (YZ) plane the value of $\epsilon'_{Y(XY)}$ at $\epsilon_Z = 0$ may be determined i.e. ϵ_Y (P_ϵ).

From eqn. (xi)

$$\epsilon'_{Y(XY)} = \epsilon_Y - \frac{\epsilon_Z}{2}$$

$$\therefore \epsilon_Y = \epsilon'_{Y(XY)} + \frac{\epsilon_Z}{2}$$

Now under normal circumstances the relative plasticity index is given by $\nu = \epsilon_i / \epsilon_m$. i.e. the strain of the inclusion to the overall strain of the matrix.

ϵ_Y is the only strain which is a dependent variable

It is sensible to measure the matrix strain in the Y direction. i.e. ϵ_{mY}

$$\nu_{P_\epsilon} = \frac{\epsilon_Y}{\epsilon_{mY}} \quad \text{for } P_\epsilon \text{ conditions } \left(\epsilon_{mY} = \ln \frac{h_o}{h_f} \right)$$

where plane strain conditions do not operate

$$\nu_{P_\epsilon}^* = \frac{\epsilon'_{Y(XY)}}{\epsilon_{mY}} + \frac{\epsilon_Z}{2 \epsilon_{mY}} \quad (\text{xvi})$$

Now earlier in eqn (xiii) ϵ_Z was defined for the (XY) and (YZ) planes as

$$\epsilon_Z = \frac{2}{3} \left[\epsilon'_{Y(YZ)} - \epsilon'_{Y(XY)} \right]$$

and substituting into eqn (xvi)

$$\nu_{P_\epsilon}^* = \frac{\epsilon'_{Y(XY)}}{\epsilon_m} + \frac{\epsilon'_{Y(YZ)} - \epsilon'_{Y(XY)}}{3 \epsilon_m}$$

$$\therefore \nu_{P_\epsilon}^* = \frac{2 \epsilon'_{Y(XY)} + \epsilon'_{Y(YZ)}}{3 \epsilon_m} \quad \text{(xvii)}$$

A similar expression may also be arrived at for $\epsilon'_{Y(XY)}$ and $\epsilon'_{Y(XZ)}$

i.e.

$$\nu_{P_\epsilon}^* = \frac{\epsilon'_{Y(XY)}}{\epsilon_m} + \frac{\epsilon'_{Y(XY)} - \epsilon'_{Y(XZ)}}{3 \epsilon_m}$$

$$\therefore \nu_{P_\epsilon}^* = \frac{4 \epsilon'_{Y(XY)} - \epsilon'_{Y(XZ)}}{3 \epsilon_m} \quad \text{(xviii)}$$

and

$$\nu_{P_z}^* = \frac{\epsilon'_{Y(XY)}}{\epsilon_m} + \frac{\epsilon'_{Y(YZ)} - \epsilon'_{Y(XZ)}}{6\epsilon_m}$$

but $\epsilon'_{Y(XY)} = \frac{\epsilon'_{Y(YZ)} + \epsilon'_{Y(XZ)}}{2}$

$$\therefore \nu_{P_z}^* = \frac{2\epsilon'_{Y(YZ)} + \epsilon'_{Y(XZ)}}{3\epsilon_m}$$

(xix)

Appendix 5.5(a)

Summary of the more useful equations used for the measurement of strains on the various planes.

Physical quantities measured are $\lambda_{(XY)}$, $\lambda_{(YZ)}$, $\lambda_{(XZ)}$.

Quantities calculated are the values

$$\epsilon'_{Y(XY)} = \frac{1}{2} \ln \lambda_{(XY)}$$

$$\epsilon'_{Y(YZ)} = \ln \lambda_{(YZ)}$$

$$\epsilon'_{Y(XZ)} = \ln \lambda_{(XZ)}$$

Planes	$\epsilon_{Z'}$	ϵ_Y Estimate (Plain strain)
$[(XY):(YZ)]^{\rightarrow}$	$\frac{2}{3} [\epsilon'_{Y(YZ)} - \epsilon'_{Y(XY)}]$	$\frac{1}{3} [2 \epsilon'_{Y(XY)} + \epsilon'_{Y(YZ)}]$
$[(XY):(XZ)]$	$\frac{2}{3} [\epsilon'_{Y(XY)} - \epsilon'_{Y(XZ)}]$	$\frac{1}{3} [4 \epsilon'_{Y(XY)} - \epsilon'_{Y(YZ)}]$
$[(YZ):(XZ)]$	$\frac{1}{3} [\epsilon'_{Y(YZ)} - \epsilon'_{Y(XZ)}]$	$\frac{1}{3} [2 \epsilon'_{Y(YZ)} + \epsilon'_{Y(XZ)}]$

+ preferred measurement planes

Also

$$\epsilon'_{Y(XY)} = \frac{\epsilon'_{Y(XZ)} + \epsilon'_{Y(YZ)}}{2}$$

REFERENCES

1. Herty C.H. & Gaines M. : Mining and Met. Invest. Bul. No.34, (1927)
2. Chipman J. & Fethers N.L. : Trans. A.S.M. (1941) 29 953
3. Taylor C.R. & Chipman J. : Trans. A.I.M.E. (1943) 154 228
4. Bell H.B. : Iron & Steel (1954) 27 493-559
5. Chipman J. : Basic open hearth steelmaking (1964) 650. (A.I.M.M.P.E. New York 3rd. Ed.)
6. Sloman H.A. : J.I.S.I. (1941) 143 311
7. Fischer W.A. & Von Ende H. : Archiv. Eisenhutt (1952) 23 21
8. Kiessling R. : Non metallic inclusions in Steel. P.III I.S.I. Publ. No 115
9. Lindon P.H. : PhD Thesis (1967) University of Aston
10. As ref. 8.
11. Sicha M. : Hutnicke Listy (1963) 17 479
12. Elliott J.F. : Elect. Fnce Proc. (1974) Vol 32 62-74
Iron & steel soc of A.I.M.E.
13. Kiessling R. : Jerkont Ann. (1969) 153 79-81
14. Simms C.E. : Trans A.I.M.E. (1959) 215 367-393
15. Pickering F.B. : The production and application of clean steels - I.S.I. London
16. Morgan E.L. et al : J.I.S.I. (1968) 987
17. Farrell J.W. et al : Elect. Fnce. Proc. (1970) 64

18. Elliott J.F., Gleiser M. & Ramakrishna V. :
'Thermochemistry for steelmaking' vols I & II
(Addison - Wesley (1963))
19. Kubaschewski O. & Evans E. : 'Metallurgical
thermochemistry' (Pergamon Press Ltd.)
20. Bodsworth C. & Bell H.B. : 'Physical chemistry of
Iron and steel manufacture' (Longman (1972))
21. Reeves G. : Unpublished work - University of Aston
22. Chipman J. & Pillay T.C.M. : Trans. A.I.M.E. (1961)
221 1277
23. Mclean A. & Ward R.J. : J.I.S.I. (1966) 204 8
24. Gokcen N.A. & Chipman J. : Trans A.I.M.E. (1953)
194 131
25. Turkdogan E.T. : J.I.S.I. (1972) 210 21
26. Korber F. & Oelsen W. : Mitt. Kaiser Wilhelm Inst.
Eisenforsch (1933) 15 271-309
27. Hilty D.C. & Crafts W. : Trans A.I.M.E. (1950)
188 425-431
28. Bell H.B. : J.I.S.I. (1963) 201 116
29. Walsh R.A. & Ramashandran S. : Trans A.I.M.E. (1963)
227 560-562
30. Turkdogan E.T. : Trans A.I.M.E. (1965) 233 2100-2112
31. Waudby P.E. & Salter W.J.M. : J.I.S.I. (1971) 219
518-522
32. Hopp H.U. : Archiv fur das Eisenhüttenwesen (1970)
41 131-138
33. Mclean A. & Ward R.J. : Jnl Metals (1965) 526-528

34. Rohde L.E. et al : Archive fur das Eisenhuttensesen
(1971) 42 165 - 174
35. Robinson S.W. : PhD Thesis Sheffield Polytechnic
(1977)
36. Lindon P.H. & Billington J.C. : Trans Met. Soc.
A.I.M.E. (1969) 245 1775
37. Mclean A. : Jnl. Metals (1968) 20 96
38. Sharma R.A. & Richardson F.D. : Trans A.I.M.E.
(1965) 233 1586
39. Abraham K.P. et al : J.I.S.I. (1960) 196 82
40. Plockinger E. & Wahlster M. : Stahl und Eisen
(1960) 80 659-669
41. Plockinger E. & Wahlster M. : 'Clean Steel' I.S.I.
Spec. Rep. No. 77 (1963) 51-56
42. Grethen E. & Philippe L. : Pre. Int. Cinf.
Balatonfured Hungary (23-26 June (1970) I.S.I.
Publn. 29-34
43. Waudby P.E. : 'Inclusions and their effects on
steel properties'. B.S.C. Conference Bodington Hall,
Leeds University Sept. 1974
44. Levin A.M. : Izvest vuz Cher Met (1965) 12 13-21
45. Ollette et al : Berg-Hutten Monatsh (1968) 113
484-492
46. Chipman J. : Trans. Met Soc A.I.M.E. (1962) 244
1288-9
47. Becker et al : Ann. Phys. (1935) 24 719-752
48. Turpin M.D. & Elliott J.F. : J.I.S.I. (1966)
204 217-225

49. Bogdandy L. Von et al : Archiv. Eisenhutt (1961)
32 451
50. Bogdandy L.Von et al : ibid (1963) 34 235
51. Woehlbier F.H. & Rengstorff G.W.P. : Jnl. Metals
(1967) 19 50-53
52. Sigworth G.K. & Elliott J.F. : Canadian Met.
Quarterly (1972) 11 (No.2) 337-346
53. Sigworth G.K & Elliott J.F. : ibid.
54. Vorobnev A.A. & Levin A.M. : Izv. V.U.Z. Chern.
Met (1967) 12 12-18
55. Straube J. Kuhnett G. & Plockinger E : Archiv. fur
das Eisenhüttenwesen(1967) 509-518
56. Froberg M.G. & Potschke J. : Friberger Forschung
(1969) 144 31-51
57. Forster E : Archiv fur das Eisenhüttenwesen (1967)
607 - 615
58. Froberg M.G.& Potschke J. : Archiv fur das
Eisenhüttenwesen (1970) 41 723 - 346
59. Forster E. & Richter J. : Proc. Int. Conf.
Balatonfüred Hungary (1970) I.S.I. Publ'n 24-28
60. Lindbourg V. & Torsell K. : Trans Met Soc A.I.M.E.
(1968) 242 94 - 102
61. Turkdogan E.T. : J.I.S.I. (1966) 914 - 919
62. Lunner. S.E. : ibid (59) 124-136
63. Salter W.B.M. & Pickering F.B. : J.I.S.I. (1969) 922

64. Herty C.H. & Fitterer G.R. : U.S. Bureau of Mines
(1930) 3054 & (1931) 3081
65. Herty C.H. et al : Min & Met. Invest. Bull. (1932) 58
66. Kawawa et al : Tetsu-to-Hagane (1965) 51 780-783
67. Tajiri I. et al : ibid (1966) 52 554-557
68. Grevillius N.F. : Jemkont Ann. (1969) 153 547-572
69. Lindon P.H. & Billington J.C. : JISI (1969) 340-347
70. Plockinger E. & Wahlster M. : Radex Rundschau (1957)
516 754-770
71. Kozakevitch P. & Ollette M. : Proc. Int Conf.
Balatonfüred Hungary (1970) ISI Pbln 42-49
72. Segal A. : PhD Thesis (1976) Univ. of Cambridge.
73. Linder S. : Scan. Jnl. Met. (1974) 3 137
74. Grevillius N.F. : Jemkont Ann. (1969) 153 547-572
75. Ohkubo M. et al : Nippon Kokan Tech. Rep. (1966) 37 161
76. Ohkubo M. et al : ibid Overseas (1965) 5 7
77. Fischer W.A. & Wahlster M. : Archiv. Eisenhütt (1957)
28 689
78. Kawawa T. et al : Tetsu-to-Hagane (1966) 52 1457
79. Kiessling R. & Lange N. : Special Report 90 ISI
(London) (1964)
80. Seward T.P. (ed Alper A.M.) : 'Phase diagrams' Vol.
6.1 Academic Press. (1970) 331.
81. Rawson H. : 'Inorganic glass forming systems'
Academic Press (1967)
83. Elliott J.F. et al : 'Thermochemistry for steel-
making' Vol II (Addison Wesley) (1963) 667
82. Condon J. : Am. Jnl. Phys (1954) 22 43
84. MacDowell J.F. & Beall G.H. : Jnl. Am. Ceram. Soc.
(1969) 52 17

85. Jones G.O. : 'Glass' (1956) Methuen London. .119.
86. Turnbull D. & Cohen M.H. : Jnl.Am.Ceram.Soc. (1958)
29 .1049.
87. Turnbull D. & Cohen M.H. : 'Modern aspects of the
vitreous state ' Vol 1. (1960).68. (Ed.Mackenzie. J.D.)
88. Turnbull D. & Cohen M.H. : Nature (1961)189.131.
89. MacMillan P.W. : 'Glass - Ceramics' (1964).229.
(Academic press.).
90. Pickering F.B. : Paper 3. Bodington Hall Conference
(1974). University of Leeds.
91. Kiessling R. & Lange N. : Special Report 110. I.S.I.
London.
92. Maunder P.H. & Charles J.A. : J.I.S.I. (1968).705.
93. Hillert M. & Hillert L. : Jnl.Mat. Sci. (1970).610.
94. Pickering F.B. : 'Iron & Steel' (1957).
95. Fischer W.A. & Fleischer H.J. : Arch. Eisenh. (1961)
32.305.
96. Simms C.E. & Dahle F.B. : Trans. A.F.A. (1938)86.796.
97. Baker T.J. & Charles J.A. : J.I.S.I. (1972).702.
98. Unkle H. : Jnl. Inst. Met. (1937)61.171.
99. Scheil E. & Schnell R. 'Stahl u Eisen.'(1952)72.683.
100. Pickering F.B. : J.I.S.I. (1958).148.
101. Malkiewicz T. & Rudnic S. : J.I.S.I. (1963).83.
102. Ekerot S. : Scand. Jnl. Met. (1974)3.151.
103. Asante J.C.B. : MSc. Thesis.(1976) - Aston University.
104. Van Vlack L.H. : Trans A.S.M. (1953)45.741.
105. 'Automatic Inclusion Assessment'. I.S.I. Publication.
106. Baker T.J. : Ph.D. Thesis. (1971) - Univ of Cambridge.

107. Baker T.J. & Charles J.A. (as ref: 97.)
108. Gladman T. : Paper 21. (as ref : 43.)
109. Gove K.B. & Charles J.A. : Met. Tech. (1974).680.
110. Warrick R.J. & Van Vlack L.H. : Trans. A.S.M. (1964)
.672.
111. Chao H.C. & Van Vlack L.H. : Trans. A.S.M. (1965)58
.335.
112. Zeisloft R.H. & Hosford W.F. : Trans. A.S.M. (1969)
62.297.
113. Sundstrom B. : Jnl.Comp.Matls. (1971)5.277.
114. McClintock J. : Jnl.App.Mech. (1968) 35.363.
115. Gove K.B. : Ph.D. Thesis. (1974) Univ of Cambridge.
116. Klevbring B.I. : Met. Trans. (1975)6A.319.
117. McClintock F.A. : 'Ductility' (1968).252. Ohio. A.S.M.
118. Gay N.C. : Tectonophysics. (1968)5(3).211.
119. Ashok S.K. : Ph.D. Thesis. (1976)- Univ of Cambridge.
120. Rice J.R. & Tracey D.M. :
121. Rudnic S. : J.I.S.I. (1966).374.
122. Smith R.B. : Geol.Soc. Am. Bul. (1975).1601.
123. Charles J.A. : Paper 6. (as ref : 43.)
124. Uchiyama I. & Sumita M. : Trans. Nat. Res. Inst. Met.
(Japan.). (1965)7.233.
125. Segal A. & Charles J.A. : Met. Tech. (1977).177.
126. Larke E.C. : 'The rolling of strip, sheet and plate.'
Science Paperback SP54. (1967) Chapman & Hall Ltd..
127. Kiessling R. : Jerkont. Ann. (1969)153.295.
128. Shiraiwa T. et al. : The Sumitomo search' (1974)11.85.
129. Cornfield & Johnson : J.I.S.I. (1973).567.
130. Rees W. & Hopkins B.E. : J.I.S.I. (1952)172.402.
131. Birkle A.J. et al. : Trans. A.S.M. (1966)59.981.

132. Cummings H.W. et al : Trans A.S.M. (1957).482.
133. Franklin A.G. et al. : J.I.S.I. (1964)202.588.
134. Leach J.C. : 'Production and application of clean steels' I.S.I. (1972).
135. Okada H. & Shimada H. : Corrosion (1974)30.97.
136. Keane D.M. : Paper 19. (as ref : 43.)
137. Kiessling R. : (as ref : 8.)
138. Goodier J.N. : Jnl.App.Mech. Trans ASME. E.(1933)55A.39.
139. Eshelby J.D. : Proc. Royal. Soc. (1957)A241.376.
140. Ashby M.F. : Phil. Mag. (1966)14.1157.
141. Gurland J. & Plateau J. : Trans. A.S.M. (1963)56.442.
142. Liu C.T. & Gurland J. : Trans A.S.M. (1968)61.156.
143. Lindsey et al : 'Effect of second phase particles on the mech. propts. of steel.' I.S.I. London (1971).
144. Knott J.F. : Paper 8. (as ref : 43.)
145. McClintock F.A. : Int. Jnl. Fract. Mech. (1968)4.101.
146. Thomason P.F. : Jnl. Inst. Met. (1968)96.360.
147. Brown L.M. & Embury J.D. : Proc 3rd. Int. Conf. 'Strength of metals and alloys' Cambridge (1973).164.
148. Hellen K. : Int. Jnl. Mech. Sci. (1975)17.369.
149. Rogers H.C. : Trans. A.I.M.E. (1960)218.498.
150. Palmer I.G. & Smith G.C. : Proc. Int. Conf. 'Oxide dispersion strengthening' N.Y. (1966).
151. Pickering F.B. : Proc. Conf. 'Toward improved ductility and toughness' Kyoto Japan. (1971).9.
152. Gangulee L. & Gurland J. : Trans. Met. Soc. A.I.M.E. (1967)239.269.
153. Tanaka K. et al. : Phil. Mag. (1970)21.267.
154. Sundstrom B. : Eng. Fract. Mech. (1974)6.483.
155. Klevebring B.I. & Mahrs R. : Scand. Jnl. Met. (1973)
.2.610.

155. Masayuki Toya. : Int. Jnl. Fract. Mech.(1973)9.463.
156. Brown L.M. & Stobbs W.M. : Phil. Mag. (1971)23.1201.
157. Cox T.B. & Low J.R. : Met. Trans. (1974)5.1457.
158. Klevebring B.I. et al. : Met. Trans. (1975)6A.319.
159. Baker T.J. : Paper 11. (as ref : 43.)
160. Roesch L. : Mem. Sci. Rev. Met. (1969)66.29.
161. Aydinceren A. & Kondic V. : Foundry Trade Jnl.
(1969)127.345.
162. Gladman T. et al. : J.I.S.I. (1970)208.172.
163. Edelson B.I. & Baldwin W.M. : Trans. A.S.M. (1962)
55.230.
164. Inoue T. & Kinoshita S. (as ref : 147.)159.
165. Zwilsky K.M. & Grant N.J. : Jnl. Metals (1957)9.1197.
166. Turkalo A.M. & Low J.R. : Trans. Met. Soc. A.I.M.E.
(1958)212.750.
167. Kinoshita S. et al. : Trans. I.S.I.Japan.(1975)15.45.
168. Gladman T. : Conf. Report 'The effect of inclusions
on the mechanical properties of steel' J.I.S.I.(1969).500
169. Argon. A.S. et al. : Met. Trans. (1975)6A.825.
170. Luyckx L. et al. : Jnl. Met. (1974).35.
171. Gladman T. et al. : (as ref ; 143.)68.
172. Baker T.J. & Charles J.A. : (as ref : 143.)
173. Vogels H.A. & Bruening F. : Arch. Eisenh.(1964)35.115.
174. Dahl. W. et al. : Stahl u Eisen (1966)86.782.&.796.
175. Bucher J.H. : J.I.S.I. (1969)207.225.
176. Mihelich J.L. et al. : J.I.S.I. (1971)209.469.
177. Luyckx L. et al. : Met. Trans.(1971)2.3203.
178. Elliott D.N. : Metal. Const. & B.W.J. (1969)1.2S.50.
179. Nagel D. & Schonherr W. : ibid .64.

180. Watkinson F. et al. : Paper 10. (as ref : 43.)
181. Baker T.J. et al. : Metals Tech. (1976).183.
182. Farrow R.J. : BSc. Project.(1975) - Aston University.
183. Trigwell N. : BSc. Project.(1976) - Aston University.
184. Smith R.F. & Knott J.F. : Proc. Conf. ' Practical implication of fracture mechanics to pressure vessel technology' Inst. Mech. Eng. (1971)65.
185. Andrews K.W. : Paper 18. (as ref ; 43.)
186. Easterling K.E. et al. : Met. Sci. Jnl.(1972)6.211.
187. Easterling K.E. et al. : Powder Met.(1973)16.128.
188. 'Lamella tearing in welded steel fabrications' Welding Institute(1972).
189. Roesch L. et al. : Mem. Sci. Rev. Met. (1966)63.941.
190. Grange R.A. : Met. Trans. (1971)2.418.
191. Walker E.F. & Barr R.R. : Paper 15. (as ref : 43.)
192. Embury J.D. et al. : Trans. A.I.M.E. (1967)239.114.
193. Atkinson M. et al. : J.I.S.I. (1960)195.64.
194. Murray J.D. & Johnson A.F. : I.S.I. Special Report 77. (1963).87.
195. Duckworth E. & Ineson E. : ibid .110.
196. Brookesbank D. & Andrews K.W. : J.I.S.I.(1972).246.
197. Andrews K.W. : Paper 18. (as ref : 43.)
198. Brookesbank D. & Andrews K.W. : J.I.S.I.(1972).765.
199. Keane D.M. : Paper 19. (as ref : 43.)
200. Trent E.M. : I.S.I. Special Report 94. (1967).11.
201. Opitz H. & Konig W. : ibid .35.
202. Robinson S.W. : Private communication.
203. Marston G.T. & Murray J.D. : J.I.S.I. (1970).568.
204. Morinaga K. et al. : Tetsu - to - Hagane Overseas. (1964)4.35.

205. Jones A. et al. : Paper 14. (as ref : 43.)
206. Mclean A. & Ward R.G. : J.I.S.I.(1966)204.8.
207. Ramsey G. et al. : Trans. Vac. Met. Conf.(1964).421.
208. Duncumb P. & Jones E.M. : T.I. Research Report 260.
(Dec.1969.)
209. Ward M. : Private communication.
210. Göhler M. : Freiburger Forschungshefte.(1963)B93 P.I.
211. Dietzel A. : Z. Electrochem(1942)48.9.
212. Kozakevitch P. & Urbain G. : Viscosité et structure
des liquides, Centre d'Etudes Supérieures de la
Siderurgie, Metz France (1954)
213. Ekerot S. & Klevebring B.I. : Scand. Jnl.Met.(1975)
214. Goursat E. : 'Mathematical Analysis' Vol.1.
chapter VI, example 9.
215. Jahnke E. & Emde F. : Funktionstabellen mit formeln und
curven von Eugen Jahnke und Fritz Emde. .52. Tubner
- Leipzig & Berlin 3rd. Ed. (1938)
216. Lawton E. : Aston University - Private communication.
217. Alder J.F. & Phillips V.A. : Jnl. Inst. Met.(1954)
83.80.
218. Hull D. : 'Introduction to dislocations' Pergamon
Press. (1969).